Polyether-based Polymer Architectures: From Pharmaceutical Application to Lithium-Ion Conductors

Dissertation
zur Erlangung des Grades
„Doktor der Naturwissenschaften“
im Promotionsfach Chemie

am Fachbereich
Chemie, Pharmazie, Geographie und Geowissenschaften
der Johannes Gutenberg-Universität Mainz

vorgelegt von

Philip Reinhard Dreier
geboren am 22.12.1990
in Worms

Mainz, Juni 2021

This thesis was carried out from February 2018 to June 2021 in the research group of Prof. Dr. Holger Frey at the Department of Chemistry, Johannes Gutenberg University, Mainz.

Dekan: Prof. Dr. Tobias Reich

Prodekanin: Prof. Dr. Tanja Schirmeister

Reviewer 1: Prof. Dr. Holger Frey

Reviewer 2: Prof. Dr. Pol Besenius

Date of oral examination: 21.07.2021

I hereby declare that I wrote the dissertation submitted without any unauthorized external assistance and used only sources acknowledged in the work. All textual passages which are appropriated verbatim or paraphrased from published and unpublished texts as well as all information obtained from oral sources are duly indicated and listed in accordance with bibliographical rules. In carrying out this research, I complied with the rules of standard scientific practice as formulated in the statutes of Johannes Gutenberg University Mainz to insure standard scientific practice.

Für meine Familie

„Wenn die Menschen nur über das sprächen, was sie begreifen, dann würde es sehr still auf der Welt sein.“

Albert Einstein

Danksagungen

Im Folgenden möchte ich mich herzlich bei den Menschen bedanken, die mich im Laufe meines Chemiestudiums und meiner Promotion unterstützt haben.

Beginnen möchte ich mit meinem Doktorvater **Prof. Dr. Holger Frey**, der mir die Möglichkeit eröffnet hat, meinem großen Interesse an der synthetischen Polymerchemie zu folgen. Vielen Dank für die stetige Motivation aber auch die Unterstützung, um meine Ideen in die Tat umzusetzen.

Auch bei **Prof. Dr. Axel H.E. Müller** möchte ich mich sehr herzlich für die hilfreiche Unterstützung und tiefgreifenden Diskussionen im Bereich der Polymerisationskinetik bedanken.

Prof. Dr. George Floudas danke ich für die zahlreichen SAXS-, DSC- und Rheologie-Messungen im Zuge der gemeinsamen Kooperation. **Junyoung Ahn**, und **Prof. Dr. Taihyun Chang** möchte ich für die Durchführung der SGIC-Messungen danken.

Weiterhin sind durch die enge Zusammenarbeit mit den (ehemaligen) Arbeitskreis-Mitgliedern **Rebecca Matthes**, **Ramona Barent**, **Sandra Schüttner**, **Dr. Patrick Verkoyen** und **Dr. Marvin Steube** spannende und innovative Kapitel meiner Arbeit entstanden. Vielen Dank für die reibungslose Kooperation und die spannenden Diskussionen!

Dr. Matthias Bros danke ich für die Einblicke in den Bereich der Biochemie und die zahlreichen Zelltests und Auswertungen der Zellstudien.

Des Weiteren bedanke ich mich für die hilfreiche Unterstützung meiner Bacheloranten **Christian Fuchs** und **Robin Mathes** im Labor.

Weiterhin möchte ich mich bei **Monika Schmelzer** für die unzähligen GPC-Messungen bedanken und dem Ertragen meiner vielfachen Nachfragen, ob die Messungen schon fertig sind. **Ulrike Kemmer-Jonas** danke ich für die Unterstützung im Laborbetrieb und die stetige Bearbeitung meiner zahlreichen Chemikalienbestellungen. Ebenfalls möchte ich mich bei **Heike Riegel-Allen** für die Hilfestellungen bei organisatorischen Problematiken bedanken. **Elena Berger-Nicoletti** danke ich für die vielfachen MALDI-ToF Messungen.

Auch für die vielen fachlichen Diskussionen möchte ich mich bei **Rebecca Matthes**, **Sandra Schüttner**, **Dr. Patrick Verkoyen**, **Dr. Marvin Steube**, **Dr. Tobias Breitbach** und **Dr. Tobias Johann** bedanken.

Bei **Rebecca Matthes**, **Sandra Schüttner**, **Marcel Fickenscher**, **Dr. Patrick Verkoyen**, **Dr. Christian Wahlen**, **Philipp Holzmüller**, **Dr. Marvin Steube**, **Dr. Jennifer Keth**, **Dr. Tobias Breitbach**, **Ramona Barent** und **Christina Gardiner** und vielen anderen für die unvergessliche Zeit bei den zahlreichen Arbeitskreis-Ausflügen bedanken.

Ein besonderer Dank gilt auch **meinen Eltern**, **meinem Bruder Martin** und **meinen Großeltern**. Ohne euch wäre die Promotion und vieles anderes gar nicht erst möglich gewesen!

Schließlich möchte ich mich insbesondere bei **Rebecca** für die allumfassende Unterstützung bedanken. Danke, dass du in sämtlichen Lebenlagen immer für mich da bist!

Content

Motivation and Objectives

Poly(ethylene oxide) (PEO), also known as poly(ethylene glycol) (PEG), is an aliphatic polyether with unique properties. Staudinger and Schweitzer were one of the first scientists who investigated PEO in thorough detail and observed its excellent water solubility.[1] Based on the hydrophilicity and high biocompatibility of the polyether backbone, PEO has been established as the "gold" standard for pharmaceutical applications. The so-called PEGylation of peptides (i.e., bioconjugation) or medical nanocarriers results in the commonly known stealth effect, which allows higher solubilities and enlarged circulation times of drugs or nanoparticles in the blood stream. As a result, multiple FDA approved drugs[2] and mRNA-based vaccines emerged from the fundamental features of PEGylation. Despite these advantages, pronounced allergic reactions were observed by the administration of PEO-based drugs, which are traced back to an immune response of the human body and the presence of anti-PEG antibodies (APA). Consequently, accelerated blood clearance of PEGylated pharmaceutics and anaphylactic shocks were observed. Recently, the underlying binding mechanism of anti-PEG APAs was revealed and is based on the selective recognition and trapping of the linear polymer in the antibody paratope.[3] Hence, the following question arises:

"Can we modify the linear chain architecture of PEO to prevent binding of APA antibodies, whilst remaining the crucial water solubility and high biocompatibility of the underlying polyether?"

This is addressed by the investigation of polyether copolymers based on EO and glycidyl ether as PEGylation substituent. For copolymerizations, the incorporation of the monomers along the chain depends on their relative reactivities. Known from carbanionic copolymerization, the structure of the monomers, chain-ends and the employed solvent have a distinct influence on the copolymerization kinetics. However, in anionic ring-opening polymerization of EO and glycidyl ethers, the influence of the solvent and the monomer structure is rather unexplored until today. Therefore, the first part additionally deals with a second question:

"What are the driving forces in the kinetics of the anionic ring-opening copolymerization of EO and glycidyl ethers?"

Besides the utilization in biomedical applications, PEO is widely applied in the field of polymer electrolytes.[4] The high polarity of the polyether backbone allows the dissolution of salts and the salt-doped material reaches high ionic conductivities. The non-flammability of the material makes it an interesting safe alternative for liquid-based electrolytes in lithium metal-based batteries. Especially PEO and polystyrene-based block copolymers have been thoroughly investigated in this field of research because they combine ionic conductivity and mechanical stability in one distinct material.[5] However, the synthetic diversity of carbanionic and oxyanionic ring-opening copolymerizations are merely gradually finding its way into the area of polymer electrolytes. Consequently, the second part of this thesis addresses the third question:

"How can we increase the performance and mechanical stability of PEO and PS-based polymer electrolytes for lithium metal-based batteries from a synthetical point of view?

References

(1) Staudinger, H.; Schweitzer, O. Über hochpolymere Verbindungen, 20. Mitteil.: Über die Poly-äthylenoxyde. *Ber. dtsch. Chem. Ges. A/B* **1929**, *62*, 2395–2405.

(2) Alconcel, S. N. S.; Baas, A. S.; Maynard, H. D. FDA-approved poly(ethylene glycol)–protein conjugate drugs. *Polym. Chem.* **2011**, *2*, 1442.

(3) Huckaby, J. T.; Jacobs, T. M.; Li, Z.; Perna, R. J.; Wang, A.; Nicely, N. I.; Lai, S. K. Structure of an anti-PEG antibody reveals an open ring that captures highly flexible PEG polymers. *Commun Chem* **2020**, *3*.

(4) Xue, Z.; He, D.; Xie, X. Poly(ethylene oxide)-based electrolytes for lithium-ion batteries. *J. Mater. Chem. A* **2015**, *3*, 19218–19253.

(5) Phan, T. N. T.; Issa, S.; Gigmes, D. Poly(ethylene oxide)-based block copolymer electrolytes for lithium metal batteries. *Polymer International* **2018**, *164*, A5019.

Abstract

Poly(ethylene oxide) (PEO), also known as poly(ethylene glycol) (PEG) is widely utilized in pharmaceutical applications and in lithium-based batteries as a polymer electrolyte due to the outstanding hydrophilicity and polarity of this aliphatic polyether. The modification of the PEO chain architecture and the combination of PEO with mechanical stable polymers in one distinct block structure results in special materials, whilst the underlying advantages of PEO are retained. This thesis focuses on both areas of research and is divided in three parts.

Chapter 1 describes the fundamental polymerization techniques for the synthesis of the herein investigated polyether copolymers and block copolymers. Therefore, the underlying kinetics of the anionic ring-opening and carbanionic (co)polymerization are discussed in detail. Additionally, an overview of the established synthesis routes of multifunctional polyethers and polystyrene-*block*-poly(ethylene oxide) (PS-*b*-PEO) structures are given. Details concerning the application of PEO and PS-*b*-PEO as polymer electrolytes are discussed. In a final part, advantages and disadvantages of PEO and alternatives as PEGylation agents are highlighted.

Chapter 2 focuses on the investigation of polyether copolymers synthesized via anionic ring-opening copolymerization based on EO and glycidyl ethers from a pharmaceutical and kinetic point of view.

In **chapter 2.1**, copolymers of EO and glycidyl methyl ether (P(EO-*co*-GME)) are discussed as alternative PEGylation agents. For the first time, anionic ring-opening copolymerization was successfully employed for the synthesis of P(EO-*co*-GME) due to novel synthesis of glycidyl methyl ether (GME). The relative incorporation of EO and GME along the polymer chain were monitored via *in situ* ^{1}H NMR measurements and Monte Carlo simulations, showing an almost ideal random copolymerization. Subsequently, fundamental enzyme-linked immunosorbent assays (ELISA) reveal that the incorporation of GME in the PEO structure results in a weakening up to complete prevention of the binding of anti-PEG antibodies to the polyether copolymers, depending on incorporated GME. Additionally, cell viability tests of murine immune cells emphasize that P(EO-*co*-GME) is non-cell toxic, shows no unspecific activation and therefore is as biocompatible as the established PEO.

The copolymerization kinetics of EO and glycidyl ethers are further investigated in **chapter 2.2** via *in situ* ^{1}H NMR spectroscopy, concerning solvent and monomer structure. A preferred incorporation of allyl glycidyl ether (AGE) and vinyloxy ethyl glycidyl ether (EVGE) compared to EO in THF and DMSO is observed, while the effect is more pronounced in the case of EVGE. Implementation of supporting density functional theory (DFT) calculations reveal that the microstructure of EO and glycidyl ether copolymers is governed by the complexation capability of glycidyl ether monomers with the cation and vice versa the underlying structure of the monomer. It is further shown that the intensity of the complexation depends on the employed solvent.

In **Chapter 3**, the influence of the polymer architecture on the morphology, mechanical and conductive properties of PEO-based block co- and terpolymers and the fundamental synthesis of the underlying materials are investigated in thorough detail.

Chapter 3.1 highlights solvent gradient interaction chromatography (SGIC) as a viable analytic method for the determination of the end-capping efficiency of EO and glycidyl ethers of living polystyryl lithium. SGIC is further employed for the investigation of the deprotection and derivatization of the resulting hydroxy functional polystyrenes.

Chapter 3.2 builds upon the obtained knowledge of chapter 2.2 and 3.1. A novel synthetic approach is elucidated for the incorporation of charged trifluoromethanesulfonamide groups in the polyether backbone of PS-*b*-PEO structures. Therefore, a synthesis protocol based on the combination of carbanionic and anionic ring-opening copolymerization is presented in detail. Herein, for the first time, the Mitsunobu reaction is employed as a post-polymerization reaction. Subsequently, the obtained single-ion conducting polymer electrolyte is investigated concerning their thermal properties and show several advantages compared to its salt-doped analogs.

Chapter 3.3 illustrates the application of solid phase peptide synthesis chemistry for the efficient linkage of tapered P(I-*co*-S) and PEO in a well-defined material with thermoplastic elastomer (TPE) behavior. Subsequent salt-doping of the block terpolymer and conductivity measurements reveal elevated ionic conductivity at higher temperatures, while rheological measurements confirm a high mechanical stability of the material.

Chapter A1 describes the synthesis and application of ABA triblock copolymers based on long-chain alkyl glycidyl ethers and PEO. Subsequent rheological measurements reveal hydrogel formation in water due to hydrophobic interactions of the alkyl chains independent of pH and salt concentration. This chapter was prepared by a joint venture with Dr. Patrick Verkoyen and was published in *Biomacromolecules* **2020**, *21*, 8, 3152–3162.

In **chapter A2**, the general concept of the synthesis of polyether copolymers based on EO and short chain glycidyl ethers and their application as PEGylation alternative is summarized in a European pending patent.

Zusammenfassung

Der aliphatische Polyether Polyethylenoxid (PEO), auch bekannt als Polyethylenglykol (PEG), findet aufgrund seiner hervorragenden Hydrophilie und Polarität breite Anwendung in pharmazeutischen Anwendungen und in Lithium-basierten Batterien als Polymerelektrolyt. Die Modifikation der PEO-Kettenarchitektur und die Kombination von PEO mit mechanisch stabilen Polymeren in einer Blockstruktur führt zu speziellen Materialien, welche die grundlegenden Vorteile von PEO beinhalten. Die vorliegende Arbeit konzentriert sich auf diese beiden Forschungsgebiete und ist in drei Teile gegliedert.

Kapitel 1 beschreibt die grundlegenden Polymerisationstechniken für die Synthese der hier untersuchten Polyethercopolymere und Blockcopolymere. Hierbei werden die zugrundeliegenden kinetischen Aspekte der anionischen Ringöffnenden und der carbanionischen (Co)polymerisation ausführlich diskutiert. Zusätzlich wird ein Überblick über die etablierten Syntheserouten von multifunktionellen Polyethern und Polystyrol-*block*-Polyethylenoxid-Strukturen (PS-*b*-PEO) gegeben. Details zur Anwendung von PEO und PS-*b*-PEO als Polymerelektrolyte werden ebenfalls diskutiert. Im letzten Teil werden Vor- und Nachteile von PEO und alternativen Strukturen für die PEGylierung gegenübergestellt.

Kapitel 2 konzentriert sich aus pharmazeutischer und kinetischer Sicht auf die Untersuchung von Polyethercopolymeren, die über anionische Ringöffnende Copolymerisation auf Basis von EO und Glycidylethern synthetisiert wurden.

In **Kapitel 2.1** werden Copolymere aus EO und Glycidylmethylether (P(EO-*co*-GME)) als alternative PEGylierungsmittel diskutiert. Aufgrund von neuartigen Synthesen von Glycidylmethylether (GME) wurde die erstmalige Synthese von P(EO-*co*-GME) durch anionische Ringöffnende Copolymerisation erfolgreich durchgeführt. Der relative Einbau von EO und GME entlang der Polymerkette wurde durch *in situ* ^{1}H-NMR-Messungen und Monte-Carlo-Simulationen untersucht und zeigt eine nahezu idealstatistische Copolymerisation. Grundlegende *Enzyme-linked Immunosorbent Assays* (ELISA) zeigen, dass der Einbau von GME in die PEO-Struktur zu einer Abschwächung bis hin zur vollständigen Verhinderung der Bindung von PEG-Antikörpern an die Polyether-Copolymere führt, in Abhängigkeit zur Menge an eingebautem GME. Darüber hinaus unterstreichen Zellviabilitätstests an murinen Immunzellen, dass P(EO-*co*-GME) nicht zelltoxisch ist, keine unspezifische Aktivierung zeigt und somit entsprechend des etablierten PEO biokompatibel ist.

Die Copolymerisationskinetik von EO und Glycidylethern wird in **Kapitel 2.2** mittels *in situ* ^{1}H-NMR-Spektroskopie hinsichtlich Lösungsmittel und Monomerstruktur tiefergehend untersucht. Es wird ein bevorzugter Einbau von Allylglycidylether (AGE) und Vinyloxyethylglycidylether (EVGE) im Vergleich zu EO in THF und DMSO beobachtet, wobei der Effekt im Falle von EVGE stärker ausgeprägt ist. Die Durchführung von unterstützender Dichtefunktionaltheorie (DFT)-Berechnungen zeigt, dass die Mikrostruktur von EO und Glycidylether-Copolymeren von der Komplexierungsfähigkeit der Glycidylether-Monomere mit dem Kation und vice versa von der

zugrundeliegenden Struktur des Monomers bestimmt wird. Es wird weiterhin gezeigt, dass die Intensität der Komplexierung vom verwendeten Lösungsmittel abhängt.

In **Kapitel 3** wird der Einfluss der Polymerarchitektur auf die Morphologie, die mechanischen und leitfähigen Eigenschaften von PEO-basierten Blockco- und -terpolymeren, sowie die grundlegende Synthese der verwendeten Materialien eingehend untersucht.

In **Kapitel 3.1** wird die Lösungsmittel-Gradienten-Interaktions-Chromatographie (SGIC) als praktikable Analysemethode für die Bestimmung der Endgruppenfunktionalisierungs-Effizienz von EO und Glycidylethern mit lebendem Polystyryl-Lithium vorgestellt. Die SGIC wird weiterhin für die Untersuchung der Deblockierung und Derivatisierung der resultierenden hydroxyfunktionellen Polystyrole eingesetzt.

Kapitel 3.2 baut auf den gewonnenen Erkenntnissen aus Kapitel 2.2 und 3.1 auf. Es wird ein neuartiger Syntheseansatz für den Einbau von geladenen Trifluormethansulfonamid-Gruppen in das Polyether-Rückgrat von PS-*b*-PEO-Strukturen aufgezeigt. Dazu wird ein Syntheseprotokoll, das auf der Kombination von carbanionischer und anionischer Ringöffnenden-Copolymerisation basiert, im Detail vorgestellt. Dabei wird zum ersten Mal die Mitsunobu-Reaktion als polymeranaloge Polymerisation etabliert. Anschließend wird der erhaltene Ein-Ionen-leitende Polymerelektrolyt auf seine thermischen Eigenschaften untersucht, wobei einige Vorteile gegenüber seinen salzdotierten Analoga aufgezeigt werden.

Kapitel 3.3 veranschaulicht die Anwendung der Festphasen-Peptidsynthesechemie für die effiziente Verknüpfung von verjüngtem P(I-*co*-S) und PEO in einem wohldefinierten Material mit thermoplastischem Elastomerverhalten. Die anschließende Salzdotierung des Blockterpolymers und Leitfähigkeitsmessungen zeigen eine erhöhte Ionenleitfähigkeit bei höheren Temperaturen, während rheologische Messungen eine hohe mechanische Stabilität des Materials bestätigen.

Kapitel A1 beschreibt die Synthese und Anwendung von ABA-Triblockcopolymeren auf Basis von langkettigen Alkylglycidylethern und PEO. Rheologische Messungen zeigen eine Hydrogelbildung in Wasser aufgrund hydrophober Wechselwirkungen der Alkylketten unabhängig von pH-Wert und Salzkonzentration. Dieses Kapitel wurde in Zusammenarbeit mit Dr. Patrick Verkoyen erstellt und in *Biomacromolecules* **2020**, *21*, 8, 3152-3162 veröffentlicht.

In **Kapitel A2** wird das allgemeine Konzept der Synthese von Polyether-Copolymeren auf der Basis von EO und kurzkettigen Glycidylethern und deren Anwendung als PEGylierungsalternative in einem angemeldeten europäischen Patent vorgestellt.

Author Contributions

Chapter 1 resulted from thorough literature research and was exclusively written by the author of this thesis.

Chapter 2.1 is the result of an equal contribution with Rebecca Matthes and the author of this thesis. Monomer and polymer synthesis as well as characterization were conducted by Rebecca Matthes and the author of this thesis. Fabian Fuß assisted within the synthesis part of this project. *In situ* ^{1}H NMR kinetics were performed by the author of this thesis together with Rebecca Matthes and Sandra Schüttner. Monte-Carlo Simulations were conducted by Ramona D. Barent. Rebecca Matthes conducted the ELISA measurements with the assistance of Fabian Fuß. Dr. Matthias Bros performed the corresponding cell tests at the University Medical Center of the Johannes Gutenberg University Mainz. Rebecca Matthes and the author of this thesis equally wrote the manuscript. All authors discussed the results and commented on the manuscript.

Chapter 2.2 is the result of an equal contribution with Rebecca Matthes and the author of this thesis, in additional collaborations with Ramona Barent and Sandra Schüttner from the research group of Prof. Dr. Holger Frey. *In situ* ^{1}H NMR kinetic measurements were performed by the author of this thesis together with Rebecca Matthes and technical assistance by Sandra Schüttner. Polymer characterization was conducted by Rebecca Matthes and the author of this thesis. Supporting DFT calculations were performed by Ramona D. Barent. Rebecca Matthes and the author of this thesis equally wrote the manuscript. Ramona D. Barent assisted with the DFT calculation section of the manuscript. All authors discussed the results and commented on the manuscript.

Chapter 3.1 is the result of a collaboration with Prof. Dr. Taihyun Chang and Junyoung Ahn from the Pohang University of Science and Technology (POSTECH), South Korea. The author of this thesis prepared and characterized the corresponding samples of this manuscript. SGIC measurements were performed by Prof. Dr. Taihyun Chang and Junyoung Ahn in South Korea. The author of this thesis wrote the manuscript. All authors discussed the results and commented on the manuscript.

In **chapter 3.2**, the author of this thesis prepared and characterized all samples from the manuscript with partial assistance from Robin Mathes. The author of this thesis wrote the manuscript. All authors discussed the results and commented on the manuscript.

Chapter 3.3 is the result of a collaboration with Prof. Dr. Floudas from the University of Ioannina, Greece. The author of this thesis prepared and characterized the corresponding samples of this manuscript in a joint venture with Dr. Marvin Steube from the research group of Prof. Dr. Frey. SAXS, rheological and conductivity measurements were performed by Prof. Dr. Floudas in the Max Planck Institute for Polymer Research (MPIP) in Mainz as well as the University of Ioannina in Greece. The author of this thesis wrote the manuscript. All authors discussed the results and commented on the manuscript.

Chapter A1 is the result of a collaboration with Dr. Patrick Verkoyen from the research group of

Prof. Dr. Frey. The author of this thesis prepared the corresponding samples of the manuscript, partially wrote the synthesis part of the publication and commented on the manuscript.

Chapter A2 is the result of the joint venture from Chapter 2.1. Rebecca Mohr, Prof. Dr. Frey and the author of this thesis equally wrote the patent in cooperation with Dr. Andrea Sommer from Patent Affairs (under assignment of the Johannes Gutenberg University of Mainz).

Graphical Abstract

Chapter 2.1

Questioning a Paradigm: Random PEG Copolymers for a Better PEGylation?

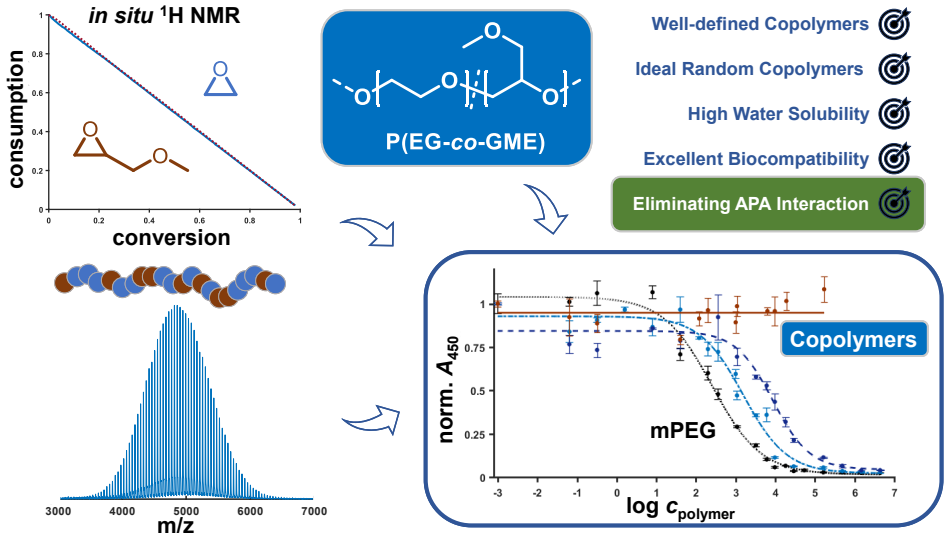

Chapter 2.2

***In situ* Kinetics is Indispensable: Influence of Solvents and Monomers on Anionic Ring-Opening Copolymerization of Epoxides**

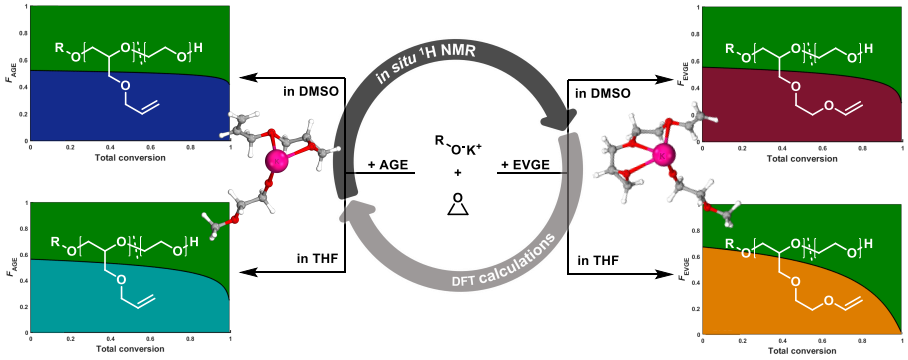

Graphical Abstract

Chapter 3.1

Epoxide Functionalization of Polystyryl-Anions Studied via Solvent Gradient Interaction Chromatography

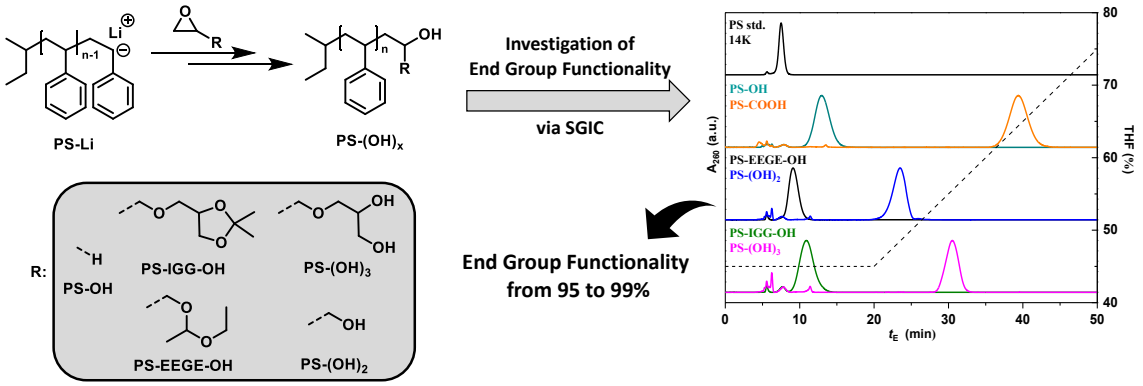

Chapter 3.2

Introduction of Multiple Charged Trifluoromethanesulfonamide Groups into Poly(ethylene oxide) Blocks of Polystyrene-Poly(ethylene oxide) Block Copolymer Electrolytes via the Mitsunobu Reaction

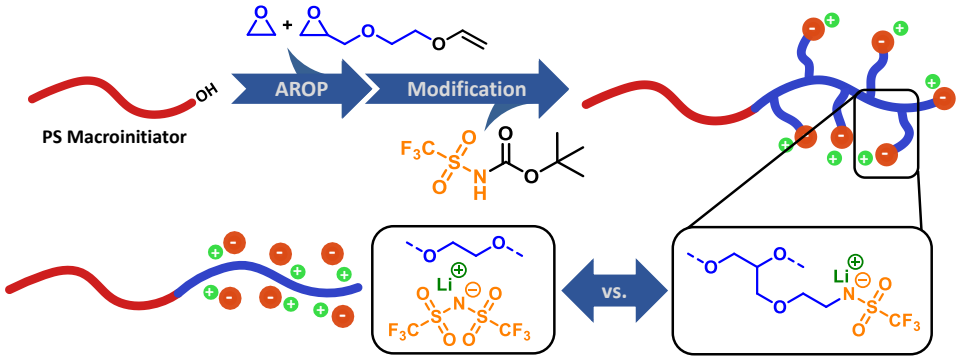

Chapter 3.3

High Yield Peptide Synthesis Strategies for Complex Block Terpolymers: Amphiphilic Thermoplastic Elastomers and their Application as Solid Polymer Electrolytes

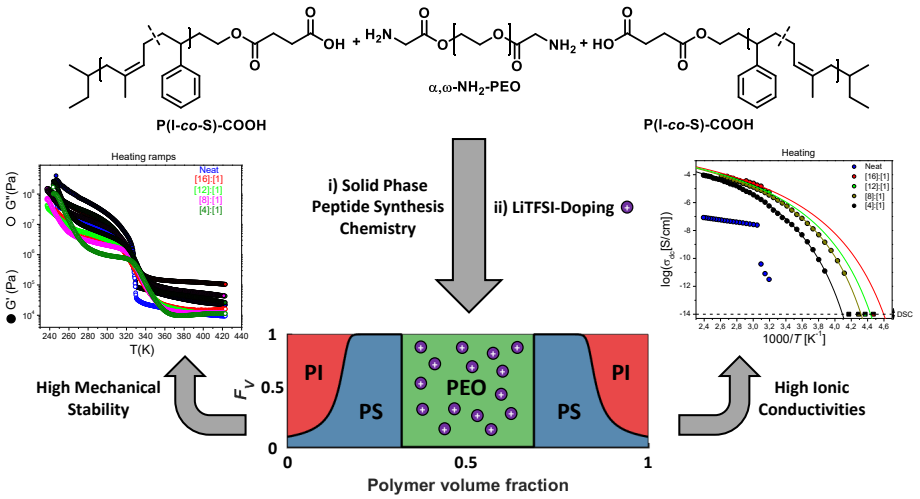

Chapter A1

“Dumb” pH-Independent and Biocompatible Hydrogels Formed by Copolymers of Long-Chain Alkyl Glycidyl Ethers and Ethylene Oxide

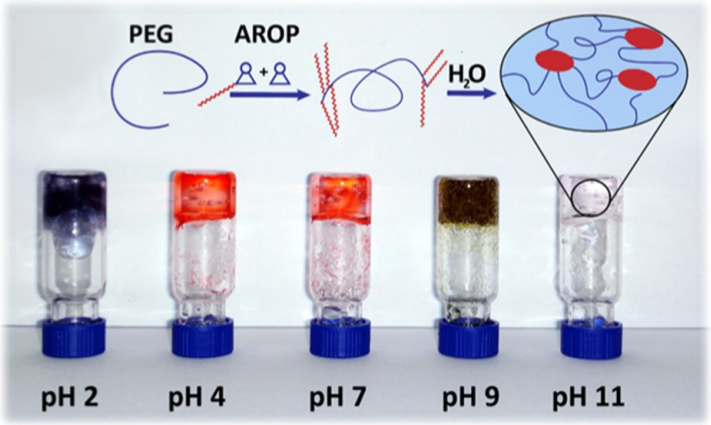

Chapter 1

Introduction

Living Carbanionic Polymerization

The revolutionary observation of the living carbanionic polymerization (LAP) by Michael Szwarc[1] in 1956 has opened a synthetic toolbox for the preparation of different materials and polymeric architectures in a well-defined manner.[2] Suitable monomers for LAP are olefins with activated double bonds through electron withdrawing groups (EWG) (Scheme 1).

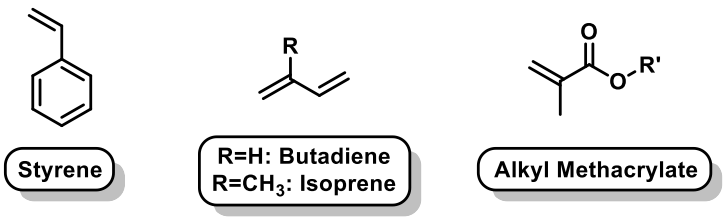

Scheme 1. Suitable general monomer structures for living carbanionic polymerization.

The LAP relies on a fast initiation step ($k_{initiation} > k_{propargation}$) (Scheme 2) with organometallic reagents (Li, Na, K or Cs), which results in a uniform chain-growth and narrow molecular weight distributions. The high sensitivity and reactivity of the carbanion demands the absence of oxygen, moisture and electrophilic impurities to prevent termination reactions.

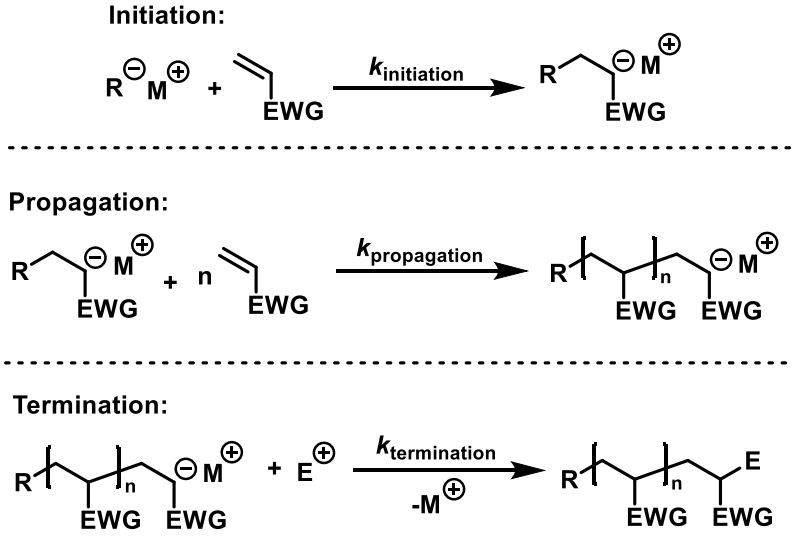

Scheme 2. Mechanism of the carbanionic polymerization of activated olefins (M: Li, Na, K or Cs, EWG: Electron withdrawing group, E: Electrophile).

This also includes thorough purification of the utilized monomers and solvents. Besides inert and apolar cyclohexane and benzene, THF is also a suitable polar solvent for LAP, especially allowing the polymerization of otherwise non-polymerizable or non-soluble vinyl monomers. With the utilization of THF, temperatures as low as -78 °C must be employed to impede proton abstraction reactions of the highly basic chain end at the solvent and to retain control over the polymerization kinetics. After full monomer consumption is reached, the chain end remains “living”, which offers a large variety of synthetic follow-up reactions with electrophiles or other monomers.[3]

Synthesis of Block Copolymers via Carbanionic Polymerization

Based on the abovementioned mechanism, the addition of other activated olefinic monomers to the active chain end results in block copolymer (BCP) structures (Scheme 3).[4] Depending on the initiation step, several BCP architectures are accessible via LAP. For example, initiation with monofunctional alkyl lithium species, e.g., butyl lithium, and sequential addition of monomer A and B results in AB-type BCP structures. In comparison, the utilization of potassium naphthalenide leads to an electron transfer reaction from the alkali metal complex to the monomer. After combination of two anion radicals a dianionic initiator species is formed, which initiates bidirectional chain-growth.

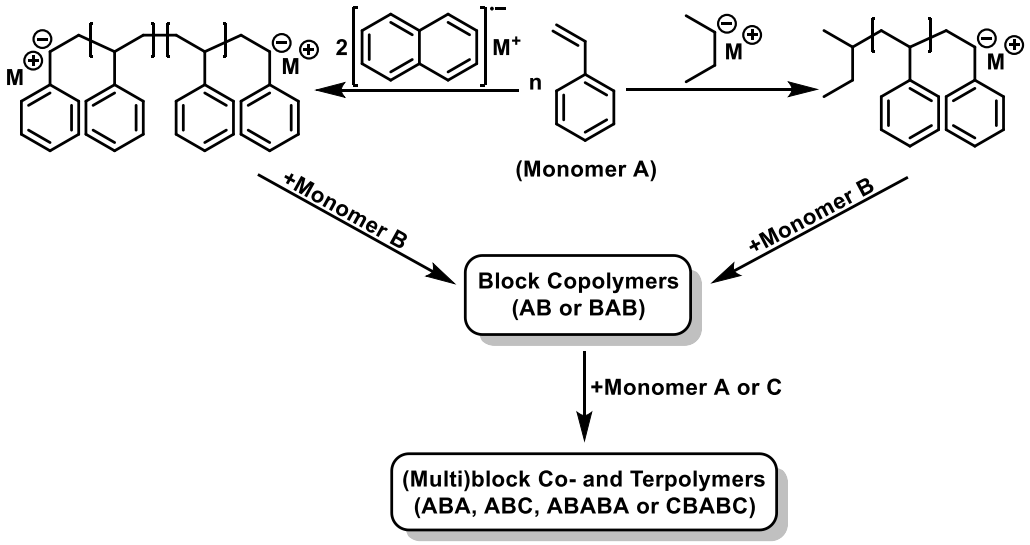

Scheme 3. Carbanionic synthesis route for (multi)block co- and terpolymers via the sequential approach.

After full monomer consumption, a homopolymer with two remaining living chain ends in α- and ω-position remains. Hence, the sequential addition of monomer B consequently results in a BAB triblock copolymer structure.[4,5] Independent of the initiator species, the chain end also remains active after quantitative incorporation of the second monomer. Therefore, multiblock copolymer structures are accessible by the combination of the LAP with the sequential monomer approach (Scheme 3).[6]

Anionic Ring-Opening (Co)polymerization of Ethylene Oxide and Monosubstituted Epoxides

Ethylene oxide (EO) and monosubstituted epoxides are typical monomers for the synthesis of polyethers with CH2-CHR-O repeating units. Epoxide monomers can be obtained via selective oxidation of double bonds with oxygen and peroxides as well as the base-catalyzed ring-closure of epichlorohydrin and chlorohydrin compounds (Figure 1). Additionally, glycidol represents a commonly utilized starting compound to obtain suitable epoxide monomer structures.

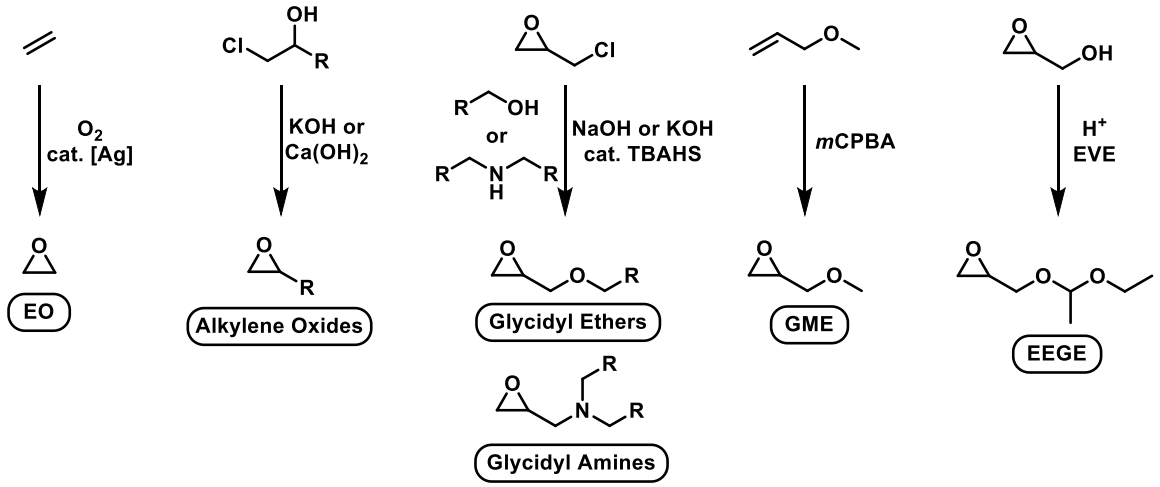

Figure 1. Overview and synthesis of EO and comonomers feasible for AROP conditions; EO: ethylene oxide, TBAHS: tetrabutylammonium hydrogensulfate, GME: glycidyl methyl ether, EVE: ethyl vinyl ether, EEGE: ethoxy ethyl glycidyl ether.

Besides special polymerization methods,[7] poly(ethylene oxide) (PEO), also known as poly(ethylene glycol) (PEG), is typically synthesized via anionic ring-opening polymerization (AROP) of ethylene oxide (EO) with a sodium, potassium or cesium alkoxide initiator in polar aprotic solvents such as THF,[8] DMSO[9,10] or HMPA.[11] Similar to the reaction conditions in LAP, the absence of moisture and polymerization under inert conditions with pure monomers and dry solvents are unavoidable precautions to prevent side reactions and obtain well-defined structures. Under AROP conditions, the initiation process is strongly accelerated in comparison to the chain propagation, which leads to uniform chain-growth and narrow Poisson-type molecular weight distributions.[12] Only a partially deprotonated initiator needs to be utilized, because a rapid proton exchange between active and dormant species is present (Scheme 4).[7] The high charge density of alkoxides favors their aggregation in solution[13] and different ionic species with different reactivities occur depending on the utilized solvent and counter ion (Scheme 5).

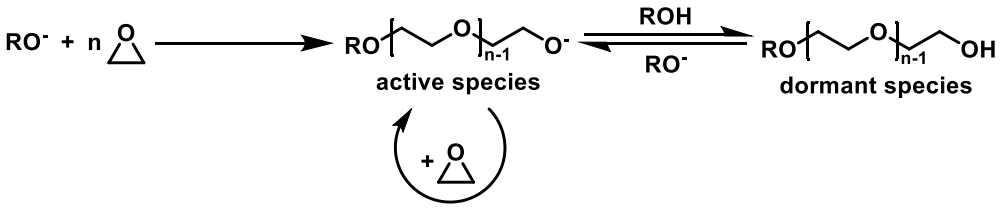

Scheme 4. Mechanism of AROP of EO; partial deprotonation of the initiator results in active and dormant species.

For example, sodium alkoxides form highly aggregated species in THF, resulting in slow polymerization kinetics.[8] In comparison, potassium und cesium cations show higher dissociation constants, and the corresponding alkoxides and ion pairs[8,14,15] (in THF) or free ions[16,17] (in DMSO) are observed.

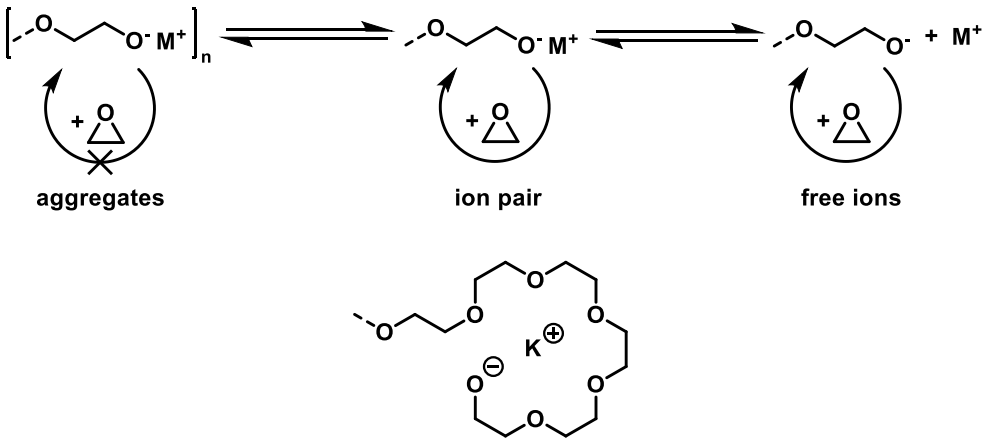

Scheme 5. Top: Different ionic species in AROP; Bottom: Crown ether effect between polyether chain and counter ion of the alkoxide chain end.

These accordingly lead to a faster chain propagation. In the case of lithium cations, the very tight ion pair of lithium and oxygen leads to strong aggregates and very slow or no chain growth at all.[7] Besides increasing the counter ion size, complexation of the cations with crown ethers or cryptands results in more reactive ionic species.[13] The crown ether effect analogously occurs with the polyether chain itself at a certain chain length of >10 repeating units,[15] leading to an auto-acceleration during polymerization.[18]

In AROP, the accessible molecular weight of homopolymers of monosubstituted epoxides is limited due to chain transfer reactions at the monomer. The active alkoxide chain end acts as a strong base and is capable of abstracting the proton of the methyl[19] or methylene group[20] in α-position of the epoxide ring of the monomer. The resulting allylic alkoxide participates as an initiator species (Scheme 6), lowering the molecular weight.

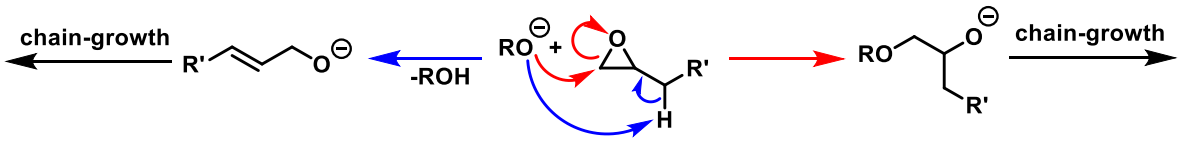

Scheme 6. Chain propagation (red) and chain-transfer reaction of substituted epoxides (blue).

In AROP, the proton abstraction can be suppressed to some extent by the addition of crown ether,[21] the utilization of cesium alkoxides[22] and a partial deprotonation of the initiator.[19]

Properties of (multifunctional) PEO

In PEO, variable amounts of chain end functionalities are accessible via mono- or multifunctional initiators. In comparison, adjustable multiple in-chain functionalities are obtained via copolymerization of EO with monosubstituted epoxides, resulting in copolymers with different properties, depending on the utilized comonomer structure (Scheme 7).[23]

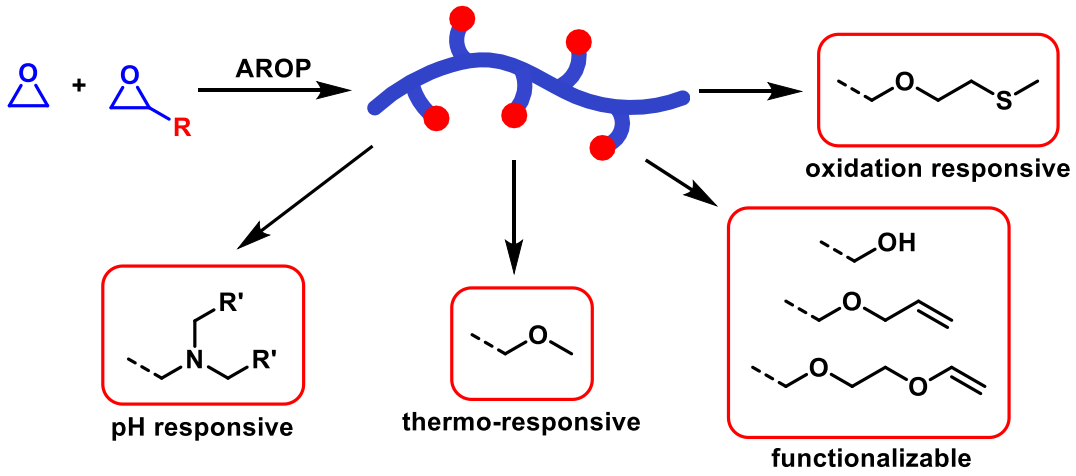

Scheme 7. Synthesis of multifunctional PEO.

For example, pH,[24,25] oxidation[26] and thermo-responsive polyether structures are accessible. Additionally, the functional groups can be addressed via post-polymerization reactions to obtain materials with functional groups insufficient for AROP conditions.[23,27,28]

Depending on the molecular weight, PEO (PEG) occurs as a viscous liquid (200-600 g mol^{-1}) or semicrystalline material (<2000 g mol^{-1}). The melting point of semicrystalline PEO ($T_{m,PEO}$) is in the range of 50 to 60 °C, depending on molecular weight. In the spherulitic crystals, the PEO chains are arranged in a lamellar structure with either elongated or folded forms.[29] Herein, the PEO molecules have a helical structure.[30] The crystallization behavior of PEO can be strongly influenced by guest molecules in the polymer matrix[31,32] or covalently attached "point defects" (deliberately included other moieties) in the polyether chain.[33–35] Additionally, the introduction of comonomer repeating units has a distinct influence on the crystallization behavior of the polyether. Each residue per comonomer repeating unit can be considered as a steric defect in the otherwise linear structure of the chain. Consequently, the degree of crystallization can be tailored via the molar amount of incorporated comonomer. For example, the crystallinity of EO-allyl glycidyl ether copolymers (P(EO-co-AGE)) monotonously decreases with increasing AGE content, until a completely amorphous polyether is obtained.[27] In comparison, BCPs of EO and monosubstituted epoxides show a distinct T_m of the PEO block, which is rather independent of the chemical structure of the comonomer and weight fraction of the second block, due to the commonly high tendency of PEO for phase separation due to crystallization.[25–28] Polyether-based block copolymers are obtainable via sequential addition of the corresponding monomers or reactivation of macroinitiators and subsequent addition of epoxides. In this manner, the comonomer can be introduced in one distinct block, and supramolecular structures in bulk or solution, based on the responsive behavior of the multifunctional groups, are accessible.

Copolymerization Kinetics in Anionic Polymerizations

The microstructure of copolymers is determined by the relative reactivities of the corresponding comonomers. Herein, the underlying copolymerization kinetics can be explained by the following elementary reaction steps (Scheme 8).

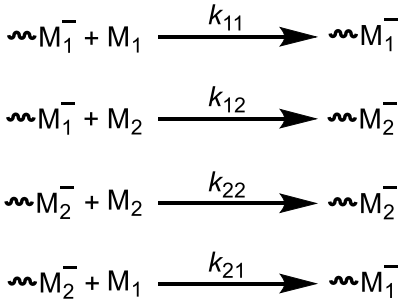

Scheme 8. Reaction steps in living carbanionic copolymerization of M_1 with M_2.

In this case, only the reaction between chain end (M_1^-, M_2^-) and the different monomers (M_1, M_2) is considered. Following the reaction steps, the monomer consumption over time can be expressed by the following equations:

$$-\frac{d[M_1]}{dt} = k_{11}[M_1][M_1^-] + k_{21}[M_1][M_2^-]$$

$$-\frac{d[M_2]}{dt} = k_{22}[M_2][M_2^-] + k_{12}[M_2][M_1^-]$$

Based on the assumption that the number of chains remains constant during LAP (steady-state assumption), the well-known Mayo Lewis equation can be obtained.

$$\frac{d[M_1]}{d[M_2]} = \frac{[M_1]}{[M_2]} \frac{\frac{k_{11}}{k_{12}}[M_1]+[M_2]}{\frac{k_{22}}{k_{21}}[M_2]+[M_1]} = \frac{[M_1]}{[M_2]} \frac{r_1[M_1]+[M_2]}{r_2[M_2]+[M_1]}$$

Herein, r_1 and $r2$ are the corresponding reactivity ratios, and their values describe the copolymerization behavior.

In anionic ring-opening copolymerization of EO and monosubstituted epoxides, the microstructure is governed by the nature of the comonomer. EO and glycidyl ethers typically possess similar reactivity ratios in the AROP, and therefore a nearly ideally random distribution of the glycidyl ether repeating units in the polyether backbone is observed.[27,28,36] In contrast, compared to EO, alkylene oxides[37] and glycidyl amines[25] have less pronounced reactivities in AROP, resulting in a preferred addition of EO to the active chain end and thus a soft gradient-like microstructure.

A special case are the so-called tapered block copolymers. The underlying gradient microstructure can be achieved via direct introduction of monomer mixtures to the initiator. Herein, the utilization of two monomers with strongly differing reactivity ratios results in a preferred addition of the more reactive monomer to the living chain end. The consumption of the less reactive monomer

continuously increases with decreasing concentration of the preferred monomer, resulting in a gradient microstructure. After full consumption of the latter, the remaining monomer homopolymerizes, and a tapered BCP is obtained.[38] For example, in the copolymerization of isoprene and styrene in cyclohexane and benzene, a preferred addition of isoprene in comparison to styrene is observed, resulting in r_I and r_S values of 10.1 and 0.013 at room temperature, respectively.[38] Therefore, a tapered BCP structure is obtained with a PI-rich area at the beginning and a pure PS block at the end of the chain.

The microstructure of poly(isoprene-*co*-styrene) (P(I-*co*-S)) can be tailored by the addition of polar additives (e.g., ethers[39] or tertiary amines[40]) (Figure 2), which is explained by the solvation of the lithium cations and the disruption of ionic aggregates by so-called randomizers.[41,42] Depending on the amount of polar additive, the microstructure can be completely reversed with a preferred incorporation of styrene instead of isoprene during copolymerization.[39]

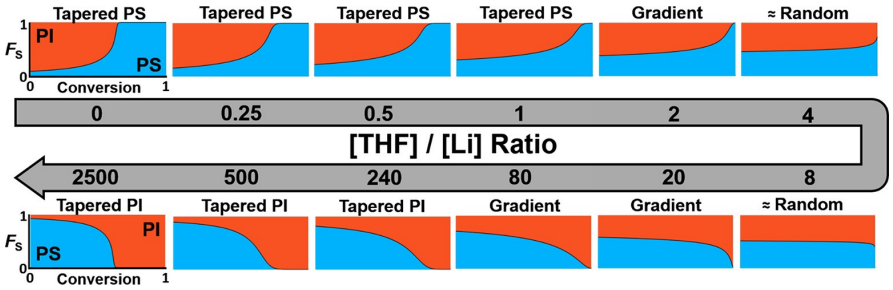

Figure 2. Influence of the THF concentration on the microstructure of PS-PI tapered block copolymers.[39]

Besides polar additives, temperature changes also show an influence on the reactivity ratios of isoprene and styrene. In this case, r_s increases with increasing temperature, resulting in a longer pure PS block.[38]

Synthesis of PS and PEO-based Block Copolymers via the Combination of Anionic Polymerization Methods

PEO is known for its highly hydrophilic characteristics, attributed to the intramolecular oxygen-oxygen distances in the backbone,[7] allowing for the aggregation of two to three water molecules at each EO repeating unit.[43] The water solubility and high dielectric constant makes PEO a highly polar polymer, which can be utilized in different applications ranging from polymer electrolytes to bioconjugation.[7] Combining the hydrophilicity of PEO, BCPs of PEO with apolar PS (PS-*b*-PEO) yields amphiphilic AB diblock structures.

The synthesis of PS-*b*-PEO via anionic polymerization methods can be achieved by a two-step procedure involving the combination of LAP and AROP. In the case of carbanions bearing a lithium counterion, the addition of EO to the living chain end results in a second-order nucleophilic substitution reaction at the methylene group of the epoxide. This enables the formation of a primary lithium alkoxide at the chain end. Propagation of EO will not occur because of the resulting tight lithium-oxygen ion pair.[44,45] This end-capping approach can be expanded to a

large variety of monosubstituted epoxide.[46,47] For example, propylene oxide (PO)[48] and butylene oxide (BO)[49] can be utilized for the introduction of a secondary hydroxyl group at the chain end. However, the end-capping efficiency decreases from EO (>99 %) to BO (99 %) and PO (96 %), because proton abstraction at the methylene group of BO and the methyl group of PO vicinal to the epoxide ring by the highly basic carbanion leads to pronounced termination reactions.[50]

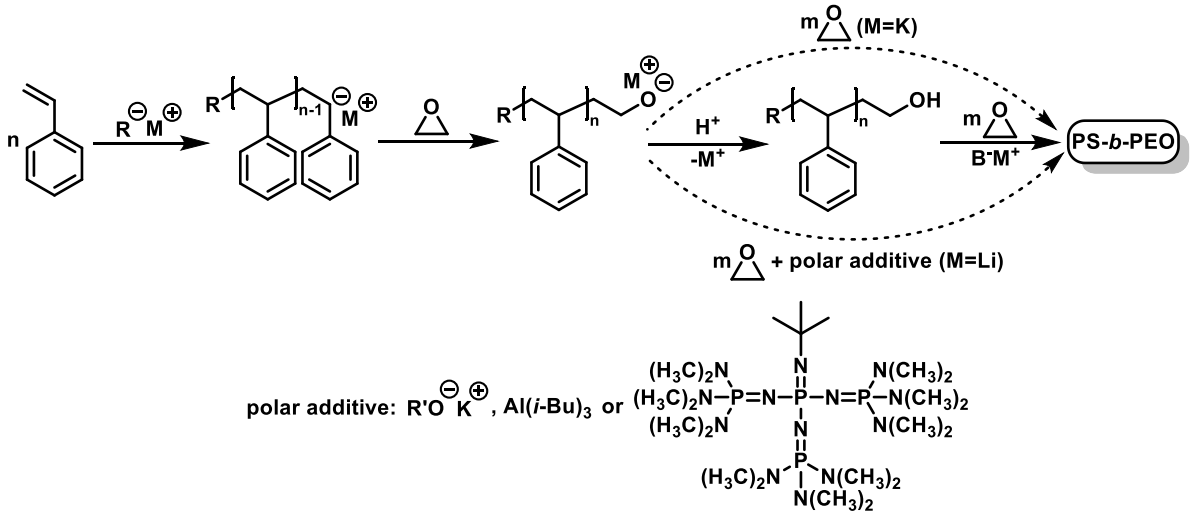

Scheme 9. Possible synthesis routes for polystyrene-block-poly(ethylene oxide); M: Li or K (depending on the synthesis route), B: base with a pKs value higher than the alcohol.

The utilization of EEGE[51] as an end-capping reagent allows for the synthesis of amphiphilic star block copolymer architectures.[52,53] In addition to EEGE, end-capping of polystyryl lithium with 1,2-isopropylidene glyceryl glycidyl ether (IGG) and trans-2-phenyl-1,3-dioxane glycidyl ether (PDGE) is also a feasible method for the introduction of multiple hydroxyl functionalities at the ω-terminus of PS after deprotection.[51] The use of potassium cation-based initiators and sequential addition of styrene and EO (Scheme 9) facilitates access to PS-*b*-PEO.[54–58] Complexation of the lithium cations[59] and polar additives[60,61] also lead to sufficient chain propagation of EO, even when lithium cations are present. However, a major drawback of these routes are partial terminations of living chains by impurities and side reactions.

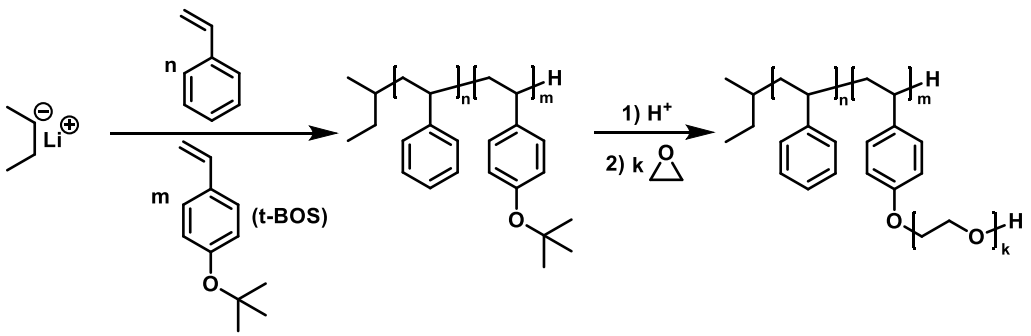

Scheme 10. Synthesis route for PS-PEO bottlebrush block copolymers.

Hence, protonation of the alkoxide, purification of the macroinitiator and re-activation via deprotonation with higher alkali metal bases are essential steps for the synthesis of well-defined PS-*b*-PEO block copolymers. Besides linear and star-like polymer architectures, the synthesis of PS-PEO bottlebrush BCPs (PS-*g*-PEO) via the combination of LAP and AROP is achievable in a comparable manner (Scheme 10). In this case, *p*-*tert*-butoxystyrene (*t*-BOS) is utilized as monomer for the LAP. After acidic deprotection of the hydroxy functionalities, PEO chains are grafted-from the phenolic groups of the polystyrene backbone in the presence of phosphazene bases.[62]

Synthesis of PS and PEO-based Block Copolymers via Controlled Radical Polymerization

PS-*b*-PEO structures are also achievable via reversible-deactivation radical polymerization (RDRP) techniques. In the first step the hydroxy functionality of the PEO chain end is modified into the required bromine,[63,64] trithiocarbonate[65] or nitroxide[66] groups via esterification reactions (Scheme 11).

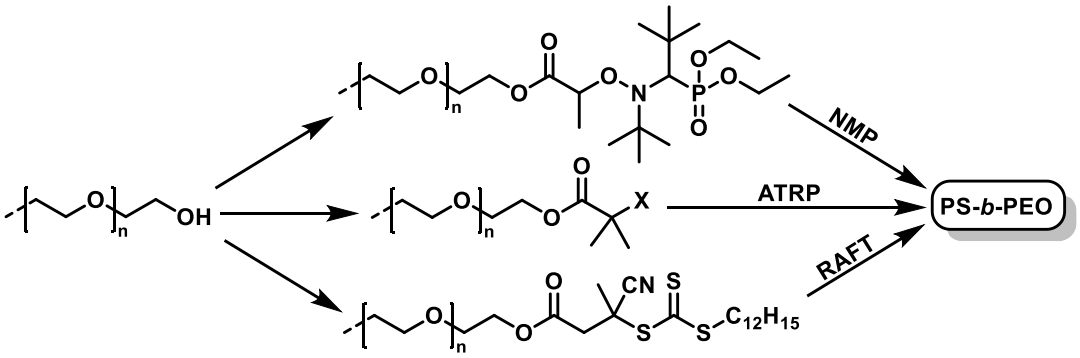

Scheme 11. Synthesis of PS-*b*-PEO via post-polymerization modification of PEO and controlled radical polymerization; X: Cl or Br.

Afterwards, PS-*b*-PEO is synthesized via RDRP, utilizing the end group functionalized PEO macroinitiator. However, for this strategy insufficient chain end modification due to the lower nucleophilicity of the hydroxyl group compared to a living carbanion is the main disadvantage compared to the LAP-AROP synthesis route. Additionally, the CRP mechanism allows the formation of homo-PS during the polymerization process.[67] Further investigations showed that the synthesis of well-defined BCP with LRP based on PEO macroinitiators is limited to low molecular weight PEO.[68]

Phase Separation of Block Copolymers

In comparison to macroscopic separated polymer blends, BCP self-assemble into well-defined nanostructures. The development of the periodic composition patterns depends on several factors, e.g., the Flory-Huggins chain-chain interaction parameter χ, which describes the interaction between the varying blocks. In case of AB BCPs, at a value of 10.5 or higher for χN (N: degree of

polymerization) and $f = 0.5$ phase separation of the blocks occurs.[69] With increasing volume fraction f of one of the distinct blocks the morphologies change from spherical (S) to hexagonal cylindrical (C) and lamellar (LAM) structures (Figure 3).[70]

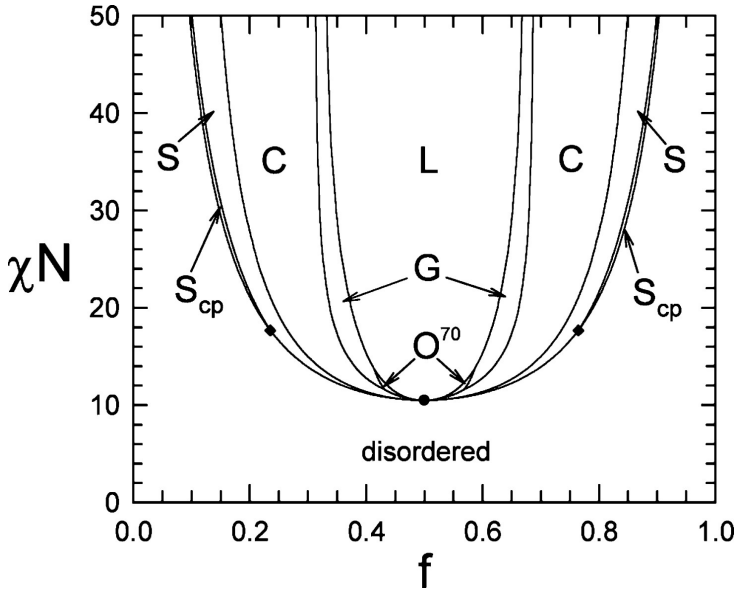

Figure 3. Phase diagram for melts of AB diblock copolymers.[71]

A special case is the gyroid (G) morphology between the C and LAM phase which was first discovered in BCPs by Fetters et al. in 1994.[72] The preferred stability of the G phase in comparison to other bicontinuous cubic morphologies can be attributed to the best compromise between chain stretching and surface tension.[73]

Although mechanical properties are tremendously increased from AB to symmetrical ABA and multiblock architectures, they show phase diagrams comparable to the simple AB case, because of the relatively unaffected free energy.[74] In the case of ABA triblock copolymers, even though the equilibrium phase diagram stays the same, a significant shift in the phase boundaries is observed.[71]

BCPs with a semicrystalline block show thermo-responsive phase behavior in bulk. Above the melting point of these materials, the expected morphologies depending on the volume fractions can be found. When cooling under the crystallization temperature, the microphase separation is no longer driven by the minimization of unlike contacts, but by the crystallization process.[75] In this case, the phase separation behavior simplifies, and only lamellar morphologies are observed.[76] For example, studies regarding PS-*b*-PEO showed that a spherulitic superstructure is formed by PEO crystallization upon cooling from the ordered melt. The crystalline block of BCPs crystallizes like its homopolymer analog, however, a reduction of crystallinity is observed. The latter can be explained by the incorporation of the amorphous phase in the interlamellar PEO regions.[77]

The addition of a third block C to AB BCPs results in an ABC structure with three underlying interaction parameters χ_{AB}, χ_{AC} and χ_{BC}. The increased complexity of parameters and possible

sequence variations have a tremendous influence on the resulting phase diagrams and the morphologies.[73] For example, PS-*b*-PI-*b*-PEO structures with a symmetric PS-*b*-PI, but different volume fractions of PEO from 0.00 to 0.33 show novel bicontinuous morphologies, which are inaccessible in common AB BCPs (Figure 4).[78] Switching the sequence to PI-PS-PEO reduces the large variety of bicontinuous morphologies from four to one between the LAM_2 and LAM_3 morphology.[79]

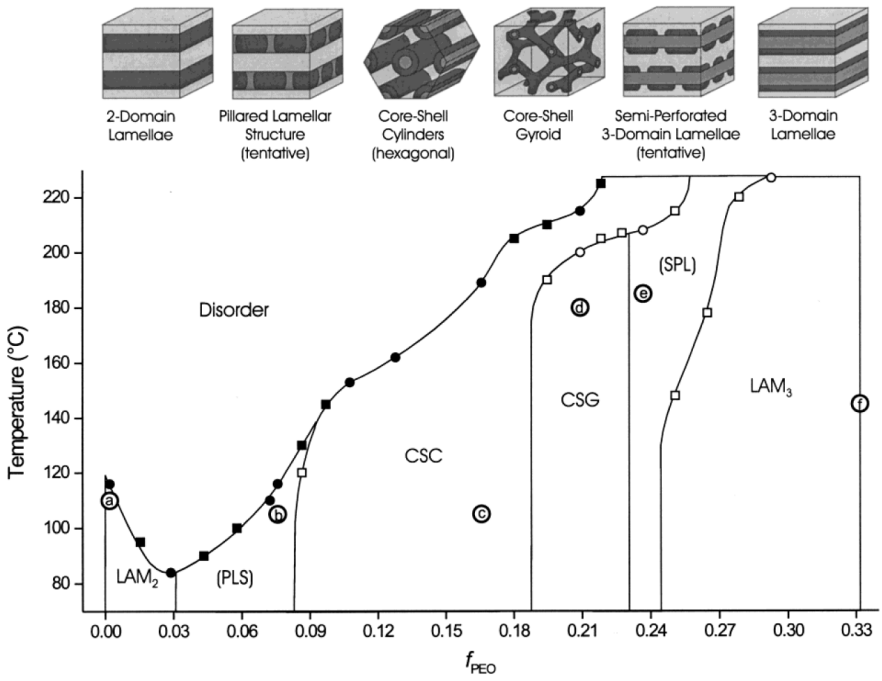

Figure 4. Phase diagramm of PS-b-PI-b-PEO with constant PS/PI ratio and increasing PEO volume fraction.[78]

This change in morphological characteristics can be attributed to the different block connectivity and interaction of the distinct blocks.[78]

Polymer Electrolytes

The combination of metal oxides as cathode material and graphene as anode material resulted in the commercialization of lithium ion batteries (LIB). Present state-of-the-art electrolytes in LIB consist of lithium salts (e.g., $LiPF_6$) dissolved in organic liquids (e.g., ethylene carbonate) with a room temperature conductivity of around 10^{-2} S cm^{-1}. Despite the excellent features of commercial LIB, there is a continuously rising demand for batteries with increased capacities. In theory, this could be fulfilled with an anode, consisting of elemental lithium.[80] Lithium has long been discussed as the perfect anode material because of its three outstanding properties: the most electronegative metal (-3.04 V against standard hydrogen electrode), the highest theoretical capacity (3.860 mAh g^{-1}) and its lightweight (0.543 g cm^{-3}).[80,81] Even though passivation reactions on the highly reactive lithium electrode surface allow for the utilization of organic

liquids as an electrolyte material, dendritic growth of lithium remains a safety issue.[80] During charge and discharge processes, the dendrite formation can propagate through the electrolyte and lead to internal short circuits when cathode and anode are connected. As a result, thermal runaways and fire issues reduced the enthusiasm for lithium metal-based batteries and stopped their commercialization in 1989.[81] Therefore, a lithium metal anode is only feasible, when a mechanically stable electrolyte is applied, which inhibits dendritic growth of lithium whilst ensuring sufficient high conductivity.

Polymer Electrolytes based on PEO

Based on the above-mentioned facts, PEO has been discussed as a nonflammable electrolyte alternative for several decades. In 1973 and 1975, Wright et al. first observed the solvation capability of PEO for salts[82] and the conductivity of PEO-salt complexes.[83] The preferred dissolution of salts is attributed to the complexation of lithium cations by the oxygens of the PEO backbone and the formation of a helical conformation of the chains around the lithium cations (Figure 5).[84]

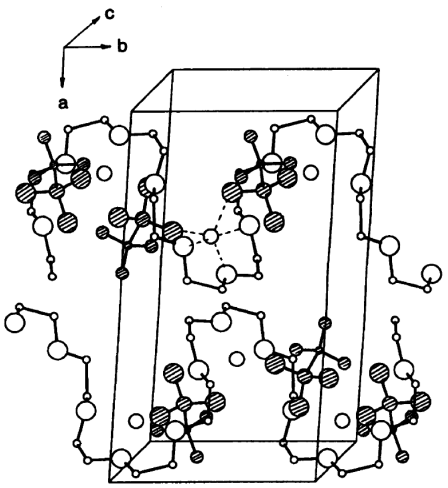

Figure 5. View of the PEO:$LiCF_3SO_3$ structure; Coordination around lithium cations is shown in dashed lines.[84]

The relation between conductivity and temperature in polymer-salt complexes is expressed by the semi-empirical Vogel-Tamman-Fulcher (VTF) equation:[85]

$$\sigma = \sigma_0 \exp\left(\frac{B}{(T-T_0)}\right)$$

with the Vogel temperature T_0 , describing the temperature at which the segmental motion drops to zero with a value of T_g-50 K.[86] An increase in ionic conductivity can be observed with increasing temperature, following a curved Arrhenius behavior (Figure 6) The ion mobility in polymers is strongly coupled with the segmental relaxation (τ_α) of the chains. As a result, the molar conductivity (Λ) correlates with τ_α and vice versa the T_g of the polymer chains, which is expressed by the Walden plot (Figure 7).[87] Based on this rationale, the highly flexible PEO with a

T_g of -60 °C can reach conductivities up to 10^{-3} S cm^{-1} after salt-doping. Unfortunately, the semi-crystalline appearance of PEO results in a sharp drop of ion conductivity at the crystallization temperature (Figure 6), because enhanced ionic mobility is only present in the amorphous domains.[88]

The conductivity also correlates with the molecular weight of PEO. An exponential decrease of the ionic conductivity is observed with increasing molecular weight until a plateau of 10^{-3} S cm^{-1} at a molecular weight of around 10 kg mol^{-1} is approached (Figure 8).[89]

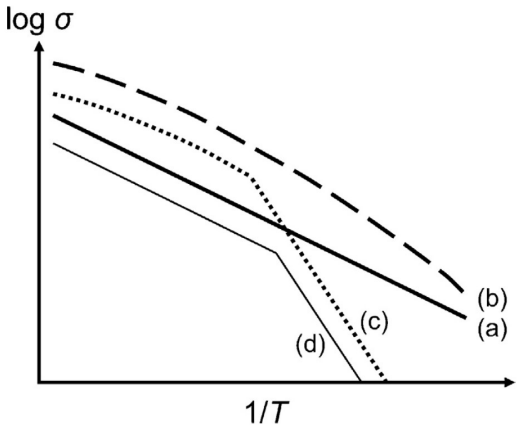

Figure 6. Comparison of conductivity-temperature-relations of a) solids (Arrhenius), b) amorphous polymers (VTF), c) and d) semi-crystalline polymers.[86]

The influence of PEO end groups on the conductivity is mostly neglectable and only observable at low molecular weights. In the latter, ion transport is mainly ensured by a vehicular mechanism, whereas lithium cations "jumping" from one coordination side to another is the dominating mechanism for high molecular weight PEO.[90]

Salt concentration plays an additional and crucial role in PEO-lithium salt electrolytes. An increase in salt concentration offers a higher amount of possible charge carriers, but simultaneously results in a higher cross-link density between different polyether chains. For example, in PEO-$LiClO_4$ mixtures, a decrease in the segmental motion of the polymer chains is observed with increasing salt concentration, resulting in lowered coductivites.[91] Simulations of PEO-LiTFSI mixtures show that the complexation of the lithium cations by the polyether chain is preferred at low salt concentrations. At higher salt concentrations ([EO]:[Li] > 6:1), the coordination sites of the PEO chains are saturated and, as a result, TFSI anions tend to interact with the lithium cations, resulting in ion clustering.[92] Therefore, the ratio between ether oxygens and Li salts ([EO]:[Li]) needs to be optimized to reach sufficiently high ionic conductivities. Further, the structures of the Li salts employed show an influence on the ionic conductivity and morphology of PEO-salt mixtures. Over the last decades, lithium bis(triflouromethylsulfonyl)imide (LiTFSI) has been assigned as the most promising salt for PEO SPEs. The negative charge of the anion is highly delocalized, which increases the mobility of the lithium cation and allows for sufficient

interaction of the latter with the oxygen atoms of the polyether chain. Furthermore, PEO-LiTFSI mixtures become fully amorphous at [EO]:[Li] ratios of 8:1 and 10:1, compared to the crystalline complexes of PEO with $LiCF_3SO_3$ and $LiClO_4$, which improves room-temperature conductivity.[31]

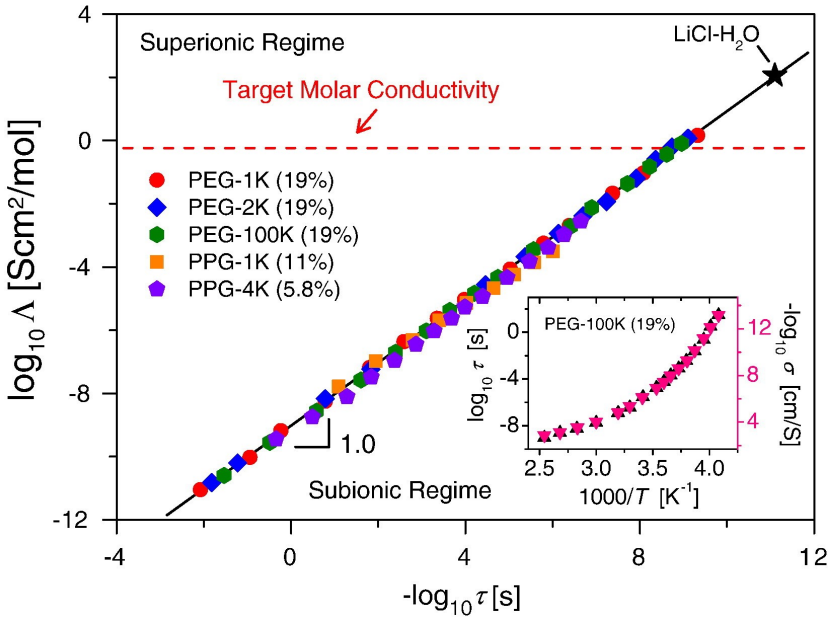

Figure 7. Walden Plot of salt-doped PEO and PPO with different molecular weights.[87]

The crystallization of PEO is also reducible by the optimization of the polyether structure, while i) keeping the oxygen-oxygen distance constant or ii) interrupting the periodic structure of the polymer. The simplest case is the replacement of PEO with amorphous poly(propylene oxide) (PPO). Despite the comparable, low T_g and similar backbone structure, PPO-lithium salt mixtures reveal lower conductivities and considerably poorer miscibility of the two components in comparison to PEO-based SPEs.[93]

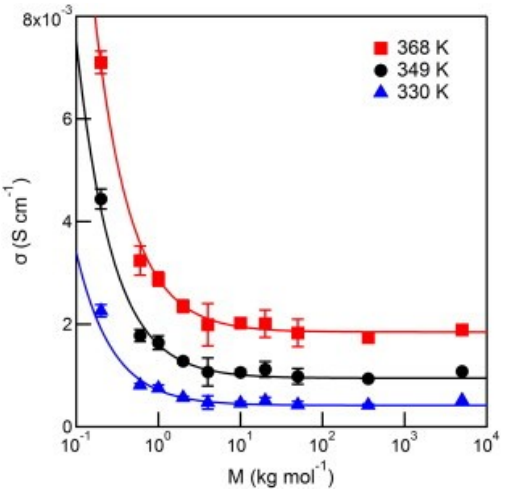

Figure 8. Molecular weight-dependent conductivity of a PEO SPE at different temperatures.[89]

Furthermore, the additional methyl groups of the PO repeating units interrupts the helical conformation of the backbone around the Li cations. This leads to larger cavities and therefore less efficient complexation of Li cations via the ether oxygens.[94] However, low molecular weight salt-doped amorphous EO-PO copolymers (P(EO-*co*-PO)) show an increased conductivity at room temperature and elevated temperatures compared to PEO.[95] Amorphous polyethers synthesized via homopolymerization or via the copolymerization of monosubstituted epoxides with EO were also explored regarding their conductivity behavior (Scheme 12). A structure-conductivity correlation is observed in these polyethers. For example, LiTFSI-doped poly(glycidyl ethers) with different residues show increased ionic conductivity with increasing polarity of the polymer matrix.[96] In these materials, the correlation between segmental motion and conductivity is decoupled, because the dielectric constants of the poly(glycidyl ethers) are below a certain threshold value for the sufficient dissolution of ionic aggregates.[97,98]

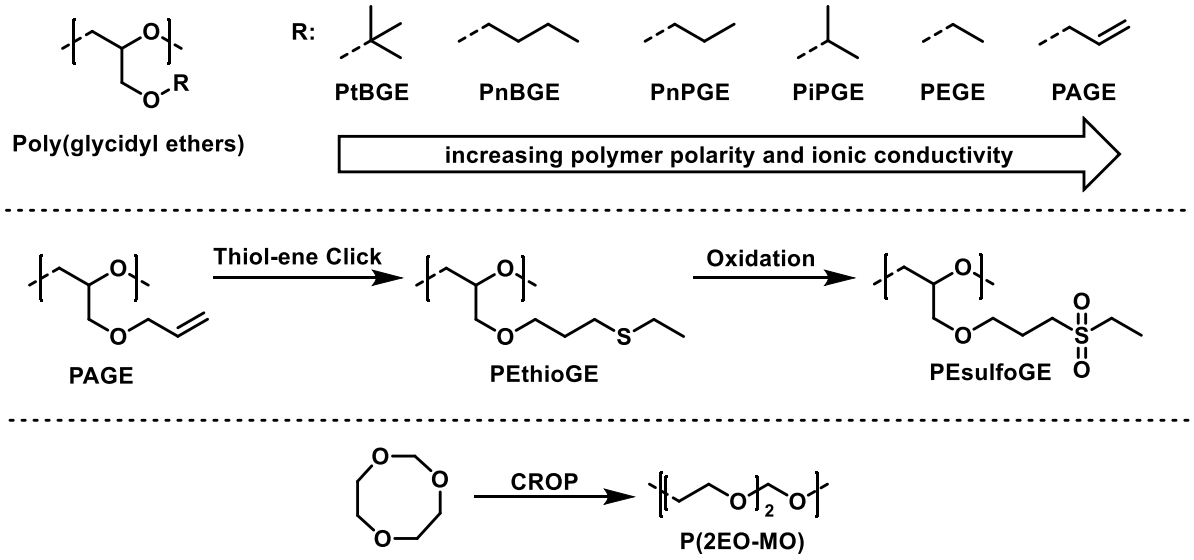

Scheme 12. Different examples for PEO analogues utilized as SPE.

Further investigations focused on the comparison of PAGE with its thioether analog (PEthioGE) and the corresponding sulfone (PEsulfoGE). The ionic conductivity of salt-doped PAGE and PEthioPGE is nearly indistinguishable, but significantly decreases in the case of PEsulfoGE. This behavior is explained by the increase of the T_g after oxidation due to the interactions of the polar sulfone groups and the resulting decrease in the segmental relaxation.[99] Another PEO-based polymer electrolyte was synthesized via cationic polymerization of 1,3,6-trioxocane.[100,101] The repeating units of the resulting P(2EO-MO) consist of two EO units and one methylene oxide unit. The interrupted PEO structure is not capable of crystallizing, but the conductivity of P(2EO-MO)/LiTFSI remains below PEO/LiTFSI for r ([Li]:[EO]) values in the range of 0.01 to 0.14. Additionally, a more pronounced increase of the T_g of P(2EO-MO) in comparison to PEO is observed with increasing salt concentrations, which can be attributed to the preferred two-chain solvation motif of P(2EO-MO).[102]

Polymer Electrolytes based on PS-PEO Block Copolymers

Even though different successful approaches have been developed to achieve high room temperature conductivities in PEO-based polymer electrolytes, the mechanical stability against dendritic growth remains an issue. Besides crosslinked PEO-based polymer electrolytes,[103–105] BCPs with conductive PEO channels and mechanically stable PS blocks have been discussed as promising candidates for several years.[106] At sufficiently high χN values, PS-*b*-PEO structures microphase separate into PEO domains, which function as conductive channels and PS domains, which possess the necessary mechanical stability against dendritic growth. Salt doping of PS-*b*-PEO leads to salt-rich PEO domains, with a non-uniform salt distribution. The highest salt concentration occurs in the middle of the PEO domain and decreases near the PS-PEO interface. This can be attributed to chain stretching events of the PEO chains at the PS-PEO interface. Chemical repulsion between the two blocks leads to unfavored chain conformations for Li ion complexation.[107,108] At low molecular weights of PS-*b*-PEO-LiTFSI mixtures, the conductivity correlates with the T_g of PS because of intermixing phenomena between PEO and PS segments.[109] Therefore, a decrease in conductivity is accompanied with an increase of the T_g of PS when the molecular weight of PS-*b*-PEO increases. However, a sharp increase in conductivity is observed for molecular weights exceeding 10 kg mol^{-1} (Figure 9).[110–112] The increasing conductivity is based on an increase of the phase separation of the BCP and neglection of the interfacial zone.[109] In comparison, a decrease in conductivity was observed with increasing molecular weight in PEO-salt mixtures.[89] Furthermore, the conductivity is independent of grain sizes and therefore from the long-range order of the material. Percolating conducting pathways are formed entirely by self-assembly processes.[111] Additionally, the influence of the morphology of the BCPs on the conductivity was investigated.

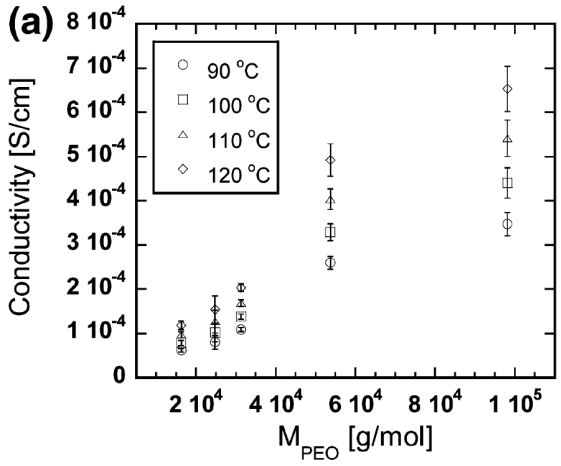

Figure 9. Ionic conductivity of PS-b-PEO-LiTFSI mixtures with $r = 0.02$.[111]

An increase in conductivity was observed for hexagonally packed cylinders and hexagonally perforated lamellae in comparison to a lamellar 2D network.[113] Therefore, the morphological complexity in salt-doped ABC block terpolymers could be utilized for microstructures with

enhanced conductivities. For instance, the addition of $LiClO_4$ to PS-PI-PEO[114] and PI-PS-PEO[115] block terpolymers results in $LiClO_4$-doped PEO domains in a bicontinuous core-shell gyroid morphology.

The variation of the polymer architecture from linear to bottlebrush structures has a direct influence on the conductivity of the SPEs. LiTf-doped polymers, consisting of low molecular weight PEO blocks grafted from a linear PS block (PS-*g*-PEO), exhibit higher room-temperature conductivities compared to PEO-LiTf mixtures with the same salt concentration ([EO]:[Li] = 8:1). This can be attributed to the decreased degree of crystallization of PEO and salt complexes inside the PEO matrix of PS-*g*-PEO.[116] Despite the different BCP architectures, linear[112] as well as bottlebrush LiTf-doped PS-PEO BCPs show transient interactions between PEO chains and salt at their highest conductivities and in the amorphous state.[116] Therefore, a similar ion mobility mechanism can be assumed for both structures.

The salt-doping of BCPs generally leads to an increase in the segregation strength, which is governed by an increasing effective interaction parameter (χ_{eff}). Depending on the utilized concentrations of the lithium salts and the respective counter ion, increased domain spacing[117] and order-order transitions (OOT) were observed.[118] The phase behavior of linear salt-doped BCPs can be expressed by the dependency of $\chi_{eff}N$ from $f_{EO,salt}$ (Figure 10).[119,120]

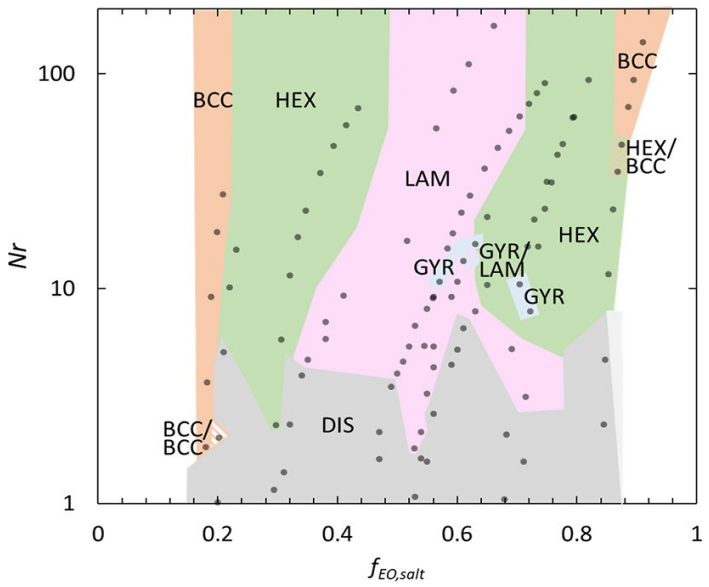

Figure 10. Phase diagram for salt-containing PS-*b*-PEO.[119]

χ_{eff} resembles the effective interaction parameter and can be expressed by a linear expression.

$$\chi_{eff} = \chi_0 + mr$$

Here, χ_0 represents the Flory-Huggins interaction parameter of the pure BCP system, m is a system dependent proportionality constant and r is the salt concentration.[119] At constant N, an increase in the salt concentration is accompanied by an increase of the segregation strength. The

added lithium salt increases the occupied volume of the PEO domains ($f_{EO,salt}$), which can be expressed by

$$f_{EO,salt} = \frac{v_{EO} + r v_{Li}}{v_{EO} + r v_{Li} + \left(\frac{M_{PS} M_{EO}}{M_S M_{PEO}} v_s\right)}$$

The experimentally obtained phase diagram of PS-*b*-PEO-LiTFSI mixtures shows a tilting of the phase boundaries, which is explained by the swelling of the PEO domains in the presence of salt.[119]

Single-Ion-Conducting Polymer Electrolytes based on PS-b-PEO Block Copolymers

In recent years, new materials with covalently attached anions to the polymer have been investigated for their application as SPEs. The main advantage of these single-ion conducting polymer electrolytes (SICPE) compared to conventional lithium salt-doped SPE is their exceptional high lithium transference number (t_{Li}). This is explained by the fact, that the anion motion is limited to the segmental motion of the polymer. As a result, the charge is mainly transported by the lithium cation, and the concentration polarization at the electrode-electrolyte interface is reduced. In recent years, SICPEs based on PS-*b*-PEO have been investigated in great detail.[121–128]

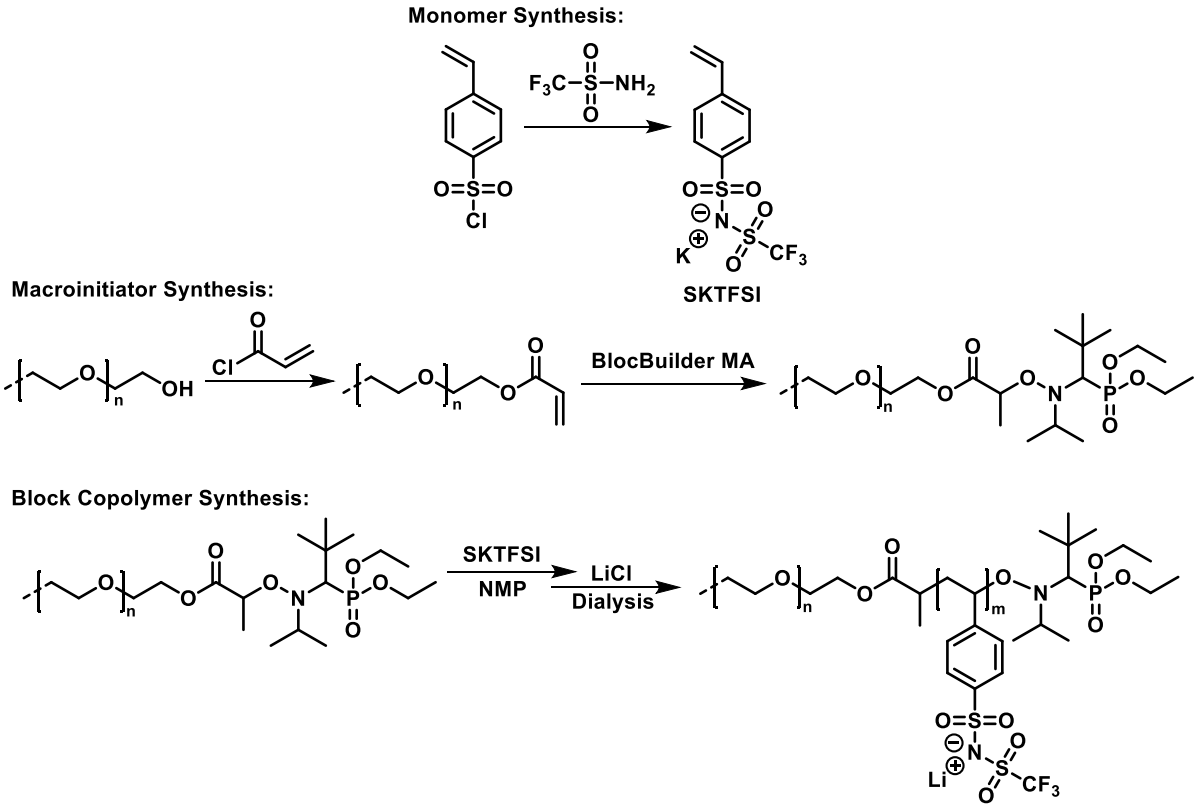

Scheme 13. Synthesis route of SICPE based on PEO and PS.

The desired BCPs were synthesized via NMP or RAFT polymerization[129] of potassium styrene trifluoromethanesulfonylimide (SKTFSI) with a modified PEO macroinitiator. In the case of

NMP, the PEO macroinitiator was synthesized via esterification of acryloyl chloride with the hydroxyl groups of PEO and addition of BlocBuilder MA (Scheme 13). Depending on the utilized mono or bifunctional PEO macroinitiator, PEO-*b*-P(SLiTFSI)[122,124–127] and P(SLiTFSI)-*b*-PEO-*b*-P(SLiTFSI)[121,128] structures are accessible. The ions in PEO-P(SLiTFSI) BCP structures with low molecular weight P(SLiTFSI) blocks are arranged in ion-clusters in the styrene domain at room temperature. Elevation of the temperature above $T_{m,PEO}$ leads to a preferred mixing of PEO and P(SLiTFSI) domains and is accompanied by a strong increase in ionic conductivity, which follows a VTF behavior.[122,124] SAXS data[122,124] and computer simulations[123] support a disordered microstructure and preferred coordination of Li cations by the ether oxygens of PEO instead of the TFSI anions in PEO-P(SLiTFSI) BCP structures above $T_{m,PEO}$ (Figure 11).

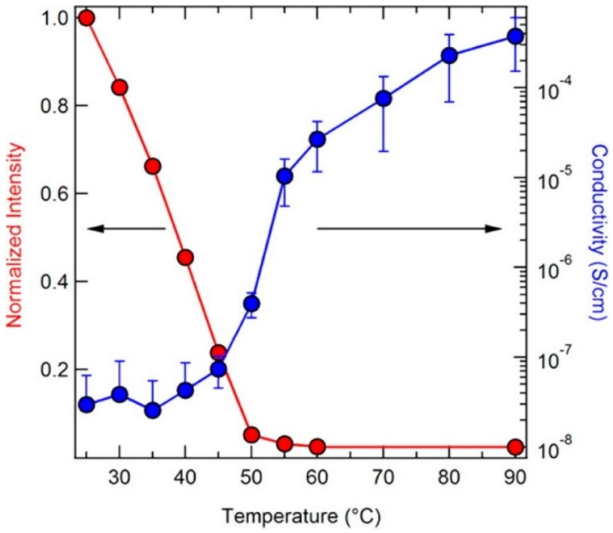

Figure 11. Temperature dependence of conductivity (blue) and SAXS intensity (red) of PEO-*b*-PSLiTFSI.[122]

The increase of the volume fraction of P(SLiTFSI) results in completely disordered and amorphous materials even at room temperature and a strong increase of $T_{g,PEO}$.[124,126] Determined negative χ values[125] and rheological measurements[126] for PEO-*b*-P(SLiTFSI) further support the preferred domain mixing and explain the uncommon conductivity behavior. In comparison, the incorporation of styrene repeating units in the P(SKTFSI) block results in phase segregation of the PEO and P(SKTFSI) domains due to unfavorable interactions of PEO and PS segments.[129]

PEGylation

Besides polymer electrolytes, PEO is widely utilized in a completely different area, namely for therapeutic protein and nanocarrier modification because of its hydrophilicity and high biocompability.[130] This so-called “PEGylation” can be considered as a grafting-to approach and is a key approach for modern nanomedicine. Herein, the hydroxyl end group functionality is modified into reactive analogues (i.e., active esters, amines) to covalently attach PEO to the proteins via amino, thiol or carboxylic acid groups (Scheme 14).[131]

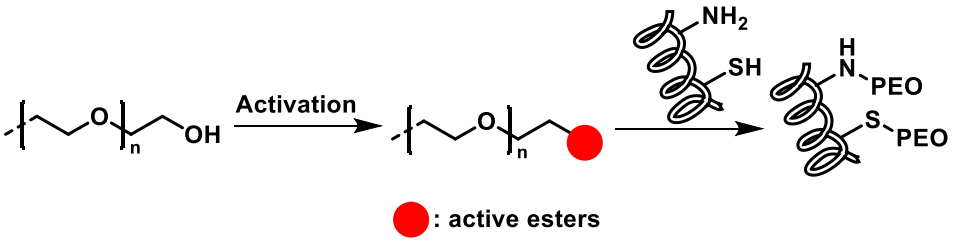

Scheme 14. Synthesis strategy for the covalent attachment of PEO to a protein, relying on lysine or cysteine residues.

Normally, peptides and proteins suffer from degradation and rapid blood clearance triggered by the immune system. In comparison, PEGylated proteins show a weakened immune system response and considerably prolonged circulation times of the therapeutics in the blood stream, due to the shielding (stealth-effect) of PEO and the increase of the hydrodynamic radii by PEO.[132] The improved pharmacological properties of these protein-polymer conjugates led to their utilization in a variety of FDA-approved drugs.[130] Additionally, PEGylation can be applied to liposomal systems, which provided the approval of the commercial drug-delivery system Doxil/Caelyx[133] and the novel mRNA-based Covid-19 vaccines. Despite the beneficial properties of PEGylation, increasing evidence for the existence of anti-PEG antibodies (APA) in a large and constantly growing part of the population raises concerns.[134] In the last decades, the immunogenicity of PEO has been detected for several PEGylated therapeutics and nanocarriers. For example, ABC of PEGylated proteins[135] and liposomes[136] induced by the formation of APAs has been observed. Recently, the unique binding mechanism between PEO and APA has been revealed. Herein, the PEO is captured in an open ring-like paratope and stabilized via Van-der-Waals interactions (Figure 12).[137]

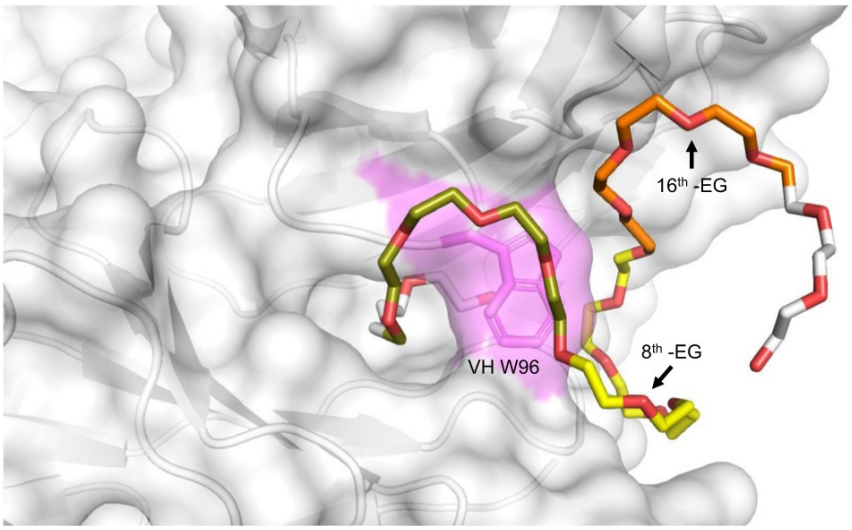

Figure 12. Binding between PEO and APA.[137]

It was further observed that the binding affinity of APAs increases with the degree of polymerization of the PEO chain and depends on the chain architecture.[138]

PEO Alternatives in PEGylation Applications

Based on the above-mentioned concerns, alternative hydrophilic polymer classes have been discussed as PEO substitutes (Scheme 15).[131,139] For example, synthetic poly(amino acid)s (especially poly(glutamic acid), poly(hydroxyethyl-L-asparagine) and poly(hydroxyethyl-L-glutamine)) are in the focus of interest due to their favorable biodegradation in non-toxic amino acids and oligomeric structures[140] combined with prolonged blood circulation time and decreased ABC.[141] Despite these advantages, the major drawback of poly(amino acid)s is the activation of the complement system.[142] Polyoxazolines (POx) are another promising candidate due to their tunable hydrophilicity, biocompatibility and non-toxicity at higher molecular weights.[143] Especially poly(2-methyl-2-oxazoline) and poly(2-ethyl-2-oxazoline) are comparable with PEO, regarding non-toxicity, biocompability[144,145] and blood circulation time.[146]

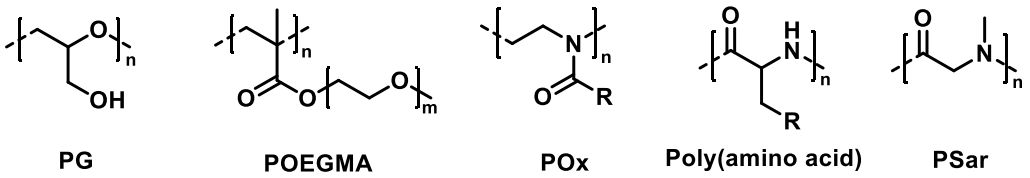

Scheme 15. Example of substitutes for PEO in PEGylation.

More recently, polysarcosines (PSar) have been introduced for their utilization in lipid nanoparticle-based mRNA delivery and possible replacement of PEO.[147] PSar and PEO show similar solution behavior and no significant complement activation in human serum.[148] Another approach to overcome the “PEG dilemma” relies on the modification of the underlying PEO structure and architecture. Exchanging the methoxy end group of mPEG with hydroxy functionalities results in a strong decrease of APA recognition.[149] A similar trend was observed for PEO-based bottlebrush polymers (POEGMA) with oligomeric side chains.[150] Linear polyglycerol (PG) is an additional potential substitute for PEO. In this polymer, the linear PEO backbone is preserved, while each repeating unit bears an additional hydroxy functionality. PG shows high biocompatibility and non-toxicity.[151] Furthermore, peptides conjugated with PG lead to half-life extensions comparable to PEO-peptide conjugates.[152]

Despite the demonstrated alternatives, PEO still remains the “gold standard”, which is utilized in polymer conjugated drug systems. Further investigations of the alternatives must be conducted to determine the suitability of these polymers as PEO substitutes.[130]

References

(1) Szwarc, M. 'Living' Polymers. *Nature* **1956**, *178*, 1168–1169.

(2) Henderson, J. F.; Szwarc, M. The use of living polymers in the preparation of polymer structures of controlled architecture. *J. Polym. Sci. Macromol. Rev*. **1968**, *3*, 317–401.

(3) Hadjichristidis, N.; Hirao, A., Eds. Anionic Polymerization: Principles, Practice, Strength, Consequences and Applications, 1st ed. **2015**.

(4) Szwarc, M.; Levy, M.; Milkovich, R. Polymerization initiated by electron transfer to monomer. A new method of formation of block copolymers. *J. Am. Chem. Soc.* **1956**, *78*, 2656–2657.

(5) Richards, D. H.; Szwarc, M. Block polymers of ethylene oxide and its analogues with styrene. *Trans. Faraday Soc.* **1959**, *55*, 1644.

(6) Steube, M.; Johann, T.; Galanos, E.; Appold, M.; Rüttiger, C.; Mezger, M.; Gallei, M.; Müller, A. H. E.; Floudas, G.; Frey, H. Isoprene/Styrene Tapered Multiblock Copolymers with up to Ten Blocks: Synthesis, Phase Behavior, Order, and Mechanical Properties. *Macromolecules* **2018**, *51*, 10246–10258.

(7) Herzberger, J.; Niederer, K.; Pohlit, H.; Seiwert, J.; Worm, M.; Wurm, F. R.; Frey, H. Polymerization of Ethylene Oxide, Propylene Oxide, and Other Alkylene Oxides: Synthesis, Novel Polymer Architectures, and Bioconjugation. *Chemical reviews* **2016**, *116*, 2170–2243.

(8) Kazanskii, K. S.; Solovyanov, A. A.; Entelis, S. G. Polymerization of ethylene oxide by alkali metal-naphthalene complexes in tetrahydrofuran. *European Polymer Journal* **1971**, *7*, 1421–1433.

(9) Price, C. C.; Carmelite, D. D. Reactions of Epoxides in Dimethyl Sulfoxide Catalyzed by Potassium t-Butoxide. *J. Am. Chem. Soc.* **1966**, *88*, 4039–4044.

(10) Bawn, C.E.H.; Ledwith, A.; McFarlane, N. R. Anionic polymerization in dimethyl sulphoxide. *Polymer* **1967**, *8*, 484–487.

(11) Price, C. C.; Akkapeddi, M. K. Kinetics of base-catalyzed polymerization of epoxides in dimethyl sulfoxide and hexamethylphosphoric triamide. *J. Am. Chem. Soc.* **1972**, *94*, 3972–3975.

(12) Flory, P. J. Molecular Size Distribution in Ethylene Oxide Polymers. *J. Am. Chem. Soc.* **1940**, *62*, 1561–1565.

(13) Penczek, S.; Duda, A. Kinetics and mechanisms in anionic ring-opening polymerization. *Makromolekulare Chemie. Macromolecular Symposia* **1993**, *67*, 15–42.

(14) Solov'yanov, A. A.; Kazanskii, K. S. The kinetics and mechanism of anionic polymerization of ethylene oxide in ether solvents. *Polymer Science U.S.S.R.* **1972**, *14*, 1186–1195.

(15) Ptitsyna, N.V.; Kazakevich, V.K.; Kazanskii, K.S. Conductometric study of "live" polyethylene oxide and its models. *Polymer Science U.S.S.R.* **1977**, *19*, 3218–3224.

(16) Kazanskii, K. S.; Solovyanov, A. A.; Dubrovsky, S. A. *Makromol. Chem.* **1978**, *179*, 969–973.

(17) Rodriguez, M.; Figueruelo, J. E. On the Anionic Polymerization Mechanism of Epoxides. *Makromol. Chem.* **1975**, *176*, 3107–3112.

(18) Penczek, S.; Cypryk, M.; Duda, A.; Kubisa, P.; Slomkowski, S. Living ring-opening polymerizations of heterocyclic monomers. *Progress in Polymer Science* **2007**, *32*, 247–282.

(19) Becker, H.; Wagner, G.; Stolarzewicz, A. Zur Übertragungsreaktion bei der anionischen Polymerisation von Oxiranen. III. Zur Dynamik der Doppelbindungsbildung bei der Propylenoxidpolymerisation. *Acta Polym.* **1982**, *33*, 34–37.

(20) Hans, M.; Keul, H.; Moeller, M. Chain transfer reactions limit the molecular weight of polyglycidol prepared via alkali metal based initiating systems. *Polymer* **2009**, *50*, 1103–1108.

(21) Becker, H.; Wagner, G. Zur Übertragungsreaktion bei der anionischen Polymerisation von Oxiranen VI. Zum Einfluß von Kronenetherzusätzen auf die Polymerisation von Propylenoxid. *Acta Polym.* **1984**, *35*, 28–32.

(22) Wegener, G.; Brandt, M.; Duda, L.; Hofmann, J.; Klesczewski, B.; Koch, D.; Kumpf, R.-J.; Orzesek, H.; Pirkl, H.-G.; Six, C.; et al. Trends in industrial catalysis in the polyurethane industry. *Applied Catalysis A: General* **2001**, *221*, 303–335.

(23) Obermeier, B.; Wurm, F.; Mangold, C.; Frey, H. Multifunctional Poly(ethylene glycol)s. *Angewandte Chemie (International ed. in English)* **2011**, *50*, 7988–7997.

(24) Kurzbach, D.; Wilms, V. S.; Frey, H.; Hinderberger, D. Impact of Amino-Functionalization on the Response of Poly(ethylene glycol) (PEG) to External Stimuli. *ACS Macro Lett.* **2013**, *2*, 128–131.

(25) Herzberger, J.; Kurzbach, D.; Werre, M.; Fischer, K.; Hinderberger, D.; Frey, H. Stimuli-Responsive Tertiary Amine Functional PEGs Based on N,N-Dialkylglycidylamines. *Macromolecules* **2014**, *47*, 7679–7690.

(26) Herzberger, J.; Fischer, K.; Leibig, D.; Bros, M.; Thiermann, R.; Frey, H. Oxidation-Responsive and "Clickable" Poly(ethylene glycol) via Copolymerization of 2-(Methylthio)ethyl Glycidyl Ether. *J. Am. Chem. Soc.* **2016**, *138*, 9212–9223.

(27) Obermeier, B.; Frey, H. Poly(ethylene glycol-co-allyl glycidyl ether)s: a PEG-based modular synthetic platform for multiple bioconjugation. *Bioconjugate chemistry* **2011**, *22*, 436–444.

(28) Mangold, C.; Dingels, C.; Obermeier, B.; Frey, H.; Wurm, F. PEG-based Multifunctional Polyethers with Highly Reactive Vinyl-Ether Side Chains for Click-Type Functionalization. *Macromolecules* **2011**, *44*, 6326–6334.

(29) Craig, D. Q.M. A review of thermal methods used for the analysis of the crystal form, solution thermodynamics and glass transition behaviour of polyethylene glycols. *Thermochimica Acta* **1995**, *248*, 189–203.

(30) Tadokoro, H.; Chatani, Y.; Yoshihara, T.; Tahara, S.; Murahashi, S. Structural studies on polyethers, [-(CH2)m-O-]n. II. Molecular structure of polyethylene oxide. *Makromol. Chem.* **1964**, *73*, 109–127.

(31) Vallée, A.; Besner, S.; Prud'Homme, J. Comparative study of poly(ethylene oxide) electrolytes made with $LiN(CF_3SO_2)_2$, $LiCF_3SO_3$ and $LiClO_4$: Thermal properties and conductivity behaviour. *Electrochimica Acta* **1992**, *37*, 1579–1583.

(32) Lascaud, S.; Perrier, M.; Vallee, A.; Besner, S.; Prud'Homme, J.; Armand, M. Phase Diagrams and Conductivity Behavior of Poly(ethylene oxide)-Molten Salt Rubbery Electrolytes. *Macromolecules* **1994**, *27*, 7469–7477.

(33) Pulst, M.; Samiullah, M. H.; Baumeister, U.; Prehm, M.; Balko, J.; Thurn-Albrecht, T.; Busse, K.; Golitsyn, Y.; Reichert, D.; Kressler, J. Crystallization of Poly(ethylene oxide) with a Well-Defined Point Defect in the Middle of the Polymer Chain. *Macromolecules* **2016**, *49*, 6609–6620.

(34) Samiullah, M. H.; Pulst, M.; Golitsyn, Y.; Busse, K.; Poppe, S.; Hussain, H.; Reichert, D.; Kressler, J. Solid State Phase Transitions in Poly(ethylene oxide) Crystals Induced by Designed Chain Defects. *Macromolecules* **2018**, *51*, 4407–4414.

(35) Samiullah, M. H.; Pulst, M.; Golitsyn, Y.; Bui, A.; Busse, K.; Hussain, H.; Reichert, D.; Kressler, J. Tailored Melting Temperatures and Crystallinity of Poly(ethylene oxide) Induced by Designed Chain Defects. *ACS Appl. Polym. Mater.* **2019**, *1*, 3130–3136.

(36) Herzberger, J.; Leibig, D.; Liermann, J. C.; Frey, H. Conventional Oxyanionic versus Monomer-Activated Anionic Copolymerization of Ethylene Oxide with Glycidyl Ethers: Striking Differences in Reactivity Ratios. *ACS Macro Lett.* **2016**, *5*, 1206–1211.

(37) Blankenburg, J.; Kersten, E.; Maciol, K.; Wagner, M.; Zarbakhsh, S.; Frey, H. The poly(propylene oxide-*co*-ethylene oxide) gradient is controlled by the polymerization method: determination of reactivity ratios by direct comparison of different copolymerization models. *Polymer chemistry* **2019**, *10*, 2863–2871.

(38) Steube, M.; Johann, T.; Plank, M.; Tjaberings, S.; Gröschel, A. H.; Gallei, M.; Frey, H.; Müller, A. H. E. Kinetics of Anionic Living Copolymerization of Isoprene and Styrene Using in Situ NIR Spectroscopy: Temperature Effects on Monomer Sequence and Morphology. *Macromolecules* **2019**, *52*, 9299–9310.

(39) Steube, M.; Johann, T.; Hübner, H.; Koch, M.; Dinh, T.; Gallei, M.; Floudas, G.; Frey, H.; Müller, A. H. E. Tetrahydrofuran: More than a "Randomizer" in the Living Anionic Copolymerization of Styrene and Isoprene: Kinetics, Microstructures, Morphologies, and Mechanical Properties. *Macromolecules* **2020**, *53*, 5512–5527.

(40) Annighöfer, F.; Gronski, W. Block copolymers with broad interphase. Determination of morphological parameters and interphase width by electron microscopy and small angle X-ray scattering. *Makromol. Chem.* **1984**, *185*, 2213–2231.

(41) Morton, M.; Bostick, E. E.; Livigni, R. A.; Fetters, L. J. Homogeneous anionic polymerization. IV. Kinetics of butadiene and isoprene polymerization with butyllithium. *J. Polym. Sci. A Gen. Pap.* **1963**, *1*, 1735–1747.

(42) Morton, M.; Fetters, L. J. Homogeneous anionic polymerization. V. Association phenomena in organolithium polymerization. *J. Polym. Sci. A Gen. Pap.* **1964**, *2*, 3311–3326.

(43) Harris, J. M.; Chess, R. B. Effect of pegylation on pharmaceuticals. *Nature reviews. Drug discovery* **2003**, *2*, 214–221.

(44) Quirk, R. P.; Ma, J.-J. Characterization of the functionalization reaction product of poly(styryl)lithium with ethylene oxide. *J. Polym. Sci. A Polym. Chem.* **1988**, *26*, 2031–2037.

(45) Quirk, R. P.; Mathers, R. T.; Wesdemiotis, C.; Arnould, M. A. Investigation of Ethylene Oxide Oligomerization during Functionalization of Poly(styryl)lithium Using MALDI−TOF MS and NMR. *Macromolecules* **2002**, *35*, 2912–2918.

(46) Quirk, R. P.; Contractor, A.; Polce, M. J.; Wesdemiotis, C. Functionalization and Linking Chemistry of Poly(styryl)lithium with 1,3-Butadiene Diepoxide. *Macromol. Chem. Phys.* **2006**, *207*, 2280–2288.

(47) Quirk, R. P.; Hasegawa, H.; Gomochak, D. L.; Wesdemiotis, C.; Wollyung, K. Functionalization of Poly(styryl)lithium with Styrene Oxide. *Macromolecules* **2004**, *37*, 7146–7155.

(48) Quirk, R. P.; Lizárraga, G. M. Investigation of the Reaction of Poly(styryl)lithium with Propylene Oxide. Macromolecules 1998, 31, 3424–3430.

(49) Quirk, R. P.; Ge, Q.; Arnould, M. A.; Wesdemiotis, C. Functionalization of Poly(styryllithium) with 1-Butene Oxide. *Macromol. Chem. Phys*. **2001**, *202*, 1761–1767.

(50) Quirk, R. P.; Cheong, T.-H.; Jiang, K.; Gomochak, D. L.; Yoo, T.; Andes, K. T.; Mathers, R. T. Recent advances in the anionic synthesis of chain-end functionalized polymers. *Macromol. Symp.* **2003**, *195*, 69–74.

(51) Tonhauser, C.; Wilms, D.; Wurm, F.; Nicoletti, E. B.; Maskos, M.; Löwe, H.; Frey, H. Multihydroxyl-Functional Polystyrenes in Continuous Flow. *Macromolecules* **2010**, *43*, 5582–5588.

(52) Wang, G.; Huang, J. Synthesis and characterization of well-defined ABC 3-Miktoarm star-shaped terpolymers based on poly(styrene), poly(ethylene oxide), and poly(ε-caprolactone) by combination of the "living" anionic polymerization with the ring-opening polymerization. *J. Polym. Sci. A Polym. Chem.* **2008**, *46*, 1136–1150.

(53) Wang, G.; Huang, J. Preparation of Star-Shaped ABC Copolymers of Polystyrene-Poly(ethylene oxide)-Polyglycidol Using Ethoxyethyl Glycidyl Ether as the Cap Molecule. *Macromol. Rapid Commun.* **2007**, *28*, 298–304.

(54) Gervais, M.; Gallot, B. Use of freeze-fracture electron microscopy to study the refolding of crystallized chains in block copolymers. *Polymer* **1981**, *22*, 1129–1133.

(55) Gervais, M.; Gallot, B. *Makromol. Chem.* **1973**, *171*, 157–178.

(56) Hruska, Z.; Hurtrez, G.; Walter, S.; Riess, G. An improved technique of the cumylpotassium preparation: application in the synthesis of spectroscopically pure polystyrene-poly(ethylene oxide) diblock copolymers. *Polymer* **1992**, *33*, 2447–2449.

(57) Barker, M. C.; Vincent, B. The preparation and characterisation of polystyrene/poly/ethylene oxide) AB block copolymers. *Colloids and Surfaces* **1984**, *8*, 289–295.

(58) Ekizoglou, N.; Hadjichristidis, N. Benzyl potassium: An efficient one-pot initiator for the synthesis of block co- and terpolymers of ethylenoxide. *J. Polym. Sci. A Polym. Chem.* **2001**, *39*, 1198–1202.

(59) Esswein, B.; Möller, M. Polymerization of Ethylene Oxide with Alkyllithium Compounds and the Phosphazene Base "tBu-P4". *Angew. Chem. Int. Ed. Engl.* **1996**, *35*, 623–625.

(60) Quirk, R. P.; Kim, J.; Kausch, C.; Chun, M. Butyllithium-Initiated Anionic Synthesis of Well-Defined Poly(styrene-block-ethylene oxide) Block Copolymers with Potassium Salt Additives. *Polymer International* **1996**, *39*, 3–10.

(61) Rejsek, V.; Desbois, P.; Deffieux, A.; Carlotti, S. Polymerization of ethylene oxide initiated by lithium derivatives via the monomer-activated approach: Application to the direct synthesis of PS-*b*-PEO and PI-*b*-PEO diblock copolymers. *Polymer* **2010**, *51*, 5674–5679.

(62) Zhao, J.; Mountrichas, G.; Zhang, G.; Pispas, S. Amphiphilic Polystyrene-*b*-poly(*p*-hydroxystyrene-*g*-ethylene oxide) Block−Graft Copolymers via a Combination of Conventional and Metal-Free Anionic Polymerization. *Macromolecules* **2009**, *42*, 8661–8668.

(63) Jankova, K.; Chen, X.; Kops, J.; Batsberg, W. Synthesis of Amphiphilic PS-*b*-PEG-*b*-PS by Atom Transfer Radical Polymerization. *Macromolecules* **1998**, *31*, 538–541.

(64) Baba, E.; Honda, S.; Yamamoto, T.; Tezuka, Y. ATRP–RCM polymer cyclization: synthesis of amphiphilic cyclic polystyrene-*b*-poly(ethylene oxide) copolymers. *Polym. Chem.* **2012**, *3*, 1903–1909.

(65) Cortez-Lemus, N. A.; Baldenebro, V.; Zizumbo-Lopez, A.; Licea-Claverie, A. Synthesis of Amphiphilic Symmetrical ABA Triblock Copolymers PS-*b*-PEG-*b*-PS Using a Bifunctional Macro RAFT Agent. *Macromol. Symp.* **2013**, 325-326, 47–55.

(66) Perrin, L.; Phan, T. N. T.; Querelle, S.; Deratani, A.; Bertin, D. Polystyrene-*block*-poly(ethylene oxide)-*block*-polystyrene: A New Synthesis Method Using Nitroxide-Mediated Polymerization from Poly(ethylene oxide) Macroinitiators and Characterization of the Architecture Formed. *Macromolecules* **2008**, *41*, 6942–6951.

(67) Chen, X.; Gao, B.; Kops, J.; Batsberg, W. Preparation of polystyrene-poly(ethylene glycol) diblock copolymer by 'living' free radical polymerisation. *Polymer* **1998**, *39*, 911–915.

(68) Perrier, S.; Haddleton, D. M. Initiating efficiency of poly(ethylene glycol)-based initiators for transition metal mediated living radical polymerisation. *European Polymer Journal* **2004**, *40*, 2277–2286.

(69) Leibler, L. Theory of Microphase Separation in Block Copolymers. *Macromolecules* **1980**, *13*, 1602–1617.

(70) Bates, F. S.; Fredrickson, G. H. Block copolymer thermodynamics: Theory and experiment. *Annual review of physical chemistry* **1990**, *41*, 525–557.

(71) Matsen, M. W. Effect of Architecture on the Phase Behavior of AB-Type Block Copolymer Melts. *Macromolecules* **2012**, *45*, 2161–2165.

(72) Hajduk, D. A.; Harper, P. E.; Gruner, S. M.; Honeker, C. C.; Kim, G.; Thomas, E. L.; Fetters, L. J. The Gyroid: A New Equilibrium Morphology in Weakly Segregated Diblock Copolymers. *Macromolecules* **1994**, *27*, 4063–4075.

(73) Bates, F. S.; Fredrickson, G. H. Block Copolymers—Designer Soft Materials. *Physics Today* **1999**, *52*, 32–38.

(74) Matsen, M. W.; Thompson, R. B. Equilibrium behavior of symmetric ABA triblock copolymer melts. *The Journal of chemical physics* **1999**, *111*, 7139–7146.

(75) Rangarajan, P.; Register, R. A.; Adamson, D. H.; Fetters, L. J.; Bras, W.; Naylor, S.; Ryan, A. J. Dynamics of Structure Formation in Crystallizable Block Copolymers. *Macromolecules* **1995**, *28*, 1422–1428.

(76) Rangarajan, P.; Register, R. A.; Fetters, L. J. Morphology of semicrystalline block copolymers of ethylene-(ethylene-*alt*-propylene). *Macromolecules* **1993**, *26*, 4640–4645.

(77) Floudas, G.; Tsitsilianis, C. Crystallization Kinetics of Poly(ethylene oxide) in Poly(ethylene oxide)−Polystyrene−Poly(ethylene oxide) Triblock Copolymers. *Macromolecules* **1997**, *30*, 4381–4390.

(78) Bailey, T. S.; Pham, H. D.; Bates, F. S. Morphological Behavior Bridging the Symmetric AB and ABC States in the Poly(styrene-*b*-isoprene-*b*-ethylene oxide) Triblock Copolymer System. *Macromolecules* **2001**, *34*, 6994–7008.

(79) Bailey, T. S.; Hardy, C. M.; Epps, T. H.; Bates, F. S. A Noncubic Triply Periodic Network Morphology in Poly(isoprene-*b*-styrene-*b*-ethylene oxide) Triblock Copolymers. *Macromolecules* **2002**, *35*, 7007–7017.

(80) Lin, D.; Liu, Y.; Cui, Y. Reviving the lithium metal anode for high-energy batteries. *Nature nanotechnology* **2017**, *12*, 194–206.

(81) Xu, K. Nonaqueous liquid electrolytes for lithium-based rechargeable batteries. *Chem. Rev.* **2004**, *104*, 4303–4417.

(82) Fenton, D. E.; Parker, J. M.; Wright, P. V. Complexes of alkali metal ions with poly(ethylene oxide). *Polymer* **1973**, *14*, 589.

(83) Wright, P. V. Electrical conductivity in ionic complexes of poly(ethylene oxide). *Brit. Poly. J.* **1975**, *7*, 319–327.

(84) Lightfoot, P.; Mehta, M. A.; Bruce, P. G. Crystal Structure of the Polymer Electrolyte Poly(ethylene oxide)$_3$:LiCF_3SO_3. *Science (New York, N.Y.)* **1993**, *262*, 883–885.

(85) Wright, P. V. Polymer electrolytes—the early days. *Electrochimica Acta* **1998**, *43*, 1137–1143.

(86) Mindemark, J.; Lacey, M. J.; Bowden, T.; Brandell, D. Beyond PEO—Alternative host materials for Li^+ -conducting solid polymer electrolytes. *Progress in Polymer Science* **2018**, *81*, 114–143.

(87) Wang, Y.; Fan, F.; Agapov, A. L.; Yu, X.; Hong, K.; Mays, J.; Sokolov, A. P. Design of superionic polymers—New insights from Walden plot analysis. *Solid State Ionics* **2014**, *262*, 782–784.

(88) Berthier, C.; Gorecki, W.; Minier, M.; Armand, M. B.; Chabagno, J. M.; Rigaud, P. Microscopic investigation of ionic conductivity in alkali metal salts-poly(ethylene oxide) adducts. *Solid State Ionics* **1983**, *11*, 91–95.

(89) Teran, A. A.; Tang, M. H.; Mullin, S. A.; Balsara, N. P. Effect of molecular weight on conductivity of polymer electrolytes. *Solid State Ionics* **2011**, *203*, 18–21.

(90) Devaux, D.; Bouchet, R.; Glé, D.; Denoyel, R. Mechanism of ion transport in PEO/LiTFSI complexes: Effect of temperature, molecular weight and end groups. *Solid State Ionics* **2012**, *227*, 119–127.

(91) Le Nest, J. F.; Gandini, A.; Cheradame, H.; Cohen-Addad, J. P. Influence of lithium perchlorate on the properties of polyether networks: specific volume and glass transition temperature. *Macromolecules* **1988**, *21*, 1117–1120.

(92) Fang, C.; Loo, W. S.; Wang, R. Salt Activity Coefficient and Chain Statistics in Poly(ethylene oxide)-Based Electrolytes. *Macromolecules* **2021**, *54*, 2873–2881.

(93) Vachon, C.; Labreche, C.; Vallee, A.; Besner, S.; Dumont, M.; Prud'Homme, J. Microphase Separation and Conductivity Behavior of Poly(propylene oxide)-Lithium Salt Electrolytes. *Macromolecules* **1995**, *28*, 5585–5594.

(94) Cowie, J. M. G.; Cree, S. H. Electrolytes Dissolved in Polymers. *Annu. Rev. Phys. Chem.* **1989**, *40*, 85–113.

(95) Andrieu, X.; Fauvarque, J. F.; Goux, A.; Hamaide, T.; M'hamdi, R.; Vicedo, T. Solid polymer electrolytes based on statistical poly (ethylene oxide-propylene oxide) copolymers. *Electrochimica Acta* **1995**, *40*, 2295–2299.

(96) Barteau, K. P. Poly(Glycidyl Ether)-Based Battery Electrolytes: Correlating Polymer Properties to Ion Transport; University of California, Santa Barbara, **2015**.

(97) Wheatle, B. K.; Keith, J. R.; Mogurampelly, S.; Lynd, N. A.; Ganesan, V. Influence of Dielectric Constant on Ionic Transport in Polyether-Based Electrolytes. *ACS Macro Lett.* **2017**, *6*, 1362–1367.

(98) Wheatle, B. K.; Lynd, N. A.; Ganesan, V. Effect of Polymer Polarity on Ion Transport: A Competition between Ion Aggregation and Polymer Segmental Dynamics. *ACS Macro Lett.* **2018**, *7*, 1149–1154.

(99) Viviani, M.; Meereboer, N. L.; Saraswati, Ni Luh Putu Ananda; Loos, K.; Portale, G. Lithium and magnesium polymeric electrolytes prepared using poly(glycidyl ether)-based polymers with short grafted chains. *Polym. Chem.* **2020**, *11*, 2070–2079.

(100) Okada, M.; Kozawa, S.; Yamashita, Y. Kinetic studies on the polymerization of 1.3.6-trioxocane catalyzed by triethyl oxonium tetrafluoroborate *Makromol. Chem.* **1969**, *127*, 66–77.

(101) Xu, B.; Lillya, C. P.; Chien, J. C. W. Cationic polymerizations of 1,3,6-trioxocane and 2-butyl-1,3,6-trioxocane. *Macromolecules* **1987**, *20*, 1445–1450.

(102) Zheng, Q.; Pesko, D. M.; Savoie, B. M.; Timachova, K.; Hasan, A. L.; Smith, M. C.; Miller, T. F.; Coates, G. W.; Balsara, N. P. Optimizing Ion Transport in Polyether-Based Electrolytes for Lithium Batteries. *Macromolecules* **2018**, *51*, 2847–2858.

(103) Alloin, F.; Sanchez, J.; Armand, M. Triblock copolymers and networks incorporating oligo(oxyethylene) chains. *Solid State Ionics* **1993**, *60*, 3–9.

(104) Alloin, F.; Sanchez, J. -Y.; Armand, M. Electrochemical Behavior of Lithium Electrolytes Based on New Polyether Networks. *J. Electrochem. Soc.* **1994**, *141*, 1915–1920.

(105) Alloin, F.; Sanchez, J.-Y. New solvating polyether networks. *Electrochimica Acta* **1995**, *40*, 2269–2276.

(106) Phan, T. N. T.; Issa, S.; Gigmes, D. Poly(ethylene oxide)-based block copolymer electrolytes for lithium metal batteries. *Polymer International* **2018**, *164*, A5019.

(107) Gomez, E. D.; Panday, A.; Feng, E. H.; Chen, V.; Stone, G. M.; Minor, A. M.; Kisielowski, C.; Downing, K. H.; Borodin, O.; Smith, G. D.; et al. Effect of ion distribution on conductivity of block copolymer electrolytes. *Nano letters* **2009**, *9*, 1212–1216.

(108) Bouchet, R.; Phan, T. N. T.; Beaudoin, E.; Devaux, D.; Davidson, P.; Bertin, D.; Denoyel, R. Charge Transport in Nanostructured PS–PEO–PS Triblock Copolymer Electrolytes. *Macromolecules* **2014**, *47*, 2659–2665.

(109) Yuan, R.; Teran, A. A.; Gurevitch, I.; Mullin, S. A.; Wanakule, N. S.; Balsara, N. P. Ionic Conductivity of Low Molecular Weight Block Copolymer Electrolytes. *Macromolecules* **2013**, *46*, 914–921.

(110) Panday, A.; Mullin, S.; Gomez, E. D.; Wanakule, N.; Chen, V. L.; Hexemer, A.; Pople, J.; Balsara, N. P. Effect of Molecular Weight and Salt Concentration on Conductivity of Block Copolymer Electrolytes. *Macromolecules* **2009**, *42*, 4632–4637.

(111) Singh, M.; Odusanya, O.; Wilmes, G. M.; Eitouni, H. B.; Gomez, E. D.; Patel, A. J.; Chen, V. L.; Park, M. J.; Fragouli, P.; Iatrou, H.; et al. Effect of Molecular Weight on the Mechanical and Electrical Properties of Block Copolymer Electrolytes. *Macromolecules* **2007**, *40*, 4578–4585.

(112) Zardalidis, G.; Gatsouli, K.; Pispas, S.; Mezger, M.; Floudas, G. Ionic Conductivity, Self-Assembly, and Viscoelasticity in Poly(styrene-*b*-ethylene oxide) Electrolytes Doped with LiTf. *Macromolecules* **2015**, *48*, 7164–7171.

(113) Young, W.-S.; Epps, T. H. Ionic Conductivities of Block Copolymer Electrolytes with Various Conducting Pathways: Sample Preparation and Processing Considerations. *Macromolecules* **2012**, *45*, 4689–4697.

(114) Epps, T. H.; Bailey, T. S.; Pham, H. D.; Bates, F. S. Phase Behavior of Lithium Perchlorate-Doped Poly(styrene-*b*-isoprene-*b*-ethylene oxide) Triblock Copolymers. *Chem. Mater.* **2002**, *14*, 1706–1714.

(115) Epps, T. H.; Bailey, T. S.; Waletzko, R.; Bates, F. S. Phase Behavior and Block Sequence Effects in Lithium Perchlorate-Doped Poly(isoprene-*b*-styrene-*b*-ethylene oxide) and Poly(styrene-*b*-isoprene-*b*-ethylene oxide) Triblock Copolymers. *Macromolecules* **2003**, *36*, 2873–2881.

(116) Zardalidis, G.; Pipertzis, A.; Mountrichas, G.; Pispas, S.; Mezger, M.; Floudas, G. Effect of Polymer Architecture on the Ionic Conductivity. Densely Grafted Poly(ethylene oxide) Brushes Doped with LiTf. *Macromolecules* **2016**, *49*, 2679–2687.

(117) Sharon, D.; Bennington, P.; Webb, M. A.; Deng, C.; Pablo, J. J. de; Patel, S. N.; Nealey, P. F. Molecular Level Differences in Ionic Solvation and Transport Behavior in Ethylene Oxide-Based Homopolymer and Block Copolymer Electrolytes. *J. Am. Chem. Soc.* **2021**, *143*, 3180–3190.

(118) Young, W.-S.; Epps, T. H. Salt Doping in PEO-Containing Block Copolymers: Counterion and Concentration Effects. *Macromolecules* **2009**, *42*, 2672–2678.

(119) Loo, W. S.; Galluzzo, M. D.; Li, X.; Maslyn, J. A.; Oh, H. J.; Mongcopa, K. I.; Zhu, C.; Wang, A. A.; Wang, X.; Garetz, B. A.; et al. Phase Behavior of Mixtures of Block Copolymers and a Lithium Salt. *The journal of physical chemistry. B* **2018**, *122*, 8065–8074.

(120) Loo, W. S.; Balsara, N. P. Organizing thermodynamic data obtained from multicomponent polymer electrolytes: Salt-containing polymer blends and block copolymers. *Journal of Polymer Science Part B: Polymer Physics* **2019**, *57*, 1177–1187.

(121) Bouchet, R.; Maria, S.; Meziane, R.; Aboulaich, A.; Lienafa, L.; Bonnet, J.-P.; Phan, T. N. T.; Bertin, D.; Gigmes, D.; Devaux, D.; et al. Single-ion BAB triblock copolymers as highly efficient electrolytes for lithium-metal batteries. *Nature materials* **2013**, *12*, 452–457.

(122) Inceoglu, S.; Rojas, A. A.; Devaux, D.; Chen, X. C.; Stone, G. M.; Balsara, N. P. Morphology–Conductivity Relationship of Single-Ion-Conducting Block Copolymer Electrolytes for Lithium Batteries. *ACS Macro Lett.* **2014**, *3*, 510–514.

(123) Kasemägi, H.; Ollikainen, M.; Brandell, D.; Aabloo, A. Molecular Dynamics Modelling of Block-Copolymer Electrolytes with High t^+ Values. *Electrochimica Acta* **2015**, *175*, 47–54.

(124) Rojas, A. A.; Inceoglu, S.; Mackay, N. G.; Thelen, J. L.; Devaux, D.; Stone, G. M.; Balsara, N. P. Effect of Lithium-Ion Concentration on Morphology and Ion Transport in Single-Ion-Conducting Block Copolymer Electrolytes. *Macromolecules* **2015**, *48*, 6589–6595.

(125) Thelen, J. L.; Inceoglu, S.; Venkatesan, N. R.; Mackay, N. G.; Balsara, N. P. Relationship between Ion Dissociation, Melt Morphology, and Electrochemical Performance of Lithium and Magnesium Single-Ion Conducting Block Copolymers. *Macromolecules* **2016**, *49*, 9139–9147.

(126) Rojas, A. A.; Thakker, K.; McEntush, K. D.; Inceoglu, S.; Stone, G. M.; Balsara, N. P. Dependence of Morphology, Shear Modulus, and Conductivity on the Composition of Lithiated and Magnesiated Single-Ion-Conducting Block Copolymer Electrolytes. *Macromolecules* **2017**, *50*, 8765–8776.

(127) Thelen, J. L.; Chen, X. C.; Inceoglu, S.; Balsara, N. P. Influence of Miscibility on Poly(ethylene oxide) Crystallization from Disordered Melts of Block Copolymers with Lithium and Magnesium Counterions. *Macromolecules* **2017**, *50*, 4827–4839.

(128) Devaux, D.; Liénafa, L.; Beaudoin, E.; Maria, S.; Phan, T. N.T.; Gigmes, D.; Giroud, E.; Davidson, P.; Bouchet, R. Comparison of single-ion-conductor block-copolymer electrolytes with Polystyrene-TFSI and Polymethacrylate-TFSI structural blocks. *Electrochimica Acta* **2018**, 250–261.

(129) Zhang, X.; Guillerm, B.; Prud'homme, R. E. Synthesis and thermal properties of a triblock copolymer for lithium metal polymer batteries. *Polymer* **2019**, *176*, 101–109.

(130) Knop, K.; Hoogenboom, R.; Fischer, D.; Schubert, U. S. Poly(ethylene glycol) in drug delivery: pros and cons as well as potential alternatives. *Angewandte Chemie (International ed. in English)* **2010**, *49*, 6288–6308.

(131) Pasut, G.; Zalipsky, S. Polymer-Protein Conjugates: From Pegylation and Beyond; Elsevier: Amsterdam, **2020**.

(132) Caliceti, P.; Veronese F. M. Pharmacokinetic and biodistribution properties of poly(ethylene glycol)–protein conjugates. *Advanced drug delivery reviews* **2003**, *55*, 1261–1277.

(133) Woodle, M. C. Sterically stabilized liposome therapeutics. *Advanced drug delivery reviews* **1995**, *16*, 249–265.

(134) Yang, Q.; Jacobs, T. M.; McCallen, J. D.; Moore, D. T.; Huckaby, J. T.; Edelstein, J. N.; Lai, S. K. Analysis of Pre-existing IgG and IgM Antibodies against Polyethylene Glycol (PEG) in the General Population. *Analytical chemistry* **2016**, *88*, 11804–11812.

(135) Cheng, T. L.; Wu, P. Y.; Wu, M. F.; Chern, J. W.; Roffler, S. R. Accelerated clearance of polyethylene glycol-modified proteins by anti-polyethylene glycol IgM. *Bioconjugate chemistry* **1999**, *10*, 520–528.

(136) Semple, S. C.; Harasym, T. O.; Clow, K. A.; Ansell, S. M.; Klimuk, S. K.; Hope, M. J. Immunogenicity and rapid blood clearance of liposomes containing polyethylene glycol-lipid conjugates and nucleic Acid. *The Journal of pharmacology and experimental therapeutics* **2005**, *312*, 1020–1026.

(137) Huckaby, J. T.; Jacobs, T. M.; Li, Z.; Perna, R. J.; Wang, A.; Nicely, N. I.; Lai, S. K. Structure of an anti-PEG antibody reveals an open ring that captures highly flexible PEG polymers. *Commun Chem* **2020**, 3.

(138) Saifer, M. G. P.; Williams, L. D.; Sobczyk, M. A.; Michaels, S. J.; Sherman, M. R. Selectivity of binding of PEGs and PEG-like oligomers to anti-PEG antibodies induced by methoxyPEG-proteins. *Molecular immunology* **2014**, *57*, 236–246.

(139) Chen, C.; Constantinou, A.; Deonarain, M. Modulating antibody pharmacokinetics using hydrophilic polymers. *Expert opinion on drug delivery* **2011**, *8*, 1221–1236.

(140) Pytela, J.; Saudek, V.; Drobník, J.; Rypáček, F. Poly(N^5-hydroxyalkylglutamines). IV. Enzymatic degradation of n^5-(2-hydroxyethyl)-L-glutamine homopolymers and copolymers. *Journal of Controlled Release* **1989**, *10*, 17–25.

(141) Romberg, B.; Oussoren, C.; Snel, C. J.; Carstens, M. G.; Hennink, W. E.; Storm, G. Pharmacokinetics of poly(hydroxyethyl-L-asparagine)-coated liposomes is superior over that of PEG-coated liposomes at low lipid dose and upon repeated administration. *Biochimica et biophysica acta* **2007**, *1768*, 737–743.

(142) Romberg, B.; Metselaar, J. M.; Baranyi, L.; Snel, C. J.; Bünger, R.; Hennink, W. E.; Szebeni, J.; Storm, G. Poly(amino acid)s: promising enzymatically degradable stealth coatings for liposomes. *International journal of pharmaceutics* **2007**, *331*, 186–189.

(143) Lorson, T.; Lübtow, M. M.; Wegener, E.; Haider, M. S.; Borova, S.; Nahm, D.; Jordan, R.; Sokolski-Papkov, M.; Kabanov, A. V.; Luxenhofer, R. Poly(2-oxazoline)s based biomaterials: A comprehensive and critical update. *Biomaterials* **2018**, *178*, 204–280.

(144) Bauer, M.; Lautenschlaeger, C.; Kempe, K.; Tauhardt, L.; Schubert, U. S.; Fischer, D. Poly(2-ethyl-2-oxazoline) as alternative for the stealth polymer poly(ethylene glycol): comparison of in vitro cytotoxicity and hemocompatibility. *Macromolecular bioscience* **2012**, *12*, 986–998.

(145) Bauer, M.; Schroeder, S.; Tauhardt, L.; Kempe, K.; Schubert, U. S.; Fischer, D. In vitro hemocompatibility and cytotoxicity study of poly(2-methyl-2-oxazoline) for biomedical applications. *J. Polym. Sci. A Polym. Chem.* **2013**, *51*, 1816–1821.

(146) Zalipsky, S.; Hansen, C. B.; Oaks, J. M.; Allen, T. M. Evaluation of blood clearance rates and biodistribution of poly(2-oxazoline)-grafted liposomes. *Journal of pharmaceutical sciences* **1996**, *85*, 133–137.

(147) Nogueira, S. S.; Schlegel, A.; Maxeiner, K.; Weber, B.; Barz, M.; Schroer, M. A.; Blanchet, C. E.; Svergun, D. I.; Ramishetti, S.; Peer, D.; et al. Polysarcosine-Functionalized Lipid Nanoparticles for Therapeutic mRNA Delivery. *ACS Appl. Nano Mater.* **2020**, *3*, 10634–10645.

(148) Weber, B.; Birke, A.; Fischer, K.; Schmidt, M.; Barz, M. Solution Properties of Polysarcosine: From Absolute and Relative Molar Mass Determinations to Complement Activation. *Macromolecules* **2018**, *51*, 2653–2661.

(149) Sherman, M. R.; Williams, L. D.; Sobczyk, M. A.; Michaels, S. J.; Saifer, M. G. P. Role of the methoxy group in immune responses to mPEG-protein conjugates. *Bioconjugate chemistry* **2012**, *23*, 485–499.

(150) Joh, D. Y.; Zimmers, Z.; Avlani, M.; Heggestad, J. T.; Aydin, H. B.; Ganson, N.; Kumar, S.; Fontes, C. M.; Achar, R. K.; Hershfield, M. S.; et al. Architectural Modification of Conformal PEG-Bottlebrush Coatings Minimizes Anti-PEG Antigenicity While Preserving Stealth Properties. *Advanced healthcare materials* **2019**, *8*, 1801177.

(151) Kainthan, R. K.; Janzen, J.; Levin, E.; Devine, D. V.; Brooks, D. E. Biocompatibility testing of branched and linear polyglycidol. *Biomacromolecules* **2006**, *7*, 703–709.

(152) Tully, M.; Dimde, M.; Weise, C.; Pouyan, P.; Licha, K.; Schirner, M.; Haag, R. Polyglycerol for Half-Life Extension of Proteins-Alternative to PEGylation? *Biomacromolecules* **2021**, *22*, 1406–1416.

Chapter 2

Pharmaceutical Application and Polymerization Kinetics of Polyether Copolymers

Chapter 2.1

Questioning a Paradigm: Random PEG Copolymers for a Better PEGylation?

Philip Dreier[†], Rebecca Matthes[†], Fabian Fuß[†], Matthias Bros[‡], Ramona D. Barent[†], Sandra Schüttner[†] and Holger Frey[†,*]

[†]**Department of Chemistry, Johannes Gutenberg University Mainz, Germany**

[‡]**Department of Dermatology, University Medical Center of the Johannes Gutenberg University Mainz, Germany**

ABSTRACT: PEGylation, the conjugation of poly(ethylene glycol) (PEG) to bioactive peptide drugs or nanocarriers, is an important tool to increase the blood stream circulation time of therapeutics due to the "stealth" effect of PEG. However, anti-PEG antibodies (APA) are becoming increasingly widespread in the population, leading to a pronounced immune-responses after drug application and advanced blood clearance of PEGylated drugs due to a loss of the stealth-effect. By introduction of statistically distributed, hydrophilic side chains at the polyether backbone in copolymers of ethylene oxide (EO) and glycidyl methyl ether (GME), the antigen recognition by the APA is effectively disturbed or prevented. Ideally random anionic ring-opening copolymerization of EO and GME is demonstrated by *in situ* ^{1}H NMR kinetics, while highly defined copolymers ($Đ < 1.09$) of $M_n = 4.2$ to 10.9 kg mol^{-1} and up to 49 mol% GME content are obtained. A competitive enzyme-linked immunosorbent assay (ELISA) of several copolymers revealed reduced (< 24 mol% GME) or fully suppressed recognition of the copolymers by APAs in comparison to the PEG homopolymer. Kinetic Monte Carlo (kMC) simulations illustrate the microstructure of the resulting copolymer chains and allow an in-depth understanding regarding the required GME amount from a theoretical point of view. Cell viability tests confirmed full biocompatibility, as known for the established PEG. Excellent aqueous solubility of P(EG-*co*-GME) copolymers is confirmed by determination of the lower critical solution temperature (LCST) of copolymer with 50% GME (> 94.5 °C). Model reactions with bovine serum albumin evidence the application of P(EG-*co*-GME) for protein bioconjugation. P(EG-*co*-GME) copolymers promise the full preservation of the excellent characteristics of PEG, while eliminating the adverse immune response.

INTRODUCTION

Polymer conjugation with polyethylene glycol (PEG, sometimes also designated “polyethylene oxide”, PEO) currently plays an eminent and still growing role for numerous medical therapeutics. In the “PEGylation” strategy introduced in the late 1970ies,[1–5] the polyether “polyethylene glycol” (PEG, or more commonly monofunctional methoxy-PEG, “mPEG”) is covalently linked to a drug. This is usually achieved via its end group, leading to considerably prolonged circulation times in the blood stream with a half-life on the order of 1-2 weeks. This consequence of PEG attachment is based on the so-called “stealth-effect”, which means that the immune system fails to recognize and eliminate the respective pharmaceuticals from the blood stream. It is commonly attributed to the highly hydrated PEG, forming a hydrophilic corona around the drug molecule or nanocarrier. The non-ionic, hydrophilic PEG thereby provides a steric shield that protects from recognition by the patient’s immune system and effectively increases the size of the biomolecule,[6] consequently reducing clearance from the bloodstream. Investigations of coated nanocarriers additionally revealed the effect of PEG on the composition of protein corona formed around the particles which is necessary to prevent non-specific cellular uptake.[7]

Depending on the procedure employed, several PEG chains or in some cases a single PEG chain are attached to the respective drug molecule, which can be a peptide or polypeptide, a protein or any type of medical nanocarrier (liposomes, micelles, degradable nanoparticles, etc.).[8–11] By increasing the half-life of protein drugs, the dosage frequency is strongly reduced. Since PEGylated therapeutics are injected and often have to be applied for extended periods, this feature is significant. Increased duration of pharmacological activity, reduction of toxic side effects, and increased quality of life due to controlled, timed release are the main effects attributed to PEGylation of therapeutics.

PEGylated drugs, such as e.g. PEGASYS (peginterferon alfa-2a) and Krystexxa (pegloticase) play a key role for the treatment of numerous chronic diseases. such as e.g. Hepatitis C or gout, requiring regular and repeated injections of the respective PEGylated therapeutic for extended periods, often for many years.[12–14] PEGylated drugs further include products such as Adynovate® and Esperoct® for the treatment of chronic haemophilia.[15] The recently approved mRNA vaccines from Moderna and Pfizer-BioNTech also require PEGylated lipids to ensure the stability of the mRNA in the lipid-based nanoparticle.[16,17] In summary, PEGylation is a crucial strategy for peptide and protein drugs, for liposomal formulations, but also for PEGylated lipids as solubilizing components of lipid nanoparticles used for the SARS-Cov-2 vaccine, enabling to disperse the respective lipid nanoparticles in aqueous solution.[18,19] It is appropriate to state that PEGylation represents the key technology of current nanomedicine. Currently, more than 40 PEGylated therapeutics are on the market or in clinical phase III, market introduction pending.[13]

PEG is a non-biodegradable polymer and must be eliminated from the body through the kidneys, which limits the molecular weight of PEG for medical therapeutics to the renal cutoff size, which for globular proteins is approximately 50 to 60 kDa.

Whereas it was initially believed that PEG is immunologically inert, it has become obvious in

recent decades that an increasing number of patients possess anti-PEG antibodies. The induction of anti-PEG antibodies in humans does not only stem from PEGylated therapeutics, but also from food, cosmetics, and other sources, where PEG is abundant. Several reports have stated that PEGylated proteins can elicit antibody responses against PEG that adversely affect their pharmacokinetics and therapeutic efficacy.[20,21] The potential antigenicity of PEG has even been confirmed by the existence of anti-PEG antibodies (APA) in individuals who have never received PEGylated therapeutics systemically.[22] A phase III clinical study regarding anti-coagulation factor IXa RNA PEG-conjugated aptamer had to be interrupted as anaphylactic reactions in 0.6% of the patients were observed which was most likely caused by the pre-existence of APAs in the blood stream.[23]

The incidence of anti-PEG antibodies observed in healthy blood donors has grown from around 1% in 1984 to more than 42%.[22] The presence of APA-Fabs leads to undesired accelerated blood clearance (ABC) i.e., lowered half-life times of PEGylated therapeutics and rapid clearance from the blood stream. This effect lowers or even disables therapeutic activity. In other cases allergic reactions and in extreme cases anaphylactic shocks were observed.[24]

The mechanism of the antibody interaction with PEG was recently studied by Lai et al., who explained the recognition capability of the binding center of the antibody with an open ring structure of the flexible PEG chain bound by the anti-PEG antibody.[25] The interaction with the antibody is stabilized via multiple, unspecific polar and Van der Waals interactions at the surface of the ring. By counting the number of monomer repeats interacting with the interior and exterior paratope of the Fab, these authors found the size of the PEG antigen epitope to be ~700 Da, equivalent to 16 monomer subunits. Other works suggest that also shorter regular chain segments of PEG as well as the methoxy end group of mPEG structure play a key role for the recognition. Sherman et al. used competitive enzyme-linked immunosorbent assays (ELISA) and reported that antibodies elicited by PEG-OH have similar affinity to both mPEG and PEG-OH, while antibodies induced by mPEG recognize mPEG more effectively than PEG-OH. These results imply that the anti-PEG antibodies elicited by PEG-OH-proteins are directed against the backbone of the PEG (backbone-specific), while antibodies induced by mPEG-protein conjugates are methoxy group specific.[26,27] It can be concluded that regular segments of at least 4-5 to 16 regularly arranged ethylene glycol units are required to achieve recognition and immunogenic reaction by APA-Fabs. Recent clinical works regarding Pegasparagase have shown that the presence of antibodies against PEG permits to predict allergic reactions and failure of rechallenge, emphasizing the clinical relevance of APA-Fabs for the success of the treatment of leukemia in this case.[28]

In the light of constantly increasing numbers of individuals with anti-PEG antibodies, mainly two solutions briefly summarized in the following have been suggested to lower antibody interaction by altering the PEG structure. Sherman et al.[26] introduced methods for the preparation of PEG conjugates that are based on end group modification of the PEG chains, aiming at minimizing interaction with anti-PEG Abs. The authors disclosed conjugates, wherein a hydroxyl group is present on all of the distal polyalkylene glycol termini. They showed that these conjugates

exhibited reduced antigenicity compared to mPEG-protein conjugates.[29] Chilkoti et al. used methacrylate monomers bearing oligoethylene oxide side chains and radical polymerization, resulting in POEGMA brushes with sidechain lengths of two and three EG repeats. These structures were identified as the optimal polymer architecture to minimize binding of anti-PEG antibodies (APAs).[30,31]

The strategy described in this work enables to prevent immune reactions due to APA-Fabs against PEGylated therapeutics by random incorporation of polar methoxymethyl side chains into PEG by statistical copolymerization. The increased spatial requirements of the PEG copolymers and their random distribution impede or even disable interaction with APA-Fabs according to the specific "lock and key principle". Besides the steric impact, we believe that the random distribution of the alkyl groups over the polymer chains additionally disables the development and formation of specific anti-polymer Fabs. In this context, it is vital that the dispersity M_w/M_n ($Đ$) of the random copolymers is as low as for the established PEG. Further, a high end-group fidelity of the resulting polymers is crucial for subsequent utilization in bioconjugations. Thus, the anionic ring-opening copolymerization (AROP) was employed to prepare the respective copolymers of ethylene oxide (EO) and the glycidyl methyl ether (GME).

RESULTS AND DISCUSSION

Synthesis of Copolymers of Ethylene Oxide (EO) and Glycidyl Methyl Ether (GME)

Poly(ethylene glycol) (PEG) is the key polymer for bioconjugation and a cornerstone of nanomedicine in general. Poly(glycidyl methyl ether) (PGME) represents a biocompatible structural isomer of PEG, consequently showing the very same ratio of carbon and oxygen and therefore high hydrophilicity. PGME has been observed to possess high biocompatibility in cell viability tests.[32] Combining EO and GME in a copolymer leads to polyethers with sterically more demanding structures, due to the incorporation of polar GME repeating units in the polyether backbone.

However, to date copolymerization of EO with GME as an isomer of two EO-units has rarely been investigated, due to synthetic challenges. Homopolymers of PGME were either synthesized as oligomers[32,33] or with a high dispersity of 1.5.[34] Copolymers of EO and GME, namely P(EG-*co*-GME) were merely accessible using an activated monomer approach,[34] resulting likewise in ill-defined materials contaminated with toxic aluminum impurities.[35] Here we present the first successful synthesis of well-defined P(EG-*co*-GME) copolymers under common anionic ring-opening polymerization (AROP) conditions (Figure 1a). This was accomplished by the utilization of pure GME (>99 %). The required degree of purity of GME is not available in commercial products, because traces of epichlorohydrin (ECH) remain in the product, even after fractional distillation (Figure 1b). The presence of ECH in AROP results in ill-defined oligomeric polyether structures due to side-reactions between the active chain end and ECH, necessitating an ECH-free synthesis route for GME (SI, Scheme S1). In the current work GME has been synthesized via two approaches: Prilezhaev-epoxidation of allyl methyl ether with *meta*-chloroperbenzoic acid (*m*-CPBA) and ring-closure of 1-chloro-3-methoxy-propan-1-ol.

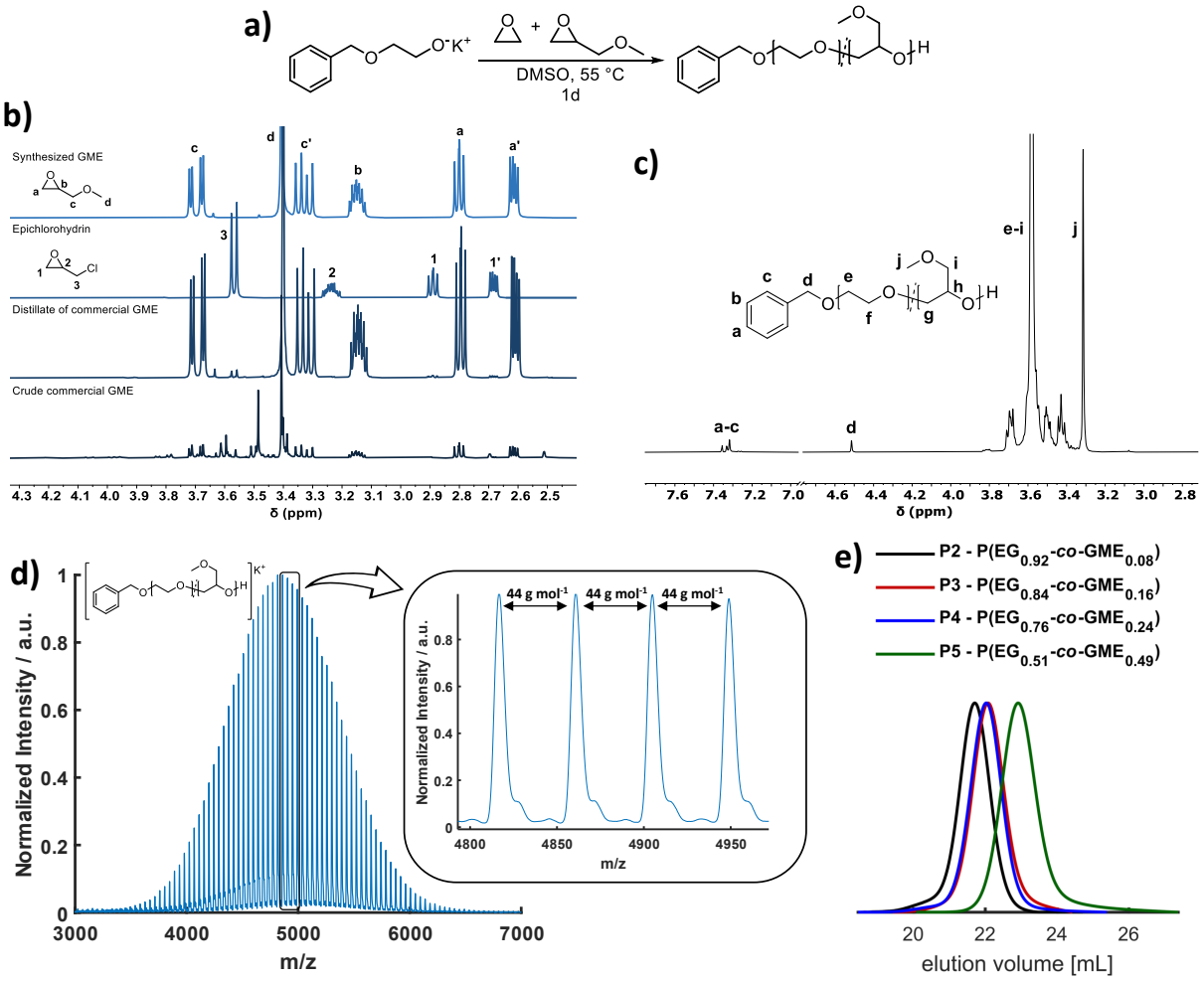

Figure 1. a) Synthesis of P(EG-*co*-GME); b) Comparison of commercial and synthesized GME; c) ^{1}H NMR spectrum of P(EG-*co*-GME); d) MALDI ToF mass spectrum of P(EG-*co*-GME); e) SEC traces of P(EG-*co*-GME).

Both routes yielded highly pure GME (> 99%), enabling the utilization in AROP (full NMR analysis, see SI section 3). Copolymerizations of EO and GME were carried out in DMSO at 55 °C under established AROP conditions, utilizing potassium or cesium 2-benzyloxy ethoxide as an initiator system. Resulting ^{1}H NMR spectra (Figure 1c) of the prepared copolymers show the expected signals of the polyether backbone and the methyl groups of the GME repeating units as well as the absence of any other undesired side-products (full NMR analysis, see SI section 4). Further monitoring of the copolymerization via size exclusion chromatography (SEC) (Figure 1e, SI, Figure S9 and S11) confirms well-defined copolymers with monomodal distributions and low dispersities (1.04-1.09) in the range of 4 to 9 kg mol^{-1} (Table 1). The molar amount of incorporated GME repeating units (mol%$_{GME}$) was varied from 4 to 100 %. Matrix-assisted laser desorption/ionization time of flight mass spectroscopy (MALDI ToF MS) of the synthesized copolymers (Figure 1d) further support the monomodal distributions, showing mass differences of 44 g mol^{-1} in the desired m/z ratio and a single molecular weight distribution.

Table 1. Overview of synthesized P(EG-*co*-GME) copolymers and PGME homopolymer.

No.	Sample	EG ratio[a)] [mol%]	GME ratio[a)] [mol%]	M_n[a)] [kg mol^{-1}]	M_n[b)] [kg mol^{-1}]	M_n[c)] [kg mol^{-1}]	$Đ$[c)]
P1	P($EG_{0.96}$-*co*-$GME_{0.04}$)	96	4	5.3	4.8	3.9	1.04
P2	P($EG_{0.92}$-*co*-$GME_{0.08}$)	92	8	5.2	5.3	4.5	1.05
P3	P($EG_{0.84}$-*co*-$GME_{0.16}$)	84	16	6.9	4.9	3.7	1.05
P4	P($EG_{0.76}$-*co*-$GME_{0.24}$)	76	24	6.0	5.2	3.8	1.06
P5	P($EG_{0.51}$-*co*-$GME_{0.49}$)	51	49	4.2	3.8	2.4	1.09
P6	P($EG_{0.96}$-*co*-$GME_{0.04}$)	96	4	10.9	8.5	7.5	1.08
P7	P($EG_{0.93}$-*co*-$GME_{0.07}$)	93	7	9.0	8.5	7.3	1.05
P8	PGME	-	100	4.2	4.0	2.7	1.05

a) Determined by ^{1}H NMR spectroscopy; b) Determined by MALDI-TOF MS; c) Determined by SEC.

Noteworthy, these statistical copolymers yield unusually clean MALDI ToF mass spectra, which is a result of GME, representing the molecular weight of two EG repeating units (M_{GME} = 2 x M_{EO} = 88.08 g mol^{-1}). The copolymerization procedure is further adaptable to other alkoxide initiators known for AROP, e.g., potassium 2-(2-methoxyethoxy) ethoxide and potassium *N*,*N*-dibenzylamino ethoxide, showing that methoxy, amino and multiple other functionalities are accessible at the α-functionality of P(EG-*co*-GME) via the presented approach (SI, Figure S10). MALDI-ToF mass spectra of the synthesized copolymers evidence an end group fidelity of > 99% for all synthesized copolymers (Figure 1d). The latter is a unique feature of AROP and an indispensable aspect for the sufficient conjugation of polymers to proteins, nanocarriers or surfaces. In comparison, this end group control cannot be achieved via the monomer activated method previously employed for the copolymerization of EO and GME by our group,[34] due to different and unreactive end-groups present at the chain end as well as aluminum impurities.[35]

Investigations of the Microstructure and the Introduction of 'Synthetic Point Mutations' to the Polyether Backbone

Recently, the hitherto elusive binding mechanism of anti-PEG antibodies (APA) with PEG was elucidated. The polyether chain interacts as an open ring structure with the APA paratope.[25] The APA relies on the flexible PEG conformation to capture the rather inert PEG chain and trap the polyether via Van-der-Waals interactions. The respective epitope is believed to consist of 16 monomer units. In order to suppress APA interaction, we propose incorporation of GME repeating units to disrupt the regular PEG chain structure, which may be viewed as introducing 'synthetic point mutations' to PEG. Both the steric demand and the random distribution of side chains are capable of inhibiting the interaction of the APAs with the polyether antigen.

We conducted *in-situ* ^{1}H NMR measurements to elucidate the incorporation of GME into the copolymer during the living anionic copolymerization process, permitting to follow the mean composition at all chain positions. The almost linear decrease of the consumption vs. total

conversion plot clearly demonstrates that the introduction of EO and GME repeating units occurs in an ideally random manner (Figure 2a+b, SI, section 6). Evaluation of the kinetic data via the non-terminal Jaacks model (R^2 = 0.9998) confirms the visible trend with reactivity ratios of r_{EO} = r_{GME} = 1 ± 0.0005 (Figure 2c). Based on the determined reactivity ratios, kinetic Monte Carlo (kMC) simulations (SI, section 7) were performed to further illustrate the random distribution of the "synthetic point mutations" along the PEG copolymer chains (Figure 2d). The chemical heterogeneity within the polymer sample is evident, as each distinct chain possesses different sequence of repeating units. The GME units as 'point mutations' are randomly introduced into the polyether backbone, but the statistical diversity within each chain within one sample is tremendously high. As an example, for a copolymer with 50 monomer units, among which 10 monomer units are GME (20%), the number of possible chain isomers with different structure is 10,272,278,170, which illustrates that the induction of polymer-specific antibodies targeting a regular chain segment will be impossible.

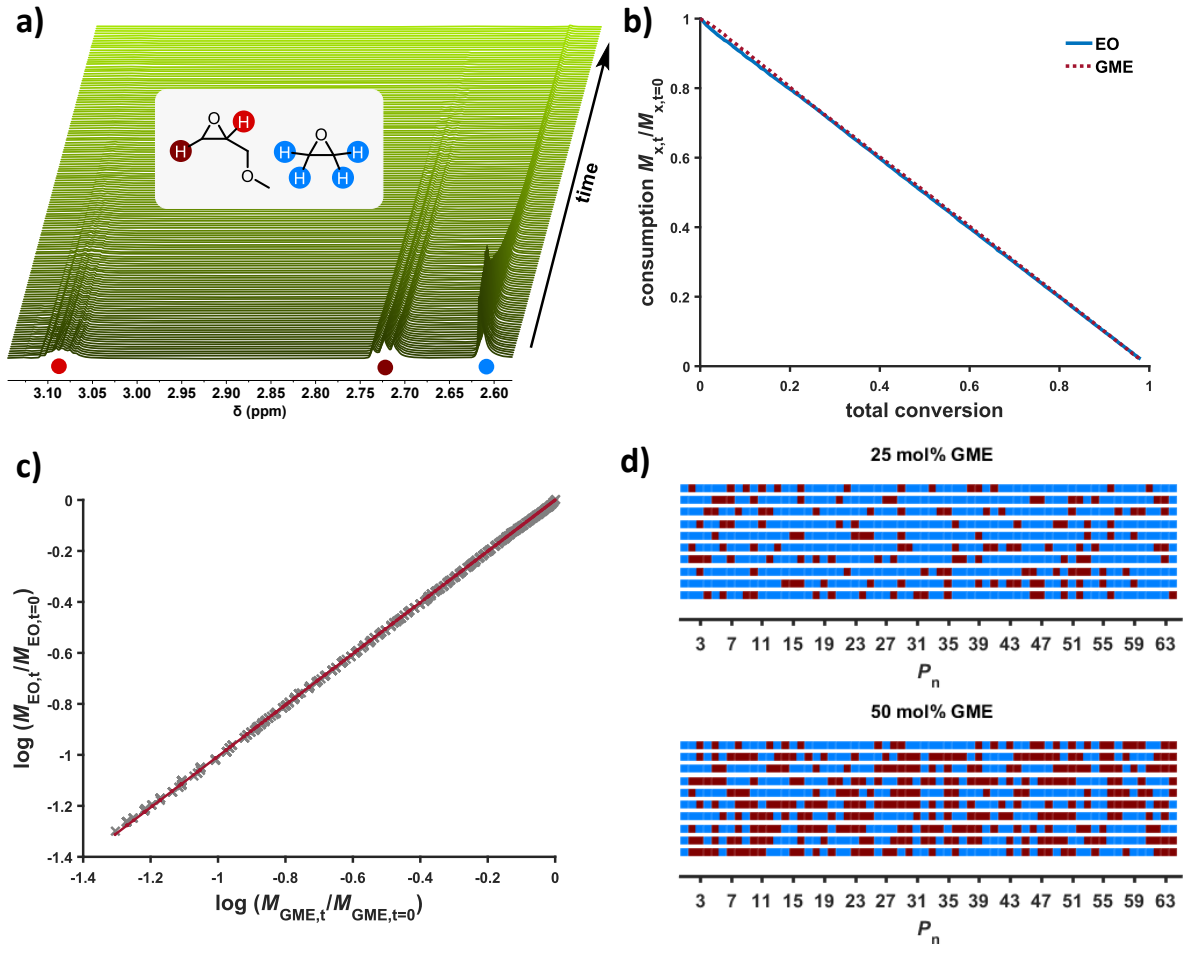

Figure 2. a) Stacked spectra of *in situ* ^{1}H NMR measurement, showing the decrease of monomer resonances over time due to monomer consumption; b) Consumption plot versus total conversion; c) Jaacks fit of the copolymerization of EO and GME; d) Section of a 65 repeating units sequence from 10 out of 1000 chains calculated by Monte-Carlo simulations for 25 and 50 mol% GME (blue dots: EG repeating units, red dots: GME repeating units).

Influence of Synthetic Point Mutations on the Interaction of APAs with Random Copolymers

The effect of a varied concentration of synthetic point mutations (16, 24 and 49 mol%$_{GME}$) on the binding capability of PEG backbone-specific APAs was investigated via competitive enzyme-linked immunosorbent assay (competitive ELISA) at different polymer concentrations. Herein, the concentration-dependent interaction between the APA and PEG homo- and copolymers is observed by a decrease of the fluorescence intensity. An explicit trend is observed: Compared to mPEG (5 kg mol^{-1}), the synthesized copolymers with GME contents > 16 mol% show strongly reduced interaction with APAs. A clear shift of the ELISA curves of 16 and 24 mol% GME to higher polymer concentrations relative to mPEG is manifest in the plot (Figure 3a). Remarkably, with an incorporation of 49 mol% GME, no recognition of the copolymer by APAs is observed. We assume that this translates to full disappearance of the undesired effects, such as ABC and allergic reactions caused by PEG.

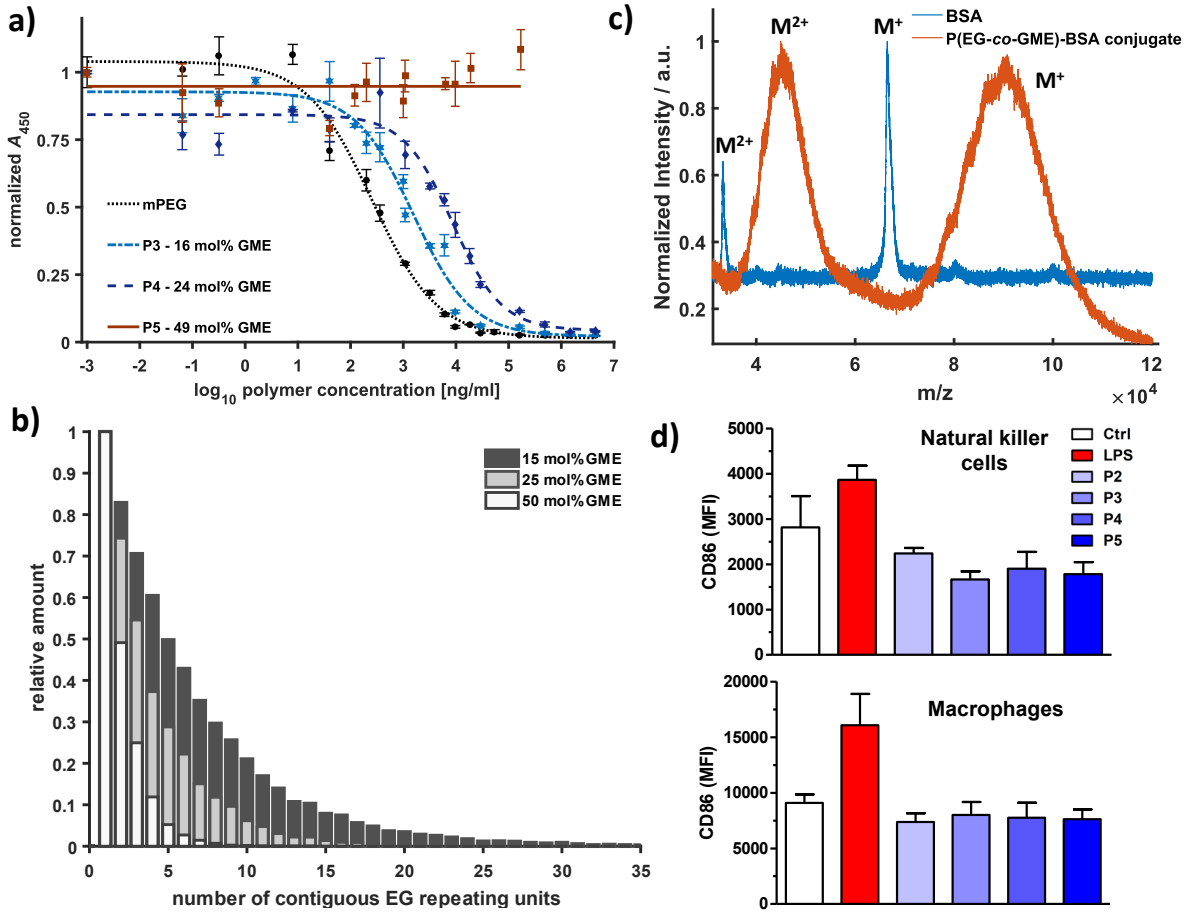

Figure 3. a) Competitive ELISA for mPEG and 16, 24 and 49 mol% GME-containing copolymers; b) Visualization of distribution of EG repeating units in the copolymers with 15, 25 and 50 mol% GME determined via Monte-Carlo-Simulations: Relative amounts of segments with a number of contiguous EG repeating units; c) Overlay of MALDI ToF mass spectra of BSA (blue) and P(EG-*co*-GME)-BSA conjugate (orange) (Matrix: Sinapinic acid); d) PEG derivatives exert no stimulatory effects on immune cells.

In their publication, Lai and co-workers[25] presented the interaction mechanism of PEG and APAs, showing that 16 sequential EG units interact with the interior and exterior paratope of the APA-Fab, regular PEG-segments of this type constitute the epitope. Quantitative analysis of the results generated by kMC simulations allow for the determination of proportional occurrences of sequential EG units in P(EG-*co*-GME) copolymers in dependence of the respective GME ratio. As shown in Figure 3b, in the case of 15 mol% GME, still segments containing > 35 EG-exclusive contiguous repeating units are observed, permitting sufficient interaction of the APA-Fab with the polyether.

This is equally applicable for the copolymer with 24 mol% GME, even though the probability to find these PEG segments in the polymer chains decreases dramatically. With incorporation of 49 mol% GME, the probability of finding longer EG-segments in the polyether almost approaches zero, and the APA-Fab is no longer capable of recognizing the polymeric antigen. Considering these statistical findings in combination with the herein presented experimental results, one may conclude that the APA binds to chain segments exceeding 10 EG subunits. Chain segments below this value are no longer recognized by the APA-Fab. This conclusion further supports the crucial importance of a random distribution of GME repeating units along the polyether chains. On the contrary, a gradient structure would result in an accumulation of contiguous EG repeating units at the beginning or end of the polymer chain, resulting in enhanced APA recognition.

Suitability of P(EG-*co*-GME) Copolymers for Medical Applications

The hydrophilicity of PEG and the resulting accumulation of water molecules in combination with protein interaction[7] play an essential role for the reduced protein adsorption of PEGylated drugs and the stealth effect.[6] To examine the solubility of the presented copolymers in aqueous solution with regard to temperature, we conducted turbidimetric experiments (SI, section 5, Figure S13). All herein prepared copolymers exhibit excellent water solubility with an LCST of 94.5 °C for 49 mol% GME and are therefore comparable with PEG with respect to their hydrophilicity. In addition to the already mentioned features, the incorporation of GME units into the polyether backbone leads to the inhibition of crystallization of the EG units, yielding amorphous materials (SI, section 10). The indispensable non-toxicity for biomedical application of the synthesized copolymers was investigated by flow cytometry of murine spleen cells. All immune cell types showed the same cell viability after treatment with P(EO-*co*-GME) (c = 0.1 to 10 mg ml^{-1}) compared to untreated cells (SI, section 11). Subsequent screening of the copolymers (c = 1 mg ml^{-1}) (Figure 3d) demonstrated no stimulatory effect on immune cells compared to untreated cells, while the utilized positive control (lipopolysaccharide, LPS) exhibited high stimulation. These results show full biocompatibility, as commonly known for the PEG homopolymer. Finally, a model bioconjugation of a P(EG-*co*-GME) copolymer to bovine serum albumin (BSA) was performed to demonstrate the chemical suitability of these copolymers for protein conjugation as an alternative to PEGylation (SI, section 8). Figure 3c shows the corresponding MALDI ToF MS of BSA and a conjugate with P3 (16 mol% GME). The absence of unfunctionalized BSA in the spectra confirms quantitative functionalization of BSA with P(EG-*co*-GME). The broadening of the P(EG-*co*-GME)-

BSA conjugate signal compared to the unfunctionalized BSA is explained by multiple conjugation with different numbers of P(EG-*co*-GME) chains. The successful conjugation was conducted using an established procedure for PEG, relying on NHS activation of the ω-chain end (SI, section 8). The results demonstrate the suitability of P(EG-*co*-GME) copolymers for protein bioconjugation, relying on procedures established for PEG.

CONCLUSION

The increasing abundance of anti-PEG antibodies (APA) in the population leads to undesired immune-responses to PEGylated drugs. This has become an increasingly severe concern over the years since it renders the stealth effect ineffective. Recently, its topicality has drastically increased, as the containment of the global COVID-19 pandemic partly relies on PEGylated lipids for the transport of the RNA vaccines. We introduce the concept of random polyether copolymers containing chemical 'point mutations' as a novel alternative to the established PEGylation. The immediately obvious advantage of the strategy described in this work lies in the fact that existing PEG technology in all steps is equally applicable. Unlike in the case of recently discussed PEG alternatives, such as polyoxazolines[8,36] or polysarcosine,[37] completely new GMP manufacturing strategies and supply chains are not required. Highly defined poly(ethylene glycol-*co*-glycidyl methyl ether) (P(EG-*co*-GME)) copolymers ($Đ < 1.09$, mostly < 1.05; end-group fidelity of > 99 %) of up to 9.4 kg mol^{-1} have been synthesized by anionic ring-opening copolymerization of ethylene oxide (EO) and glycidyl methyl ether (GME). Detailed *in situ* ^{1}H NMR kinetic experiments revealed an ideally random copolymerization of both monomers, enabling a random incorporation of chemical 'point mutations' into the PEG backbone. The highly hydrophilic copolymers demonstrate dramatically reduced recognition by APAs (< 24 mol% GME) in a competitive enzyme-linked immunosorbent assay (ELISA). while incorporation of 49 mol% of GME lead to a full suppression of any APA interaction, which is crucial for PEGylation type bioconjugation. Kinetic Monte Carlo (kMC) simulations regarding the microstructure of such copolymers further supported the experimental ELISA results. A wide range of structural diversity of the P(EG-*co*-GME) copolymers, determined by statistics, is present in the copolymers, despite the highly controlled chain length due to the living synthesis method. A further adjustment of GME ratios enables further variation possibilities. Versatile conjugation chemistry has been established for PEG for more than 3 decades and is fully transferrable to the GME-PEG copolymers, as demonstrated in this study by a model conjugation with bovine serum albumin (BSA). Further architectural variation may include different bi- to multifunctional initiators, block copolymers as well as the utilization of varied alkyl side chains by incorporation of ethyl, propyl or *iso*-propyl glycidyl ether units. On the other hand, the possibility of segregating the medical and pharmaceutical application by use of GME-PEGs may aid to avoid antibody induction.

We firmly believe that PEGylation with random copolymers as outlined here bears immense potential for the treatment of chronic diseases. One can for instance imagine giving drugs that are GME-PEGylated with different contents upon repeated administration, thereby disabling the immune system from developing an antibody response. Hence, "Beyond PEG" – as it was

mentioned in the title of recent critical reviews, may simply mean randomizing the PEG structure by the introduction of suitable comonomers.

REFERENCES

(1) Harris, J. M.; Chess, R. B. Effect of pegylation on pharmaceuticals. Nature reviews. *Drug discovery* **2003**, *2*, 214–221.

(2) Kolate, A.; Baradia, D.; Patil, S.; Vhora, I.; Kore, G.; Misra, A. PEG - a versatile conjugating ligand for drugs and drug delivery systems. *Journal of controlled release: official journal of the Controlled Release Society* **2014**, *192*, 67–81.

(3) Mishra, P.; Nayak, B.; Dey, R. K. PEGylation in anti-cancer therapy: An overview. *Asian Journal of Pharmaceutical Sciences* **2016**, *11*, 337–348.

(4) Hoffman, A. S. The early days of PEG and PEGylation (1970s-1990s). *Acta biomaterialia* **2016**, *40*, 1–5.

(5) Ostuni, E.; Chapman, R. G.; Holmlin, R. E.; Takayama, S.; Whitesides, G. M. A Survey of Structure−Property Relationships of Surfaces that Resist the Adsorption of Protein. *Langmuir* **2001**, *17*, 5605–5620.

(6) Pelegri-O'Day, E. M.; Lin, E.-W.; Maynard, H. D. Therapeutic protein-polymer conjugates: advancing beyond PEGylation. *Journal of the American Chemical Society* **2014**, *136*, 14323–14332.

(7) Schöttler, S.; Becker, G.; Winzen, S.; Steinbach, T.; Mohr, K.; Landfester, K.; Mailänder, V.; Wurm, F. R. Protein adsorption is required for stealth effect of poly(ethylene glycol)- and poly(phosphoester)-coated nanocarriers. *Nature nanotechnology* **2016**, *11*, 372–377.

(8) Knop, K.; Hoogenboom, R.; Fischer, D.; Schubert, U. S. Poly(ethylene glycol) in drug delivery: pros and cons as well as potential alternatives. *Angewandte Chemie International Edition* **2010**, *49*, 6288–6308.

(9) Alconcel, S. N. S.; Baas, A. S.; Maynard, H. D. FDA-approved poly(ethylene glycol)–protein conjugate drugs. *Polym. Chem.* **2011**, *2*, 1442.

(10) D'souza, A. A.; Shegokar, R. Polyethylene glycol (PEG): a versatile polymer for pharmaceutical applications. *Expert opinion on drug delivery* **2016**, *13*, 1257–1275.

(11) Roberts, M. J.; Bentley, M. D.; Harris, J. M. Chemistry for peptide and protein PEGylation. *Advanced drug delivery reviews* **2012**, *64*, 116–127.

(12) Heredia, K. L.; Maynard, H. D. Synthesis of protein-polymer conjugates. *Organic & biomolecular chemistry* **2007**, *5*, 45–53.

(13) Zalipsky, S.; Pasut, G. Evolution of polymer conjugation to proteins. *Polymer-Protein Conjugates; Elsevier*, **2020**; 3–22.

(14) Irizarry Rovira, A. R.; Bennet, B. M.; Bolon, B.; Braendli-Baiocco, A.; Chandra, S.; Fleurance, R.; Garman, R.; Hutto, D.; Lane, J.; Romeike, A.; et al. Scientific and Regulatory Policy Committee Points to Consider: Histopathologic Evaluation in Safety Assessment Studies for PEGylated Pharmaceutical Products. *Toxicologic pathology* **2018**, *46*, 616–635.

(15) Valentino, L. A.; Cong, L.; Enockson, C.; Song, X.; Scheiflinger, F.; Muchitsch, E. M.; Turecek, P. L.; Hakobyan, N. The biological efficacy profile of BAX 855, a PEGylated recombinant factor VIII molecule. *Haemophilia : the official journal of the World Federation of Hemophilia* **2015**, *21*, 58–63.

(16) Michael McCoy. Lipids, the unsung COVID-19 vaccine component, get investment: Several specialty chemical companies are adding capacity to supply Moderna and Pfizer-BioNTech. *American Chemical Society*, **2021**.

(17) Pastor, F.; Berraondo, P.; Etxeberria, I.; Frederick, J.; Sahin, U.; Gilboa, E.; Melero, I. An RNA toolbox for cancer immunotherapy. *Nature reviews. Drug discovery* **2018**, *17*, 751–767.

(18) Pardi, N.; Hogan, M. J.; Porter, F. W.; Weissman, D. mRNA vaccines - a new era in vaccinology. *Nature reviews. Drug discovery* **2018**, *17*, 261–279.

(19) Schoenmaker, L.; Witzigmann, D.; Kulkarni, J. A.; Verbeke, R.; Kersten, G.; Jiskoot, W.; Crommelin, D. J. A. mRNA-lipid nanoparticle COVID-19 vaccines: Structure and stability. *International Journal of Pharmaceutics* **2021**, *601*, 120586.

(20) d'Avanzo, N.; Celia, C.; Barone, A.; Carafa, M.; Di Marzio, L.; Santos, H. A.; Fresta, M. Immunogenicity of Polyethylene Glycol Based Nanomedicines: Mechanisms, Clinical Implications and Systematic Approach. *Adv. Therap.* **2020**, *3*, 1900170.

(21) Barz, M.; Luxenhofer, R.; Zentel, R.; Vicent, M. J. Overcoming the PEG-addiction: well-defined alternatives to PEG, from structure–property relationships to better defined therapeutics. *Polym. Chem.* **2011**, *2*, 1900.

(22) Yang, Q.; Jacobs, T. M.; McCallen, J. D.; Moore, D. T.; Huckaby, J. T.; Edelstein, J. N.; Lai, S. K. Analysis of Pre-existing IgG and IgM Antibodies against Polyethylene Glycol (PEG) in the General Population. *Analytical chemistry* **2016**, *88*, 11804–11812.

(23) Lincoff, A. M.; Mehran, R.; Povsic, T. J.; Zelenkofske, S. L.; Huang, Z.; Armstrong, P. W.; Steg, P. G.; Bode, C.; Cohen, M. G.; Buller, C.; et al. Effect of the REG1 anticoagulation system versus bivalirudin on outcomes after percutaneous coronary intervention (REGULATE-PCI): a randomised clinical trial. *The Lancet* **2016**, *387*, 349–356.

(24) Sellaturay, P.; Nasser, S.; Islam, S.; Gurugama, P.; Ewan, P. W. Polyethylene glycol (PEG) is a cause of anaphylaxis to the Pfizer/BioNTech mRNA COVID-19 vaccine. *Clin Exp Allergy.* **2021**, *51*, 861-863.

(25) Huckaby, J. T.; Jacobs, T. M.; Li, Z.; Perna, R. J.; Wang, A.; Nicely, N. I.; Lai, S. K. Structure of an anti-PEG antibody reveals an open ring that captures highly flexible PEG polymers. *Commun Chem* **2020**, 3.

(26) Sherman, M. R.; Williams, L. D.; Sobczyk, M. A.; Michaels, S. J.; Saifer, M. G. P. Role of the methoxy group in immune responses to mPEG-protein conjugates. *Bioconjugate chemistry* **2012**, *23*, 485–499.

(27) Saifer, M. G. P.; Williams, L. D.; Sobczyk, M. A.; Michaels, S. J.; Sherman, M. R. Selectivity of binding of PEGs and PEG-like oligomers to anti-PEG antibodies induced by methoxyPEG-proteins. *Molecular immunology* **2014**, *57*, 236–246.

(28) Liu, Y.; Smith, C. A.; Panetta, J. C.; Yang, W.; Thompson, L. E.; Counts, J. P.; Molinelli, A. R.; Pei, D.; Kornegay, N. M.; Crews, K. R.; et al. Antibodies Predict Pegaspargase Allergic Reactions and Failure of Rechallenge. *Journal of Clinical Oncology* **2019**, *37*, 2051–2061.

(29) Alexa L Martinez, Merry R Sherman, Mark G. P. Saifer, L David Williams. Polymer conjugates with decreased antigenicity, methods of preparation and uses thereof.

(30) Joh, D. Y.; Zimmers, Z.; Avlani, M.; Heggestad, J. T.; Aydin, H. B.; Ganson, N.; Kumar, S.; Fontes, C. M.; Achar, R. K.; Hershfield, M. S.; et al. Architectural Modification of Conformal PEG-Bottlebrush Coatings Minimizes Anti-PEG Antigenicity While Preserving Stealth Properties. *Advanced healthcare materials* **2019**, *8*, e1801177.

(31) Chilkoti, A. e. a. Polymer conjugates having reduced antigenicity and methods of using the same.

(32) Weinhart, M.; Grunwald, I.; Wyszogrodzka, M.; Gaetjen, L.; Hartwig, A.; Haag, R. Linear poly(methyl glycerol) and linear polyglycerol as potent protein and cell resistant alternatives to poly(ethylene glycol). *Chemistry, an Asian journal* **2010**, *5*, 1992–2000.

(33) Isono, T.; Miyachi, K.; Satoh, Y.; Sato, S.; Kakuchi, T.; Satoh, T. Design and synthesis of thermoresponsive aliphatic polyethers with a tunable phase transition temperature. *Polym. Chem.* **2017**, *8*, 5698–5707.

(34) Müller, S. S.; Moers, C.; Frey, H. A Challenging Comonomer Pair: Copolymerization of Ethylene Oxide and Glycidyl Methyl Ether to Thermoresponsive Polyethers. *Macromolecules* **2014**, *47*, 5492–5500.

(35) Sakakibara, K.; Nakano, K.; Nozaki, K. Regio-controlled ring-opening polymerization of perfluoroalkyl-substituted epoxides. *Chemical communications* **2006**, 3334–3336.

(36) Lorson, T.; Lübtow, M. M.; Wegener, E.; Haider, M. S.; Borova, S.; Nahm, D.; Jordan, R.; Sokolski-Papkov, M.; Kabanov, A. V.; Luxenhofer, R. Poly(2-oxazoline)s based biomaterials: A comprehensive and critical update. *Biomaterials* **2018**, *178*, 204–280.

(37) Nogueira, S. S.; Schlegel, A.; Maxeiner, K.; Weber, B.; Barz, M.; Schroer, M. A.; Blanchet, C. E.; Svergun, D. I.; Ramishetti, S.; Peer, D.; et al. Polysarcosine-Functionalized Lipid Nanoparticles for Therapeutic mRNA Delivery. *ACS Appl. Nano Mater.* **2020**, *3*, 10634–10645.

SUPPORTING INFORMATION

Materials and Instrumentation

Reagents and Equipment

All chemicals and solvents were purchased from Acros Organics, Roth, TCI, Sigma-Aldrich, Fisher Scientific and Fluka, unless otherwise noted. Deuterated solvents were received from Deutero GmbH. Ethylene Oxide was acquired from Air Liquide. THF was flashed over basic aluminum oxide before usage. Glycidyl methyl ether was dried over CaH_2 and cryo-transferred before the polymerizations.

Size Exlcusion Chromatography

Size exclusion chromatography (SEC) measurements were performed in dimethylformamide (DMF) with 1 g L^{-1} lithium bromide as an eluent at 50 °C. An Agilent 1100 Series was used, equipped with HEMA 300/100/40 columns, and calibration was carried out using polyethylene glycol (PEG) standards, both provided by Polymer Standard Service (PSS), Mainz.

Differential Scanning Calorimetry

DSC measurements were carried out in the temperature range of -100 to 100 °C with a heating rate of 10 K min^{-1} at a PerkinElmer DSC 8500. The thermal history of the samples was excluded via two cooling and two heating cycles. For each sample, the glass transition and the melting temperatures were obtained from the second heating curve.

MALDI-ToF Mass Spectrometry (MS)

MALDI-ToF MS measurements were carried out at a Bruker autoflex maX MALDI-TOF/TOF. For copolymers, the potassium salt of triflouroacetic acid and DCTB were utilized as ionization salt and matrix, respectively. For conjugates, sinapinic acid was utilized as matrix.

NMR Spectroscopy and *in situ* ^{1}H NMR Kinetic Experiments

^{1}H and ^{13}C NMR spectra were recorded on a Bruker Avance III HD 300 spectrometer with 300 MHz and 75 MHz, respectively, and referenced internally to residual proton signals of the deuterated solvent. The herein performed online ^{1}H NMR kinetic study was conducted according to a protocol by Herzberger et al. in a Norell S-500-VT-7 NMR tube.[1] The monomer consumption over time was recorded by online ^{1}H NMR spectra with a Bruker Avance III HD 400 MHz spectrometer which was equipped with a 5 mm BFFO SmartProbe. Prior to the experiment, KO*t*Bu (19.2 mg, 172 μmol) was dissolved in a THF/water mixture and transferred to a septum and stop cock-equipped flame-dried Schlenk flask. Benzyl alcohol (29.0 mg, 191 μmol) was dissolved in benzene and added to the base solution. The initiator salt was dried under high vacuum at 60 °C after the solvent was slowly evaporated under high vacuo. The dry initiator salt was dissolved in dry DMSO-d_6 (1 mL) and stirred for 30 min. Simultaneously, EO (96 mg, 100 μL,

2.2 μmol) was cryo-transferred under static vacuum at -50 °C with an acetone/nitrogen bath to the evacuated NMR tube which was attached to the Schlenk-line. Following, GME (95 mg, 95 μL, 1.1 μmol) and 200 μL initiator solution were transferred under inert argon-atmosphere to the NMR tube. Subsequently, the solution was cooled by liquid nitrogen, evacuated and sealed with a Teflon stop cock. After warming to room temperature, the reaction mixture was shaken vigorously to ensure a homogenous mixture and then paced in the preheated (55 °C) NMR spectrometer. After the temperature was stable ($T = 0.1$ K), one spectrum was recorded every 30 sec with 1 scan. The experimental data was analyzed by help of NIREVAL software from Johann, Steube and Frey.[2]

Regarding ethylene oxide: EO is a toxic, highly flammable gas. Therefore, careful handling and specific precautions are necessary. The addition of EO to the NMR tube was carried out in a reproducible procedure. Hence, a very small amount was utilized (< 0.1 ml) which might cause small deviations in the measured volumes. The targeted monomer ratios might therefore differ from the actual monomer ratios to a small extent.

Turbidimetric Measurements

Turbidimetry measurements were performed with a UV/VIS-spectrometer V-630 by JASCO for determination of the cloud point T_{cp}. Samples were measured at a wavelength of 600 nm and with a heating rate of 1 K min^{-1}. Samples were prepared in Milli-Q® water, which was utilized as reference prior to each experiment. The sample concentration was 2.5 mg ml^{-1} while the T_{cp} was determined at a transmission of 50%.

Competitive Enzyme-linked Immunsorbent Assay (ELISA)

The interaction of the copolymers with APA was evaluated by a competitive PEG ELISA kit using a murine monoclonal, horseradish peroxidase conjugated anti PEG antibody (HRP anti-PEG) (Life diagnostics, West Chester, PA, USA). Samples of concentrations ranging from 0 to 4600 μg mL^{-1} were prepared in dilution buffer. Additionally, mPEG with a molecular weight of 5 kg mol^{-1} was utilized as an internal standard for comparison. 50 μL of each prepared sample was dispensed to a PEG pre-coated 96-well plate and 50 μL of HRP anti-PEG was added to each well. The solutions were incubated for 1 h at 25 °C with a micro-plate shaker and then washed six times with 400 μL of wash buffer per each well. After removal of residual droplets, 100 μL of 3,3′,5,5′-tetramethylbiphenyl-4,4'-diamine (TMB) was added to each well and the solutions were mixed on a micro-plate shaker for 20 min. The reaction was stopped by addition of 100 μL of stop solution and the absorbance at 450 nm was read within 5 min.

The determined absorbance values were normalized to visualize the percent of maximal binding. The sample concentrations were transformed to a function of $\log_{10}$. Sigmoidal fits were calculated using the following equation with a representing the upper limit b the lower limit c the inflection point and d the hill slope.

$$y = \frac{a+(b-a)}{1+10^{(c-x)d}}$$

Flow cytometry

Potential cytotoxic and stimulatory effects of the various copolymers on primary immune cell populations were assessed using mouse spleen cells. For this purpose, spleens retrieved from C57BL/6 mice were mechanically dissected, and erythrocytes were lysed using a hypotonic lysis buffer. Spleen cells were resuspended in IMDM culture medium (107 mL) and aliquots (200 μL) were transferred into sterile FACS tubes. Then, the different PEG derivatives were applied at the concentrations indicated (0.1-10 mg mL^{-1}). In some experiments, lipopolysaccharide (LPS; Sigma-Aldrich, Deisenhofen, Germany) was applied as a positive control for immune cell activation (1 μg mL^{-1}). On the next day, samples were washed and preincubated (20 min, 4 °C) with a Fcγ receptor-blocking antibody (clone 2.4G2) to prevent unspecific binding of receptor-specific antibodies. Then, samples were incubated (20 min, 4 °C) with antibodies specific for CD3 (labeled with eFl500), CD11b (SB600), CD11c (BV421), CD19 (SB702), NK1.1 (PE), Ly6G (PE-eFl610), and CD86 (FITC) was added (20 min at 4 °C. Cell viability was assessed by applying Fixable viability dye (FVD)-eFl780 (30 min, 4° C). Subsequently, samples were fixed (0.7% paraformaldehyde) and subjected to flow cytometric analysis using an Attune NxT flow cytometer (Thermo Fisher) equipped with Attune Nxt Software v3.1.1. The different spleen cell populations were identified by sequential gating as described.[3] Polymers were dialyzed against deionized water before incubation.

Experimental Procedures

Synthesis of Glycidyl Methyl ether

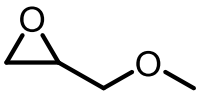

The monomer glycidyl methyl ether (GME) is commercially available with a purity rate of 85 % including high amounts of epichlorohydrin (ECH). The contamination of ECH leads to undesired termination reactions, shown in Scheme S1. The potassium alkoxide of either the initiator or the living chain end leads to nucleophilic ring opening of ECH, followed by ring closure under precipitation of potassium chloride, while either the chain end is terminated by epoxidation or the respective glycidyl ether is formed.

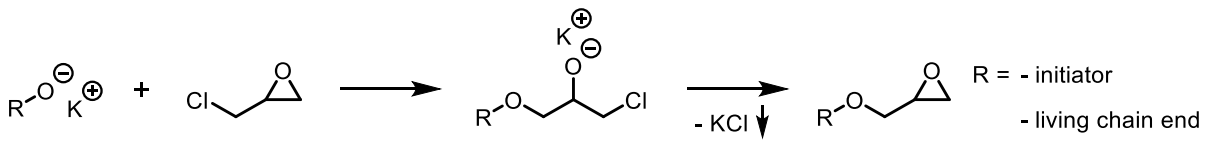

Scheme S1. Side reaction during anionic ring-opening polymerization of epoxides with epichlorohydrin impurities present.

Route (a). Synthesis of GME by Prileschajew epoxidation.[4] Allyl methyl ether (10.0 g, 139 mmol) was dissolved in 274 mL dichloromethane (DCM) and *m*-chloroperoxybenzoic acid (*m*-CPBA)

(70%, 37.6 g, 153 mmol (based on *m*-CPBA)) was added to the solution. After stirring overnight, the solution was filtrated and slowly concentrated under reduced pressure. Crude glycidyl methyl ether was separated from solid impurities via cryo-transfer. Slow evaporation of residual dichloromethane in vacuo gave pure glycidyl methyl ether as a colorless liquid; Yield 41%.

Route (b). Synthesis of GME by ring-closure. 1-Chloro-3-methoxy-propan-2-ol (3.00 g, 2.56 mL, 24.1 mmol) and anhydrous sodium sulfate (1.02 g, 7.23 mmol) were added to a flask equipped with a magnetic stirrer and cooled with a water bath. Finely grounded sodium hydroxide (1.25 g, 31.3 mmol) was added under stirring. After complete reaction (TLC control) the crude product was cryo-transferred in vacuo from the reaction flask and dried over CaH_2 under cooling. After an additional cryo-transfer, GME was obtained as a colorless liquid with a yield of 93%.

^{1}H NMR ($CDCl_3$) δ [ppm]: 3.72-3.67 (dd, 1H, CH_2-O-CH-), 3.41 (s, 3H, -CH_3), 3.36-3.30 (dd, 1H, CH_2-O-CH-), 3.17-3.12 (m, 1H, CH_2-O-CH-),), 2.82-2.79 (dd, 1H, -CH_2-CH_3), 2.63-2.60 (dd, 1H, -CH_2-CH_3).

Synthesis of PGME

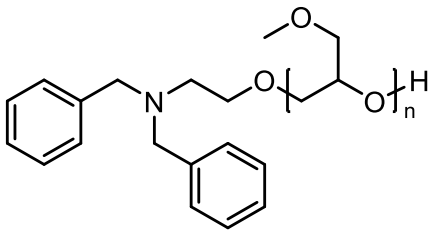

Cesium hydroxide monohydrate (25.0 mg, 149 μmol) was dissolved in a THF/water mixture and transferred to a flame-dried reaction flask, equipped with a septum and a Teflon stopcock. The initiator salt was produced by dissolving *N*,*N*-dibenzyl-2-aminoethanol (40.0 mg, 166 μmol) in benzene and addition to the reaction flask. After slow evaporation of the solvent, the resulting solid was dried at 60 °C under high vacuum overnight. Subsequently, the salt was dissolved in dry DMSO (5 mL) and the mixture was cooled to -78 °C. After addition of GME (660 mg, 670 μL, 7.46 mmol) via syringe, the solution was stirred for 48 h at room temperature under vacuum. After polymerization, the reaction solution was dissolved in excess chloroform and extracted against water (3 times) and brine, dried over $MgSO_4$ and filtrated. Poly(glycidyl methyl ether) (PGME) was obtained in quantitative yield as a viscous liquid after evaporation of the solvent and drying under high vacuo.

^{1}H NMR (DMSO-d_6) δ [ppm]: 7.38-7.21 (m, 10H, Ar-*H*), 3.75-3.40 (m, polyether backbone, Ar-CH_2-N), 3.31 (OCH_3), 2.54 (t, 2H, N-CH_2-CH_2-O).

Synthesis of P(EG-*co*-GME)

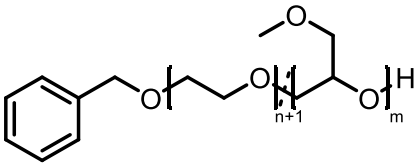

An exemplary procedure for the synthesis of random P(EG-*co*-GME) copolymers is given in the following. Additional polymers were synthesized with the same procedure. Potassium *tert*-butoxide (13.0 mg, 118 μmol) was dissolved in a THF/water mixture and transferred to a flame-dried reaction flask, equipped with a septum and a Teflon stopcock. The initiator, 2-benzyloxy-ethanol (20.0 mg, 18.7 μL, 131 μmol) was dissolved in benzene and added to the flame-dried reaction flask. After slow evaporation of the solvent, the resulting solid was dried at 60 °C under high vacuum overnight. Subsequently, the salt was dissolved in dry DMSO (5 mL) and the mixture was cooled to -78 °C. GME (119 mg, 122 μL, 1.35 mmol) was added via syringe and ethylene oxide (537 mg, 553 μL, 12.2 mmol) was cryo-transferred into the reaction flask. The solution was heated to 55 °C and stirred for 24 h under vacuum. After polymerization, the reaction solution was dissolved in excess chloroform and extracted against water (3 times) and brine, dried over $MgSO_4$ and filtrated. α-BzO-P($EG_{0.92}$-*co*-$GME_{0.08}$) was obtained in quantitative yield as a colorless solid after evaporation of the solvent and drying under high vacuo.

^{1}H NMR ($CDCl_3$) δ [ppm]: 7.35-7.27 (m, 5H, Ar-*H*), 4.56 (s, 2H, Ph-CH_2), 3.75-3.40 (m, polyether backbone), 3.31 (s, GME-OCH_3).

Synthesis of mPEG-*b*-PGME

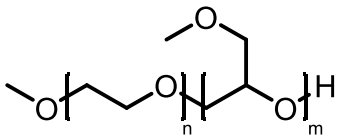

mPEG-*b*-PGME was synthesized in a similar procedure as the random copolymers. The initiator mPEG (M_n = 2 kg mol^{-1}; 250 mg, 125 μmol) was utilized for this purpose. mPEG-*b*-PGME 4k was obtained as a colorless solid after precipitation in ice-cold diethyl ether with quantitative yield.

^{1}H NMR ($CDCl_3$) δ [ppm]: 3.75-3.40 (m, polyether backbone), 3.31 (s, GME-OCH_3 + PEG-O-CH_3).

Synthesis of α-BzO-ω-*N*-succinimidyl carbonate-P(EG-*co*-GME)

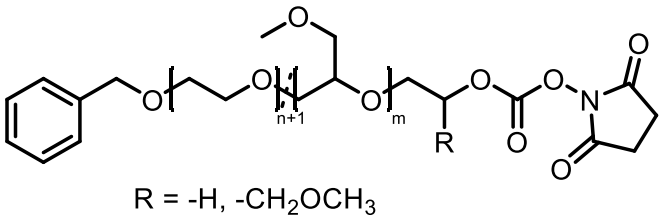

N,*N*'-disuccinimidyl carbonate (3.5 mg, 13.8 μmol) was added to a stirred solution of α-BzO-P(EG-*co*-GME) (50.0 mg, 4.6 μmol) in dry CH_3CN (1 mL) at room temperature for 18 h. The reaction mixture was dissolved in dichloromethane, extracted with a saturated $NaHCO_3$, water and brine, dried over $MgSO_4$ and filtered. The solvent was removed under reduced pressure and the polymer dried under vacuum. The product was obtained as a white solid in quantitative yield.

^{1}H NMR ($CDCl_3$) δ [ppm]: 7.35-7.27 (m, 5H, Ar-*H*), 4.56 (s, 2H, Ph-CH_2), 4.49-4.45 (t, 2H, CH_2-OCOO-succinimidyl), 3.86-3.27 (m, polyether backbone), 3.36 (s, GME-OCH_3), 2.86 (s, 4H, OCCH_2CH_2CO).

Conjugation of α-BzO-ω-*N*-succinimidyl carbonate-P(EG-*co*-GME) to bovine serum albumin (BSA)

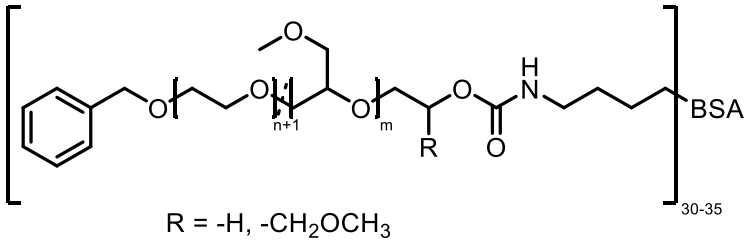

For conjugation of P(EG-*co*-GME) copolymers to BSA, the surface-accessible lysine groups (30-35) were targeted for conjugation. For this purpose, BSA (5.00 mg, 0.07 μmol) and α-BzO-ω-*N*-succinimidyl carbonate-P(EG-*co*-GME) (16.9 mg, 2.6 μmol) were stirred in PBS buffer for 1 h. The unreacted polymer was removed by dialysis in deionized water with a 25 kDa membrane filter. The conjugate was then dried by lyophilization and obtained in quantitative yield.

Additional Spectra of GME

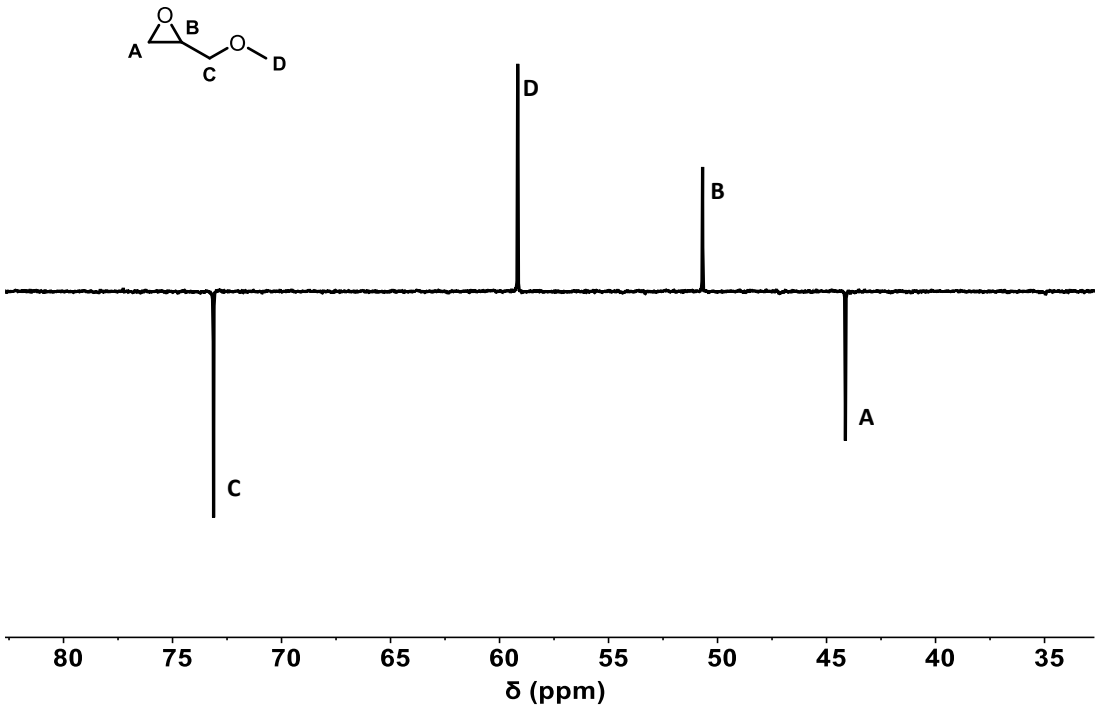

Figure S1. ^{13}C DEPT NMR spectrum ($CDCl_3$) of GME.

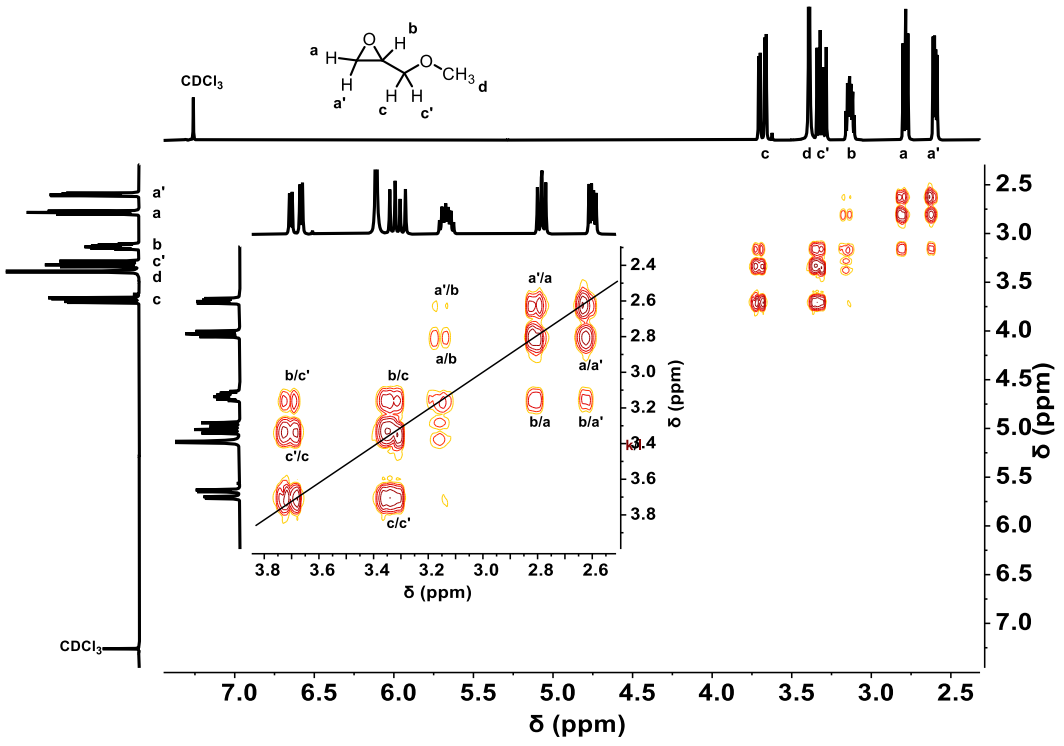

Figure S2. $^{1}H,^{1}H$ COSY NMR spectrum ($CDCl_3$) of GME.

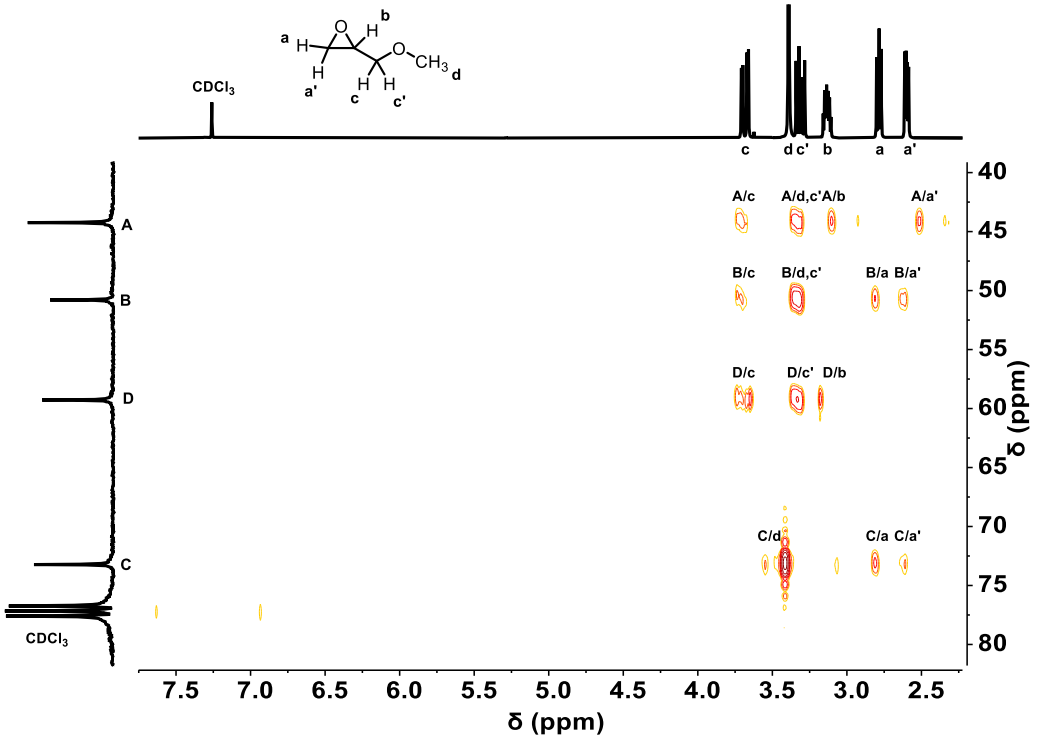

Figure S3. $^{1}H,^{13}C$ HMBC NMR spectrum ($CDCl_3$) of GME.

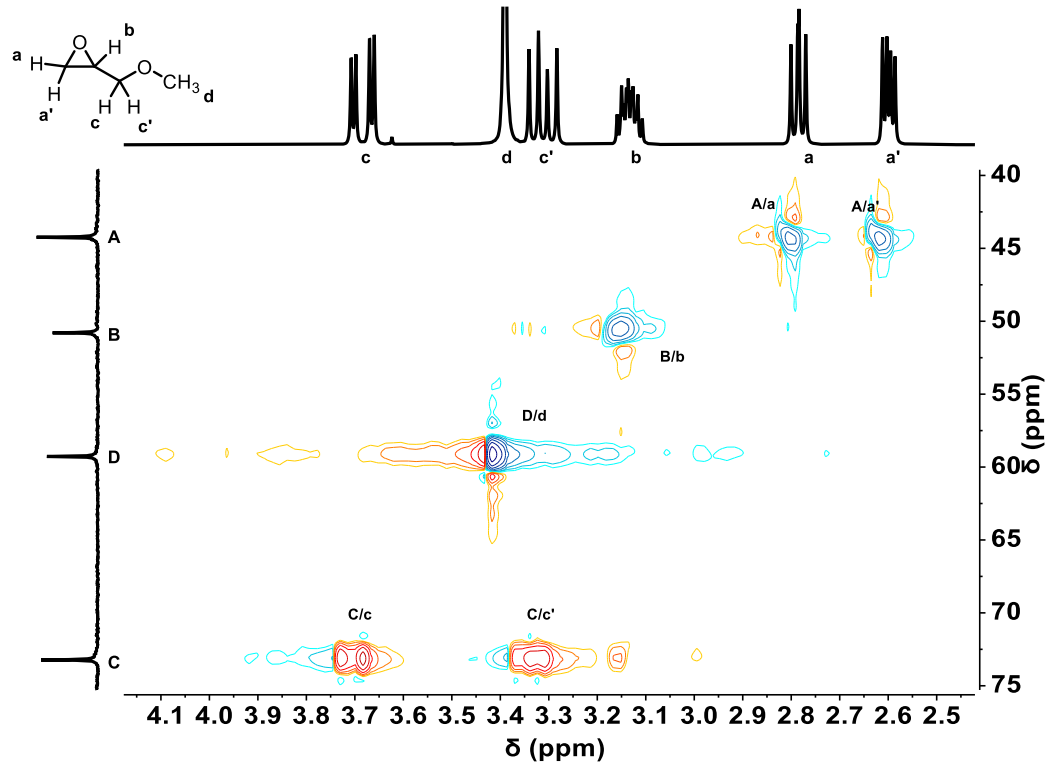

Figure S4. $^{1}H,^{13}C$ HSQC NMR spectrum ($CDCl_3$) of GME.

Additional Spectra and Plots of P(EG-*co*-GME) and PGME

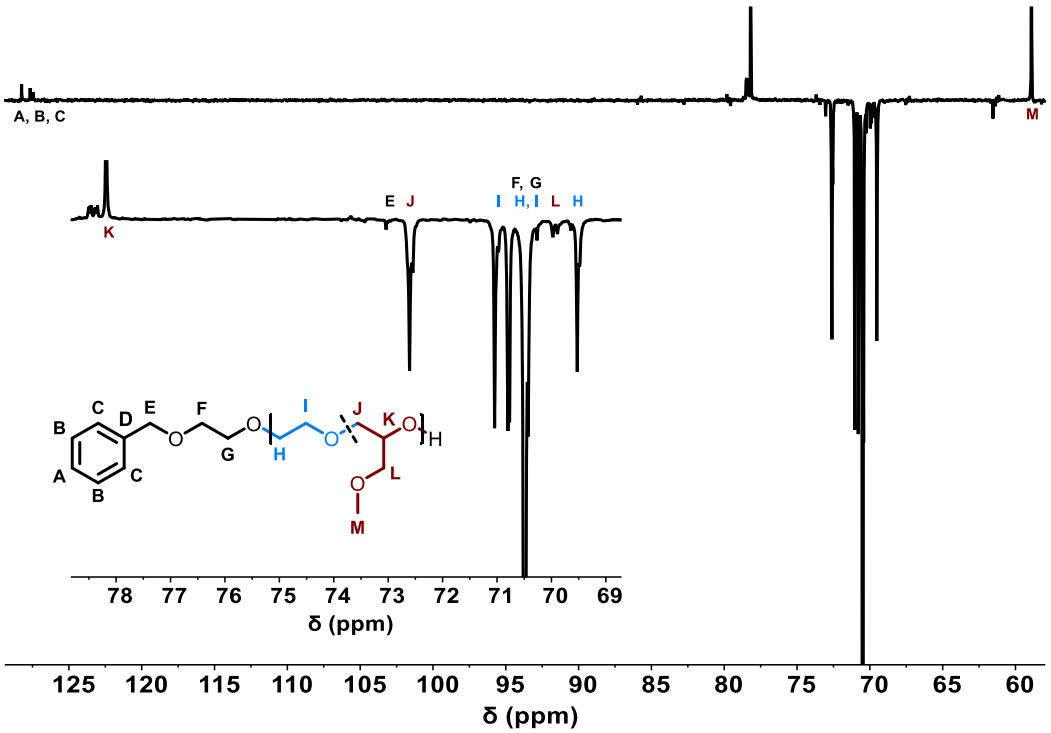

Figure S5. ^{13}C DEPT NMR spectrum (CD_2Cl_2) of P(EG-*co*-GME).

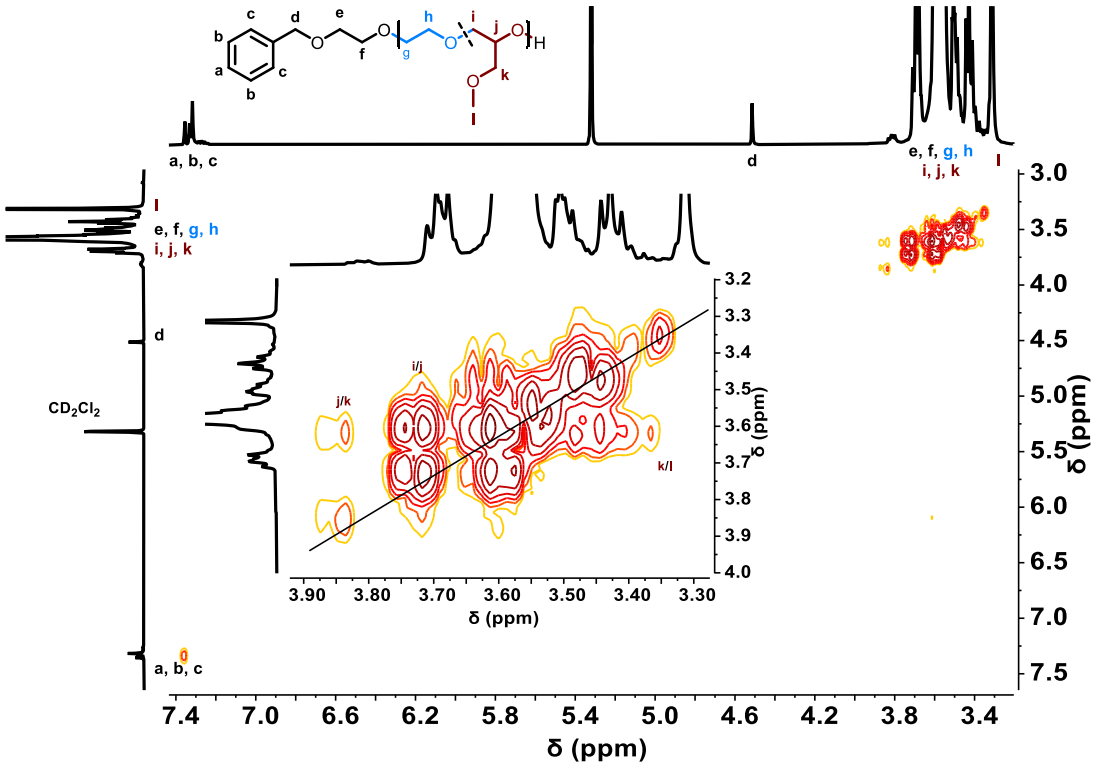

Figure S6. ^{1}H,^{1}H COSY NMR spectrum (CD_2Cl_2) of P(EG-*co*-GME).

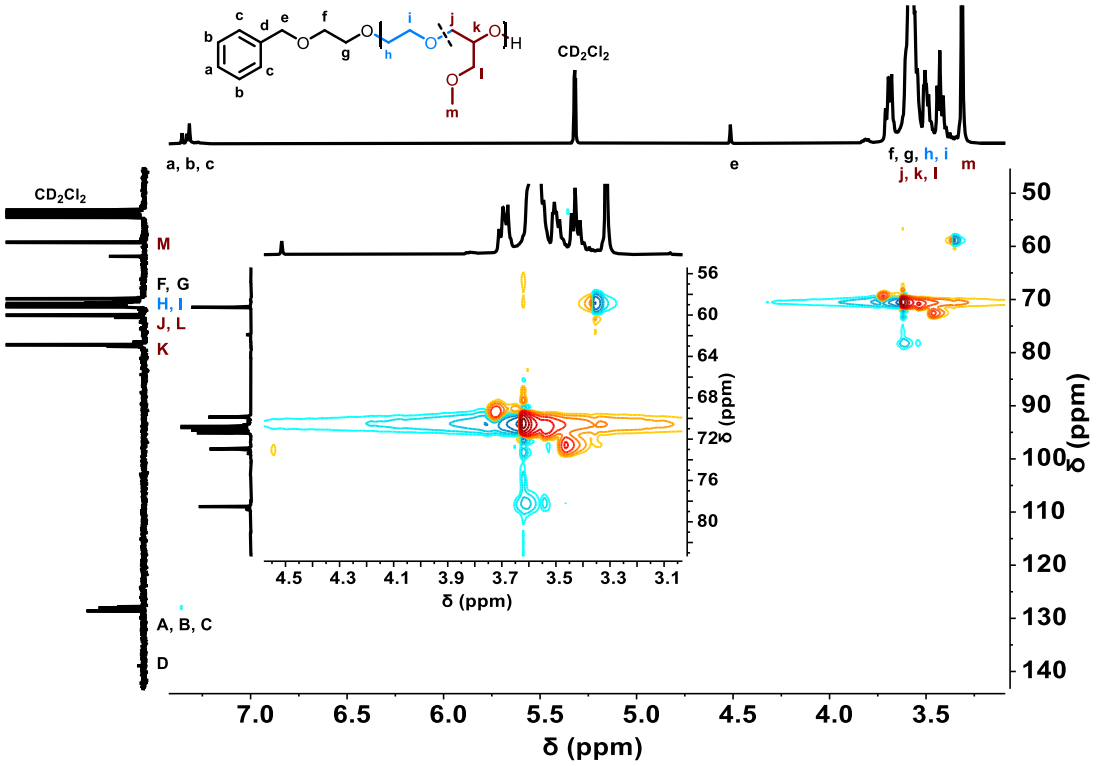

Figure S7. $^{1}H,^{13}C$ HSQC NMR spectrum CD_2Cl_2) of P(EG-*co*-GME).

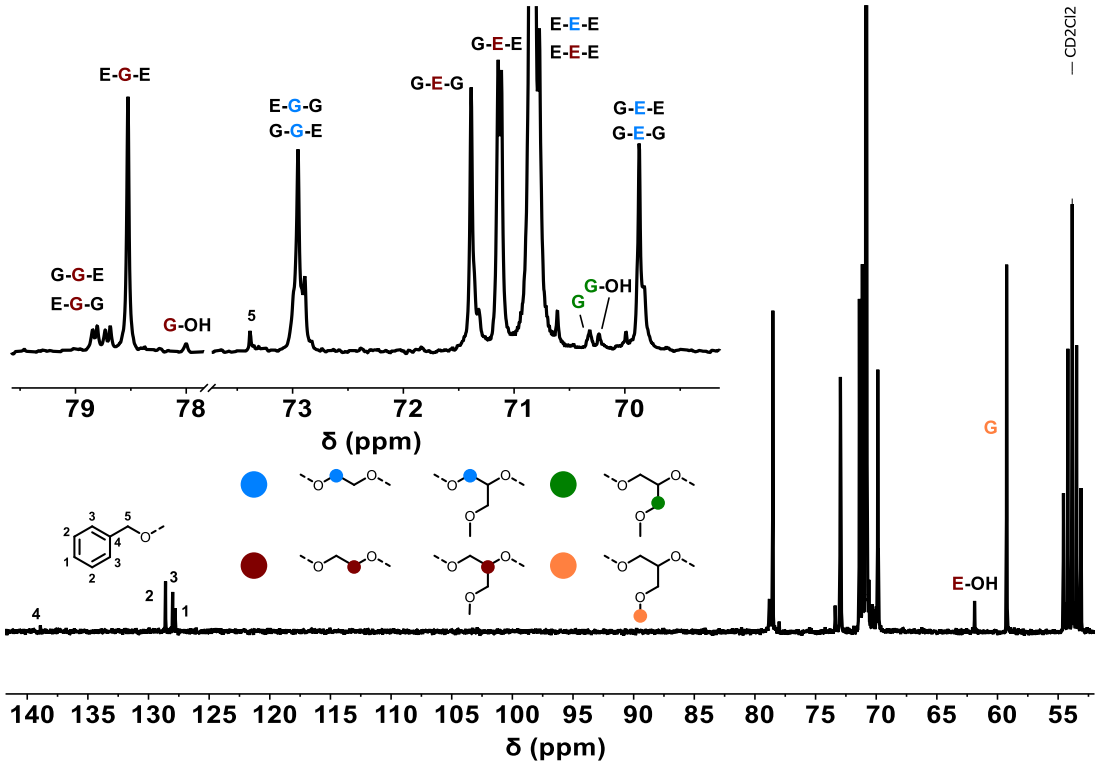

Figure S8. ^{13}C IG NMR spectrum (CD_2Cl_2, 75 MHz) of P(EG-*co*-GME).

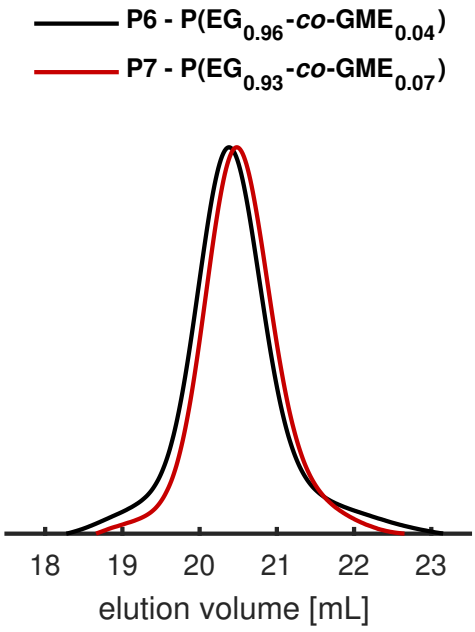

Figure S9. SEC (DMF, PEG calibration) of P6 and P7.

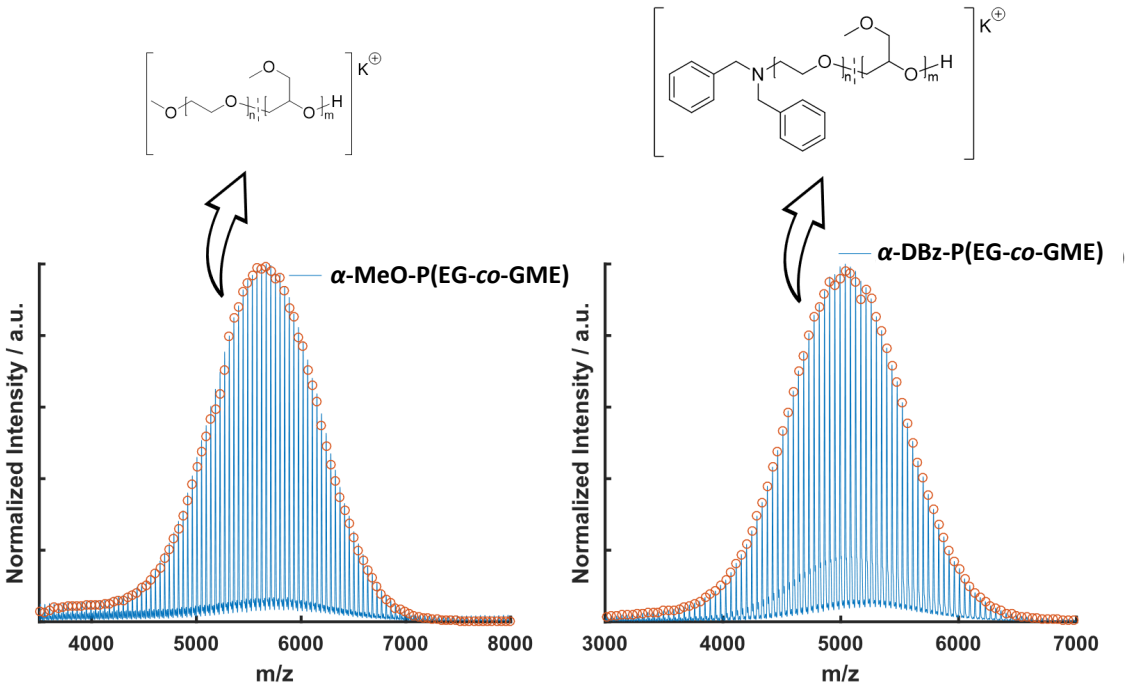

Figure S10. MALDI ToF mass spectra of α-methoxy (left) and α-*N*,*N*-dibenzylamino-P(EG-*co*-GME) (right).

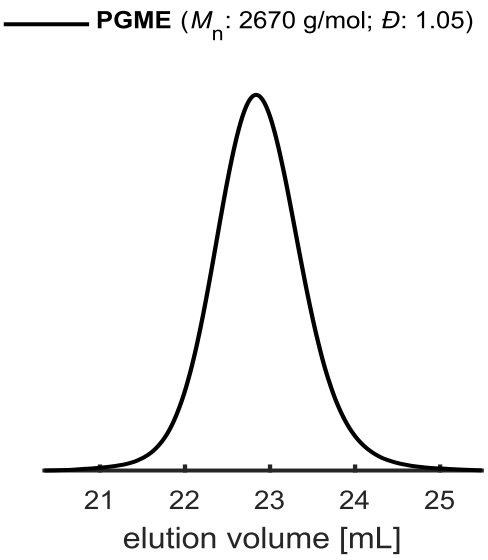

Figure S11. SEC (DMF, PEG calibration) of PGME (P8).

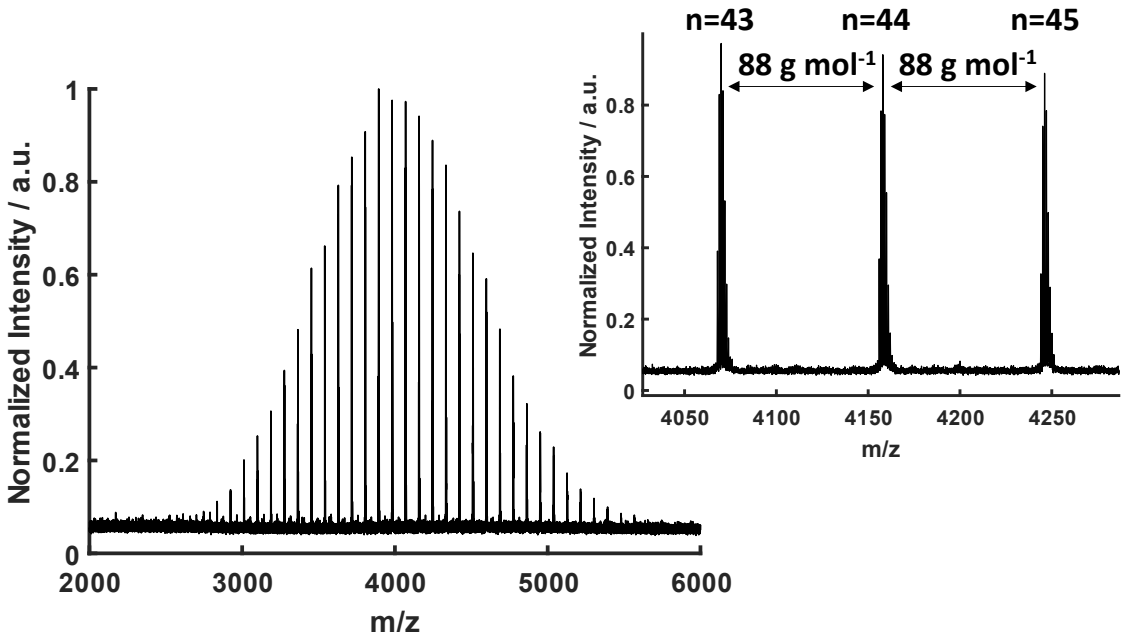

Figure S12. MALDI ToF MS of PGME (P8).

Investigation of Thermoresponsivity

Investigations concerning the LCST of P(EG-*co*-GME) copolymers was conducted by turbidimetric measurements for calculation of the cloud point T_{cp}. The highly hydrophilic PEG exhibits a LCST above 100 °C, underlining its excellent aqueous solubility.[9] The LCST of PGME was investigated in several papers, showing a T_{cp} between 45 to 64 °C depending on factors like M_n and concentration.[10-12] However, the herein investigated random P(EG-*co*-GME) copolymers with GME amounts < 49 mol% exhibited no thermoresponsive behavior, while a 49 mol% of GME incorporation lead to a T_{cp} of 94.5 °C. These results strongly support the high hydrophilicity of the random copolymers as well as their possible bioapplication at body temperature of 37 °C without formation of aggregates and subsequent precipitation.

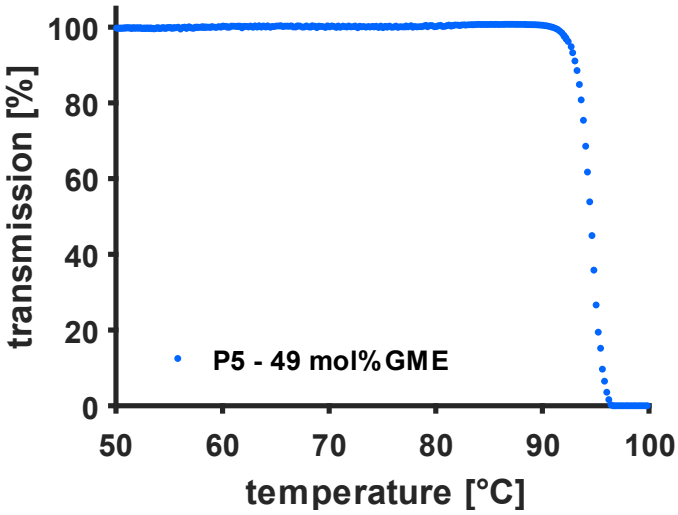

Figure S13. Determination of the cloud point T_{cp} by turbidimetry in 2.5 mg mL^{-1} for copolymer with 49% GME in aqueous solution. The heat rate was 1 °C min^{-1} while the T_{cp} was determined at 50% transmission.

Additional Plots *in situ* Kinetics

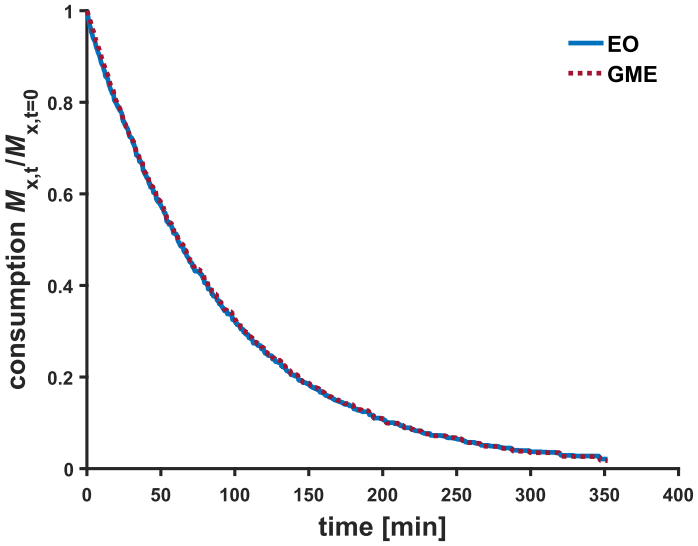

Figure S14. Consumption $M_{x,t}/M_{x,t=0}$ vs. time plot of the copolymerization of EO and GME determined by *in situ* ^{1}H NMR kinetics.

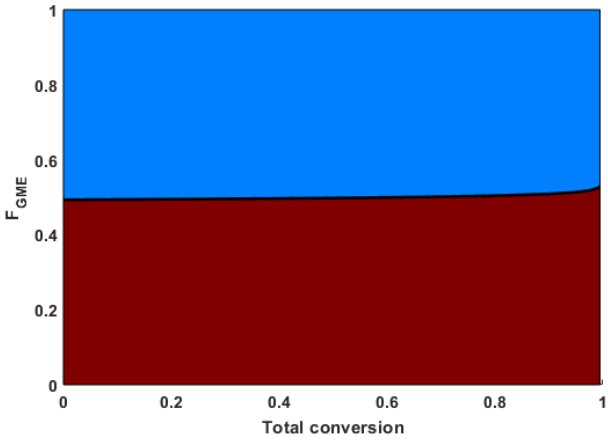

Figure S15. Visualization of the polymer microstructure of P(EG-*co*-GME) by plotting the molar mean incorporation of GME (F_{GME}) (red) as a function of total conversion.

Analysis of Microstructure Based on DFT Calculations

As recently shown by Lai and co-workers[9] the anti-PEG antibody (APA) captures around 16 ethylene glycol units within its paratope. Based on these findings, the P(EG-*co*-GME) copolymers are examined regarding the occurrence of 16 sequential EG units, so called hektakaidekads. In this manner, the interaction of the APA with the herein presented copolymers can be quantified on a theoretical level. To enable the analysis of the P(EG-*co*-GME) copolymers with respect to their microstructure, kinetic Monte-Carlo (kMC) simulations were conducted. The model of the kMC simulation originates in the stochastic simulation algorithm by Gillespie and relies on the conversion of the continuum-based reaction rates into number-based probabilities.[10-12] In order to provide an insight into chemical composition distribution, more precisely the distribution of consecutive EG repeating units in EO/GME copolymers, kMC simulations represent a versatile tool and hence eight polymerizations were performed *in silico*. For this purpose, the rationale of a living anionic polymerization was taken as a basis, what implies the absence of chain termination or chain transfer reactions. The copolymerization reaction can simply be described by the four rate constants: the homopropagation rate constants k_{11} and k_{22} aa well as the cross-propagation rate constants k_{12} and k_{21}. These rate constants are transformed into number-based probabilities, where A_i denotes the corresponding aggregation number of the chain ends ($A_\mathrm{i} = 2 \rightarrow$ dimers, $A_\mathrm{i} = 4 \rightarrow$ tetramers, etc.) and concentrations are converted by multiplying with the Avogadro's number N and the simulation volume V.

$$kMC_{11} = \frac{k_{11}}{(NV)^{1/A_1}}$$

$$kMC_{22} = \frac{k_{22}}{(NV)^{1/A_2}}$$

$$kMC_{12} = \frac{k_{12}}{(NV)^{1/A_1}}$$

$$kMC_{21} = \frac{k_{21}}{(NV)^{1/A_2}}$$

The copolymerization is then determined based on the cumulative probabilities P_v by a uniformly distributed random number $rn_1 = [0 \ldots 1]$.

$$P_v = \frac{R_v}{\sum_M^{v=1} R_v}$$

$$\sum_{v=1}^{\mu=1} P_v < rn_1 < \sum_v^{\mu} P_v$$

The copolymerization kinetics was assumed to be perfectly random, implying $k_{11} = k_{22} = k_{12} = k_{21} = 1$. Furthermore, no aggregated chain ends ($A_1 = A_2 = 1$) were supposed. For each polymerization, 1000 chains were simulated. The simulations were run with the listed degrees of polymerizations of the individual monomers, a targeted conversion of 99.9%, initiator concentrations of 1 mmol L^{-1} and polymerization volumes of 1.66 10^{-18} L. For every polymerization, an overall molecular weight of 5 kg mol^{-1} was targeted, leading to the listed degrees of polymerization with molar ratios of 20 up to 50% of GME with a stepwise increase by 5 mol%. In Table S1 the seven simulated polymerizations and the respective proportional occurrence of hektakaidekads are listed.

Table S1. Analysis concerning the occurrence of hektakaidekads (16 EG units) within the P(EG-*co*-GME) copolymers with varying GME ratios (20 to 50 $mol\%_{GME}$). Results were obtained by DFT calculations which were performed based on the estimated reactivity ratios of the copolymerization of EO and GME.

Polymer	$mol\%_{GME}$ [%]	hektakaidekad analysis (16 EG units) [%]	number of chains (16 EG units) [%]
P($EG_{0.80}$-*co*-$GME_{0.20}$)	20	44.4	38.5
P($EG_{0.75}$-*co*-$GME_{0.25}$)	25	19.6	17.7
P($EG_{0.70}$-*co*-$GME_{0.30}$)	30	7.2	6.9
P($EG_{0.65}$-*co*-$GME_{0.35}$)	35	2.9	2.9
P($EG_{0.60}$-*co*-$GME_{0.40}$)	40	0.5	0.5
P($EG_{0.55}$-*co*-$GME_{0.45}$)	45	0.4	0.4
P($EG_{0.50}$-*co*-$GME_{0.50}$)	50	0	0

The investigations regarding the recognition of P(EG-*co*-GME) by APAs revealed a decrease (< 24 mol% GME) up to the full prevention (49 mol% GME) of recognition with increasing GME content. This observation is supported by the theoretical consideration revealing the full exclusion of 16 sequential EG units if 50 mol% of GME are incorporated to the polyether. On the contrary, polymers containing 25 mol% of GME still 17.7% of 1000 simulated chains possess at least one EG-hektakaidekad. To graphically transfer the results of kMC simulations, ten exemplary chains for each respective GME ratio are shown in Figure S16. As the GME units are statistically distributed throughout the polyether, the occurrence of EG-rich regions consequently decreases with increasing GME ratio.

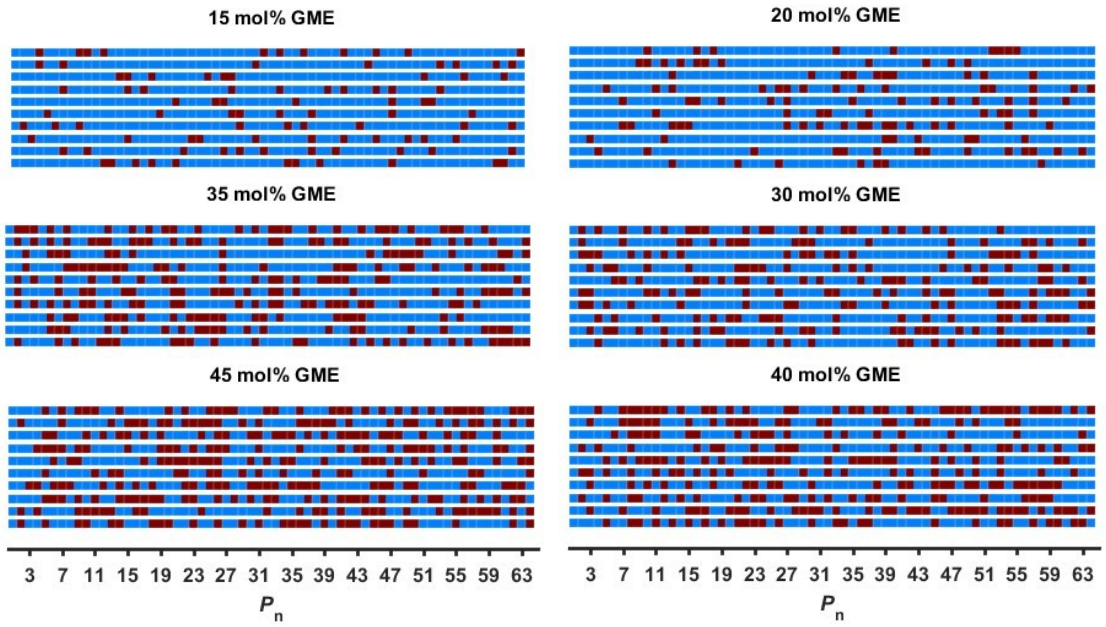

Figure S16. Graphical illustration of individual chains of P(EG-*co*-GME) copolymers with varying GME ratio calculated by DFT calculations (EG = blue, GME = red).

Conjugation of BSA with P(EG-co-GME)

Figure S17 shows the ^{1}H NMR spectrum of α-BzO-ω-*N*-succinimidyl carbonate-P(EG-*co*-GME). The copolymer was synthesized with a GME content of 16 mol%. Considering the random copolymerization demonstrated by the described *in situ* ^{1}H NMR kinetics, statistically 84% of *N*,*N*'-disuccinimidyl carbonate is attached to an EO chain end. The overall degree of functionalization for terminal EG as well as GME units is calculated by the integral of the methylene protons m and n at 2.86 ppm of the succinimidyl-substituent in comparison to the benzylic initiator protons at 4.58 ppm. The calculation reveals a successful functionalization of 68%. Integration of the corresponding methylene protons l at 4.45 to 4.49 ppm shows 88% of functionalized EG units which consequently results in 12% terminal GME units, which is a similar value compared to the determined 16 mol% of the precursor.

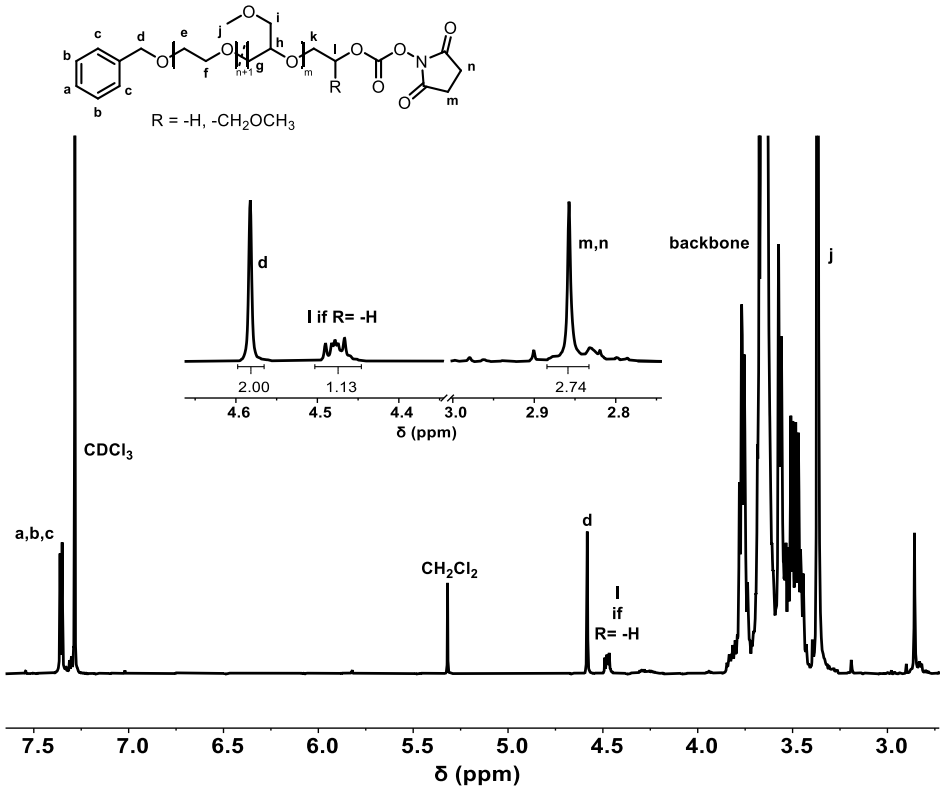

Figure S17. ^{1}H NMR spectrum of α-BzO-ω-*N*-succinimidyl carbonate-P(EG-*co*-GME).

Block Copolymer Synthesis

Besides random copolymers, the synthesis of mPEG-*b*-PGME is achieved by the utilization of mPEG as macroinitiator.

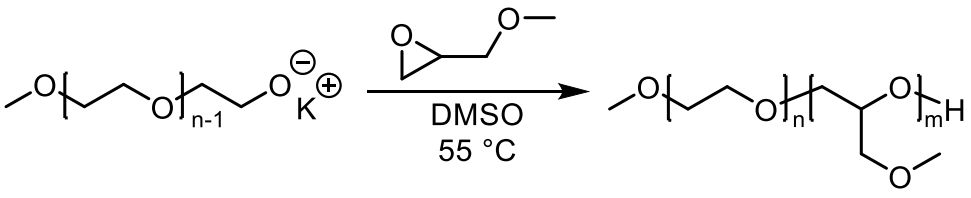

Scheme S2. Synthesis of mPEG-*b*-PGME.

The corresponding SEC (Figure S18) and MALDI-ToF mass spectra (Figure S19) show a clear shift to lower elution volume and higher molecular weights, respectively, of the block copolymer relative to the precursor mPEG and the absence of homopolymer traces. Additionally, the molecular weight distribution of mPEG-*b*-PGME exhibits a 44 g mol^{-1} difference between the signals in the MALDI-ToF MS, showing successful block copolymer formation.

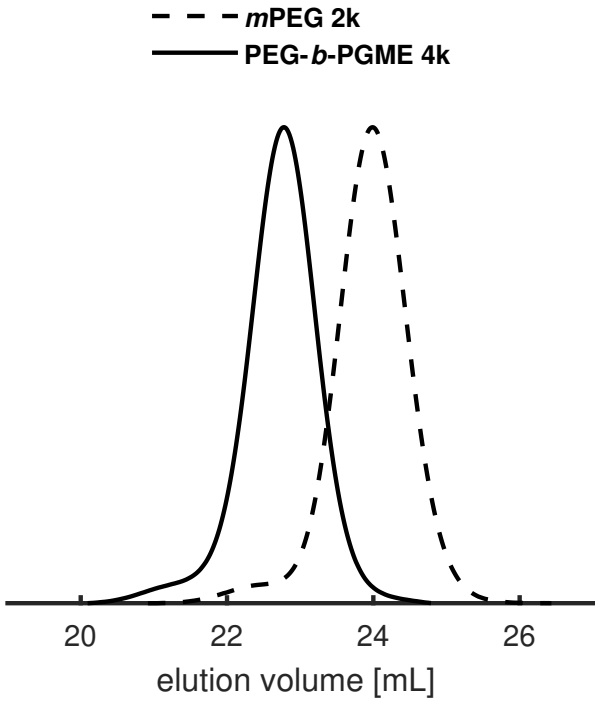

Figure S18. SEC (DMF, PEG calibration) of mPEG and mPEG-*b*-PGME.

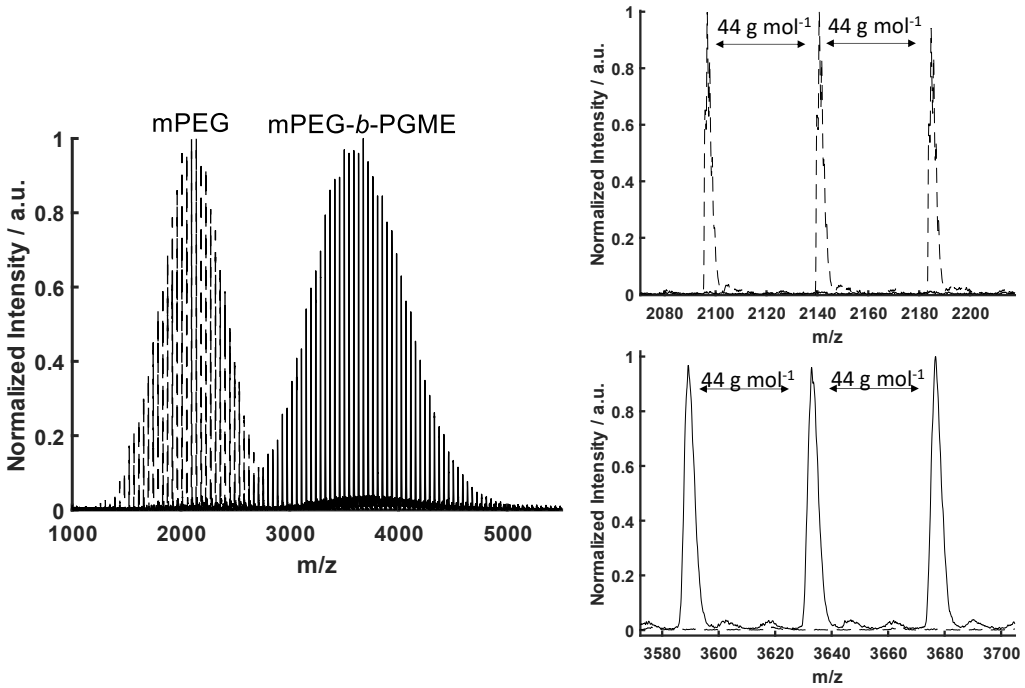

Figure S19. Overlay MALDI ToF mass spectra of mPEG and mPEG-*b*-PGME (Matrix: DCTB, KTFA).

Thermal Properties of Random and Block Copolymers

The melting temperature and degree of crystallinity of the random copolymers strongly depends on the molar amount of incorporated GME. With increasing GME content, the melting temperature and melting enthalpy of the copolymers decreases, independent of molecular weight (Table S2). In the case of mPEG-*b*-PGME only a minor influence of the PGME block on crystallinity of PEG is observed compared to random copolymers with similar molar amounts of GME. These results are in accordance with the literature[13] and support the ideal random incorporation of GME in the polyether during the copolymerization.

Table S2. Thermal Properties of Random and Block Copolymers; Determined via DSC (10 K min^{-1}) (xk = x kg mol^{-1}).

Sample	mol%$_{GME}$ [%]	T_g [°C]	T_m [°C]	ΔH_{PEG} [J g^{-1}]	$X_{c,PEG}$
P(EG$_{0.96}$-*co*-GME$_{0.04}$) 5k	4	-56	46	88.63	0.45
P(EG$_{0.92}$-*co*-GME$_{0.08}$) 5k	8	-59	35	58.22	0.30
P(EG$_{0.85}$-*co*-GME$_{0.15}$) 6k	15	-61	7	32.62	0.16
P(EG$_{0.96}$-*co*-GME$_{0.04}$) 10k	4	-56	45	76.79	0.39
P(EG$_{0.93}$-*co*-GME$_{0.07}$) 10k	7	-59	37	56.26	0.28
PEG-*b*-PGME 4k	22	-59	45	80.16	0.41

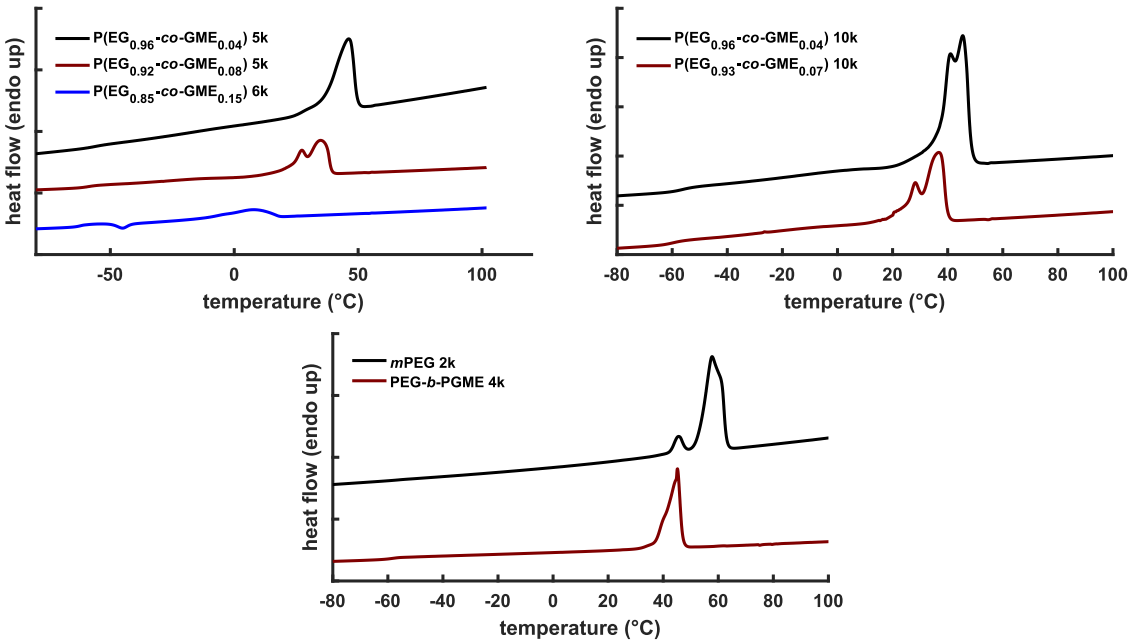

Figure S20. 2nd DSC heating curves (10 K min^{-1}) of random and block copolymers.

Cell Viability Tests

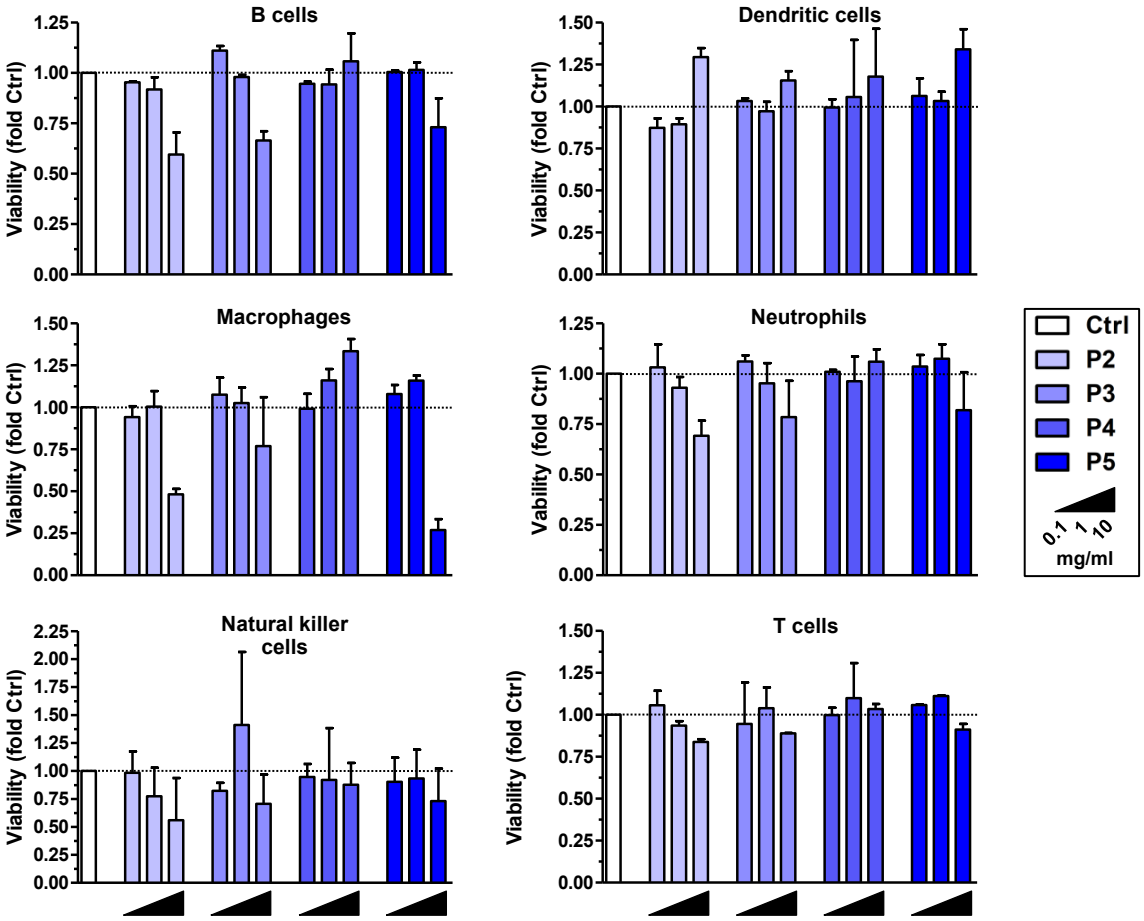

Figure S21. PEG derivatives influence the viability of immune cells in a formulation- and cell type-specific manner at high concentrations. Murine spleen cells were incubated over-night with different PEG derivatives at various concentrations as indicated (0.1-10 mg mL^{-1}). Graphs show the viability of the various leukocyte populations in response to treatment given relative to the viability of untreated cells (Ctrl). Data denote the mean ± SD of two independent experiments.

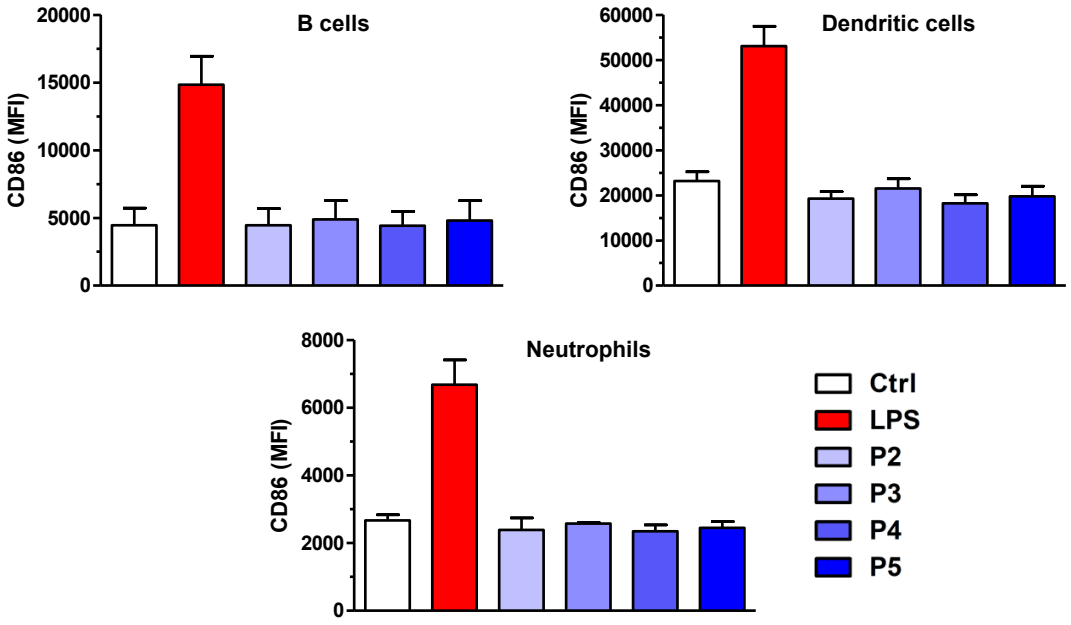

Figure S22. PEG derivatives exert no stimulatory effects on immune cells. Murine spleen cells were incubated over-night with different PEG derivatives at subtoxic concentration (1 mg mL^{-1}) and LPS (1 μg mL^{-1}) as a positive control. On the next day, expression of the costimulatory receptor CD86 was assessed for the different leukocyte populations. Data denote the mean fluorescence intensity (MFI) ± SEM of three independent experiments.

REFERENCES

(1) Herzberger, J.; Leibig, D.; Liermann, J. C.; Frey, H. Conventional Oxyanionic versus Monomer-Activated Anionic Copolymerization of Ethylene Oxide with Glycidyl Ethers: Striking Differences in Reactivity Ratios. *ACS Macro Lett.* **2016**, *5*, 1206–1211.

(2) Steube, M.; Johann, T.; Plank, M.; Tjaberings, S.; Gröschel, A. H.; Gallei, M.; Frey, H.; Müller, A. H. E. Kinetics of Anionic Living Copolymerization of Isoprene and Styrene Using in Situ NIR Spectroscopy: Temperature Effects on Monomer Sequence and Morphology. *Macromolecules* **2019**, *52*, 9299–9310.

(3) Wagener, K.; Bros, M.; Krumb, M.; Langhanki, J.; Pektor, S.; Worm, M.; Schinnerer, M.; Montermann, E.; Miederer, M.; Frey, H.; et al. Targeting of Immune Cells with Trimannosylated Liposomes. *Adv. Therap.* **2020**, *3*, 1900185.

(4) Prileschajew, N. Oxydation ungesättigter Verbindungen mittels organischer Superoxyde. *Ber. Dtsch. Chem. Ges.* **1909**, *42*, 4811–4815.

(5) Saeki, S.; Kuwahara, N.; Nakata, M.; Kaneko, M. Upper and lower critical solution temperatures in poly (ethylene glycol) solutions. *Polymer* **1976**, *17*, 685–689.

(6) Fellin, C. R.; Adelmund, S. M.; Karis, D. G.; Shafranek, R. T.; Ono, R. J.; Martin, C. G.; Johnston, T. G.; DeForest, C. A.; Nelson, A. Tunable temperature- and shear-responsive hydrogels based on poly(alkyl glycidyl ether)s. *Polym. Int.* **2019**, *68*, 1238–1246.

(7) Müller, S. S.; Moers, C.; Frey, H. A Challenging Comonomer Pair: Copolymerization of Ethylene Oxide and Glycidyl Methyl Ether to Thermoresponsive Polyethers. *Macromolecules* **2014**, *47*, 5492–5500.

(8) Isono, T.; Miyachi, K.; Satoh, Y.; Sato, S.-i.; Kakuchi, T.; Satoh, T. Design and synthesis of thermoresponsive aliphatic polyethers with a tunable phase transition temperature. *Polym. Chem.* **2017**, *8*, 5698–5707.

(9) Huckaby, J. T.; Jacobs, T. M.; Li, Z.; Perna, R. J.; Wang, A.; Nicely, N. I.; Lai, S. K. Structure of an anti-PEG antibody reveals an open ring that captures highly flexible PEG polymers. *Commun Chem* **2020**, 3.

(10) Gillespie, D. T. Exact stochastic simulation of coupled chemical reactions. *J. Phys. Chem.* **1977**, *81*, 2340–2361.

(11) Gillespie, D. T. A general method for numerically simulating the stochastic time evolution of coupled chemical reactions. *Journal of Computational Physics* **1976**, *22*, 403–434.

(12) Steube, M.; Johann, T.; Galanos, E.; Appold, M.; Rüttiger, C.; Mezger, M.; Gallei, M.; Müller, A. H. E.; Floudas, G.; Frey, H. Isoprene/Styrene Tapered Multiblock Copolymers with up to Ten Blocks: Synthesis, Phase Behavior, Order, and Mechanical Properties. *Macromolecules* **2018**, *51*, 10246–10258.

(13) Mangold, C.; Wurm, F.; Obermeier, B.; Frey, H. Hetero-Multifunctional Poly(ethylene glycol) Copolymers with Multiple Hydroxyl Groups and a Single Terminal Functionality. *Macromolecular rapid communications* **2010**, *31*, 258–264.

Chapter 2.2

In situ Kinetics is Indispensable: Influence of Solvents and Monomers on Anionic Ring-Opening Copolymerization of Epoxides

Philip Dreier[†], Rebecca Matthes[†], Ramona D. Barent[†], Sandra Schüttner[†], Axel H. E. Müller[†] and Holger Frey[†,*]

[†]Department of Chemistry, Johannes Gutenberg University Mainz, Germany

---

ABSTRACT: In-depth understanding of copolymerization kinetics and the resulting polymer microstructure is crucial for the design of materials with well-defined properties. *In situ* ^{1}H NMR spectroscopy enables precise monitoring of the living anionic ring-opening copolymerization (AROP) of ethylene oxide (EO) with the glycidyl ethers allyl glycidyl ether (AGE) and ethoxy vinyl glycidyl ether (EVGE), respectively. Determination of reactivity ratios revealed slightly higher reactivity of both glycidyl ethers compared to EO, emphasizing a pronounced counterion chelation effect by glycidyl ethers in AROP. Implementation of density functional theory (DFT) calculations further illustrated the complexation capability of ether-containing side groups in glycidyl ethers, in analogy to crown ethers ("crown ether effect"). Investigation of the copolymerization both in THF-d_8 and DMSO-d_6 showed the increasing reactivity disparity of both glycidyl ethers compared to EO with decreasing solvent polarity. Furthermore, a comparison of the determined reactivity ratios via the herein utilized *in situ* ^{1}H NMR spectroscopy and the end-group-dyad (EGD) analysis introduced by Lynd, Hawker et al. was conducted, showing significant differences with respect to the reactivity ratios. Hence, supporting DFT calculations were implemented, illustrating the different preferential incorporation at the initiator and in the course of the further growth of the polymer chains. The results evidence the crucial importance of detailed *in situ* studies by initiator-independent methods in the living copolymerization, encompassing the entire monomer consumption range for the evaluation of copolymerization kinetics. Information derived merely from the initiating dyad provides only insufficient tendencies rather than accurate reactivity ratios.

INTRODUCTION

In depth kinetic studies of the statistical copolymerization of different monomers, have received renewed interest in recent years, particularly for living polymerization (LP) techniques. Besides the controlled radical polymerization, the anionic LP remains the most efficient method for the synthesis of well-defined copolymers with narrow molecular weight distribution and controlled monomer gradients. Detailed knowledge regarding the compositional profile of the comonomers along the polymer chains is of key importance in gradient or tapered copolymers to adjust the thermal properties in bulk[1–6] and solution and consequently to control the morphology[1,4,7] of the resulting materials.

In the past, common methods for the evaluation of the reactivity ratios and the corresponding comonomer gradient in the copolymer chains formed were determination of the comonomer content at different stages of the copolymerization after precise termination[8,9] and subsequent gas chromatographic analysis of the residual monomers.[10] These monitoring techniques are time-consuming, often rather difficult to implement and may hold uncertainties due to missing reproducibility, since the data have to be obtained from different polymerization experiments. In comparison, triad analysis via ^{13}C inverse gated (IG) spectroscopy[11–13] is a more reliable method for determination of the microstructure, but a large variety of samples must be synthesized for correct assignment and evaluation of the corresponding triads. More recently, *in situ* monitoring via near infrared (NIR) spectroscopy[7,14,15] was established as a feasible analytical set-up to directly correlate the polymerization kinetics with the copolymer microstructure for carbanionic copolymerization. The *in situ* methods advantageously permit to follow the mean composition over the whole conversion range, i.e. at all given chain positions, resulting in a complete compositional profile of the copolymers.[7,16] For instance, the influence of temperature[7] and polar additives[14,15] on the compositional drift and steepness of the gradient in isoprene/styrene-based tapered block copolymers, synthesized via carbanionic copolymerization, was recently investigated in great detail via NIR spectroscopy.

In comparison to the living carbanionic polymerization, the relatively slow polymerization kinetics of the anionic ring-opening polymerization (AROP) in polar aprotic solvents facilitates monitoring. This has been exploited to follow the monomer consumption of epoxides[13,17–24] as well as activated aziridines[25–28] via *in situ* ^{1}H NMR spectroscopy. Depending on the comonomer employed, the copolymerization of EO with monosubstituted epoxides may result in rather different polymer microstructures. For example, preferred addition of EO over alkylene oxides[20] and glycidyl amines[17,19] to the active chain end has been observed. In contrast, the copolymerization of EO with various glycidyl ethers (GE) generally revealed an almost ideally random distribution of the comonomer units along the polyether backbone.[18,21,22,29] Considering the underlying reactivity ratios, r, and rate constants, k ($r_{EO} = k_{EO,EO}/k_{EO,GE}$, $r_{EO} = k_{GE,GE}/k_{GE,EO}$), this copolymerization behavior necessitates $k_{EO,EO} = k_{GE,EO}$ as well as $k_{GE,GE} = k_{EO,GE}$ and thus

strictly results in the product $r_{EO} \cdot r_{GE}$ being unity. Consequently , non-terminal models, e.g., the Jaacks method[30] can be employed to investigate the underlying copolymerization kinetics in AROP.[18,24,29]

In 2012, Lynd, Hawker and coworkers reported a novel initiator-based method for the calculation of the reactivity ratios in the AROP copolymerization of EO and monosubstituted epoxides based on ^{1}H NMR spectroscopy. This method relies solely on evaluating the dyad containing the benzylic alkoxide initiator and the following two monomer units (end-group-dyad (EGD) analysis). Surprisingly, a dramatically preferred incorporation of ethoxy vinyl glycidyl ether (EVGE) relative to EO and consequently a gradient microstructure was observed by the authors in THF, relying on the EGD method.[31,32] These findings contradict the current knowledge regarding EO/glycidyl ether copolymerizations under AROP conditions in THF and are inconsistent with the results obtained in our group via ^{13}C inverse gated spectroscopy in a preceding publication. For the statistical copolymerization of ethoxy vinyl glycidyl ether (EVGE) and EO a random distribution of the EVGE units along the polymer backbone was obtained by comparison of the triad distribution.[12] In addition to the chemical nature of the monomers, the polarity of the solvent and its potential interaction with the counterion affect the kinetics of AROP copolymerization. EO or substituted epoxides have been investigated with regard to polymerization kinetics in different aprotic polar solvents ranging from linear and cyclic ethers[33–36] to polar solvents like dimethyl sulfoxide (DMSO)[37–41] and hexamethylphosphoramide (HMPA).[39,42] Depending on the polarity of the solvents, ion pairs were observed as reactive species in ethers,[34,36] whereas free ions were found to be present in the case of the more polar DMSO[43] and HMPA.[42] Nevertheless, although the homopolymerization kinetics in these solvents is well understood, the influence of the solvent on the copolymerization kinetics of EO with monosubstituted epoxides remains largely unexplored. To the best of our knowledge, only the variation of the reactivity ratios in the presence of electron donors has been investigated in detail for the copolymerization of epoxides to date.[10]

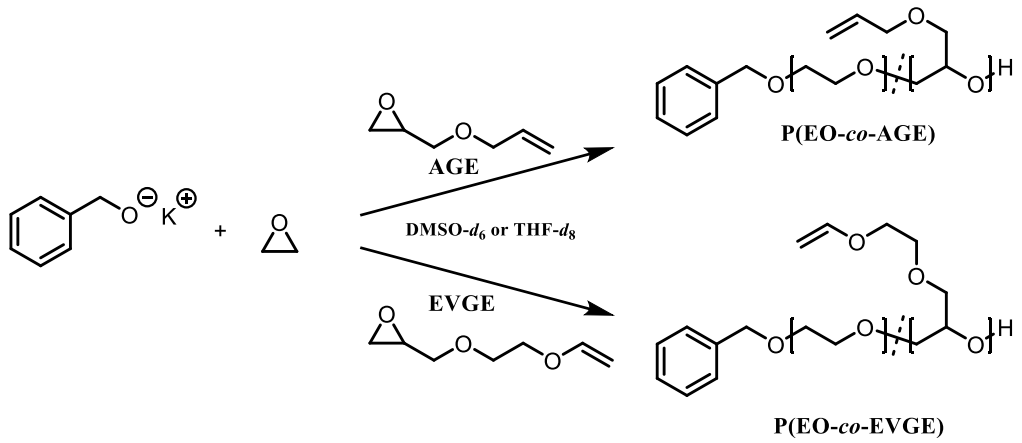

Scheme 1. Synthesis route of P(EO-*co*-AGE) and P(EO-*co*-EVGE) initiated by potassium phenylmethanolate in DMSO-d_6 and THF-d_8.

In the current work we utilize *in situ* ^{1}H NMR kinetics monitoring to evaluate and compare the reactivity ratios of the copolymerization of EO with EVGE and AGE, respectively, both in the presence of tetrahydrofuran-d_8 (THF-d_8) and DMSO-d_6 (Scheme 1). DFT calculations were employed, leading to an in-depth understanding of the copolymerization kinetics. Additionally, the values obtained from *in situ* monitoring are directly compared to the reactivity ratios reported by Lynd, Hawker et al. via ^{1}H NMR end group dyad (EGD) analysis, where only the first two chain units are considered.

RESULTS AND DISCUSSION

Impact of Solvents on AROP Copolymerization Kinetics of EO and Glycidyl Ethers

The anionic ring-opening polymerization (AROP) of epoxides is commonly performed in polar solvents to sufficiently dissolve the involved ionic species. DMSO with a dipole moment of 3.96 D is the solvent with the highest polarity that can be utilized in AROP apart from HMPA, which was not used in this study for safety reasons. Thus, DMSO can be considered as the ideal polar system with a high extent of ion dissociation and free ions as the active species.[43] On the contrary, THF exhibits a lower dipole moment of 1.63 D and accordingly is a less polar solvent implemented in AROP, permitting only partial dissociation of alkali metal alkoxides.[44] The reactive species of the alkoxide chain ends in THF can be characterized as ion pairs, which are in equilibrium with unreactive aggregates,[34] and most likely mimics the behavior in bulk polymerizations of epoxides. Therefore, the outlined solvents represent the upper and lower limit of polarity for AROP. Although several studies targeted at the copolymerization of EO with substituted epoxides have been conducted in either THF, DMSO or mixtures of both, their influence on the copolymerization kinetics has not been compared in a detailed manner to date. Based on this lack of data, we elucidated the impact of solvent polarity on the incorporation of different epoxides in the polyether during the copolymerization of EO with monosubstituted epoxides via *in situ* ^{1}H NMR kinetics. To this end, model copolymerizations of EO with the two glycidyl ethers AGE and EVGE were performed, initiated by potassium phenylmethanolate at 45 °C in DMSO-d_6 and THF-d_8, respectively.

As shown in Figure 1, in DMSO, the copolymerization of EO with AGE and EVGE exhibits high propagation rates, with a half-life (50 % conversion) of the respective glycidyl ether of 13 (AGE) and 20 min (EVGE), respectively. By recording one spectrum every 30 s, the monomer consumption was monitored over time (Figure S1), enabling the determination of the comonomer consumption versus total conversion, as shown in Figure 1 (bottom). The data show that in both cases the glycidyl ether is incorporated slightly faster than EO. Implementation of the Jaacks equation[30] enabled the calculation of reactivity ratios for both copolymerizations with a coefficient of determination (R^2) of 0.9995 (AGE) and 0.998 (EVGE), respectively (Figure S2). The Jaacks model is a non-terminal, integrated model for ideal copolymerizations that originates in the simplification $r_1 = r_2^{-1}$ and relies on the linearization of the Meyer-Lowry equation.

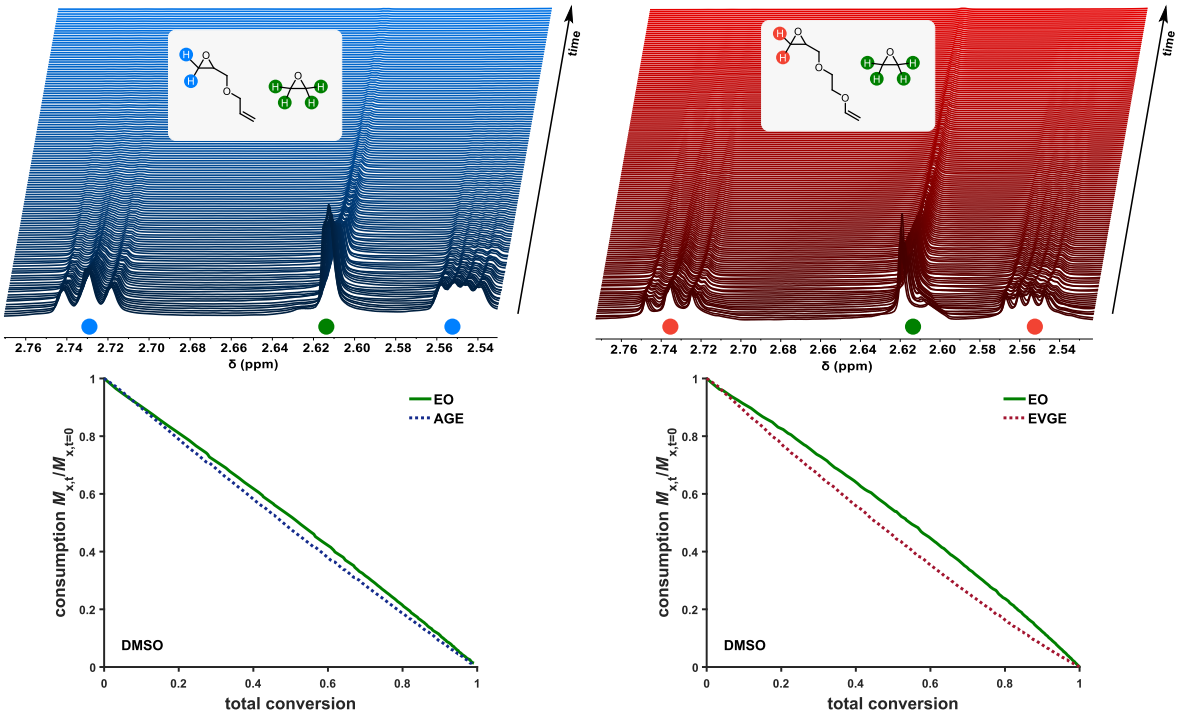

Figure 1. top: *in situ* ^{1}H NMR kinetics of the anionic copolymerization of EO with AGE in DMSO-d_6 (left) and with EVGE (right), initiated by potassium phenylmethanolate at 45 °C; bottom: conversion of both comonomers vs. total conversion.

The latter is applicable, if the rate of monomer incorporation does not show a strong dependence on the identity of the terminal unit, but on the nature of the reacting monomers. Its strength lies in the reduction of potential errors caused by overfitting. The implementation of the non-terminal model is further justified by DFT calculations, as discussed in a later section. Note that reactivity ratios are defined as $r_1 = k_{1,1}/k_{1,2}$ and $r_2 = k_{2,2}/k_{2,1}$ with index 1 representing EO and 2 the respective glycidyl ether. Both glycidyl ethers demonstrate rate constants of $k_{\mathrm{AGE,AGE}} > k_{\mathrm{AGE,EO}}$ and $k_{\mathrm{EVGE,EVGE}} > k_{\mathrm{EVGE,EO}}$, resulting in the preferential incorporation of AGE and EVGE in the early stages of the copolymerization compared to EO. The herein performed *in situ* kinetic experiments in DMSO consequently revealed reactivity ratios of $r_{\mathrm{EO}}^{\mathrm{DMSO}} = 0.92 \pm 0.002$ and $r_{\mathrm{AGE}}^{\mathrm{DMSO}} = 1.08 \pm 0.002$ as well as $r_{\mathrm{EO}}^{\mathrm{DMSO}} = 0.81 \pm 0.001$ and $r_{\mathrm{EVGE}}^{\mathrm{DMSO}} = 1.23 \pm 0.002$. Collectively, the copolymerization of EO and AGE in DMSO shows a nearly ideally random character, whereas the copolymerization with EVGE results in a very slight gradient microstructure. Based on the obtained reactivity ratios, the molar composition diagrams FGE versus total conversion illustrate the close to random (AGE) and slight gradient (EVGE) structure (Figure S3).

Subsequently, similar *in situ* ^{1}H NMR kinetic experiments were performed in THF to determine the polymerization kinetics of ion pairs in equilibrium with unreactive aggregates. As expected, both copolymerizations revealed significantly decreased propagation rates compared to DMSO, leading to a half-life of 17.3 h (AGE) and 7.6 h (EVGE), respectively (Figure S4). The experiment was not carried out to full conversion due to limited measurement time. Nevertheless, the amount

of data points reaching > 70 % conversion ensures a reliable evaluation of reactivity ratios by the Jaacks equation (R^2 of 0.997 (AGE) and 0.992 (EVGE)) (Figure S5). The differences in reactivity between EO and both glycidyl ethers are notably increased in THF in comparison to the polar DMSO system, albeit without affecting the overall trend.

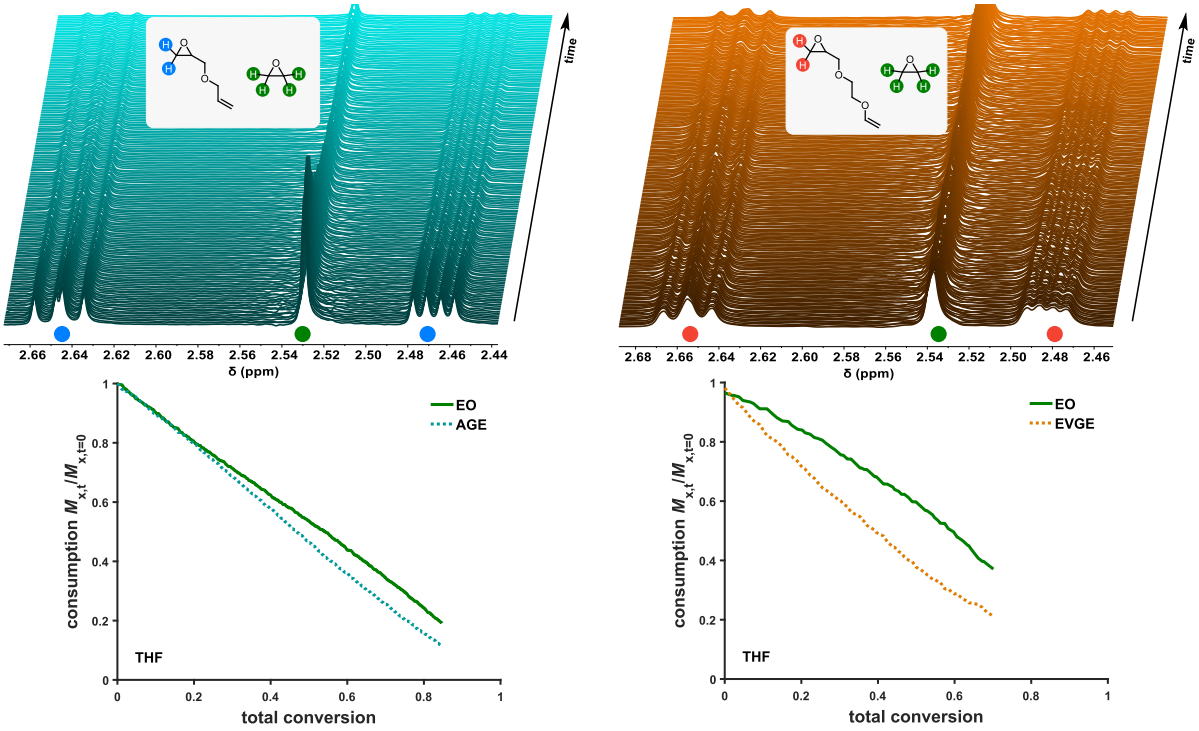

Figure 2. top: *in situ* ^{1}H NMR kinetics in THF-d_8 investigating the anionic copolymerization of P(EO-*co*-AGE) (blue) and P(EO-*co*-EVGE) (red) initiated by potassium phenylmethanolateat 45 °C; bottom: consumption $M_{x,t}/M_{x,t=0}$ versus total conversion of P(EO-*co*-AGE) (blue) and P(EO-*co*-EVGE) (red).

Accordingly, reactivity ratios were determined as $r_{EO}^{THF} = 0.78 \pm 0.001$ and $r_{AGE}^{THF} = 1.29 \pm 0.002$ as well as $r_{EO}^{THF} = 0.48 \pm 0.004$ and $r_{EVGE}^{THF} = 2.05 \pm 0.015$. In THF, both copolymerizations exhibit soft gradient microstructures, illustrated in the molar composition diagrams (Figure S6). In the case of of P(EO-*co*-EVGE) the gradient determines the nature of the terminal units, consisting almost exclusively of EO repeating units. The investigated polymerizations in DMSO as well as THF resulted in polymers of narrow dispersities ($Đ < 1.19$) (Figure S9). A summary of the evaluated reactivity ratios compared to the values reported by Lynd, Hawker et al.[31] (based on the EGD method) is given in Table 1. Comparison of the herein presented results with the reactivity ratios evaluated by the EGD method show a strong discrepancy between the different methods. The end-group dyad (EGD) analysis yields a more pronounced reactivity of the respective glycidyl ethers compared to the established *in situ* methods. These findings are discussed in the following.

Table 1. Reactivity ratios evaluated by *in situ* ^{1}H NMR experiments using the Jaacks method[30] and EGD analysis.[31]

Comonomer	Method	Solvent	r_{EO}	r_{EO}^{err}	r_{GE}	r_{GE}^{err}	$r_{EO}*r_{GE}$	R^2
AGE	Jaacks	DMSO	0.92	0.002	1.08	0.002	1.00	0.9995
	Jaacks	THF	0.78	0.001	1.29	0.002	1.00	0.997
	EGD	THF	0.54	0.03	1.31	0.26	0.71	-
EVGE	Jaacks	DMSO	0.81	0.001	1.23	0.002	1.00	0.998
	Jaacks	THF	0.48	0.004	2.05	0.015	1.00	0.992
	EGD	THF	0.32	0.10	3.50	0.90	1.12	-

In addition to the Jaacks equation,[30] the reactivity ratios were evaluated by ideal integrated equation of Meyer-Lowry[20] as well as the Beckingham-Sanoja-Lynd (BSL)[45] method (Table S1 and Figures S7 and S8).

Impact of transition state on monomer reactivity

The described results demonstrate that the influence of cation complexation on monomer reactivities during the polymerization is more pronounced in THF rather than DMSO. Following these findings, we postulate the transient "crown ether-effect" of the investigated glycidyl ethers causing the enhanced reactivity of both glycidyl ethers compared to EO in THF. It is a known phenomenon that the addition of 18 crown-6, a cyclic oligo(ethylene glycol) consisting of six EO repeating units, strongly complexes potassium cations in THF.[46] The distance of two methylene units between the oxygens of 18-crown-6 is similarly found for the three oxygens in EVGE. Based on this rationale, a preferential combined complexation of the potassium cation with EVGE monomer and the alkoxide of the propagating chain via chelation can be hypothesized and investigated by quantum chemistry methods, namely density functional theory (DFT) (Figure 3, right). In contrast, EO exhibits only one coordination site per monomer and therefore a lower complex coordination constant with potassium cations. Consequently, this results in a higher probability to find EVGE rather than EO in the chain segments close to the initiator, explaining the preferential incorporation of EVGE ($r_{EVGE} > r_{EO}$) during chain propagation. The chelation of potassium cations is less pronounced for AGE, as only two possible coordination sites are present in each AGE monomer (Figure 3, center). Therefore, the stability constant of AGE complexes is lower than that of EVGE, but still somewhat higher than for EO, resulting in a merely slightly preferred addition of AGE to the chain end in THF ($r_{AGE} > r_{EO}$). DFT calculations further provide information concerning the geometry of the precursor complexes of the chain ends with the different monomers. The enhanced coordination of the potassium counterion by the monomer going from EO and AGE to EVGE was observed as a local energy minimum. Hence, the inherent entropic benefit is a determining factor for the preferred chelation of the potassium cation.

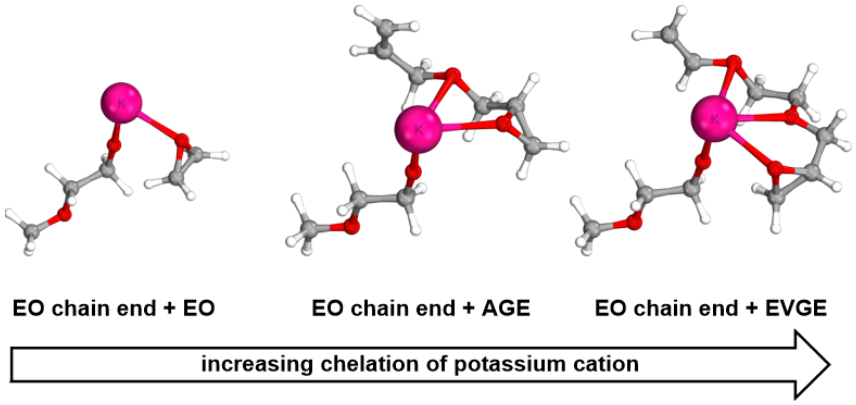

Figure 3. Complexation of potassium by EO chain end with EO, AGE and EVGE calculated by DFT.

Furthermore, we compared the electron densities of the electrophilic methylene groups of the epoxides calculated by DFT, which are attacked by the alkoxide during polymerization. Since the bond angles of the different epoxides and hence the ring strain of the monomers are comparable, the electron density is the pivotal parameter for the monomer reactivity. In Table 2, the partial charges of the three monomers simulated in vacuum as well as in THF and DMSO are given, using the implicit solvation model CPCM.

Table 2. Partial charges of the unsubstituted methylene carbon of the epoxide moiety of the monomers ethylene oxide (EO), allyl glycidyl ether (AGE) and ethoxy vinyl glycidyl ether (EVGE) calculated by DFT without taking solvation into account or rather in THF and DMSO using CPCM.

System	EO	AGE	EVGE
vacuum	-0.285 e	-0.251 e	-0.251 e
THF	-0.275 e	-0.242 e	-0.249 e
DMSO	-0.273 e	-0.240 e	-0.243 e

Both investigated glycidyl ethers exhibit lower electron density at their electrophilic carbon relative to EO. The trend is further decreased for all epoxides with increasing dipole moment of the respective solvent. Consequently, the partial charges give a first indication for preferential incorporation of the glycidyl ethers at the chain end compared to EO. This is in accordance with the observed trend from the *in situ* ^{1}H NMR kinetic experiments. Surprisingly, the unsubstituted methylene carbon of AGE exhibits a higher electrophilicity than the respective carbon of EVGE in all solvents. Considering the afore described reactivity ratios, the potassium complexation of glycidyl ethers appears to be the major contributing factor to the copolymerization kinetics in THF, rather than the electrophilicity itself. These findings suggest that the monomer, but not the respective chain, primarily affects the incorporation with its specific complexation behavior. This further supports the implementation of the non-terminal model for the determination of reactivity ratios by *in situ* ^{1}H NMR measurements.

Additional considerations are required to understand the impact of solvent polarity on the differences of the reactivity ratios in THF and DMSO (r_{GE}^{DMSO} and r_{GE}^{THF}). Compared to THF, DMSO

is a solvent with a high dipole moment. The resulting high polarity of the solvent allows an excellent dissolution of ions. Therefore, free ions are the primary active species, which mainly contribute to propagation.[43] The strong solvation effect of DMSO has a documented impact on complexes, e.g. it is known to decrease the stability constants of crown ether complexes.[47] This influence is clearly visible when comparing the reactivity ratios obtained via *in situ* ^{1}H NMR measurements in the different solvents. In DMSO, only a slightly preferred incorporation of EVGE over EO is observed. Therefore, the previously proposed crown ether-effect of EVGE in THF (Figure 3) is less pronounced in the case of DMSO. This is additionally confirmed by the increasing r_{EO} values from THF (0.57) to DMSO (0.81) and the increasing similarity of r_{EVGE}^{DMSO} (1.23) and r_{AGE}^{DMSO} (1.08). The described influence of DMSO is equally observed in the copolymerization of EO with AGE, resulting in an almost ideally random copolymerization with $r_{EO} \approx r_{AGE}$. Similar values of the reactivity ratios were previously reported by our group for the copolymerization of ethoxyethyl glycidyl ether (EEGE) with EO in DMSO under AROP conditions.[18]

In summary, variation of the chemical structure of a glycidyl ether, e.g., the addition of an ethylene glycol spacer at the monomer side chain, has a distinct influence on the behavior of epoxide monomers in copolymerizations with EO and consequently the microstructure of the resulting copolymers. In this context, the choice of solvent thus has a pronounced effect on the copolymerization reaction kinetics.

Comparison of *in situ* kinetics and end-group dyad (EGD) analysis

The presented results describe the reactivities of the epoxide monomers throughout the copolymerization process. When *in situ* kinetic experiments are utilized to monitor the AROP, monomer consumption is observed over time and translated to reactivity ratios by non-terminal evaluation methods, such as the herein applied Jaacks[30] or the Beckingham-Sanoja-Lynd (BSL)[45] method or alternatively the ideal integrated copolymerization equation.[20,48] On the contrary, the ^{1}H NMR EGD analysis by Lynd, Hawker and coworkers relies on the splitting of the benzylic proton signals based on the dyads formed directly upon initiation of the polymer chain. In this manner, the reactivity of the initiator towards the first monomer and the following initiator-monomer adduct towards the second monomer can be quantified via ^{1}H NMR EGD analysis in a simple manner. However, the reactivity ratio r_{EVGE}^{THF} determined via EGD analysis (3.50) significantly differs from r_{EVGE}^{THF} obtained via our *in situ* ^{1}H NMR spectroscopy measurements (2.05). Furthermore, the product of r_{EVGE} and r_{EO} deviates from unity in the case of the EGD method (Table 1) and therefore contradicts the assumption of a non-terminal model. The latter is surprising, as non-terminal-based methods were successfully implemented for various copolymerizations of EO and glycidyl ethers.[18,24,29] To explain these contradictory results, the presence of chain end-dependent polymerization kinetics can be emphasized at the beginning of the copolymerization process. As mentioned by Kazanskii et al., an auto-acceleration of the EO homopolymerization kinetics in THF is observed at low monomer conversion, until a critical number of repeating units is reached. At this point, the polymerization process becomes stationary. These peculiar kinetics are explained by the poor solubility of alkoxides in THF: A sufficient chain length must be reached

to permit the abovementioned multidentate chelation of the potassium cation via the backbone ether oxygens and the subsequent full dissolution of the oligo-PEO.[34] A similar behavior is highly probable for the copolymerization of EVGE and EO. The nucleophilic attack of the initiator at an EVGE monomer (I-EVGE) results in a product with four ether oxygens. Therefore, the coordination sites of the potassium cation can be saturated by at least three oxygens of the EVGE chain end, increasing the solubility of I-EVGE. Multidentate chelation of I-EVGE is supported by the implemented DFT calculations of the initiator-monomer adducts (Figure 4) and suggests a preferred addition of EVGE over EO to the initiator. A similar rationale can be considered for the AGE adduct, even though only two oxygens (chain end and side chain ether oxygen) coordinate the potassium cation, as observed via DFT calculations (Figure 4). Therefore, the additional oxygen of EVGE compared to AGE results in an enhanced complexation behavior and supports the preferred incorporation of EVGE. In the case of the initiator-EO adduct, due to the lack of side-chain ether oxygens, only weak coordination with the oxygen of the initiator is present. The overestimation of the reactivity gap of EO and AGE by the EGD method compared to our findings support the conclusion that the side-chain ether oxygens of glycidyl ethers result in an enhanced crown ether-effect compared to the single oxygen of the initiator.

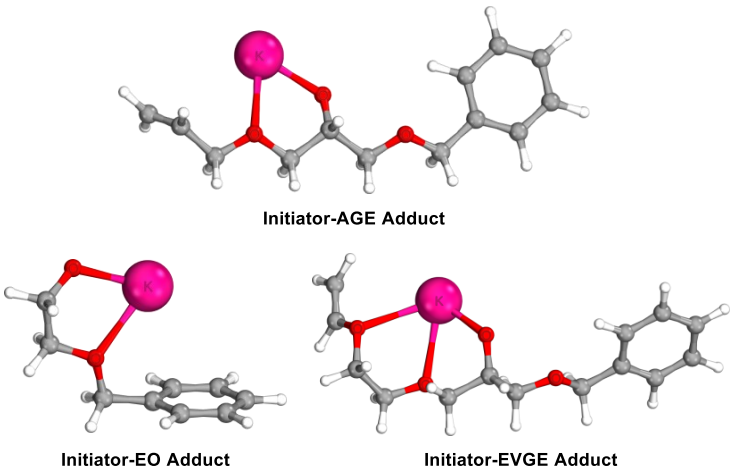

Figure 4. Complexation of potassium cation by initiator-monomer adducts calculated by DFT.

Following this line of thought, the coordination of the addition product and an additional EVGE monomer further saturates the complexation sites of the potassium cation, independent of an EO or EVGE chain end. In both cases, the addition of the second EVGE monomer would allow for a better solubility of the chain due the multidentate chelation observed by Kazanskii et al..[34]

Having reached a critical conversion, the polymer chains are solubilized, because the polyether chain possesses a sufficient length, and subsequent multidentate chelation with the potassium cation occurs (Figure 5 and Figure S10).[34] At this point, the copolymerization becomes merely monomer-dependent, resulting in the non-terminal polymerization kinetics discussed above. These considerations are supported by the aforementioned successful implementation of the Jaacks method. A similar behavior is observed for copolymerizations in DMSO, although the

enhanced ion dissolution in the more polar solvent reduces the proposed crown ether-effect, resulting in less pronounced reactivity disparity between EO and both glycidyl ethers. Based on this explanation, it is important to note that the complexation of the cation by the monomer remains in equilibrium with the coordination of the backbone. However, r_{GE} determined via *in situ* ^{1}H NMR spectroscopy in THF shows a slightly preferred complexation by the monomer rather than the polyether backbone, underlined by the observation that r_{EO} and r_{GE} are not approaching equality ($r_{EO} \neq r_{GE}$).

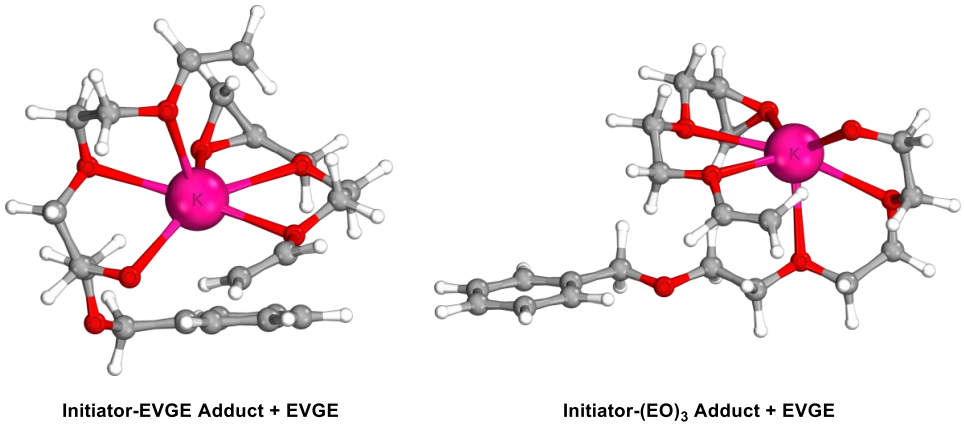

Figure 5. Complexation of potassium cation via EVGE chain end and EVGE monomer (left) and polyether backbone and EVGE monomer (right).

These considerations underline the observation of the pronounced presence of EVGE repeating units near the initiator compared to the residual polymer chain, resulting in differing reactivity ratios observed via EGD and *in situ* ^{1}H NMR analysis. As a result, EGD analysis is exclusively applicable in the beginning of the copolymerization. Vice versa, determination of the compositional drift is not feasible by the employed EGD method.

Only a single *in situ* experiment is necessary to obtain reliable and reproducible reactivity ratios in case of *in situ* ^{1}H NMR spectroscopy. The integration of the overlapping signals of the benzylic protons in the EGD analysis is prone to errors as it relies on a user-dependent estimation. *In situ* ^{1}H NMR monitoring ultimately provides normalized data determined by a constant integration area, which eliminates possible errors.

CONCLUSION

With this study we aim at a general understanding of the anionic ring-opening copolymerization kinetics of ethylene oxide (EO) with glycidyl ethers (GE) via online ^{1}H NMR measurements. Allyl glycidyl ether (AGE) and ethoxy vinyl glycidyl ether (EVGE) were chosen as typical and synthetically valuable representatives of glycidyl ether monomers, and copolymerization was carried out either in THF or DMSO. Online ^{1}H NMR kinetics enables *in situ* monitoring of monomer consumption, leading to precise and reliable determination of reactivity ratios by common non-terminal models. Both investigated glycidyl ethers exhibited slightly higher reactivity ratios than

EO in DMSO as well as in THF, while the difference increased with reduced solvent polarity. These results emphasize the crown ether-effect and the underlying multidentate cation complexation as the driving force for the enhanced reactivity of glycidyl ethers compared to EO in the anionic copolymerization. The impact of the crown ether-like complexation consequently increased with reduced cation dissociation in less polar media on going from DMSO to THF. Supplementary calculations by density functional theory (DFT) support the presented crown ether-effect, showing the stronger complexation with increasing number of oxygen atoms comparing EO with ethylene glycol spacer containing GEs (EO < AGE < EVGE). Furthermore, the superiority of *in situ* ^{1}H NMR kinetics over end-group dyad (EGD) analysis for the evaluation of reactivity ratios with non-terminal models has been demonstrated. In general, the EGD analysis is strongly affected by the limited solubility of the initiator and the respective first comonomer pair. Consequently, this method enables the exclusive investigation of the reactivity of the applied monomers at the beginning of polymerization rather than the determination of true reactivity ratios of the considered copolymerization process at any given time.

Overall, the results disclose the underlying effects of the slightly preferred glycidyl ether incorporation over EO. This is crucial for the design of glycidyl ether-based copolymerizations, since the resulting microstructure is tunable by choice of solvent as well as the introduction of ethylene glycol spacers in the monomer structures. The monomer gradient governs the behavior of the resulting materials in bulk or solution. In summary, our results manifest the importance of *in situ* experiments for in-depth analysis of epoxide copolymerizations and demonstrate that there is no simple shortcut to determine reactivity ratios.

REFERENCES

(1) Steube, M.; Johann, T.; Galanos, E.; Appold, M.; Rüttiger, C.; Mezger, M.; Gallei, M.; Müller, A. H. E.; Floudas, G.; Frey, H. Isoprene/Styrene Tapered Multiblock Copolymers with up to Ten Blocks: Synthesis, Phase Behavior, Order, and Mechanical Properties. *Macromolecules* **2018**, *51*, 10246–10258.

(2) Grune, E.; Johann, T.; Appold, M.; Wahlen, C.; Blankenburg, J.; Leibig, D.; Müller, A. H. E.; Gallei, M.; Frey, H. One-Step Block Copolymer Synthesis versus Sequential Monomer Addition: A Fundamental Study Reveals That One Methyl Group Makes a Difference. *Macromolecules* **2018**, *51*, 3527–3537.

(3) Hodrokoukes, P.; Floudas, G.; Pispas, S.; Hadjichristidis, N. Microphase Separation in Normal and Inverse Tapered Block Copolymers of Polystyrene and Polyisoprene. 1. Phase State. *Macromolecules* **2001**, *34*, 650–657.

(4) Lach, R.; Weidisch, R.; Knoll, K. Morphology and mechanical properties of binary triblock copolymer blends. *J. Polym. Sci. B Polym. Phys.* **2005**, *43*, 429–438.

(5) Singh, N.; Tureau, M. S.; Epps, T. H. Manipulating ordering transitions in interfacially modified block copolymers. *Soft Matter* **2009**, *5*, 4757.

(6) Thunga, M.; Staudinger, U.; Satapathy, B. K.; Weidisch, R.; Abdel-Goad, M.; Janke, A.; Knoll, K. Influence of molecular architecture of S-S/B-S triblock copolymers on rheological properties. *J. Polym. Sci. B Polym. Phys.* **2006**, *44*, 2776–2788.

(7) Steube, M.; Johann, T.; Plank, M.; Tjaberings, S.; Gröschel, A. H.; Gallei, M.; Frey, H.; Müller, A. H. E. Kinetics of Anionic Living Copolymerization of Isoprene and Styrene Using *in Situ* NIR Spectroscopy: Temperature Effects on Monomer Sequence and Morphology. *Macromolecules* **2019**, *52*, 9299–9310.

(8) Korotkov, A. A.; Rakova, G. V. The copolymerization of isoprene and styrene with butyllithium as catalyst. *Polymer Science U.S.S.R.* **1962**, *3*, 990–1000.

(9) Price, C. C.; Atarashi, Y.; Yamamoto, R. Polymerization and copolymerization of some epoxides by potassium tert-butoxide in DMSO. *J. Polym. Sci. A-1 Polym. Chem.* **1969**, *7*, 569–574.

(10) Stolarzewicz, A.; Becker, H.; Wagner, G. Zum Einfluß von Elektronendonatoren auf die anionische Copolymerisation von Oxiranen. *Acta Polym.* **1980**, *31*, 743–745.

(11) Heatley, F.; Yu, G.-e.; Booth, C.; Blease, T. G. Determination of reactivity ratios for the anionic copolymerization of ethylene oxide and propylene oxide in bulk. *European Polymer Journal* **1991**, *27*, 573–579.

(12) Mangold, C.; Dingels, C.; Obermeier, B.; Frey, H.; Wurm, F. PEG-based Multifunctional Polyethers with Highly Reactive Vinyl-Ether Side Chains for Click-Type Functionalization. *Macromolecules* **2011**, *44*, 6326–6334.

(13) Reuss, V. S.; Obermeier, B.; Dingels, C.; Frey, H. *N*,*N*-Diallylglycidylamine: A Key Monomer for Amino-Functional Poly(ethylene glycol) Architectures. *Macromolecules* **2012**, *45*, 4581–4589.

(14) Steube, M.; Johann, T.; Hübner, H.; Koch, M.; Dinh, T.; Gallei, M.; Floudas, G.; Frey, H.; Müller, A. H. E. Tetrahydrofuran: More than a “Randomizer” in the Living Anionic Copolymerization of Styrene and Isoprene: Kinetics, Microstructures, Morphologies, and Mechanical Properties. *Macromolecules* **2020**, *53*, 5512–5527.

(15) Kim, J. M.; Chakrapani, S. B.; Beckingham, B. S. Tuning Compositional Drift in the Anionic Copolymerization of Styrene and Isoprene. *Macromolecules* **2020**, *53*, 3814–3821.

(16) Natalello, A.; Werre, M.; Alkan, A.; Frey, H. Monomer Sequence Distribution Monitoring in Living Carbanionic Copolymerization by Real-Time ^{1}H NMR Spectroscopy. *Macromolecules* **2013**, *46*, 8467–8471.

(17) Obermeier, B.; Wurm, F.; Frey, H. Amino Functional Poly(ethylene glycol) Copolymers via Protected Amino Glycidol. *Macromolecules* **2010**, *43*, 2244–2251.

(18) Herzberger, J.; Leibig, D.; Liermann, J. C.; Frey, H. Conventional Oxyanionic versus Monomer-Activated Anionic Copolymerization of Ethylene Oxide with Glycidyl Ethers: Striking Differences in Reactivity Ratios. *ACS Macro Lett.* **2016**, *5*, 1206–1211.

(19) Herzberger, J.; Kurzbach, D.; Werre, M.; Fischer, K.; Hinderberger, D.; Frey, H. Stimuli-Responsive Tertiary Amine Functional PEGs Based on *N*,*N*-Dialkylglycidylamines. *Macromolecules* **2014**, *47*, 7679–7690.

(20) Blankenburg, J.; Kersten, E.; Maciol, K.; Wagner, M.; Zarbakhsh, S.; Frey, H. The poly(propylene oxide-*co*-ethylene oxide) gradient is controlled by the polymerization method: determination of reactivity ratios by direct comparison of different copolymerization models. *Polymer chemistry* **2019**, *10*, 2863–2871.

(21) Blankenburg, J.; Maciol, K.; Hahn, C.; Frey, H. Poly(ethylene glycol) with Multiple Aldehyde Functionalities Opens up a Rich and Versatile Post-Polymerization Chemistry. *Macromolecules* **2019**, *52*, 1785–1793.

(22) Niederer, K.; Schüll, C.; Leibig, D.; Johann, T.; Frey, H. Catechol Acetonide Glycidyl Ether (CAGE): A Functional Epoxide Monomer for Linear and Hyperbranched Multi-Catechol Functional Polyether Architectures. *Macromolecules* **2016**, *49*, 1655–1665.

(23) Zhang, W.; Allgaier, J.; Zorn, R.; Willbold, S. Determination of the Compositional Profile for Tapered Copolymers of Ethylene Oxide and 1,2-Butylene Oxide by *in situ*-NMR. *Macromolecules* **2013**, *46*, 3931–3938.

(24) Verkoyen, P.; Dreier, P.; Bros, M.; Hils, C.; Schmalz, H.; Seiffert, S.; Frey, H. "Dumb" pH-Independent and Biocompatible Hydrogels Formed by Copolymers of Long-Chain Alkyl Glycidyl Ethers and Ethylene Oxide. *Biomacromolecules* **2020**, *21*, 3152–3162.

(25) Homann-Müller, T.; Rieger, E.; Alkan, A.; Wurm, F. R. *N*-Ferrocenylsulfonyl-2-methylaziridine: the first ferrocene monomer for the anionic (co)polymerization of aziridines. *Polymer chemistry* **2016**, *7*, 5501–5506.

(26) Rieger, E.; Alkan, A.; Manhart, A.; Wagner, M.; Wurm, F. R. Sequence-Controlled Polymers via Simultaneous Living Anionic Copolymerization of Competing Monomers. *Macromolecular rapid communications* **2016**, *37*, 833–839.

(27) Rieger, E.; Blankenburg, J.; Grune, E.; Wagner, M.; Landfester, K.; Wurm, F. R. Controlling the Polymer Microstructure in Anionic Polymerization by Compartmentalization. *Angewandte Chemie (International ed. in English)* **2018**, *57*, 2483–2487.

(28) Gleede, T.; Markwart, J. C.; Huber, N.; Rieger, E.; Wurm, F. R. Competitive Copolymerization: Access to Aziridine Copolymers with Adjustable Gradient Strengths. *Macromolecules* **2019**, *52*, 9703–9714.

(29) Herzberger, J.; Fischer, K.; Leibig, D.; Bros, M.; Thiermann, R.; Frey, H. Oxidation-Responsive and "Clickable" Poly(ethylene glycol) via Copolymerization of 2-(Methylthio)ethyl Glycidyl Ether. *Journal of the American Chemical Society* **2016**, *138*, 9212–9223.

(30) Jaacks, V. A Novel Method of Determination of Reactivity Ratios in Binary and Ternary Copolymerizations. *Makromol. Chem.* **1972**, *161*, 161–172.

(31) Lee, B. F.; Wolffs, M.; Delaney, K. T.; Sprafke, J. K.; Leibfarth, F. A.; Hawker, C. J.; Lynd, N. A. Reactivity ratios, and mechanistic insight for anionic ring-opening copolymerization of epoxides. *Macromolecules* **2012**, *45*, 3722–3731.

(32) Lee, A.; Lundberg, P.; Klinger, D.; Lee, B. F.; Hawker, C. J.; Lynd, N. A. Physiologically relevant, pH-responsive PEG-based block and statistical copolymers with N,N-diisopropylamine units. *Polymer chemistry* **2013**, *4*, 5735–5742.

(33) Majdanski, T. C.; Vitz, J.; Meier, A.; Brunzel, M.; Schubert, S.; Nischang, I.; Schubert, U. S. “Green” ethers as solvent alternatives for anionic ring-opening polymerizations of ethylene oxide (EO): *In-situ* kinetic and advanced characterization studies. *Polymer* **2018**, *159*, 86-94.

(34) Kazanskii, K. S.; Solovyanov, A. A.; Entelis, S. G. Polymerization of ethylene oxide by alkali metal-naphthalene complexes in tetrahydrofuran. *European Polymer Journal* **1971**, *7*, 1421–1433.

(35) Ptitsyna, N.V.; Kazakevich, V.K.; Kazanskii, K.S. Conductometric study of “live” polyethylene oxide and its models. *Polymer Science U.S.S.R.* **1977**, *19*, 3218–3224.

(36) Solov’yanov, A. A.; Kazanskii, K. S. The kinetics and mechanism of anionic polymerization of ethylene oxide in ether solvents. *Polymer Science U.S.S.R.* **1972**, *14*, 1186–1195.

(37) Bawn, C.E.H.; Ledwith, A.; McFarlane, N. R. Anionic polymerization in dimethyl sulphoxide. *Polymer* **1967**, *8*, 484–487.

(38) Bawn, C.E.H.; Ledwith, A.; McFarlane, N. Anionic polymerization of ethylene oxide in dimethyl sulphoxide. *Polymer* **1969**, *10*, 653–659.

(39) Price, C. C.; Akkapeddi, M. K. Kinetics of base-catalyzed polymerization of epoxides in dimethyl sulfoxide and hexamethylphosphoric triamide. *J. Am. Chem. Soc.* **1972**, *94*, 3972–3975.

(40) Price, C. C.; Carmelite, D. D. Reactions of Epoxides in Dimethyl Sulfoxide Catalyzed by Potassium *t*-Butoxide. *J. Am. Chem. Soc.* **1966**, *88*, 4039–4044.

(41) Solov'yanov, A. A.; Kazanskii, K. S. Polymerization of ethylene oxide in dimethyl sulphoxide (DMS). *Polymer Science U.S.S.R.* **1972**, *14*, 1196–1206.

(42) Figueruelo, J. E.; Worsfold, D. J. The anionic polymerization of ethylene oxide in hexamethyl phosphoramide. *European Polymer Journal* **1968**, *4*, 439–444.

(43) Kazanskii, K. S.; Solovyanov, A. A.; Dubrovsky, S. A. Some Remarks to the Kinetics of Anionic Polymerization of Ethylene Oxide in Dimethyl Sulfoxide. *Makromol. Chem.* **1978**, *179*, 969–973.

(44) Penczek, S.; Cypryk, M.; Duda, A.; Kubisa, P.; Slomkowski, S. Living ring-opening polymerizations of heterocyclic monomers. *Progress in Polymer Science* **2007**, *32*, 247–282.

(45) Beckingham, B. S.; Sanoja, G. E.; Lynd, N. A. Simple and Accurate Determination of Reactivity Ratios Using a Nonterminal Model of Chain Copolymerization. *Macromolecules* **2015**, *48*, 6922–6930.

(46) Ding, J.; Heatley, F.; Price, C.; Booth, C. Use of crown ether in the anionic polymerization of propylene oxide—2. Molecular weight and molecular weight distribution. *European Polymer Journal* **1991**, *27*, 895–899.

(47) Solov'ev, V. P.; Strakhova, N. N.; Raevsky, O. A.; Rüdiger, V.; Schneider, H.-J. Solvent Effects on Crown Ether Complexations. *J. Org. Chem.* **1996**, *61*, 5221–5226.

(48) Meyer, V. E.; Lowry, G. G. Integral and differential binary copolymerization equations. *J. Polym. Sci. A Gen. Pap.* **1965**, *3*, 2843–2851.

SUPPORTING INFORMATION

Materials and Experimental Procedures

Reagent and Equipment

All chemicals and solvents were purchased from Acros Organics, TCI, Sigma-Aldrich and Fluka. Deuterated solvents were received from Deutero GmbH. Ethyl vinyl glycidyl ether (EVGE) was synthesized according to the procedure established by our group in 2011.[1] Allyl glycidyl ether (AGE) was purchased from TCI and purified before use by fractional distillation. Both glycidyl ethers were dried prior to the experiments by cryo-transfer after stirring over CaH_2 for 30 min.

In situ ^{1}H NMR Kinetic Experiments

Online ^{1}H NMR kinetic measurements were performed according to a protocol by Herzberger et al.[2] in a Norell S-500-VT-7 NMR tube. The *in situ* ^{1}H NMR spectra were recorded on a Bruker Avance III HD 400 MHz spectrometer equipped with a 5 mm BBFO SmartProbe. An exemplary protocol for P(EO-*co*-AGE) in DMSO-d_6 is described in the following, other experiments were performed equivalently. KO*t*Bu (24.6 mg, 219 μmol) was dissolved in a THF/water mixture and transferred in a flame-dried Schlenk flask equipped with a septum and stop cock. Benzyl alcohol (24.9 mg, 23.9 μl, 230 μmol) was dissolved in benzene and added to the base solution. After slow evaporation of the solvent under high vacuo, the initiator salt was dried at 60 °C under high vacuum. The dried initiator salt was then dissolved in 1.12 ml DMSO-d_6 and stirred for 30 min. Concurrently, EO (0.05 ml, 23 eq) was cryo-transferred to the evacuated NMR tube attached to the Schlenk-line under static vacuum at -50 °C with an acetone/nitrogen bath. Subsequently, 0.21 ml of the initiator solution and AGE (0.11 ml, 20 eq) were transferred to the NMR tube under an inert argon-atmosphere. The reaction mixture was then cooled by liquid nitrogen, evacuated and finally sealed with a Teflon stop cock. The reaction mixture was warmed to room temperature, shaken vigorously to ensure a homogenous solution and placed in the preheated (45 °C) NMR spectrometer. One spectrum every 30 sec. was recorded in DMSO-d_6 with one scan after the temperature was stable ($T = \pm 0.1$ K). In THF, spectra were recorded in a 10 min interval. The experimental data was analyzed by using NIREVAL software from Johann, Steube and Frey.[3]

Note regarding ethylene oxide: EO is a highly flammable and toxic gas. It therefore has to be handled with care and the necessary precautions. The addition of EO throughout this study was carried out in a reproducible procedure. Yet, small deviations in the measured volumes are possible considering the very small amounts utilized (< 0.1 ml). The evaluated reaction times depend on the overall concentration, which may therefore vary with each measurement. The targeted monomer ratios might differ to a small extent as well.

DFT Calculations

DFT calculations were performed on MOGON II at the high-performance computing center of the Johannes Gutenberg University Mainz using ORCA 4.2.1. software.[4,5] The B3LYP hybrid density functionals[6,7] were used as the calculation of the analytical Hessian matrix is available. Furthermore, the D3BJ[8,9] atom-pairwise dispersion correction to the DFT energy with Becke-Johnson damping was enabled. The def2-TZVP valence triple-zeta basis set[10,11] was selected and for an accurate single point energy TightSCF was chosen together with a Grid6 integration grid. The RIJCOSX approximation[12] was implemented together with a GridX8 for accurate geometry optimization, as it offers large accelerations. Finally, geometrical Counterpoise Corrections (gCP)[13] were enabled to prevent artificial overbinding effects. To take solvation into account, the implicit solvation model of the conductor-like polarizable continuum (CPCM)[14] simulating the solvate in a solvent cavity was utilized where appropriate. Furthermore, the maximum amount of memory to be used for integral buffering was defined by %maxcore and parallel jobs were invoked by %pal nprocs. The number of parallel jobs was set to the threefold of the number of atoms. The SCF calculations were specified in terms of their integral direct integration, by a maximal number of iterations and by a very tight convergence as threshold. An exemplary ORCA inputfile allowing the calculation of a local energy minimum is shown below:

!B3LYP D3BJ def2-TZVP CPCM(*solvent*) TightSCF RIJCOSX Opt Grid6 NoFinalGrid GridX8 FREQ NORMALPRINT GCP(DFT/TZ)

%maxcore *8000*

%PAL NPROCS 64 END

%scf MaxIter *2000*

SCFMode Direct

Convergence VeryTight

End

* xyzfile *Charge Multiplicity 3d_coordinates.xyz*

Size Exclusion Chromatography

Size exclusion chromatography (SEC) measurements were performed in dimethylformamide (DMF) with 1 g L^{-1} lithium bromide as an eluent at 50 °C. An Agilent 1100 Series was used, equipped with HEMA 300/100/40 columns, and calibration was carried out using polyethylene glycol (PEG) standards, both provided by Polymer Standard Service (PSS), Mainz.

Results of *in situ* ^{1}H NMR Kinetic Experiments

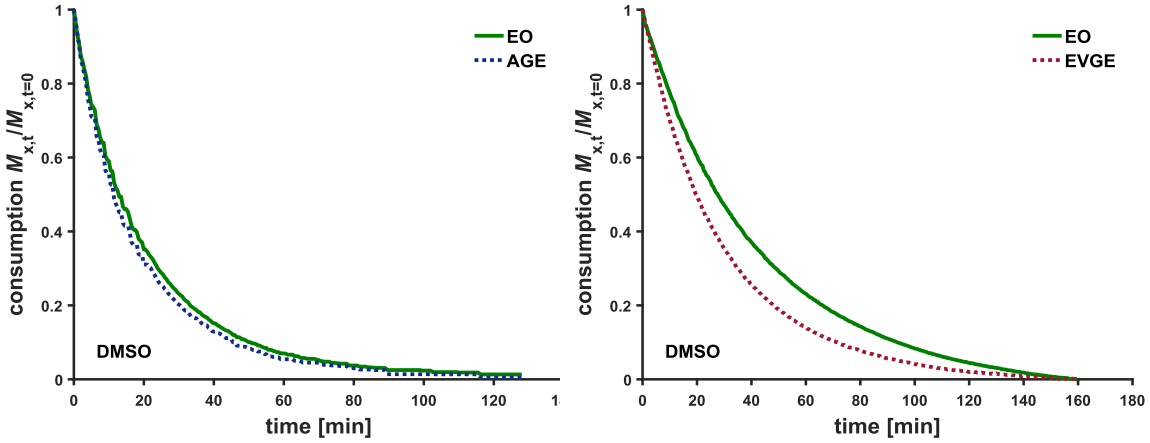

Figure S1. Time-conversion plot of of the copolymerization of EO with AGE (left) and with-EVGE (right) determined via *in situ* ^{1}H NMR kinetics in DMSO-d_6 at 45 °C.

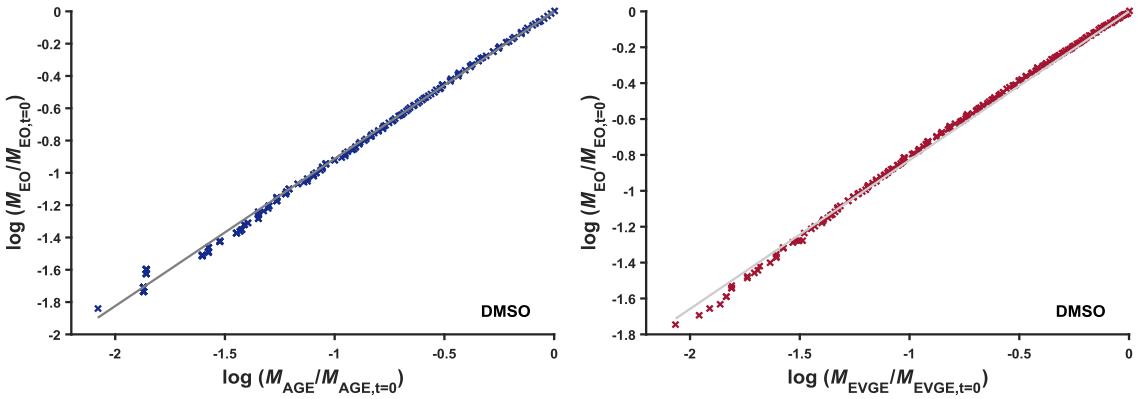

Figure S2. Jaacks plot for the copolymerization of EO with AGE (left, $R^2 = 0.99$) and with EVGE (right, $R^2 = 0.99$) determined via *in situ* ^{1}H NMR kinetics in DMSO-d_6 at 45 °C.

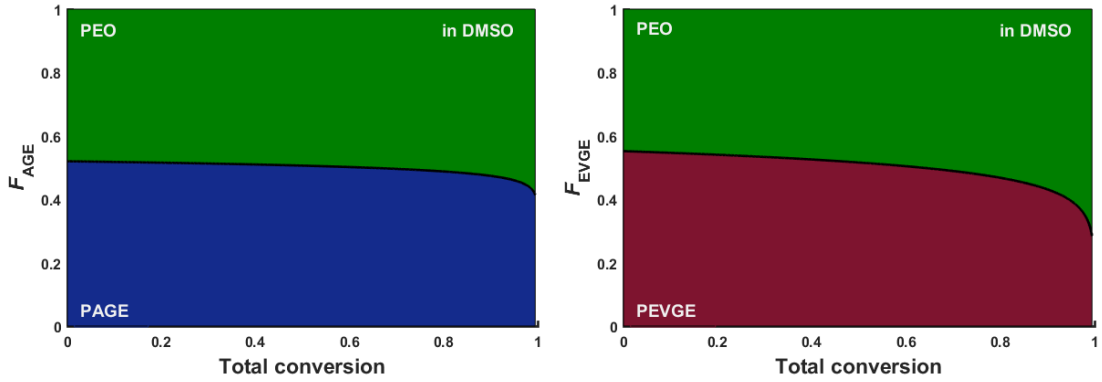

Figure S3. Molar-based composition diagram of P(EO-*co*-AGE) (left) and P(EO-*co*-EVGE) (right) in DMSO-d_6 with an initial equimolar ratio; F_{AGE} = AGE incorporation, F_{EVGE} = EVGE incorporation.

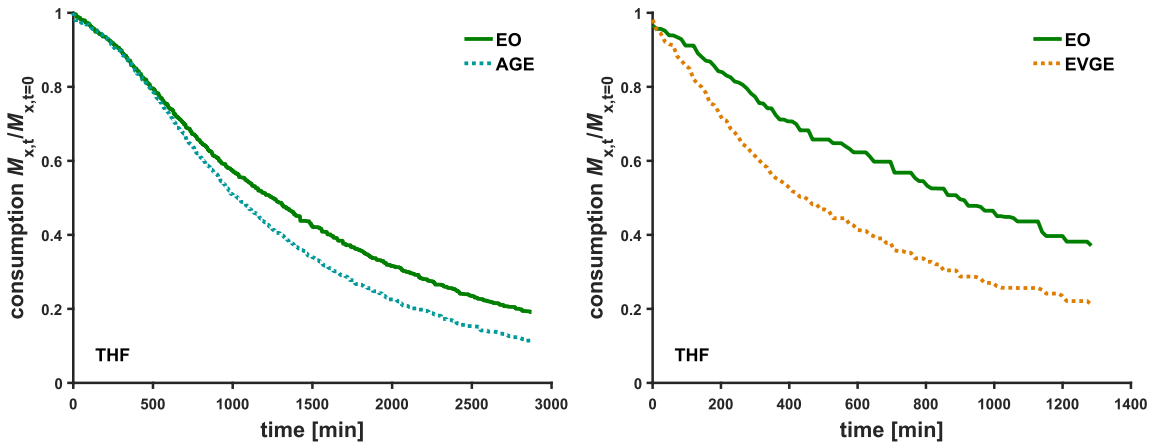

Figure S4. Time-conversion plot of the copolymerization of EO with AGE (left) and with-EVGE (right), determined via *in situ* ^{1}H NMR kinetics in THF-d_8 at 45 °C.

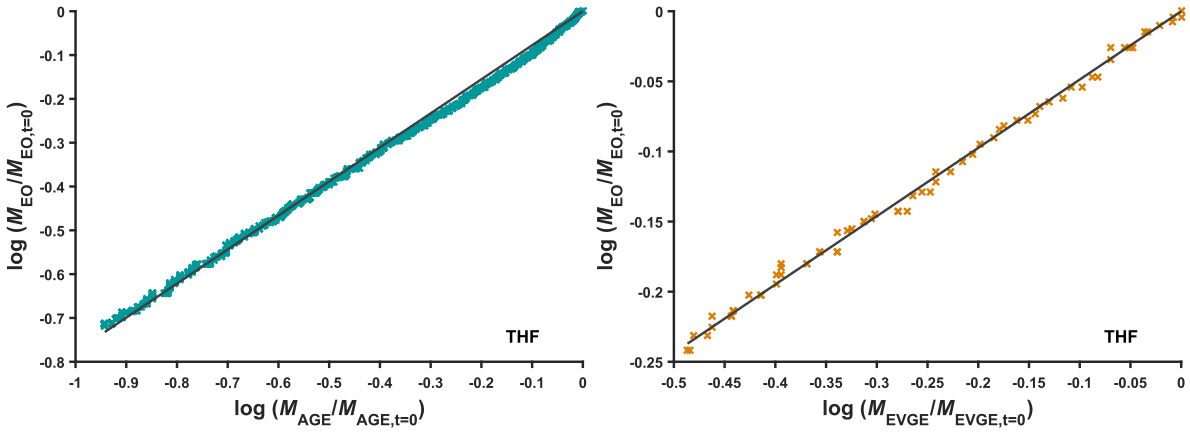

Figure S5. Jaacks plot for the copolymerization of EO with AGE (left, $R^2 = 0.99$) and with EVGE (right, $R^2 = 0.99$) determined via *in situ* ^{1}H NMR kinetics in THF-d_8 at 45 °C.

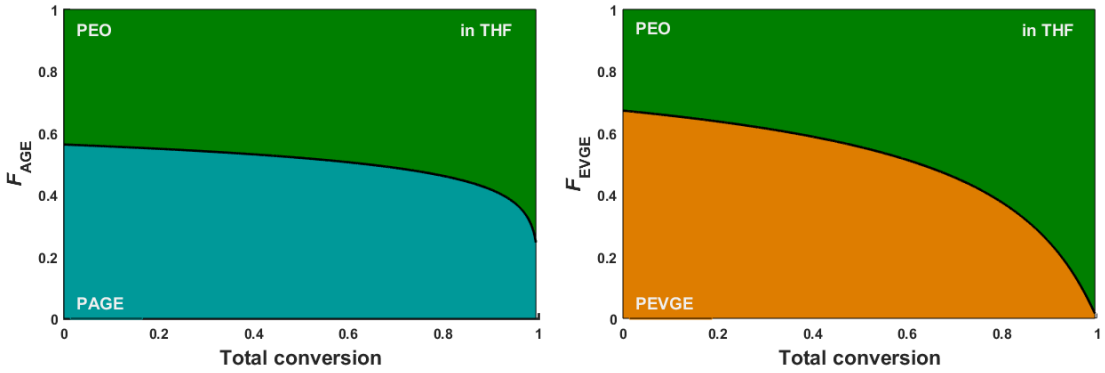

Figure S6. Molar-based composition diagram of P(EO-*co*-AGE) (left) and P(EO-*co*-EVGE) (right) in THF-d_8 with an initial equimolar monomer ratio; F_{AGE} = AGE incorporation, F_{EVGE} = EVGE incorporation.

Table S1. Reactivity ratios r_{EO} and r_{GE} from *in situ* ^{1}H NMR spectroscopy of the copolymerization of EO with AGE and EVGE evaluated by implementation of Jaacks,[15] Meyer-Lowry ideal integrated,[16] Beckingham-Sanoja-Lynd (BSL)[17] and end group dyad analysis (EGD).[18]

Method	Comonomer	Solvent	r_{EO}	r_{EO}^{err}	r_{GE}	r_{GE}^{err}	$r_{EO}*r_{GE}$
Jaacks	AGE	DMSO	0.92	0.002	1.08	0.002	1.000
Meyer-Lowry ideal			0.91	0.003	1.09	0.004	1.000
BSL			0.91	0.003	1.10	0.003	1.002
Jaacks	AGE	THF	0.78	0.001	1.29	0.002	1.000
Meyer-Lowry ideal			0.76	0.002	1.31	0.004	1.000
BSL			0.79	0.002	1.25	0.004	0.990
EGD			0.54	0.03	1.31	0.26	0.71
Jaacks	EVGE	DMSO	0.81	0.001	1.23	0.002	1.00
Meyer-Lowry ideal			0.80	0.003	1.25	0.007	1.00
BSL			0.79	0.002	1.27	0.002	1.01
Jaacks	EVGE	THF	0.48	0.004	2.05	0.015	1.00
Meyer-Lowry ideal			0.48	0.01	2.08	0.03	1.00
BSL			0.49	0.002	2.04	0.02	1.00
EGD			0.32	0.10	3.50	0.90	1.09

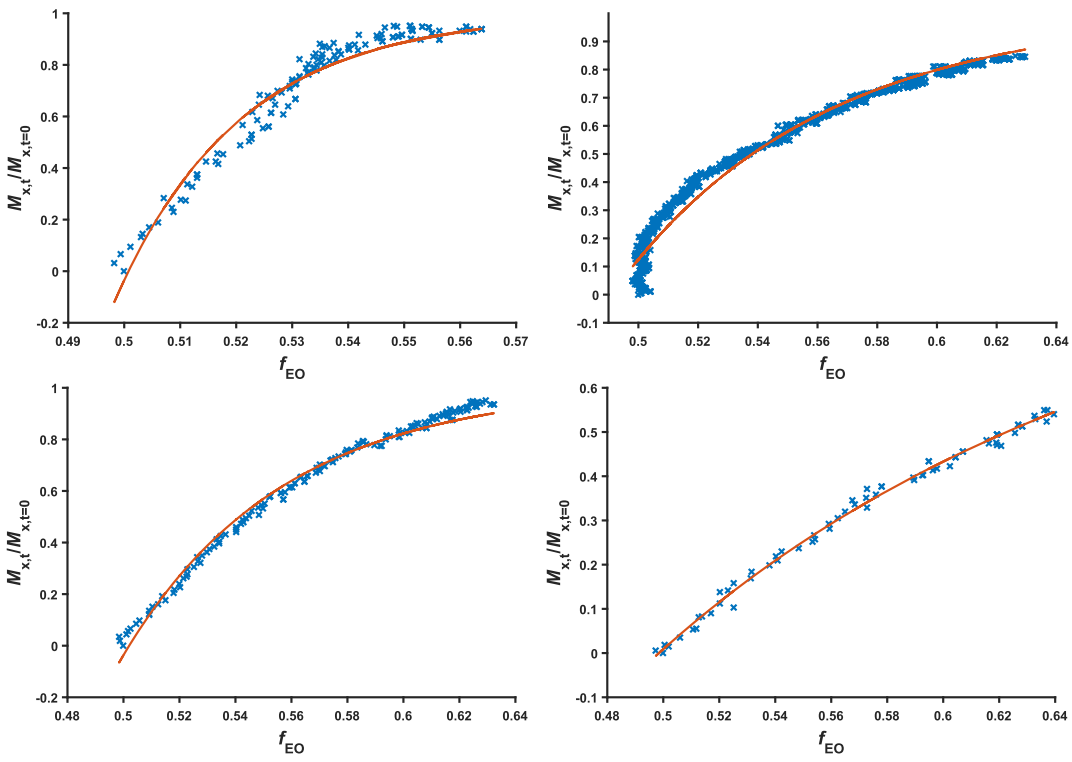

Figure S7. Ideal integrated equation fits of P(EO-*co*-AGE) (top) and P(EO-*co*-EVGE) (bottom) in DMSO (left) and THF (right) determined via *in situ* ^{1}H NMR kinetics at 45 °C.

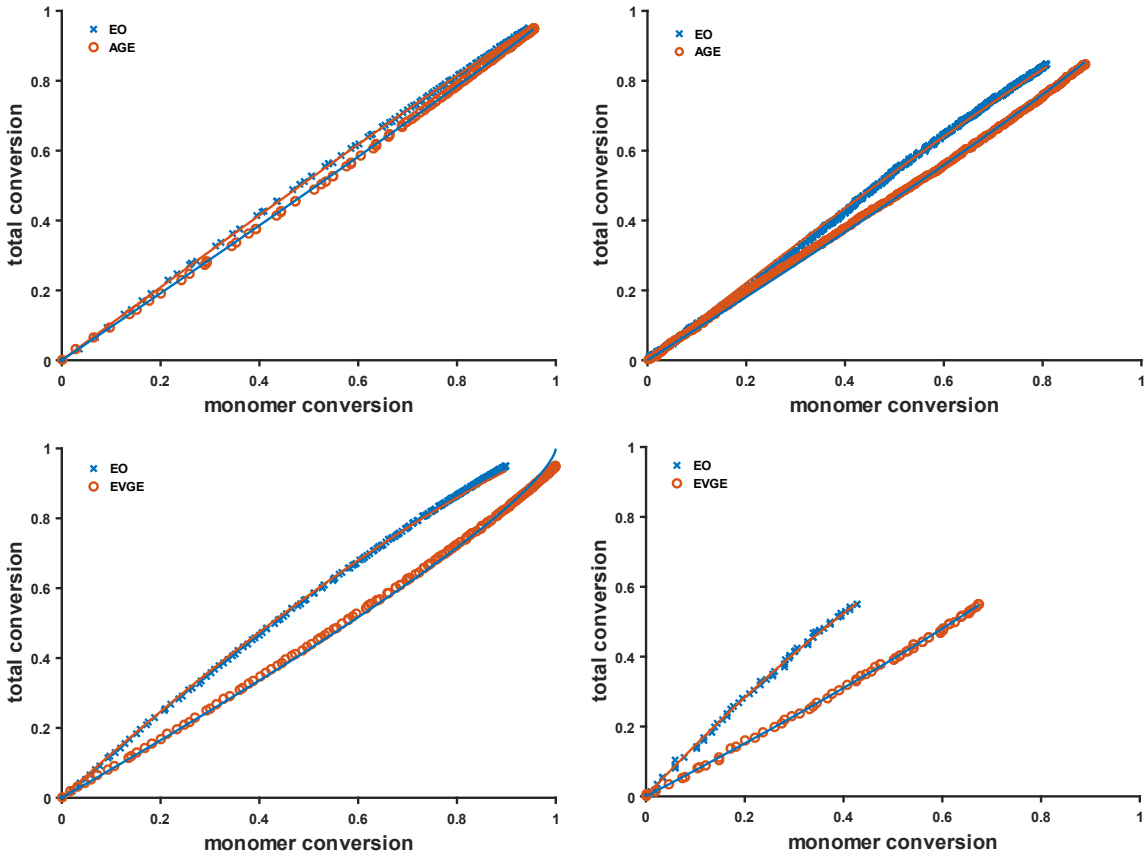

Figure S8. Beckingham-Sanoja-Lynd (BSL) fits of P(EO-*co*-AGE) (top) and P(EO-*co*-EVGE) (bottom) in DMSO (left) and THF (right) determined via *in situ* ^{1}H NMR kinetics at 45 °C.

Molecular Weight Distribution of Copolymers Prepared

The SEC traces of the *in situ* ^{1}H NMR kinetic show molecular weight distribution from 3000 to 3700 g mol^{-1} with dispersities ranging from 1.08 to 1.19 (Figure S9). Please note that the samples were formed in the NMR tube. In the case of the THF samples, high molecular weight shoulders can be observed, which can be explained by the presence of traces of water in the polymerization process. However, the presence of water has no influence on the concentration of active chain-ends and the monomer consumption. Therefore, online monitoring results regarding monomer consumption via *in situ* ^{1}H NMR measurements are independent of the dispersity of the samples.

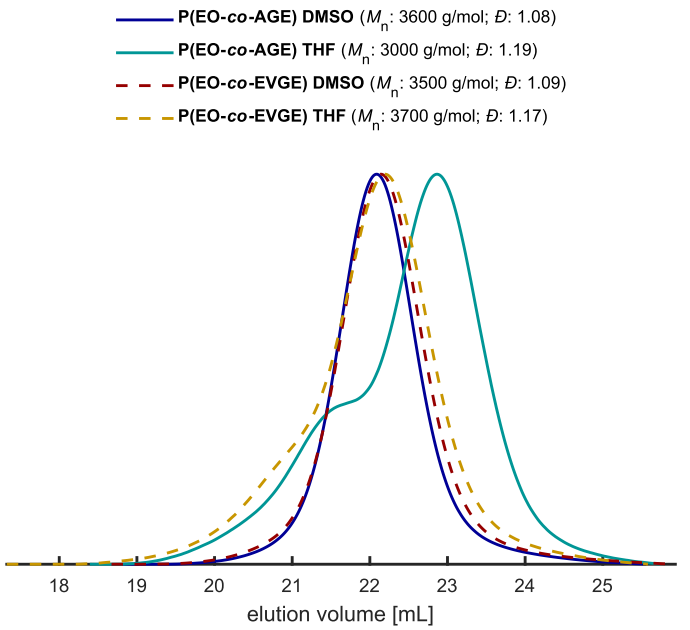

Figure S9. SEC traces of P(EO-*co*-AGE) and P(EO-*co*-EVGE) copolymers synthesized in DMSO-d_6 und THF-d_8 at 45 °C (solvent: DMF, standard: PEG).

Supplementary DFT Calculations

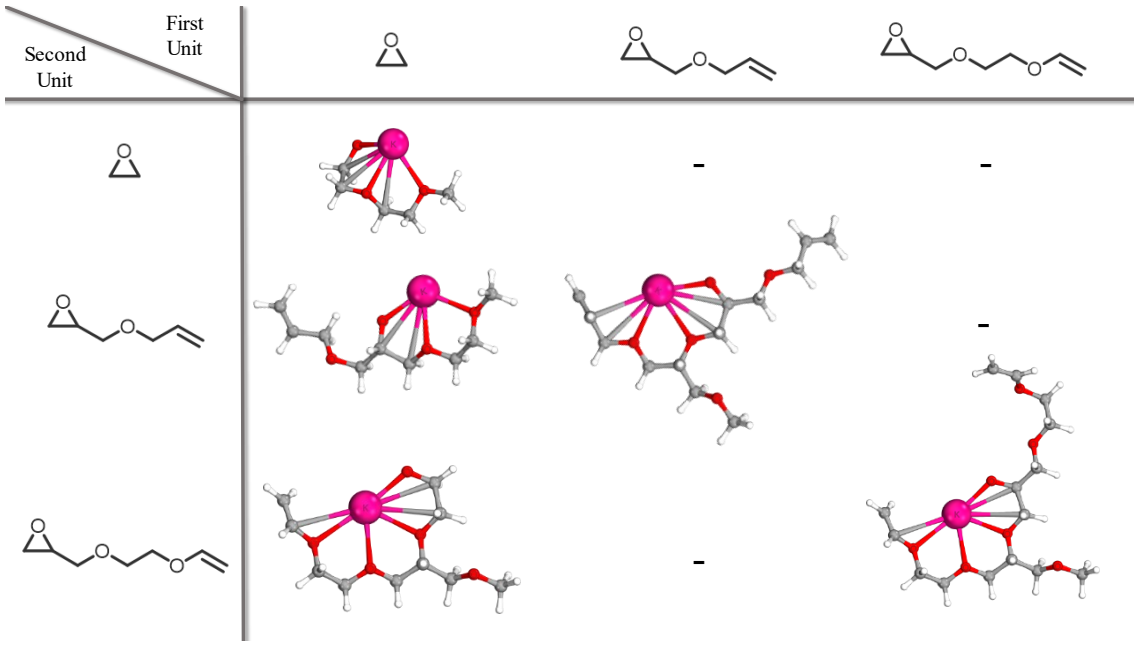

Figure S10. Complexation of the potassium counterion within the two penultimate monomer units. Potassium methanolate was utilized as a model initiator for this simulation. The multidentate chelation with the potassium counterion is shown for combined incorporated monomer units, visualizing the comparably poor complexation by solely EO repeating units.

REFERENCES

(1) Mangold, C.; Dingels, C.; Obermeier, B.; Frey, H.; Wurm, F. PEG-based Multifunctional Polyethers with Highly Reactive Vinyl-Ether Side Chains for Click-Type Functionalization. *Macromolecules* **2011**, *44*, 6326–6334.

(2) Herzberger, J.; Leibig, D.; Liermann, J. C.; Frey, H. Conventional Oxyanionic versus Monomer-Activated Anionic Copolymerization of Ethylene Oxide with Glycidyl Ethers: Striking Differences in Reactivity Ratios. *ACS Macro Lett.* **2016**, *5*, 1206–1211.

(3) Steube, M.; Johann, T.; Plank, M.; Tjaberings, S.; Gröschel, A. H.; Gallei, M.; Frey, H.; Müller, A. H. E. Kinetics of Anionic Living Copolymerization of Isoprene and Styrene Using *in Situ* NIR Spectroscopy: Temperature Effects on Monomer Sequence and Morphology. *Macromolecules* **2019**, *52*, 9299–9310.

(4) Neese, F. Software update: the ORCA program system, version 4.0. *WIREs Comput Mol Sci* **2018**, 8.

(5) Neese, F. The ORCA program system. WIREs *Comput Mol Sci* **2012**, *2*, 73–78.

(6) Lee; Yang; Parr. Development of the Colle-Salvetti correlation-energy formula into a functional of the electron density. *Phys. Rev. B* **1988**, *37*, 785–789.

(7) Becke, A. D. A new mixing of Hartree–Fock and local density-functional theories. *The Journal of chemical physics* **1993**, *98*, 1372–1377.

(8) Grimme, S.; Antony, J.; Ehrlich, S.; Krieg, H. A consistent and accurate ab initio parametrization of density functional dispersion correction (DFT-D) for the 94 elements H-Pu. *The Journal of chemical physics* **2010**, *132*, 154104.

(9) Grimme, S.; Ehrlich, S.; Goerigk, L. Effect of the damping function in dispersion corrected density functional theory. *Journal of computational chemistry* **2011**, *32*, 1456–1465.

(10) Schäfer, A.; Horn, H.; Ahlrichs, R. Fully optimized contracted Gaussian basis sets for atoms Li to Kr. *The Journal of chemical physics* **1992**, *97*, 2571–2577.

(11) Weigend, F.; Ahlrichs, R. Balanced basis sets of split valence, triple zeta valence and quadruple zeta valence quality for H to Rn: Design and assessment of accuracy. *Physical chemistry chemical physics: PCCP* **2005**, *7*, 3297–3305.

(12) Neese, F.; Wennmohs, F.; Hansen, A.; Becker, U. Efficient, approximate and parallel Hartree–Fock and hybrid DFT calculations. A 'chain-of-spheres' algorithm for the Hartree–Fock exchange. *Chemical Physics* **2009**, 356, 98–109.

(13) Kruse, H.; Grimme, S. A geometrical correction for the inter- and intra-molecular basis set superposition error in Hartree-Fock and density functional theory calculations for large systems. *The Journal of chemical physics* **2012**, *136*, 154101.

(14) Barone, V.; Cossi, M. Quantum Calculation of Molecular Energies and Energy Gradients in Solution by a Conductor Solvent Model. *J. Phys. Chem. A* **1998**, *102*, 1995–2001.

(15) Jaacks, V. A Novel Method of Determination of Reactivity Ratios in Binary and Ternary Copolymerizations. *Makromol. Chem.* **1972**, *161*, 161–172.

(16) Blankenburg, J.; Kersten, E.; Maciol, K.; Wagner, M.; Zarbakhsh, S.; Frey, H. The poly(propylene oxide-*co*-ethylene oxide) gradient is controlled by the polymerization method: determination of reactivity ratios by direct comparison of different copolymerization models. *Polym. Chem.* **2019**, *116*, 2170.

(17) Beckingham, B. S.; Sanoja, G. E.; Lynd, N. A. Simple and Accurate Determination of Reactivity Ratios Using a Nonterminal Model of Chain Copolymerization. *Macromolecules* **2015**, *48*, 6922–6930.

(18) Lee, B. F.; Wolffs, M.; Delaney, K. T.; Sprafke, J. K.; Leibfarth, F. A.; Hawker, C. J.; Lynd, N. A. Reactivity ratios, and mechanistic insight for anionic ring-opening copolymerization of epoxides. *Macromolecules* **2012**, *45*, 3722–3731.

Chapter 3

Synthesis and Application of Poly(ethlyene oxide)-based Block Co- and Terpolymers

Chapter 3.1

Epoxide Functionalization of Polystyryl-Anions Studied via Solvent Gradient Interaction Chromatography

Philip Dreier[†], Junyoung Ahn[‡], Taihyun Chang[*,‡] and Holger Frey[*,†]

[†]**Department of Chemistry, Johannes Gutenberg University Mainz, Germany**

[‡]**Department of Chemistry and Division of Advanced Materials Science, Pohang University of Science and Technology (POSTECH), Korea**

ABSTRACT: The end group functionality is of great importance for the utilization of polymers as macroinitiators or the linkage of macromolecules to surfaces. We investigated the end-capping efficiency of living polystyryl lithium with various epoxides, namely ethylene oxide (EO), ethoxy ethyl glycidyl ether (EEGE) and isopropylidene glyceryl glycidyl ether (IGG), relying on solvent gradient interaction chromatography (SGIC). Generally, end-capping efficiencies of > 95% were observed, which are in pronounced contrast to previously reported terminal functionalities of 84 to 91% for controlled radical techniques (ATRP and RAFT). Hydroxyl functional polystyrenes (PS-OH, PS-EEGE-OH and PS-IGG-OH) were obtained with molecular weights ranging from 13.8 to 15.0 kg mol^{-1} (size exclusion chromatography (SEC), with dispersities of 1.05-1.06). Furthermore, the acid-catalyzed deprotection of the acetal (PS-EEGE-OH) and ketal protective group (PS-IGG-OH) was investigated. In both cases, nearly quantitative deprotection (> 99%) resulting in the corresponding multihydroxy functional PS (PS-$(OH)_2$ and PS-$(OH)_3$) was observed via SGIC. Esterification of PS-OH with succinic anhydride showed a conversion of 98% of the hydroxyl group to the corresponding ester. An extremely detailed picture of side reactions during the carbanionic polymer synthesis and epoxide termination was obtained, demonstrating 95 – 99% terminal functionality). Depending on the polarity of the end group, an elution order of PS-OH < PS-$(OH)_2$ < PS-$(OH)_3$ < PS-COOH was obtained in SGIC. The study demonstrates the unrivalled terminal functionalization efficiency of the anionic polymerization methods for the generation of well-defined polymer chains, which is crucial for the further use of such polymers for the generation of block copolymers and other polymer architectures.

INTRODUCTION

Living carbanionic polymerization (LAP) is the crucial polymerization technique for the precise synthesis of well-defined homo- and copolymers as well as a vast variety of complex polymer architectures. It is a characteristic feature of this method that transfer and termination reactions are absent, resulting in a Poisson distribution of the molecular weights.[1,2] In LAP, the α-functionality is commonly varied by the implementation of organolithium-based initiators bearing protected functionalities.[3–6] For the ω-terminus, functionalization is achieved by the end-capping reaction of the living chain end with a large variety of electrophiles, i.e., epoxides,[7–13] thiiranes,[14] carbon dioxide,[15,16] alkyl halides,[17] aldehydes[18] and sultones.[19] Especially ω-hydroxy-functionalized polymers are of growing interest, as they are widely utilized as macroinitiators in ring-opening polymerizations of epoxides,[20–22] cyclic esters (i.e., lactones)[23,24] and cyclic carbonates to generate block copolymers.[25] These materials are employed for different applications[26,27] ranging from polymer electrolytes[28] to nanoporous membranes.[24] ω-Hydroxyl-functionalized polystyrene (PS-OH) is obtained via LAP of styrene and end-capping with ethylene oxide (EO),[7,8] as first described by Michael Szwarc.[29] For the end-capping step, a high reactivity of the electrophile and the absence of side-reactions are crucial to achieve high end group functionality and reduce traces of non-initiating homopolymer. Consequently, the structure of the electrophile used for termination is of great importance. For example, Quirk et al. investigated the addition of propylene oxide (PO)[9] and butylene oxide (BO)[10] to the living chain end of polystyryl lithium (PS-Li) in a detailed manner. They concluded that the end-capping efficiency drops from EO to BO and PO, which is explained by the proton abstraction at the methyl or methylene group in α-position to the oxirane ring of PO and BO, respectively.[30] The portfolio of epoxide reagents for the end-functionalization of PS-Li was further extended to different glycidyl ethers.[11] Herein, glycidyl ethers are utilized for the introduction of additional (protected) functionalities to the chain end, resulting in multifunctional materials.[31]

The end-capping efficiency cannot be determined by the widely established size exclusion chromatography (SEC), as the method is incapable of differentiating between chains with the same hydrodynamic radius but different chain end functionalities.[32] Hence, ^{1}H nuclear magnetic resonance (NMR) spectroscopy and matrix-assisted light desorption/ionization time of flight mass spectrometry (MALDI-ToF MS)[33] have been applied as suitable methods. However, their sensitivity and resolution capacity for end groups are dependent on the molecular weight of the investigated polymer. Additionally, in MALDI-ToF MS, the ionization efficiency strongly differs from unfunctionalized to functionalized species. The mass discrimination effect and fragmentation[34,35] during ionization of the samples are additional disadvantages of the MALDI-ToF MS technique. In contrast, high-performance liquid chromatography (HPLC) has been established as a suitable method for the quantitative determination of end groups.[33,36,37] For example, our group successfully quantified different species of α- and ω-functionalized telechelic poly(ethylene oxide).[38] Additionally, Chang et al. separated and determined living and dead chains of PS synthesized via RAFT[39] and ATRP[40] by the utilization of solvent gradient interaction chromatography (SGIC) and specially designed polar agents, demonstrating limited terminal

functionalization by these popular synthesis methods in the range of 84% to 91%.

Although the latter method shows reliable results, to the best of our knowledge, the end-capping reaction of PS-Li with monosubstituted epoxides, especially glycidyl ethers, has not been investigated by SGIC until today. Therefore, we prepared different PS-$(OH)_x$ (x = 0,1,2) samples exceeding 10 kg mol^{-1} via end-capping of PS-Li with EO and two hydroxyl-protected glycidyl ethers (i) ethoxy ethyl glycidyl ether (EEGE) and (ii) isopropylidene glyceryl glycidyl ether (IGG), respectively. End-capping efficiency, deprotection to multi hydroxyl-functional PS and functionalization of the hydroxyl group were investigated via HPLC, and all results were supported with conventional NMR measurements.

RESULTS AND DISCUSSION

Synthesis of PS-$(OH)_x$

Monohydroxy functional polystyrenes PS-OH, PS-EEGE-OH and PS-IGG-OH were synthesized via carbanionic polymerization of styrene in cyclohexane and subsequent addition of excess EO, EEGE or IGG[41] to living polystyryl lithium (PS-Li), respectively (Scheme 1).[7,8,11] Before the addition to the living chain end, the epoxides were dried with aliquots of *sec*-butyllithium to remove traces of protic impurities and water, which is an essential step to prevent undesired termination reactions.

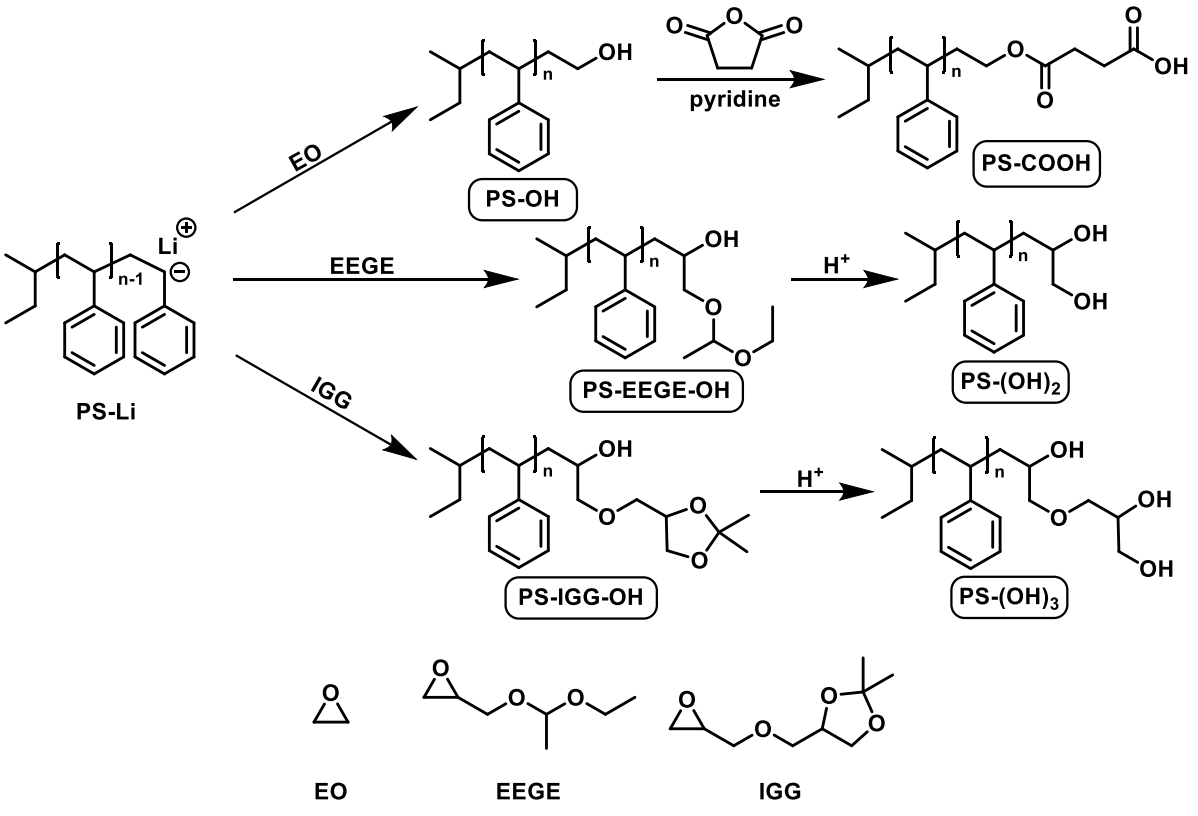

Scheme 1. Synthesis protocol of PS-$(OH)_x$ (x = 1,2,3) and PS-COOH.

PS-EEGE-OH and PS-IGG-OH were further deprotected under acidic conditions in THF to yield bifunctional (PS-$(OH)_2$) and trifunctional polystyrene (PS-$(OH)_3$), respectively. Molecular weights (M_n) of PS-$(OH)_x$ were determined via ^{1}H NMR spectroscopy end group analysis. Comparison of the integrals of the *sec*-butyl initiator group (0.70 ppm) and the signals of the aromatic region (7.36-6.28 ppm) show M_n in the range of 13.7-15.0 kg mol^{-1} (Table 1, Figure S1-S5).

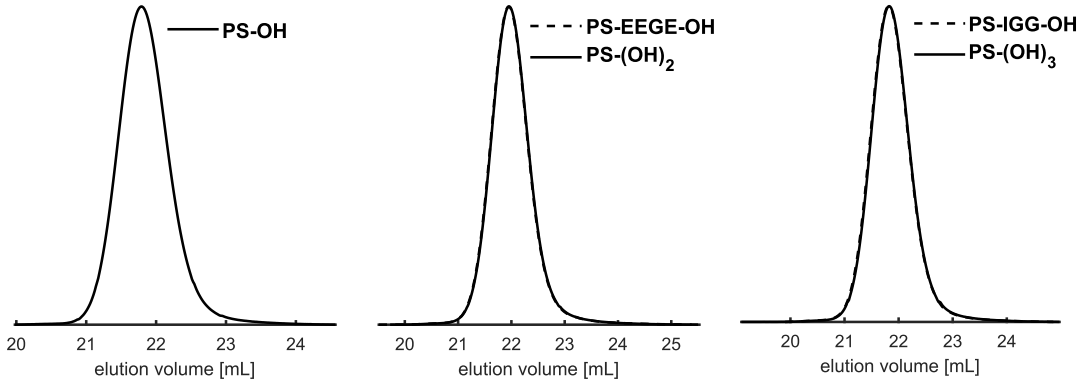

Figure 1. SEC traces (THF, PS calibration, RI detector) of the synthesized polymers.

Additionally, SEC traces of all hydroxyl-functionalized PS show narrow monomodal molecular weight distributions with low dispersities ranging from 1.05 to 1.06 (Table 1 and Figure 1). For protected (PS-EEGE-OH and PS-IGG-OH) and deprotected samples (PS-$(OH)_2$ and PS-$(OH)_3$), scarcely distinguishable SEC traces are obtained, due to the weak influence of the end group on the hydrodynamic radii of the corresponding polymers.[32]

Table 1. Overview of the synthesized samples and their end-group functionality.

Sample	$M_{n,SEC}$ [a)] [kg mol^{-1}]	$M_{n,NMR}$ [b)] [kg mol^{-1}]	$Đ$ [a)]	End Group Functionality [c)]
PS-OH	15.0	15.0	1.05	0.99
PS-EEGE-OH	13.8	14.8	1.06	0.96
PS-$(OH)_2$	13.7	15.0	1.06	0.96
PS-IGG-OH	14.9	14.6	1.06	0.96
PS-$(OH)_3$	14.8	14.7	1.06	0.95
PS-COOH	15.0	15.0	1.05	0.98

a) Determined by THF-SEC (PS calibration, RI detector); b) Determined by ^{1}H NMR spectroscopy; c) Determined by SGIC.

Consequently, precise determination of the end-capping and subsequent deprotection efficiency cannot be obtained by SEC measurements. In comparison, ^{1}H NMR spectra of PS-EEGE-OH (Figure S2) and PS-IGG-OH (Figure S4) and their deprotected analogs support the quantitative deprotection by the complete disappearance of the methine proton of the acetal group at 4.56 ppm (PS-$(OH)_2$) and the methyl protons of the ketal group at 1.44 ppm (PS-$(OH)_3$) (Figure S3 and S5).

Synthesis of PS-(COOH)

The functionalization of PS-OH to its carboxylic acid analogue (PS-COOH) was adapted from Ferruti et al.[42] The esterification reaction was carried out with succinic anhydride in dry $CHCl_3$ in the presence of pyridine.

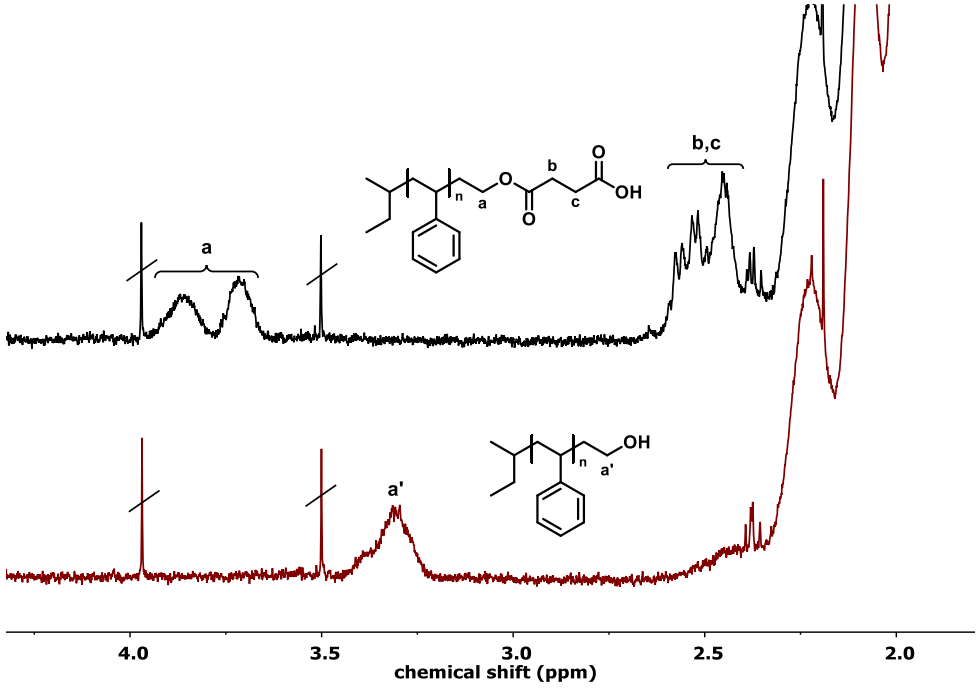

Figure 2. Section of ^{1}H NMR spectra ($CDCl_3$, 400 MHz) of PS-OH (bottom) and PS-COOH (top).

New resonances are observed between 4.00-3.60 and 2.60-2.40 ppm in the ^{1}H NMR spectrum of PS-COOH (Figure 2) which are assigned to the methylene groups next to the ester oxygen (a) and carbonyl groups of the succinic half-ester (b+c), respectively. Additionally, the signal of the methylene group next to the hydroxyl group (a') at 3.30 ppm of the PS-OH precursor is absent in the spectrum, which supports quantitative esterification.

HPLC fractionation

Solvent gradient interaction chromatography (SGIC) with a bare silica stationary phase and a THF/*n*-hexane mobile phase was employed to further separate the different polymeric species and to quantify the end-capping as well as deprotection efficiency of the above-mentioned synthesis. In contrast to SEC, in interaction chromatography, the separation of different end-functionalized species with the same molecular weights and hydrodynamic radii depends on the polarity of the samples´ functional end group.[32] Therefore, as-prepared samples were investigated with respect to their interaction behavior under SGIC conditions (Figure 3).

At first, the solvent mixture was held constant at 25%$_{vol}$ of THF for 20 min. Subsequently, the THF content was increased to 75%$_{vol}$ over a 30 min time frame. A qualitative trend is obtained:

With increasing polarity of the PS end group an increase in the elution time (t_E) of the samples is observed. Consequently, it is emphasized that the primary hydroxyl group of PS-OH shows stronger interaction and a higher t_E of the sample compared to the secondary hydroxyl groups of PS-EEGE-OH and PS-IGG-OH. Furthermore, the additional ether oxygen of PS-IGG-OH appears to result in a more pronounced adsorption compared to PS-EEGE-OH.

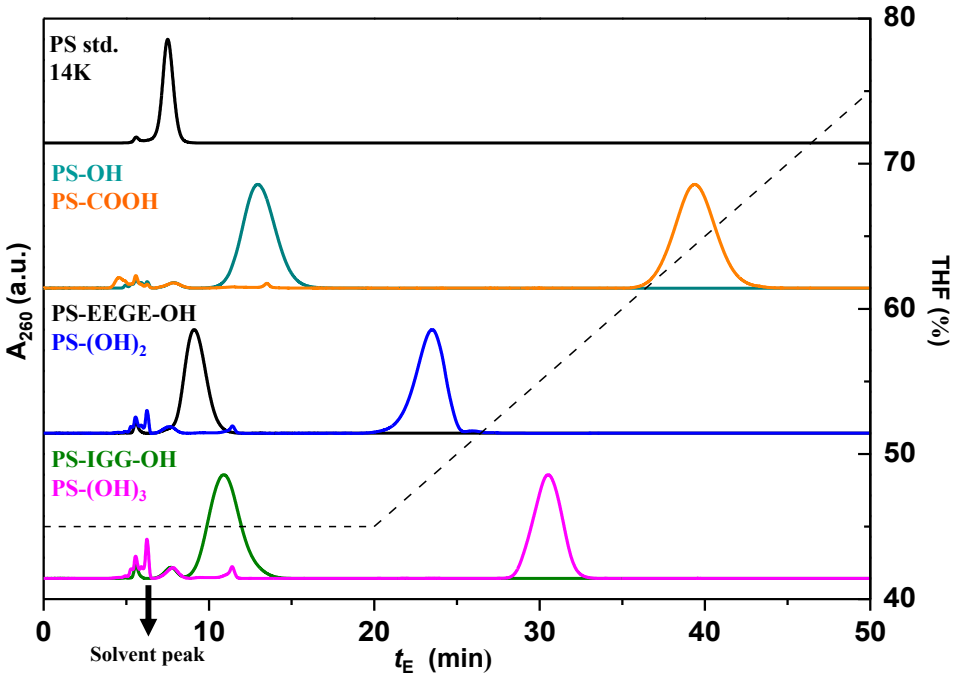

Figure 3. HPLC chromatograms of PS standard (top), PS-OH and PS-COOH (overlay, top middle), PS-EEGE-OH and PS-$(OH)_2$ (overlay, bottom middle) and PS-IGG-OH and PS-$(OH)_3$ (overlay, bottom).

In the case of PS-$(OH)_2$ and PS-$(OH)_3$, t_E strongly increases compared to their protected analogues due to the stronger interaction of the multiple hydroxyl groups per chain-end with the stationary phase.[37,39] On the other hand, PS-COOH exhibits the highest elution time of all samples, which is explained by the higher polarity of carboxylic acid groups in comparison to multiple hydroxyl groups. Therefore, the elution order of the different functional polymers is PS-OH < PS-$(OH)_2$ < PS-$(OH)_3$ < PS-COOH.

In all samples, traces of non-functionalized (proton-terminated) PS are observed, which exhibit t_E comparable to the PS standard. The undesired termination reactions might be explained by the reactions discussed in the following. Traces of protic impurities or water could be present during the end-capping step and react with the living chain-end. On the other hand, EEGE and IGG exhibit weakly acidic protons at the methylene group next to the oxirane ring.[43] Consequently, the highly basic PS-Li can abstract a proton, resulting in an unfunctionalized chain.

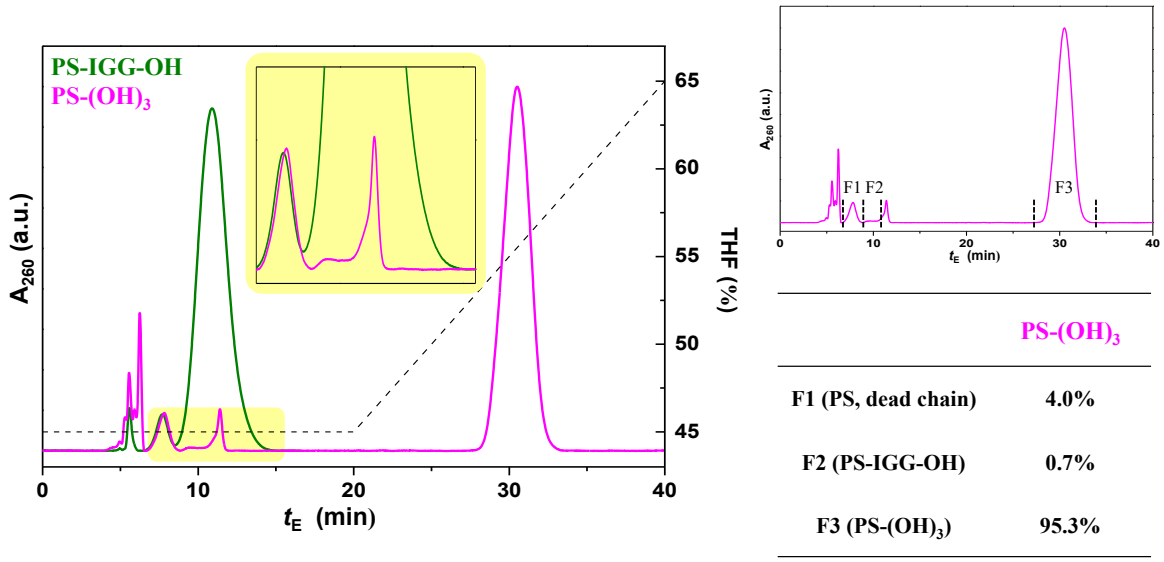

	PS-(OH)$_3$
F1 (PS, dead chain)	4.0%
F2 (PS-IGG-OH)	0.7%
F3 (PS-(OH)$_3$)	95.3%

Figure 4. Overlay of HPLC chromatograms of PS-IGG-OH and PS-(OH)$_3$ (left); overview and quantification of the different fractions in the PS-(OH)$_3$ sample (right).

The latter reaction was observed by Quirk et al. for the end-capping of PS-Li with propylene oxide[9] and butylene oxide,[10] which would explain the considerable increase of "dead" PS chains from 0.7% to 2.5% (Figure 5) and 4.0% (Figure 4) when comparing PS-EEGE-OH and PS-IGG-OH with PS-OH, since EO-termination does not lead to this kind of proton abstraction. The high end-capping efficiency (>99%) for PS-OH (Figure S7) is in accordance with MALDI-ToF MS results presented by Quirk et al. for the end-capping efficiency of low molecular weight PS-Li with EO.[7,8] These observations highlight the advantage of carbanionic polymerization over controlled radical polymerization techniques. In the latter case, terminal functionalities of merely 84%[40] and 91%[39] are reported for atom transfer radical polymerization (ATRP) and reversible addition-fragmentation chain-transfer (RAFT) polymerization, respectively.

A more detailed examination of the HPLC chromatograms of PS-(OH)$_3$ (Figure 4) allows for quantification of the deprotection efficiency. Besides fraction 3 (F3) (PS-(OH)$_3$) (95.3%) and fraction 1 (F1) (4.0%) (dead PS), fraction 2 (F2) (0.7%) is assigned to PS-IGG-OH by the overlay of the HPLC chromatograms of PS-(OH)$_3$. This is a crucial observation, for instance regarding the subsequent synthesis of AB$_3$ star block copolymers. Insufficient deprotection leads to the formation of ≈1% impurities in form of linear block copolymers, which are formed along with the targeted star block copolymers. The unprotected species (0.7%) was equally observed in the case of PS-(OH)$_2$ (Figure 5). However, in both cases a high deprotection efficiency of > 99% was obtained. Additionally, a sharp peak at t_E = 12 min was observed in the chromatograms of both PS-(OH)$_3$ and PS-(OH)$_2$, whose insignificant light scattering intensity points to a non-polymeric impurity.

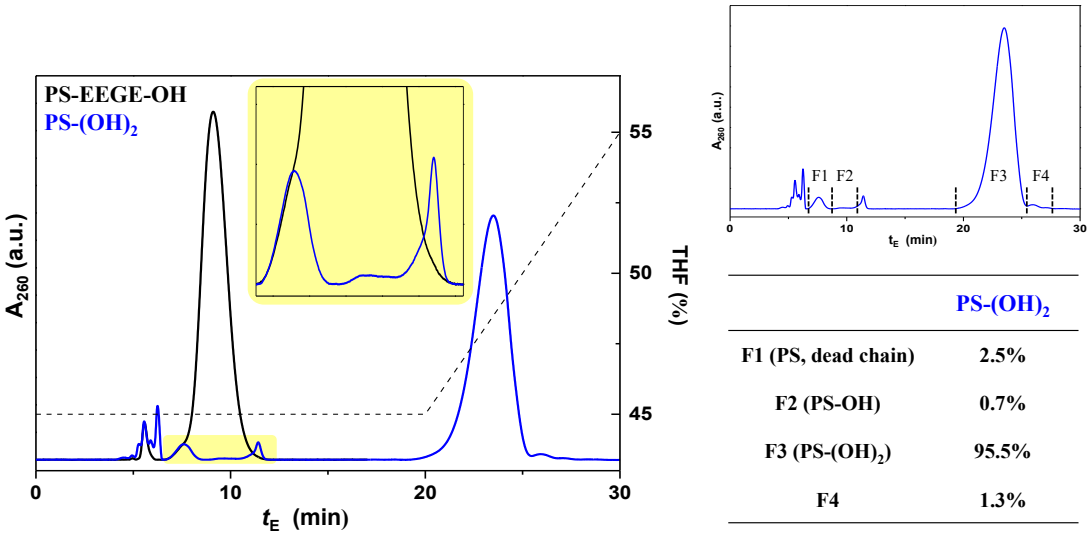

	PS-(OH)$_2$
F1 (PS, dead chain)	2.5%
F2 (PS-OH)	0.7%
F3 (PS-(OH)$_2$)	95.5%
F4	1.3%

Figure 5. Overlay of HPLC chromatograms of PS-EEGE-OH and PS-(OH)$_2$ (left); Overview of the different fractions in the PS-(OH)$_2$ sample (right).

In case of the esterification reaction of PS-OH with succinic anhydride, small traces of non-functionalized chains (< 0.2%) and PS-OH precursor (2.1%) are observed in the chromatogram of PS-COOH (Figure S7). However, nearly all (97.7%) hydroxyl groups undergo the targeted esterification reaction, which is remarkable for a post-polymerization reaction and proves excellent addressability of the hydroxy functionality.

CONCLUSION

This study relies on the SGIC-method to shed light on the end-capping efficiency of the well-known epoxide termination strategy for anionic polymerization, using PS-Li in combination with EO and two glycidyl ethers EEGE and IGG. End-capping efficiency has been quantified with unprecedented precision via solvent gradient interaction chromatography. A chain-end functionalization of > 99% with EO and > 95% with EEGE and IGG was observed, and all occurring side-reactions could be quantified. The ensuing deprotection efficiency of the acetal and ketal groups was determined to be > 99% by HPLC. Traces of unfunctionalized PS were observed. Functionalization of PS-OH with succinic anhydride showed a conversion of 98% of the hydroxyl groups to the carboxylic acid moiety. All results are in line with NMR measurements.

In summary, these results clearly demonstrate the power of SGIC to determine end-capping and deprotection efficiency at polymer chains. Our observations further highlight the advantage of carbanionic polymerization over widely used controlled radical polymerization techniques (84-91% end group functionality) concerning the introduction of functional groups at the chain end, which is of crucial importance for the synthesis of block copolymers or complex polymer architectures in general.

REFERENCES

(1) Hadjichristidis, N.; Pitsikalis, M.; Pispas, S.; Iatrou, H. Polymers with complex architecture by living anionic polymerization. *Chem. Rev.* **2001**, *101*, 3747–3792.

(2) Hadjichristidis, N.; Hirao, A., Eds. Anionic Polymerization: Principles, Practice, Strength, Consequences and Applications, 1st ed. 2015; Springer Japan: Tokyo, **2015**.

(3) Elkins, C. L.; Viswanathan, K.; Long, T. E. Synthesis and Characterization of Star-Shaped Poly(ethylene-*co*-propylene) Polymers Bearing Terminal Self-Complementary Multiple Hydrogen-Bonding Sites. *Macromolecules* **2006**, *39*, 3132–3139.

(4) Hirao, A.; Matsuo, Y.; Oie, T.; Goseki, R.; Ishizone, T.; Sugiyama, K.; Gröschel, A. H.; Müller, A. H. E. Facile Synthesis of Triblock Co- and Terpolymers of Styrene, 2-Vinylpyridine, and Methyl Methacrylate by a New Methodology Combining Living Anionic Diblock Copolymers with a Specially Designed Linking Reaction. *Macromolecules* **2011**, *44*, 6345–6355.

(5) Lee, I.; Bates, F. S. Synthesis, Structure, and Properties of Alternating and Random Poly(styrene-*b*-butadiene) Multiblock Copolymers. *Macromolecules* **2013**, *46*, 4529–4539.

(6) Touris, A.; Lee, S.; Hillmyer, M. A.; Bates, F. S. Synthesis of Tri- and Multiblock Polymers with Asymmetric Poly(ethylene oxide) End Blocks. *ACS Macro Lett.* **2012**, *1*, 768–771.

(7) Quirk, R. P.; Ma, J.-J. Characterization of the functionalization reaction product of poly(styryl)lithium with ethylene oxide. *J. Polym. Sci. A Polym. Chem.* **1988**, *26*, 2031–2037.

(8) Quirk, R. P.; Mathers, R. T.; Wesdemiotis, C.; Arnould, M. A. Investigation of Ethylene Oxide Oligomerization during Functionalization of Poly(styryl)lithium Using MALDI−TOF MS and NMR. *Macromolecules* **2002**, *35*, 2912–2918.

(9) Quirk, R. P.; Lizárraga, G. M. Investigation of the Reaction of Poly(styryl)lithium with Propylene Oxide. *Macromolecules* **1998**, *31*, 3424–3430.

(10) Quirk, R. P.; Ge, Q.; Arnould, M. A.; Wesdemiotis, C. Functionalization of Poly(styryllithium) with 1-Butene Oxide. *Macromol. Chem. Phys.* **2001**, *202*, 1761–1767.

(11) Tonhauser, C.; Wilms, D.; Wurm, F.; Nicoletti, E. B.; Maskos, M.; Löwe, H.; Frey, H. Multihydroxyl-Functional Polystyrenes in Continuous Flow. *Macromolecules* **2010**, *43*, 5582–5588.

(12) Quirk, R. P.; Contractor, A.; Polce, M. J.; Wesdemiotis, C. Functionalization and Linking Chemistry of Poly(styryl)lithium with 1,3-Butadiene Diepoxide. *Macromol. Chem. Phys.* **2006**, *207*, 2280–2288.

(13) Quirk, R. P.; Hasegawa, H.; Gomochak, D. L.; Wesdemiotis, C.; Wollyung, K. Functionalization of Poly(styryl)lithium with Styrene Oxide. *Macromolecules* **2004**, *37*, 7146–7155.

(14) Quirk, R. P.; Ocampo, M.; Polce, M. J.; Wesdemiotis, C. Functionalization of Poly(styryl)lithium with Thiiranes: Sulfur Extrusion vs Ring-Opening Mechanisms. *Macromolecules* **2007**, *40*, 2352–2360.

(15) Park, S.; Cho, D.; Ryu, J.; Kwon, K.; Chang, T.; Park, J. Temperature gradient interaction chromatography and matrix-assisted laser desorption/ionization time-of-flight mass spectrometry analysis of air terminated polystyryllithium. *Journal of Chromatography A* **2002**, *958*, 183–189.

(16) Quirk, R. P.; Yin, J.; Fetters, L. J. Carbonation and related reactions of poly(styryl)lithium. *Macromolecules* **1989**, *22*, 85–90.

(17) Ueda, K.; Hirao, A.; Nakahama, S. Synthesis of polymers with amino end groups. 3. Reactions of anionic living polymers with α-halo-ι-aminoalkanes with a protected amino functionality. *Macromolecules* **1990**, *23*, 939–945.

(18) Quirk, R. P.; Kuang, J. Anionic synthesis and characterization of ω-formyl-functionalized polystyrenes. *Polymer International* **1994**, *33*, 181–186.

(19) Quirk, R. P.; Kim, J. Anionic synthesis of model ionomers: ι-lithium poly(styrene)sulfonates. *Macromolecules* **1991**, *24*, 4515–4522.

(20) Hillmyer, M. A.; Bates, F. S. Synthesis and Characterization of Model Polyalkane−Poly(ethylene oxide) Block Copolymers. *Macromolecules* **1996**, *29*, 6994–7002.

(21) Quirk, R. P.; Kim, J.; Rodrigues, K.; Mattice, W. L. Anionic synthesis and characterization of poly(styrene-block-ethylene oxide) polymers with fluorescent probes at the block junctions. Makromolekulare Chemie. *Macromolecular Symposia* **1991**, *42-43*, 463–473.

(22) Bailey, T. S.; Pham, H. D.; Bates, F. S. Morphological Behavior Bridging the Symmetric AB and ABC States in the Poly(styrene-*b*-isoprene-*b*-ethylene oxide) Triblock Copolymer System. *Macromolecules* **2001**, *34*, 6994–7008.

(23) Schmidt, S. C.; Hillmyer, M. A. Synthesis and Characterization of Model Polyisoprene−Polylactide Diblock Copolymers. *Macromolecules* **1999**, *32*, 4794–4801.

(24) Zalusky, A. S.; Olayo-Valles, R.; Wolf, J. H.; Hillmyer, M. A. Ordered nanoporous polymers from polystyrene-polylactide block copolymers. *J. Am. Chem. Soc.* **2002**, *124*, 12761–12773.

(25) Vora, A.; Wojtecki, R. J.; Schmidt, K.; Chunder, A.; Cheng, J. Y.; Nelson, A.; Sanders, D. P. Development of polycarbonate-containing block copolymers for thin film self-assembly applications. *Polym. Chem.* **2016**, *7*, 940–950.

(26) Thomas H. Epps, III; O'Reilly, R. K. Block copolymers: Controlling nanostructure to generate functional materials – synthesis, characterization, and engineering. *Chem. Sci.* **2016**, *7*, 1674–1689.

(27) Bates, C. M.; Bates, F. S. 50th Anniversary Perspective: Block Polymers—Pure Potential. *Macromolecules* **2016**, *50*, 3–22.

(28) Ketkar, P. M.; Shen, K.-H.; Hall, L. M.; Epps, T. H. Charging toward improved lithium-ion polymer electrolytes: exploiting synergistic experimental and computational approaches to facilitate materials design. *Mol. Syst. Des. Eng.* **2019**, *4*, 223–238.

(29) Richards, D. H.; SZWARC, M. Block polymers of ethylene oxide and its analogues with styrene. *Trans. Faraday Soc.* **1959**, *55*, 1644.

(30) Quirk, R. P.; Cheong, T.-H.; Jiang, K.; Gomochak, D. L.; Yoo, T.; Andes, K. T.; Mathers, R. T. Recent advances in the anionic synthesis of chain-end functionalized polymers. *Macromol. Symp.* **2003**, *195*, 69–74.

(31) Tonhauser, C.; Frey, H. A road less traveled to functional polymers: epoxide termination in living carbanionic polymer synthesis. *Macromolecular rapid communications* **2010**, *31*, 1938–1947.

(32) Chang, T. Polymer characterization by interaction chromatography. *Journal of Polymer Science Part B: Polymer Physics* **2005**, *43*, 1591–1607.

(33) Jiang, X.; Schoenmakers, P. J.; van Dongen, J. L. J.; Lou, X.; Lima, V.; Brokken-Zijp, J. Mass spectrometric characterization of functional poly(methyl methacrylate) in combination with critical liquid chromatography. *Anal. Chem.* **2003**, *75*, 5517–5524.

(34) Pasch, H.; Deffieux, A.; Ghahary, R.; Schapacher, M.; Rique-Lurbet, L. Analysis of Macrocyclic Polystyrenes. 2. Mass Spectrometric Investigations. *Macromolecules* **1997**, *30*, 98–104.

(35) Muscat, D.; Henderickx, H.; Kwakkenbos, G.; van Benthem, R.; Koster, C. G. de; Fokkens, R.; Nibbering, N. M. M. In-source decay of hyperbranched polyesteramides in matrix-assisted laser desorption/ionization time-of-flight mass spectrometry. *Journal of the American Society for Mass Spectrometry* **2000**, *11*, 218–227.

(36) Guo, R.; Shi, Z.; Wang, X.; Dong, A.; Zhang, J. Separation and quantification of dead species in styrene RAFT polymerization by gradient polymer elution chromatography. *Polym. Chem.* **2012**, *3*, 1314–1321.

(37) Gao, H.; Louche, G.; Sumerlin, B. S.; Jahed, N.; Golas, P.; Matyjaszewski, K. Gradient Polymer Elution Chromatographic Analysis of α,ω-Dihydroxypolystyrene Synthesized via ATRP and Click Chemistry. *Macromolecules* **2005**, *38*, 8979–8982.

(38) Pohlit, H.; Worm, M.; Langhanki, J.; Berger-Nicoletti, E.; Opatz, T.; Frey, H. Silver Oxide Mediated Monotosylation of Poly(ethylene glycol) (PEG): Heterobifunctional PEG via Polymer Desymmetrization. *Macromolecules* **2017**, *50*, 9196–9206.

(39) Kim, K.; Ahn, J.; Park, M.; Lee, H.; Kim, Y. J.; Chang, T.; Jeon, H. B.; Paik, H.-j. Molecular-Weight Distribution of Living Chains in Polystyrene Prepared by Reversible Addition–Fragmentation Chain-Transfer Polymerization. *Macromolecules* **2019**, *52*, 7448–7455.

(40) Oh, J.; Kuk, J.; Lee, T.; Ye, J.; Paik, H.-j.; Lee, H. W.; Chang, T. Molecular Weight Distribution of Living Chains in Polystyrene Prepared by Atom Transfer Radical Polymerization. *ACS Macro Lett.* **2017**, *6*, 758–761.

(41) Wurm, F.; Nieberle, J.; Frey, H. Synthesis and Characterization of Poly(glyceryl glycerol) Block Copolymers. *Macromolecules* **2008**, *41*, 1909–1911.

(42) Ferruti, P.; Tanzi, M. C.; Rusconi, L.; Cecchi, R. *Makromol. Chem.* **1981**, *182*, 2183–2192.

(43) Hans, M.; Keul, H.; Moeller, M. Chain transfer reactions limit the molecular weight of polyglycidol prepared via alkali metal based initiating systems. *Polymer* **2009**, *50*, 1103–1108.

SUPPORTING INFORMATION

Experimental Part

Reagents

All reagents were purchased either from Acros Organics, Roth, Fischer Chemical or VWR Chemicals unless otherwise noticed. Chloroform-*d* was purchased from Deutero GmbH. Ethylene oxide (EO) was purchased from Air Liquide. Cyclohexane was dried with *sec*-BuLi/DPE, degassed and freshly distilled into the reaction flask for each polymerization. Ethoxy ethyl glycidyl ether (EEGE) was synthesized from glycidol and ethyl vinyl ether according to Fitton et al.[1] Isopropylidene glyceryl glycidyl ether (IGG) was synthesized from epichlorohydrin and 2,2-dimethyl-4-hydroxymethyl-1,3-dioxolane, according to Frey et al.[2] EEGE and IGG were purified by fractional distillation. Succinic anhydride was recrystallized from THF before usage. Styrene was flushed through basic aluminum oxide before usage.

Instrumentation

^{1}H NMR spectra were recorded on a Bruker Avance III HD 400 spectrometer with 400 MHz and referenced internally to residual proton signals of the deuterated solvent.

SEC measurements were performed with THF as the mobile phase (flow rate 1 mL min^{-1}) on an SDV column set from PSS (SDV 103, SDV 105, SDV 106) at 30 °C. Polymer concentrations were 1 mg mL^{-1}. Calibration was carried out using polystyrene standards (from Polymer Standard Service, Mainz).

For HPLC analysis, a bare silica column (Agilent Zorbax SIL, 5 μm, 80 Å, 250 × 4.6 mm) was used. The mobile phase was a THF/*n*-hexane mixture delivered by an HPLC pump (Shimadzu LC-20AD) at a flow of 0.6 mL min^{-1}. The column temperature was kept at 10 °C using a homemade column jacket and a water bath circulator (JulaboF25). Chromatograms were recorded with a UV/Vis absorption detector (Younglin UV730D). All samples for HPLC analysis were dissolved in the eluent at 1 mg mL^{-1} and the injection volume was 100 μL. For the solvent gradient elutions, the eluent composition was kept at 50/50 vol% for the first 20 min and then changed linearly to 75% THF for the next 30 min.

End-Capping of PS-Li with epoxides

The following procedure was adapted for the synthesis of PS-EEGE-OH. PS-OH and PS-IGG-OH were synthesized in the same manner but EO or IGG was used instead of EEGE. Styrene (4.55 g, 5.00 mL, 0.43 mol) was dried over fine-powdered CaH_2 for one day, degassed by three cycles of freeze-thaw and transferred under high vacuum (10^{-3} mbar) in a flask connected to a Schlenk line and equipped with a stopcock and a septum. Dry cyclohexane (25 mL) was added via distillation under high vacuum. The flask was flushed with argon and *sec*-BuLi (1.3 M stock solution in cyclohexane/*n*-hexane, 0.24 mL, 0.31 mmol) was added through the septum with a syringe under vigorous stirring. The orange solution was heated at 40 °C and stirred for 2.5 h. After

cooling to room temperature, the flask was evacuated by repeated opening of the stopcock to the vacuum line. EEGE (280 mg, 280 μL, 1.94 mmol) was dried with sec-BuLi (1.3 M stock solution in cyclohexane/*n*-hexane, 0.08 mL, 0.11 mmol), degassed and transferred to the living polymer solution via cryo-distillation. After stirring for 2 h at room temperature, the polymerization was quenched with degassed MeOH (100 μL). The polymer was purified by precipitation of the reaction solution in a ten-fold excess of MeOH/i-PrOH (1:1) and repeated precipitation from DCM in a ten-fold excess of MeOH. PS-EEGE-OH was dried under high vacuum for several days.

PS-OH: ^{1}H NMR ($CDCl_3$), δ (ppm): 7.19-6.15 (m (broad), H_{ar}), 3.30 (m (broad), H_a), 2.50-0.71 (m (broad), H_b-H_d), 0.71-0.44 (m, H_e+H_f).

PS-EEGE-OH: 1H NMR (CD_2Cl_2), δ (ppm): 7.45-6.27 (m (broad), H_{ar}), 4.58 (m, H_h), 3.60-3.00 (m (broad, H_a+H_g+H_j), 2.60-0.83 (m (broad), H_b-H_d), 1.22 (d (broad), H_i), 1.13 (t (broad), H_k), 0.83-0.56 (m (broad), H_e+H_f).

PS-IGG-OH: 1H NMR (CD_2Cl_2), δ (ppm): 7.45-6.27 (m (broad), H_{ar}), 4.18 (m (broad), H_i), 4.07-3.02 (m (broad), H_a+H_g+H_h+H_j), 2.60-0.83 (m (broad), H_b-H_d), 1.10 (s, H_k+H_l), 0.83-0.56 (m (broad), H_e+H_f).

Deprotection of PS-EEGE-OH and PS-IGG-OH

The following procedure was adapted for the deprotection of PS-EEGE-OH. PS-IGG-OH was deprotected in the same manner. PS-EEGE-OH (2.00 g, 130 μmol) was dissolved in THF (40 mL) in a flask equipped with a condenser. the solution was treated with 2N HCl (6 mL) and stirred under reflux for one day. THF was evaporated and the residue was dissolved in $CHCl_3$. The solution was extracted with saturated $NaHCO_3$ (50 mL) and Brine (50 mL). The organic phase was dried over $MgSO_4$, filtered and concentrated to around 25 mL. The polymer was precipitated in an excess of MeOH to yield PS-$(OH)_2$.

PS-$(OH)_2$: ^{1}H NMR ($CDCl_3$), δ (ppm): 7.19-6.15 (m (broad), H_{ar}), 3.56-3.13 (m (broad), H_a+H_g), 2.50-0.71 (m (broad), H_b-H_d), 0.71-0.44 (m, H_e+H_f).

PS-$(OH)_3$: ^{1}H NMR ($CDCl_3$), δ (ppm): 7.19-6.15 (m (broad), H_{ar}), 3.90-3.04 (m (broad), H_a+H_g-H_j), 2.50-0.71 (m (broad), H_b-H_d), 0.71-0.44 (m, H_e+H_f).

Functionalization of PS-OH

PS-OH (7.00 g, 470 μmol) was added to a flame-dried round bottom flask equipped with a stir bar and condenser, dissolved in benzene and freeze-dried overnight. Succinic anhydride (470 mg, 4.70 mmol) was added and the mixture was dissolved in dry DCM (30 mL). Dry pyridine (370 mg, 380 μL, 4.70 mmol) was added and the solution was heated under reflux and argon for one week. The reaction was quenched with DCM (470 mL) and extracted with saturated Na_2CO_3 (100 mL, two times), 0.1 N HCl (100 mL, two times) and Brine (100 mL). The organic phase was dried over $MgSO_4$ and the solvent was evaporated after filtration to yield PS-COOH.

PS-COOH: ^{1}H NMR ($CDCl_3$), δ (ppm): 7.19-6.15 (m (broad), H_{ar}), 3.96-3.62 (m (broad), H_a), 2.64-2.33 (m (broad), H_g+H_h), 2.33-0.71 (m (broad), H_b-H_d), 0.71-0.44 (m, H_e+H_f).

Additional Spectra

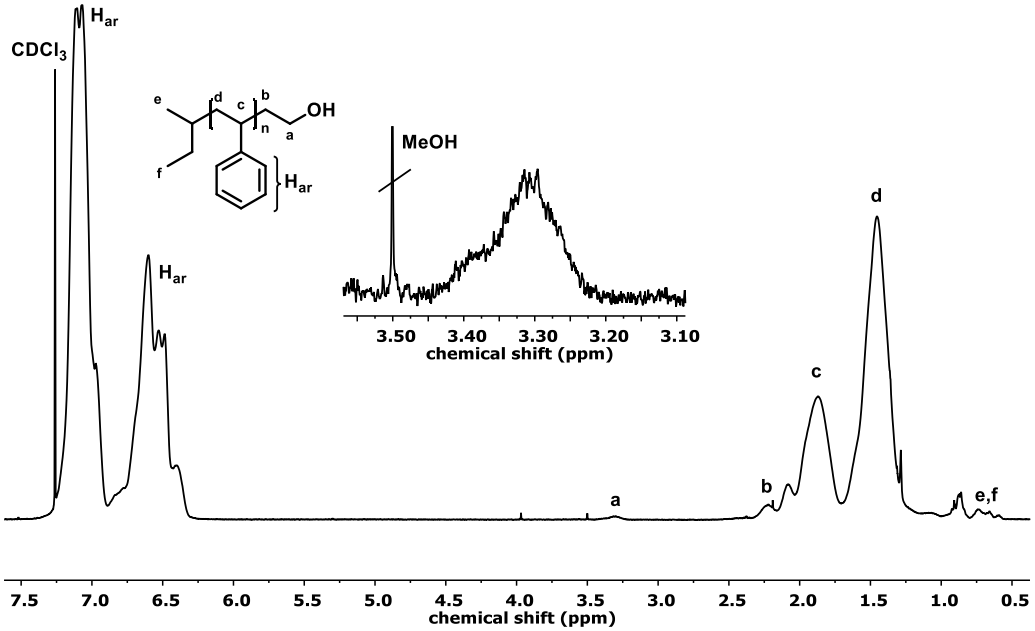

Figure S1. ^{1}H NMR spectrum ($CDCl_3$, 400 MHz) of PS-OH.

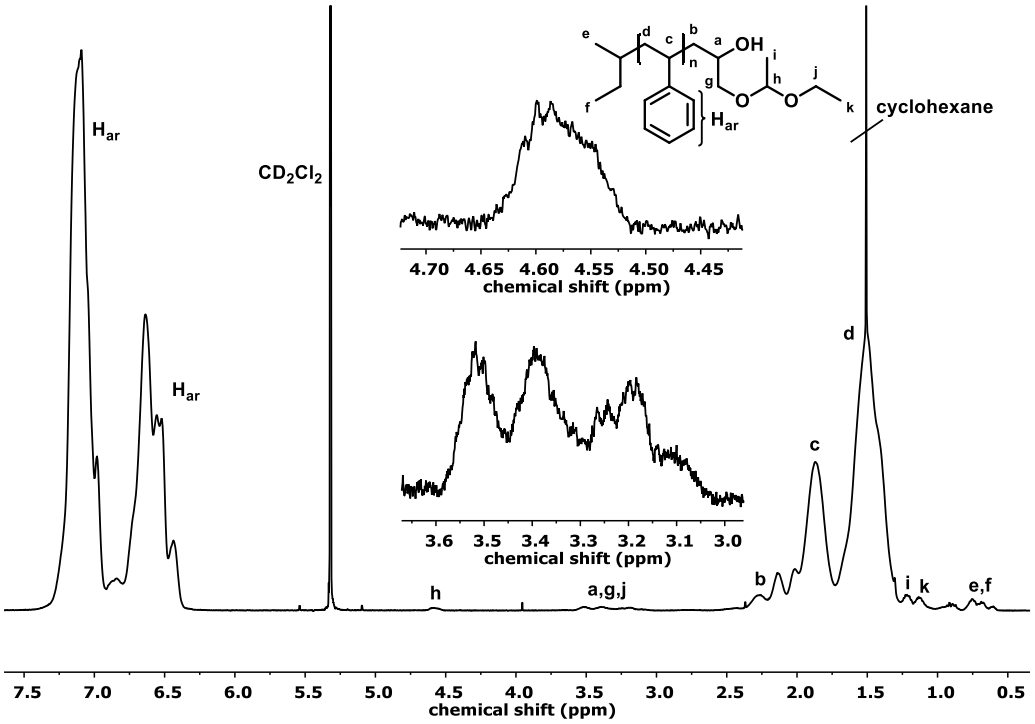

Figure S2. ^{1}H NMR spectrum (CD_2Cl_2, 400 MHz) of PS-EEGE-OH.

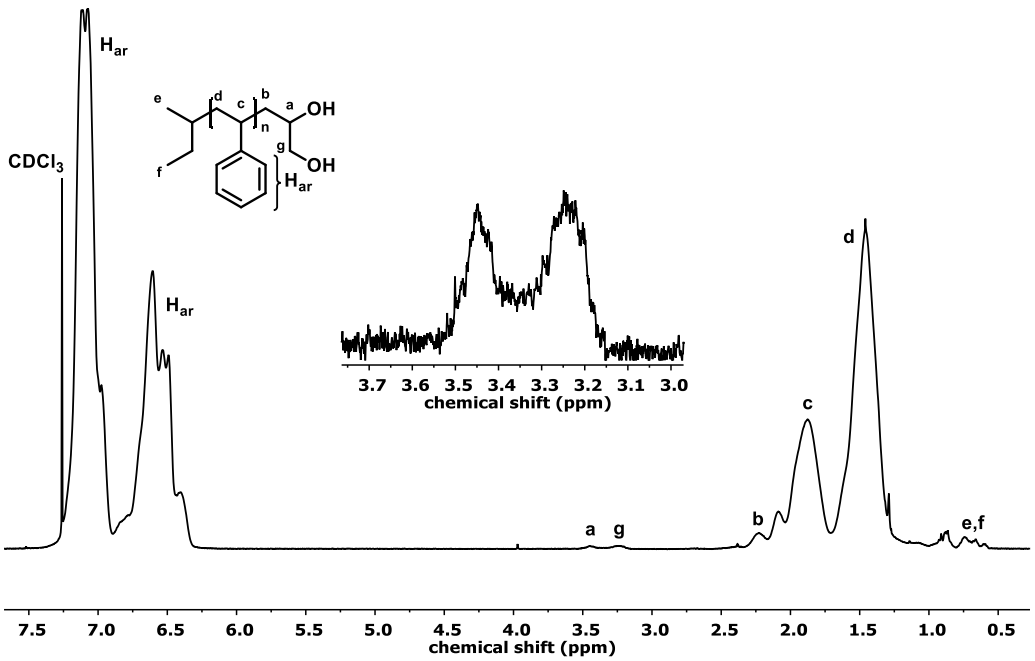

Figure S3. ^{1}H NMR spectrum ($CDCl_3$, 400 MHz) of PS-$(OH)_2$.

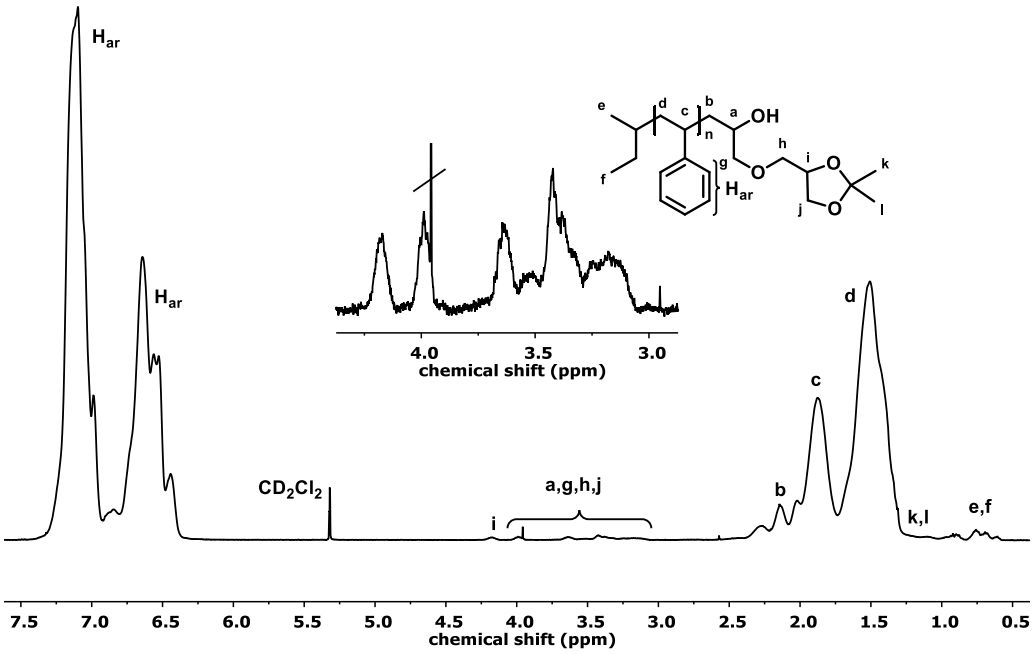

Figure S4. ^{1}H NMR spectrum (CD_2Cl_2, 400 MHz) of PS-IGG-OH.

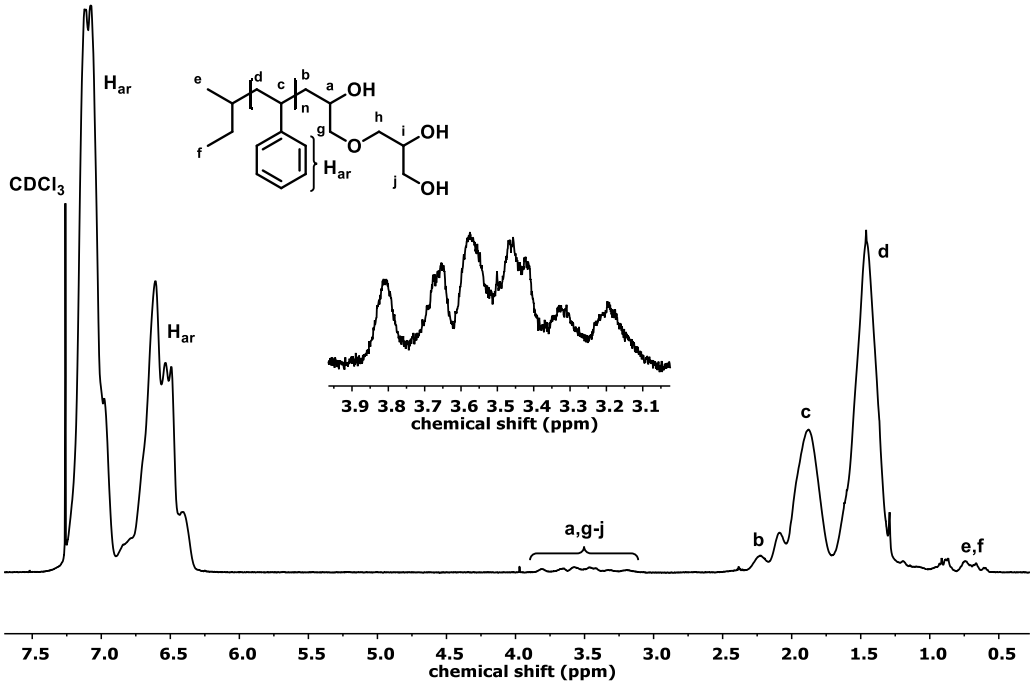

Figure S5. ^{1}H NMR spectrum ($CDCl_3$, 400 MHz) of PS-$(OH)_3$.

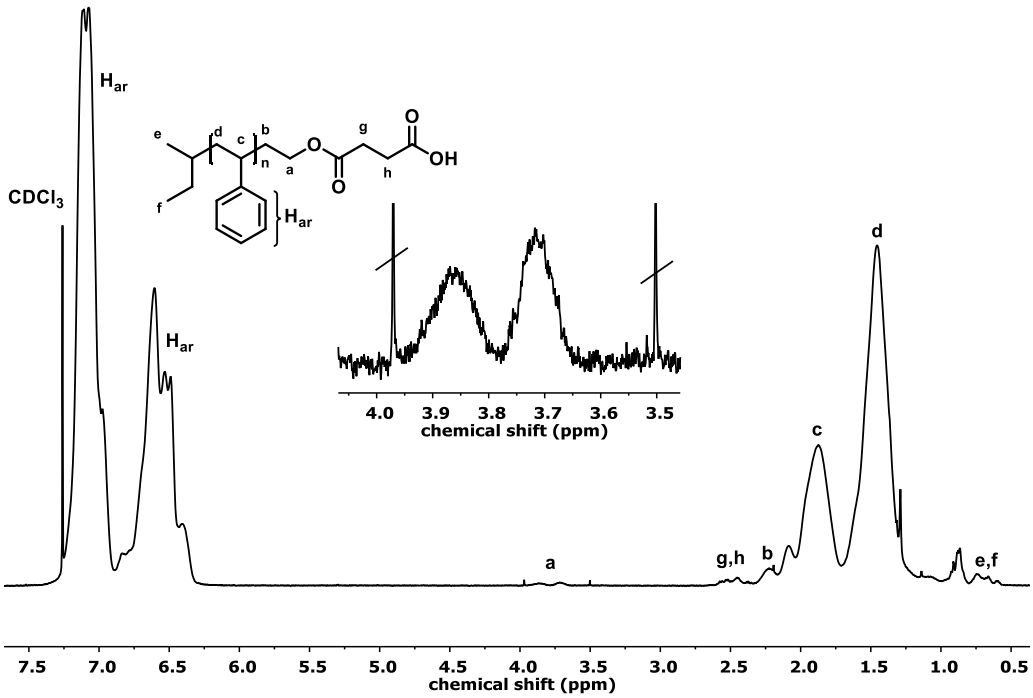

Figure S6. ^{1}H NMR spectrum ($CDCl_3$, 400 MHz) of PS-COOH.

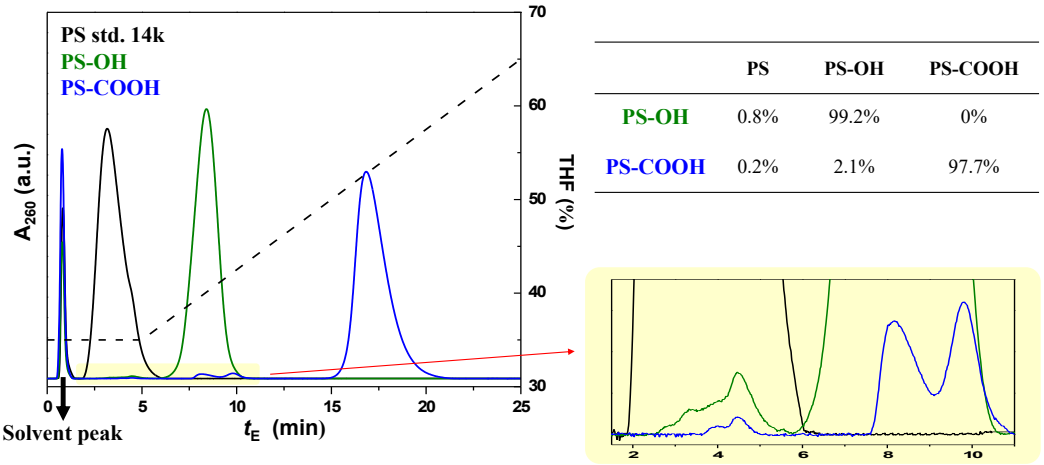

	PS	PS-OH	PS-COOH
PS-OH	0.8%	99.2%	0%
PS-COOH	0.2%	2.1%	97.7%

Figure S7. Overlay of HPLC chromatograms of PS standard, PS-OH and PS-COOH (left); Zoom in (bottom right); Overview of the different fractions in the PS-OH and PS-COOH sample (top right). Experimental conditions: bare silica column (Macherey-Nagel Nucleosil diol, 5 μm, 100 Å, 100 × 2.1 mm); flow rate of 0.6 mL min^{-1} at the column temperature of 5 °C; the eluent composition was kept at 35/65%$_{vol}$ THF/*n*-hexane for the first 5 min and then changed linearly to 65% THF for the next 20 min.

REFERENCES

(1) Fitton, A. O.; Hill, J.; Jane, D. E.; Millar, R. Synthesis of Simple Oxetanes Carrying Reactive 2-Substituents. *Synthesis* **1987**, 1140–1142.

(2) Wurm, F.; Nieberle, J.; Frey, H. Synthesis and Characterization of Poly(glyceryl glycerol) Block Copolymers. *Macromolecules* **2008**, *41*, 1909–1911.

Chapter 3.2

Introduction of Multiple Charged Trifluoromethanesulfonamide Groups into Poly(ethylene oxide) Blocks of Polystyrene-Poly(ethylene oxide) Block Copolymer Electrolytes via the Mitsunobu Reaction

Philip Dreier[†], Robin Mathes[†] and Holger Frey[*,†]

[†]**Department of Chemistry, Johannes Gutenberg University Mainz, Germany**

ABSTRACT: Single ion-conducting polymer electrolytes (SICPE) based on polystyrene and poly(ethylene oxide) block copolymers (PS-*b*-PEO) are promising materials due to their combination of high stability and exclusive current transport via lithium cations. However, the incorporation of covalently attached anions into the flexible polyether block remains a synthetic challenge. For this purpose, a polystyrene-multifunctional poly(ethylene oxide) block copolymer precursor (M_n = 15.1 kg mol^{-1}, $Đ$ = 1.09) with randomly distributed multiple hydroxyl functional groups (6 %$_{mol}$) in the polyether block was synthesized by the combination of living carbanionic and anionic ring-opening polymerization (AROP). First, living polystyryl lithium was end-functionalized with ethylene oxide (EO). Subsequently, AROP of EO and ethoxy vinyl glycidyl ether (EVGE) was initiated by an alkoxide-functional polystyrene macroinitiator, followed by deprotection of the vinyl ether groups. A novel post-polymerization Mitsunobu reaction was employed to quantitatively substitute the hydroxyl groups with *tert*-butyloxycarbonyl (BOC)-protected trifluoromethanesulfonamide (TFSA) functionalities, monitored via detailed NMR, IR and SEC characterization. DSC measurements show a strong dependence of the glass transition and melting temperature of the PEO block on the structure of the functional group. Further deprotection and deprotonation of the TFSA groups were conducted to yield the underlying SICPE material with a salt concentration of r = 0.06. DSC measurements reveal a fully amorphous polyether block with thermal properties ($T_{g,PEO}$ = -37 °C) comparable to lithium salt-doped PS-*b*-PEO. The investigated material combines high PEO chain flexibility and absence of crystallinity, necessary for high room temperature conductivity, while retaining the advantageous features of a block copolymer-based SICPE.

INTRODUCTION

Poly(ethylene oxide) (PEO) is a well-known matrix polymer for the dissolution of alkali metal salts.[1] The high flexibility of the polyether chains permits a helical conformation of the oxygens around the alkali metal cations, which results in a favorable interaction between PEO and the respective salt.[2] This behavior renders PEO a suitable and safer alternative to common liquid electrolytes in lithium-ion batteries or even lithium metal batteries. Commonly used salts for this purpose are lithium triflate (LiTf) and lithium bis(trifluoromethanesulfonyl)imide (LiTFSI). Even though the conductivity of PEO-lithium salt mixtures reaches values of 10^{-3} S cm^{-1} above the melting temperature of PEO ($T_{m,PEO} \approx 60$ °C), the semi-crystalline nature of PEO leads to low conductivity at room temperature.[3] In numerous works, a variety of modifications of PEO was implemented to increase the ionic conductivity of the polymer electrolyte. Most commonly, an increase in conductivity of several orders of magnitude at room temperature is observed in PEO-based polymer electrolytes upon introduction of side chains at the PEO backbone.[4–6] This can for instance be achieved by the copolymerization of ethylene oxide (EO) with different epoxide comonomers.[7] In this case incorporation of side-chains gradually decreases the degree of crystallization of PEO and leads to amorphous materials at a certain comonomer concentration.[4,5] Unfortunately, a decrease of the degree of crystallization is also accompanied by deterioration of the mechanical properties of the material, leading to dendritic growth of lithium through the electrolyte matrix during charge-discharge cycles. The undesired dendritic growth can be minimized by the combination of PEO with mechanically stable (i.e., high T_g) materials, e.g., polystyrene (PS), to block copolymer (BCP) structures. Herein, the nature of the microphase separation of BCPs in well-defined microstructures[8,9] determines the conductive pathways for lithium cations, while the mechanical properties of the material are governed by the PS block. In this context, lithium salt-doped PS-*b*-PEO based BCPs represent one of the most intensely studied systems at present (Figure 1).[10–12]

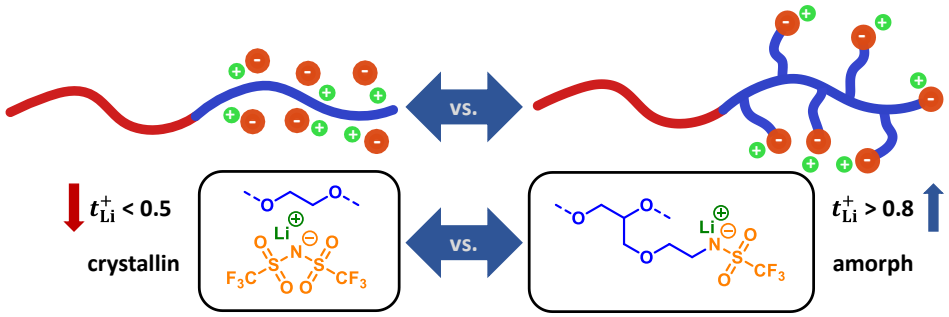

Figure 1. Comparison of established PS-b-PEO-based SPE in literature (left) and employed SICPE in this study (right).

In recent years, the interest in so called single-ion conducting polymer electrolytes (SICPE) increased constantly, mainly because of their exceptionally high lithium transference number (t^+).[13] In SICPEs, the counter anion of the lithium cation is covalently attached to the polymer and therefore its mobility is connected to the segmental motion of the polymer. As a result, the

charge is almost exclusively transported by the lithium cations, and undesirable concentration polarization is reduced.[14] In comparison to SICPEs, t^+ values lower than 0.5 are observed in PEO lithium salt-mixtures[15] because of the preferred solvation of lithium cations relative to the bulky anion by the oxygens of the polyether.[16] The negative charge of the attached anions in SICPEs should lead to a high delocalization, i.e. a Tf^- or $TFSI^-$ structure, to permit sufficient separation of the lithium cations from the counter anion.[14] SICPE BCPs are most commonly based on PEO macroinitiators and synthesized via controlled radical polymerization of negatively charged monomers or by the introduction of charges via post-polymerization reactions.[13] As result, the charged groups are localized in the glassy domains, which leads to insulating characteristics at room temperature and insufficient conductivity at elevated temperatures because of mixing between the conductive and the insulating (high T_g) domains.[14] Although several attempts have been reported to date to incorporate anions into the conductive blocks of SICPE BCPs,[17] the well-defined synthesis of these materials remains elusive. To the best of our knowledge, covalent attachment of multiple negatively charged trifluoromethanesulfonamide (TFSA) groups in the polyether block of PS-*b*-PEO structures has not been reported to date. Overcoming this synthesis predicament, the Mitsunobu reaction is employed as a key synthesis step for the incorporation of protected TFSA groups in the polyether block of polystyrene-*block*-poly(ethylene oxide-*co*-hydroxyethyl glycidyl ether) (PS-*b*-P(EO-*co*-HEGE)). Additionally, a detailed synthesis protocol was elaborated for the deprotection and deprotonation of the TFSA groups to achieve the desired SICPE material. The thermal properties of the latter are further compared to its established salt-doped analogues.

RESULTS AND DISCUSSION

Synthesis of BOC-protected trifluoromethanesulfonamide

In Mitsunobu reactions, a suitable pK_a value of the pronucleophile below 11 is necessary to achieve quantitative protonation of the betaine and consequently high product yields without undesired side reactions.[18] Although primary sulfonamides already possess suitable pK_a values, they are known for their side reaction to phosphine imides under typical Mitsunobu reaction conditions.[19] Fortunately, this side reaction can be suppressed by monoacylation or alkylation of the primary sulfonamide.[20] Additionally, *N*-acylation further decreases the pK_a values of the corresponding sulfonamides[21] which renders them efficient pronucleophiles for Mitsunobu reactions.[18] Based on this rationale, *tert*-butyl ((trifluoromethyl)sulfonyl) carbamate (BTFSA) was utilized as a suitable sulfonamide for the post-polymerization Mitsunobu reaction (PPMR). The *tert*-butyloxycarbonyl (BOC) protection group was chosen because of its facile cleavage under acidic conditions[22] or thermolysis.[20] BTFSA was synthesized via the mono acetylation of trifluoromethanesulfonamide with di-tert-butyl dicarbonate ($(BOC)_2O$) under basic catalysis in DCM (Scheme 1).

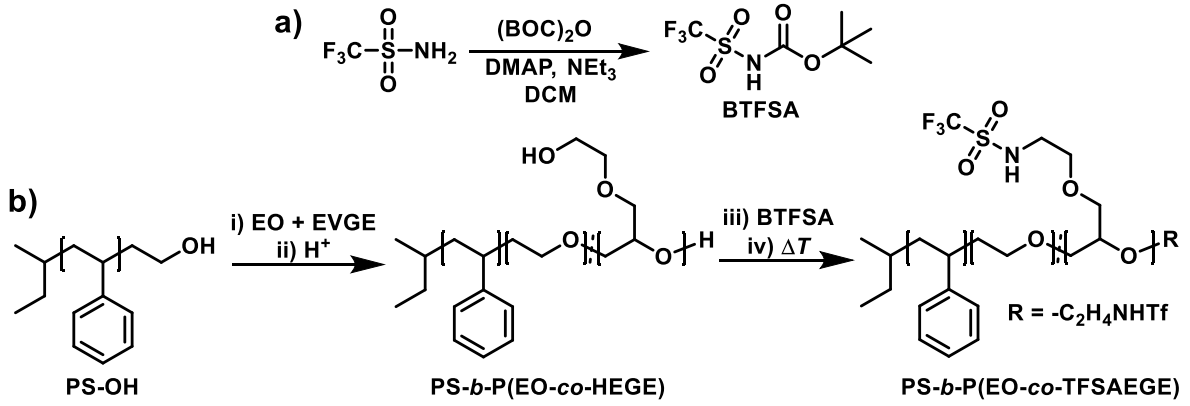

Scheme 1. a) Synthesis of *tert*-butyl ((trifluoromethyl)sulfonyl)carbamate (BTFSA); b) Synthesis route for the incorporation of TFSA groups into the polyether block.

The respective ^{1}H (Figure S1) and ^{13}C NMR spectra (Figure S2) of BTFSA show the corresponding signals for the protons (1.51 ppm) and carbons (147.11, 87.08 and 27.81 ppm) of the BOC protection group as well as the sulfonamide proton (7.49 ppm). Additionally, one distinct peak is observed in the ^{19}F NMR spectrum (Figure S3), confirming the absence of fluorinated impurities.

Synthesis of the Precursor Block Copolymer Structure

To achieve the desired BCP structure, the macroinitiator *ω*-hydroxy-polystyrene (PS-OH) was synthesized via the end-capping of living polystyryl lithium with ethylene oxide (EO) in cyclohexane.[23,24] The resulting SEC trace (Figure 2) shows a monomodal distribution and narrow polydispersity (*Đ*) at the desired molecular weight. A single, distinct distribution is observed in the MALDI-ToF mass spectrum (Figure S5), confirming quantitative functionalization of the PS chain end with EO.[24]

The following BCP synthesis and incorporation of multiple hydroxyl groups into the PEO block was achieved via copolymerization of EO with ethoxy vinyl glycidyl ether (EVGE) under AROP conditions, using PS-OH as a macroinitiator and subsequent deprotection of the vinyl ether groups of the EVGE repeating units under acidic conditions (Scheme 1).[25] The ^{1}H NMR spectrum of PS-*b*-P(EO-*co*-EVGE) (Figure S6) shows the corresponding peaks of the vinyl ether protons at 6.53, 4.21 and 4.02 ppm, while a content of 6 $\%_{mol}$ EVGE in the PEO block was determined, which is in accordance with the theoretical value. A single diffusion coefficient is observed for all PS-*b*-P(EO-*co*-EVGE) peaks in the DOSY NMR (Figure S8) and confirms the block formation.

Table 1. Overview of synthesized polymers.

Sample	$M_{n,NMR}$ [a)] [kg mol^{-1}]	$M_{n,SEC}$ [b)] [kg mol^{-1}]	Functionality [a)] [%$_{mol,PEO}$]	$Đ$ [b)]	f_{PEO} [a)]	$T_{g,PEO}$ [c)] [°C]	$T_{m,PEO}$ [c)] [°C]	$X_{c,PEO}$ [c)] [%]
PS-OH	8.6	8.2	-	1.05	-	-	-	-
PS-*b*-P(EO-*co*-EVGE)	15.4	16.9	6.0	1.10	0.39	-60	30	34
PS-*b*-P(EO-*co*-HEGE)	15.1	15.6	6.0	1.09	0.39	-59	30	33
PS-*b*-P(EO-*co*-BTFSAEGE)	17.3	17.8	6.0	1.14	0.39	-51	22	24
PS-*b*-P(EO-*co*-TFSAEGE)	16.4	17.1	6.0	1.12	0.39	.48	23	22
PS-*b*-P(EO-*co*-LiTFSAEGE)	16.5	17.5	6.0	1.13	0.39	-37	-	-

a) Determined via ^{1}H NMR spectroscopy; b) Determined via SEC (PS calibration); c) Determined via DSC.

The latter was also followed by SEC (Figure 2) with a clear shift of the SEC trace of PS-*b*-P(EO-*co*-EVGE) to lower elution volume relative to PS-OH. The total volume fraction of the PEO block (f_{PEO}) was estimated via ^{1}H NMR spectroscopy to be 0.39 (Table 1, Figure 2) based on the densities of PS and PEO reported in the literature.[26]

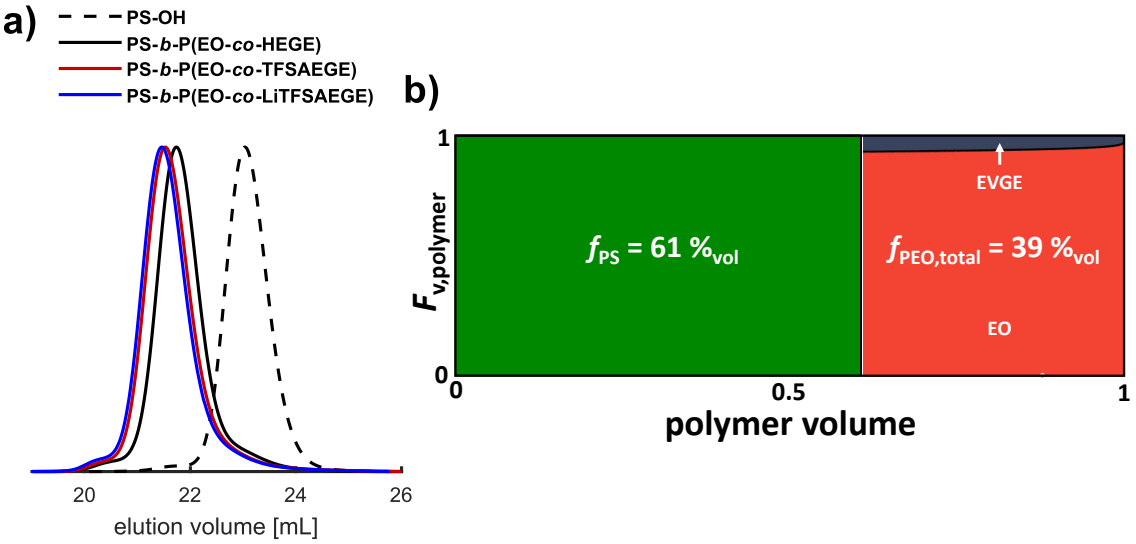

Figure 2. a) SEC traces (THF, PS calibration) of PS-OH, PS-*b*-P(EO-*co*-HEGE), PS-*b*-P(EO-*co*-TFSAEGE) and PS-*b*-P(EO-*co*-LiTFSAEGE); b) Composition profile according to volume fraction of PS-*b*-P(EO-*co*-EVGE).

Quantitative deprotection of the hydroxyl groups was achieved under acidic conditions and monitored by a shift of the SEC trace of PS-*b*-P(EO-*co*-HEGE) to higher elution volume relative to PS-*b*-P(EO-*co*-EVGE) and the disappearance of the vinyl protection group protons and carbons in the ^{1}H NMR (Figure S9) and ^{13}C NMR spectrum (Figure 3), respectively. The BCPs were obtained with low $Đ$ ranging from 1.09 to 1.10 and monomodal distributions (Table 1, Figure 2).

Introduction of Sulfonamide Groups via Post-Polymerization Mitsunobu Reaction

The substitution of the hydroxyl groups of PS-*b*-P(EO-*co*-HEGE) with BTFSA under Mitsunobu reaction conditions to PS-*b*-P(EO-*co*-BTFSAEGE) (Scheme 1) was monitored via IR spectroscopy (Figure S12). The disappearance of the OH band (3480 cm^{-1}) and the appearance of C=O and O=S=O bands of the incorporated TFSA groups are observable at 1755 and 1211 cm^{-1}, respectively. The resulting SEC trace of PS-*b*-P(EO-*co*-BTFSAEGE) (Figure S13) shows a slight shift to lower elution volume relative to PS-*b*-P(EO-*co*-HEGE). A conclusive interpretation of the substitution efficiency via ^{1}H NMR spectroscopy (Figure S10) is not possible because of an overlap of the resonances of the methylene group protons adjacent to the hydroxyl groups with the signal of the polyether backbone. However, quantitative determination of the substitution efficiency is feasible by ^{13}C NMR spectroscopy (Figure 3) because of the differing chemical shifts of the peaks corresponding to the methylene carbons next to the hydroxyl (61.83 ppm) and the BTFSA groups (48.14 ppm) at the side chains.

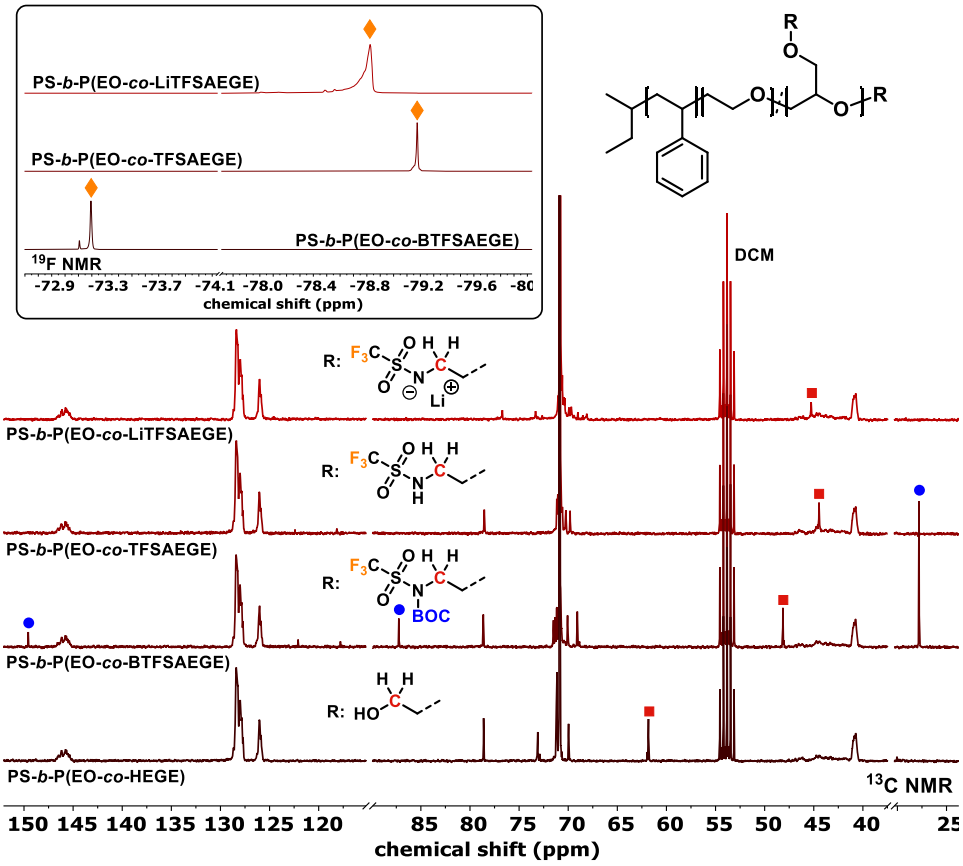

Figure 3. ^{13}C and ^{19}F NMR spectra (inset) of PS-*b*-P(EO-*co*-HEGE), PS-*b*-P(EO-*co*-BTFSAEGE), PS-*b*-P(EO-*co*-TFSAEGE) and PS-*b*-P(EO-*co*-LiTFSAEGE); BOC protection group (blue dots), fluorine atom (orange diamonds) and methylene carbon signals (red cubes) are highlighted.

After the PPMR, the signal of the methylene carbons adjacent to the hydroxyl groups completely disappeared, and new peaks of the BOC protection group carbons are present in the ^{13}C NMR

spectrum at 149.57 (*C*O), 87.24 (*C*(CH_3)$_3$) and 27.80 ppm (C(*C*H_3)$_3$). Additionally, two distinct resonances of the trifluoromethyl groups (side groups and ω-end group) are visible in the ^{19}F NMR spectrum (Figure 3). The mentioned observations confirm the quantitative introduction of BOC protected TFSA groups in the polyether block. To the best of our knowledge, Mitsunobu reactions have not been employed for post-functionalization of polymers until today. BOC protection groups were cleaved via thermolysis[20] in DMF. The ^{1}H (Figure S11) and ^{13}C NMR spectrum of the resulting PS-*b*-P(EO-*co*-TFSAEGE) (Figure 3) show a high-field shift of the methylene protons and carbons adjacent to the deprotected TFSA groups to 3.46 and 44.47 ppm, respectively, in accordance with the altered chemical environment. The ^{13}C NMR signals of the BOC protection groups disappeared, demonstrating complete deprotection. Additional evidence for the quantitative deprotection was observed via ^{19}F NMR spectroscopy (Figure 3) by the appearance of a distinct high-field shifted peak compared to the two peaks of the BOC protected species. Deprotection of the TFSA groups was further followed via IR spectroscopy (Figure S12) by the disappearance of the C=O band of the corresponding BOC protection groups at 1755 cm^{-1} and appearance of the N-H band (3510 cm^{-1}) of the free sulfonamide groups.

The described synthesis for the introduction and deprotection of TFSA groups was equally applied to the single hydroxyl end group of mPEO 5k as a model compound. For this structural model SEC, NMR and MALDI-ToF mass spectra (Figure S15-S18) further confirm a controlled and quantitative substitution of the hydroxyl group with BTFSA.

Introduction of Charges

In the final step of the synthesis sequence the TFSA groups of PS-*b*-P(EO-*co*-TFSAEGE) were deprotonated with lithium hydroxide to obtain PS-*b*-P(EO-*co*-LiTFSAEGE) (Scheme 2). After deprotonation of the acidic sulfonamide proton, the stability of the TFSA groups against base-catalyzed hydrolysis is secured by the resulting delocalized negative charge, which results in shielding of the electrophilic sulfur.[27,28] Therefore, partial hydrolysis of the TFSA groups can be excluded under the deprotonation conditions employed.

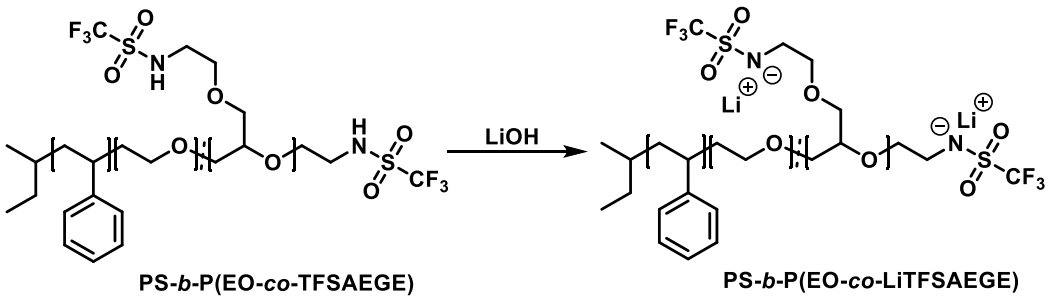

Scheme 2. Synthesis of the SICPE material.

The SEC trace of PS-*b*-P(EO-*co*-LiTFSAEGE) (Figure 2) shows a monomodal distribution with a $Đ$ of 1.13 (Table 1). A broad singlet at 3.28 ppm and a signal at 45.27 ppm is visible in the resulting ^{1}H (Figure 4) and ^{13}C NMR spectra of PS-*b*-P(EO-*co*-LiTFSAEGE) (Figure 3), respectively, which

can be assigned to the protons and carbons of the methylene groups adjacent to the deprotonated TFSA groups. Additionally, the ^{19}F NMR spectrum of PS-*b*-P(EO-*co*-LiTFSAEGE) (Figure 3) shows a broad peak with a slight down-field shift relative to PS-*b*-P(EO-*co*-TFSAEGE).

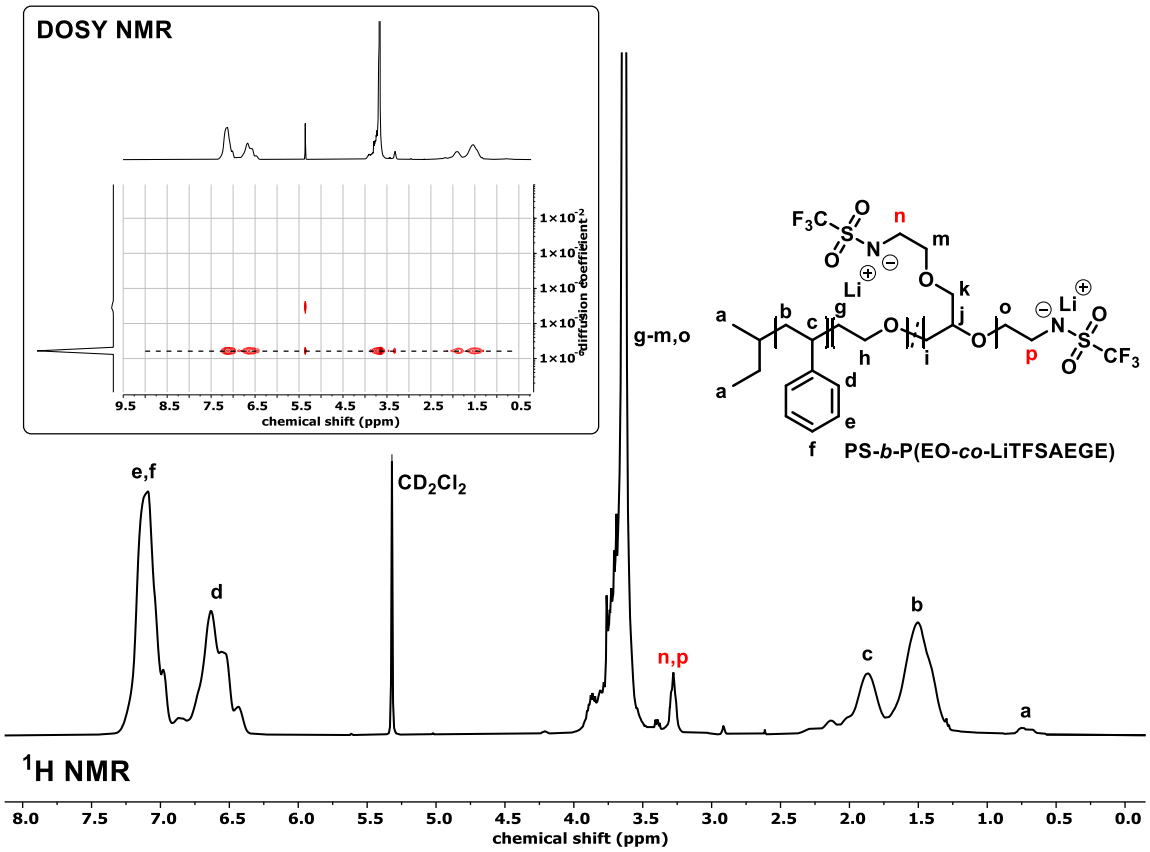

Figure 4. ^{1}H (300 MHz) and DOSY NMR spectrum (400 MHz, CD_2Cl_2) of PS-*b*-P(EO-*co*-LiTFSAEGE).

The DOSY NMR spectrum of PS-*b*-P(EO-*co*-LiTFSAEGE) (Figure 4) further confirms the covalent attachment of the charged TFSA groups at the polymer by the uniform diffusion coefficient of the polymer resonances and the side group signals.

Thermal Properties

The random distribution of comonomer units in the polymer chain is a key feature to decrease the degree of crystallization and consequently the melting temperature of the polyether block, even when a low comonomer content is present. An earlier study by our group revealed the desired random incorporation of the utilized glycidyl ether EVGE in the PEO backbone.[25] In case of strongly differing reactivity ratios between EO and less reactive epoxides, a gradient-microstructure is formed with the comonomer, having only a small influence on the PEO melting temperature.[29]

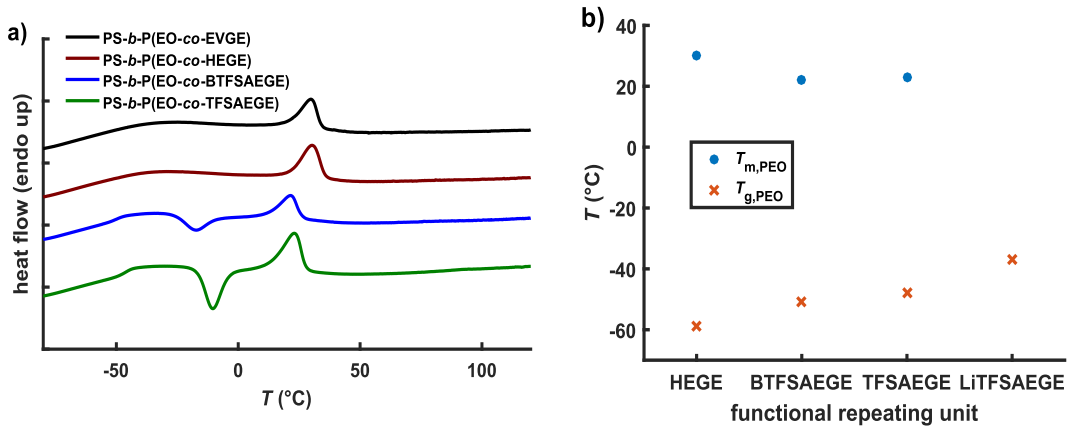

Figure 5. a) 2nd DSC heating curves (10 K min^{-1}); b) Trend of $T_{m,PEO}$ and $T_{g,PEO}$ with differing functional repeating units.

Additionally, the introduction of charged side groups should also influence the segmental motion and the crystallization behavior of the PEO block.

Addressing this question, the thermal properties of the synthesized BCPs were investigated via differential scanning calorimetry (DSC) (Table 1, Figure 5). In comparison to PEO with a typical $T_{m,PEO}$ of 60 °C, the incorporated side chains of PS-*b*-P(EO-*co*-HEGE) decrease the $T_{m,PEO}$ to 30 °C, which is consistent with an earlier study by our group.[25] Exchange of the hydroxyl functionalities with TFSA groups shows a more pronounced effect on the $T_{m,PEO}$. The additional inter- and intramolecular polar interactions between different TFSA groups lead to a $T_{m,PEO}$ of 22 °C.

Table 2. Composition and DSC data for neat, salt-doped PS-*b*-PEO and SICPE.

Sample	[EO]:[Li]	r[a)] ([Li]:[EO])	f_{PEO}[b)]	$T_{g,PEO}$[c)] [°C]	$T_{m,PEO}$[c)] [°C]	ΔH_{PEO}[c)] [J g^{-1}]	$X_{c,PEO}$[c)] [%]
PS-*b*-PEO	-	-	0.41	n.d.	54	43.5	54
PS-*b*-PEO + LiTf	16	0.06	0.41	-44	50	30.1	36
PS-*b*-PEO + LiTFSI	16	0.06	0.41	-42	38	2.4	3
PS-*b*-P(EO-*co*-LiTFSAEGE)	16	0.06	0.39	-37	-	-	-

a) r = [Li]/[EO]; b) Determined via ^{1}H NMR spectroscopy; c) Determined via DSC.

An opposite trend was observed for the $T_{g,PEO}$ in comparison to the $T_{m,PEO}$. The incorporation of TFSA groups before and after deprotection results in an increase of the $T_{g,PEO}$ to -51 °C and -48 °C, respectively, compared to the precursor BCP PS-*b*-P(EO-*co*-HEGE) ($T_{g,PEO}$ = -59 °C). This can also be explained by pronounced hydrogen bond formation, i.e., non-covalent cross-links between the polymer chains. After further deprotonation of the TFSA groups, an additional increase of the $T_{g,PEO}$ up to -37 °C is observed. This effect is caused by inter- and intramolecular non-covalent cross-linkages between the chains, which results in a decrease of the segmental motion of the PEO block.[30,31]

Comparison of the thermal properties of PS-b-P(EO-co-LiTFSAEGE) with lithium salt-doped PS-*b*-PEO

Furthermore, the thermal properties of the SICPE material PS-*b*-P(EO-*co*-LiTFSAEGE) were compared with established SPEs based on PS-*b*-PEO and lithium salt additives. Therefore, LiTFSI- and LiTf-doped PS-*b*-PEO with similar $M_{n,total}$ (15.2 kg mol^{-1}), f_{PEO} (0.41) and r (0.06) (r = [Li]/[EO]) were prepared and investigated via DSC (Figure 6). A distinct decrease of ΔH_{PEO} and $T_{m,PEO}$ in lithium salt-doped PS-*b*-PEO compared to pure PS-*b*-PEO is observed, whereas the effect is more pronounced in the case of LiTFSI rather than in LiTf (Table 2). The differing influence of the added salts on the degree of crystallization inhibition was similarly observed in related studies.[32,33] The reduction of crystallization can be attributed to the accumulation of the salt in the polar PEO domains and the interaction of the polymer backbone oxygens with the lithium cations.[32] At the same r value, PS-*b*-P(EO-*co*-LiTFSAEGE) is obtained as a completely amorphous material (Figure 6) due to the additive disruption of the crystallization by the introduced charges and the additional steric hindrance of the side chains.

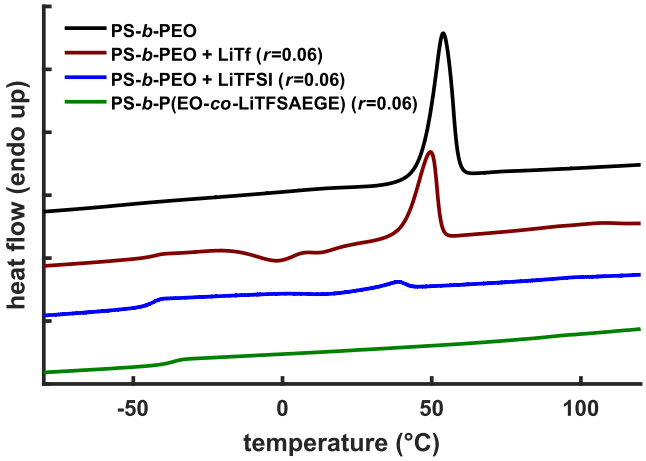

Figure 6. 2nd DSC heating curves (10 K min^{-1}) of neat and salt-doped PS-*b*-PEO and PS-*b*-P(EO-*co*-LiTFSAEGE) with r = 0.06.

This is an important observation, as a sufficiently high room-temperature ionic conductivity is only possible in PEO-based SPEs, if the ion mobility is not disturbed by insulating crystalline areas in the conductive polyether matrix.[3] Additionally, a similar decrease of the segmental motion of PEO in LiTf-doped, LiTFSI-doped PS-*b*-PEO and PS-*b*-P(EO-*co*-LiTFSAEGE) is observed, which is emphasized by an increase of the $T_{g,PEO}$ to -44 °C, -42 °C and -37 °C, respectively (Table 2). Thus, a comparable distribution and complexation of the lithium cations inside the PEO domains is assumed for PS-*b*-P(EO-*co*-LiTFSAEGE) and lithium salt-doped PS-*b*-PEO. Fortunately, the presence of the ions only slightly influences the segmental motion of the PEO chains in the SICPE material. This contrasts with PS-*b*-PEO-based SICPEs with anions located in the glassy PS domains. Herein, the SICPEs exist as an insulator at room temperature with ionic clusters trapped inside the glassy domains. Mixing of the domains due to temperature elevation leads to

conductive behavior, but also a sharp increase in the T_g of the PEO domains.[34,35] In the case of PS-*b*-P(EO-*co*-LiTFSAEGE), the ionic species are already dissolved inside the PEO domains and therefore mixing of the domains is interrupted.

CONCLUSION

We successfully established a novel synthesis protocol for the controlled introduction of neutral and charged TFSA groups in the polyether block of polystyrene-*block*-poly(ethylene oxide-*co*-hydroxyethyl glycidyl ether) diblock copolymers via a post-polymerization Mitsunobu reaction. In-depth analyses revealed both, complete substitution of hydroxyl groups with BTFSA and the quantitative deprotection as well as deprotonation of the sulfonamide groups under preservation of the underlying block copolymer structure. DSC measurements show a correlation of the nature of the functional group and the thermal properties of the PEO block. Subsequent investigations regarding the thermal properties of the resulting amorphous single-ion-conducting polymer electrolytes (SICPE) material and comparison with lithium salt-doped PS-*b*-PEO (LiTFSI and LiTf) via DSC measurements indicate a similar value of the $T_{g,PEO}$ at the same salt concentration ($r = 0.06$). Hence, a comparable coordination and aggregation of the ionic species with the PEO backbone can be emphasized for lithium salt-doped PS-*b*-PEO and PS-*b*-P(EO-*co*-LiTFSAEGE). Fortunately, the $T_{g,PEO}$ of the SICPE (-37 °C) is scarcely influenced by the introduction of the ionic species, which is in pronounced contrast to earlier reported SICPEs based on PS-*b*-PEO. We believe that the established synthesis protocol and discussed features of PS-*b*-P(EO-*co*-LiTFSAEGE) offer interesting potential for the utilization of this material as SICPE in lithium ion and lithium metal batteries. Investigations concerning the morphology, transference numbers and ionic conductivity of the novel SICPE material with varying salt concentrations will be reported in further studies by our group.

REFERENCES

(1) Fenton, D. E.; Parker, J. M.; Wright, P. V. Complexes of alkali metal ions with poly(ethylene oxide). *Polymer* **1973**, *14*, 589.

(2) Cowie, J. M. G.; Cree, S. H. Electrolytes Dissolved in Polymers. *Annu. Rev. Phys. Chem.* **1989**, *40*, 85–113.

(3) Berthier, C.; Gorecki, W.; Minier, M.; Armand, M. B.; Chabagno, J. M.; Rigaud, P. Microscopic investigation of ionic conductivity in alkali metal salts-poly(ethylene oxide) adducts. *Solid State Ionics* **1983**, *11*, 91–95.

(4) Geng, Z.; Schauser, N. S.; Lee, J.; Schmeller, R. P.; Barbon, S. M.; Segalman, R. A.; Lynd, N. A.; Hawker, C. J. Role of Side-Chain Architecture in Poly(ethylene oxide)-Based Copolymers. *Macromolecules* **2020**, *53*, 4960–4967.

(5) Marco Viviani; Niels Laurens Meereboer; Ni Luh Putu Ananda Saraswati; Katja Loos; Giuseppe Portale. Lithium and magnesium polymeric electrolytes prepared using poly(glycidyl ether)-based polymers with short grafted chains. *Polym. Chem.* **2020**, *11*, 2070–2079.

(6) Barteau, K. P.; Wolffs, M.; Lynd, N. A.; Fredrickson, G. H.; Kramer, E. J.; Hawker, C. J. Allyl Glycidyl Ether-Based Polymer Electrolytes for Room Temperature Lithium Batteries. *Macromolecules* **2013**, *46*, 8988–8994.

(7) Herzberger, J.; Niederer, K.; Pohlit, H.; Seiwert, J.; Worm, M.; Wurm, F. R.; Frey, H. Polymerization of Ethylene Oxide, Propylene Oxide, and Other Alkylene Oxides: Synthesis, Novel Polymer Architectures, and Bioconjugation. *Chemical reviews* **2016**, *116*, 2170–2243.

(8) Leibler, L. Theory of Microphase Separation in Block Copolymers. *Macromolecules* **1980**, *13*, 1602–1617.

(9) Bates, F. S.; Fredrickson, G. H. Block copolymer thermodynamics: Theory and experiment. *Annual review of physical chemistry* **1990**, *41*, 525–557.

(10) Loo, W. S.; Balsara, N. P. Organizing thermodynamic data obtained from multicomponent polymer electrolytes: Salt-containing polymer blends and block copolymers. *Journal of Polymer Science Part B: Polymer Physics* **2019**, *57*, 1177–1187.

(11) Ketkar, P. M.; Shen, K.-H.; Hall, L. M.; Epps, T. H. Charging toward improved lithium-ion polymer electrolytes: exploiting synergistic experimental and computational approaches to facilitate materials design. *Mol. Syst. Des. Eng.* **2019**, *4*, 223–238.

(12) Young, W.-S.; Kuan, W.-F.; Epps, T. H. Block copolymer electrolytes for rechargeable lithium batteries. *J. Polym. Sci. Part B: Polym. Phys.* **2014**, *52*, 1–16.

(13) Zhang, H.; Li, C.; Piszcz, M.; Coya, E.; Rojo, T.; Rodriguez-Martinez, L. M.; Armand, M.; Zhou, Z. Single lithium-ion conducting solid polymer electrolytes: Advances and perspectives. *Chem. Soc. Rev.* **2017**, *46*, 797–815.

(14) Morris, M. A.; An, H.; Lutkenhaus, J. L.; Epps, T. H. Harnessing the Power of Plastics: Nanostructured Polymer Systems in Lithium-Ion Batteries. *ACS Energy Lett.* **2017**, *2*, 1919–1936.

(15) Rosenwinkel, M. P.; Schönhoff, M. Lithium Transference Numbers in PEO/LiTFSA Electrolytes Determined by Electrophoretic NMR. *J. Electrochem. Soc.* **2019**, *166*, A1977-A1983.

(16) Diederichsen, K. M.; McShane, E. J.; McCloskey, B. D. Promising Routes to a High Li^+ Transference Number Electrolyte for Lithium Ion Batteries. *ACS Energy Lett.* **2017**, *2*, 2563–2575.

(17) Li, S.; Mohamed, A. I.; Pande, V.; Wang, H.; Cuthbert, J.; Pan, X.; He, H.; Wang, Z.; Viswanathan, V.; Whitacre, J. F.; et al. Single-Ion Homopolymer Electrolytes with High Transference Number Prepared by Click Chemistry and Photoinduced Metal-Free Atom-Transfer Radical Polymerization. *ACS Energy Lett.* **2017**, *3*, 20–27.

(18) S. Fletcher. The Mitsunobu reaction in the 21st century. *Org. Chem. Front.* **2015**, *2*, 739–752.

(19) Bittner, S.; Assaf, Y.; Krief, P.; Pomerantz, M.; Ziemnicka, B. T.; Smith, C. G. Synthesis of *N*-acyl-, *N*-sulfonyl-, and *N*-phosphinylphospha(PV)azenes by a redox-condensation reaction using amides, triphenylphosphine, and diethyl azodicarboxylate. *J. Org. Chem.* **1985**, *50*, 1712–1718.

(20) Henry, J. R.; Marcin, L. R.; McIntosh, M. C.; Scola, P. M.; Davis Harris, G.; Weinreb, S. M. Mitsunobu reactions of *n*-alkyl and *n*-acyl sulfonamides-an efficient route to protected amines. *Tetrahedron Letters* **1989**, *30*, 5709–5712.

(21) Koppel, I.; Koppel, J.; Degerbeck, F.; Grehn, L.; Ragnarsson, U. Acidity of imidodicarbonates and tosylcarbamates in dimethyl sulfoxide. Correlation with yields in the Mitsunobu reaction. *J. Org. Chem.* **1991**, *56*, 7172–7174.

(22) Fukuyama, T.; Cheung, M.; Kan, T. N -Carboalkoxy-2-Nitrobenzenesulfonamides: A Practical Preparation of *N*-Boc-, *N*-Alloc-, and *N*-Cbz-Protected Primary Amines. *Synlett* **1999**, 1301–1303.

(23) Quirk, R. P.; Ma, J.-J. Characterization of the functionalization reaction product of poly(styryl)lithium with ethylene oxide. *J. Polym. Sci. A Polym. Chem.* **1988**, *26*, 2031–2037.

(24) Quirk, R. P.; Mathers, R. T.; Wesdemiotis, C.; Arnould, M. A. Investigation of Ethylene Oxide Oligomerization during Functionalization of Poly(styryl)lithium Using MALDI−TOF MS and NMR. *Macromolecules* **2002**, *35*, 2912–2918.

(25) Mangold, C.; Dingels, C.; Obermeier, B.; Frey, H.; Wurm, F. PEG-based Multifunctional Polyethers with Highly Reactive Vinyl-Ether Side Chains for Click-Type Functionalization. *Macromolecules* **2011**, *44*, 6326–6334.

(26) Fetters, L. J.; Lohse, D. J.; Richter, D.; Witten, T. A.; Zirkel, A. Connection between Polymer Molecular Weight, Density, Chain Dimensions, and Melt Viscoelastic Properties. *Macromolecules* **1994**, *27*, 4639–4647.

(27) Sowada, R. Synthesen mit N,N'-disubstituierten Schwefelsäurediamiden. IV. Über die Acetylierung 1,3-disubstituierter Schwefelsäurediamide. *J. Prakt. Chem.* **1964**, *26*, 184–194.

(28) Searles, S.; Nukina, S. Cleavage And Rearrangement Of Sulfonamides. *Chem. Rev.* **1959**, *59*, 1077–1103.

(29) Herzberger, J.; Kurzbach, D.; Werre, M.; Fischer, K.; Hinderberger, D.; Frey, H. Stimuli-Responsive Tertiary Amine Functional PEGs Based on N,N -Dialkylglycidylamines. *Macromolecules* **2014**, *47*, 7679–7690.

(30) Krimalowski, A.; Thelakkat, M. Sequential Co-Click Reactions with Poly(glycidyl propargyl ether) toward Single-Ion Conducting Electrolytes. *Macromolecules* **2019**, *52*, 4042–4051.

(31) Ho, H. T.; Tintaru, A.; Rollet, M.; Gigmes, D.; Phan, T. N. T. A post-polymerization functionalization strategy for the synthesis of sulfonyl (trifluoromethanesulfonyl)imide functionalized (co)polymers. *Polym. Chem.* **2017**, *8*, 5660–5665.

(32) Young, W.-S.; Epps, T. H. Salt Doping in PEO-Containing Block Copolymers: Counterion and Concentration Effects. *Macromolecules* **2009**, *42*, 2672–2678.

(33) Vallée, A.; Besner, S.; Prud'Homme, J. Comparative study of poly(ethylene oxide) electrolytes made with $LiN(CF_3SO_2)_2$, $LiCF_3SO_3$ and $LiClO_4$: Thermal properties and conductivity behaviour. *Electrochimica Acta* **1992**, *37*, 1579–1583.

(34) Inceoglu, S.; Rojas, A. A.; Devaux, D.; Chen, X. C.; Stone, G. M.; Balsara, N. P. Morphology–Conductivity Relationship of Single-Ion-Conducting Block Copolymer Electrolytes for Lithium Batteries. *ACS Macro Lett.* **2014**, *3*, 510–514.

(35) Bouchet, R.; Maria, S.; Meziane, R.; Aboulaich, A.; Lienafa, L.; Bonnet, J.-P.; Phan, T. N. T.; Bertin, D.; Gigmes, D.; Devaux, D.; et al. Single-ion BAB triblock copolymers as highly efficient electrolytes for lithium-metal batteries. *Nature materials* **2013**, *12*, 452–457.

SUPPORTING INFORMATION

Experimental Part

Reagents

All reagents were purchased either from Acros Organics, Roth, Fischer Chemical, VWR Chemicals or Carbolution Chemicals GmbH unless otherwise noticed. Chloroform-*d* and Methylene chloride-d_2 were purchased from Deutero GmbH. Ethylene oxide (EO) was purchased from Air Liquide. Ethoxy vinyl glycidyl ether (EVGE) was synthesized according to the literature.[1] Styrene was flushed through basic aluminum oxide before usage. Dowex was activated with conc. HCl and dried before usage. LiTFSI was purchased from IoLiTec Liquids Technologies GmbH, dried at 120 °C in high vacuo and transferred in a glove box before usage. LiTf was purchased from ABCR and directly transferred into a glove box before opening and usage. Cyclohexane was dried over sodium/benzophenone, degassed and freshly distilled into the reaction flask for each polymerization.

Instrumentation

NMR spectra were recorded on a Bruker Avance III HD 300 spectrometer with 300 MHz and referenced internally to residual proton or carbon peaks of the deuterated solvent. DOSY NMR spectra were recorded on a Bruker Avance III HD 400 spectrometer with 400 MHz.

SEC measurements were performed with THF as the mobile phase (flow rate 1 mL min^{-1}) on an SDV column set from PSS (SDV 103, SDV 105, SDV 106) at 30 °C. Polymer concentrations were 1 mg mL^{-1}. Calibration was carried out using polystyrene standards (from Polymer Standard Service, Mainz).

DSC measurements were conducted on a PerkinElmer DSC 8500 differential scanning calorimeter and calibrated with n-decane and indium standards. Two cooling and heating cycles were performed between -100 and 120 °C at a heating rate of 10 K min^{-1}. Melting and glass transition temperatures were obtained from the second heating cycle.

MALDI-ToF mass spectra were recorded on a Bruker MALDI ToF MS Autoflex Max. Measurements were performed in the linear modus. For PS-OH, AgTFA and dithranol were used as a salt additive and matrix, respectively. In the case of ω-BTFSA-PEO and ω-TFSA-PEO, KTFA and DCTB were utilized as a salt additive and matrix, respectively.

Salt-doping of block copolymers with lithium salts

PS-*b*-PEO was dissolved in benzene and a solution of LiTFSI or LiTf in THF was added under stirring. After homogenization, the solution was poured into a Teflon mold and the solvent was slowly evaporated until a thin film was obtained. The film was further dried under high vacuo at 60 °C to ensure the absence of solvent traces.

Experimental Procedures

***tert*-Butyl ((trifluoromethyl)sulfonyl)carbamate (BTFSA)**

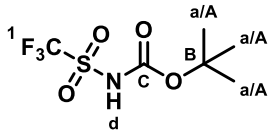

Trifluoromethanesulfonamide (3.00 g, 20.1 mmol) was suspended in DCM (50 mL) and TEA (2.04 g, 2.79 mL, 20.1 mmol) and DMAP (246 mg, 2.01 mmol) were added. Di-tert-butyl dicarbonate (4.03 g, 3.95 mL, 23.1 mmol) was added dropwise to the ice-cooled solution. After stirring for 2 h at room temperature, DCM was evaporated in vacuo and the residue was dissolved in EtOAc (240 mL). The organic phase was extracted with 1N HCl (160 mL), H_2O (160 mL, two times) and brine (160 mL). The organic phase was dried over $MgSO_4$, filtered and the solvent was evaporated to yield colorless crystals. Pure BTFSA (4.13 g, 16.6 mmol, 82 %) was obtained as colorless crystals after sublimation of unreacted trifluoromethanesulfonamide from the crystal mixture at room temperature and high vacuum (10^{-3} mbar).

^{1}H NMR (CD_2Cl_2), δ (ppm): 7.49 (s, 1H, H_d), 1.51 (s, 9H, H_a).

^{13}C NMR (CD_2Cl_2), δ (ppm): 147.11 (C_C), 87.08 (C_B), 27.81 (C_A).

^{19}F NMR (CD_2Cl_2), δ (ppm): -77.22.

***ω*-Hydroxy-polystyrene (PS-OH)**

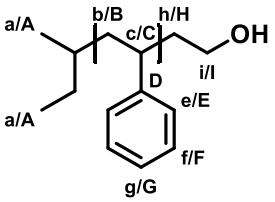

Styrene (8.65 g, 9.50 mL, 830 mmol) was dried over CaH_2 for 1 d and transferred in the reaction flask via cryo-distillation. Cyclohexane (50 mL) was cryo-transferred in the reaction flask and the flask was flushed with argon. The polymerization was initiated with sec-BuLi (1.3 M stock solution, 0.45 mL, 580 μmol) and stirred for 3 h at 35 °C. The flask was evacuated and dry EO (162 mg, 167 μL, 3.69 mmol) was transferred to the reaction mixture at -78 °C. The solution was warmed to room temperature and stirred for 1 d. Quantitative yield of PS-OH was obtained via precipitation of the polymer solution in a ten-fold excess of MeOH-*i*PrOH (50:50 vol-%) and drying in vacuo.

^{1}H NMR ($CDCl_3$), δ (ppm): 7.19-6.15 (m (broad), H_e-H_g), 3.18 (s (broad), H_i), 2.50-0.71 (m (broad), H_b+H_c+H_h), 0.71-0.44 (m, H_a).

Polystyrene-*block*-poly(ethylene oxide-*co*-ethoxy vinyl glycidyl ether) (PS-*b*-P(EO-*co*-EVGE))

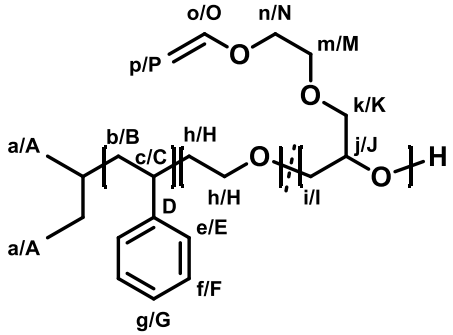

PS-OH (1.00 g, 117 μmol) was dissolved in benzene, lyophilized and dried at 80 °C under high vacuum for 18 h. THF (7.5 mL) was cryo-transferred into the reaction flask and potassium naphthalenide (0.44 M stock solution in THF, 210 μL, 93.4 μmol) was added dropwise to the solution. DMSO (2.5 mL) was added via syringe and the solution was cooled to -78 °C. EVGE (200 mg, 200 μL, 4.53 mmol) and EO (970 mg, 1.00 mL, 22.0 mmol) were added and the polymerization was carried out at 50 °C for 1 d. The polymer was precipitated in a ten-fold excess of H_2O under stirring and redissolved in benzene. Lyophilized PS-*b*-P(EO-*co*-EVGE) (1.71 g, 111 μmol, 95 %) was obtained as a colorless solid.

^{1}H NMR (CD_2Cl_2), δ (ppm): 7.34-6.34 (m (broad), H_e-H_g), 6.53 (m, H_o), 4.21 (dd, H_p), 4.02 (dd, H_p), 3.90-3.28 (m (broad), H_h-H_n), 2.40-0.83 (m (broad), H_b+H_c), 0.75 (m, H_a).

^{13}C NMR (CD_2Cl_2), δ (ppm): 152.23 (C_O) 145.80 (C_D), 128.03 (C_F+C_G), 126.06 (C_E), 86.74 (C_P), 78.68 (C_J), 70.88 (C_H+C_I+C_K+C_M), 67.89 (C_N), 47.27-41.45 (C_B), 40.76 (C_C).

Polystyrene-*block*-poly(ethylene oxide-*co*-hydroxyethyl glycidyl ether) (PS-*b*-P(EO-*co*-HEGE))

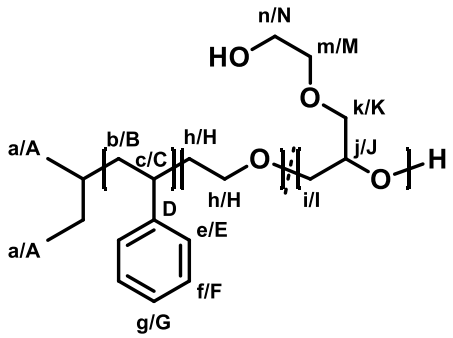

PS-*b*-P(EO-*co*-EVGE) (1.39 g, 90.0 μmol) was dissolved in DCM (35 mL) and MeOH (7 mL) and Dowex (70.0 mg) were added. The reaction mixture was stirred for 20 h and quenched with DCM (20 mL). The suspension was filtered, and the filtrate was dried over $MgSO_4$. The solvent was evaporated and the polymer was redissolved in benzene. Lyophilized PS-*b*-P(EO-*co*-HEGE) was obtained in quantitative yields as a colorless solid.

^{1}H NMR (CD_2Cl_2), δ (ppm): 7.34-6.34 (m (broad), H_e-H_g), 3.90-3.28 (m (broad), H_h-H_n), 2.40-0.83 (m (broad), H_b+H_c), 0.75 (m, H_a).

^{13}C NMR (CD_2Cl_2), δ (ppm): 145.80 (C_D), 128.03 (C_F+C_G), 126.06 (C_E), 78.61 (C_J), 70.87 (C_H+C_I+C_K+C_M), 61.83 (C_N), 47.27-41.45 (C_B), 40.76 (C_C).

Polystyrene-*block*-poly(ethylene oxide-*co*-*tert*-butyl ((trifluoromethyl)sulfonyl)carbamate ethyl glycidyl ether) (PS-*b*-P(EO-*co*-BTFSAEGE))

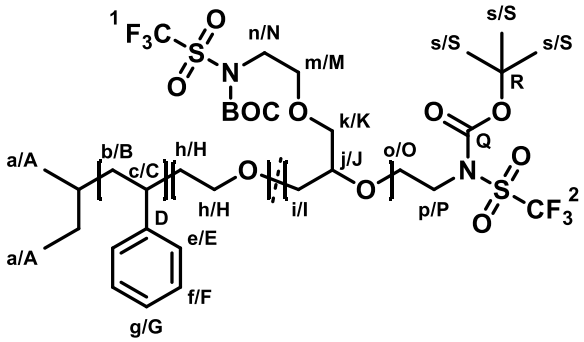

PS-*b*-P(EO-*co*-HEGE) (1.20 g, 79.4 μmol) was dissolved in benzene and lyophilized for 18 h. The polymer was dissolved in dry THF (18 mL) and PPh_3 (506 mg, 1.93 mmol) and BTFSA (481 mg, 1.93 mmol) were added. DIAD (390 mg, 380 μL, 1.93 mmol) was added dropwise and the solution was stirred for 16 h. The polymer was precipitated in a ten-fold excess of isopropanol and centrifuged. The precipitate was redissolved in THF (15 mL) and precipitated in a ten-fold excess of *n*-hexane. The last step was repeated four times. The polymer was redissolved in benzene. Lyophilized PS-*b*-P(EO-*co*-BTFSAEGE) (1.25 g, 72.2 μmol, 91 %) was obtained as a colorless solid.

^{1}H NMR (CD_2Cl_2), δ (ppm): 7.34-6.34 (m (broad), H_e-H_g), 3.97 (t, H_n+H_p), 3.80-3.28 (m (broad), H_h-H_m+H_o), 2.40-0.83 (m (broad), H_b+H_c), 1.55 (s, H_s), 0.75 (m, H_a).

^{13}C NMR (CD_2Cl_2), δ (ppm): 149.57 (C_Q), 145.80 (C_D), 128.03 (C_F+C_G), 126.06 (C_E), 87.24 (C_R), 78.64 (C_J), 70.89 (C_H+C_I+C_K+C_M+C_O), 48.14 (C_N+C_P), 47.27-41.45 (C_B), 40.76 (C_C), 27.80 (C_S).

^{19}F NMR (CD_2Cl_2), δ (ppm): -73.11 (F_2), -73.19 (F_1).

Polystyrene-*block*-poly(ethylene oxide-*co*-(trifluoromethanesulfonamide)ethyl glycidyl ether) (PS-*b*-P(EO-*co*-TFSAEGE))

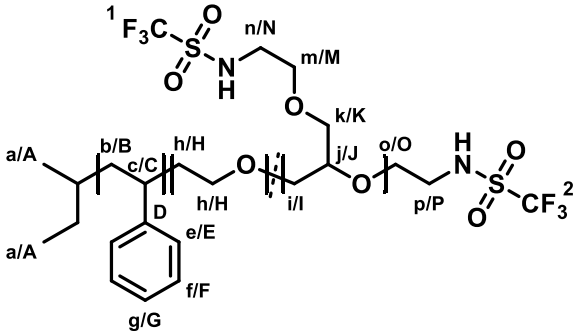

PS-*b*-P(EO-*co*-BTFSAEGE) (1.13 g, 65.2 μmol) was dissolved in DMF (45 mL) and the solution was heated at 100 °C under stirring for 3 h. DMF was evaporated under high vacuum and the resulting solid was redissolved in benzene. Lyophilized PS-*b*-P(EO-*co*-TFSAEGE) was obtained in quantitative yields as a colorless solid.

^{1}H NMR (CD_2Cl_2), δ (ppm): 7.34-6.34 (m (broad), H_e-H_g), 3.80-3.28 (m (broad), H_h-H_m+H_o), 3.45 (m (broad), H_n+H_p), 2.40-0.83 (m (broad), H_b+H_c), 0.75 (m, H_a).

^{13}C NMR (CD_2Cl_2), δ (ppm): 145.80 (C_D), 128.03 (C_F+C_G), 126.06 (C_E), 78.54 (C_J), 70.86 (C_H+C_I+C_K+C_M+C_O), 47.27-41.45 (C_B), 44.47 (C_N+C_P), 40.76 (C_C).

^{19}F NMR (CD_2Cl_2), δ (ppm): -79.18 (F_1+F_2).

Polystyrene-*block*-poly(ethylene oxide-*co*-(lithium trifluoromethanesulfonamide)ethyl glycidyl ether) (PS-*b*-P(EO-*co*-LiTFSAEGE))

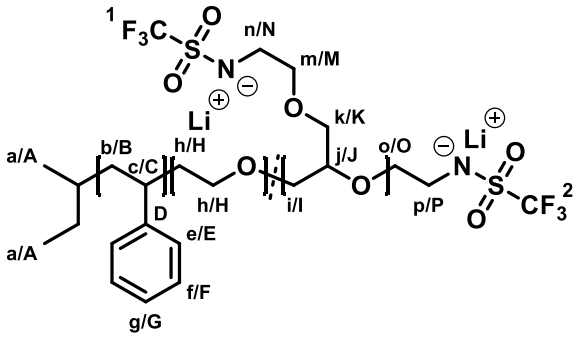

PS-*b*-P(EO-*co*-TFSAEGE) (980 mg, 59.8 μmol) was dissolved in $CHCl_3$ (4.5 mL) and MeOH (1.5 mL) and the solution was transferred in a dialysis tube (1 kDa MWCO). The polymer was dialyzed for 1 d against 0.1 M LiOH in MeOH (1 L) and 2 d against MeOH (1 L). The polymer solution was transferred from the dialysis tube in a flask, the solvent was evaporated in vacuo and the polymer was redissolved in benzene. Lyophilized PS-*b*-P(EO-*co*-LiTFSAEGE) (914 mg, 55.4 μmol, 93 %) was obtained as a colorless solid.

^{1}H NMR (CD_2Cl_2), δ (ppm): 7.34-6.34 (m (broad), H_e-H_g), 3.80-3.28 (m (broad), H_h-H_m+H_o), 3.28 (m (broad), H_n+H_p), 2.40-0.83 (m (broad), H_b+H_c), 0.75 (m, H_a).

^{13}C NMR (CD_2Cl_2), δ (ppm): 145.80 (C_D), 128.03 (C_F+C_G), 126.06 (C_E), 76.70 (C_J), 70.86 (C_H+C_I+C_K+C_M+C_O), 47.27-41.45 (C_B), 45.27 (C_N+C_P), 40.76 (C_C).

^{19}F NMR (CD_2Cl_2), δ (ppm): -78.83 (broad, F_1+F_2).

Additional Spectra

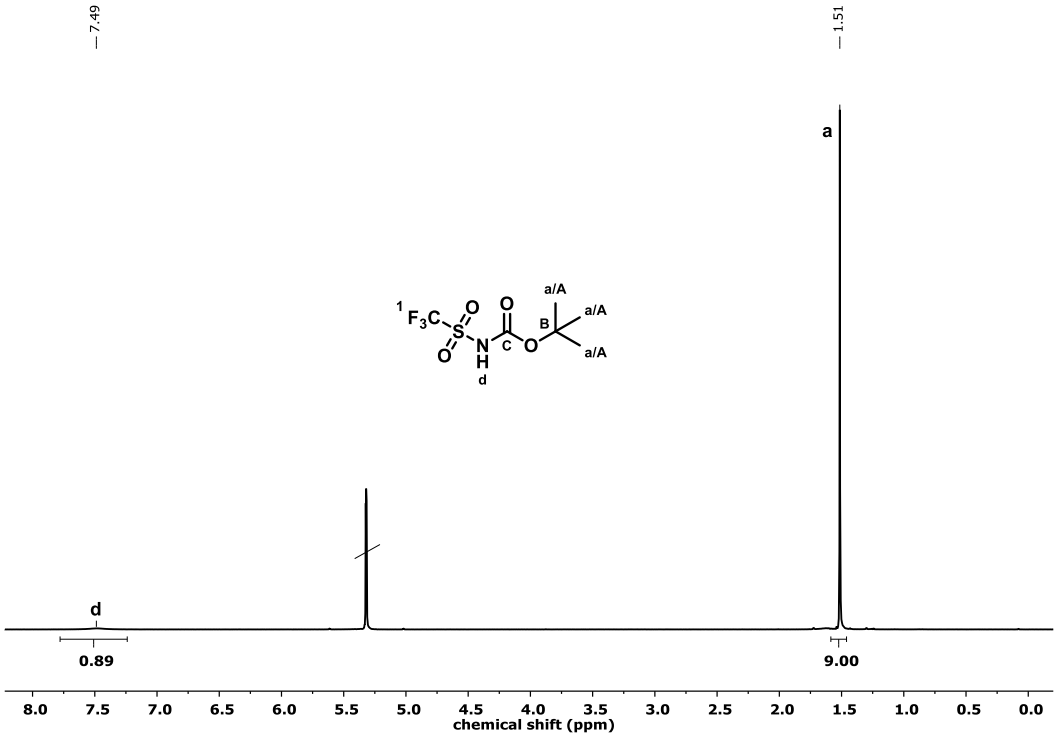

Figure S1. ^{1}H NMR spectrum (300 MHz, CD_2Cl_2) of BTFSA.

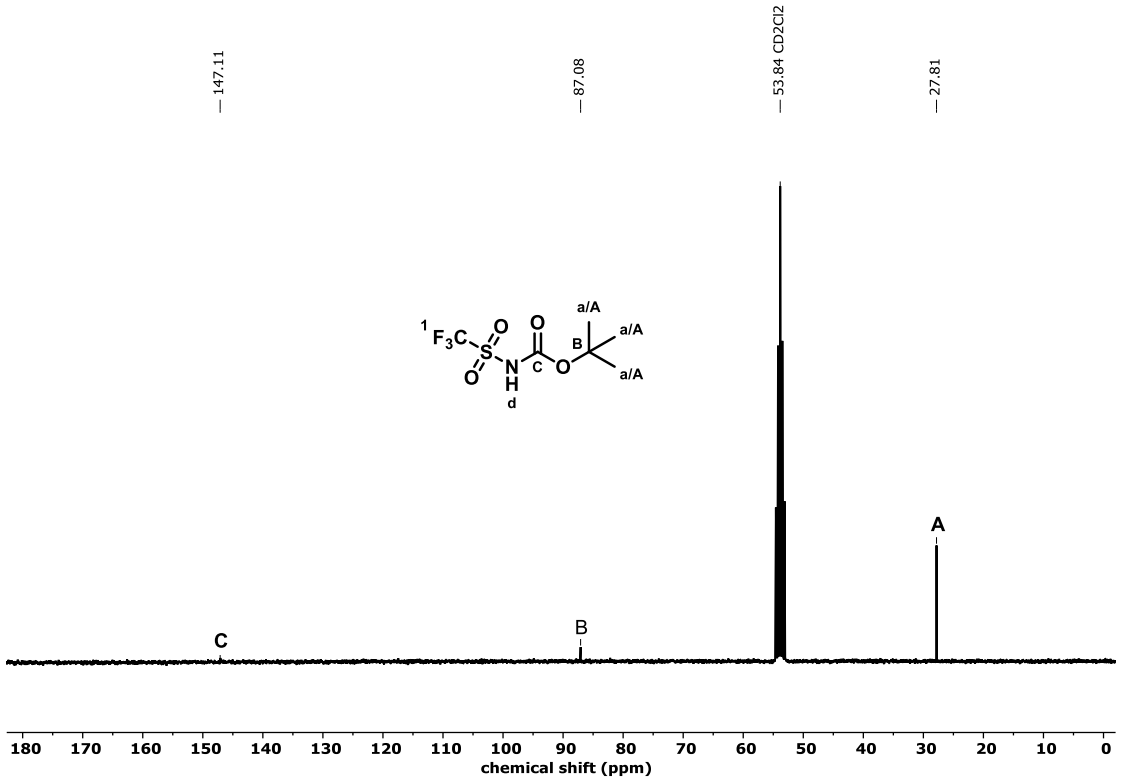

Figure S2. ^{13}C NMR spectrum (75 MHz, CD_2Cl_2) of BTFSA.

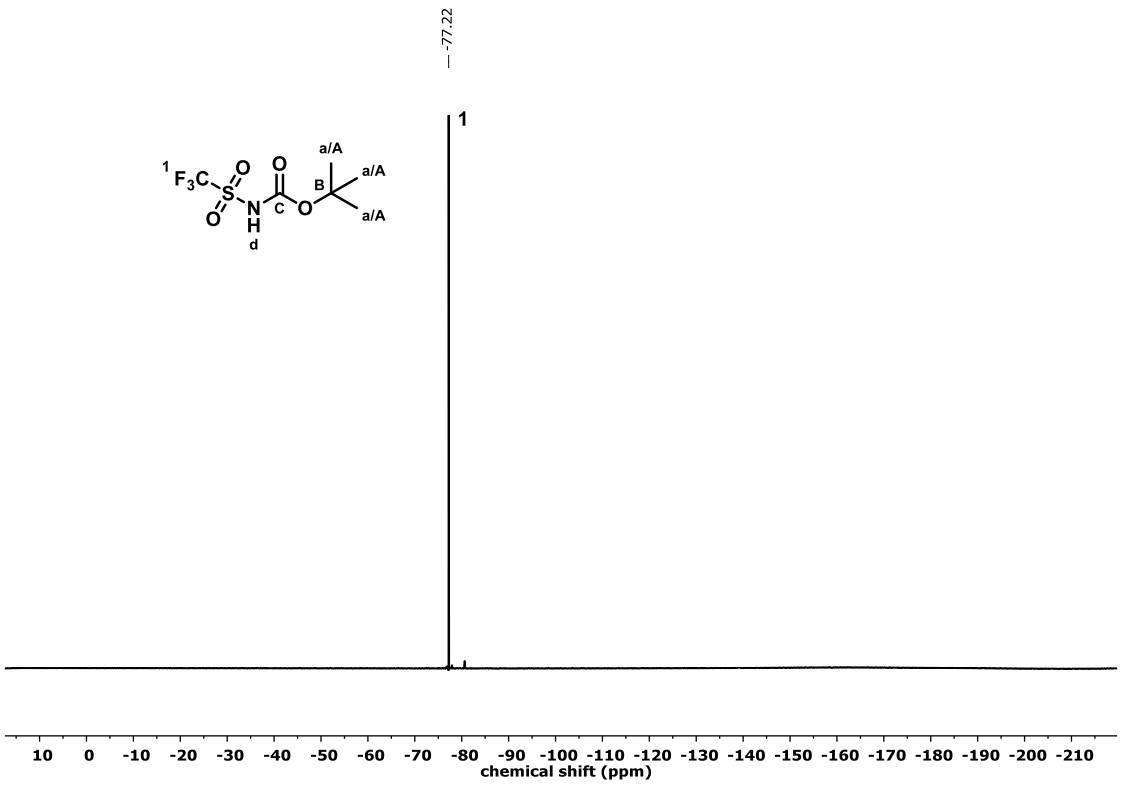

Figure S3. ^{19}F NMR spectrum (300 MHz, CD_2Cl_2) of BTFSA.

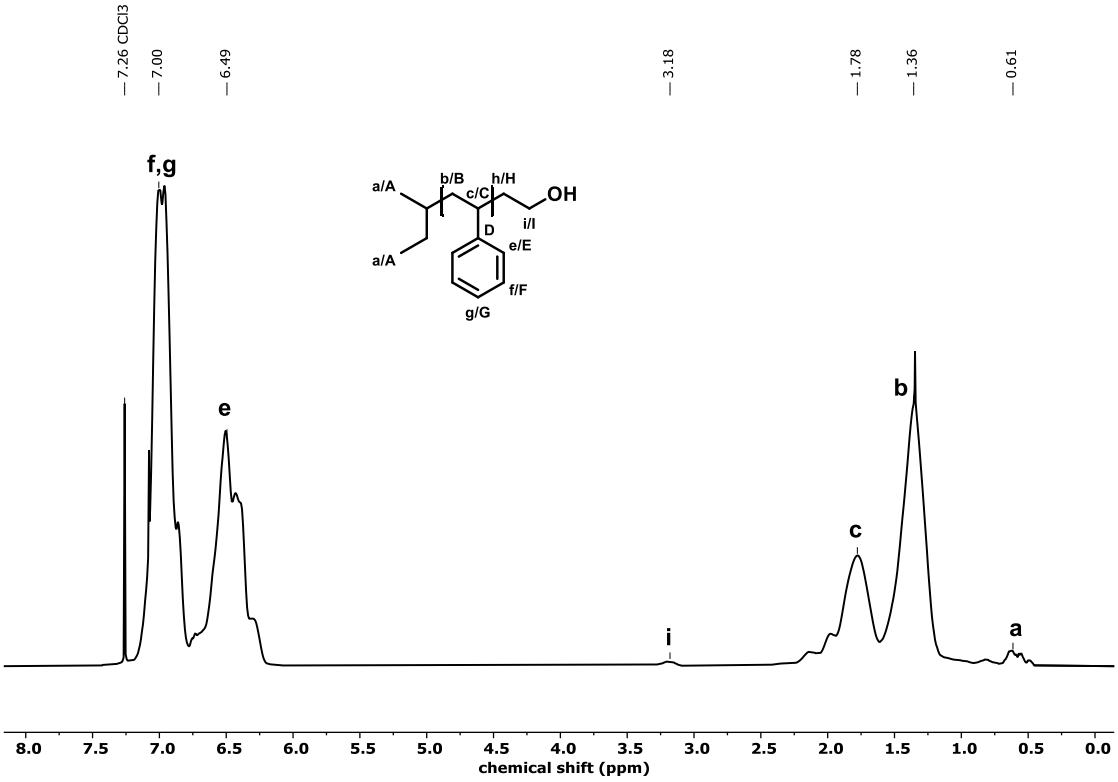

Figure S4. ^{1}H NMR spectrum (300 MHz, $CDCl_3$) of PS-OH.

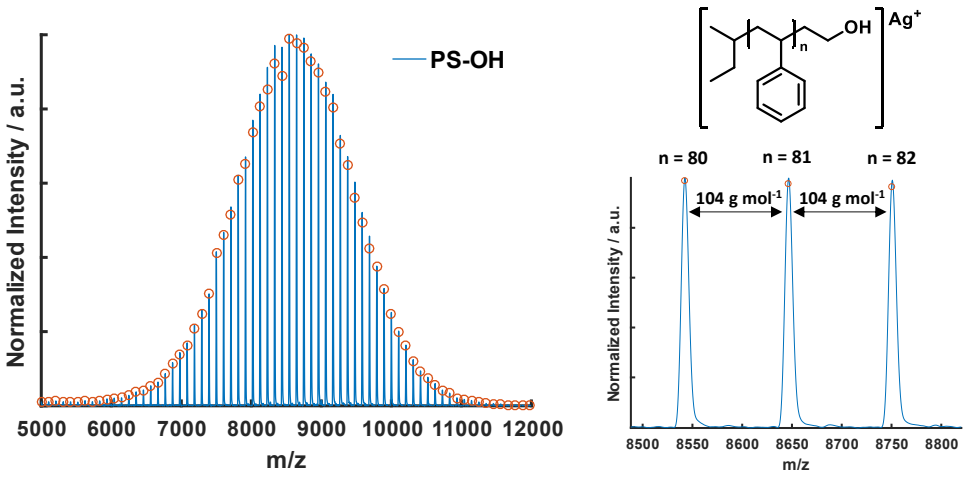

Figure S5. MALDI-ToF MS (dithranol, AgTFA, linear mode) of PS-OH.

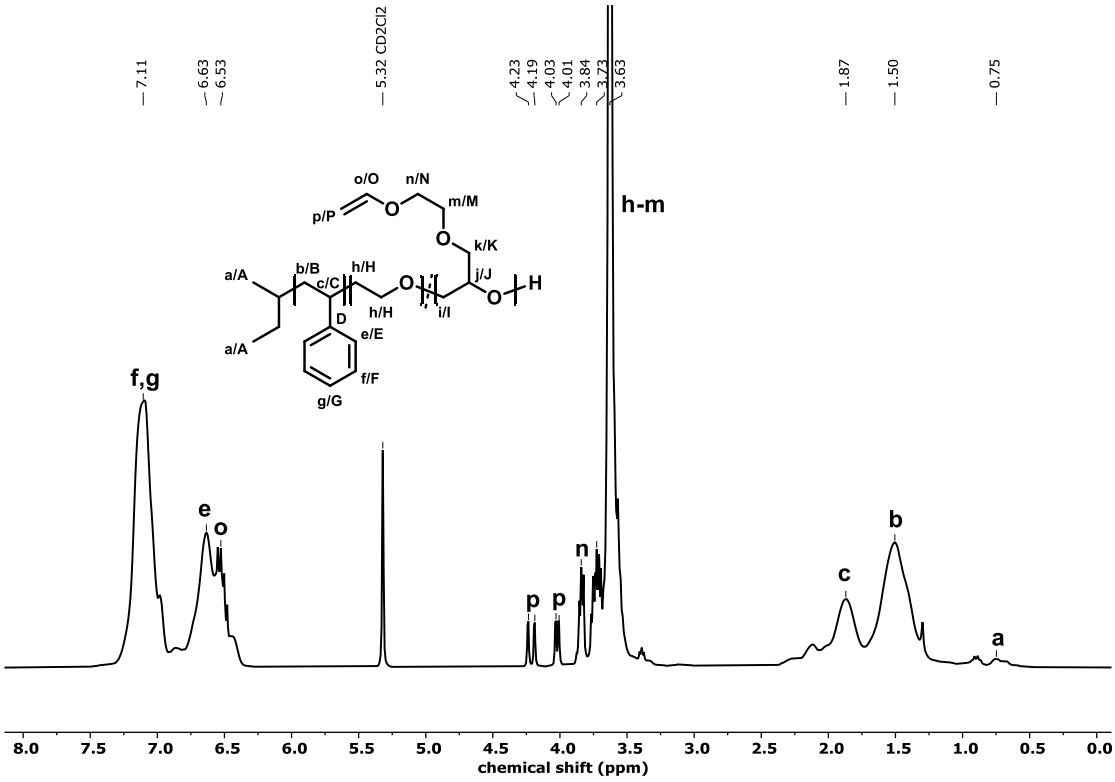

Figure S6. ^{1}H NMR spectrum (300 MHz, CD_2Cl_2) of PS-*b*-P(EO-*co*-EVGE).

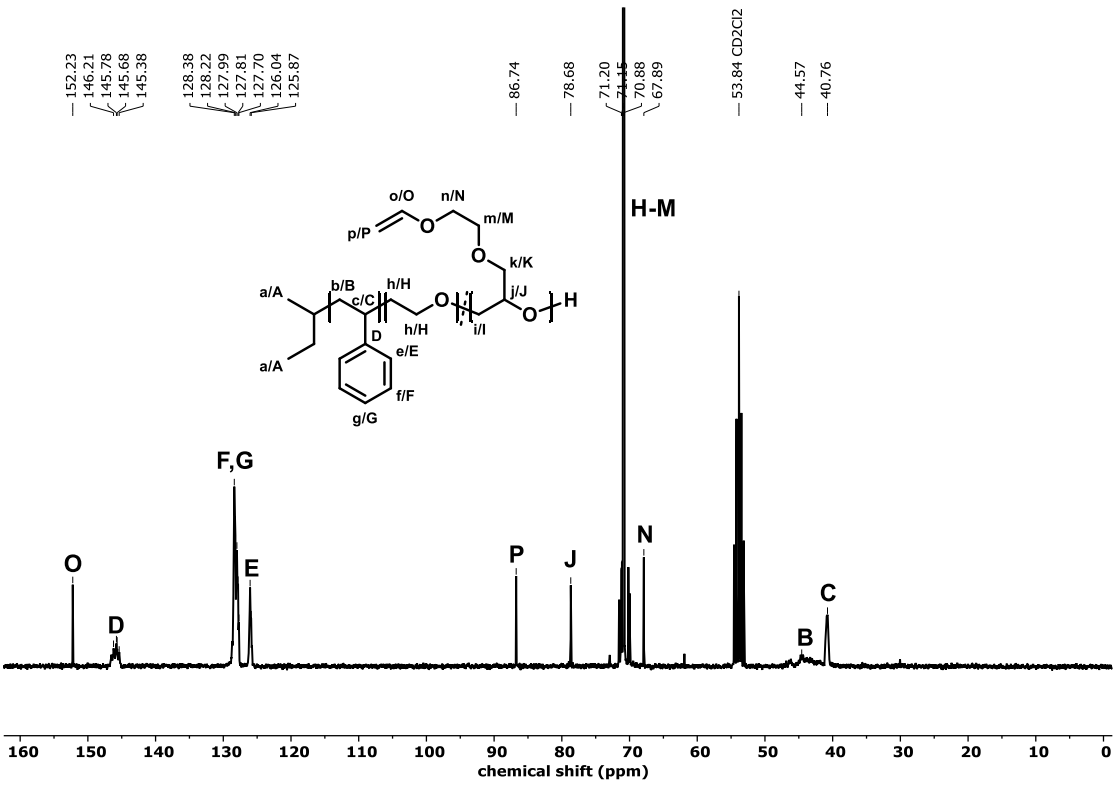

Figure S7. ^{13}C NMR spectrum (75 MHz, CD_2Cl_2) of PS-*b*-P(EO-*co*-EVGE).

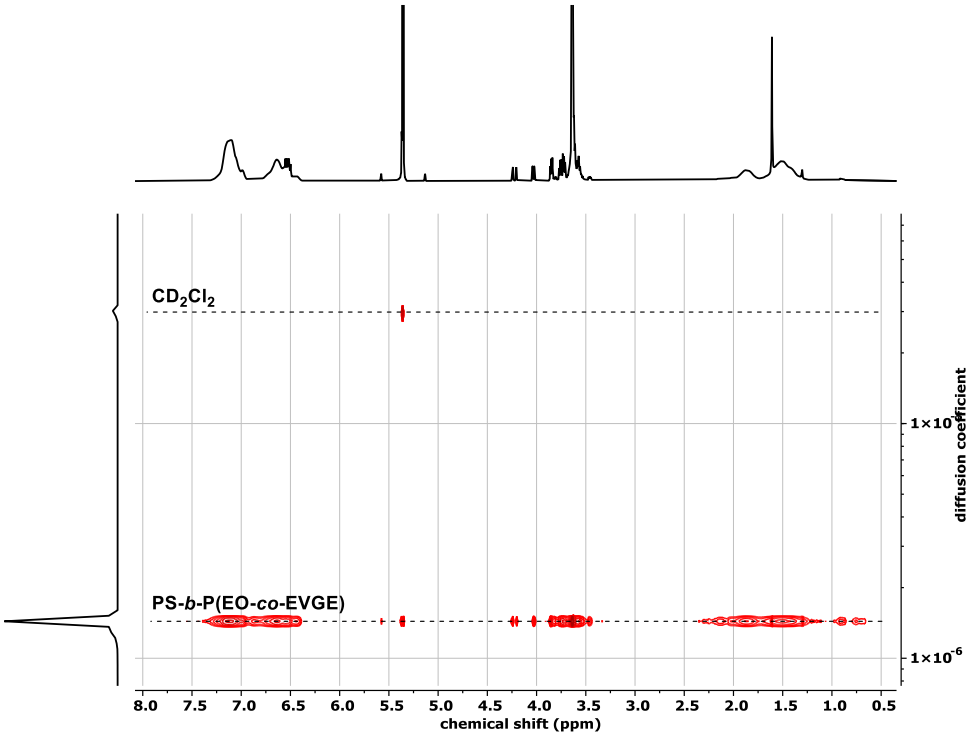

Figure S8. DOSY NMR spectrum (400 MHz, CD_2Cl_2) of PS-*b*-P(EO-*co*-EVGE).

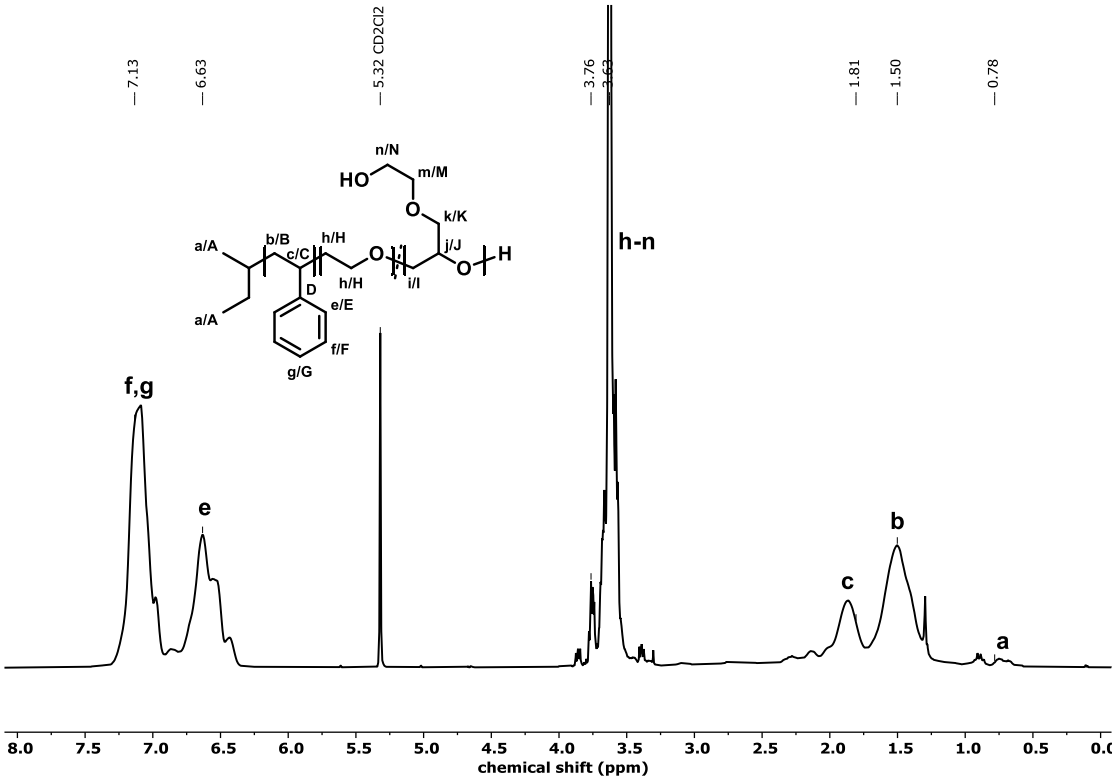

Figure S9. ^{1}H NMR spectrum (300 MHz, CD_2Cl_2) of PS-*b*-P(EO-*co*-HEGE).

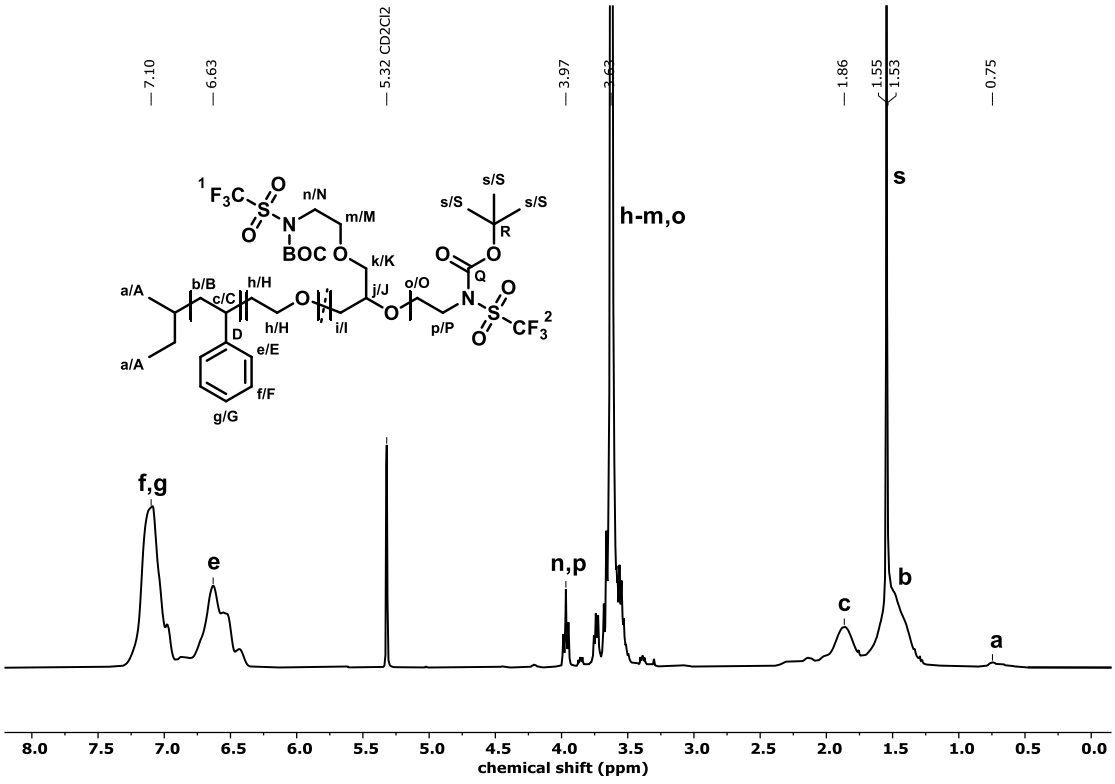

Figure S10. ^{1}H NMR spectrum (300 MHz, CD_2Cl_2) of PS-*b*-P(EO-*co*-BTFSAEGE).

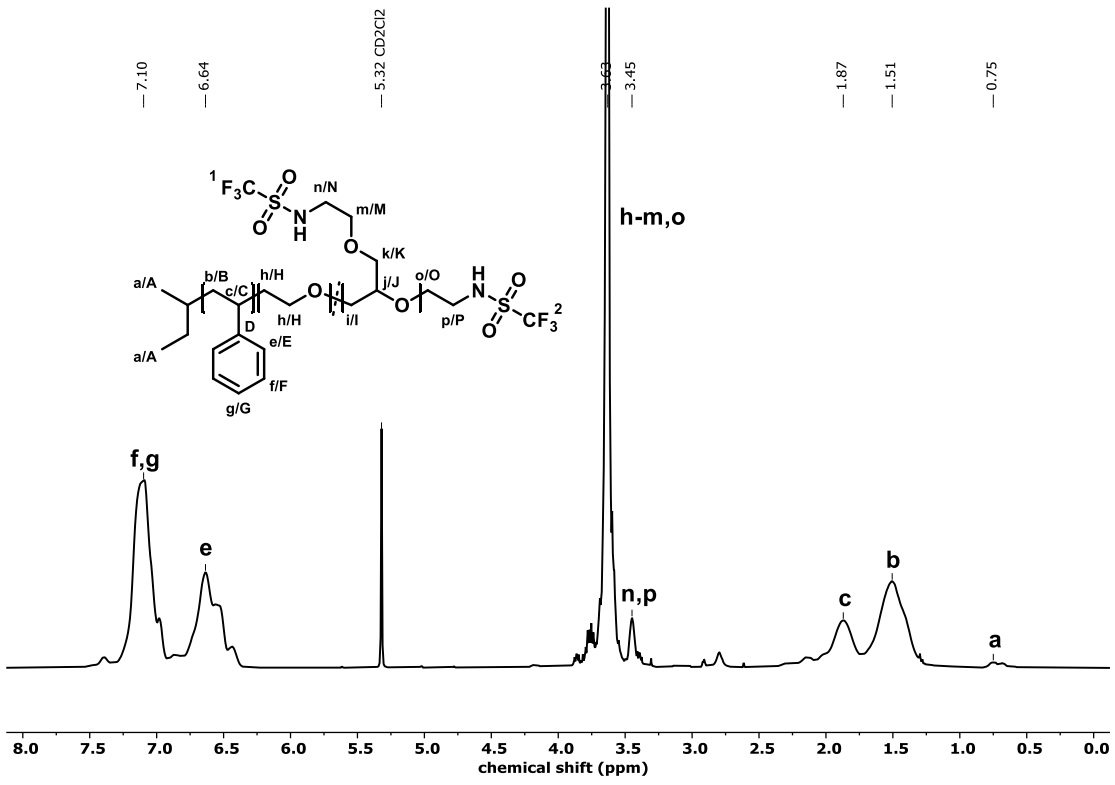

Figure S11. ^{1}H NMR spectrum (300 MHz, CD_2Cl_2) of PS-*b*-P(EO-*co*-TFSAEGE).

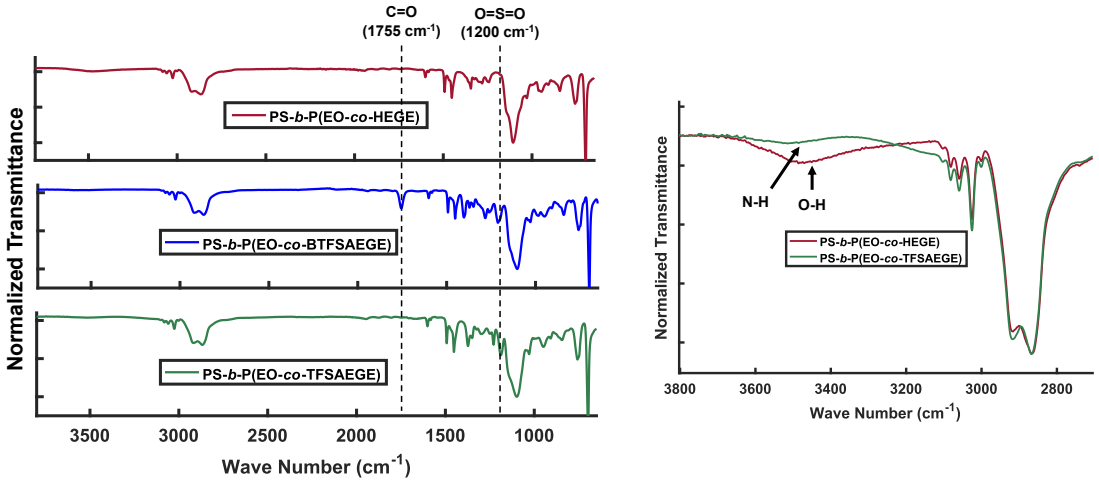

Figure S12. Stacked IR spectra of PS-*b*-P(EO-*co*-HEGE), PS-*b*-P(EO-*co*-BTFSAEGE) and PS-*b*-P(EO-*co*-TFSAEGE).

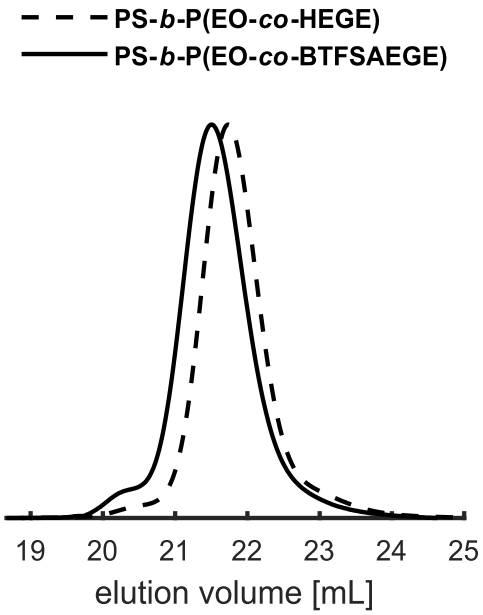

Figure S13. SEC traces (THF, PS calibration) of PS-*b*-P(EO-*co*-HEGE) and PS-*b*-P(EO-*co*-BTFSAEGE).

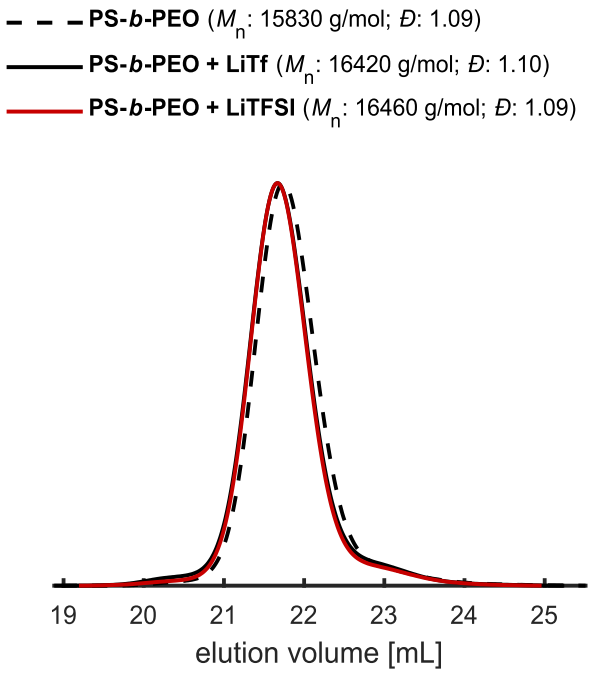

Figure S14. SEC traces (THF, PS calibration) of neat and salt-doped PS-*b*-PEO.

Investigation of the PPMR with mPEO

The *ω*-chain end of mPEO 5k was substituted with BTFSA under the reaction conditions utilized for PS-*b*-P(EO-*co*-HEGE) (Scheme S1). After the PPMR, the disappearance of the proton of the hydroxyl group of PEO 5k (a) in the ^{1}H NMR spectrum of *ω*-BTFSA-PEO (Figure S15) confirms a quantitative substitution of the hydroxyl end group with BTFSA.

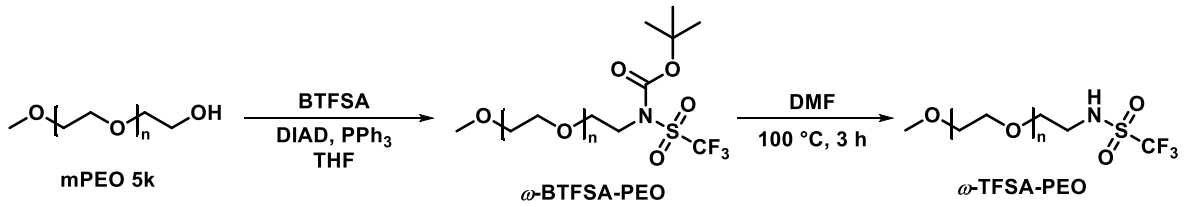

Scheme S1. Synthesis of *ω*-BTFSA-PEO and *ω*-TFSA-PEO.

Additionally, the protons of the methylene group next to the BTFSA group (a', b') are present in the spectrum. The SEC trace of *ω*-BTFSA-PEO (Figure S16) shows a monomodal distribution ($Đ = 1.05$) with a slight shift to lower elution volume, compared to mPEO 5k. MALDI-ToF MS was utilized to further investigate the substitution efficiency of the PPMR. In the case of PS-*b*-P(EO-*co*-HEGE) and PS-*b*-P(EO-*co*-BTFSAEGE), MALDI-ToF MS was not feasible due to the increased variety of linear combinations in the spectrum. Two distributions are observed in the MALDI-ToF mass spectrum of *ω*-BTFSA-PEO (Figure S17), which can be attributed to *ω*-BTFSA-PEO and

ω-TFSA-PEO, ionized with a potassium cation. Even though the ionization process or utilized matrix seem to promote partial cleavage of the BOC protection group, quantitative substitution of the hydroxyl end group was confirmed based on the absence of a mPEO 5k species. Further cleavage of the BOC protection group was achieved via thermolysis in DMF with the utilized reaction conditions for PS-*b*-P(EO-*co*-TFSAEGE) (Scheme S1). The corresponding proton of the free sulfonamide group (a") is present while the BOC protection group signal (b') disappeared. Additionally, the signal of the protons of the methylene group next to the sulfonamide group shifted to higher fields (a"). The deprotection of the TFSA group results in a noticeable change in the hydrodynamic radius because a strong shift to lower elution volume of the SEC trace of ω-TFSA-PEO ($Đ$ = 1.04) (Figure S16) is observed, compared to ω-BTFSA-PEO. The single distribution of ω-TFSA-PEO in the MALDI-ToF mass spectrum (Figure S18) further confirms the quantitative cleavage of the BOC protection group and the absence of side reactions during the deprotection step.

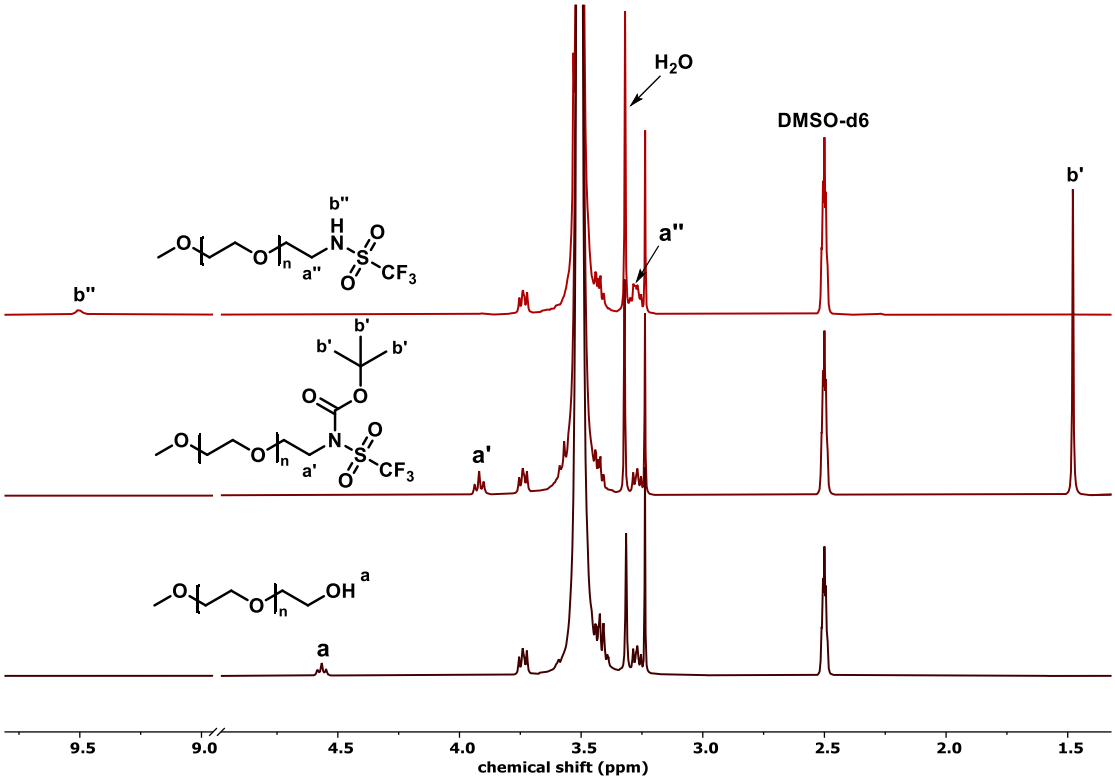

Figure S15. ^{1}H NMR spectra ((300 MHz, CD_2Cl_2)) of PEO 5k, ω-BTFSA-PEO and ω-TFSA-PEO.

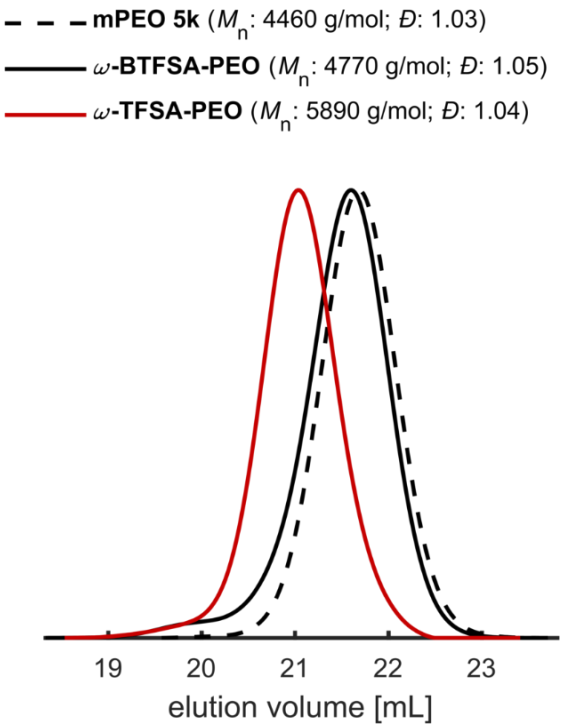

Figure S16. SEC traces of PEO 5k, ω-BTFSA-PEO and ω-TFSA-PEO.

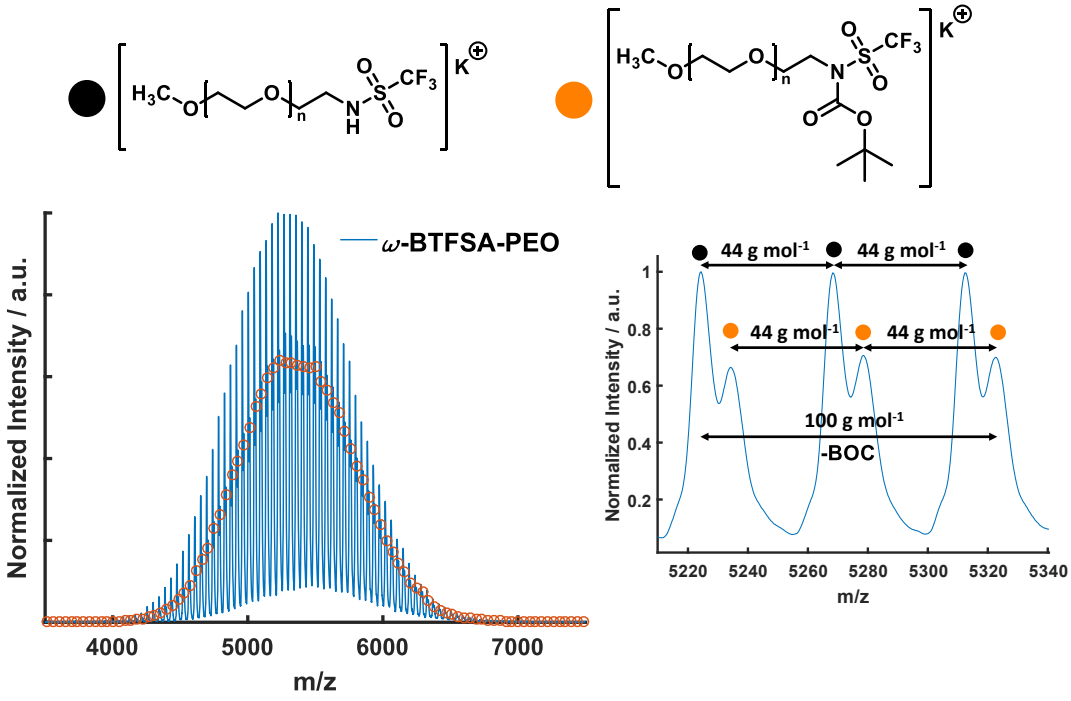

Figure S17. MALDI ToF MS (DCTB, KTFA, linear mode) of ω-BTFSA-PEO (orange).

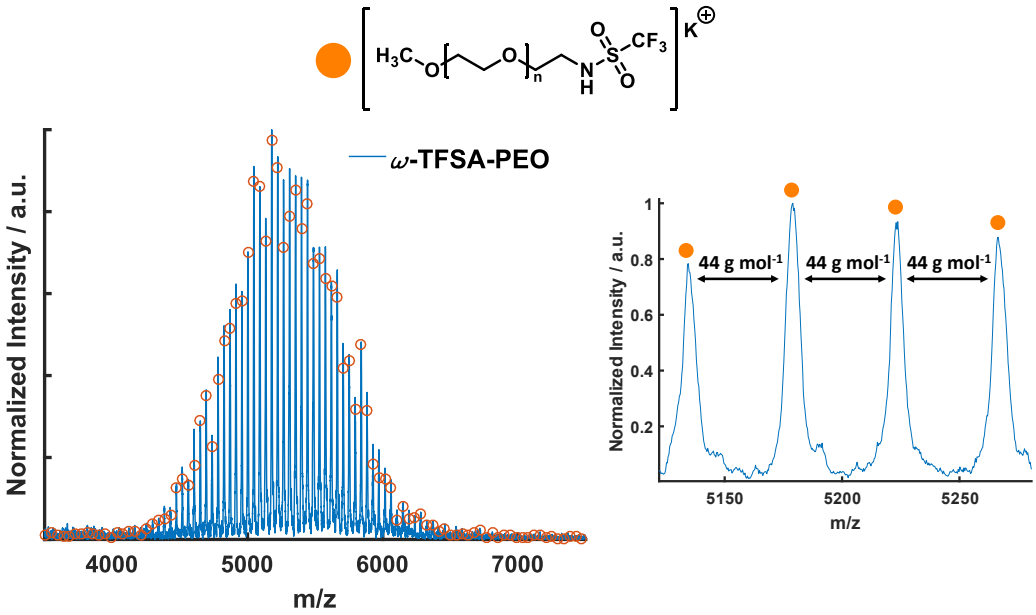

Figure S18: MALDI ToF MS (DCTB, KTFA, linear mode) of ω-TFSA-PEO (orange).

REFERENCES

(1) Mangold, C.; Dingels, C.; Obermeier, B.; Frey, H.; Wurm, F. PEG-based Multifunctional Polyethers with Highly Reactive Vinyl-Ether Side Chains for Click-Type Functionalization. *Macromolecules* **2011**, *44*, 6326–6334.

Chapter 3.3

High Yield Peptide Synthesis Strategies for Complex Block Terpolymers: Amphiphilic Thermoplastic Elastomers and their Application as Solid Polymer Electrolytes

Philip Dreier[†], Marvin Steube[†], George Floudas[*,‡,⊥] and Holger Frey[*,†]

[†]**Department of Chemistry, Johannes Gutenberg University Mainz, Germany**

[‡]**Department of Physics, University of Ioannina, Greece**

[⊥]**Max Planck Institute for Polymer Research, Mainz, Germany**

ABSTRACT: Polystyrene and poly(ethylene oxide) containing block copolymers are promising candidates for solid polymer electrolytes (SPE) in lithium-based batteries. In this work, we introduce the combination of PEO with mechanically adjusted tapered polystyrene copolymers into an thermoplastic elastomer electrolyte (TPEE) via efficient coupling chemistry. Solid-phase peptide synthesis chemistry was employed for the coupling of two carboxylic acid end-group functionalized tapered poly(isoprene-*co*-styrene) (P(I-*co*-S)-COOH) with diamino functional poly(ethylene oxide) (α,ω-NH_2-PEO). The resulting tapered pentablock material P(I-*co*-S)-*b*-PEO-*b*-P(S-*co*-I) was doped with lithium bis(trifluoromethane)sulfonylimide (LiTFSI) and investigated regarding its application as SPE. Rheological investigations of neat and salt-doped material reveal TPE mechanics and toughness over a broad temperature range, facilitating processing of the material. With increasing salt concentration, a decrease in the melting point of the polar PEO block and an increase in the ordering of the lamellar morphologies were revealed by DSC and SAXS measurements, respectively. Further conductivity measurements show an increase in conductivity with decreasing lithium ion concentration in the SPE and an increase of the segmental behavior, whereas [EO]:[Li] = 16:1 exhibited the highest ionic conductivity of all investigated samples. Vogel-Tammann-Fulcher behavior was observed in all salt-doped samples for the temperature dependent conductivities, and ionic conductivities up to 10^{-4} S cm^{-1} above 353 K were obtained.

INTRODUCTION

Block copolymers (BCP) are materials that combine the physical properties of different polymer chains in one well-defined polymer structure. Materials of this type can self-assemble into ordered, microphase-separated nanoscale structures, depending both on the constituents´ volume fraction and the extent of immiscibility of the polymer blocks involved, expressed by the Flory-Huggins interaction parameter. In the simplest diblock copolymer (AB) case, the resulting morphologies can be of spherical, cylindrical, gyroid or lamellar nature.[1] ABA triblock copolymers based on a glassy (i.e. high glass transition) block A (e.g. polystyrene (PS)) and a rubbery middle block B (e.g. polydienes) possess high mechanical stability and toughness[2–5] and are widely used technical products, known as "thermoplastic elastomers" (TPEs).[6]

BCPs are obtained by sequential addition of the different monomers, i.e. living polymerization techniques, or the covalent linkage of distinct homopolymers. Additionally, (multi)block copolymers are generated via carbanionic polymerization capitalizing on the repeated addition of 1,3-diene/styrene-mixtures to the living chain-end in hydrocarbons.[7] This strategy relies on the preferential incorporation of isoprene during the copolymerization with styrene and subsequent formation of a tapered block copolymer P(I-*co*-S) structure in nonpolar solvents, such as cyclohexane.[7–10] The steepness of the taper is further adjustable by variation of the applied temperature[11] or via addition of polar additives, so called "modifiers".[12] Consequently, depending on the molecular weight and amount of modifier, the introduction of the low glass transition temperature (T_g) PI segments in the glassy PS structure alters the mechanical properties and morphologies of the resulting copolymers.[11]

In sequential ABA triblock copolymers, replacing the polydiene block with semi-crystalline poly(ethylene oxide) (PEO) results in amphiphilic polystyrene-*block*-poly(ethylene oxide)-*block*-polystyrene (PS-*b*-PEO-*b*-PS) structures. As a result of the low T_g (≈-60 °C), PEO is a highly flexible material and hence a suitable middle block for TPEs. However, the semicrystalline nature of PEO below the melting point (≈ 55-60 °C) constitutes an obstacle for such applications. The high polarity of the PEO backbone further allows the solvation of salts in the polyether, thus functions as a conductive matrix for ions in polymer electrolytes.[13] Fortunately, the salt-doping affects crystallization behaviour and amorphous PEO is obtained depending on the utilized salt and the resulting PEO-salt ratio.[14] The lack of crystalline domains is advantageous both with respect to mechanical properties and ion mobility.

Lithium salt-doped PS-*b*-PEO of different molecular weights and compositions has been investigated in a variety of works with respect to application as a solid polymer electrolyte (SPE) in lithium-based batteries,[15–18] because the material combines high ionic conductivity of the salt-containing PEO block (10^{-4} S cm^{-1})[18] with the required mechanical stability of the PS block against dendritic growth of lithium.

PS-*b*-PEO is typically synthesized by the combination of the living anionic polymerization of styrene and subsequent anionic ring-opening polymerization of EO.[19–24] In contrast, PS-*b*-PEO-*b*-PS structures are not accessible by this type of sequential approach, since the alkoxide chain end of PEO is incapable of initiating the polymerization of styrene.[21] Therefore, controlled radical polymerization techniques such as ATRP or RAFT, based on PEO macroinitiators must be employed to achieve the desired PS-*b*-PEO-*b*-PS structure.[25–27] However, these synthesis routes result in materials with rather low molecular weight PEO blocks and corresponding homopolymer traces cannot be avoided due to the limitations of the polymerization mechanism.[28] On the other hand, the implementation of coupling strategies for the covalent linkage of the respective PEO and PS homopolymers resulted in insufficient coupling of the corresponding blocks and ill-defined ABA structures.[29–31]

In comparison, solid-phase peptide synthesis (SPPS) relies on efficient coupling and protection group chemistry to achieve desired peptide sequences. Long term efforts in this area resulted in the development of coupling reagents, which support a selective and nearly quantitative amide bond formation of the corresponding carboxylic acid and amine functionalities.[32] These approaches can be adapted to non-solid synthesis procedures. As an example, the SPPS chemistry was successfully employed in a recent publication by Besenius et al. for the synthesis of monomers for supramolecular polymerization.[33]

In the following, we describe how the underlying coupling chemistry of SPPS is adaptable to the efficient covalent linkage of tapered block copolymers, in our case P(I-*co*-S) with PEO, yielding well-defined high molecular weight P(I-*co*-S)-*b*-PEO-*b*-P(S-*co*-I) structures. To the best of our knowledge, for the first time this approach combines the versatile and defined tapered block copolymer obtained from statistical copolymerization of I and S with the polar PEO block into a TPE material. Subsequent salt doping with lithium bis(trifluoromethane)sulfonylimide (LiTFSI) results in a TPE with SPE properties. The resulting salt-doped block terpolymer structures are investigated with respect to their application as thermoplastic elastomer electrolyte (TPEE).

RESULTS AND DISCUSSION

Synthesis of P(I-*co*-S)-*b*-PEO-*b*-P(S-*co*-I)

In a first step, hydroxyl functional tapered poly(isoprene-*co*-styrene) (P(I-*co*-S)-OH) was synthesized via anionic copolymerization of a 50/50%$_{mol}$ mixture of isoprene and styrene in cyclohexane[7] and subsequent addition of excess ethylene oxide (EO) to the living chain end.[34,35] The resulting ^{1}H NMR spectrum of P(I-*co*-S)-OH shows the typical PI and PS signals and the resonance of the methylene group next to the hydroxyl group at 3.30 ppm (Figure S1).

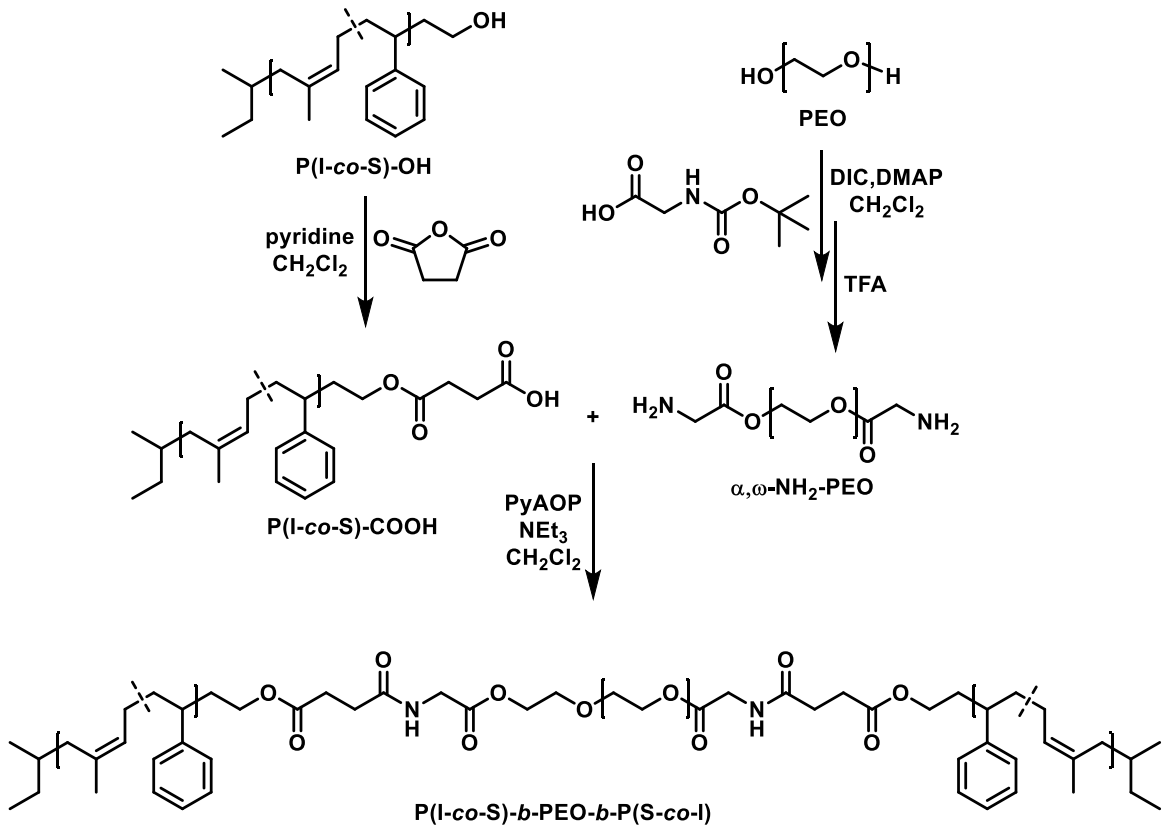

Scheme 1. Synthesis route of P(I-*co*-S)-*b*-PEO-*b*-P(S-*co*-I).

The tapered microstructure of isoprene and styrene (Figure S9) is obtained due to the preferred incorporation of isoprene to the living chain end in cyclohexane, which has been investigated with detailed online kinetics in recent years.[7–10] P(I-*co*-S)-OH was transferred into its carboxylic acid analog (P(I-*co*-S)-COOH) by the base-catalyzed esterification reaction with succinic anhydride (Scheme 1). The functionalization procedure was followed via ^{1}H NMR spectroscopy monitoring the disappearance of the methylene group signal (3.31 ppm) next to the hydroxyl group of P(I-*co*-S)-OH (Figure S1) and the appearance of a new resonance at 3.78 ppm, corresponding to the methylene group next to the ester oxygen (Figure S2). In the ensuing step, the amino component for the SPPS analogue reaction was obtained via Steglich esterification of the α and ω-hydroxyl groups of PEO with *N*-(*tert*-butyloxycarbonyl) glycine (*N*-BOC glycine) and subsequent deprotection of the BOC protection group (Scheme 1). The viability of the Steglich esterification as an efficient post-polymerization reaction of hydroxyl groups with *N*-BOC glycine was recently demonstrated by Gallei et al.[36] After the Steglich reaction, new signals in the ^{1}H NMR spectrum (Figure S3), assigned to the covalently attached *N*-BOC glycine and the methylene group next to the ester oxygen (4.27 ppm) confirm the successful derivatization reaction of PEG. Quantitative deprotection of the amino functionality was achieved via acidic work-up with trifluoracetic acid (TFA) and was monitored via ^{1}H NMR spectroscopy by the vanishing of the protection group signal at 1.42 ppm and a shift of the methylene group signal next to the ester oxygen from 4.27 to 4.36 ppm (Figure S8). Additionally, the ^{1}H NMR spectrum of α,ω-NH_2-PEO

shows the corresponding signal of the methylene groups of the glycine residue at 3.93 ppm (Figure S4), confirming the stability of the ester group under the chosen deprotection conditions.

In the final step, the amidation reaction conditions of solid phase peptide synthesis were adapted for the coupling of P(I-*co*-S)-COOH and α,ω-NH_2-PEO. The amide bond formation was achieved in dichloromethane with the coupling reagent PyAOP in the presence of triethylamine at room temperature (Scheme 1).[37] A slide excess of P(I-*co*-S)-COOH (1.1 equivalents per amino group) was employed to ensure quantitative reaction of the amino groups with the carboxylic acid functionalities. Excess of P(I-*co*-S)-COOH precursor was removed from the coupling product via precipitation of the block terpolymer in ice-cold diethyl ether, which is an essential purification step to achieve the well-defined block structure. P(I-*co*-S)-*b*-PEO-*b*-P(S-*co*-I) with a molecular weight of 50 kg mol^{-1} and a PEO volume fraction of 0.36 (Table 1) was obtained.

Table 1. Sample Overview of P(I-*co*-S)-*b*-PEO-*b*-P(S-*co*-I).

Sample	$M_{n,P(I\text{-}co\text{-}S)}$ [a] [kg mol^{-1}]	$M_{n,PEO}$ [a] [kg mol^{-1}]	$M_{n,total}$ [a] [kg mol^{-1}]	$M_{n,total}$ [b] [kg mol^{-1}]	$Đ$ [b]	$f_{P(I\text{-}co\text{-}S)}$ [a]	f_{PEO} [a]
P(I-*co*-S)-*b*-PEO-*b*-P(S-*co*-I)	30.0	20.0	50.0	49.5	1.18	0.64	0.36

a) Determined by ^{1}H NMR spectroscopy; b) Determined by SEC (THF, PS calibration, RI detector).

The corresponding microstructure is visualized in Figure 1b. Based on the above-mentioned observations, we emphasize that the presented synthesis route can be transferred to coupling reactions of PEO with other polymers, if the COOH-precursor polymer is soluble in diethyl ether. To the best of our knowledge, this is the first time P(I-*co*-S)-*b*-PEO-*b*-P(S-*co*-I) architectures have been synthesized. Consequently, a distinct shift of the SEC trace of P(I-*co*-S)-*b*-PEO-*b*-P(I-*co*-S) to lower elution volume and therefore higher molecular weight relative to the precursors is observed (Figure 1a).

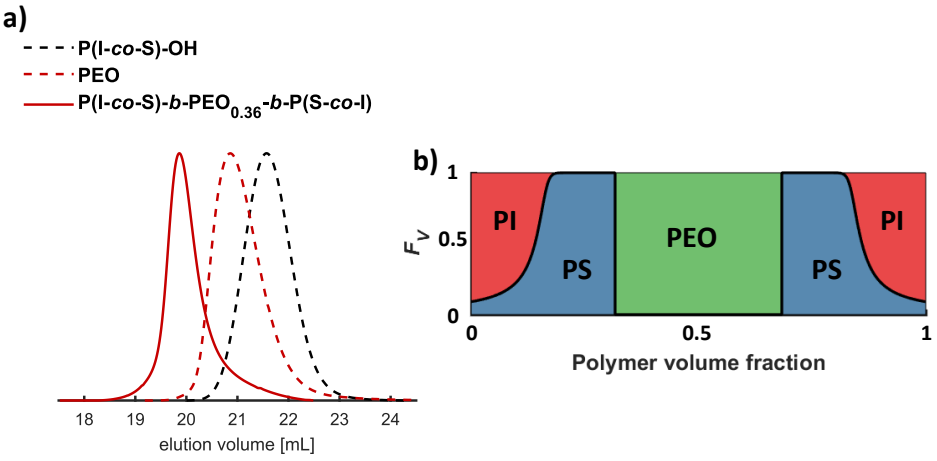

Figure 1. a) Stacked SEC traces of PEO, P(I-*co*-S)-OH and P(I-*co*-S)-*b*-PEO-*b*-P(S-*co*-I) with 36 $\%_{vol}$ PEO (THF, PS calibration, RI detector); b) Mean incorporation volume (F_V) of the different monomers (PI: red, PS: blue. PEO: green) as a function of the polymer volume fraction.

Additionally, the SEC trace of P(I-*co*-S)-*b*-PEO-*b*-P(S-*co*-I) shows a monomodal distribution with a narrow dispersity of 1.18 (Table 1). The corresponding ^{1}H (Figure 2) and ^{13}C NMR spectra (Figure S5) of P(I-*co*-S)-*b*-PEO-*b*-P(S-*co*-I) confirm quantitative coupling by comparison of the integral of the aromatic protons of P(I-*co*-S) with the integral of the methylene group of the glycine residue. The ratio between the aromatic protons of PS and the methylene group protons of the PEO backbone is in good accordance with the theoretical value. Further, the DOSY NMR spectrum of P(I-*co*-S)-*b*-PEO-*b*-P(S-*co*-I) shows one exclusive diffusion coefficient for all P(I-*co*-S) and PEO resonances (Figure 2). In a comparative study, the direct coupling of P(I-*co*-S)-COOH with unmodified PEO under the employed reaction conditions was investigated, revealing a merely moderate coupling efficiency (Figure S8).

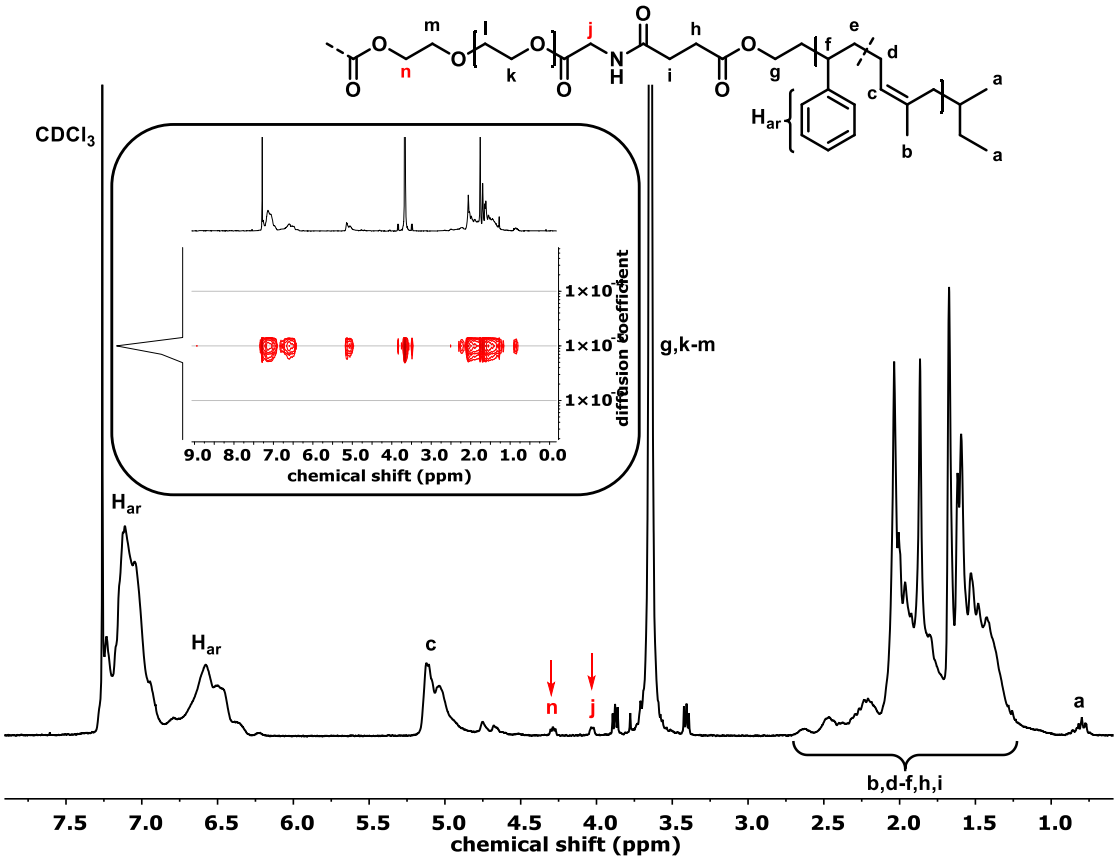

Figure 2. ^{1}H NMR and DOSY spectrum (inset) ($CDCl_3$, 300 MHz) of P(I-*co*-S)-*b*-PEO-*b*-P(S-*co*-I); Important resonances are highlighted in red with arrows.

The prepared block terpolymer and LiTFSI-doped analogs with different concentrations of salt were investigated concerning their thermal properties, viscoelastic behavior, structural characteristics and ionic conductivities (Table 2).

Table 2. Overview of thermal and structural properties of neat and salt-doped P(I-*co*-S)-*b*-PEO-*b*-P(S-*co*-I).

[EO]:[Li]	*r* ([Li]:[EO])	$T_{g,PEO}$ [a)] [°C (K)]	$T_{m,PEO}$ [a)] [°C (K)]	$X_{c,PEO}$ [a)] [%]	$T_{g,PS}$ [b)] [°C (K)]	Morphology[c)]
neat	0.00	-30 (243)	52 (325)	72	44 (317)	LAM_2
16:1	0.06	-50 (223)	42 (315)	21	53 (326)	LAM_2
12:1	0.08	-47 (226)	-	-	56 (329)	LAM_2
8:1	0.13	-40 (233)	-	-	60 (333)	LAM_2
4:1	0.25	-32 (241)	-	-	63 (336)	LAM_2

a) Determined via DSC (second heating curve, heating rate: 10 K min^{-1}); b) Determined via rheology; c) Determined via SAXS at 393 K.

Thermal Properties of salt-doped BCPs

The influence of salt-doping on the thermal properties of P(I-*co*-S)-*b*-PEO-*b*-P(S-*co*-I) was investigated via differential scanning calorimetry (DSC) (Figure 3).

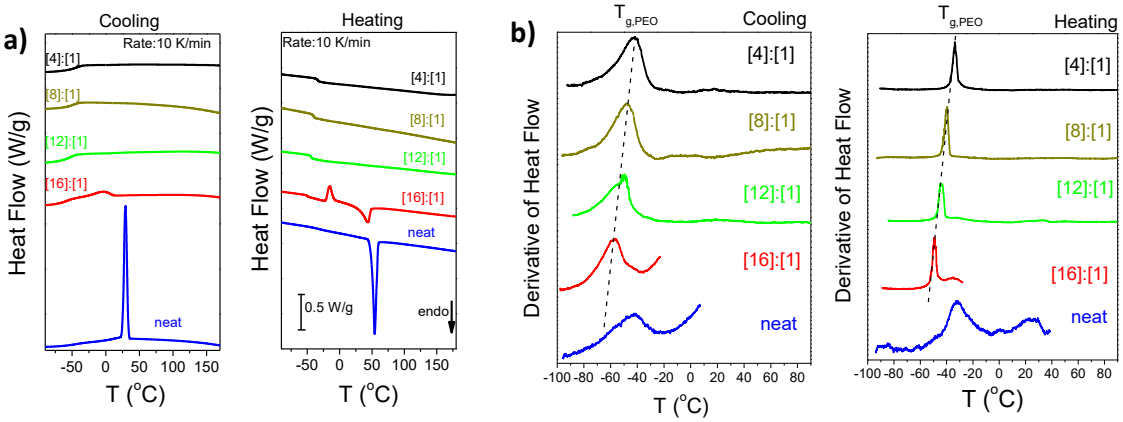

Figure 3. a) Stacked DSC curves of P(I-*co*-S)-*b*-PEO-*b*-P(S-*co*-I) with different salt concentrations; b) Derivatives of the DSC curves.

At low salt-concentration ([EO]:[Li] = 16:1), a decrease of $T_{m,PEO}$ and degree of crystallization (X_c) in comparison to neat P(I-*co*-S)-*b*-PEO-*b*-P(S-*co*-I) is observed, accompanied with cold crystallization upon heating. With further increase of the LiTFSI concentration (from 12:1 to 4:1), completely amorphous materials are obtained (Figure 3). For the latter, merely a glass transition for the PEO block was observed, with $T_{g,PEO}$ increasing with larger salt concentration from 223 ([EO]:[Li] = 16:1) up to 241 K ([EO]:[Li] = 4:1) (Figure 4, Table 2).

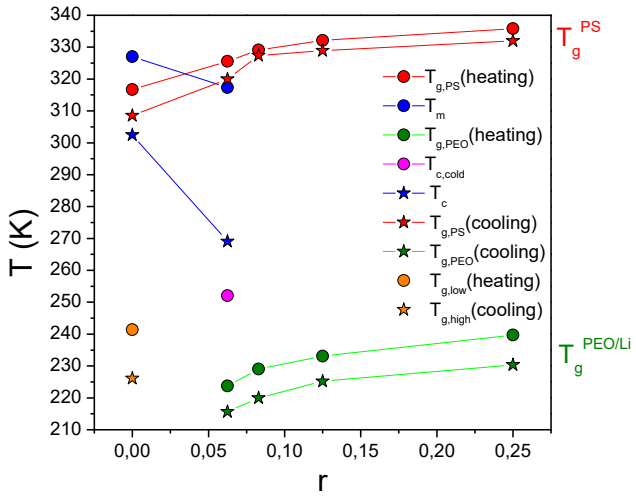

Figure 4. Overview of the thermal properties of the samples in dependence of the salt concentration.

In summary, the concentration dependent influence of salt addition on the $T_{g,PEO}$ confirms the exclusive accumulation of LiTFSI in the polar PEO domains and are in line with the results obtained from comparable salt-doped BCP systems.[38–40]

Viscoelastic Behavior

The glass transition temperature of the P(I-co-S) block ($T_{g,PS}$) is not observed in the DSC measurements. However, values of $T_{g,PS}$ (Figure 4, Table 2) for all samples were obtained from rheological measurements (Figure 5). Herein, the glass transition event of neat P(I-*co*-S)-*b*-PEO-*b*-P(S-*co*-I) was observed at 317 K.

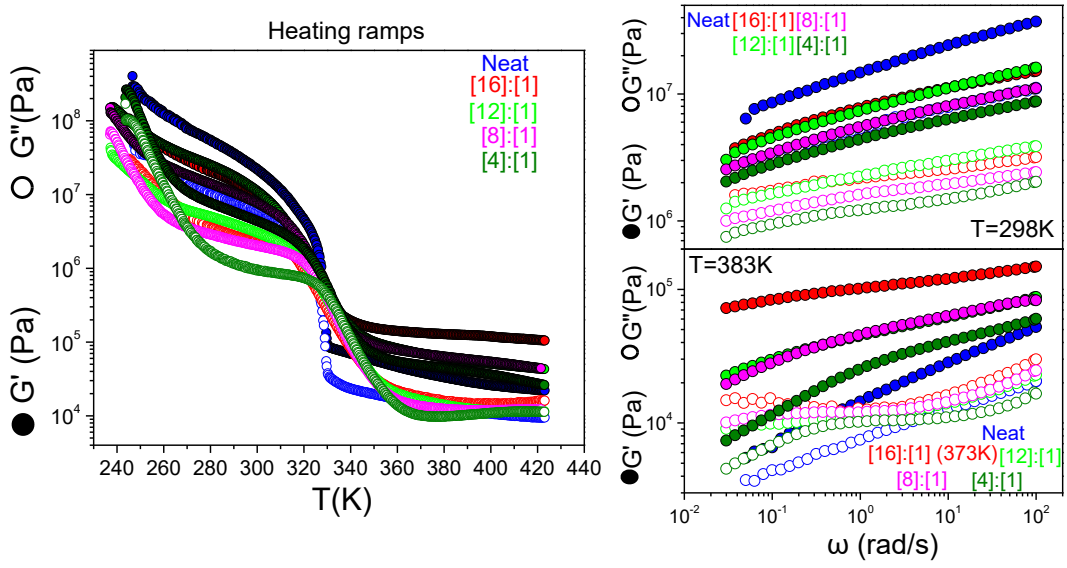

Figure 5. Left: Storage (filled symbols) and loss (open symbols) moduli (heating rate: 2 K min^{-1}, frequency: 10 rad s^{-1}); Right: Frequency scans of the samples at 298 and 383 K.

This value is significantly lower than $T_{g,PS}$ obtained for polystyrene (353 K) in PS-*b*-PEO,[15] showing the expected impact of incorporated PI segments on the thermal properties of the P(I-*co*-S) block. In addition, an increase of $T_{g,PS}$ of the P(I-*co*-S) block upon salt-doping is observed from 326 (16:1) to 336 K (4:1) (Figure 4 and 5), which is explained by the stiffening of the P(I-*co*-S) block at the PEO/P(I-*co*-S) interface,[15] and this effect is more pronounced in case of higher LiTFSI concentrations.

At temperatures below the glass transition, the storage modulus G' of the salt-doped samples decreases with increasing salt concentration due to a reduction of the degree of crystallization, whereas neat P(I-*co*-S)-*b*-PEO-*b*-P(S-*co*-I) exhibits the largest storage modulus. Upon heating above $T_{g,PS}$, G' remains higher than the corresponding loss modulus G" for neat and salt-doped samples. This demonstrates the TPE-like behavior of the triblock terpolymers. Interestingly, G' of all salt-doped samples remains at higher values than G' for neat P(I-*co*-S)-*b*-PEO-*b*-P(S-*co*-I), which is attributed to additional non-covalent intramolecular interaction of the PEO chains due to interactions between lithium cations and ether oxygens.[15]

Isothermal frequency scans at 298 K of neat and salt-doped P(I-*co*-S)-*b*-PEO-*b*-P(S-*co*-I) show a frequency independence of G' and at all measured frequencies G' remains larger than G", indicating elastic behavior. At 383 K, salt-doped samples exhibit frequency dependent moduli, while G' values are higher with respect to neat P(I-*co*-S)-*b*-PEO-*b*-P(S-*co*-I). Herein, a salt concentration of [EO]:[Li] = 16:1 results in the highest storage modulus (10^5 Pa) of all investigated samples. The viscoelastic response of the salt-doped material suggests the formation of transient network structures of LiTFSI with the PEO chains[15,41] at temperatures above $T_{g,PS}$.

Structural Characteristics of salt-doped BCPs

In the following, phase separation behavior of neat and salt-doped samples was investigated via small-angle X-ray scattering (SAXS) measurements. A disordered state was observed at room temperature for the tapered precursor diblock copolymer P(I-*co*-S)-OH.

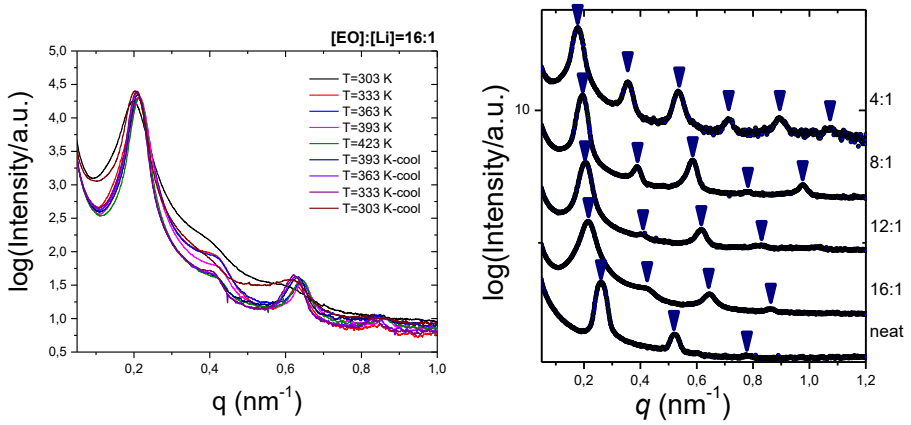

Figure 6. Left: SAXS patterns of 16:1 sample at different temperatures (cool: cooling); Right: Stacked SAXS patterns of neat and salt-doped P(I-*co*-S)-*b*-PEO-*b*-P(S-*co*-I) (M_n = 50 kg mol^{-1}, f_{PEO} = 0.39) at 393 K.

In comparison, based on the obtained SAXS patterns (Figure 6 and S10), neat and salt-doped tapered pentablock copolymers P(I-*co*-S)-*b*-PEO-*b*-P(S-*co*-I) form lamellar morphologies (LAM_2) at 393 K. Upon cooling, the recrystallization of neat and [EO]:[Li] = 16:1 samples was monitored by broadening of the SAXS reflections (Figure 6). With increasing salt concentration, a pronounced increase both in the long-range order and the domain spacing (d) is observed (Figure 7).

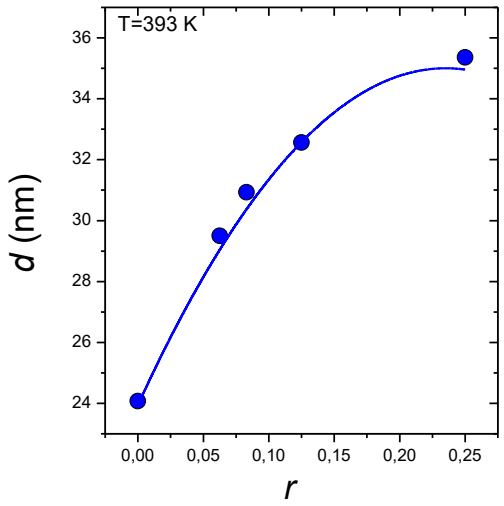

Figure 7. Domain spacing dependent on the salt concentration obtained via SAXS at 393 K.

This is indicated by the occurrence of higher-order reflections up to the sixth order and a shift of the first-order reflection (q^*) to smaller values (Figure 6). The increase of d from 24 nm (neat) to 35 nm (4:1) (Figure 7) with increasing salt content is in accordance with earlier studies[15,38,39] and is attributed to the accumulation of LiTFSI in the PEO domains as well as an increase in the salt-dependent effective interaction parameter ($\chi_{\text{eff}}(N,r)$) (N: degree of polymerization, r: [Li]:[EO]).[15,42]

Ionic Conductivity of salt-doped BCPs

Further investigations concerning the temperature-dependent dc conductivities of neat and salt-doped samples reveal a qualitative trend: With increasing salt concentration from 16:1 to 4:1, a decrease in conductivity is observed (Figure 7). Additionally, a typical Vogel-Tammann-Fulcher-behaviour[18] was observed for the ionic conductivity of the salt-doped samples. Consequently, the ionic conductivity of salt-doped P(I-*co*-S)-*b*-PEO-*b*-P(S-*co*-I)) depends on the segmental mobility of the PEO block and scales with $T_{\text{g,PEO}}$.

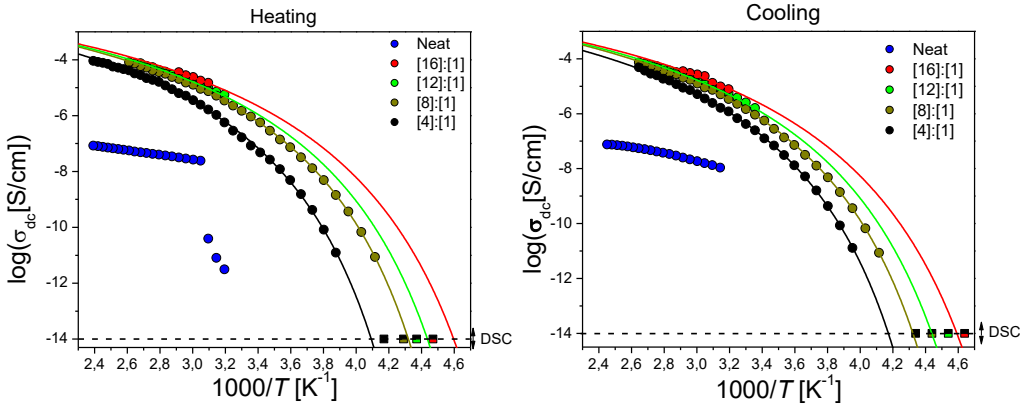

Figure 8. Temperature dependence of ionic conductivity of neat and salt-doped P(I-co-S)-b-PEO-b-P(S-co-I) upon heating (left) and cooling (right); Conductivity decreases with increasing salt concentrations because of VTF behavior of the salt-doped samples.

Consequently, P(I-*co*-S)-*b*-PEO-*b*-P(S-*co*-I) with a salt concentration of 16:1 and the lowest $T_{g,PEO}$ of all investigated samples (223 K) (Figure 3, Table 2) exhibits the highest ionic conductivity. Above 353 K, ionic conductivities up to 10^{-4} S cm^{-1} are obtained for [EO]:[Li] = 16:1, which is in the typical range for salt-doped PS-b-PEO BCPs.[18]

CONCLUSION

The highly efficient coupling chemistry developed for solid-phase peptide synthesis has been adapted for the covalent linkage of carboxylic acid end-group functionalized tapered poly(isoprene-*co*-styrene) (P(I-*co*-S)-COOH) and diamino functionalized poly(ethylene oxide) (α,ω-NH_2-PEO) to generate tapered pentablock terpolymers. The precursors were obtained via quantitative end group esterification reactions with succinic anhydride and BOC-protected glycine of P(I-*co*-S)-OH and PEO, respectively. The resulting block terpolymer (P(I-*co*-S)-*b*-PEO-*b*-P(S-*co*-I)) (M_n = 50 kg mol^{-1}, f_{PEO} = 0.36) exhibited a monomodal molecular weight distribution with a narrow polydispersity of 1.18. For the first time, the herein presented coupling chemistry allowed the synthesis of the otherwise inaccessible complex tapered block terpolymer structure.

Investigations of the thermal properties revealed that the polyisoprene segments in the tapered P(I-*co*-S) permit tailoring of the glass transition temperature of the apolar block, compared to the PS homopolymer, which is also relevant in view of processing.

The resulting well-defined block terpolymer P(I-*co*-S)-*b*-PEO-*b*-P(S-*co*-I) was further mixed with different amounts of LiTFSI to produce solid polymer electrolyte (SPE) materials. Neat and salt-doped samples exhibit lamellar morphologies, while the presence of salt results in chain stretching at the interfaces of the block domains and, as a result, an increase of glass transition temperatures (T_gs) of the and P(I-*co*-S) block ($\Delta T_{g,PS}$ up to 9 K). The viscoelastic properties of salt-doped block terpolymers differ substantially from neat P(I-*co*-S)-*b*-PEO-*b*-P(S-*co*-I). The presence of LiTFSI salt in the PEO domain results in an increased stability of the material above $T_{g,PS}$, relative to the pure block terpolymer, which is attributed to interactions of the PEO chains with the added

lithium salt. Ionic conductivity measurements show typical Vogel-Tammann-Fulcher behavior for all salt-doped samples with conductivities comparable to PS-*b*-PEO and PS-*b*-PEO-*b*-PEO-based SPEs.

In conclusion, salt-doped P(I-*co*-S)-*b*-PEO-*b*-P(S-*co*-I) represents a mechanically stable SPE material with sufficient ionic conductivities. We emphasize that the peptide coupling-based synthesis route is further applicable for the covalent linkage of a wide range of other polymer classes to PEO and other polymer architectures. Furthermore, the influence of a modified tapered structure in P(I-*co*-S) on the thermal and viscoelastic properties of the material are content of further investigations.

REFERENCES

(1) Leibler, L. Theory of Microphase Separation in Block Copolymers. *Macromolecules* **1980**, *13*, 1602–1617.

(2) Georgopanos, P.; Handge, U. A.; Abetz, C.; Abetz, V. Influence of block sequence and molecular weight on morphological, rheological and dielectric properties of weakly and strongly segregated styrene-isoprene triblock copolymers. *Polymer* **2016**, *104*, 279–295.

(3) Holden, G.; Bishop, E. T.; Legge, N. R. Thermoplastic elastomers. *J. polym. sci., C Polym. symp.* **1969**, *26*, 37–57.

(4) Mai, S.-M.; Mingvanish, W.; Turner, S. C.; Chaibundit, C.; Fairclough, J. P. A.; Heatley, F.; Matsen, M. W.; Ryan, A. J.; Booth, C. Microphase-Separation Behavior of Triblock Copolymer Melts. Comparison with Diblock Copolymer Melts. *Macromolecules* **2000**, *33*, 5124–5130.

(5) Qiao, L.; Leibig, C.; Hahn, S. F.; Winey, K. I. Isolating the Effects of Morphology and Chain Architecture on the Mechanical Properties of Triblock Copolymers. *Ind. Eng. Chem. Res.* **2006**, *45*, 5598–5602.

(6) Scheirs, J.; Priddy, D. B. Modern Styrenic Polymers: Polystyrenes and Styrenic Copolymers; John Wiley & Sons, Ltd: Chichester, UK, **2003**.

(7) Steube, M.; Johann, T.; Galanos, E.; Appold, M.; Rüttiger, C.; Mezger, M.; Gallei, M.; Müller, A. H. E.; Floudas, G.; Frey, H. Isoprene/Styrene Tapered Multiblock Copolymers with up to Ten Blocks: Synthesis, Phase Behavior, Order, and Mechanical Properties. *Macromolecules* **2018**, *51*, 10246–10258.

(8) Kraus, G.; Childers, C. W.; Gruver, J. T. Properties of random and block copolymers of butadiene and styrene. I. Dynamic properties and glassy transition temperatures. *Journal of Applied Polymer Science* **1967**, *11*, 1581–1591.

(9) Kraus, G.; Rollmann, K. W. *Angew. Makromol. Chemie* **1971**, *16*, 271–296.

(10) Worsfold, D. J. Anionic copolymerization of styrene and isoprene in cyclohexane. *J. Polym. Sci. A-1 Polym. Chem.* **1967**, *5*, 2783–2789.

(11) Steube, M.; Johann, T.; Plank, M.; Tjaberings, S.; Gröschel, A. H.; Gallei, M.; Frey, H.; Müller, A. H. E. Kinetics of Anionic Living Copolymerization of Isoprene and Styrene Using in Situ NIR Spectroscopy: Temperature Effects on Monomer Sequence and Morphology. *Macromolecules* **2019**, *52*, 9299–9310.

(12) Steube, M.; Johann, T.; Hübner, H.; Koch, M.; Dinh, T.; Gallei, M.; Floudas, G.; Frey, H.; Müller, A. H. E. Tetrahydrofuran: More than a “Randomizer” in the Living Anionic Copolymerization of Styrene and Isoprene: Kinetics, Microstructures, Morphologies, and Mechanical Properties. *Macromolecules* **2020**, *53*, 5512–5527.

(13) Wright, P. V. Electrical conductivity in ionic complexes of poly(ethylene oxide). *Brit. Poly. J.* **1975**, *7*, 319–327.

(14) Lascaud, S.; Perrier, M.; Vallee, A.; Besner, S.; Prud'Homme, J.; Armand, M. Phase Diagrams and Conductivity Behavior of Poly(ethylene oxide)-Molten Salt Rubbery Electrolytes. *Macromolecules* **1994**, *27*, 7469–7477.

(15) Zardalidis, G.; Gatsouli, K.; Pispas, S.; Mezger, M.; Floudas, G. Ionic Conductivity, Self-Assembly, and Viscoelasticity in Poly(styrene- b -ethylene oxide) Electrolytes Doped with LiTf. *Macromolecules* **2015**, *48*, 7164–7171.

(16) Thelen, J. L.; Wang, A. A.; Chen, X. C.; Jiang, X.; Schaible, E.; Balsara, N. P. Correlations between Salt-Induced Crystallization, Morphology, Segmental Dynamics, and Conductivity in Amorphous Block Copolymer Electrolytes. *Macromolecules* **2018**, *51*, 1733–1740.

(17) Devaux, D.; Glé, D.; Phan, T. N. T.; Gigmes, D.; Giroud, E.; Deschamps, M.; Denoyel, R.; Bouchet, R. Optimization of Block Copolymer Electrolytes for Lithium Metal Batteries. *Chem. Mater.* **2015**, *27*, 4682–4692.

(18) Panday, A.; Mullin, S.; Gomez, E. D.; Wanakule, N.; Chen, V. L.; Hexemer, A.; Pople, J.; Balsara, N. P. Effect of Molecular Weight and Salt Concentration on Conductivity of Block Copolymer Electrolytes. *Macromolecules* **2009**, *42*, 4632–4637.

(19) Gervais, M.; Gallot, B. Use of freeze-fracture electron microscopy to study the refolding of crystallized chains in block copolymers. *Polymer* **1981**, *22*, 1129–1133.

(20) Richards, D. H.; SZWARC, M. Block polymers of ethylene oxide and its analogues with styrene. *Trans. Faraday Soc.* **1959**, *55*, 1644.

(21) Baer, M. Anionic block polymerization. II. Preparation and properties of block copolymers. *J. Polym. Sci. A Gen. Pap.* **1964**, *2*, 417–436.

(22) Tsitsilianis, C.; Staikos, G.; Dondos, A.; Lutz, P.; Rempp, P. Influence of annealing and casting solvent on the morphology of poly(ethylene oxide)-*b*-polystyrene-*b*-poly(ethylene oxide) triblock copolymer: Compatibility effects. *Polymer* **1992**, *33*, 3369–3374.

(23) Xie, H.; Zhou, P. Synthesis of poly(oxyethylene-styrene-oxyethylene) triblock copolymers and their phase behavior. *Polym. Eng. Sci.* **1985**, *25*, 32–36.

(24) Floudas, G.; Tsitsilianis, C. Crystallization Kinetics of Poly(ethylene oxide) in Poly(ethylene oxide)−Polystyrene−Poly(ethylene oxide) Triblock Copolymers. *Macromolecules* **1997**, *30*, 4381–4390.

(25) Cortez-Lemus, N. A.; Baldenebro, V.; Zizumbo-Lopez, A.; Licea-Claverie, A. Synthesis of Amphiphilic Symmetrical ABA Triblock Copolymers PS-*b*-PEG-*b*-PS Using a Bifunctional Macro RAFT Agent. *Macromol. Symp.* **2013**, *325-326*, 47–55.

(26) Jankova, K.; Chen, X.; Kops, J.; Batsberg, W. Synthesis of Amphiphilic PS-*b*-PEG-*b*-PS by Atom Transfer Radical Polymerization. *Macromolecules* **1998**, *31*, 538–541.

(27) Perrin, L.; Phan, T. N. T.; Querelle, S.; Deratani, A.; Bertin, D. Polystyrene-*block*-poly(ethylene oxide)-*block*-polystyrene: A New Synthesis Method Using Nitroxide-Mediated Polymerization

from Poly(ethylene oxide) Macroinitiators and Characterization of the Architecture Formed. *Macromolecules* **2008**, *41*, 6942–6951.

(28) Rollet, M.; Pelletier, B.; Berek, D.; Maria, S.; Phan, T. N.T.; Gigmes, D. Separation of parent homopolymers from polystyrene and poly(ethylene oxide) based block copolymers by liquid chromatography under limiting conditions of desorption—3. Study of barrier efficiency according to block copolymers' chemical composition. *Journal of Chromatography A* **2016**, *1462*, 63–72.

(29) Das, P. J.; Barak, A.; Kawakami, Y.; Kannan, T. Synthesis and characterization of ABA-type amphiphilic tri-block copolymers through anionic polymerization using end functionalized poly(ethylene oxide) oligomers. *J. Polym. Sci. A Polym. Chem.* **2011**, *49*, 1376–1386.

(30) Orhan, E.H.; Yilgör, I.; Baysal, B.M. Block polymers from poly(ethylene oxide) and styrene. *Polymer* **1977**, *18*, 286–290.

(31) Uyanik, N.; Baysal, B. M. Preparation of polystyrene-*block*-(ethylene oxide)s and characterization of the products. *Journal of Applied Polymer Science* **1990**, 41.

(32) Albericio, F.; El-Faham, A. Choosing the Right Coupling Reagent for Peptides: A Twenty-Five-Year Journey. *Org. Process Res. Dev.* **2018**, *22*, 760–772.

(33) Otter, R.; Berac, C. M.; Seiffert, S.; Besenius, P. Tuning the life-time of supramolecular hydrogels using ROS-responsive telechelic peptide-polymer conjugates. *European Polymer Journal* **2019**, *110*, 90–96.

(34) Quirk, R. P.; Ma, J.-J. Characterization of the functionalization reaction product of poly(styryl)lithium with ethylene oxide. *J. Polym. Sci. A Polym. Chem.* **1988**, *26*, 2031–2037.

(35) Quirk, R. P.; Mathers, R. T.; Wesdemiotis, C.; Arnould, M. A. Investigation of Ethylene Oxide Oligomerization during Functionalization of Poly(styryl)lithium Using MALDI−TOF MS and NMR. *Macromolecules* **2002**, *35*, 2912–2918.

(36) Schöttner, S.; Brodrecht, M.; Uhlein, E.; Dietz, C.; Breitzke, H.; Tietze, A. A.; Buntkowsky, G.; Gallei, M. Amine-Containing Block Copolymers for the Bottom-Up Preparation of Functional Porous Membranes. *Macromolecules* **2019**, *52*, 7, 2631–2641.

(37) Frérot, E.; Coste, J.; Pantaloni, A.; Dufour, M.-N.; Jouin, P. PyBOP® and PyBroP: Two reagents for the difficult coupling of the α,α-dialkyl amino acid, Aib. *Tetrahedron* **1991**, *47*, 259–270.

(38) Young, W.-S.; Epps, T. H. Salt Doping in PEO-Containing Block Copolymers: Counterion and Concentration Effects. *Macromolecules* **2009**, *42*, 2672–2678.

(39) Epps, T. H.; Bailey, T. S.; Waletzko, R.; Bates, F. S. Phase Behavior and Block Sequence Effects in Lithium Perchlorate-Doped Poly(isoprene-*b*-styrene-*b*-ethylene oxide) and Poly(styrene-*b*-isoprene-*b*-ethylene oxide) Triblock Copolymers. *Macromolecules* **2003**, *36*, 2873–2881.

(40) Xu, H.; Greve, E. M.; Mahanthappa, M. K. Morphological Impact of Segment Dispersity in Lithium Salt-Doped Poly(styrene)/Poly(ethylene oxide) Triblock Polymers. *Macromolecules* **2019**, *52*, 5722–5734.

(41) Zardalidis, G.; Pipertzis, A.; Mountrichas, G.; Pispas, S.; Mezger, M.; Floudas, G. Effect of Polymer Architecture on the Ionic Conductivity. Densely Grafted Poly(ethylene oxide) Brushes Doped with LiTf. *Macromolecules* **2016**, *49*, 2679–2687.

(42) Hou, K. J.; Loo, W. S.; Balsara, N. P.; Qin, J. Comparing Experimental Phase Behavior of Ion-Doped Block Copolymers with Theoretical Predictions Based on Selective Ion Solvation. *Macromolecules* **2020**, *53*, 3956–3966.

SUPPORTING INFORMATION

Experimental Section

Reagents

All reagents were purchased either from Acros Organics, Roth, Fischer Chemical, VWR Chemicals or Carbolution Chemicals GmbH unless otherwise noticed. Chloroform-*d* was purchased from Deutero GmbH. Ethylene oxide (EO) was purchased from Air Liquide. Cyclohexane was dried over sodium/benzophenone, degassed and freshly distilled into the reaction flask for each polymerization. Succinic anhydride was recrystallized before usage. Styrene and isoprene were flushed through basic aluminum oxide before usage.

Instrumentation

^{1}H and ^{13}C NMR spectra were recorded on a Bruker Avance III HD 300 spectrometer with 300 and 75 MHz, respectively, and referenced internally to residual proton signals of the deuterated solvent.

SEC measurements were performed with THF as the mobile phase (flow rate 1 mL min^{-1}) on an SDV column set from PSS (SDV 103, SDV 105, SDV 106) at 30 °C. Polymer concentrations were 1 mg mL^{-1}. Calibration was carried out using polystyrene standards (from Polymer Standard Service, Mainz).

The thermal properties of the block copolymer electrolytes were studied with a Q2000 (TA Instruments) differential scanning calorimeter (DSC). Cooling and heating cycles were performed at a rate of 10 K min^{-1} and in a temperature range between 173 and 473 K.

Small-angle X-ray scattering (SAXS) measurements were made using Cu K_α radiation (Rigaku MicroMax 007 X-ray generator, Osmic Confocal Max-Flux curved multilayer optics). 2D scattering patterns were recorded on a Mar345 image plate. Radial intensity distributions are presented as a function of the modulus of the scattering vector $q = (4\pi/\lambda)\sin(2\theta/2)$, where 2θ is the scattering angle. Temperature dependent SAXS measurements in the range from 303 to 423 K in steps of 30 K were made on heating and on subsequent cooling.

A TA Instruments AR-G2 with a magnetic bearing that allows for nanotorque control was used for recording the viscoelastic properties of the polymer electrolytes. Measurements were made with the environmental test chamber as a function of temperature. Samples were prepared on the lower rheometer plate (8 mm), the upper plate was brought into contact, and the gap thickness was adjusted. The linear and nonlinear viscoelastic regions were determined by the strain amplitude dependence of the complex shear modulus $|G^*|$ at $\omega = 10\,\mathrm{rad\,s^{-1}}$. Measurements involved isothermal frequency scans within the range $10^{-1} < \omega < 10^{2}$ rad s^{-1} at selected temperatures and isochronal temperature ramps with $\omega = 10$ rad s^{-1} between 233 and 423 K.

For dielectric spectroscopy (DS), Sample capacitors were prepared in a glovebox under a controlled nitrogen atmosphere. Samples were heated up to the melting temperature of the complex and

hot pressed between two mirror polished brass electrodes to a thickness of 100 μm maintained with Teflon spacers. Dielectric spectroscopy measurements were made with a Novocontrol BDS system composed of a frequency response analyzer (Solartron Schlumberger FRA 1260) and a broadband dielectric converter. The experiments were performed at atmospheric pressure in the temperature range from 193 to 473 K and for frequencies in the range from 0.01 to 10^6 Hz.

Synthesis Protocols

Synthesis of P(I-*co*-S)-OH

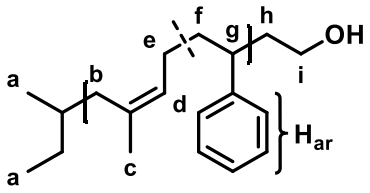

A mixture of styrene (17.6 g, 19.4 mL, 169 mmol) and isoprene (11.5 g, 16.9 mL, 169 mmol) was dried and degassed (as mentioned in a recent publication from our group[1]) and transferred in a reaction flask under high vacuum (10^{-3} mbar). Dry cyclohexane (135 mL) was added, the flask was flushed with argon and sec-BuLi (1.3 M stock solution in cyclohexane/n-hexane, 1.50 mL, 1.95 mmol) was added via a gastight syringe under vigorous stirring. The solution was heated to 40 °C and stirred for 2.5 h. After cooling to room temperature, the flask was evacuated by repeated opening of the stopcock to the vacuum line. EO (500 mg, 500 μL, 11.3 mmol) was dried with sec-BuLi (1.3 M stock solution in cyclohexane/n-hexane, 300 μL, 390 μmol), degassed and transferred to the living polymer solution via cryo-distillation. After stirring overnight at room temperature, the polymerization was quenched with degassed MeOH (100 μL). The polymer was purified by precipitation of the reaction solution in a ten-fold excess of MeOH/i-PrOH (1:1). P(I-*co*-S)-OH was obtained as a colorless solid in quantitative yields after drying at 40 °C under high vacuum for several days.

^{1}H NMR ($CDCl_3$), δ (ppm): 7.36-6.28 (m (broad), H_{ar}), 5.28-4.51 (m (broad), H_d), 3.30 (m (broad), H_i), 2.76-0.98 (m (broad), H_b+H_c+H_e-H_h), 0.83 (m, H_a).

Synthesis of P(I-*co*-S)-COOH

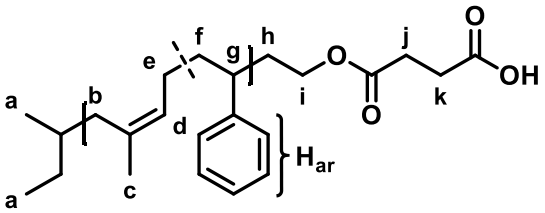

P(I-*co*-S)-OH (10.0 g, 665 μmol) was added to a flame-dried round bottom Schlenk flask equipped with a stir bar and condenser, dissolved in benzene and freeze-dried overnight. Succinic anhydride

(665 mg, 6.65 mmol) was added under argon and the mixture was dissolved in dry DCM (40 mL). Dry pyridine (526 mg, 537 μL, 6.65 mmol) was added and the solution was heated under reflux and argon for 6 d. The reaction was quenched with DCM (500 mL) and extracted with saturated Na_2CO_3 (100 mL, two times), 0.1 N HCl (100 mL, two times) and Brine (100 mL). The organic phase was dried over $MgSO_4$ and the solvent was evaporated after filtration to yield P(I-*co*-S)-COOH (7.01 g, 463 μmol, 70 %) as a colorless solid.

^{1}H NMR ($CDCl_3$), δ (ppm): 7.36-6.28 (m (broad), H_{ar}), 5.28-4.51 (m (broad), H_d), 3.98-3.61 (m (broad), H_d), 2.76-0.98 (m (broad), H_b+H_c+H_e-H_h+H_j+H_k), 0.83 (m, H_a).

Synthesis of α,ω-*N*-BOC-glycine-PEO

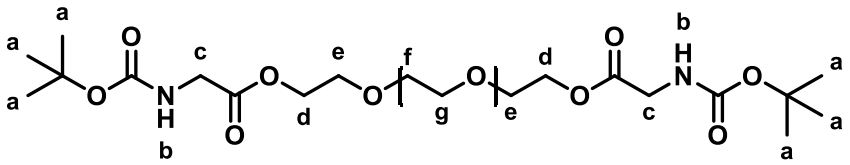

PEO (10.0 g, 500 μmol) was added to a flame-dried round bottom Schlenk flask equipped with a septum, dissolved in benzene and freeze-dried at 70 °C overnight. After addition of DMAP (24.0 mg, 200 μmol), *N*-BOC glycine (701 mg, 4.00 mmol) and dry DCM (20 mL) were added under argon, the solution was cooled to 0 °C and DIC (505 mg, 619 μL, 4.00 mmol) was added under stirring. The solution was heated to room temperature and stirred for 3 h. Repeated precipitation in a ten-fold excess of Et_2O from DCM yielded α,ω-*N*-BOC-glycine-PEO (6.78 g, 334 μmol, 67 %) as a colorless solid after drying under high vacuum.

^{1}H NMR ($CDCl_3$), δ (ppm): 5.11 (s (broad), H_b), 4.26 (m, H_d), 3.90 (s (broad), H_c), 3.76-3.44 (s (broad), H_e-H_g), 1,42 (s, H_a).

Synthesis of α,ω-NH_2-PEO

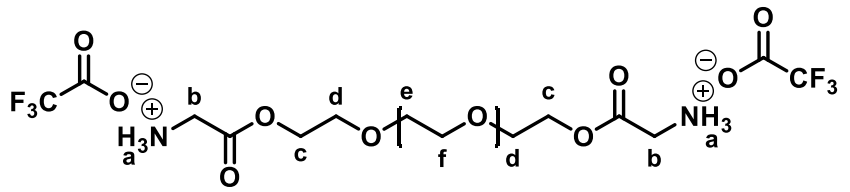

α,ω-*N*-BOC-glycine-PEO (2.00 g, 98.4 μmol) was dissolved in DCM (5 mL). The solution was cooled to 0 °C and TFA (5 mL) was added under stirring. After 1 d, the polymer solution was poured in a ten-fold excess of cold Et_2O. α,ω-NH_2-PEO (1.70 g, 83.5 μmol, 85 %) was obtained as a colorless solid after repeated precipitation in a ten-fold excess of cold Et_2O from DCM.

^{1}H NMR ($CDCl_3$), δ (ppm): 6.32 (s (broad), H_a), 4.36 (m, H_c), 3.94 (s (broad), H_b), 3.80-3.44 (s (broad), H_d-H_f).

Synthesis of P(I-*co*-S)-*b*-PEO-*b*-P(S-*co*-I)

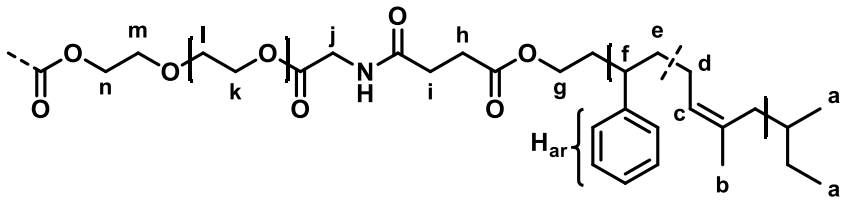

α,ω-NH_2-PEO (1.50 g, 73.7 μmol) and P(I-*co*-S)-COOH (2.46 g, 162 μmol) were dissolved in benzene and freeze-dried overnight. The polymer mixture was dissolved in dry DCM (25 mL) and PyAOP (92.0 μg, 177 μmol) was added under stirring. After the addition of dry NEt_3 (117 mg, 160 μL, 1.13 mmol), the solution was stirred for 4 h and poured into a ten-fold excess of Et_2O. The crude polymer was washed three times with distilled H_2O (50 mL), dissolved in benzene and freeze-dried for several days. P(I-*co*-S)-*b*-PEO-*b*-P(S-*co*-I) (2.24 g, 44.8 μmol, 61 %) was obtained as a colorless solid.

^{1}H NMR ($CDCl_3$), δ (ppm): 7.36-6.28 (m (broad), H_{ar}), 5.28-4.51 (m (broad), H_c), 4.28 (m (broad), H_n), 4.03 (s, H_j), 3.82-3.47 (s (broad), H_g+H_k-H_m), 2.76-0.98 (m (broad), H_b+H_d-H_f+H_h+H_i), 0.80 (m, H_a).

Additional Spectra and Plots

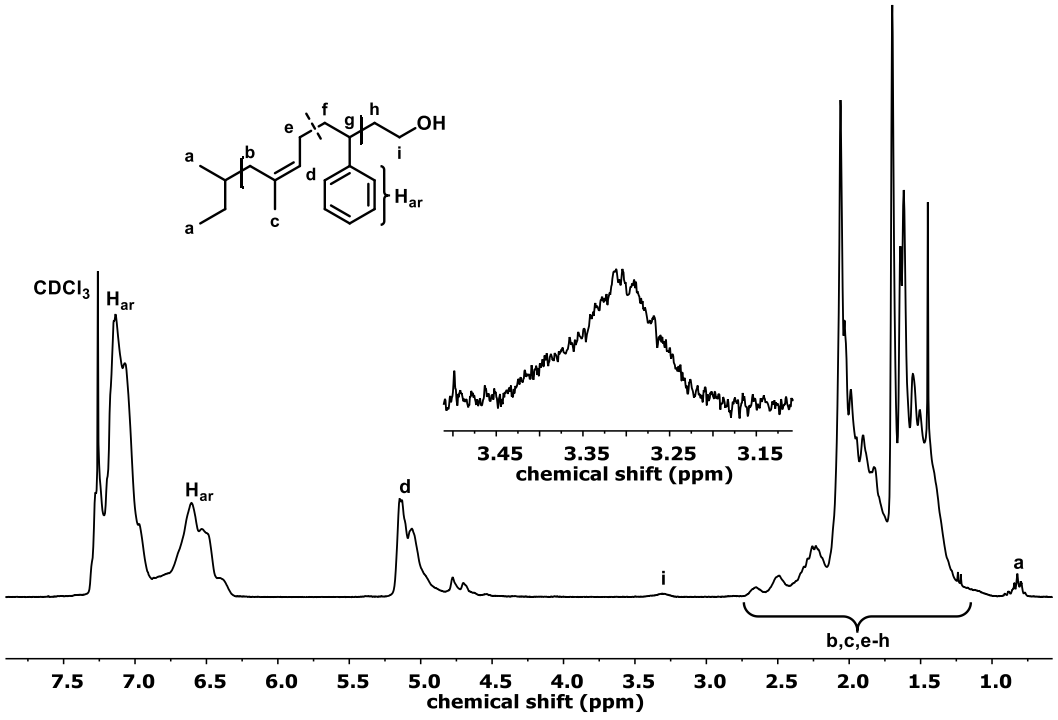

Figure S1. ^{1}H NMR spectrum ($CDCl_3$, 300 MHz) of P(I-*co*-S)-OH.

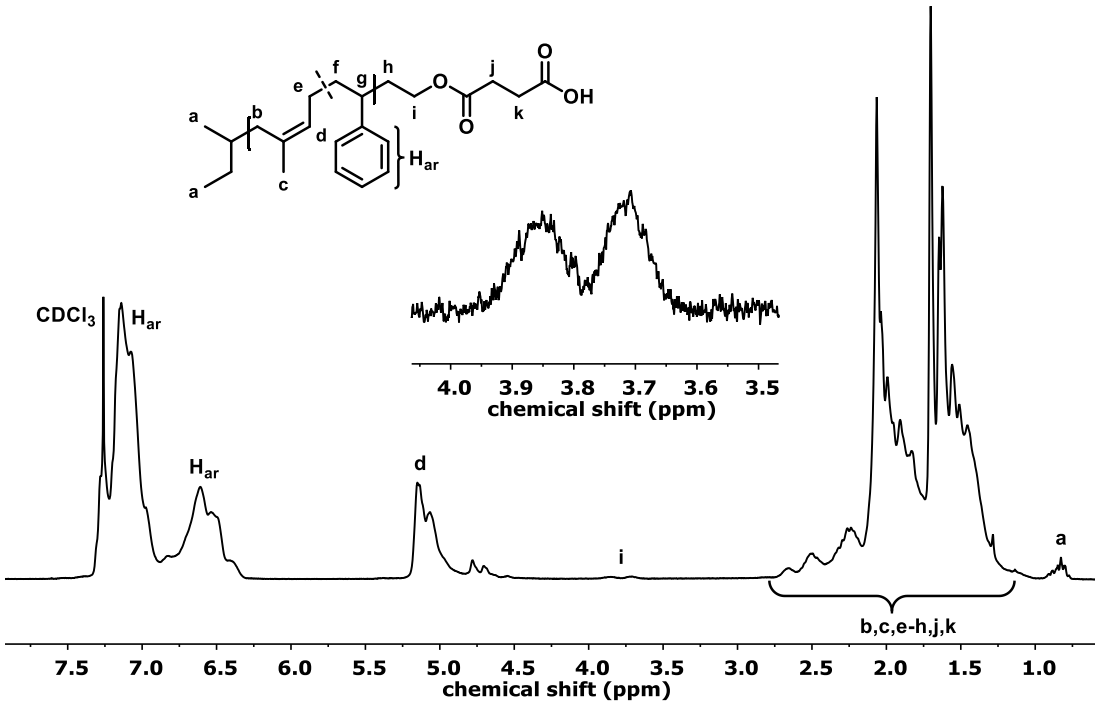

Figure S2. ^{1}H NMR spectrum ($CDCl_3$, 300 MHz) of P(I-*co*-S)-COOH.

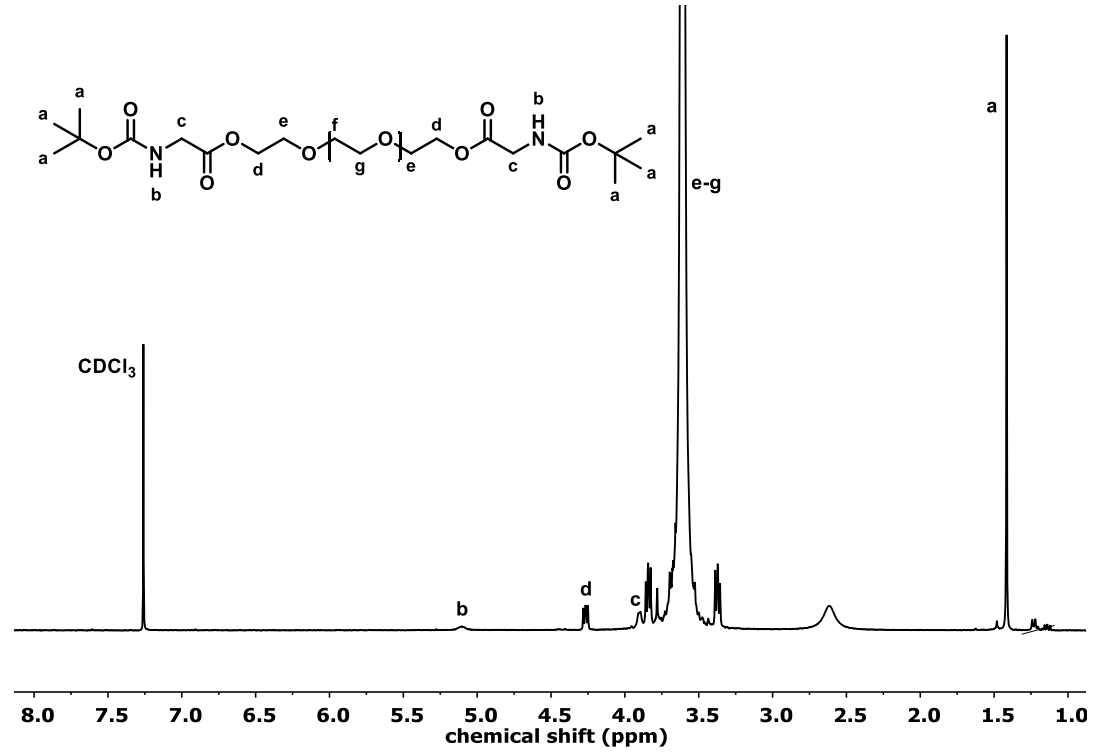

Figure S3. ^{1}H NMR spectrum ($CDCl_3$, 300 MHz) of α,ω-*N*-BOC-glycine-PEO.

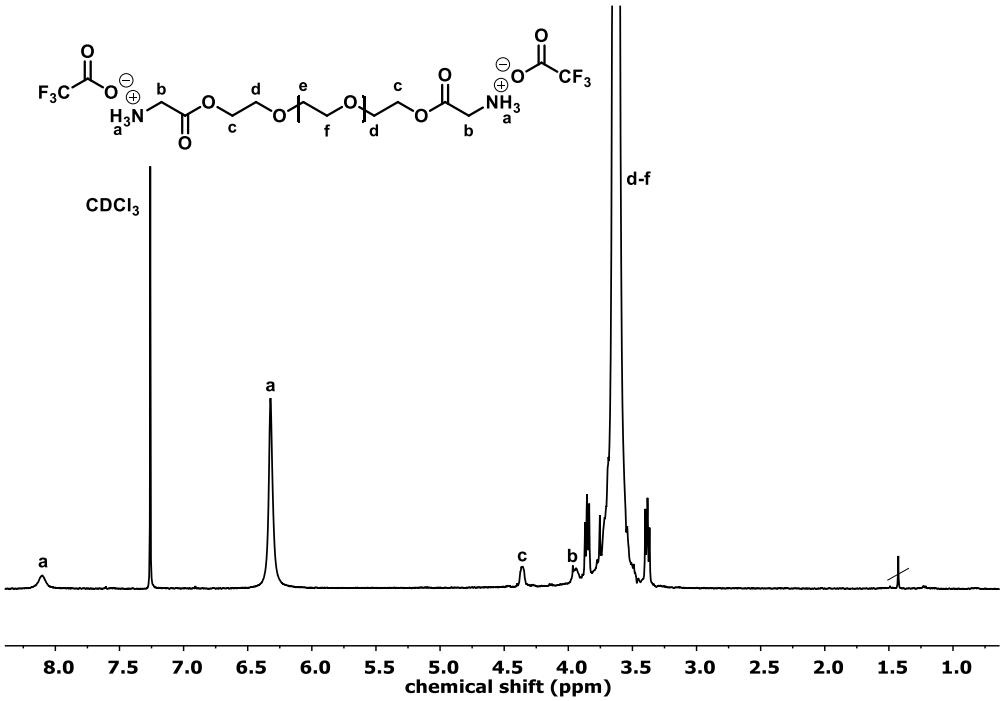

Figure S4. ^{1}H NMR spectrum ($CDCl_3$, 300 MHz) of α,ω-NH_2-PEO.

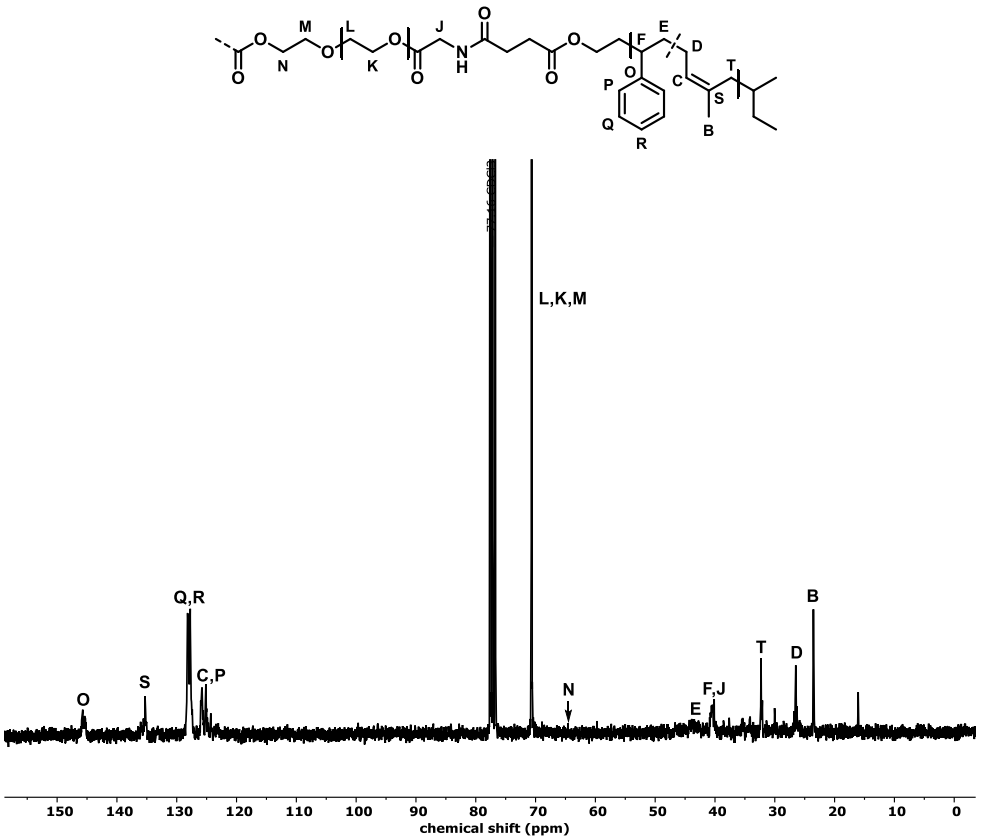

Figure S5. ^{13}C NMR spectrum ($CDCl_3$, 75 MHz) of P(I-*co*-S)-*b*-PEO-*b*-P(S-*co*-I).

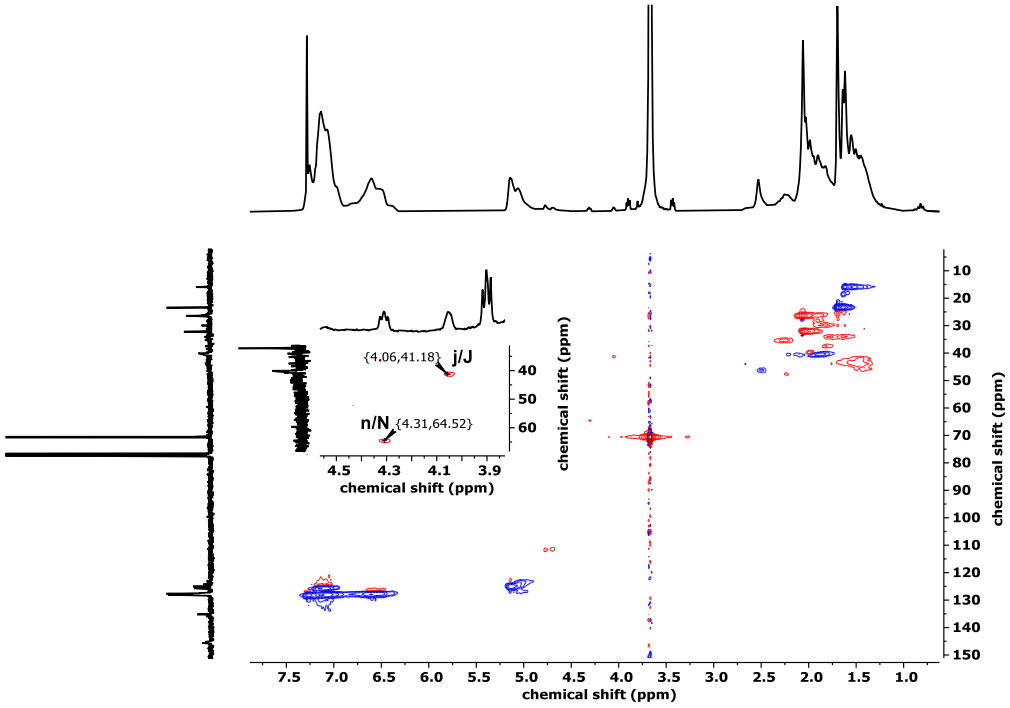

Figure S6. HSQC NMR spectrum ($CDCl_3$) of P(I-*co*-S)-*b*-PEO-*b*-P(S-*co*-I).

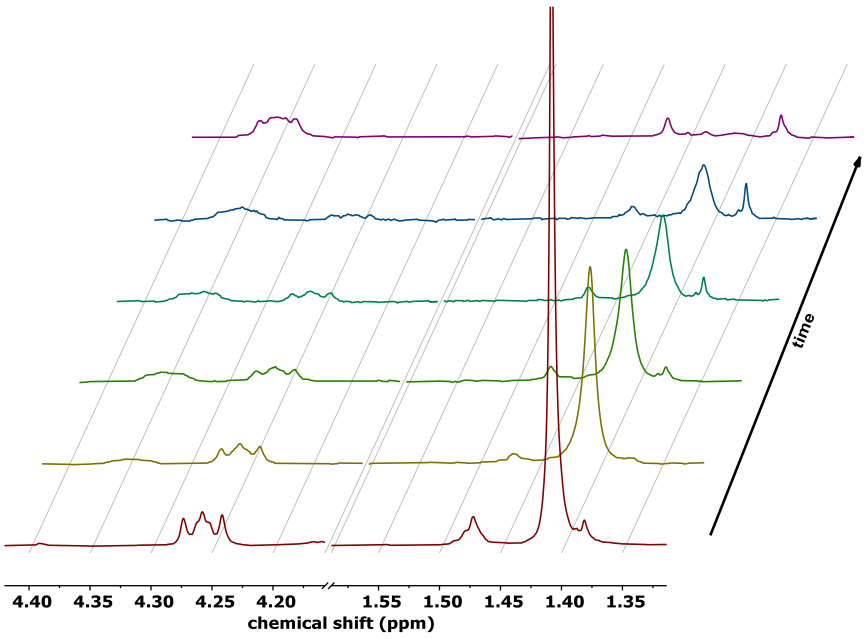

Figure S7. Stacked ^{1}H NMR spectra ($CDCl_3$, 300 MHz) of the deprotection of α,ω-*N*-BOC-glycine-PEO over time.

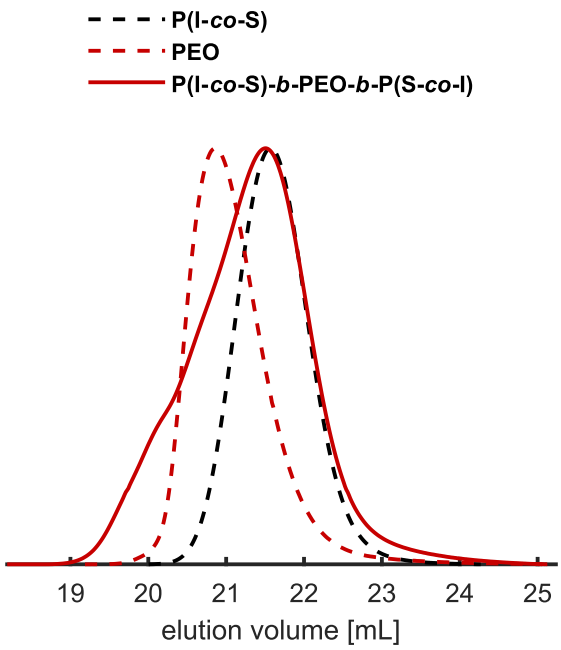

Figure S8. SEC traces of coupling reaction with unmodified PEO.

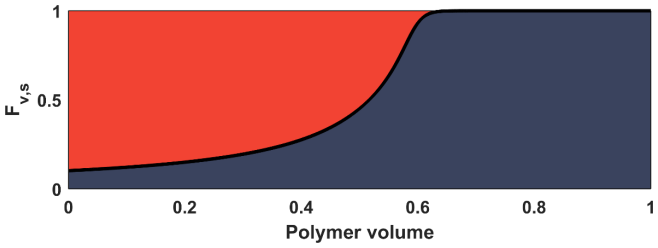

Figure S9. Visualization of the polymer microstructure of P(I-*co*-S) by plotting the mean incorporation volume of styrene ($F_{V,S}$) (blue) as a function of the polymer volume fraction.

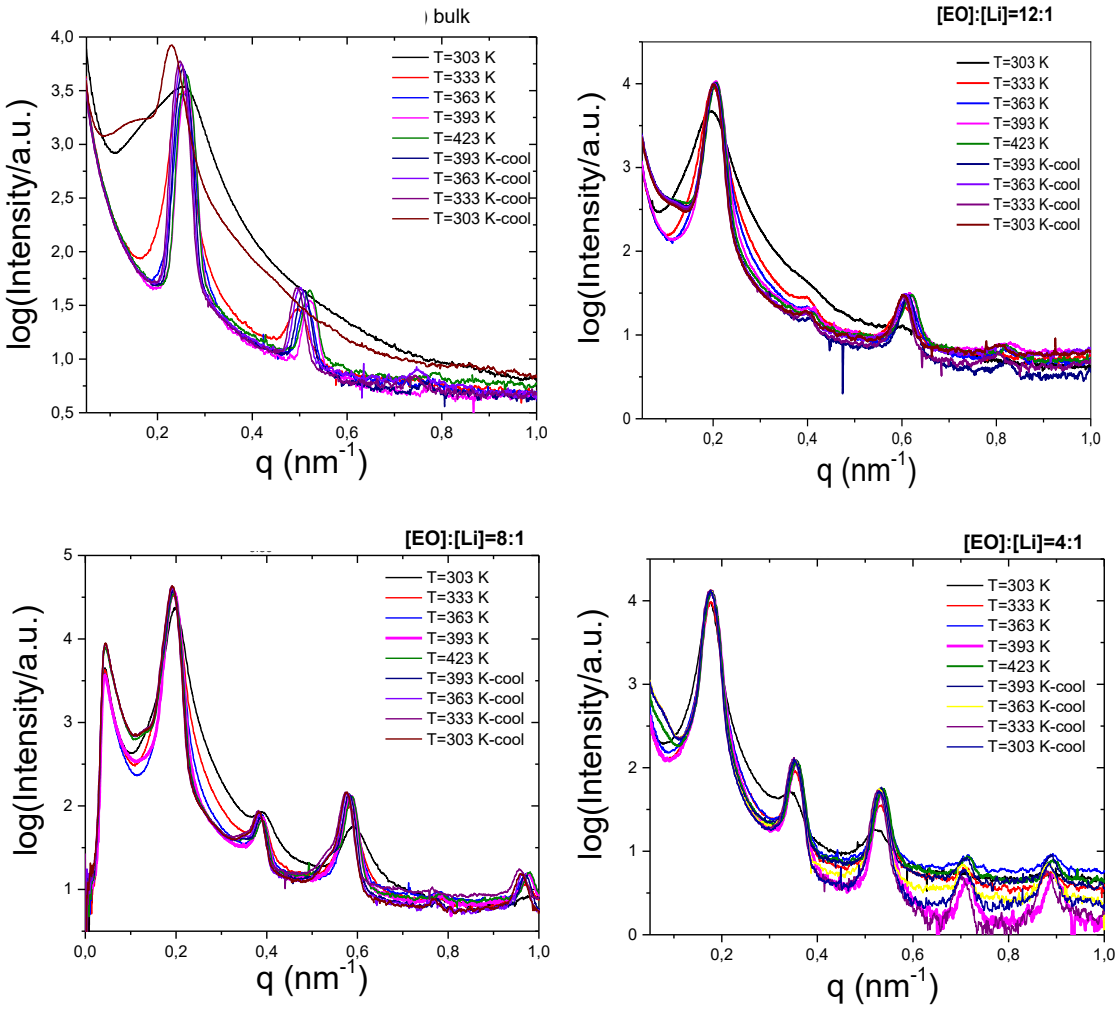

Figure S10. SAXS patterns of neat and salt-doped P(I-*co*-S)-*b*-PEO-*b*-P(S-*co*-I) at different temperatures.

REFERENCES

(1) Steube, M.; Johann, T.; Galanos, E.; Appold, M.; Rüttiger, C.; Mezger, M.; Gallei, M.; Müller, A. H. E.; Floudas, G.; Frey, H. Isoprene/Styrene Tapered Multiblock Copolymers with up to Ten Blocks: Synthesis, Phase Behavior, Order, and Mechanical Properties. *Macromolecules* **2018**, *51*, 10246–10258.

Chapter A

Appendix

Chapter A1

“Dumb” pH-Independent and Biocompatible Hydrogels Formed by Copolymers of Long-Chain Alkyl Glycidyl Ethers and Ethylene Oxide

Patrick Verkoyen[†], Philip Dreier[†], Matthias Bros[‡], Christian Hils[⊥], Holger Schmalz[⊥], Sebastian Seiffert[†], and Holger Frey[*,†]

[†]**Department of Chemistry, Johannes Gutenberg University Mainz, Germany**

[‡]**Department of Dermatology, University Medical Center of the Johannes Gutenberg University Mainz, Germany**

[⊥]**Makromolekulare Chemie II, University of Bayreuth, Germany**

The author of this thesis prepared the corresponding samples of the manuscript, partially wrote the synthesis part of the publication and commented on the manuscript.

---

pubs.acs.org/Biomac Article

"Dumb" pH-Independent and Biocompatible Hydrogels Formed by Copolymers of Long-Chain Alkyl Glycidyl Ethers and Ethylene Oxide

Patrick Verkoyen, Philip Dreier, Matthias Bros, Christian Hils, Holger Schmalz, Sebastian Seiffert, and Holger Frey*

Cite This: *Biomacromolecules* 2020, 21, 3152−3162 Read Online

ACCESS | Metrics & More | Article Recommendations | Supporting Information

ABSTRACT: The formation and rheological properties of hydrogels based on amphiphilic ABA triblock polyether copolymers are described, relying solely on the hydrophobic interaction of long-chain alkyl glycidyl ether (AlkGE)- based A-blocks that are combined with a hydrophilic poly(ethylene glycol) (PEG) midblock. Via anionic ring-opening copolymerization (AROP), ethylene oxide (EO) and long-chain alkyl glycidyl ethers (AlkGEs) were copolymerized, using deprotonated poly(ethylene glycol) (PEG) macroinitiators (M_n of 10, 20 kg mol^{-1}). The polymerization afforded amphiphilic ABA triblock copolymers with molar masses in the range of 21−32 kg mol^{-1} and dispersities ($Đ$) of $Đ$ = 1.07−1.17. Kinetic studies revealed random copolymerization of EO and AlkGE, indicating random spacing of the hydrophobic AlkGE units by polar EO units. Following this approach, the hydrophobicity of the apolar blocks of amphiphilic ABA triblock polyethers can be tailored. Detailed rheological measurements confirmed the successful formation of hydrogels at different pH values as a consequence of nonpolar interactions and alkyl chain crystallization. Hydrogel formation was also observed at different ionic strengths (i.e., varied salt concentration), based on the hydrophobic aggregates. This behavior is in contrast to other often-used supramolecular cross-linking strategies, such as Coulomb interactions, complexation, or hydrogen bonding. Micro-differential scanning calorimetry (μ-DSC) measurements of the hydrogels revealed crystalline hydrophobic domains with melting temperatures in the physiological temperature range. In 3-[4,5-dimethylthiazol-2-yl]-2,5-diphenyltetrazoliumbromide (MTT) assays, diblock copolymers possessing structural analogy to the triblock copolymers were studied to assess the general cytotoxicity of amphiphilic polyethers bearing long alkyl chains at the polyether backbone, using splenic immune cells. At intermediate polymer concentrations, no cytotoxic effects were observed. This indicates that long-chain alkyl glycidyl ethers are promising for the introduction of highly hydrophobic as well as crystalline motifs at the polyether backbone in hydrogels for biomedical purposes.

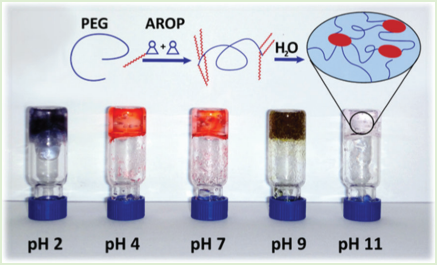

Downloaded via UNIV MAINZ on May 31, 2021 at 12:40:38 (UTC).
See https://pubs.acs.org/sharingguidelines for options on how to legitimately share published articles.

INTRODUCTION

Hydrogels are three-dimensional networks formed by cross-linked, hydrophilic polymers. Synthetic hydrogels have been diversified for a vast variety of applications in the past decades. For instance, scaffolds for tissue engineering, artificial implants, or drug delivery systems are key applications of hydrogels.[1−7] Gelation is achieved by chemical cross-linking of hydrophilic polymer chains.[8,9] However, noncovalent interactions, such as ion−ion interactions,[10] hydrogen bonding,[11,12] or hydrophobic interactions,[9,13−15] are commonly utilized to form reversible, supramolecular hydrogel systems.[16] Additionally, so-called secondary interactions lead to high flexibility and reversibility of the gel formation, allowing further adjustment to specific applications. A key feature of noncovalent, i.e., supramolecular cross-linked hydrogels based on Coulomb interactions or hydrogen bonding is the strong dependence on specific pH values and on the concentration of electrolytes, i.e., the ionic strength of the aqueous medium.[17−19] In contrast, hydrophobic interactions show little dependency on the aforementioned parameters, if the chemical structure of the polymer is otherwise inert.

It is well known that amphiphilic polymer systems can show concentration-dependent gelation behavior, forming flowerlike micelles in a dilute aqueous solution, while an increase of the polymer concentration leads to the formation of different aggregates, resulting in three-dimensional networks of cross-linked micellar structures.[20−22] In this context, strongly hydrophobic epoxides such as long-chain alkyl glycidyl ethers (AlkGEs) represent an interesting class of epoxide monomers

Received: April 17, 2020
Revised: June 30, 2020
Published: June 30, 2020

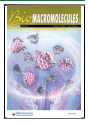

ACS Publications © 2020 American Chemical Society

https://dx.doi.org/10.1021/acs.biomac.0c00576
Biomacromolecules 2020, 21, 3152−3162

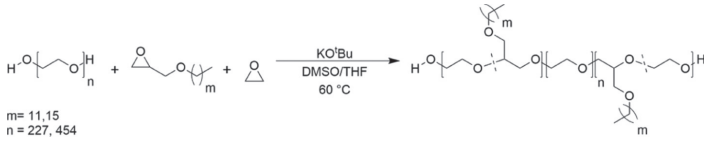

Figure 1. Synthesis of ABA triblock copolymers using deprotonated PEG as a bifunctional macroinitiator (hydrophilic midblock) and long-chain alkyl glycidyl ethers (AlkGE)[32] C12-AlkGE and C16-AlkGE copolymerized with ethylene oxide (EO) for the A-blocks.

that have been little exploited to date. Due to the tunable melting temperatures and hydrophobicity that can be adjusted by the length of the alkyl chain, the resulting polyethers enable the design of a variety of temperature-dependent physical properties. The combination of these monomers with hydrophilic polyethers, such as poly(ethylene glycol) (PEG), affords strongly amphiphilic block copolymer systems.

Poloxamers, also known as Pluronics, represent a widely used class of amphiphilic polyethers based on poly(ethylene glycol) (PEG) and poly(propylene oxide) (PPO), arranged in an ABA triblock structure with a central apolar PPO segment.[15] Reverse poloxamer-like ABA block structures acting as noncovalent hydrogels have been reported. ABA triblock copolymers containing poly(lactic acid) (PLA), poly(caprolactone) (PCL), or PPO A-blocks as hydrophobic components have been extensively investigated in the past decades.[23−28] To understand the different gelation mechanisms of poloxamer-like polymers compared to the reverse structures, Ding and co-workers recently studied amphiphilic block copolymers with different architectures (ABA, AB, BAB), using PLA as a hydrophobic component and PEG as a hydrophilic component.[29] Murakami et al. investigated amphiphilic ABA triblock copolymer structures and their impact on viscosity in aqueous solutions in dependence of the alkyl chain length in the hydrophobic A-block, obtained from copolymerization of ethylene oxide (EO) and allyl glycidyl ether (AGE), followed by postmodification via a thiol−ene reaction.[30] In previous work, our group introduced the polymerization of dodecyl glycidyl ether (C12-AlkGE) and hexadecyl glycidyl ether (C16-AlkGE), relying on anionic ring-opening polymerization (AROP) conditions. We employed bifunctional PEG macroinitiators, a crown ether, and potassium as a counterion. With this procedure, amphiphilic ABA triblock copolymers were accessible that showed swelling in water/ethanol mixtures (not in pure water) and formed gels with thermoresponsive mechanical behavior.[31]

In the current work, we report the preparation of hydrogels based on amphiphilic ABA triblock polyethers with a hydrophilic PEG midblock, capitalizing on the hydrophobic interaction of the long alkyl chains. Rheological measurements of the hydrogels revealed successful gelation at different pH values and with different electrolyte concentrations. In copolymerization reactions of C12-AlkGE or C16-AlkGE with EO, hydrophobic blocks with deliberately altered apolar character were generated in a single reaction step. As a consequence of the copolymerization, and in pronounced contrast to our previous work,[31] EO units are placed in between the highly hydrophobic alkyl chains, permitting to adjust the hydrophobicity of the hydrophobic A-blocks (Figure 1). Melting temperatures of the hydrophobic blocks were adjusted using the C12-AlkGE or the C16-AlkGE monomer, leading to lower or higher melting temperatures, respectively. Following this approach, a variety of amphiphilic ABA triblock polyether structures with molar masses ranging from M_n = 21 000 to 32 000 g mol^{-1} and narrow dispersities in the range of $Đ$ = 1.07−1.17 were synthesized (Figure 2 and Table 1), starting from common bifunctional PEG as a macroinitiator (10 000 and 20 000 g mol^{-1}) (Figure 1).

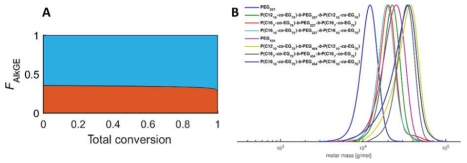

Figure 2. (A) Molar chain composition of BnO-P(C12-AlkGE-*co*-EG) copolymers (in situ NMR). Ethylene oxide is shown in blue and C12-AlkGE is shown in red. (B) SEC traces of the synthesized P(AlkGE$_x$-*co*-EG$_{75}$)-*b*-PEG$_y$-*b*-P(AlkGE$_x$-*co*-EG$_{75}$) triblock polyethers (eluent: DMF, calibration: PEG standards).

EXPERIMENTAL SECTION

Reagents. Solvents and reagents were purchased from Acros Organics, TCI, Sigma-Aldrich, or Fluka and used as received unless otherwise stated. Deuterated solvents were obtained from Deutero GmbH. Both C12-AlkGE and C16-AlkGE were dissolved in benzene and dried overnight under reduced pressure before polymerization. The dispersity ($Đ$) of the purchased macroinitiators was determined by SEC (eluent: DMF, calibration: PEG standards); for 10 000 g mol^{-1} PEG, $Đ$ = 1.07, and for 20 000 g mol^{-1} PEG, $Đ$ = 1.12.

Instrumentation. ^{1}H NMR (300 MHz) spectra were recorded on a Bruker Avance III HD (300 MHz, 5 mm BBFO-head with a *z*-gradient and automated tuning and matching (ATM), BACS 60 sample changer) and referenced internally to the proton signal of the deuterated solvent ($CDCl_3$). ^{1}H NMR kinetic measurements were carried out using a Bruker Avance III HD (400 MHz, 5 mm BBFO-SmartProbe with a *z*-gradient and ATM, SampleXPress 60 sample changer) at 298 K.

Size exclusion chromatography (SEC) was performed in dimethylformamide (DMF) with 1 g L^{-1} lithium bromide as an eluent and MZ-Analysentechnik HEMA 300/100/40 columns at 50 °C, using a refractive index (RI) detector at a flow rate of 1 mL min^{-1}. Calibration was carried out using low-dispersity poly(ethylene oxide) (PEG) standards provided by the company PSS.

Differential scanning calorimetry (DSC) measurements were carried out under a nitrogen atmosphere using a PerkinElmer DSC 8500 in the temperature range of −80 to 70 °C, with heating rates of 20, 10, and 5 K min^{-1}, respectively. To exclude the effects of the thermal history of the polymer samples, the first heating cycle was carried out at a heating rate of 20 K min^{-1}, followed by a temperature plateau at 70 °C for 10 min. Subsequently, a cooling run was applied to the polymer sample at rates of 20, 10, and 5 K min^{-1}, respectively. At −80 °C, a temperature plateau of 3 min was introduced, followed by a second heating run at heating rates of 20, 10, and 5 K min^{-1}, respectively. For evaluation of the melting temperatures, the second heating run was always used.

https://dx.doi.org/10.1021/acs.biomac.0c00576
Biomacromolecules 2020, 21, 3152−3162

Table 1. Synthesized ABA-Type Triblock Copolymers

polymer sample	M_n/g mol^{-1} (theoretical)	M_n/g mol^{-1} [a]	M_n/g mol^{-1} [b]	$Đ$[b]	T_m/°C[c]
P(C12$_{10}$-*co*-EG$_{75}$)-*b*-PEG$_{227}$-*b*-P(C12$_{10}$-*co*-EG$_{75}$)	21 428	21 400	22 000	1.17	−13/52
P(C12$_{10}$-*co*-EG$_{75}$)-*b*-PEG$_{454}$-*b*-P(C12$_{10}$-*co*-EG$_{75}$)	31 416	29 800	30 300	1.11	−17/54
P(C16$_{10}$-*co*-EG$_{75}$)-*b*-PEG$_{227}$-*b*-P(C16$_{10}$-*co*-EG$_{75}$)	22 548	22 300	15 400	1.07	25/51
P(C16$_{10}$-*co*-EG$_{75}$)-*b*-PEG$_{454}$-*b*-P(C16$_{10}$-*co*-EG$_{75}$)	32 536	32 200	31 600	1.14	18/55
P(C16$_{7}$-*co*-EG$_{75}$)-*b*-PEG$_{227}$-*b*-P(C16$_{7}$-*co*-EG$_{75}$)	20 760	20 700	19 100	1.06	20/51
P(C16$_{7}$-*co*-EG$_{75}$)-*b*-PEG$_{454}$-*b*-P(C16$_{7}$-*co*-EG$_{75}$)	30 748	30 700	30 600	1.07	20/55

[a]Determined by ^{1}H NMR (300 MHz, $CDCl_3$). [b]Determined by SEC (eluent: dimethylformamide (DMF), calibration: PEG). [c]Melting temperatures determined by differential scanning calorimetry (DSC) (heating rate 5 K min^{-1}). The first and second melting temperatures can be assigned to the P(AlkGE-*co*-EG), and the PEG block, respectively.

Micro-differential scanning calorimetry (μ-DSC) measurements were performed on a SETARAM Micro DSC III using sealed measuring cells ("batch cells", V = 1 mL) filled with the polymer gel (see Tables S8 and S9). A scanning rate of 0.5 K min^{-1} was employed and pure water (deionized water (filtered through a Millipore Milli-Q Plus system, QPAK 2, conductivity: 18.2 MΩ cm)) was used as a reference. The measurements were performed in a range of 2−60 °C, with the following temperature program: (1) isothermal plateau 1 at 2 °C for 30 min, (2) heating 1 from 2 to 60 °C, (3) isothermal plateau 2 at 60 °C for 5 min, (4) cooling 1 from 60 to 2 °C, (5) isothermal plateau 3 at 2 °C for 5 min, (6) heating 2 from 2 to 60 °C, (7) isothermal plateau 4 at 60 °C for 5 min, (8) cooling 2 from 60 to 2 °C, (9) isothermal plateau 5 at 2 °C for 60 min, (10) heating 3 from 2 to 60 °C, and (11) isothermal plateau 6 at 60 °C for 5 min.

Viscoelastic properties were investigated by oscillatory shear measurements at 10 °C. For these measurements, a rheometer (Anton Paar, MCR302) equipped with a parallel-plate geometry (25 mm i.d.) was used. For the measurements, the prepared, homogeneous hydrogels were applied in the rheometer geometry (see the section on "Swelling Experiments and Hydrogel Formation"). To confirm full contact between the plates, a force with a threshold of 1 N was applied to the hydrogel sample. After reaching a force of 1 N, the approaching parallel-plate setup automatically stopped, and the distance was kept constant during the measurements. Subsequently, the sample was kept at the designated temperature for 300 s with a constant frequency of 1 rad s^{-1} and an amplitude of 1% to achieve an equilibrium situation of the hydrogel sample between the plates with respect to the temperature and the mechanical history of the sample. Amplitude-sweep measurements were carried out at 10 °C and at a constant frequency of 1 rad s^{-1}, unless otherwise stated. Frequency-sweep measurements were performed in the linear viscoelastic regime, which has been extracted by the amplitude-sweep measurements before, usually at an amplitude of 1%, unless otherwise stated.

Synthesis. Synthesis and purification of the long-chain alkyl glycidyl ether monomers C12- and C16-AlkGE were carried out as reported before.[31] Tetrahydrofuran (THF) used for copolymerization was dried with sodium and benzophenone as an indicator, followed by additional drying with butyl lithium and 1,1-diphenylethylene as an indicator.

Triblock Copolymer Synthesis. In the following, a general reaction procedure is exemplified for P(C16-AlkGE-*co*-EG$_{75}$)-*b*-PEG$_{227}$-*b*-P(C16-AlkGE-*co*-EG$_{75}$). In a 50 mL custom-made anionic flask, equipped with a poly(tetrafluoroethylene) (PTFE) valve and a septum, 750 mg (0.075 mmol, 1 equiv) of PEG (M_n = 10 000 g mol^{-1}) and 5 mg (0.045 mmol, 0.6 equiv) of KO^{t}Bu were dissolved in 5 mL of a benzene/methanol mixture (9/1). Subsequently, the mixture was dried overnight under reduced pressure at 60 °C to afford the partially deprotonated initiator. The reaction mixture was cooled to −80 °C, and 6 mL of a mixture of dried dimethyl sulfoxide (DMSO)/THF (5/1) was added. After the addition of the solvent mixture, 500 mg (11.3 mmol, 150 equiv) of EO and 450 mg (1.5 mmol, 20 equiv) of the dried C16-AlkGE were added. Subsequently, the reaction mixture was stirred at 60 °C for 72 h. After completion of the reaction, 1 mL of methanol and 15 mL of dichloromethane were added to the viscous solution at room temperature. The mixture was washed three times with deionized water, and the organic phases were combined, dried over $MgSO_4$, and subsequently the solvent was evaporated under reduced pressure. The product was precipitated in diethyl ether at room temperature. ^{1}H NMR (300 MHz, chloroform-*d*) δ (ppm) = 3.92−3.35 (m, 1648H, backbone), 1.64−1.46 (m, 39H, O CH$_2$ CH_2), 1.37−1.17 (m, 482H, OCH$_2$ CH$_2$ (CH_2)$_9$ CH$_3$), 0.87 (t, 55H, J = 7.0 Hz, CH_3) (Figures S45−S50).

^{1}H NMR Kinetic Study. Statistical copolymerization of C12-AlkGE and EO under the reaction conditions described above was performed in a sealable NMR tube. To this end, a mixture of THF/DMSO, KO^{t}Bu, and benzyloxy ethanol (BnO) was added to the sealable NMR tube via a syringe. At −80 °C, a defined amount of EO was transferred to the NMR tube. The NMR tube was evacuated, sealed, and then transferred to the NMR spectrometer. To prevent pressure buildup in the sealed NMR tube, the reaction was performed at 25 °C for 6 h, recording a spectrum every 30 s.

Determination of the Cytotoxicity. To assess the cytotoxic character of the amphiphilic polyethers, 3-[4,5-dimethylthiazol-2-yl]-2,5-diphenyltetrazoliumbromide (MTT) assays have been carried out. Since no homogeneous solution of the synthesized amphiphilic triblock copolymers could be prepared, due to the formation of aggregates in an aqueous solution, a diblock copolymer (mPEG$_{113}$-*b*-P(C16-AlkGE)$_3$) was synthesized according to the synthesis protocol discussed above. Murine spleen cells derived from C57BL/6 mice were seeded into wells of 96-well cluster plates (each 10^6 cells/100 μL per well). The diblock copolymer mPEG$_{113}$-*b*-P(C16-AlkGE)$_3$ was applied at different concentrations in triplicate. Samples left untreated or incubated with DMSO at a high cytotoxic dose (10%) were employed as controls. After overnight incubation, 20 μL of water-soluble 3-[4,5-dimethylthiazol-2-yl]-2,5-diphenyltetrazoliumbromide (MTT) reagent was added (Promega, Madison, WI). MTT is reduced by mitochondrial dehydrogenases to a purple, water-insoluble formazan product. After 5 h, the reaction was terminated by the addition of 100 μL of Stop/lysis buffer (Promega). The absorbance was measured at 570 nm using a Spark multimode microplate reader (TECAN, Männedorf, Switzerland).

Swelling Experiments and Hydrogel Formation. Swelling experiments of the synthesized block copolymer structures were performed in 2.5 mL high-performance liquid chromatography (HPLC) vials by adding a defined amount of water or aqueous salt solution, such as NaCl solutions (0.5, 1 mol L^{-1}), and solutions with varied pH values (pH = 4 and 9) to the respective amount of polymer. For the ultrahigh molar mass (UHMW) PEO addition (M_n = 1 000 000 g mol^{-1}), the respective triblock copolymer was mixed with a defined amount of UHMW PEO before the addition of water to generate the hydrogels. For all samples, a polymer concentration of 10 wt % was used to achieve gelation. For the preparation of the hydrogels, a defined amount of the respective powderlike polymer was weighed into a 2.5 mL vial, followed by the addition of the premixed aqueous solution. Subsequently, vigorous mixing was carried out using a vortex mixer to achieve a homogeneous distribution of the polymer. The mixture was then stored at 40 °C for at least 24 h to obtain homogeneous hydrogels. Gelation was indicated by the inversed vial test. Due to the nature of the noncovalent cross-links in the hydrogels, additional mechanical mixing of the gels can be applied to ensure uniformity of the hydrogels after gelation by mixing the respective sample with a spatula. After 12 h, homogeneously distributed

https://dx.doi.org/10.1021/acs.biomac.0c00576
Biomacromolecules 2020, 21, 3152−3162

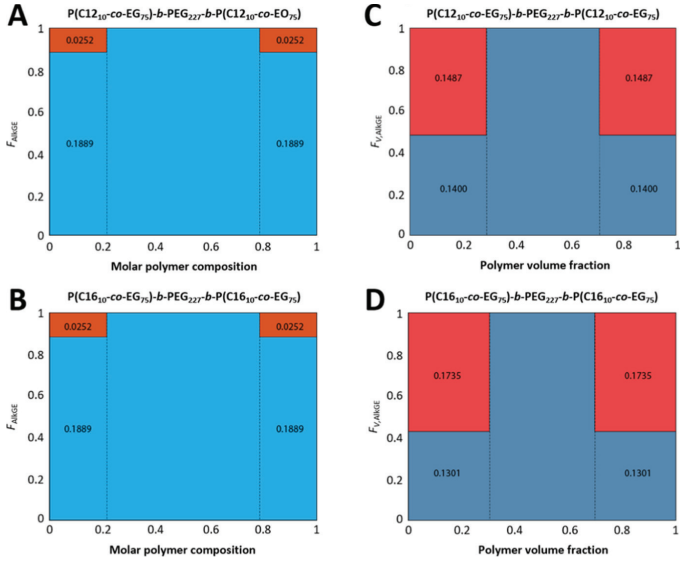

Figure 3. Calculated volume fractions of the synthesized ABA structures using either C12-AlkGE or C16-AlkGE in combination with EO, and PEG (M_n 10 000 g mol^{-1}) as a macroinitiator. (A, B) Calculated molar fraction in the P(AlkGE-*co*-EG)-*b*-PEG$_{227}$-*b*-P(AlkGE-*co*-EG) triblock. The respective AlkGE is displayed in light red and EO is displayed in light blue. Molar fractions of the different components are shown by the respective areas, resulting in a molar hydrophobic/hydrophilic monomer ratio of 1:7.5 for both polyethers. (C, D) Approximate volume fraction in the triblock copolymers. AlkGE (dark red) and EO (dark blue).

hydrogels were obtained, due to the self-healing properties based on the reversible physical cross-links. Finally, the hydrogels were applied to the rheometer using a parallel-plate geometry to conduct the rheology measurements. For better visualization of the different pH values that were applied to the hydrogels, different pH indicators were mixed with the hydrogels (table of content, TOC graphics). For pH = 2−7 Congo red, for pH = 9 bromothymol blue, and for pH = 11 phenolphthalein were used, respectively.

Abbreviation and Nomenclature. To provide a consistent nomenclature of the synthesized polyethers, ethylene glycol units formed by ring-opening of EO will be denoted "EG". Furthermore, the abbreviation PEG will be used for the macroinitiators, whereas the common "PEO" will be used for the ultrahigh molar mass polyether added to some of the hydrogel samples.

RESULTS AND DISCUSSION

To obtain amphiphilic triblock copolymers in a one-step reaction, PEG (M_n = 10 000 and 20 000 g mol^{-1}) was partially deprotonated and used as a bifunctional macroinitiator. Utilizing the copolymerization of EO and long-chain alkyl glycidyl ethers (AlkGE), a variation of the composition and thus hydrophobic properties of the apolar blocks was possible, mitigating the hydrophobicity of the telechelic A-blocks of the ABA structures. This enabled homogeneous swelling in an aqueous solution. To prevent insufficient mixing and high pressure in the sealed reaction flask during the copolymerization, all polymerizations were performed in solution, using a mixture of dry DMSO/THF (5/1) (Table 1).

In clear contrast to the recently reported homopolymerization of AlkGE monomers, no crown ether was required to obtain full conversion and triblock copolymers with narrow molar mass distributions (Figure 2). This can be explained by the addition of the solvent mixture THF/DMSO (5/1), whereas the previously reported structures[31] were polymerized in bulk. Due to the strong solvation effect of cations, such as K^+ or Ag^+ by DMSO, an increased propagation rate of the ion pair is achieved, leading to increased reactivity of the active chain end.[33,34] The effect of cation solvation by DMSO has been investigated in several epoxide polymerization reactions.[35−39]

To gain further insight into the copolymerization reaction and the reactivity ratios of the EO/AlkGE monomer pair with respect to the microstructure of the apolar blocks formed, a real-time ^{1}H NMR kinetics study of the copolymerization of EO/C12-AlkGE was carried out. The reactivity ratios of r(EO) = 0.97 and r(C12-AlkGE) = 1.03 were calculated using the ideal Jaacks model[40] and indicate a random copolymerization, which is in line with other previously reported copolymerization data of EO with various glycidyl ethers, regardless of the long alkyl chain.[41−43] Thus, a random distribution of the AlkGE units within the hydrophobic block of the polyether triblocks can be confirmed (Figure S1 and Table S1). For a quantitative visualization of the monomer distribution along the polymer chains, the calculated reactivity ratios were used in combination with the Meyer−Lowry equation (Figure 2A).

We emphasize that the determined chain composition shown in Figure 2A is based on the molar ratio of the epoxide monomers. To visualize the volume fraction of the long-chain AlkGE monomers versus EO, the volume fraction values of the resulting ABA triblock copolymers have been calculated. For this purpose, the calculated reactivity ratios (Figure S1 and Table S1) and the molar composition have been combined with the densities of the polymers, as reported in previous

https://dx.doi.org/10.1021/acs.biomac.0c00576
Biomacromolecules 2020, 21, 3152−3162

studies of our group (Figure 3).[44] Due to the lack of reported density values of the AlkGE monomers, the known densities of the respective alcohols (1-dodecanol, 1-hexadecanol) have been used as a first approximation. We emphasize that the volume fractions shown in Figure 3C,D should only be seen as an approximate visualization and do not represent the exact volume ratios, since the density changes of the alkyl monomer and ethylene oxide in the copolymer were not considered. However, significant differences between the molar fractions and the volume fractions can be observed (Figures 3, S2, and S3). The volume fractions displayed in the respective areas result in hydrophobic/hydrophilic ratios of 1:0.94 and 1:0.75 for the P(C12-AlkGE-*co*-EG)- and the P(C16-*co*-EG)-block, respectively.

Furthermore, the hydrophobic/hydrophilic ratio of the telechelic blocks based either on C12- or C16-AlkGE was determined and translated to the respective areas shown in the graphs (Figure 3 and Tables S2 and S3). This underlines the outstanding hydrophobic character of the polymerized AlkGE units caused by the high molar masses and the long alkyl chains of the respective epoxide monomers (hydrophobic/hydrophilic ratio determined by molar fraction vs volume fraction: 1:7.5 vs 1:0.94). To vary the hydrophobicity of the P(AlkGE-*co*-EG) blocks, a constant amount of EO was copolymerized with different molar ratios of C16-AlkGE. Therefore, the amount of C16-AlkGE was adjusted to obtain a similar hydrophobic/hydrophilic ratio compared to the C12-AlkGE-containing block by calculating the theoretical volume fraction (Figures S4 and S5 and Tables S2–S4).

Hydrogel Formation and Thermal Characterization. For the formation of hydrogels, the different ABA triblock copolymers were dissolved in deionized water and stored at 40 °C for 24 h with subsequent slow cooling to room temperature. Homogeneous gelation of the triblock polyethers was achieved in aqueous solutions with 10 wt % of the respective ABA triblock copolymer. Visual inspection of the C12-AlkGE-containing gels showed soft materials at room temperature, whereas the C16-AlkGE-containing hydrogels yielded tough, elastic hydrogels. This can be explained by the different melting temperatures of the AlkGE epoxide monomers leading to crystallization of the alkyl chains in the case of the longer C16-AlkGE monomer units. In our previous work, the melting temperatures of the PC12- and PC16-AlkGE homopolymers in bulk were reported to be 14 and 43 °C, respectively.[31]

Differential scanning calorimetry (DSC) measurements have been carried out to investigate the thermal properties of the synthesized triblock copolymers in bulk. In analogy to the reported ABA triblock structures with PAlkGE homo blocks, we expected similar melting temperatures of the alkyl chain block.[31] However, thermal investigation revealed significantly decreased melting temperatures compared to the PAlkGE homopolymer blocks (Table 1 and Figures 4 and S25).

This can be explained by the random distribution of the long alkyl groups of the glycidyl ethers in the polyether backbone, impeding ordering and crystallization of the alkyl chains, resulting in lowered melting temperatures and lowered melting enthalpies. Additionally, the cooling cycles have been evaluated to obtain crystallization temperatures and enthalpies. Furthermore, different heating and cooling rates (5, 10, and 20 K min^{-1}) were used during the thermal investigation to determine the glass transition temperatures. However, no glass transition temperatures could be observed (Figures S7–S24 and Tables S5–S7). Despite the varying degrees of polymerization (DP) of the C16-AlkGE in the triblock copolymers, similar thermal behavior for the polymer samples (DP = 7 vs 10) was observed (Figures S21 and S22 vs Figures S23 and S24).

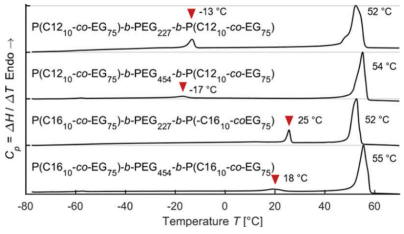

Figure 4. DSC measurements of the synthesized ABA triblock copolymers in bulk (heating rate: 5 K min^{-1}).

Via μ-DSC measurements with higher sensitivity, the prepared hydrogels have also been investigated. The melting temperatures for the C16-AlkGE-containing blocks were observed in the hydrogel state, with melting temperatures in the physiological temperature range between 29 and 39 °C (Table S8 and Figures S26–S31). Interestingly, the melting temperatures of the hydrophobic domains in the hydrogels showed higher values compared to the respective polymer samples in bulk. This unexpected result is tentatively explained by the relatively low order and crystallization of the alkyl chains in bulk. In the hydrogels, the significant contrast in the polarity of the water-swollen PEG domains and the alkyl chains obviously leads to higher order of the alkyl chains, resulting in an increased degree of crystallization and higher melting temperatures. Furthermore, the significantly lower heating/cooling rates applied by the μ-DSC measurements compared to the lowest heating/cooling rate applied by the standard DSC measurements (0.5 vs 5 K min^{-1}) may also contribute to higher order for the alkyl crystallites, leading to higher melting temperatures and increased values of the crystallization and melting enthalpy. For analogous systems containing C18 alkyl chains, albeit based on a poly(acrylic acid) polymer backbone, a hexagonal packing of the alkyl chains could be observed in the hydrophobic domains via X-ray diffraction measurements.[45] Further investigations on related systems based on double-semicrystalline triblock copolymers containing *it*-PPO and PEO blocks revealed hydrophobic domains in the prepared hydrogels resulting from ordered crystalline *it*-PPO domains.[25,26] No melting temperatures could be observed for the C12-AlkGE-containing hydrogels, underlining the importance of the alkyl chain length and its impact on the melting temperature.

Rheological Characterization of the Hydrogels. Oscillatory shear measurements, which represent a standard method for gel analysis, specifically in conjunction with data evaluation on the basis of common rubber-network elasticity models, which commonly directly lead to the prediction of the shear modulus that is probed in shear rheology, were performed to investigate the mechanical properties of the prepared hydrogels. For this purpose, the addition of (i) different pH values, (ii) varied salt concentrations, i.e., different ionic strengths, and (iii) the addition of ultrahigh molar mass (UHMW) PEO (M_n 1 000 000 g mol^{-1}) were investigated. Since the gelation mechanism of the prepared structures in

https://dx.doi.org/10.1021/acs.biomac.0c00576
Biomacromolecules 2020, 21, 3152–3162

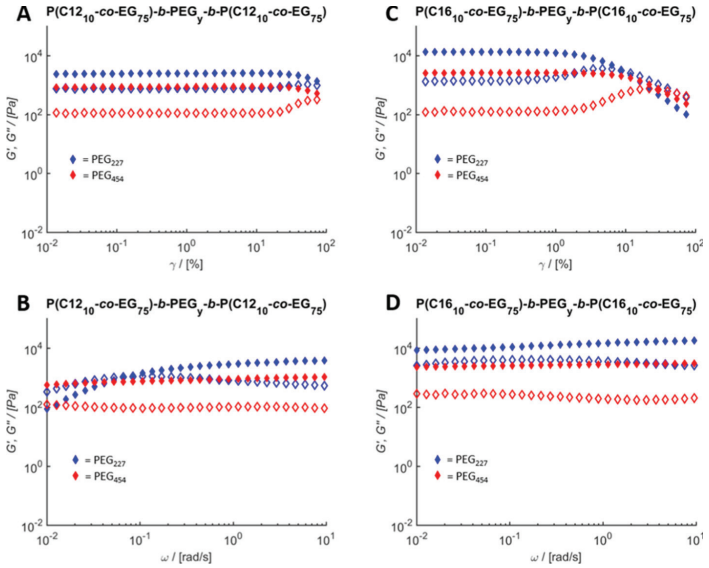

Figure 5. Comparison of the amplitude and frequency-sweep measurements of C12-AlkGE- and C16-AlkGE-containing triblock polyether hydrogels (deionized water, pH = 7). (A) Amplitude-sweep measurements of P(C12-AlkGE$_{10}$-*co*-EG$_{75}$)-*b*-PEG$_y$-*b*-P(C12-AlkGE$_{10}$-*co*-EG$_{75}$)-containing gels. (B) Corresponding frequency-sweep of the hydrogel in (A). (C) Amplitude-sweep data of P(C16-AlkGE$_{10}$-*co*-EG$_{75}$)-*b*-PEG$_y$-*b*-P(C16-AlkGE$_{10}$-*co*-EG$_{75}$) hydrogels. (D) Corresponding frequency-sweep of the hydrogel in (C). Filled and open symbols indicate the storage and loss modulus, respectively.

Table 2. Comparison of the G' Values (Pa) Determined via the Amplitude-Sweep Measurements[a]

	C12-EG-PEG$_{227}$-C12-EG	C12-EG-PEG$_{454}$-C12-EG	C16-EG-PEG$_{227}$-C16-EG	C16-EG-PEG$_{454}$-C16-EG
pH 7 deionized	2300	800	13200	2500
pH 4	3700	200	9200	1000
pH 9	1600	4700	11000	9000
0.5 N NaCl	700	3000	9200	8000
1 N NaCl	800	2400	12000	5400
1wt% UHMW PEO	4500	3500	3200	2600
5wt% UHMW PEO	500	900	800	500

[a]The values in the table represent the determined values of the storage modulus (G'/Pa) for the respective hydrogel. For better comparison of the mechanical behavior, a color code based on the values of the storage modulus has been chosen: light blue, weak; blue, medium; and dark blue, tough hydrogels. All measurements have been carried out at 10 °C and at a constant frequency of ω = 1 rad s^{-1}. The values in the table were obtained from the rheological measurements.

water is based on the hydrophobic association of the alkyl chains, a rather small influence of pH values and ionic strength was expected, which is considered to be a peculiarity of this type of micellar hydrogel structure that in the case of C16 exhibits crystallinity in the hydrophobic domains with melting temperatures in the physiological temperature range.

As a further strategy for improvement of the mechanical properties of the prepared hydrogels, small amounts of UHMW PEO (M_n = 1 000 000 g mol^{-1}; 1 and 5 wt %) were added to the respective triblock copolymers prior to the addition of water. We expected the long PEO chains to act as additional cross-links due to multiple entanglements of the PEO chains and aimed at improving mechanical properties, such as modulus and stretchability of the hydrogel systems.[46] All hydrogel samples contained a total amount of 10 wt % polymer and were characterized at 10 °C.

https://dx.doi.org/10.1021/acs.biomac.0c00576
Biomacromolecules 2020, 21, 3152−3162

The rheological data shown in Figure 5A,C show a general gel-like behavior for the different polyether structures swollen in deionized water at pH = 7. For a better comparison of the mechanical properties of the hydrogels at varied pH values and ion concentrations, the trends obtained for amplitude-sweep measurements are summarized in Table 2. To this end, the obtained values for G' are displayed. Furthermore, additional data concerning the values of G', G'', and the end of the linear viscoelastic region at the corresponding shear value are displayed in Table S10.

Amplitude-Sweep Measurements. Generally, the modulus values of the amplitude-sweep measurements for all synthesized polyether structures show a behavior typical for gels. However, differences in the modulus values and the linear viscoelastic regions of the hydrogels can be observed. For all samples, the addition of UHMW PEO (1 wt %) first led to higher moduli when added to C12-EG-PEG_{227}-C12-EG, while further addition (5 wt %) led to significantly decreased moduli (Figures S32 and S33). This observation is tentatively explained by the high amount of UHMW PEO, which may impede assembly of the hydrophobic blocks. Furthermore, the linear viscoelastic region is narrowed (maximum amplitude of 10%) compared to the gels containing pure, deionized water. For better comparison of the mechanical properties before and after the addition of the UHMW PEO, an overlay of the determined data is provided in the Supporting Information (Figure S34).

For the C16-AlkGE-containing samples, higher modulus values were observed compared to the C12-AlkGE-containing gels, whereas the latter showed shifts of the modulus values for different pH values or ion concentrations. For the absolute modulus values, no systematic trend was observed. While a decrease of the modulus values for the P(C12-*co*-EG)-*b*-PEG_{454}-*b*-P(C12-*co*-EG) and P(C16-*co*-EG)-*b*-PEG_{454}-*b*-P(C16-*co*-EG) at pH = 7 and 4 was observed, the respective polyethers containing PEG_{227} as a midblock showed higher modulus values. An increase of the pH to 9 for the PEG_{454}-containing samples resulted in an increased modulus, whereas no significant shift of the modulus values was observed for the respective gels C12-AlkGE or C16-AlkGE using PEG_{227} as a midblock. Increasing the electrolyte concentration resulted in an increased modulus for the C16-AlkGE-containing hydrogels, whereas for the P(C12-*co*-EG)-*b*-PEG_{227}-*b*-P(C12-*co*-EG) sample, a decrease of the modulus values was observed compared to the results using deionized water at pH = 7. Furthermore, similar mechanical properties for the C16-AlkGE-containing hydrogels with varied hydrophobicities ($DP_{C16\text{-}AlkGE}$ = 7 vs 10) with values of the same order of magnitude could be observed (Figure S39).

Despite the observed variations of the moduli of the hydrogel samples at different pH values, we emphasize that the relatively low values of the loss modulus compared to the storage modulus confirm the gel-like character of all samples even under strongly acidic or basic conditions, as well as at different electrolyte concentrations (Figures S32−S39).

Frequency-Sweep Measurements. Frequency-sweep measurements for the samples with different UHMW PEO contents (1 and 5 wt %) indicate a linear trend. The crossover from $G' < G''$ to $G' > G''$ is shifted to higher frequencies with increasing amount of UHMW PEO (1 and 5 wt %). Additionally, the modulus values are lowered (Figures S32 and S33). These observations can tentatively be explained by the UHMW PEO chains impeding the association of the hydrophobic alkyl chains. This results in a more fluidlike behavior at low frequencies and lower moduli. For better comparison, the determined rheological data of the hydrogels before and after PEO doping are plotted in Figure S34. A similar trend is observed for the variation of the pH value. For the C12-AlkGE-containing polyethers, a shift of the $G'-G''$ crossover to higher frequencies is present. In analogy to the other measured parameters, no crossover could be observed for the C16-AlkGE-containing hydrogels, as expected. Furthermore, variation of the ion concentration did not show a significant impact on the mechanical properties of the measured hydrogels. The frequency-sweep measurements of the gels at pH = 7 in deionized water show overall constant modulus values of around 10^3-10^4 Pa for the C16-AlkGE-containing polyethers, while the values for the C12-AlkGE-containing polyethers are around 10^2-10^3 Pa (Figure 5B,D). For the gel containing P(C12-$AlkGE_{10}$-*co*-EG_{75})-*b*-PEG_{227}-*b*-P(C12-$AlkGE_{10}$-*co*-EG_{75}), a crossover of $G' < G''$ to $G' > G''$ at low frequencies can be observed, which is in line with recently reported polyether structures with varied alkyl chain lengths.[30] In contrast, no crossover is observed for the respective gels containing P(C16-$AlkGE_{10}$-*co*-EG_{75})-*b*-PEG_{227}-*b*-P(C16-$AlkGE_{10}$-*co*-EG_{75}) and P(C16-$AlkGE_7$-*co*-EG_{75})-*b*-PEG_{227}-*b*-P(C16-$AlkGE_7$-*co*-EG_{75}) (Figure S39). This can tentatively be explained by the length of the alkyl chains (C12 vs C16) and their behavior regarding crystallization. Since the mechanical behavior of all gels is similar at higher frequencies, the cross-linking interactions can be attributed to hydrophobic, noncrystalline interactions, which is in line with the μ-DSC measurements of the hydrogels. In contrast, a non-fluid-like behavior of the P(C16-$AlkGE_{10}$-*co*-EG_{75})-*b*-PEG_{227}-*b*-P(C16-$AlkGE_{10}$-*co*-EG_{75})-based gel at lower frequencies can tentatively be explained by combined hydrophobic and additional crystalline associations. These two cross-linking mechanisms could also explain the convergency of G' and G'' at moderate frequencies, resulting in a local maximum in the frequency-dependent curve of G'' and a step in the frequency-dependent curve of G' (Figure 5D), whereas the P(C12-$AlkGE_{10}$-*co*-EG_{75})-*b*-PEG_{227}-*b*-P(C12-$AlkGE_{10}$-*co*-EG_{75})-containing gel switches to a fluidlike behavior ($G' < G''$). This can also be observed for the gels with varied pH values and different salt concentrations (Figures S35d, S36d S37d, and S38d). For a better comparison, the two discussed frequency measurements have also been plotted in one diagram (Figure S40). Similar behavior was also described for double-network hydrogel systems containing different cross-linking mechanisms on different time scales, such as terpyridine, carboxyl, or hydroxyl functionalities, and the complexation of different metal ions.[47,48]

To support this hypothesis, additional frequency and amplitude-sweep measurements of the C16-AlkGE-containing PEG_{227} triblock copolymer in the gel state have been carried out at an elevated temperature (50 °C) (Figure S41). Compared to the measurements at 10 °C, no convergency of G' and G'' can be observed. However, no fluidlike behavior at lower frequencies can be observed. For better visualization, the loss factor of the two discussed samples have been plotted as a function of frequency (Figure S42). The observations lead to the conclusion that at elevated temperatures above the melting point of the apolar alkyl chain domains, the mechanical properties of the P(C16-$AlkGE_{10}$-*co*-EG_{75})-*b*-PEG_{227}-*b*-P(C16-$AlkGE_{10}$-*co*-EG_{75})-containing hydrogel are similar to those of the P(C16-$AlkGE_{10}$-*co*-EG_{75})-*b*-PEG_{454}-*b*-P(C16-$AlkGE_{10}$-*co*-

https://dx.doi.org/10.1021/acs.biomac.0c00576
Biomacromolecules 2020, 21, 3152−3162

EG_{75})-containing hydrogels at 10 °C. It is noteworthy that the molar concentration of the PEG_{227}-containing polyether in the gel is higher than the concentration of the PEG_{454}-containing polyether in the hydrogel since the hydrogels have been prepared using a mixture of 10 wt % of the polymer in water. Consequently, the molar concentration of the PEG_{227}-containing hydrogels is higher compared to the PEG_{454}-containing hydrogels, which leads to increased molarity of the hydrophobic block in the gel. This most likely also leads to an improvement of the mechanical properties caused by crystalline domains in the gel containing P(C16-AlkGE_{10}-*co*-EG_{75})-*b*-PEG_{227}-*b*-P(C16-AlkGE_{10}-*co*-EG_{75}). This is in line with the results of the DSC measurements (Figure 4, samples containing PEG_{227} vs PEG_{454}), where the melting temperatures of the hydrophobic block show higher intensities for the PEG_{227}-containing triblock copolymers compared to the PEG_{454}-containing triblock copolymers.

In summary, the frequency-sweep measurements reveal two different cross-linking mechanisms: (i) weak hydrophobic interactions showing a relaxation behavior for the C12-AlkGE-containing hydrogels at lower frequencies. The frequency at the crossover point marks the inverse time of dissociation of these hydrophobic associations. (ii) Strong crystalline interactions for the C16-AlkGE-containing gels resulting in a stepwise course of $G'(\omega)$ and in a maximum of $G''(\omega)$ in the same frequency region. Due to the combination of these two different cross-linking mechanisms in the C16-AlkGE-containing gels, similar dissociation of the hydrophobic associations at the designated frequency can be observed, but the strong crystalline associations lead to a gel response even at lower frequencies. This results in two plateaus of $G'(\omega)$: (i) one plateau in the low-frequency region caused by the strong crystalline associations and (ii) a second plateau in the high-frequency region caused by the combination of strong crystalline and weak hydrophobic associations. The combination of both plateaus leads to a step at the designated frequency at which the weak interactions show dissociation, causing a maximum in $G''(\omega)$, due to the energy dissipation of the breaking cross-linking mechanism.

Systems capitalizing on the described convergent behavior of G' and G'' possess highly interesting mechanical properties. Since the storage modulus exceeds the loss modulus, solid structures are obtained. However, due to the high value of the loss modulus in the convergent region, unique material properties with high energy dissipation are obtained, which possess potential for various industrial applications, e.g., in the field of vibration damping, as has been suggested for double-network hydrogel systems capitalizing on Coulomb interactions, H bonds, or hydrophobic interaction in combination with covalent cross-links.[10,13,47−51] Further tuning of this behavior might be possible by variation of the alkyl chain length and the resulting degree of crystallization of the apolar domains. Furthermore, a mixture of different supramolecular interaction mechanisms, such as $\pi-\pi$ stacking in combination with hydrophobic interaction, could lead to tailoring of convergent regions in hydrogel systems. To sum up, the rheological investigation reveals that a variation of the swelling aqueous solution, for instance by changing the pH value or the ionic strength via the salt concentration, does not lead to a breakdown of the hydrogel system.

Cytotoxicity of the Amphiphilic Polyethers. It is well known that some amphiphilic systems, such as nonionic surfactants, show cell toxicity, due to interaction with cell membranes.[52,53] In contrast, PEG is known to exhibit low toxicity and is widely used in various biomedical applications, such as in "PEGylation" applications for pharmaceutically active drugs.[54−57] Furthermore, amphiphilic systems, such as poloxamers, are widely used as amphiphilic drug carrier systems in various biomedical applications or in self-care products and are approved by the U.S. Food and Drug Administration (FDA).[58] In the synthesized triblock copolymers, long alkyl chains resembling fatty acids are combined with poly(ethylene glycol), forming amphiphilic structures with polyether backbones that are similar to reverse poloxamer-type structures.[59−61] For instance, polyethers bearing two C16 alkyl chains as end-functionality have been reported for the shielding agents of liposomes utilizing the so-called "stealth-effect" of polyethers, such as PEG or hyperbranched polyglycerol (*hb*PG).[62−65] Based on these reports, a general interaction of the alkyl chains with the cell membrane can be assumed.

To examine the cytotoxicity of the synthesized triblock copolymers used in the resulting hydrogels, cell viability tests have been carried out. Due to the gelation of the triblock polyethers in an aqueous solution, no homogeneous solutions could be prepared, since even at low polymer concentrations, the polyether structures could not be dissolved homogeneously.

To assess the potential cytotoxicity of polyethers bearing long alkyl chains, despite the challenges for the preparation of homogeneous aqueous solutions, the amphiphilic AB diblock copolymer $mPEG_{113}$-*b*-P(C16-Alk$GE)_3$ ($Đ$ = 1.04) (Figure S43) was synthesized to mimic the potential interactions of the alkyl chains attached to poly(ethylene glycol) with a cell membrane. To judge potential adverse effects of $mPEG_{113}$-*b*-P(C16-Alk$GE)_3$ on immune cells, their metabolic activity after incubation with varying doses of $mPEG_{113}$-*b*-P(C16-Alk$GE)_3$ was determined.

As indicated in Figure 6, low and intermediate concentrations of the diblock copolymer did not show any effect on

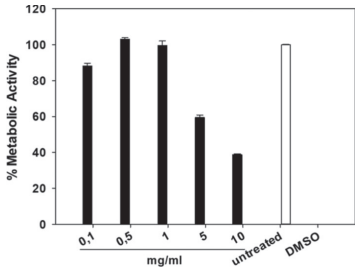

Figure 6. MTT assays of the diblock copolymer $mPEG_{113}$-*b*-P(C16-Alk$GE)_3$ at different concentrations using murine spleen cells derived from C57BL/6 mice. Data denote the results of one experiment (mean ± scanning electron microscopy (SEM) of triplicates) representative for three independent experiments.

the metabolic activity of splenic immune cells. At higher concentrations (10 mg mL^{-1}), a considerable decrease in their metabolic activity was observed. Therefore, potential cytotoxic effects of $mPEG_{113}$-*b*-P(C16-Alk$GE)_3$ on primary immune cells were evaluated by performing viability assays. As depicted in Figure S44, $mPEG_{113}$-*b*-P(C16-Alk$GE)_3$ exerted no detrimen-

https://dx.doi.org/10.1021/acs.biomac.0c00576
Biomacromolecules 2020, 21, 3152−3162

tal effects on the viability of any splenic immune cell population monitored (B cells, T cells, dendritic cells, natural killer cells, polymorphonuclear granulocytes, and macrophages). Altogether, these results suggest that $mPEG_{113}$-*b*-$P(C16\text{-}AlkGE)_3$ may affect the metabolic activity only at higher concentrations (10 mg mL^{-1}), but does not reduce the viability of primary immune cells.

We emphasize that the cytotoxic character of the diblock copolymer $mPEG_{113}$-*b*-$P(C16\text{-}AlkGE)_3$ was assessed to generally estimate the potential cytotoxicity of polyethers bearing long alkyl chains at the polymer backbone since the examination of the triblock copolymers was not possible. However, we hope to carry out further investigation on the field of polyethers bearing long alkyl chains, since a generally low cytotoxic character was observed in these exploratory measurements, rendering these structures promising candidates for biomedical applications, showing an inherent thermoresponsiveness.

CONCLUSIONS

Random copolymerization of ethylene oxide (EO) and different long-chain AlkGE monomers[32] (C12- and C16-AlkGE) with difunctional PEG macroinitiators afforded amphiphilic ABA triblock copolymers with tunable hydrophobicity of the telechelic A-block in a single polymerization step. Upon addition of water, supramolecular hydrogels are formed, merely due to physical cross-linking by micellar aggregation. Capitalizing on the variation of the molar fraction of ethylene oxide and long-chain AlkGE monomers, the hydrophobicity of the telechelic A blocks can be adjusted. Calculations of the resulting volume fractions of the respective blocks visualized the significant impact of the long alkyl chains since the incorporation of only a few repeating units of AlkGE already results in high hydrophobicity of the A-blocks. Differential scanning calorimetry measurements of the synthesized polymers in bulk revealed two melting temperatures, depending on the respective AlkGE monomer C12-AlkGE or C16-AlkGE. Interestingly, μ-DSC measurements showed melting temperatures of the hydrophobic aggregates in the prepared hydrogels for all C16-AlkGE-containing gels in the physiological region, indicating highly ordered, crystalline micelles in solution. Besides deionized water (pH = 7), aqueous solutions at different pH values (pH = 4 and 9) and at different salt concentrations (NaCl, 0.5; 1 mol L^{-1}) have been used as swelling agents to demonstrate the robust nature of these hydrogels. Additionally, UHMW PEO was added to investigate the impact of very long polyether structures in combination with the ABA triblock structures on the mechanical properties of the hydrogels. Rheological measurements of the prepared hydrogels indicated a gel-like behavior for all samples at distinct pH values and ion concentrations, due to hydrophobic cross-linking associations as expected. Furthermore, frequency-dependent behavior for the different AlkGE monomers in the hydrogels was found. While the C12-AlkGE-containing hydrogels showed a crossover to liquidlike behavior below a designated frequency, a stepwise change for G' and a maximum in G'' for the C16-AlkGE-containing hydrogels were observed. This is attributed to crystalline domains of the long alkyl chains formed in the C16-AlkGE-containing hydrogels, representing an additional cross-linking mechanism with dissociation times clearly exceeding the time of dissociation for the weaker hydrophobic interactions. Due to the high energy dissipation in the respective frequency region, materials with the found mechanical properties represent a highly interesting class of hydrogels for several applications, e.g., for vibration damping. Cell viability tests of a representative AB diblock copolymer mimicking the interaction of a dangling chain end with cells in the hydrogel system indicated low cytotoxicity in a wide range of concentrations for splenic immune cells. These findings render the hydrogel systems promising candidates for biomedical applications, such as drug carrier systems or as a long-term hydrogel release matrix for hydrophobic drugs. For several applications, the "dumb" nature of this hydrogel—the robust gelation regardless of ionic strength and pH—may even constitute an advantage.

ASSOCIATED CONTENT

Supporting Information

The Supporting Information is available free of charge at https://pubs.acs.org/doi/10.1021/acs.biomac.0c00576.

^{1}H NMR spectra; ^{1}H NMR kinetic measurements; molar and volume fraction calculations; rheological measurement data; heating and cooling curves from DSC measurements; cell test graphs (PDF)

AUTHOR INFORMATION

Corresponding Author

Holger Frey − *Department of Chemistry, Johannes Gutenberg University Mainz, 55128 Mainz, Germany*; orcid.org/0000-0002-9916-3103; Email: hfrey@uni-mainz.de

Authors

Patrick Verkoyen − *Department of Chemistry, Johannes Gutenberg University Mainz, 55128 Mainz, Germany*

Philip Dreier − *Department of Chemistry, Johannes Gutenberg University Mainz, 55128 Mainz, Germany*

Matthias Bros − *Department of Dermatology, University Medical Center of the Johannes Gutenberg University Mainz, 55131 Mainz, Germany*

Christian Hils − *Makromolekulare Chemie II, University of Bayreuth, 95440 Bayreuth, Germany*

Holger Schmalz − *Makromolekulare Chemie II, University of Bayreuth, 95440 Bayreuth, Germany*; orcid.org/0000-0002-4876-0450

Sebastian Seiffert − *Department of Chemistry, Johannes Gutenberg University Mainz, 55128 Mainz, Germany*; orcid.org/0000-0002-5152-1207

Complete contact information is available at: https://pubs.acs.org/10.1021/acs.biomac.0c00576

Author Contributions

This manuscript was written through contributions of all authors. All authors have given approval to the final version of the manuscript.

Notes

The authors declare no competing financial interest.

ACKNOWLEDGMENTS

The authors thank Monika Schmelzer for SEC measurements, and Kamil Maciol and Jan Blankenburg for technical assistance and help with the data evaluation for the ^{1}H NMR kinetic study. P.V. thanks Tobias Johann for his assistance regarding DSC data evaluation and Willi Schmolke for technical assistance during the rheological measurements. Marvin Steube and Martha Koziol are acknowledged for helpful discussions.

https://dx.doi.org/10.1021/acs.biomac.0c00576
Biomacromolecules 2020, 21, 3152−3162

■ ABBREVIATIONS

AlkGE, alkyl glycidyl ether; UHMW, ultrahigh molar mass (M_n = 1 000 000 g mol^{-1})

■ REFERENCES

(1) Drury, J. L.; Mooney, D. J. Hydrogels for tissue engineering: scaffold design variables and applications. *Biomaterials* **2003**, *24*, 4337−4351.

(2) Hoffman, A. S. Stimuli-responsive polymers: biomedical applications and challenges for clinical translation. *Adv. Drug Delivery Rev.* **2013**, *65*, 10−16.

(3) Huynh, C. T.; Nguyen, M. K.; Lee, D. S. Injectable Block Copolymer Hydrogels: Achievements and Future Challenges for Biomedical Applications. *Macromolecules* **2011**, *44*, 6629−6636.

(4) Peppas, N. A.; Hilt, J. Z.; Khademhosseini, A.; Langer, R. Hydrogels in Biology and Medicine: From Molecular Principles to Bionanotechnology. *Adv. Mater.* **2006**, *18*, 1345−1360.

(5) Lee, K. Y.; Mooney, D. J. Hydrogels for Tissue Engineering. *Chem. Rev.* **2001**, *101*, 1869−1880.

(6) Karis, D. G.; Ono, R. J.; Zhang, M.; Vora, A.; Storti, D.; Ganter, M. A.; Nelson, A. Cross-linkable multi-stimuli responsive hydrogel inks for direct-write 3D printing. *Polym. Chem.* **2017**, *8*, 4199−4206.

(7) Pertici, V.; Trimaille, T.; Gigmes, D. Inputs of Macromolecular Engineering in the Design of Injectable Hydrogels Based on Synthetic Thermoresponsive Polymers. *Macromolecules* **2020**, *53*, 682−692.

(8) Buwalda, S. J.; Vermonden, T.; Hennink, W. E. Hydrogels for Therapeutic Delivery: Current Developments and Future Directions. *Biomacromolecules* **2017**, *18*, 316−330.

(9) Chang, H.; Li, C.; Huang, R.; Su, R.; Qi, W.; He, Z. Amphiphilic hydrogels for biomedical applications. *J. Mater. Chem. B* **2019**, *7*, 2899.

(10) Sun, J.-Y.; Zhao, X.; Illeperuma, W. R. K.; Chaudhuri, O.; Oh, K. H.; Mooney, D. J.; Vlassak, J. J.; Suo, Z. Highly stretchable and tough hydrogels. *Nature* **2012**, *489*, 133.

(11) Hu, X.; Vatankhah-Varnoosfaderani, M.; Zhou, J.; Li, Q.; Sheiko, S. S. Weak Hydrogen Bonding Enables Hard, Strong, Tough, and Elastic Hydrogels. *Adv. Mater.* **2015**, *27*, 6899−6905.

(12) Qin, Z.; Yu, X.; Wu, H.; Li, J.; Lv, H.; Yang, X. Nonswellable and Tough Supramolecular Hydrogel Based on Strong Micelle Cross-Linkings. *Biomacromolecules* **2019**, *20*, 3399−3407.

(13) Tuncaboylu, D. C.; Sari, M.; Oppermann, W.; Okay, O. Tough and Self-Healing Hydrogels Formed via Hydrophobic Interactions. *Macromolecules* **2011**, *44*, 4997−5005.

(14) Miyazaki, T.; Yamaoka, K.; Kaneko, T.; Gong, J. P.; Osada, Y. Hydrogels with the ordered structures. *Sci. Technol. Adv. Mater.* **2000**, *1*, 201−210.

(15) Almeida, M.; Magalhães, M.; Veiga, F.; Figueiras, A. Poloxamers, poloxamines and polymeric micelles: Definition, structure and therapeutic applications in cancer. *J. Polym. Res.* **2018**, *25*, No. 31.

(16) Hoare, T. R.; Kohane, D. S. Hydrogels in drug delivery: Progress and challenges. *Polymer* **2008**, *49*, 1993−2007.

(17) Rajagopal, K.; Lamm, M. S.; Haines-Butterick, L. A.; Pochan, D. J.; Schneider, J. P. Tuning the pH responsiveness of beta-hairpin peptide folding, self-assembly, and hydrogel material formation. *Biomacromolecules* **2009**, *10*, 2619−2625.

(18) Zarzhitsky, S.; Shlomo, Z.; Vinod, T. P.; Jelinek, R.; Rapaport, H. Stacking interactions by two Phe side chains stabilize and orient assemblies of even the minimal amphiphilic *β*-sheet motif. *Chem. Commun.* **2015**, *51*, 3154−3157.

(19) Knerr, P. J.; Branco, M. C.; Nagarkar, R.; Pochan, D. J.; Schneider, J. P. Heavy metal ion hydrogelation of a self-assembling peptideviacysteinyl chelation. *J. Mater. Chem.* **2012**, *22*, 1352−1357.

(20) Lundberg, D. J.; Glass, J. E.; Eley, R. R. Viscoelastic behavior among HEUR thickeners. *J. Rheol.* **1991**, *35*, 1255−1274.

(21) Annable, T.; Buscall, R.; Ettelaie, R.; Whittlestone, D. The rheology of solutions of associating polymers: Comparison of experimental behavior with transient network theory. *J. Rheol.* **1993**, *37*, 695−726.

(22) Zinn, T.; Willner, L.; Knudsen, K. D.; Lund, R. Self-Assembly of Mixtures of Telechelic and Monofunctional Amphiphilic Polymers in Water: From Clusters to Flowerlike Micelles. *Macromolecules* **2017**, *50*, 7321−7332.

(23) Sanabria-DeLong, N.; Agrawal, S. K.; Bhatia, S. R.; Tew, G. N. Controlling Hydrogel Properties by Crystallization of Hydrophobic Domains. *Macromolecules* **2006**, *39*, 1308−1310.

(24) Agrawal, S. K.; Sanabria-DeLong, N.; Tew, G. N.; Bhatia, S. R. Structural Characterization of PLA−PEO−PLA Solutions and Hydrogels: Crystalline vs Amorphous PLA Domains. *Macromolecules* **2008**, *41*, 1774−1784.

(25) McGrath, A. J.; Shi, W.; Rodriguez, C. G.; Kramer, E. J.; Hawker, C. J.; Lynd, N. A. Synthetic strategy for preparing chiral double-semicrystalline polyether block copolymers. *Polym. Chem.* **2015**, *6*, 1465−1473.

(26) Shi, W.; McGrath, A. J.; Li, Y.; Lynd, N. A.; Hawker, C. J.; Fredrickson, G. H.; Kramer, E. J. Cooperative and Sequential Phase Transitions in it -Poly(propylene oxide)-b-poly(ethylene oxide)-b-it-poly(propylene oxide) Triblock Copolymers. *Macromolecules* **2015**, *48*, 3069−3079.

(27) Shin, D.; Shin, K.; Aamer, K. A.; Tew, G. N.; Russell, T. P.; Lee, J. H.; Jho, J. Y. A Morphological Study of a Semicrystalline Poly(L-lactic acid-b-ethylene oxide-b-L-lactic acid) Triblock Copolymer. *Macromolecules* **2005**, *38*, 104−109.

(28) Gjerde, N.; Zhu, K.; Nyström, B.; Knudsen, K. D. Effect of PCL end-groups on the self-assembly process of Pluronic in aqueous media. *Phys. Chem. Chem. Phys.* **2018**, *20*, 2585−2596.

(29) Cui, S.; Yu, L.; Ding, J. Thermogelling of Amphiphilic Block Copolymers in Water: ABA Type versus AB or BAB Type. *Macromolecules* **2019**, *52*, 3697−3715.

(30) Murakami, T.; Kawamori, T.; Gopez, J. D.; McGrath, A. J.; Klinger, D.; Saito, K. Synthesis of PEO-based physical gels with tunable viscoelastic properties. *J. Polym. Sci., Part A: Polym. Chem.* **2018**, *56*, 1033−1038.

(31) Verkoyen, P.; Johann, T.; Blankenburg, J.; Czysch, C.; Frey, H. Polymerization of long chain alkyl glycidyl ethers: a platform for micellar gels with tailor-made melting points. *Polym. Chem.* **2018**, *9*, 5327−5338.

(32) Verkoyen, P.; Frey, H. Long-Chain Alkyl Epoxides and Glycidyl Ethers: An Underrated Class of Monomers. *Macromol. Rapid Commun.* **2020**, *41*, No. 2000225.

(33) Solov'ev, V. P.; Strakhova, N. N.; Raevsky, O. A.; Rüdiger, V.; Schneider, H.-J. Solvent Effects on Crown Ether Complexations 1. *J. Org. Chem.* **1996**, *61*, 5221−5226.

(34) Reichardt, C. *Solvents and Solvent Effects in Organic Chemistry*, 3rd, updated and enl. ed., 2nd reprint; Wiley-VCH: Weinheim, 2005.

(35) Price, C. C.; Carmelite, D. D. Reactions of Epoxides in Dimethyl Sulfoxide Catalyzed by Potassium t-Butoxide. *J. Am. Chem. Soc.* **1966**, *88*, 4039−4044.

(36) Bawn, C. E. H.; Ledwith, A.; McFarlane, N. R. Anionic polymerization in dimethyl sulphoxide. *Polymer* **1967**, *8*, 484−487.

(37) Bawn, C. E. H.; Ledwith, A.; McFarlane, N. Anionic polymerization of ethylene oxide in dimethyl sulphoxide. *Polymer* **1969**, *10*, 653−659.

(38) Price, C. C.; Akkapeddi, M. K. Kinetics of base-catalyzed polymerization of epoxides in dimethyl sulfoxide and hexamethyl-phosphoric triamide. *J. Am. Chem. Soc.* **1972**, *94*, 3972−3975.

(39) Kazanskii, K. S.; Solovyanov, A. A.; Dubrovsky, S. A. Some remarks to the kinetics of anionic polymerization of ethylene oxide in dimethyl sulfoxide. *Makromol. Chem.* **1978**, *179*, 969−973.

(40) Jaacks, V. A novel method of determination of reactivity ratios in binary and ternary copolymerizations. *Makromol. Chem.* **1972**, *161*, 161−172.

(41) Herzberger, J.; Leibig, D.; Liermann, J. C.; Frey, H. Conventional Oxyanionic versus Monomer-Activated Anionic Co-polymerization of Ethylene Oxide with Glycidyl Ethers: Striking

https://dx.doi.org/10.1021/acs.biomac.0c00576
Biomacromolecules 2020, 21, 3152−3162

Differences in Reactivity Ratios. *ACS Macro Lett.* **2016**, *5*, 1206−1211.
(42) Herzberger, J.; Fischer, K.; Leibig, D.; Bros, M.; Thiermann, R.; Frey, H. Oxidation-Responsive and "Clickable" Poly(ethylene glycol) via Copolymerization of 2-(Methylthio)ethyl Glycidyl Ether. *J. Am. Chem. Soc.* **2016**, *138*, 9212−9223.
(43) Niederer, K.; Schüll, C.; Leibig, D.; Johann, T.; Frey, H. Catechol Acetonide Glycidyl Ether (CAGE): A Functional Epoxide Monomer for Linear and Hyperbranched Multi-Catechol Functional Polyether Architectures. *Macromolecules* **2016**, *49*, 1655−1665.
(44) Steube, M.; Johann, T.; Galanos, E.; Appold, M.; Rüttiger, C.; Mezger, M.; Gallei, M.; Müller, A. H. E.; Floudas, G.; Frey, H. Isoprene/Styrene Tapered Multiblock Copolymers with up to Ten Blocks: Synthesis, Phase Behavior, Order, and Mechanical Properties. *Macromolecules* **2018**, *51*, 10246−10258.
(45) Bilici, C.; Can, V.; Nöchel, U.; Behl, M.; Lendlein, A.; Okay, O. Melt-Processable Shape-Memory Hydrogels with Self-Healing Ability of High Mechanical Strength. *Macromolecules* **2016**, *49*, 7442−7449.
(46) Ebagninin, K. W.; Benchabane, A.; Bekkour, K. Rheological characterization of poly(ethylene oxide) solutions of different molecular weights. *J. Colloid Interface Sci.* **2009**, *336*, 360−367.
(47) Czarnecki, S.; Rossow, T.; Seiffert, S. Hybrid Polymer-Network Hydrogels with Tunable Mechanical Response. *Polymers* **2016**, *8*, 82−98.
(48) Zhu, L.; Qiu, J.; Sakai, E. A high modulus hydrogel obtained from hydrogen bond reconstruction and its application in vibration damper. *RSC Adv.* **2017**, *7*, 43755−43763.
(49) Zhao, X.; Huebsch, N.; Mooney, D. J.; Suo, Z. Stress-relaxation behavior in gels with ionic and covalent crosslinks. *J. Appl. Phys.* **2010**, *107*, No. 063509.
(50) Hao, J.; Weiss, R. A. Mechanical behavior of hybrid hydrogels composed of a physical and a chemical network. *Polymer* **2013**, *54*, 2174−2182.
(51) Zhao, X. Multi-scale multi-mechanism design of tough hydrogels: building dissipation into stretchy networks. *Soft Matter* **2014**, *10*, 672−687.
(52) Hofland, H. E. J.; Bouwstra, J. A.; Verhoef, J. C.; Buckton, G.; Chowdry, B. Z.; Ponec, M.; Junginger, H. E. Safety Aspects of Non-ionic Surfactant Vesicles: A Toxicity Study Related to the Physicochemical Characteristics of Non-ionic Surfactants. *J. Pharm. Pharmacol.* **1992**, *44*, 287−294.
(53) Arechabala, B.; Coiffard, C.; Rivalland, P.; Coiffard, L. J. M.; de Roeck-Holtzhauer, Y. Comparison of cytotoxicity of various surfactants tested on normal human fibroblast cultures using the neutral red test, MTT assay and LDH release. *J. Appl. Toxicol.* **1999**, *19*, 163−165.
(54) Veronese, F. M.; Pasut, G. PEGylation, successful approach to drug delivery. *Drug Discovery Today* **2005**, *10*, 1451−1458.
(55) Abuchowski, A.; van Es, T.; Palczuk, N. C.; Davis, F. F. Alteration of immunological properties of bovine serum albumin by covalent attachment of polyethylene glycol. *J. Biol. Chem.* **1977**, *252*, 3578−3581.
(56) Knop, K.; Hoogenboom, R.; Fischer, D.; Schubert, U. S. Poly(ethylene glycol) in drug delivery: pros and cons as well as potential alternatives. *Angew. Chem., Int. Ed.* **2010**, *49*, 6288−6308.
(57) Herzberger, J.; Niederer, K.; Pohlit, H.; Seiwert, J.; Worm, M.; Wurm, F. R.; Frey, H. Polymerization of Ethylene Oxide, Propylene Oxide, and Other Alkylene Oxides: Synthesis, Novel Polymer Architectures, and Bioconjugation. *Chem. Rev.* **2016**, *116*, 2170−2243.
(58) Yadav, H. K. S.; Dibi, M.; Mohammed, A.; Emad, A. Thermoresponsive Drug Delivery Systems, Characterization, and Applications. In *Characterization and Biology of Nanomaterials for Drug Delivery: Nanoscience and Nanotechnology in Drug Delivery*; Mohapatra, S. S.; Ranjan, S.; Dasgupta, N.; Mishra, R. K.; Thomas, S., Eds.; Micro & Nano Technologies Series; Elsevier: Amsterdam, Netherlands, 2019; pp 351−373.
(59) Kwon, J. W.; Han, Y. K.; Lee, W. J.; Cho, C. S.; Paik, S. J.; Cho, D. I.; Lee, J. H.; Wee, W. R. Biocompatibility of poloxamer hydrogel as an injectable intraocular lens: A pilot study. *J. Cataract Refractive Surg.* **2005**, *31*, 607−613.
(60) Ricci, E. J.; Lunardi, L. O.; Nanclares, D. M. A.; Marchetti, J. M. Sustained release of lidocaine from Poloxamer 407 gels. *Int. J. Pharm.* **2005**, *288*, 235−244.
(61) Issa, J. P. M.; do Nascimento, C.; Iyomasa, M. M.; Siéssere, S.; Regalo, S. C. H.; Defino, H. L. A.; Sebald, W. Bone healing process in critical-sized defects by rhBMP-2 using poloxamer gel and collagen sponge as carriers. *Micron* **2008**, *39*, 17−24.
(62) Wagener, K.; Bros, M.; Krumb, M.; Langhanki, J.; Pektor, S.; Worm, M.; Schinnerer, M.; Montermann, E.; Miederer, M.; Frey, H.; Opatz, T.; Rösch, F. Targeting of Immune Cells with Trimannosylated Liposomes. *Adv. Ther.* **2020**, No. 1900185.
(63) Wagener, K.; Worm, M.; Pektor, S.; Schinnerer, M.; Thiermann, R.; Miederer, M.; Frey, H.; Rösch, F. Comparison of Linear and Hyperbranched Polyether Lipids for Liposome Shielding by ^{18}F-Radiolabeling and Positron Emission Tomography. *Biomacromolecules* **2018**, *19*, 2506−2516.
(64) Hofmann, A. M.; Wurm, F.; Hühn, E.; Nawroth, T.; Langguth, P.; Frey, H. Hyperbranched polyglycerol-based lipids via oxyanionic polymerization: toward multifunctional stealth liposomes. *Biomacromolecules* **2010**, *11*, 568−574.
(65) Amado, E.; Kressler, J. Interactions of amphiphilic block copolymers with lipid model membranes. *Curr. Opin. Colloid Interface Sci.* **2011**, *16*, 491−498.

https://dx.doi.org/10.1021/acs.biomac.0c00576
Biomacromolecules 2020, 21, 3152−3162

Supporting Information

"Dumb" pH-Independent and Biocompatible Hydrogels Formed by Copolymers of Long-Chain Alkyl Glycidyl Ethers and Ethylene Oxide

*Patrick Verkoyen[a], Philip Dreier[a], Matthias Bros[b], Christian Hils[c], Holger Schmalz[c], Sebastian Seiffert[a], Holger Frey[a]**

a. Department of Chemistry, Johannes Gutenberg University Mainz, Duesbergweg 10-14, D-55128 Mainz, Germany.

b. Department of Dermatology, University Medical Center of the Johannes Gutenberg University Mainz, Langenbeckstrasse 1, D-55131 Mainz, Germany.

c. Makromolekulare Chemie II, University of Bayreuth, 95440 Bayreuth, Germany

^{1}H NMR Kinetics Studies

Table S1. Determined reactivity ratios r using the Ideal Jaacks method.

Method	r (EO)	r (C12-AlkGE)
Ideal Jaacks	0.97	1.03

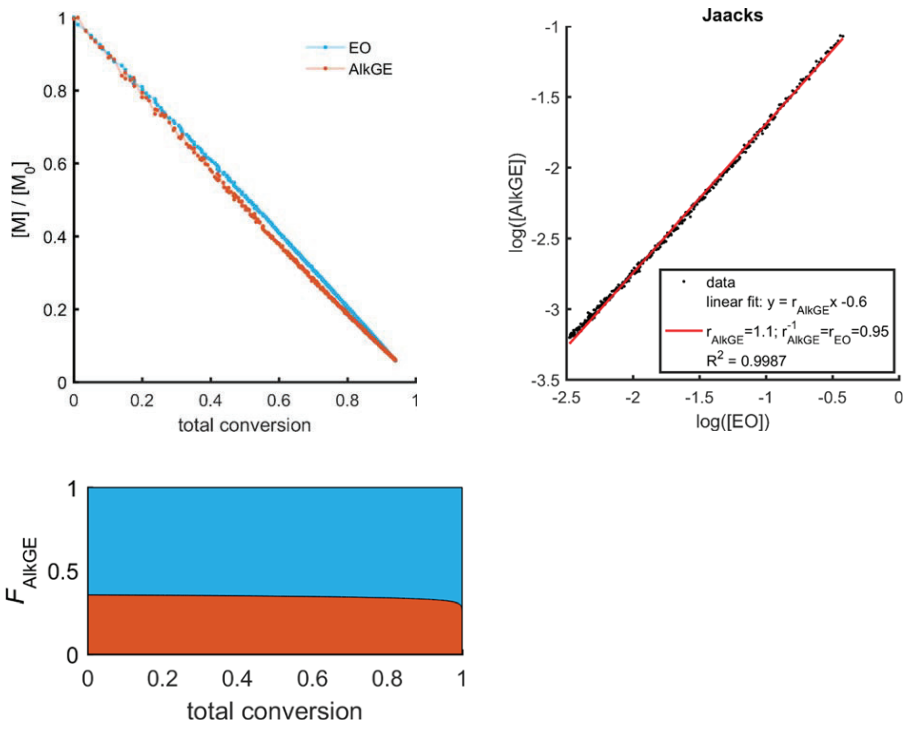

Figure S1. ^{1}H NMR kinetical studies using the Ideal Jaacks method. Observed conversion of EO (blue) und C12-AlkGE (red) during the experiment, Jaacks plot. Graphical illustration of the polymer composition with monomer conversion.

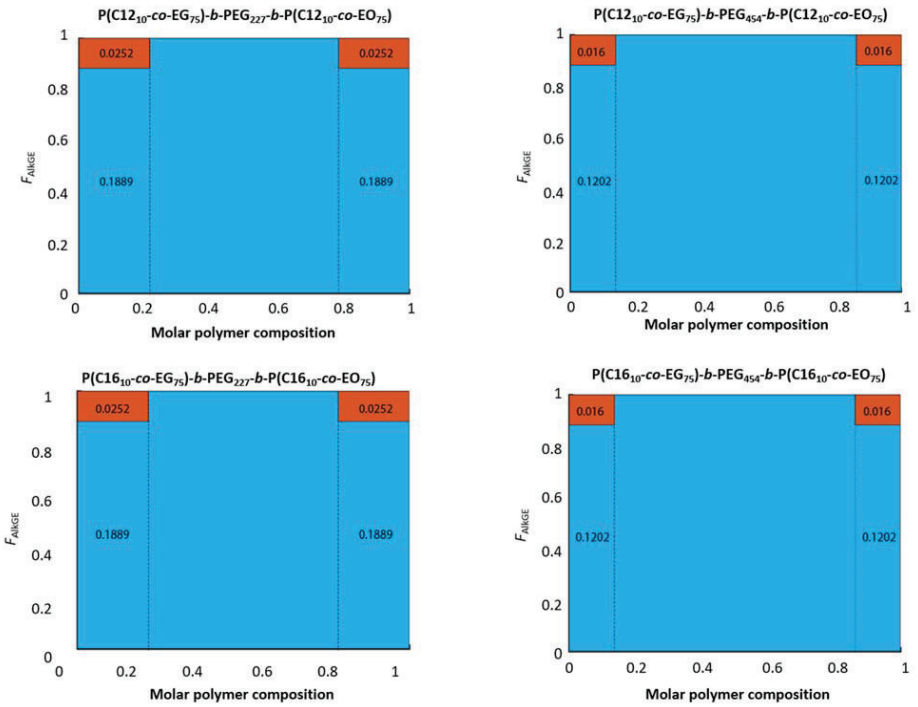

Figure S2. Calculated molar conversion plots of the synthesized ABA triblock copolymers using PEG (M_n 10 000, 20 000 g mol^{-1}) macroinitiators in combination with EO (blue) and C12-, or C16-AlkGE (red) copolymer segments.

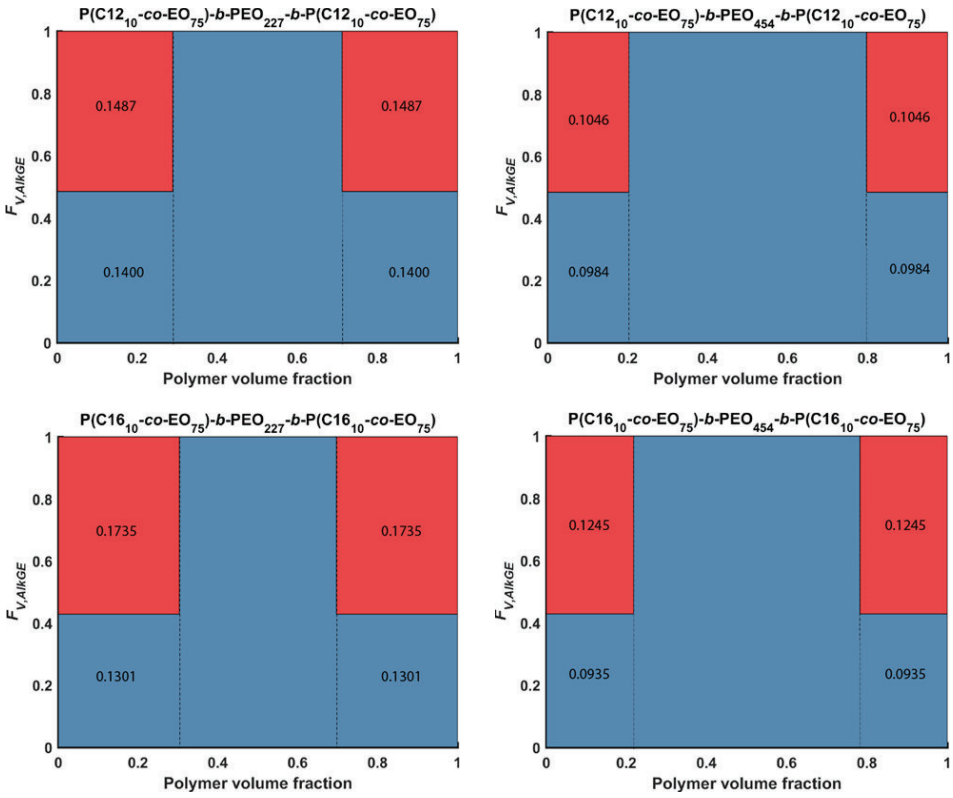

Figure S3. Calculated molar volume fraction plots of the synthesized ABA triblock copolymers using PEG (M_n 10 000, 20 000 g mol^{-1}) macroinitiators in combination of EO (blue) and C12-, or C16-AlkGE (red), respectively. For the volume calculation, densities of PEG and the respective alkyl alcohol have been used.

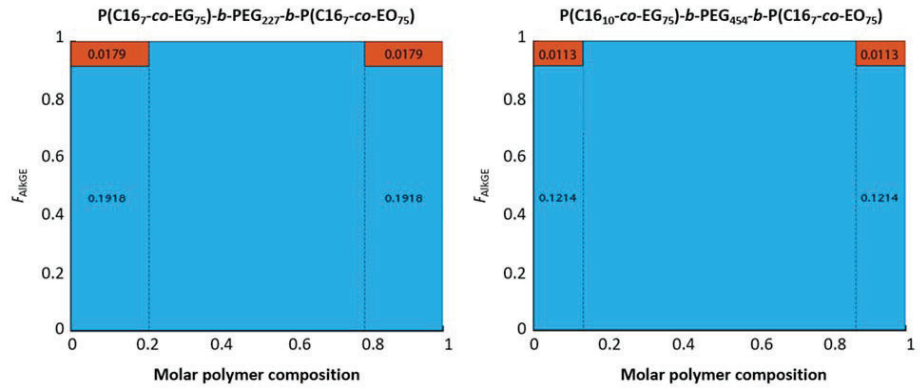

Figure S4. Calculated molar conversion plots of the synthesized ABA triblock copolymers using PEG (M_n 10 000, 20 000 g mol^{-1}) macroinitiators in combination of EO (blue) and C16-AlkGE (red), with variated molarities calculated to theoretical volume fraction of C12-AlkGE.

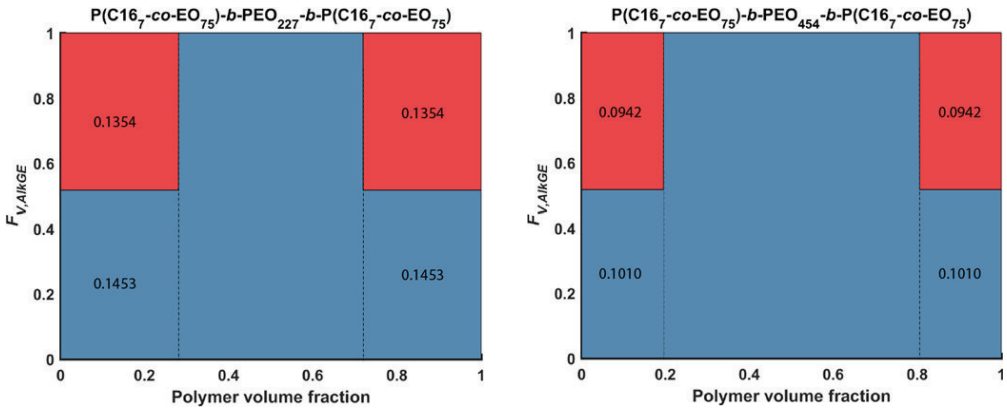

Figure S5. Calculated molar volume fraction plots of the synthesized ABA triblock copolymers using PEG (M_n 10 000, 20 000 g mol^{-1}) macroinitiators in combination of EO (blue) and C16-AlkGE (red). For the volume calculation, densities of PEG and the alkyl alcohol have been used.

Table S2. Comparison of the fraction values calculated by using the Meyer-Lowry equation in combination with the determined reactivity ratios and the densities of the different polymers PAlkGE (approximation using the densities of the alcohols) and PEG for the ABA triblock copolymers with PEG_{227} (M_n 10 000 g mol^{-1}) as macroinitiator.

Structure	Molar fraction of AlkGE [a]	Molar fraction of EO[a]	Volume fraction of AlkGE[a]	Volume fraction of EO[a]
P($C12_{10}$-*co*-EG_{75})-*b*-PEG_{227}-*b*-P($C12_{10}$-*co*-EG_{75})	0.0252	0.1889	0.1487	0.1400
P($C16_{10}$-*co*-EG_{75})-*b*-PEG_{227}-*b*-P($C16_{10}$-*co*-EG_{75})	0.0252	0.1889	0.1735	0.1301
P($C16_{7}$-*co*-EG_{75})-*b*-PEG_{227}-*b*-P($C16_{7}$-*co*-EG_{75})	0.0179	0.1918	0.1354	0.1453

[a] The values of the integrals relate to the area of the respective blocks AlkGE (red) and EO (blue) of the hydrophobic A-block in the ABA triblock copolymer for one A-Block. The total relative area value of one P(AlkGE-co-EG) A-Block can be obtained by adding the values of AlkGE and EO.

Table S3. Comparison of the fraction values calculated by using the Meyer-Lowry equation in combination with the determined reactivity ratios and the densities of the different polymers PAlkGE (approximation using the densities of the alcohols) and PEG for the ABA triblock copolymers with PEG_{454} (M_n 20 000 g mol^{-1}) as macroinitiator.

Structure	Molar fraction of AlkGE[a]	Molar fraction of EO[a]	Volume fraction of AlkGE[a]	Molar fraction of EO[a]
P($C12_{10}$-*co*-EG_{75})-*b*-PEG_{454}-*b*-P($C12_{10}$-*co*-EG_{75})	0.0160	0.1202	0.1046	0.0984
P($C16_{10}$-*co*-EG_{75})-*b*-PEG_{454}-*b*-P($C16_{10}$-*co*-EG_{75})	0.0160	0.1202	0.1245	0.0935
P($C16_7$-*co*-EG_{75})-*b*-PEG_{454}-*b*-P($C16_7$-*co*-EG_{75})	0.0113	0.1214	0.0942	0.1010

[a] The values of the integrals relate to the area of the respective blocks AlkGE (red) and EO (blue) of the hydrophobic A-block in the ABA triblock copolymer for one A-Block. The total relative area value of one P(AlkGE-co-EG) A-Block can be obtained by adding the values of AlkGE and EO.

The values shown in Table S3 are calculated relatively to the normalization of the values shown in Table S2. Due to the normalization of the polymer volume fraction, no direct comparison of the PEG_{227} (M_n 10.000 g mol^{-1}) (Table S2) and PEG_{454} (M_n 20.000 g mol^{-1}) (Table S3) can be made. Using the specific conversion factor (F_{conv}), which can be obtained by calculating the theoretical area values of the PEG_{454} middle block in the PEG_{227} normalized plot (Equation ES3), the fraction values of Table S3 times F_{conv} can be compared to the values shown in Table S2.

The theoretical approach to equation ES3 is as follows. The triblock copolymer structures ABA is built by two A-blocks with constant fraction values A and one middle B-block with the fraction value B for PEG_{227}. For the normalized plots of PEG_{227} the values in Table S2 can be used and the equation

$$Area_{total} = 2 * A + B \quad \text{(ES1)}$$

can be obtained. For the total area of the plot, using PEG_{454} instead of PEG_{227} the equation is:

$$Area_{total} = 2 * A + 2 * B \quad \text{(ES2)}$$

since the molecular weight of the middle block is two times larger compared to (ES1). The specific conversion factor (F_{conv}) can be obtained by the fraction of ES2 and ES1:

$$F_{conv} = \frac{2*A+2*B}{2*A+B} \quad \text{(ES3)}$$

Table S4 shows the fraction values of the PEG_{227} consisting ABA structures and the fraction values of the PEG_{454} structures, which have been multiplied by the conversion factor F_{conv} for a better comparison.

Table S4. Comparison of the calculated fraction values obtained by the polymer conversion and polymer volume plots using the conversion factor F_{conv} for the PEG_{454} consisting ABA structures for a better comparison.

Structure	Molar fraction of AlkGE[a]	Molar fraction of EO[a]	Volume fraction of AlkGE[a]	Volume fraction of EO[a]
P($C12_{10}$-*co*-EG_{75})-b-PEG_{227}-*b*-P($C12_{10}$-*co*-EG_{75})	0.0252	0.1889	0.1488	0.1400
P($C16_{10}$-*co*-EG_{75})-b-PEG_{227}-*b*-P($C16_{10}$-*co*-EG_{75})	0.0252	0.1889	0.1735	0.1302
P($C12_{10}$-*co*-EG_{75})-b-PEG_{454}-*b*-P($C12_{10}$-*co*-EG_{75})	0.0252	0.1889	0.1488	0.1400
P($C16_{10}$-*co*-EG_{75})-b-PEG_{454}-*b*-P($C16_{10}$-*co*-EG_{75})	0.0252	0.1889	0.1735	0.1302
P($C16_{7}$-*co*-EG_{75})-b-PEG_{227}-*b*-P($C16_{7}$-*co*-EG_{75})	0.0179	0.1918	0.1354	0.1453
P($C16_{7}$-*co*-EG_{75})-b-PEG_{454}-*b*-P($C16_{7}$-*co*-EG_{75})	0.0179	0.1918	0.1355	0.1453

Figure S6. Inversed-vial test of the P(C16$_7$-*co*-EG$_{75}$)-*b*-PEG$_{227}$-*b*-P(C16$_7$-*co*-EG$_{75}$) containing hydrogel (10 wt% polymer) in deionized water, indicating a homogeneously swollen hydrogel.

Table S5. Thermal properties of the synthesized triblock copolymers in bulk (heating rate: 20 K min^{-1}).

Structure	T_m / °C [a]	ΔH_m / J/g [a]	T_c / °C [b]	ΔH_c / J/g [b]
P($C12_{10}$-*co*-EG_{75})-*b*-PEG_{227}-*b*-P($C12_{10}$-*co*-EG_{75})	-11 / 55	5.5 / 60.4	-27 / 19	-8.1 / -74.9
P($C16_{10}$-*co*-EG_{75})-*b*-PEG_{227}-*b*-P($C16_{10}$-*co*-EG_{75})	26 / 53	11.7 / 87.7	18 / 30	-13.0 / -93.7
P($C12_{10}$-*co*-EG_{75})-*b*-PEG_{454}-*b*-P($C12_{10}$-*co*-EG_{75})	-16 / 56	2.3 / 80-9	-27 / 25	-3.46 / -89.7
P($C16_{10}$-*co*-EG_{75})-*b*-PEG_{454}-*b*-P($C16_{10}$-*co*-EG_{75})	21 / 56	4.4 / 80.4	9 / 23	-4.35 / -90.8
P($C16_7$-*co*-EG_{75})-*b*-PEG_{227}-*b*-P($C16_7$-*co*-EG_{75})	20 / 53	5.1 / 72.1	10 / 22	-5.4 / -78.9
P($C16_7$-*co*-EG_{75})-*b*-PEG_{454}-*b*-P($C16_7$-*co*-EG_{75})	22 / 61	3.6 / 74.9	7 / 21	-4.3 / -97.7

[a] First and second melting temperature can be assigned to the P(AlkGE-*co*-EG), and the PEG block, respectively. [b] First and second crystallization temperature can be assigned to the P(AlkGE-*co*-EG), and the PEG block, respectively.

Table S6. Thermal properties of the synthesized triblock copolymers in bulk (heating rate: 10 K min^{-1}).

Structure	T_m / °C [a]	ΔH_m / J/g [a]	T_c / °C [b]	ΔH_c / J/g [b]
P($C12_{10}$-*co*-EG_{75})-*b*-PEG_{227}-*b*-P($C12_{10}$-*co*-EG_{75})	-13 / 52	6.9 / 66.9	-23 / 25	-8.2 / -75.4
P($C16_{10}$-*co*-EG_{75})-*b*-PEG_{227}-*b*-P($C16_{10}$-*co*-EG_{75})	26 / 53	12.3 / 89.5	18 / 30	-13.8 / -93.9
P($C12_{10}$-*co*-EG_{75})-*b*-PEG_{454}-*b*-P($C12_{10}$-*co*-EG_{75})	-16 / 55	2.7 / 82.4	-25 / 29	-4.0 / -90.7
P($C16_{10}$-*co*-EG_{75})-*b*-PEG_{454}-*b*-P($C16_{10}$-*co*-EG_{75})	20 / 55	3.9 / 85.4	12 / 28	-6.8 / 93.9
P($C16_{7}$-*co*-EG_{75})-*b*-PEG_{227}-*b*-P($C16_{7}$-*co*-EG_{75})	20 / 51	6.9 / 75.5	12 / 24	-7.9 / -84.6
P($C16_{7}$-*co*-EG_{75})-*b*-PEG_{454}-*b*-P($C16_{7}$-*co*-EG_{75})	20 / 57	5.6 / 92.7	11 / 28	-7.4 / -106.4

[a] First and second melting temperature can be assigned to the P(AlkGE-*co*-EG), and the PEG block, respectively. [b] First and second crystallization temperature can be assigned to the P(AlkGE-*co*-EG), and the PEG block, respectively.

Table S7. Thermal properties of the synthesized triblock copolymers in bulk (heating rate: 5 K min^{-1}).

Structure	T_m / °C [a]	ΔH_m / J/g [a]	T_c / °C [b]	ΔH_c / J/g [b]
P($C12_{10}$-*co*-EG_{75})-*b*-PEG_{227}-*b*-P($C12_{10}$-*co*-EG_{75})	-13 / 52	7.2 / 69.4	-21 / 29	-8.5 / 75.8
P($C16_{10}$-*co*-EG_{75})-*b*-PEG_{227}-*b*-P($C16_{10}$-*co*-EG_{75})	25 / 52	12.5 / 92.7	21 / 36	-13.8 / 95.7
P($C12_{10}$-*co*-EG_{75})-*b*-PEG_{454}-*b*-P($C12_{10}$-*co*-EG_{75})	-17 / 54	3.7 / 84.9	-24 / 34	-4.5 / -91.6
P($C16_{10}$-*co*-EG_{75})-*b*-PEG_{454}-*b*-P($C16_{10}$-*co*-EG_{75})	18 / 55	5.8 / 89.3	13 / 37	-7.0 / -97.7
P($C16_7$-*co*-EG_{75})-*b*-PEG_{227}-*b*-P($C16_7$-*co*-EG_{75})	20 / 51	8.5 / 76.6	14 / 28	-9.4 / -86.8
P($C16_7$-*co*-EG_{75})-*b*-PEG_{454}-*b*-P($C16_7$-*co*-EG_{75})	20 / 55	4.3 / 89.1	12 / 33	-8.1 / -106.1

[a] First and second melting temperature can be assigned to the P(AlkGE-*co*-EG), and the PEG block, respectively. [b] First and second crystallization temperature can be assigned to the P(AlkGE-*co*-EG), and the PEG block, respectively.

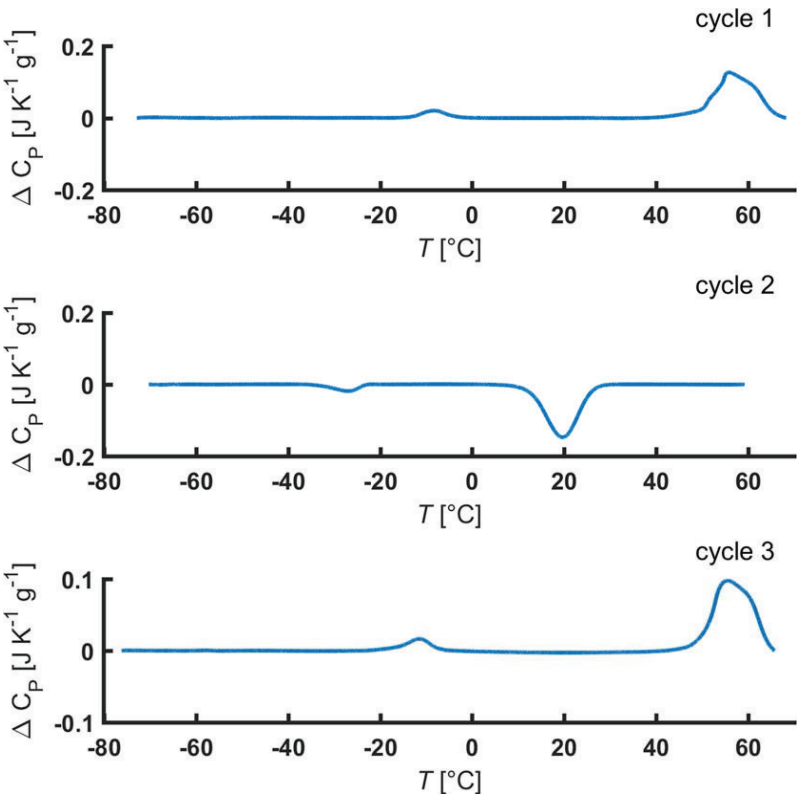

Figure S7. DSC results for heating and cooling cycles of the synthesized triblock copolymer P(C12$_{10}$-*co*-EG$_{75}$)-*b*-PEG$_{227}$-*b*-P(C12$_{10}$-*co*-EG$_{75}$); Heating rate: 20 K min^{-1}.

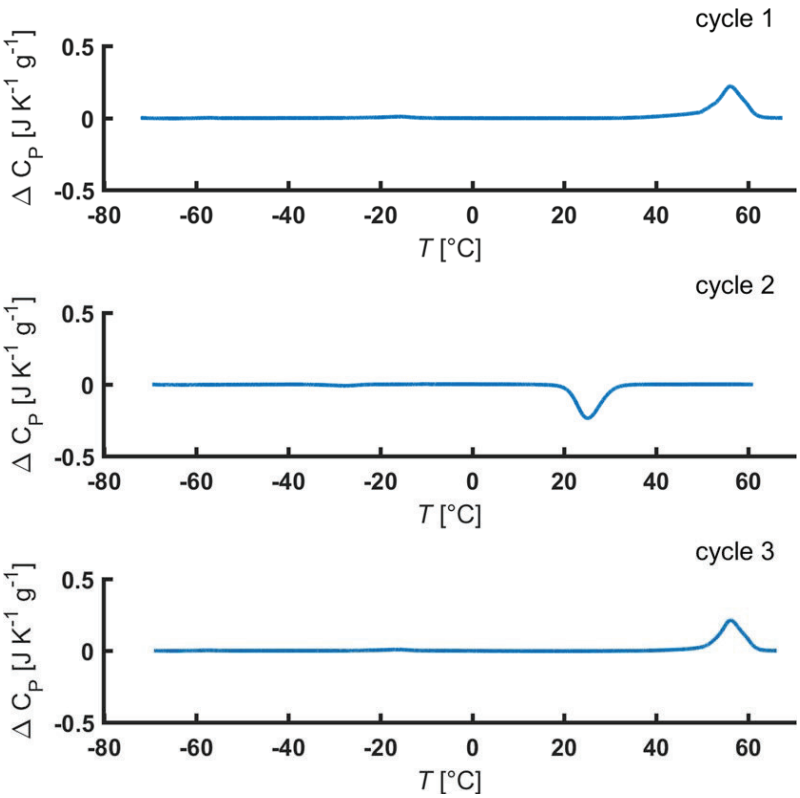

Figure S8. DSC results for heating and cooling cycles of the synthesized triblock copolymer P(C12$_{10}$-*co*-EG$_{75}$)-*b*-PEG$_{454}$-*b*-P(C12$_{10}$-*co*-EG$_{75}$); Heating rate: 20 K min^{-1}.

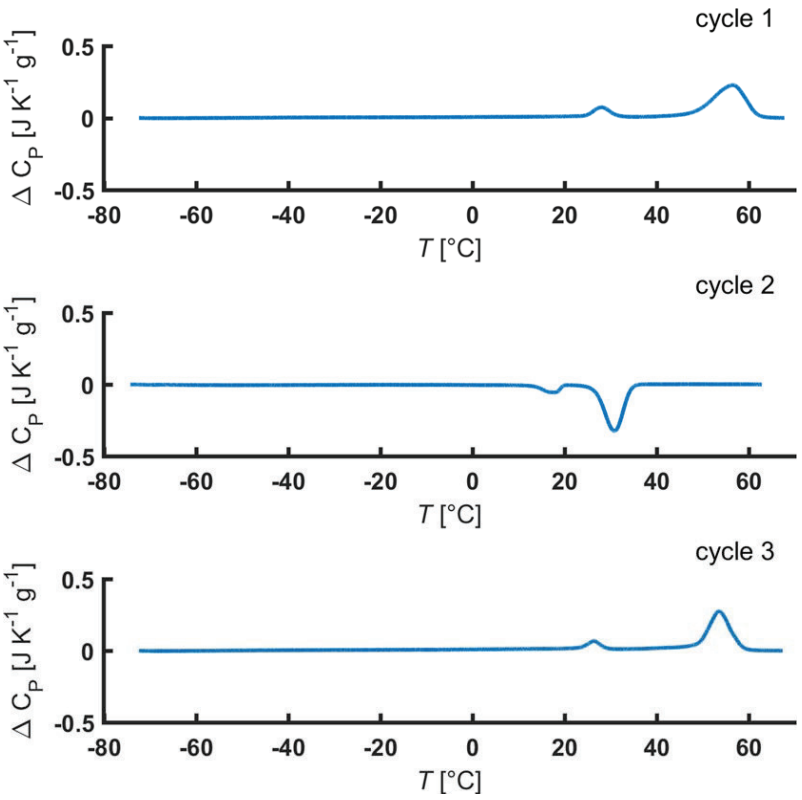

Figure S9. DSC results for heating and cooling cycles of the synthesized triblock copolymer P(C16$_{10}$-*co*-EG$_{75}$)-*b*-PEG$_{227}$-*b*-P(C16$_{10}$-*co*-EG$_{75}$); Heating rate: 20 K min^{-1}.

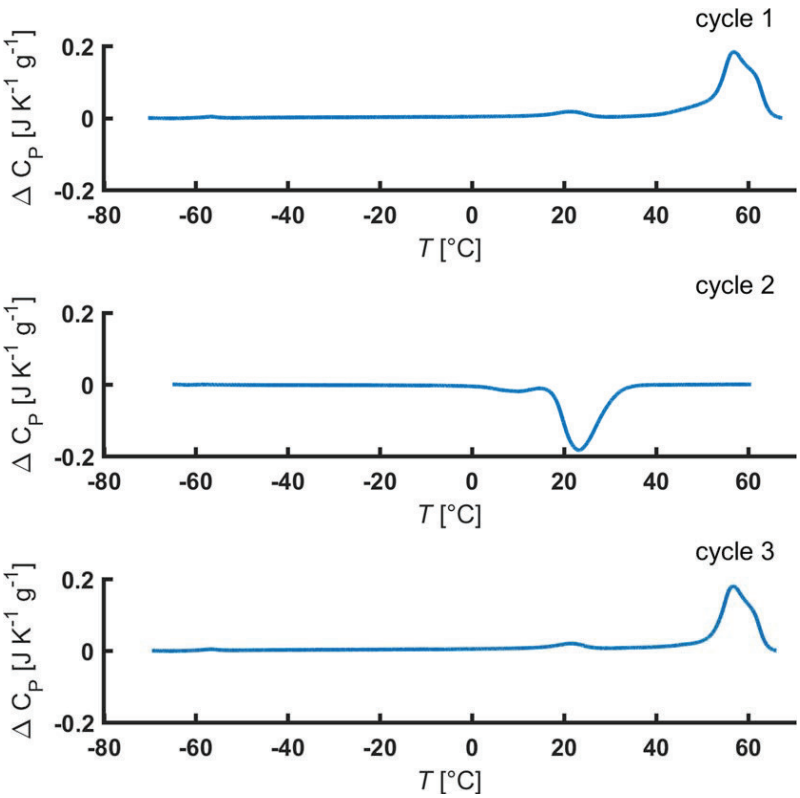

Figure S10. DSC results for heating and cooling cycles of the triblock copolymer P(C16$_{10}$-*co*-EG$_{75}$)-*b*-PEG$_{454}$-*b*-P(C16$_{10}$-*co*-EG$_{75}$); Heating rate: 20 K min^{-1}.

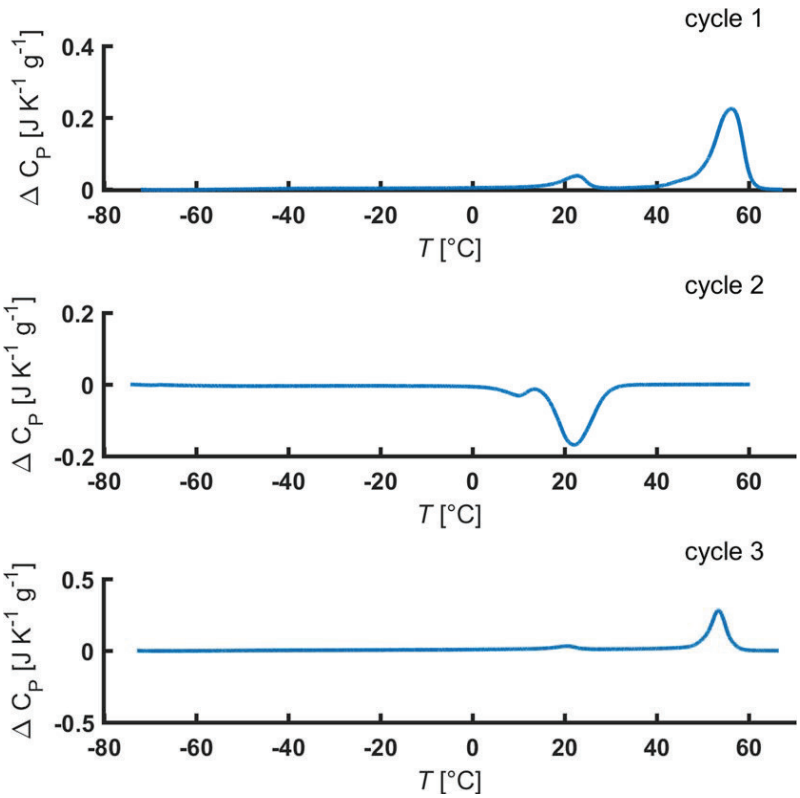

Figure S11. DSC results for heating and cooling cycles of the triblock copolymer P(C16$_7$-*co*-EG$_{75}$)-*b*-PEG$_{227}$-*b*-P(C16$_7$-*co*-EG$_{75}$); Heating rate: 20 K min^{-1}.

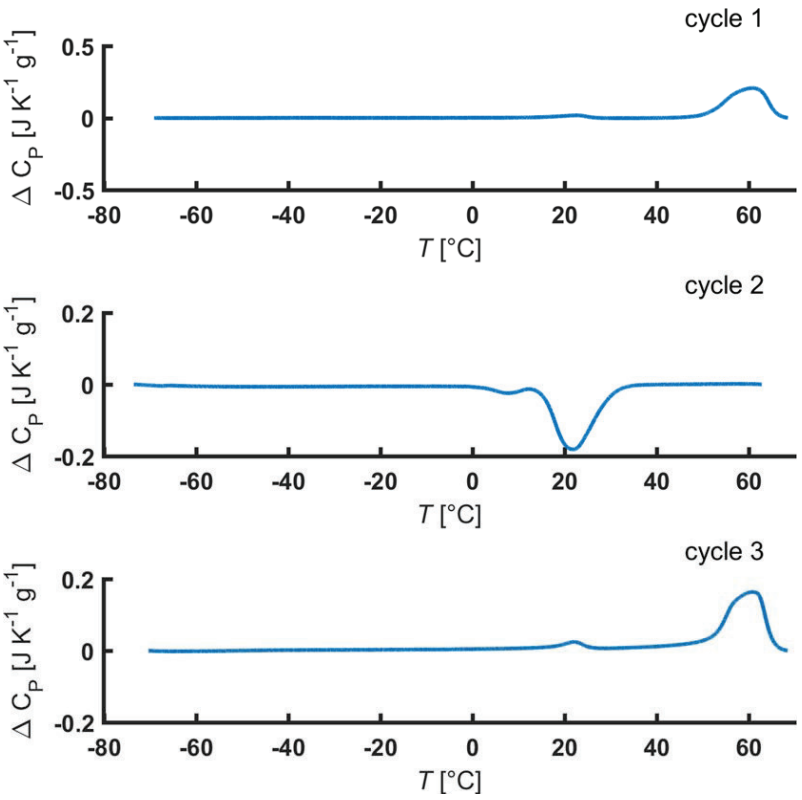

Figure S12. DSC results for heating and cooling cycles of the synthesized triblock copolymer P(C16$_7$-*co*-EG$_{75}$)-*b*-PEG$_{454}$-*b*-P(C16$_7$-*co*-EG$_{75}$); Heating rate: 20 K min^{-1}.

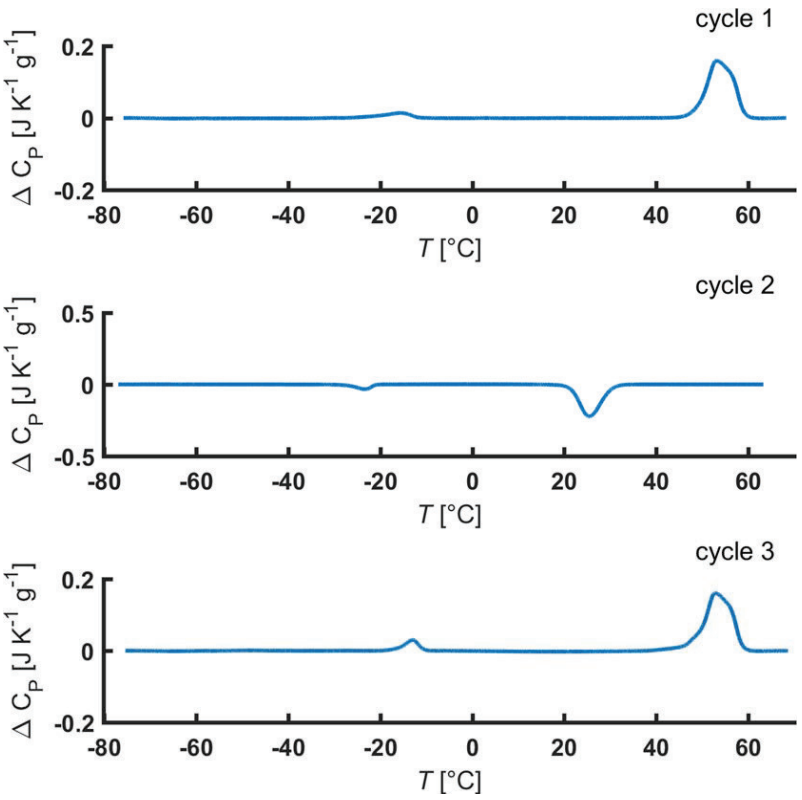

Figure S13. DSC results for heating and cooling cycles of the synthesized triblock copolymer P(C12$_{10}$-*co*-EG$_{75}$)-*b*-PEG$_{227}$-*b*-P(C12$_{10}$-*co*-EG$_{75}$); Heating rate: 10 K min^{-1}.

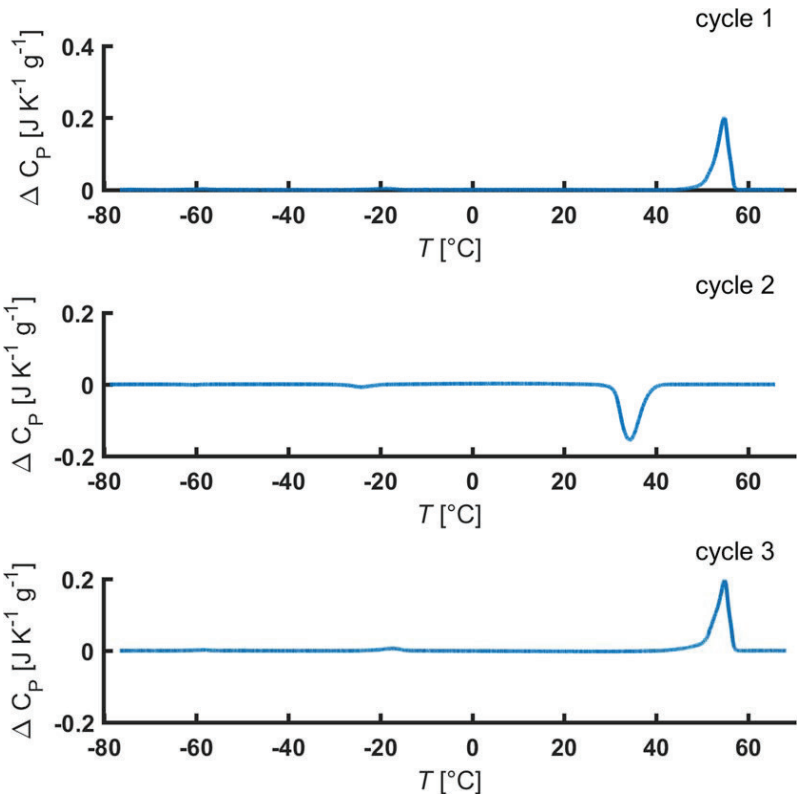

Figure S14. DSC results for heating and cooling cycles of the synthesized triblock copolymer P(C12$_{10}$-*co*-EG$_{75}$)-*b*-PEG$_{454}$-*b*-P(C12$_{10}$-*co*-EG$_{75}$); Heating rate: 10 K min^{-1}.

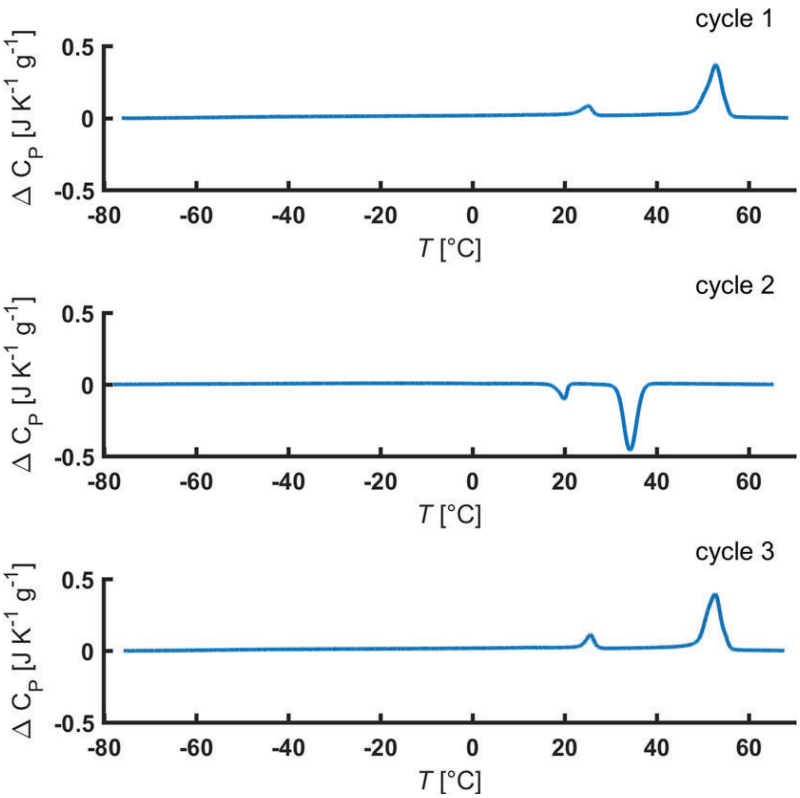

Figure S15. DSC results for heating and cooling cycles of the synthesized triblock copolymer P(C16$_{10}$-*co*-EG$_{75}$)-*b*-PEG$_{227}$-*b*-P(C16$_{10}$-*co*-EG$_{75}$); Heating rate: 10 K min^{-1}.

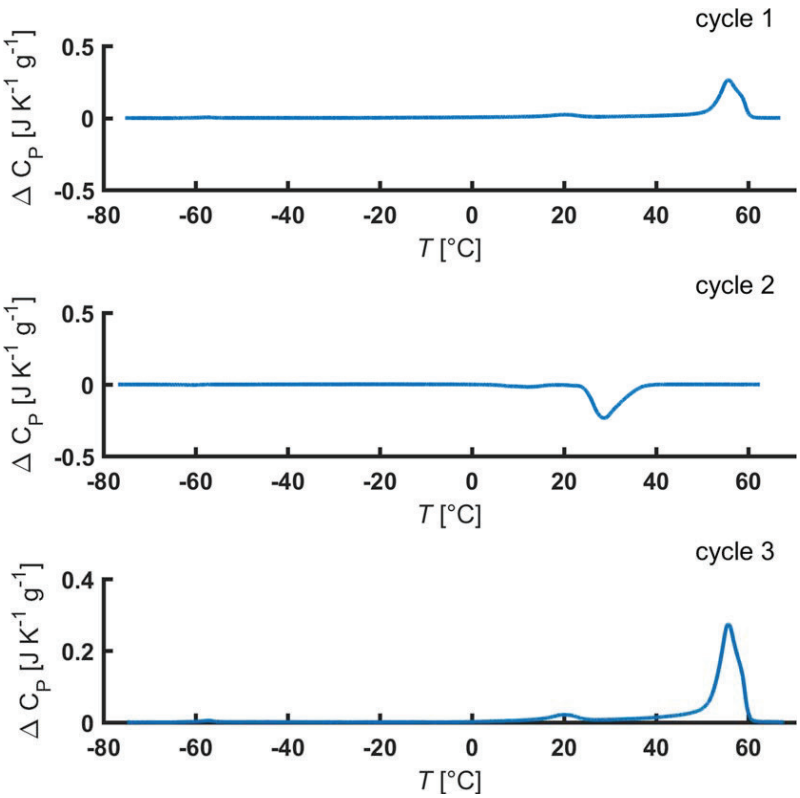

Figure S16. DSC results for heating and cooling cycles of the synthesized triblock copolymer P(C16$_{10}$-*co*-EG$_{75}$)-*b*-PEG$_{454}$-*b*-P(C16$_{10}$-*co*-EG$_{75}$); Heating rate: 10 K min^{-1}.

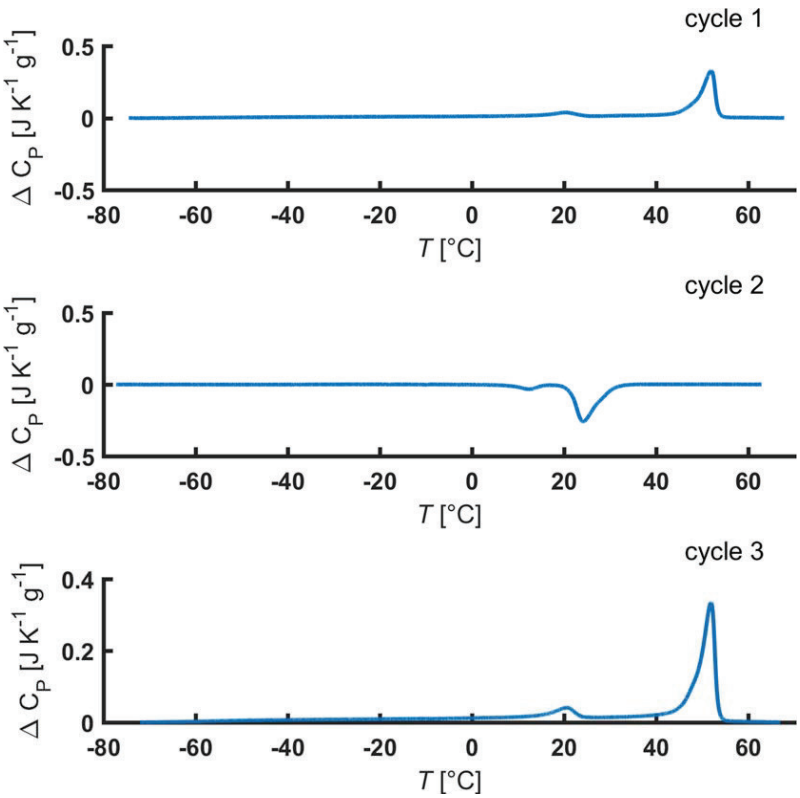

Figure S17. DSC results for heating and cooling cycles of the synthesized triblock copolymer P(C16$_7$-*co*-EG$_{75}$)-*b*-PEG$_{227}$-*b*-P(C16$_7$-*co*-EG$_{75}$); Heating rate: 10 K min^{-1}.

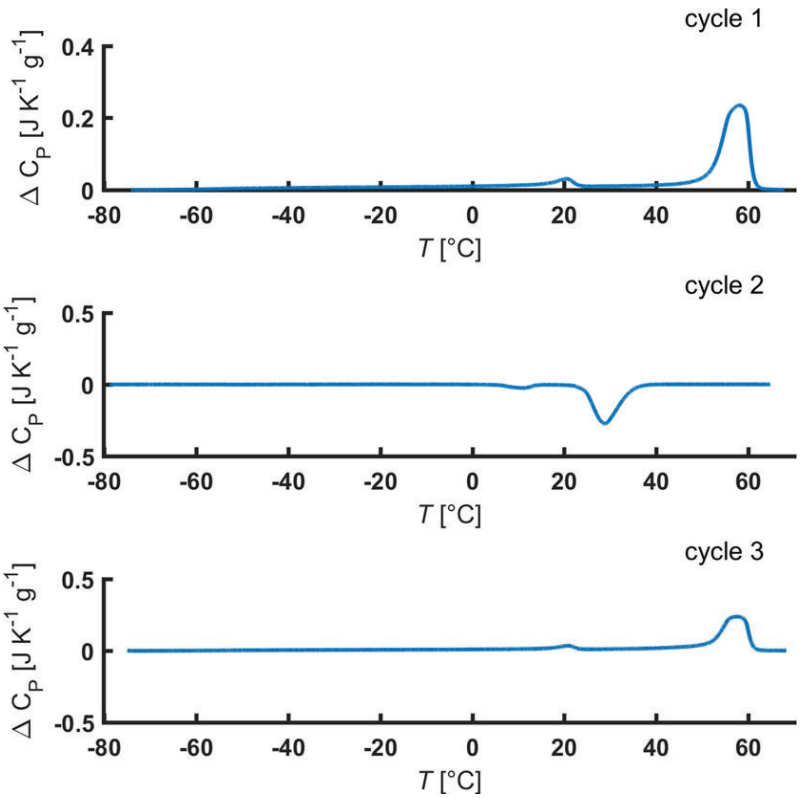

Figure S18. DSC results for heating and cooling cycles of the synthesized triblock copolymer P(C16$_7$-*co*-EG$_{75}$)-*b*-PEG$_{454}$-*b*-P(C16$_7$-*co*-EG$_{75}$); Heating rate: 10 K min^{-1}.

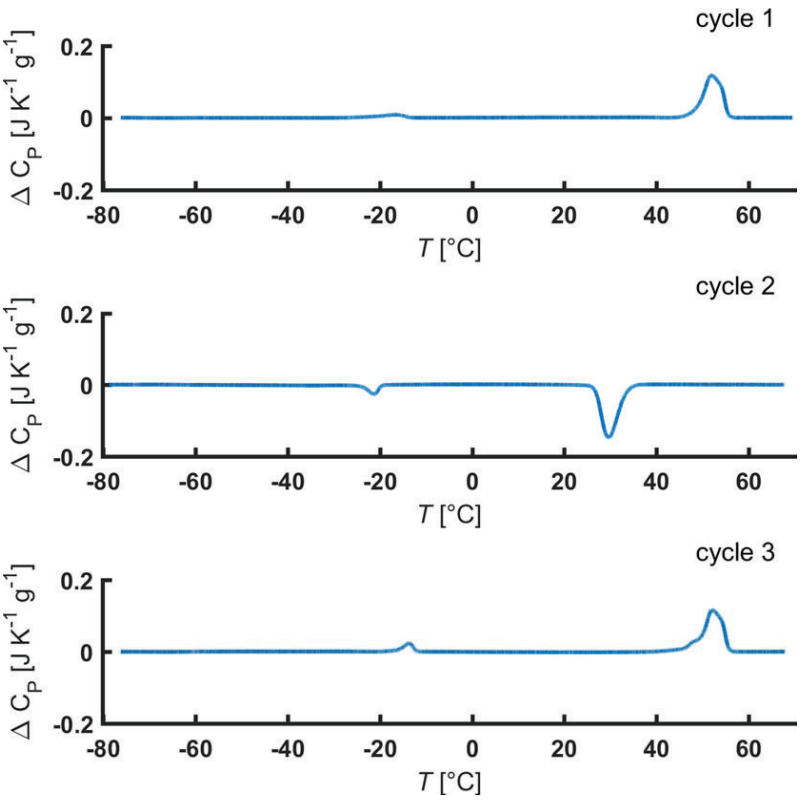

Figure S19. DSC results for heating and cooling cycles of the synthesized triblock copolymer P(C12$_{10}$-*co*-EG$_{75}$)-*b*-PEG$_{227}$-*b*-P(C12$_{10}$-*co*-EG$_{75}$); Heating rate: 5 K min^{-1}.

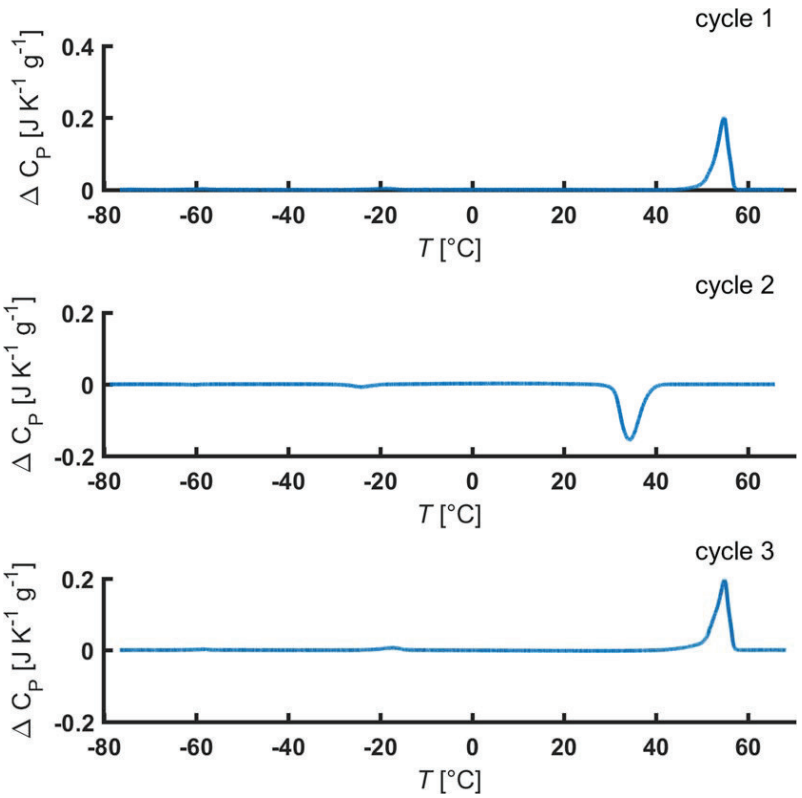

Figure S20. DSC results for heating and cooling cycles of the triblock copolymer P($C12_{10}$-*co*-EG_{75})-*b*-PEG_{454}-*b*-P($C12_{10}$-*co*-EG_{75}); Heating rate: 5 K min^{-1}.

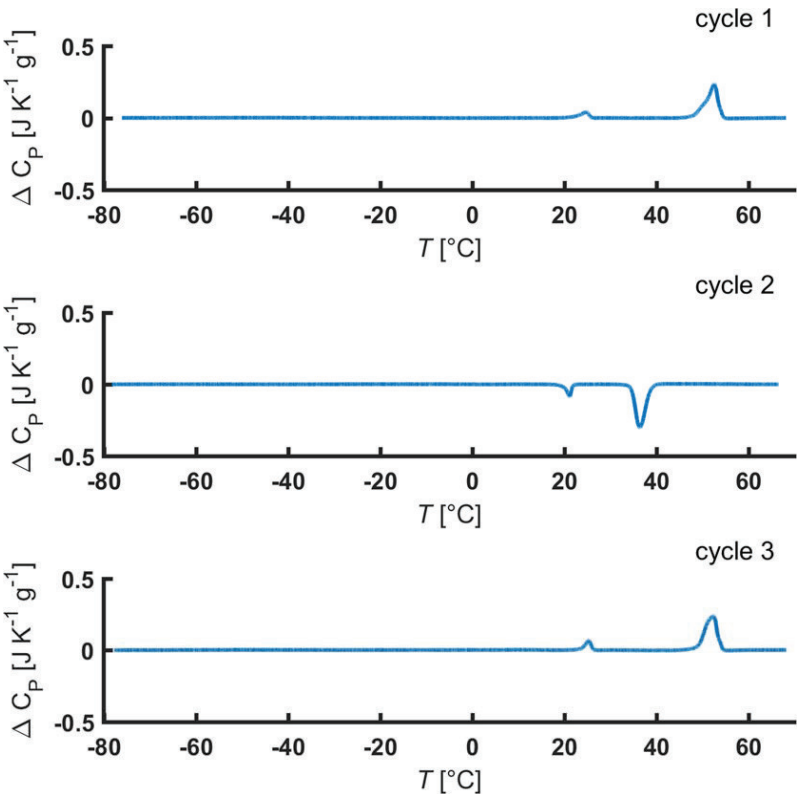

Figure S21. DSC results for heating and cooling cycles of the synthesized triblock copolymer P(C16$_{10}$-*co*-EG$_{75}$)-*b*-PEG$_{227}$-*b*-P(C16$_{10}$-*co*-EG$_{75}$); Heating rate: 5 K min^{-1}.

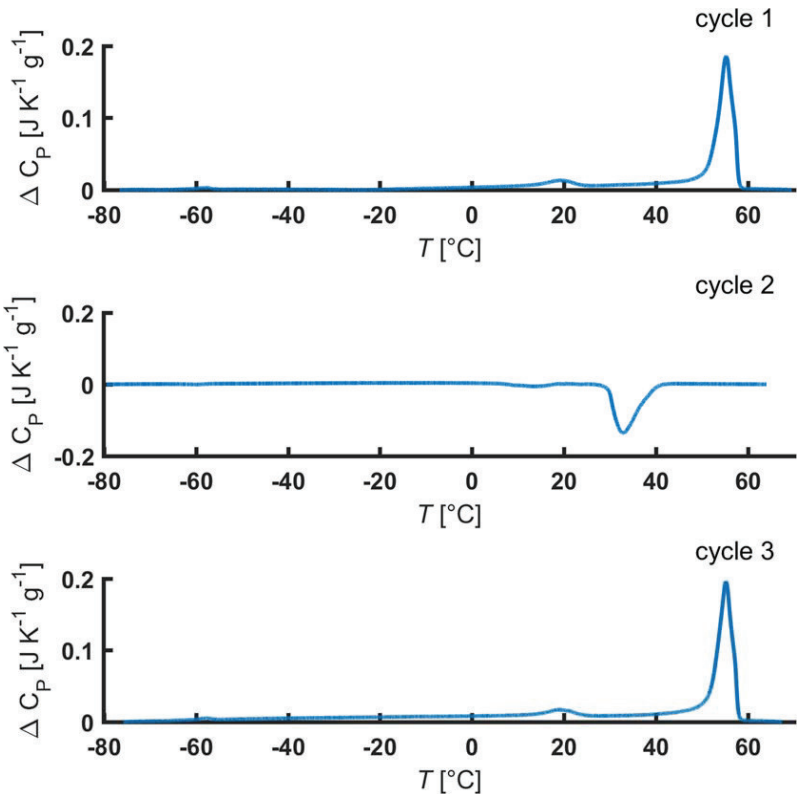

Figure S22. DSC results for heating and cooling cycles of the synthesized triblock copolymer P(C16$_{10}$-*co*-EG$_{75}$)-*b*-PEG$_{454}$-*b*-P(C16$_{10}$-*co*-EG$_{75}$); Heating rate: 5 K min^{-1}.

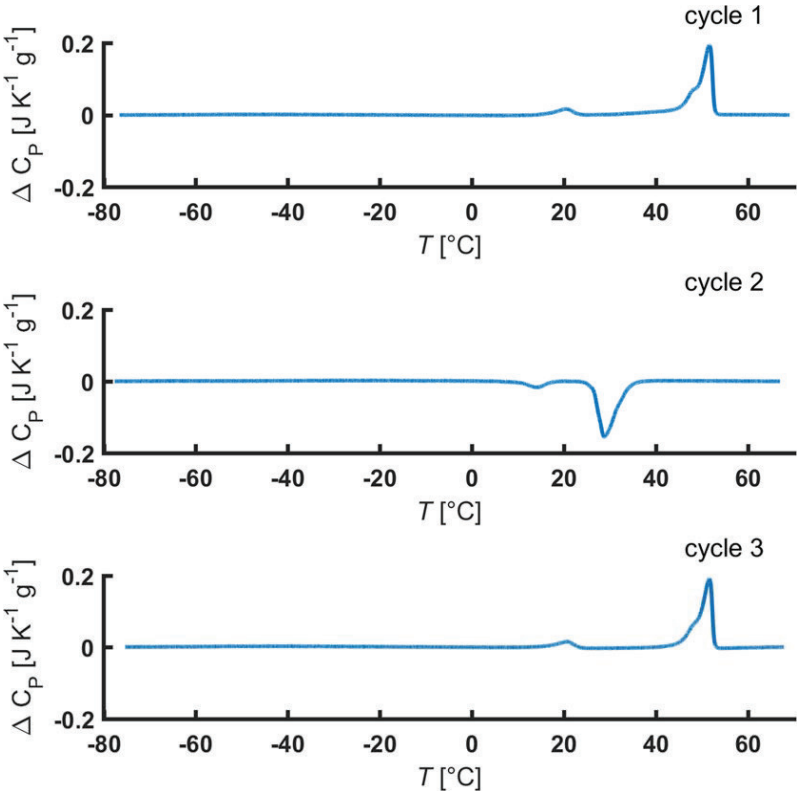

Figure S23. DSC results for heating and cooling cycles of the synthesized triblock copolymer P(C16$_7$-*co*-EG$_{75}$)-*b*-PEG$_{227}$-*b*-P(C16$_7$-*co*-EG$_{75}$); Heating rate: 5 K min^{-1}.

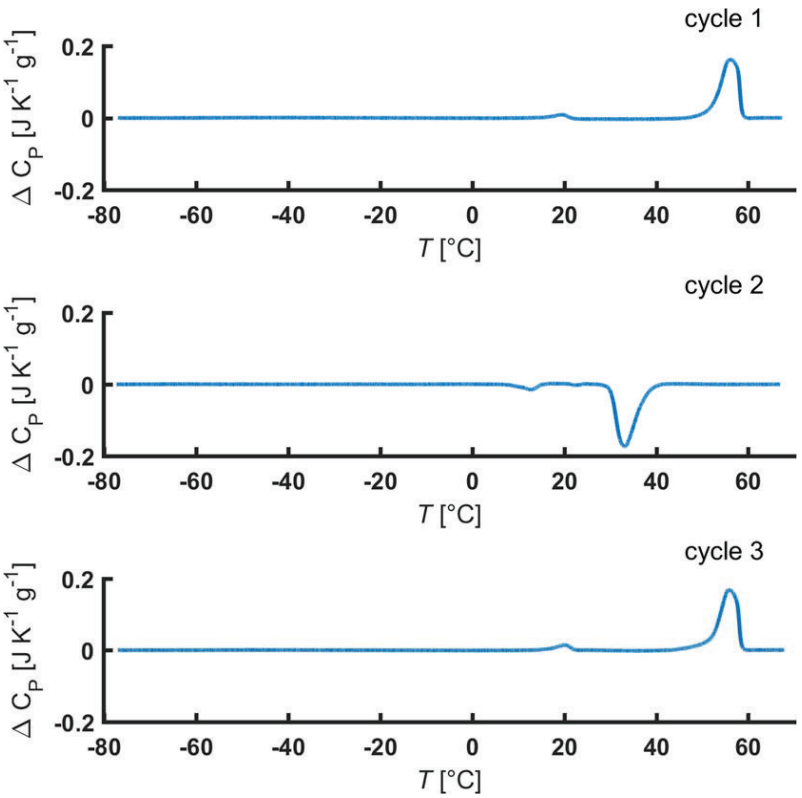

Figure S24. DSC results for heating and cooling cycles of the triblock copolymer P(C16$_7$-*co*-EG$_{75}$)-*b*-PEG$_{454}$-*b*-P(C16$_7$-*co*-EG$_{75}$); Heating rate: 5 K min^{-1}.

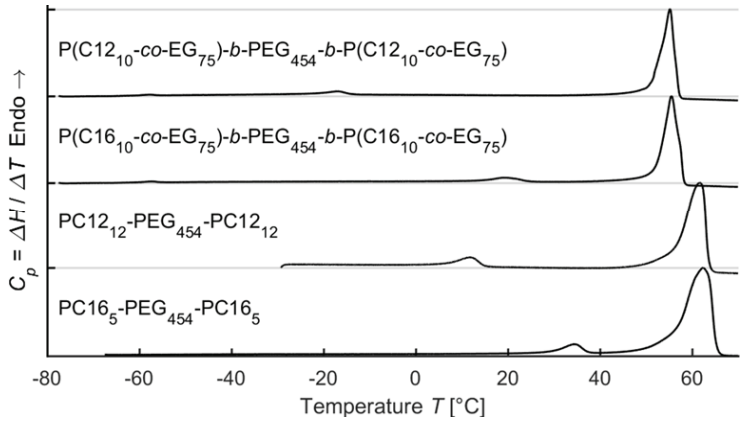

Figure S25. DSC results for heating and cooling cycles of triblock copolymers bearing P(AlkGE-*co*-EG) and P(AlkGE) blocks for better comparison concerning the shift of the melting temperatures; Heating rate: 5 K min^{-1}. The P(AlkGE) containing triblock copolymers have been previously synthesized and reported before.[1]

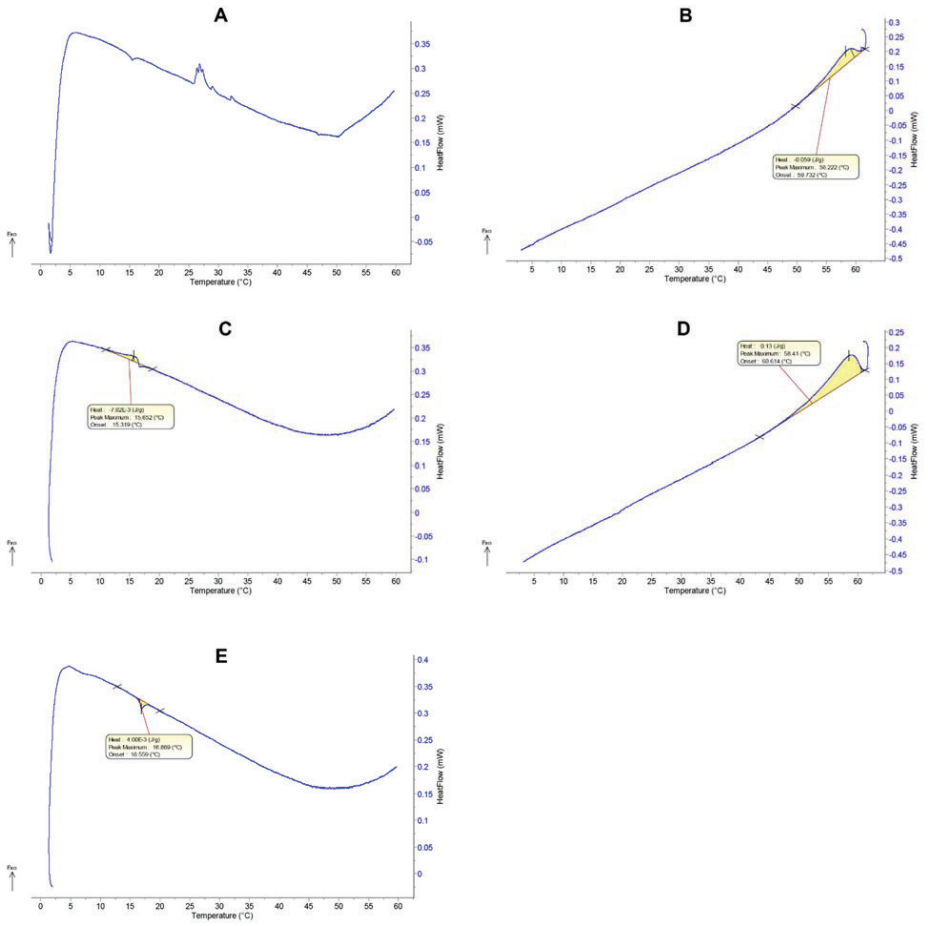

Figure S26. μ-DSC measurements of the prepared hydrogel containing P($C12_{10}$-*co*-EG_{75})-*b*-PEG_{227}-*b*-P($C12_{10}$-*co*-EG_{75}) (10 wt%; rate: 0.5 K min^{-1}). **A:** Heating cycle 1, **B:** cooling cycle 1, **C:** heating cycle 2, **D:** cooling cycle 2, **E:** heating cycle 3.

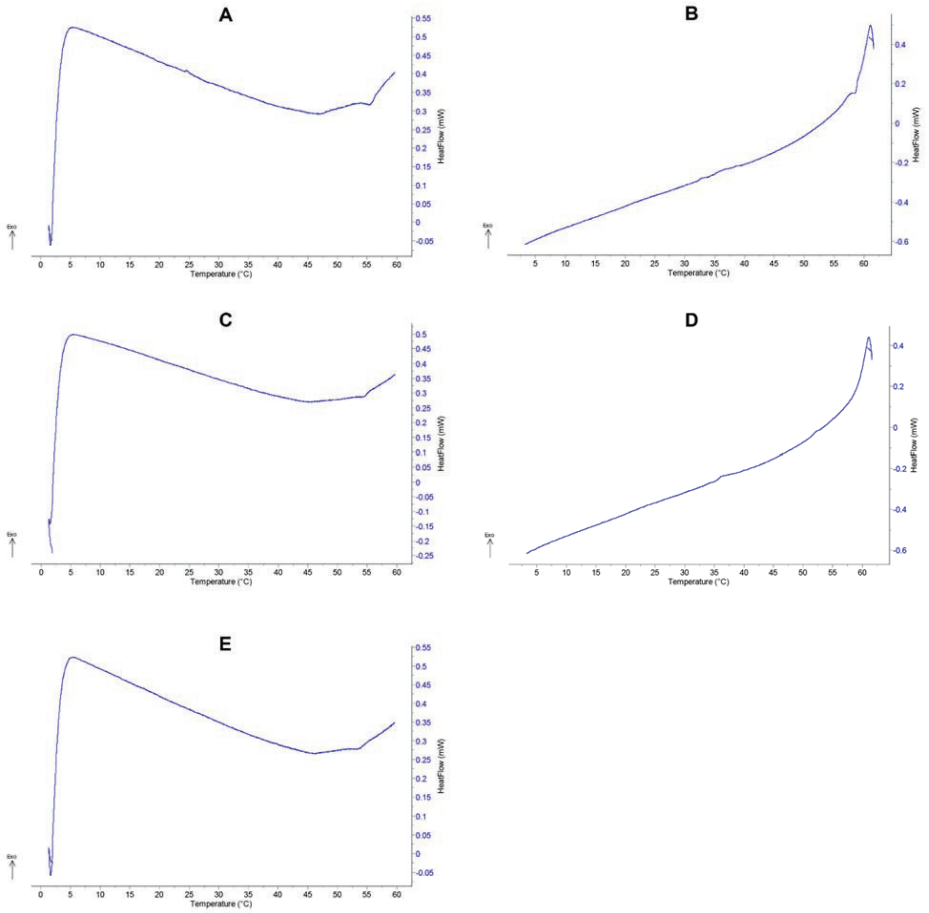

Figure S27. µ-DSC measurements of the prepared hydrogel containing P($C12_{10}$-*co*-EG_{75})-*b*-PEG_{454}-*b*-P($C12_{10}$-*co*-EG_{75}) (10 wt%; rate: 0.5 K min^{-1}). **A:** Heating cycle 1, **B:** cooling cycle 1, **C:** heating cycle 2, **D:** cooling cycle 2, **E:** heating cycle 3.

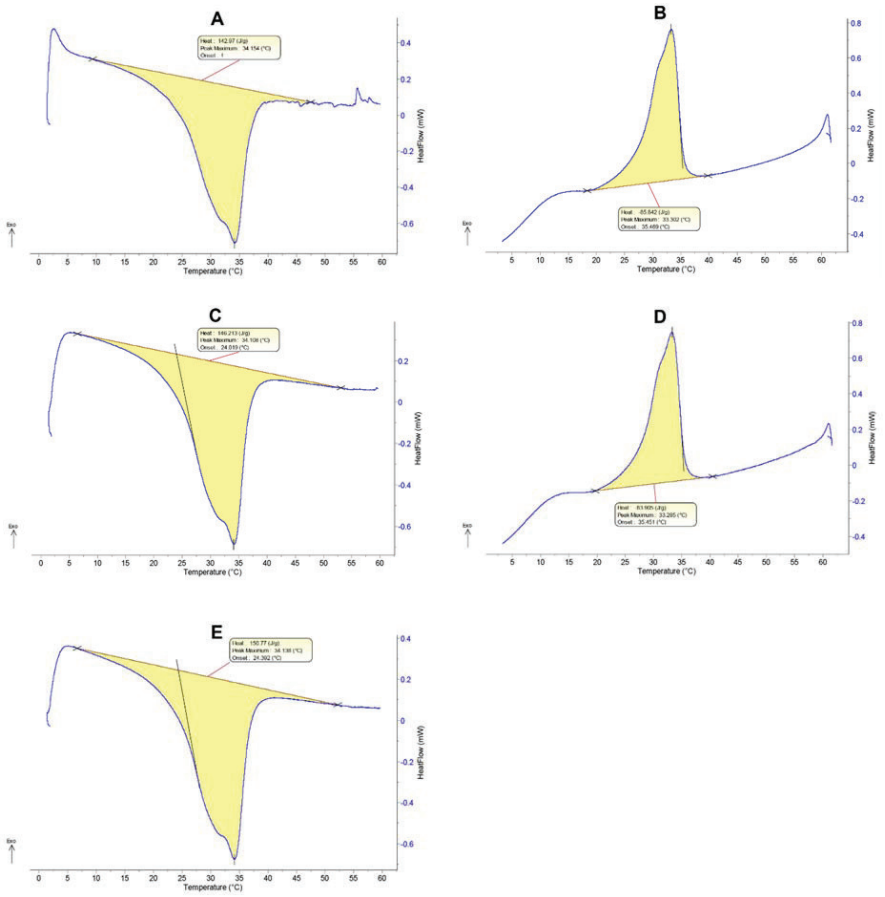

Figure S28. µ-DSC measurements of the prepared hydrogel containing P(C16$_{10}$-*co*-EG$_{75}$)-*b*-PEG$_{227}$-*b*-P(C16$_{10}$-*co*-EG$_{75}$) (10 wt%; rate: 0.5 K min^{-1}). **A:** Heating cycle 1, **B:** cooling cycle 1, **C:** heating cycle 2, **D:** cooling cycle 2, **E:** heating cycle 3.

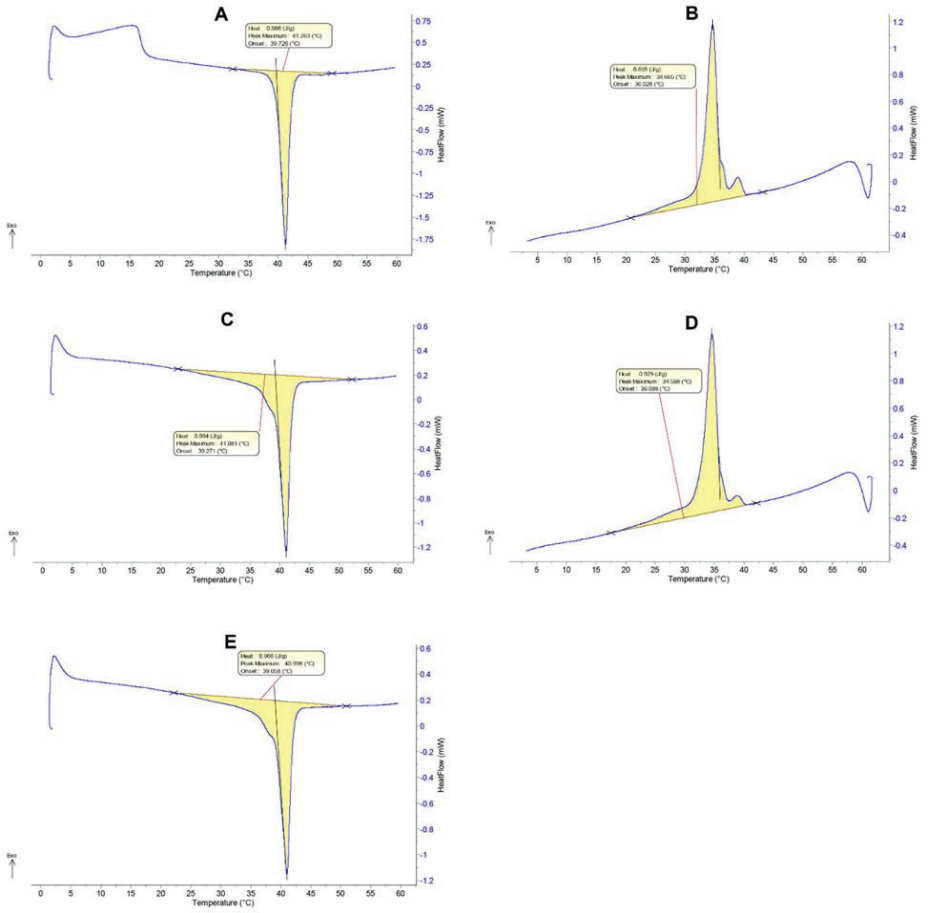

Figure S29. µ-DSC measurements of the prepared hydrogel containing P($C16_{10}$-*co*-EG_{75})-*b*-PEG_{454}-*b*-P($C16_{10}$-*co*-EG_{75}) (10 wt%; rate: 0.5 K min^{-1}). **A:** Heating cycle 1, **B:** cooling cycle 1, **C:** heating cycle 2, **D:** cooling cycle 2, **E:** heating cycle 3.

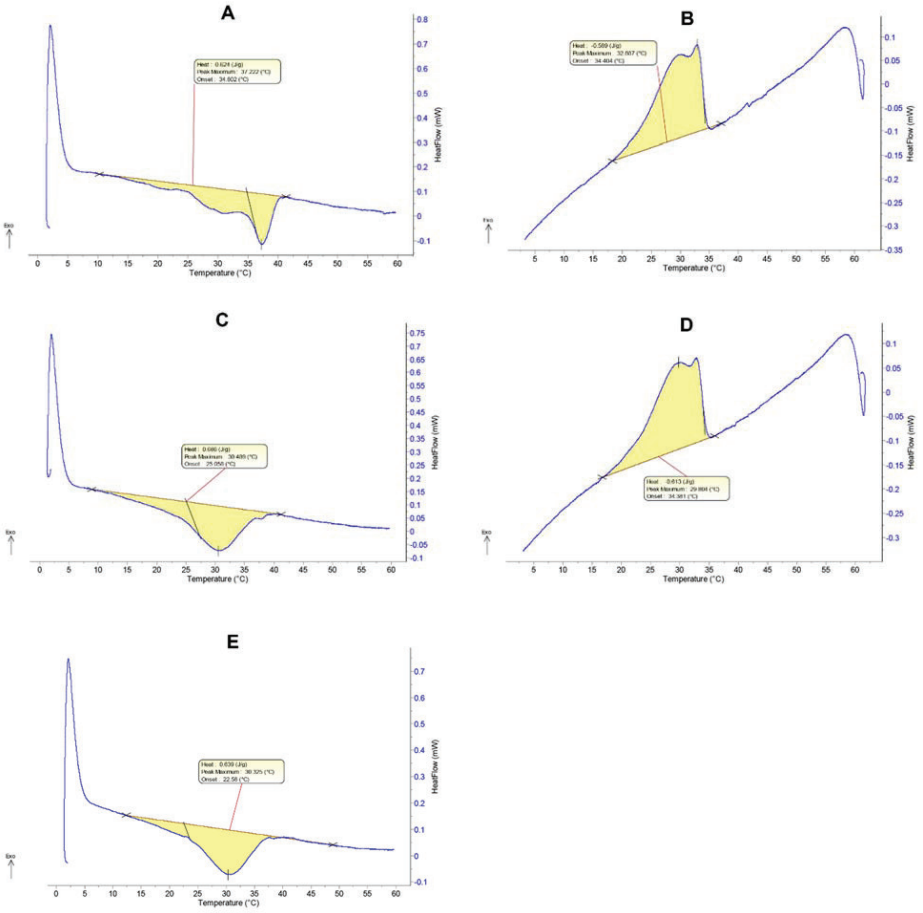

Figure S30. μ-DSC measurements of the prepared hydrogel containing P(C16$_7$-*co*-EG$_{75}$)-*b*-PEG$_{227}$-*b*-P(C16$_7$-*co*-EG$_{75}$) (10 wt%; rate: 0.5 K min^{-1}). **A:** Heating cycle 1, **B:** cooling cycle 1, **C:** heating cycle 2, **D:** cooling cycle 2, **E:** heating cycle 3.

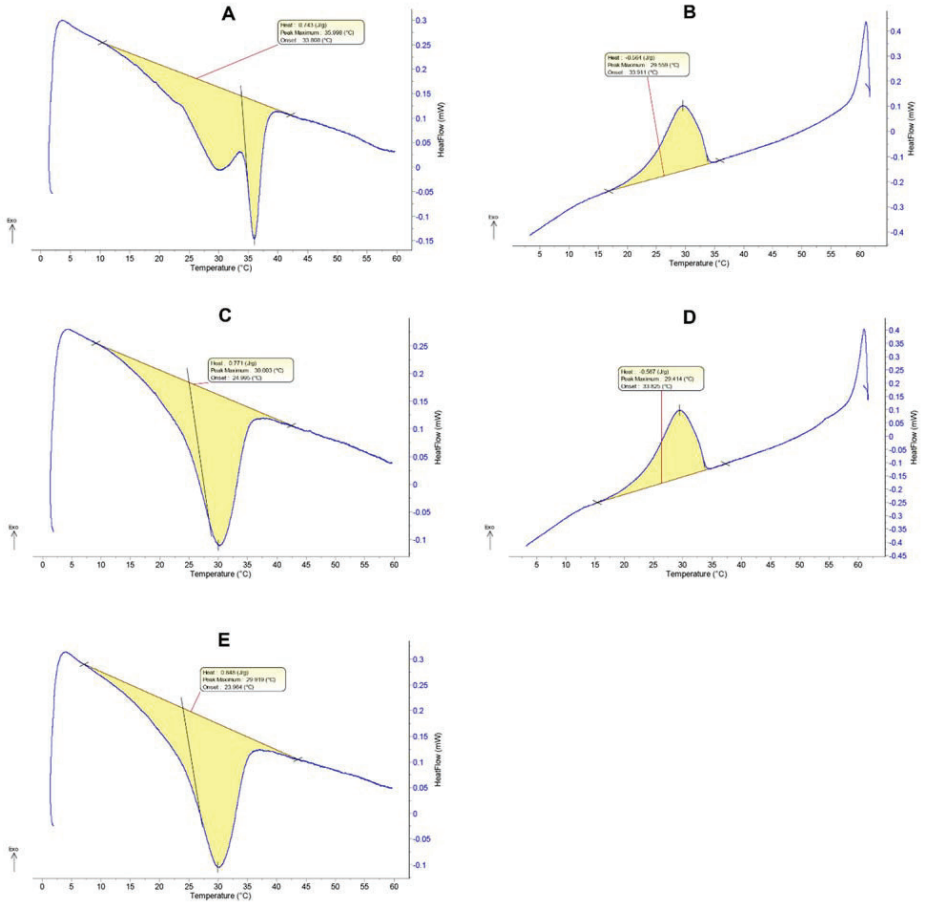

Figure S31. μ-DSC measurements of the prepared hydrogel containing P(C16$_7$-*co*-EG$_{75}$)-*b*-PEG$_{454}$-*b*-P(C16$_7$-*co*-EG$_{75}$) (10 wt%; rate: 0.5 K min^{-1}). **A:** Heating cycle 1, **B:** cooling cycle 1, **C:** heating cycle 2, **D:** cooling cycle 2, **E:** heating cycle 3.

Table S8. Thermal properties of the prepared gels of the triblock copolymers measured by μ-DSC measurements.

Structure	T_m / °C [a]	ΔH_m / J/g [a]	T_C / °C [a]	ΔH_c / J/g [a]
P(C12$_{10}$-*co*-EG$_{75}$)-*b*-PEG$_{227}$-*b*-P(C12$_{10}$-*co*-EG$_{75}$)	16.559	0.004	58.410	-0.130
P(C16$_{10}$-*co*-EG$_{75}$)-*b*-PEG$_{227}$-*b*-P(C16$_{10}$-*co*-EG$_{75}$)	34.138	2.019	35.451	-1.123
P(C12$_{10}$-*co*-EG$_{75}$)-*b*-PEG$_{454}$-*b*-P(C12$_{10}$-*co*-EG$_{75}$)	-	-	-	-
P(C16$_{10}$-*co*-EG$_{75}$)-*b*-PEG$_{454}$-*b*-P(C16$_{10}$-*co*-EG$_{75}$)	39.058	0.966	34.598	-0.929
P(C16$_7$-*co*-EG$_{75}$)-*b*-PEG$_{227}$-*b*-P(C16$_7$-*co*-EG$_{75}$)	30.325	0.639	29.804	-0.613
P(C16$_7$-*co*-EG$_{75}$)-*b*-PEG$_{454}$-*b*-P(C16$_7$-*co*-EG$_{75}$)	29.919	0.848	33.825	-0.567

[a] Melting (T_m) and crystallization temperatures (T_C) listed have been measured in heating cycle 3 and cooling cycle 2, respectively.

Table S9. Sample weights of the hydrogels used for μ-DSC measurements.

Structure	Sample weight$_{hydrogel}$	Sample weight$_{water}$
P(C12$_{10}$-*co*-EG$_{75}$)-*b*-PEG$_{227}$-*b*-P(C12$_{10}$-*co*-EG$_{75}$)	426.9	426.5
P(C16$_{10}$-*co*-EG$_{75}$)-*b*-PEG$_{227}$-*b*-P(C16$_{10}$-*co*-EG$_{75}$)	289.3	291.1
P(C12$_{10}$-*co*-EG$_{75}$)-*b*-PEG$_{454}$-*b*-P(C12$_{10}$-*co*-EG$_{75}$)	522.8	523.3
P(C16$_{10}$-*co*-EG$_{75}$)-*b*-PEG$_{454}$-*b*-P(C16$_{10}$-*co*-EG$_{75}$)	496.2	495.7
P(C16$_{7}$-*co*-EG$_{75}$)-*b*-PEG$_{227}$-*b*-P(C16$_{7}$-*co*-EG$_{75}$)	323.1	324.6
P(C16$_{7}$-*co*-EG$_{75}$)-*b*-PEG$_{454}$-*b*-P(C16$_{7}$-*co*-EG$_{75}$)	395.9	396.4

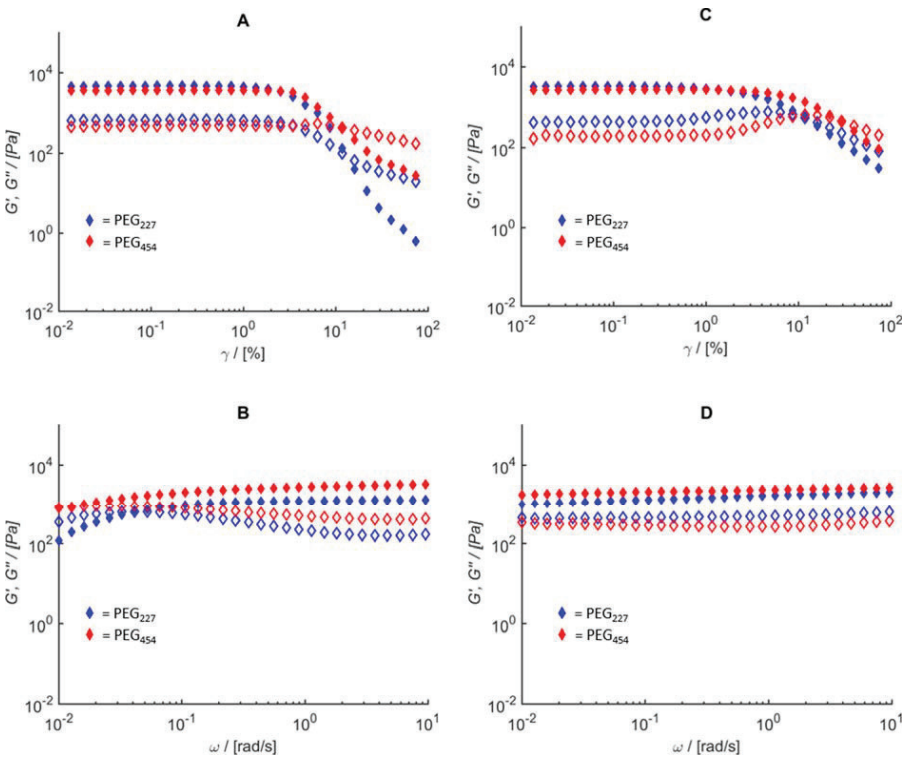

Figure S32. Comparison of the amplitude and frequency sweep measurements of the C12-AlkGE, C16-AlkGE containing triblock polyethers in gel state (deionized water with **1 wt% UHMW PEO**). A: Amplitude sweep measurements of the P(C12-AlkGE$_{10}$-*co*-EG$_{75}$)-*b*-PEG$_y$-*b*-P(C12-AlkGE$_{10}$-*co*-EG$_{75}$) containing gels. B: Frequency sweep measurements of the P(C12-AlkGE$_{10}$-*co*-EG$_{75}$)-*b*-PEG$_y$-*b*-P(C12-AlkGE$_{10}$-*co*-EG$_{75}$) containing gels. C: Amplitude sweep measurements of the P(C16-AlkGE$_{10}$-*co*-EG$_{75}$)-*b*-PEG$_y$-*b*-P(C16-AlkGE$_{10}$-*co*-EG$_{75}$) containing gels. D: Frequency sweep measurements of the P(C16-AlkGE$_{10}$-*co*-EG$_{75}$)-*b*-PEG$_y$-*b*-P(C16-AlkGE$_{10}$-*co*-EG$_{75}$) containing gels. Filled and open symbols indicate the storage and loss modulus, respectively.

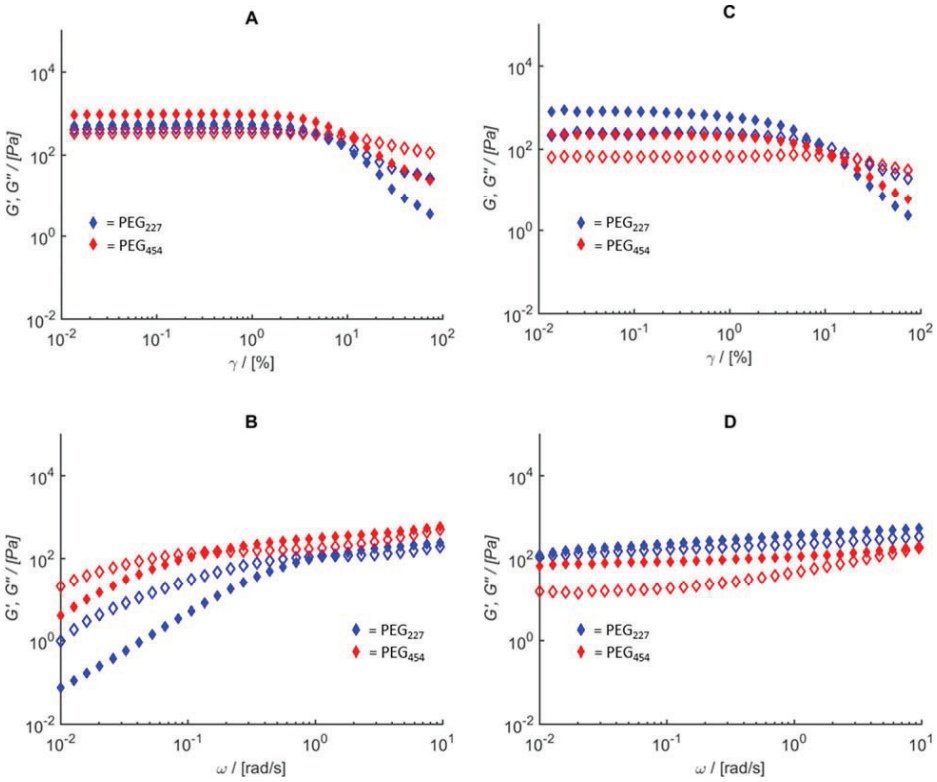

Figure S33. Comparison of the amplitude and frequency sweep measurements of the C12-AlkGE, C16-AlkGE containing triblock polyethers in gel state (deionized water with **5 wt% UHMW PEO**). A: Amplitude sweep measurements of the P(C12-AlkGE$_{10}$-*co*-EG$_{75}$)-*b*-PEG$_y$-*b*-P(C12-AlkGE$_{10}$-*co*-EG$_{75}$) containing gels. B: Frequency sweep measurements of the P(C12-AlkGE$_{10}$-*co*-EG$_{75}$)-*b*-PEG$_y$-*b*-P(C12-AlkGE$_{10}$-*co*-EG$_{75}$) containing gels. C: Amplitude sweep measurements of the P(C16-AlkGE$_{10}$-*co*-EG$_{75}$)-*b*-PEG$_y$-*b*-P(C16-AlkGE$_{10}$-*co*-EG$_{75}$) containing gels. D: Frequency sweep measurements of the P(C16-AlkGE$_{10}$-*co*-EG$_{75}$)-*b*-PEG$_y$-*b*-P(C16-AlkGE$_{10}$-*co*-EG$_{75}$) containing gels. Filled and open symbols indicate the storage and loss modulus, respectively.

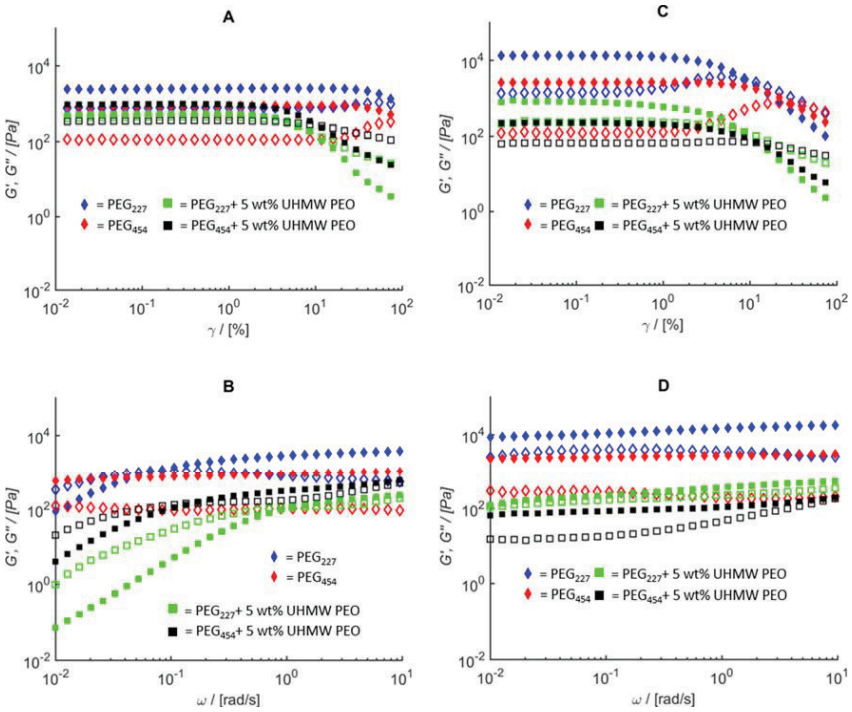

Figure S34. Comparison of the amplitude and frequency sweep measurements of the C12-AlkGE, C16-AlkGE containing triblock polyethers in gel state before and after PEO doping (deionized water **pure gels** vs. **5 wt% UHMW PEO**). A: Amplitude sweep measurements of the P(C12-AlkGE$_{10}$-*co*-EG$_{75}$)-*b*-PEG$_y$-*b*-P(C12-AlkGE$_{10}$-*co*-EG$_{75}$) containing gels. B: Frequency sweep measurements of the P(C12-AlkGE$_{10}$-*co*-EG$_{75}$)-*b*-PEG$_y$-*b*-P(C12-AlkGE$_{10}$-*co*-EG$_{75}$) containing gels. C: Amplitude sweep measurements of the P(C16-AlkGE$_{10}$-*co*-EG$_{75}$)-*b*-PEG$_y$-*b*-P(C16-AlkGE$_{10}$-*co*-EG$_{75}$) containing gels. D: Frequency sweep measurements of the P(C16-AlkGE$_{10}$-*co*-EG$_{75}$)-*b*-PEG$_y$-*b*-P(C16-AlkGE$_{10}$-*co*-EG$_{75}$) containing gels. Filled and open symbols indicate the storage and loss modulus, respectively.

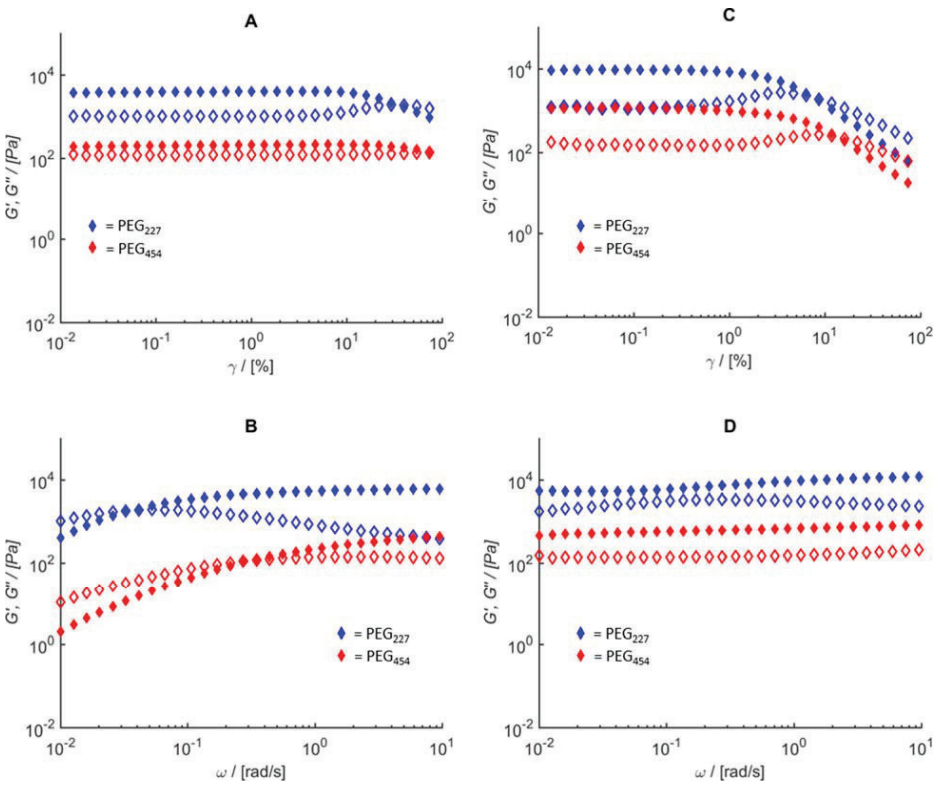

Figure S35. Comparison of the amplitude and frequency sweep measurements of the C12-AlkGE, C16-AlkGE containing triblock polyethers in gel state (**pH = 4**). A: Amplitude sweep measurements of the P(C12-AlkGE$_{10}$-*co*-EG$_{75}$)-*b*-PEG$_y$-*b*-P(C12-AlkGE$_{10}$-*co*-EG$_{75}$) containing gels. B: Frequency sweep measurements of the P(C12-AlkGE$_{10}$-*co*-EG$_{75}$)-*b*-PEG$_y$-*b*-P(C12-AlkGE$_{10}$-*co*-EG$_{75}$) containing gels. C: Amplitude sweep measurements of the P(C16-AlkGE$_{10}$-*co*-EG$_{75}$)-*b*-PEG$_y$-*b*-P(C16-AlkGE$_{10}$-*co*-EG$_{75}$) containing gels. D: Frequency sweep measurements of the P(C16-AlkGE$_{10}$-*co*-EG$_{75}$)-*b*-PEG$_y$-*b*-P(C16-AlkGE$_{10}$-*co*-EG$_{75}$) containing gels. Filled and open symbols indicate the storage and loss modulus, respectively.

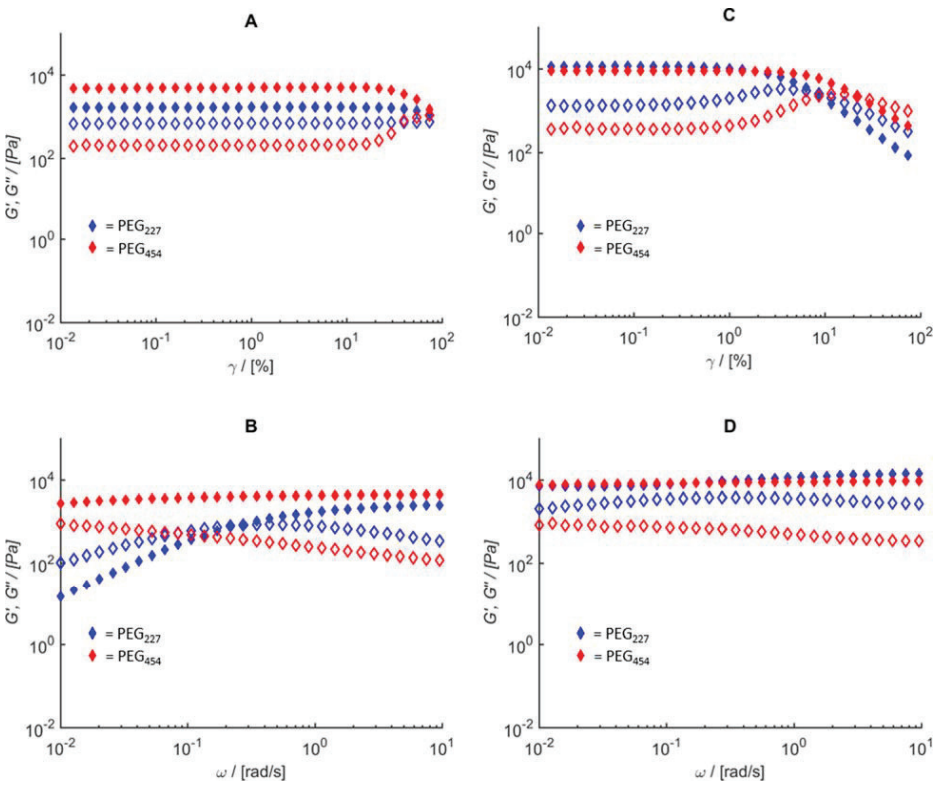

Figure S36. Comparison of the amplitude and frequency sweep measurements of the C12-AlkGE, C16-AlkGE containing triblock polyethers in gel state (**pH = 9**). A: Amplitude sweep measurements of the P(C12-AlkGE$_{10}$-*co*-EG$_{75}$)-*b*-PEG$_y$-*b*-P(C12-AlkGE$_{10}$-*co*-EG$_{75}$) containing gels. B: Frequency sweep measurements of the P(C12-AlkGE$_{10}$-*co*-EG$_{75}$)-*b*-PEG$_y$-*b*-P(C12-AlkGE$_{10}$-*co*-EG$_{75}$) containing gels. C: Amplitude sweep measurements of the P(C16-AlkGE$_{10}$-*co*-EG$_{75}$)-*b*-PEG$_y$-*b*-P(C16-AlkGE$_{10}$-*co*-EG$_{75}$) containing gels. D: Frequency sweep measurements of the P(C16-AlkGE$_{10}$-*co*-EG$_{75}$)-*b*-PEG$_y$-*b*-P(C16-AlkGE$_{10}$-*co*-EG$_{75}$) containing gels. Filled and open symbols indicate the storage and loss modulus, respectively.

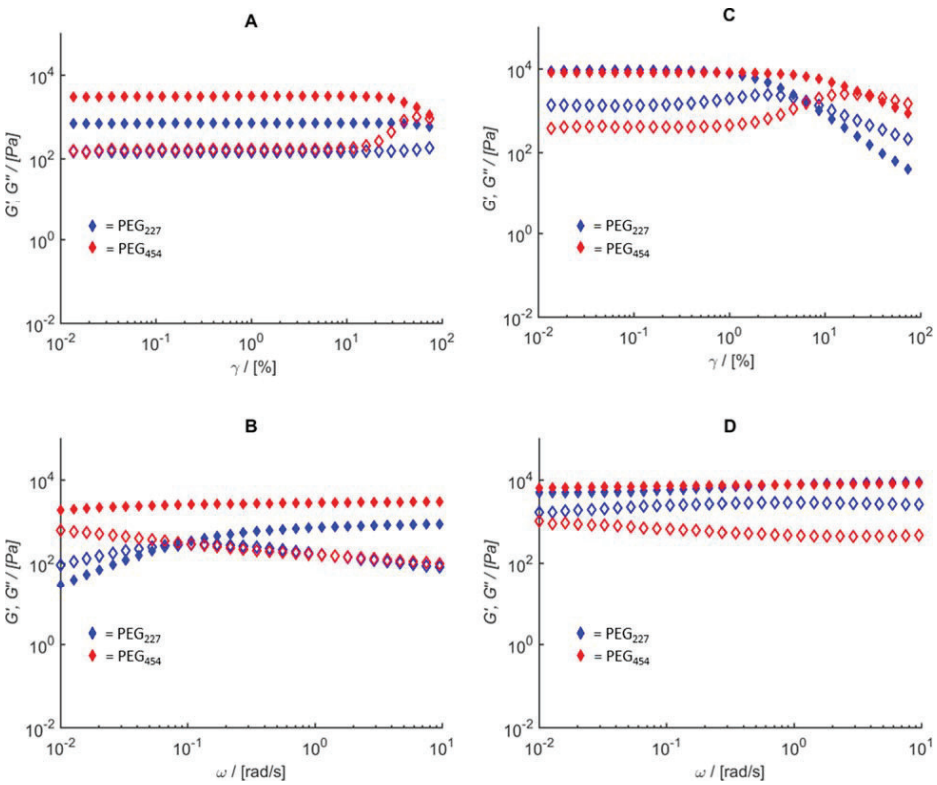

Figure S37. Comparison of the amplitude and frequency sweep measurements of the C12-AlkGE, C16-AlkGE containing triblock polyethers in gel state (**NaCl solution in deionized water; c = 0.5 mol L^{-1}**). A: Amplitude sweep measurements of the P(C12-AlkGE$_{10}$-*co*-EG$_{75}$)-*b*-PEG$_y$-*b*-P(C12-AlkGE$_{10}$-*co*-EG$_{75}$) containing gels. B: Frequency sweep measurements of the P(C12-AlkGE$_{10}$-*co*-EG$_{75}$)-*b*-PEG$_y$-*b*-P(C12-AlkGE$_{10}$-*co*-EG$_{75}$) containing gels. C: Amplitude sweep measurements of the P(C16-AlkGE$_{10}$-*co*-EG$_{75}$)-*b*-PEG$_y$-*b*-P(C16-AlkGE$_{10}$-*co*-EG$_{75}$) containing gels. D: Frequency sweep measurements of the P(C16-AlkGE$_{10}$-*co*-EG$_{75}$)-*b*-PEG$_y$-*b*-P(C16-AlkGE$_{10}$-*co*-EG$_{75}$) containing gels. Filled and open symbols indicate the storage and loss modulus, respectively.

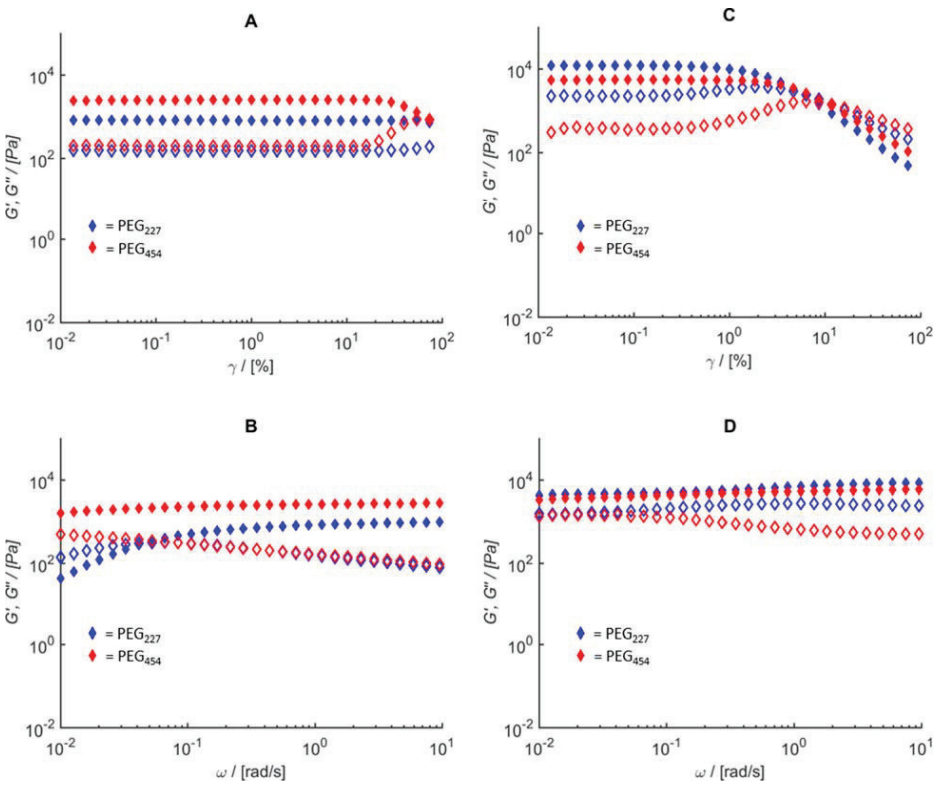

Figure S38. Comparison of the amplitude and frequency sweep measurements of the C12-AlkGE, C16-AlkGE containing triblock polyethers in gel state (**NaCl solution with deionized water; c = 1 mol L^{-1}**). A: Amplitude sweep measurements of the P(C12-AlkGE$_{10}$-*co*-EG$_{75}$)-*b*-PEG$_y$-*b*-P(C12-AlkGE$_{10}$-*co*-EG$_{75}$) containing gels. B: Frequency sweep measurements of the P(C12-AlkGE$_{10}$-*co*-EG$_{75}$)-*b*-PEG$_y$-*b*-P(C12-AlkGE$_{10}$-*co*-EG$_{75}$) containing gels. C: Amplitude sweep measurements of the P(C16-AlkGE$_{10}$-*co*-EG$_{75}$)-*b*-PEG$_y$-*b*-P(C16-AlkGE$_{10}$-*co*-EG$_{75}$) containing gels. D: Frequency sweep measurements of the P(C16-AlkGE$_{10}$-*co*-EG$_{75}$)-*b*-PEG$_y$-*b*-P(C16-AlkGE$_{10}$-*co*-EG$_{75}$) containing gels. Filled and open symbols indicate the storage and loss modulus, respectively.

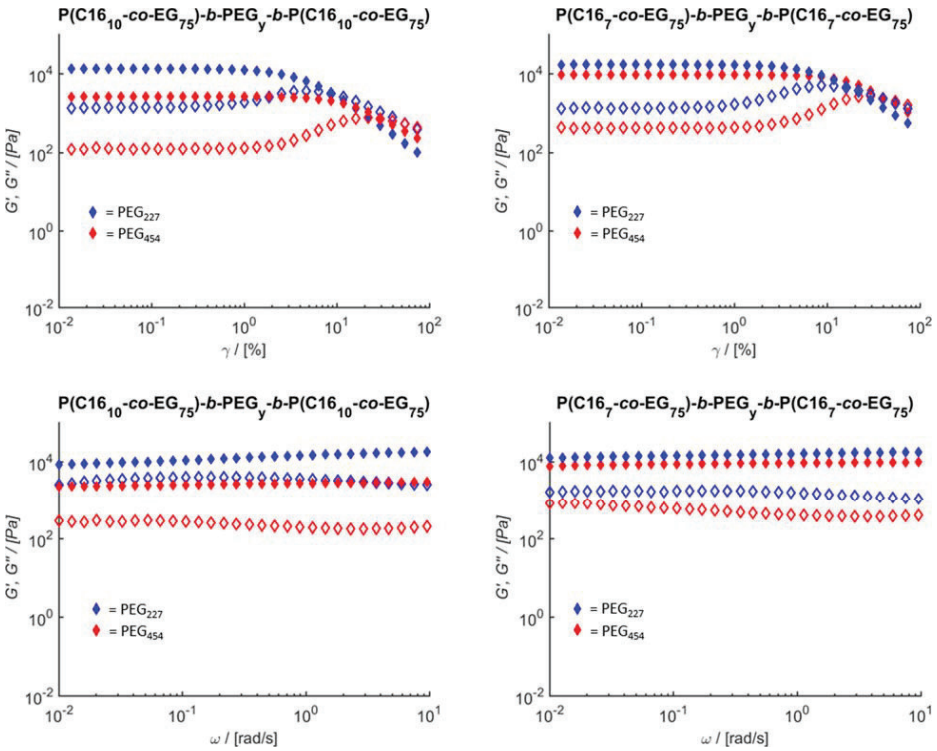

Figure S39. Comparison of the amplitude and frequency sweep measurements of the C16-AlkGE containing triblock polyethers in gel state with varied C16-AlkGE content (**deionized water, pH = 7**). Filled and open symbols indicate the storage and loss modulus, respectively.

Table S10. Comparison of the results of the amplitude sweep measurements concerning the values of G', G'' and the maximum shear rate at the end of the linear viscoelastic region.

	C12-EG-PEG$_{227}$-C12-EG	C12-EG-PEG$_{454}$-C12-EG	C16-EG-PEG$_{227}$-C16-EG	C16-EG-PEG$_{454}$-C16-EG
pH 7 deionized	2 300 / 700 / 70	800 / 100 / 70	13 200 / 1400 / 10	2 500 / 100 / 30
pH 4	3 700 / 1000 / 30	200 / 100 / 70	9 200 / 1200 / 10	1 000 / 150 / 15
pH 9	1 600 / 600 / 100	4 700 / 200 / 100	11 000 / 1300 / 10	9 000 / 400 / 30
0,5 N NaCl	700 / 100 / 100	3 000 / 200 / 100	9 200 / 1300 / 10	8 000 / 400 / 30
1 N NaCl	800 / 150 / 100	2 400 / 200 / 70	12 000 / 2200 / 5	5 400 / 400 / 10
1wt% UHMW PEO	4 500 / 600 / 10	3 500 / 400 / 10	3 200 / 400 / 10	2 600 / 200 / 20
5wt% UHMW PEO	500 / 40 / 10	900 / 630 / 10	800 / 200 / 10	500 / 60 / 10

The values in the table can be read as follows: value (storage modulus) [Pa] / value (loss modulus) [Pa] / end of the linear viscoelastic region (shear [%]). For better comparison of the mechanical behavior, a color-code based on the values of the storage modulus has been chosen. Light blue: weak, blue: medium, and dark blue: tough hydrogels. All measurements have been carried out at 10 °C and at constant frequency of $\omega = 1$ rad/s. The values in the table were obtained by comparison of the respective values determined *via* the rheological measurements.

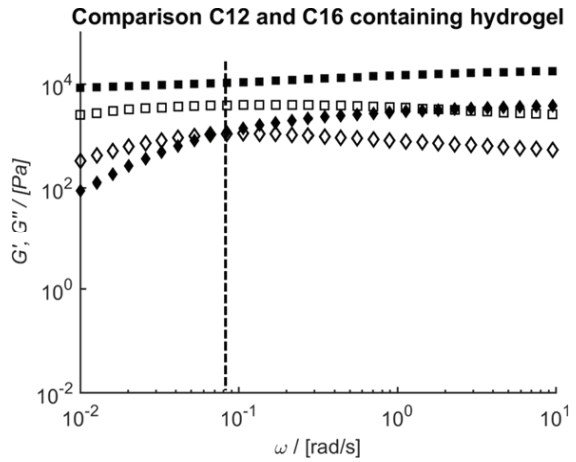

Figure S40. Comparison of P(C12-AlkGE$_{10}$-*co*-EG$_{75}$)-*b*-PEG$_{227}$-*b*- P(C12-AlkGE$_{10}$-*co*-EG$_{75}$) (◇), and P(C16-AlkGE$_{10}$-*co*-EG$_{75}$)-*b*-PEG$_{227}$-*b*- P(C16-AlkGE$_{10}$-*co*-EG$_{75}$) (□) in frequency sweep measurements. Filled and open symbols indicate the storage and loss modulus, respectively. The dotted line indicates the cross-over of $G' > G''$ for the C12-AlkGE containing hydrogel, and the observed local minimum, and maximum of the C16-AlkGE containing hydrogel, respectively.

As shown in **Figure S40**, the cross-over point of the C12-AlkGE containing gel lies in the same frequency region as the convergent region of the C16-AlkGE containing gel, indicating a second cross-link mechanism.

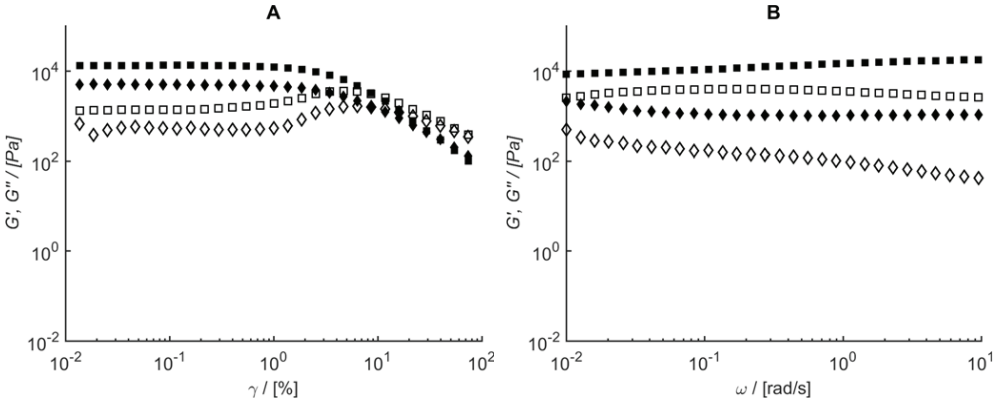

Figure S41. A: Amplitude sweep measurements of the hydrogel swollen in pure water (pH = 7) containing 10 wt% of P(C16-AlkGE$_{10}$-*co*-EG$_{75}$)-*b*-PEG$_{227}$-*b*-P(C16-AlkGE$_{10}$-*co*-EG$_{75}$). **B:** Frequency sweep measurements of the hydrogel swollen in pure water (pH = 7) containing 10 wt% of P(C16-AlkGE$_{10}$-*co*-EG$_{75}$)-*b*-PEG$_{227}$-*b*-P(C16-AlkGE$_{10}$-*co*-EG$_{75}$). The symbols (□) and (◇) indicate the temperatures during the measurements at 10 °C and 50 °C, respectively. Filled and open symbols indicate the storage and loss modulus, respectively.

As indicated in **Figure S41**, a loss of the crystalline interactions can be observed at higher temperatures. However, the modulus values are only slightly shifted to lower values.

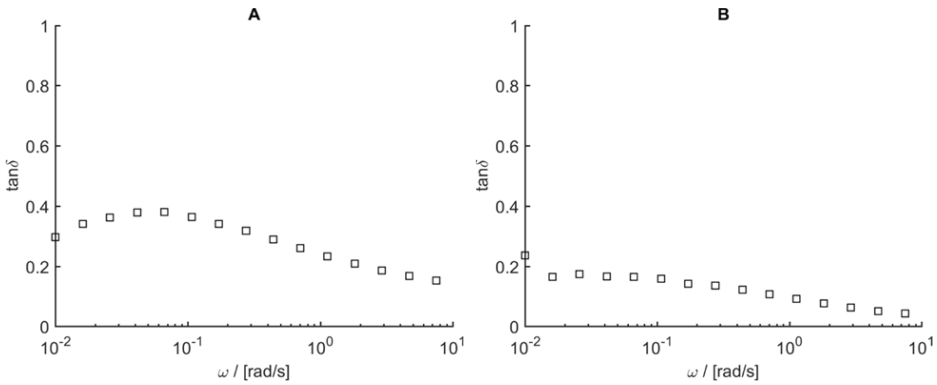

Figure S42. Comparison of the loss factor as a function if the frequency. **A:** Loss modulus of the hydrogel containing P(C16-AlkGE$_{10}$-*co*-EG$_{75}$)-*b*-PEG$_{227}$-*b*-P(C16-AlkGE$_{10}$-*co*-EG$_{75}$) swollen in pure water (pH = 7) measured at 10 °C**. B:** Loss modulus of the hydrogel containing P(C16-AlkGE$_{10}$-*co*-EG$_{75}$)-*b*-PEG$_{227}$-*b*-P(C16-AlkGE$_{10}$-*co*-EG$_{75}$) swollen in pure water (pH = 7) measured at 50 °C.

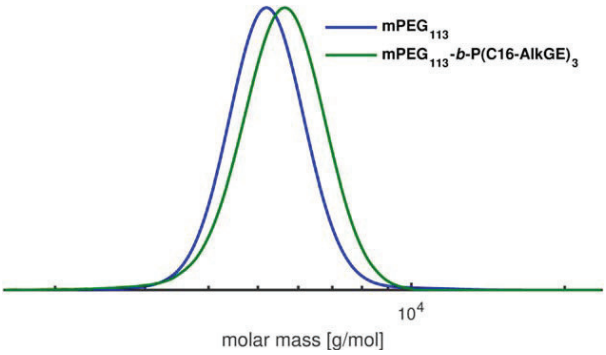

Figure 43. SEC trace of the synthesized AB diblock copolymer mPEG$_{113}$-*b*-P(C16-AlkGE)$_3$ for the biocompatibility tests.

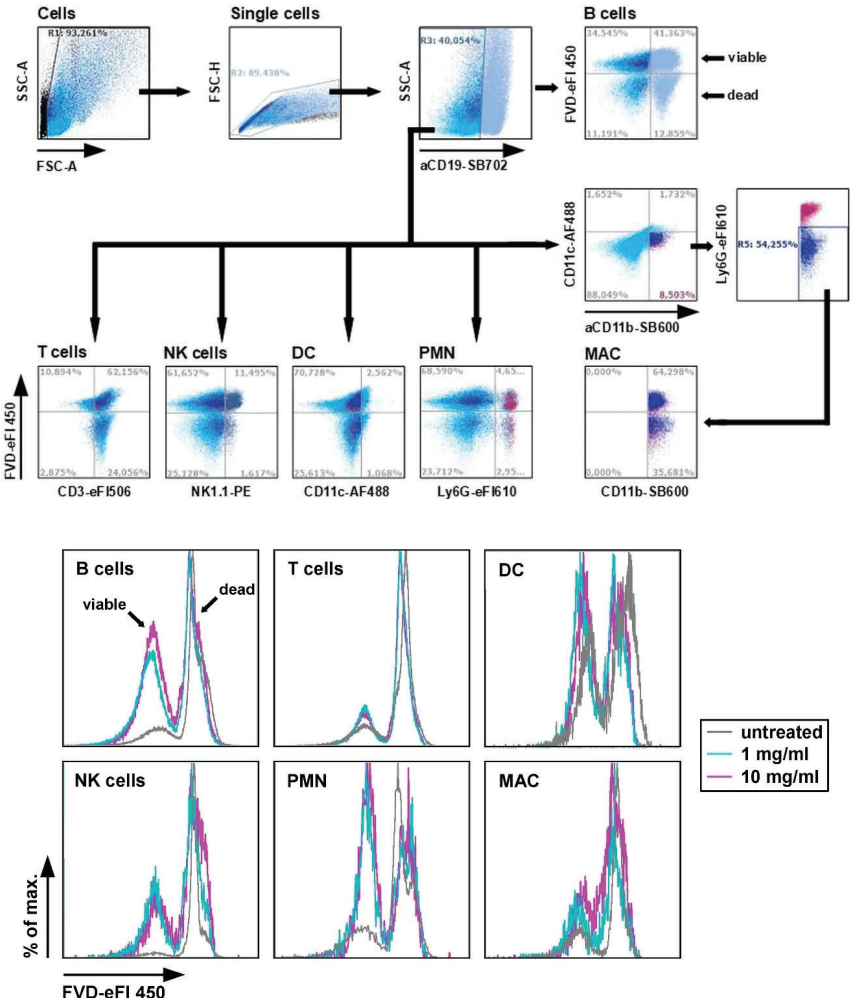

Figure S44. The viability of spleen immune cell populations is not impaired by mPEG$_{113}$-*b*-P(C16-AlkGE)$_3$. Mouse spleens (C57BL/6 background) were mechanically disrupted, and erythrocytes were lysed by using a hypotonic buffer. Leukocytes were kept in IMDM culture medium (4x106/mL), and aliquots were transferred into sterile FACS tubes (500 µL). In parallel settings, mPEG$_{113}$-*b*-P(C16-AlkGE)$_3$ was applied at the concentrations indicated or spleen cells were left

untreated. On the next day, samples were thoroughly washed, and incubated with a CD16/CD32-specific antibody (clone 4.G2) to avoid binding of subsequently applied antibodies to Fc receptors. Samples were incubated with antibodies specific for cell type-specific lineage markers (see below), and FVD-450 to identify dead cells. All antibodies were obtained from Thermo Fisher (Waltham, MA) or BioLegend (San Diego, CA). Samples incubated with single antibodies or left untreated, respectively, served as controls. After repetitive washing, all samples were fixed (PBS, 2mM EDTA, 0.7 %PFA) and subjected to flow cytometric analysis (Attune NxT flow cytometer, Attune Nxt Software v3.1.1; Thermo Fisher). Upper panel: Gating strategy applied to delineate potential cytotoxic effects of $mPEG_{113}$-b-$P(C_{16}$-AlkGE$)_3$ on mouse splenic immune cells in a cell type-specific manner. Cellular debris and non-single cells were gated out. CD19+ cells constitute B cells. To differentiate other spleen cell populations, CD19+ B cells were gated out. T cells (CD3+), natural killer (NK) cells (NK1.1+), dendritic cells (DC, CD11c+), and polymorphonuclear granulocytes (PMN, Ly6G+) were identified according to expression of the respective surface marker. Macrophages (MAC) were identified as positive for CD11b, but negative for the DC marker CD11c and the PMN marker Ly6G. In each spleen cell population, dead cells were identified as FVD+. Dot plots show the gating strategy for untreated spleen cells and are representative for 2 independent experiments. Lower panel: Spleen cells were incubated over-night with mPEG113-b-P(C16-AlkGE)3 at the indicated concentrations or were left untreated. On the next day, cell populations were identified by flow cytometric analysis of lineage marker expression, and dead cells were delineated using FVD. Histograms denote the relative distribution of viable (FVD-, left peak), and dead (FVD+, right peak) cells in response to differential treatment. Plots are representative for 2 independent experiments.

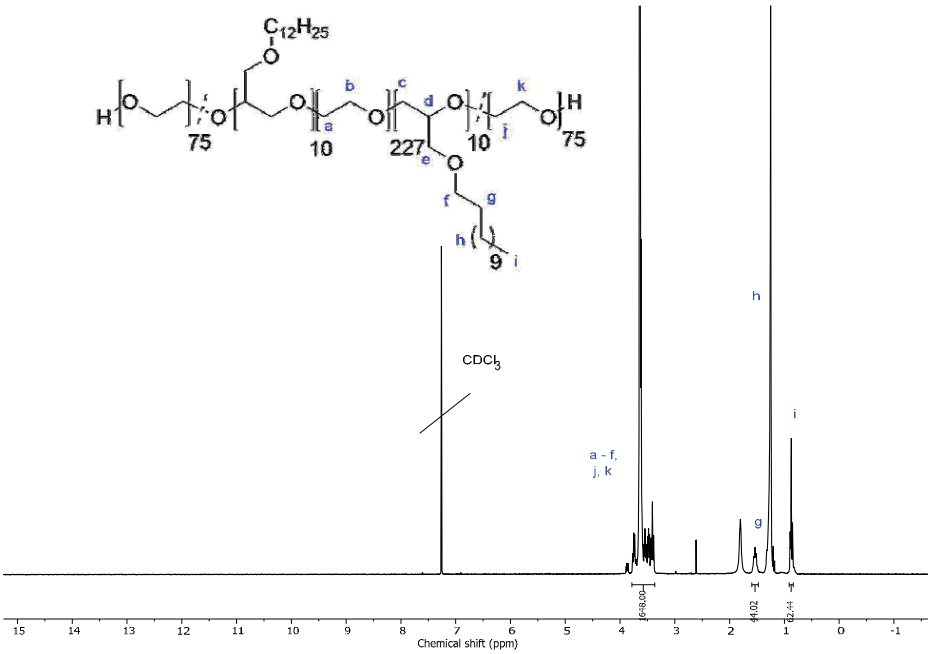

Figure S45. ^{1}H NMR spectrum (300 MHz, chloroform-*d*) of P(C12$_{10}$-*co*-EG$_{75}$)-*b*-PEG$_{227}$-*b*-P(C12$_{10}$-*co*-EG$_{75}$).

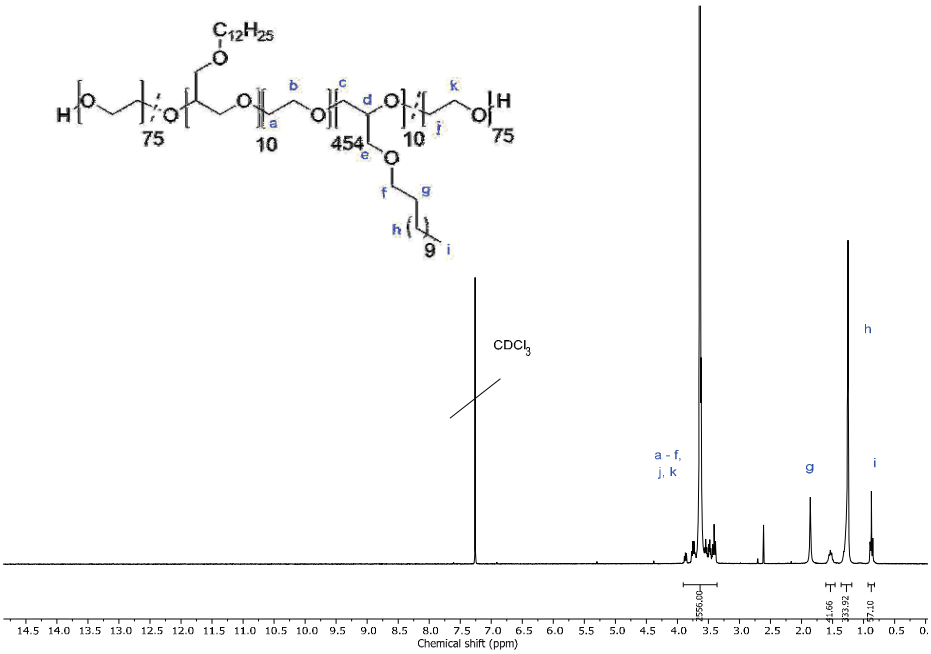

Figure S46. ^{1}H NMR spectrum (300 MHz, chloroform-*d*) of P(C12$_{10}$-*co*-EG$_{75}$)-*b*-PEG$_{454}$-*b*-P(C12$_{10}$-*co*-EG$_{75}$).

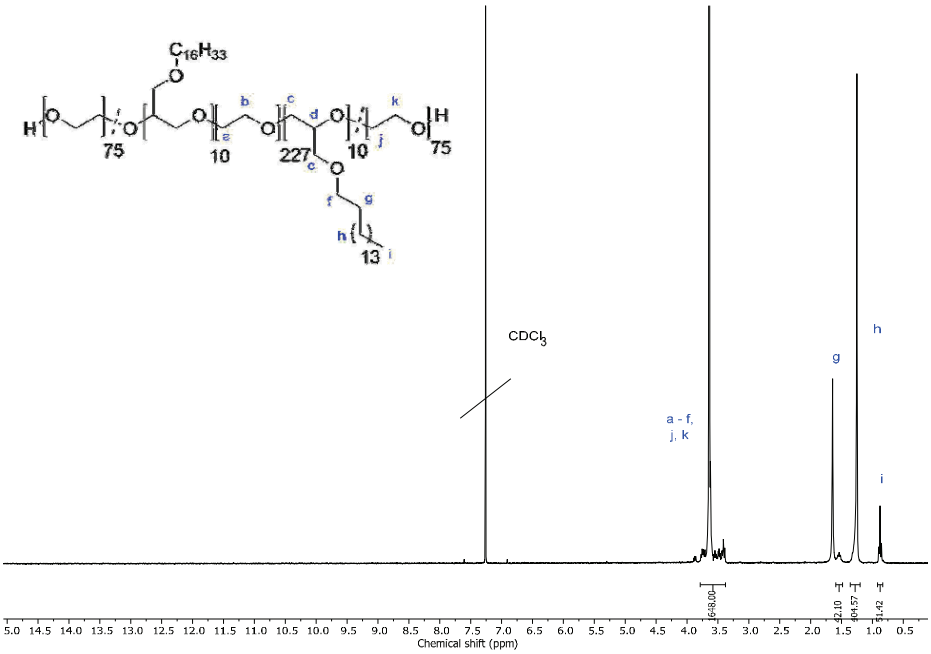

Figure S47. ^{1}H NMR spectrum (300 MHz, chloroform-*d*) of P(C16$_{10}$-*co*-EG$_{75}$)-*b*-PEG$_{227}$-*b*-P(C16$_{10}$-*co*-EG$_{75}$).

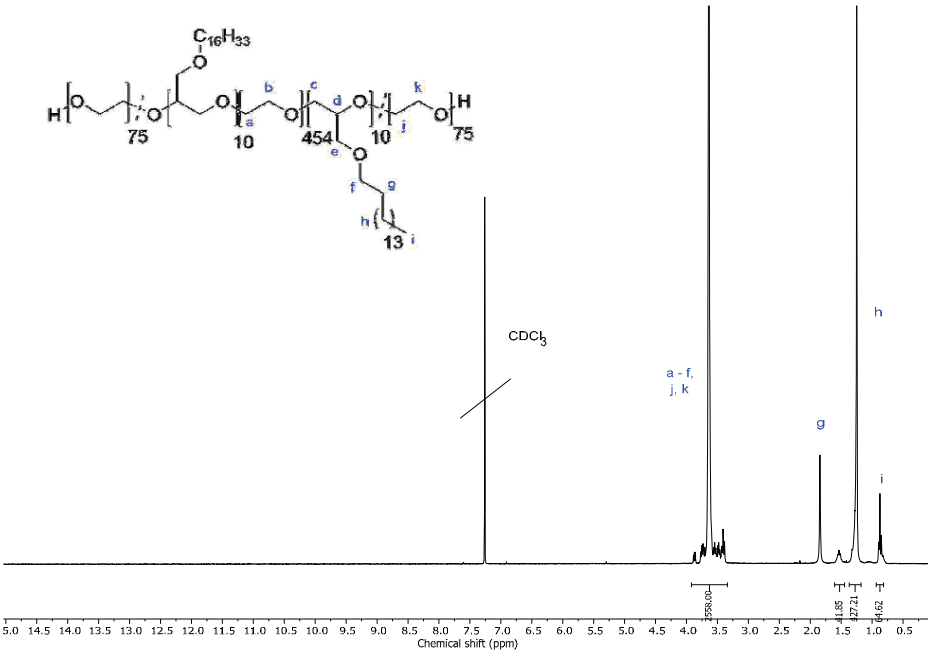

Figure S48. ^{1}H NMR spectrum (300 MHz, chloroform-*d*) of P(C16$_{10}$-*co*-EG$_{75}$)-*b*-PEG$_{454}$-*b*-P(C16$_{10}$-*co*-EG$_{75}$).

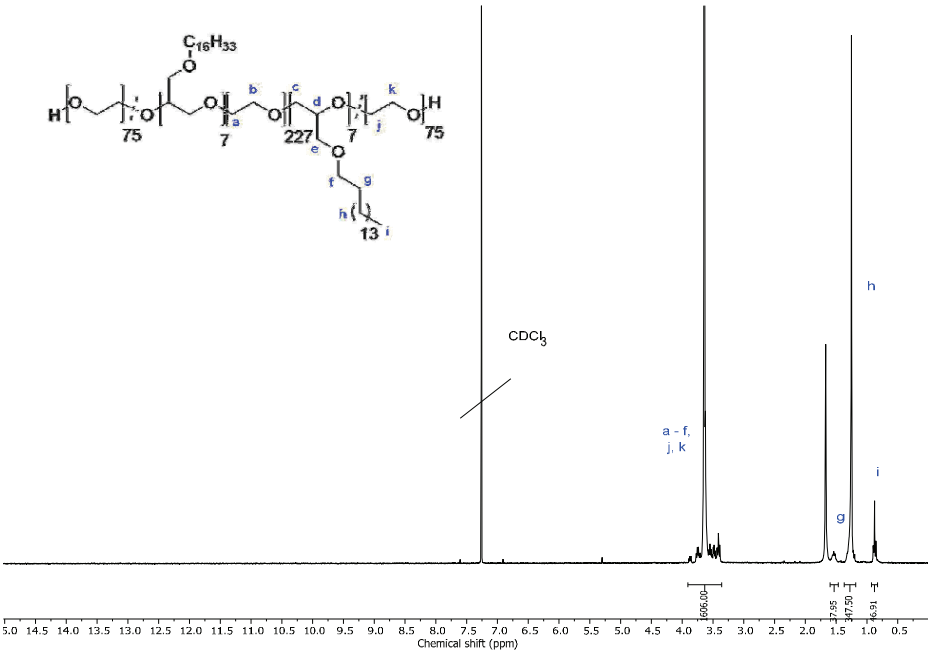

Figure S49. ^{1}H NMR spectrum (300 MHz, chloroform-*d*) of P(C16$_{7}$-*co*-EG$_{75}$)-*b*-PEG$_{227}$-*b*-P(C16$_{7}$-*co*-EG$_{75}$).

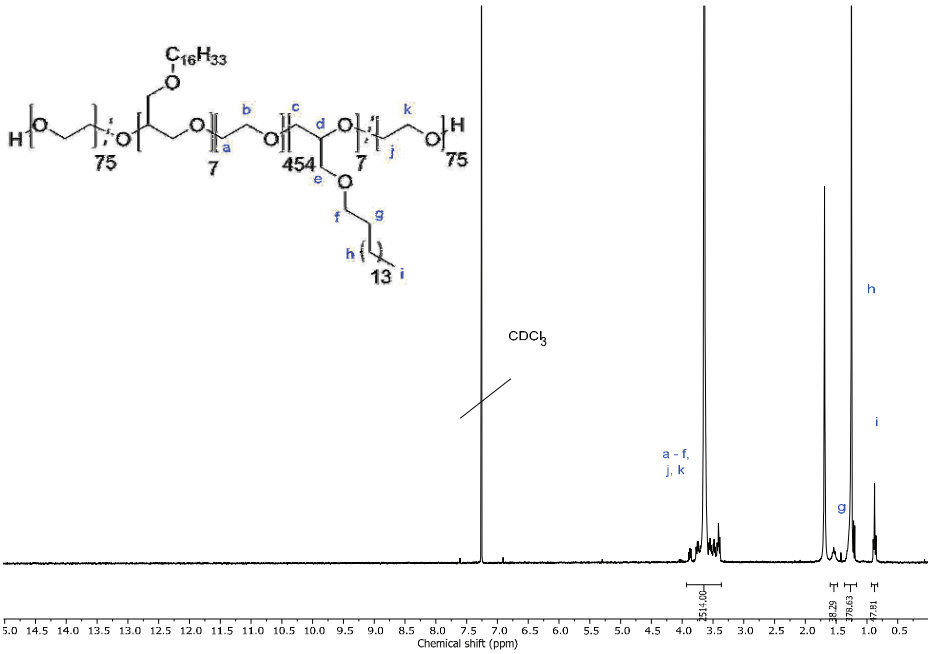

Figure S50. ^{1}H NMR spectrum (300 MHz, chloroform-*d*) of P(C16$_{7}$-*co*-EG$_{75}$)-*b*-PEG$_{454}$-*b*-P(C16$_{7}$-*co*-EG$_{75}$).

References

(1) Verkoyen, P.; Johann, T.; Blankenburg, J.; Czysch, C.; Frey, H. Polymerization of long chain alkyl glycidyl ethers: a platform for micellar gels with tailor-made melting points. *Polym. Chem.* **2018**, *9*, 5327–5338.

Chapter A2

Poly(ethylene glycol) having C1 to C3-alkyloxymethyl side chains, bioconjugates thereof, process for its preparation and its use

Philip Dreier[†], Rebecca Mohr[†] and Holger Frey[*,†]

[†]Department of Chemistry, Johannes Gutenberg University Mainz, Germany

---

The author of this thesis contributed to this work by synthesis of the corresponding copolymer structures and partially writing of the patent. The patent was submitted on 14.5.2021 and is currently reviewed by the european patent office (EPO).

Title:

Poly(ethylene glycol) having C1 to C3-alkyloxymethyl side chains, bioconjugates thereof, process for its preparation and its use

Introduction

The present invention concerns polyether polymers represented by the following formula [I]:

$$-(CH_2CHR\text{-}O\text{-})_m-$$

[I],

wherein residues R are hydrogen or C1-C3 alkoxymethyl, 1 to 100 % are methoxymethyl and up to 50% of R may be C2-C3 alkoxymethyl with the proviso that at least one R is hydrogen, if at least one R is C2-C3 alkoxymethyl; and m is in the range of from 10 to 1000, wherein the dispersity is 1.15 or less. The invention further concerns a process for their preparation, conjugates thereof and the use thereof.

Background of the invention

The aliphatic polyether poly(ethylene glycol) (PEG) is the most widely employed polymer in pharmaceutics, medicine and drug delivery. PEGylation, i.e. the attachment of PEG to peptide drugs, was introduced in the 1970ies and has since then led to numerous highly efficient drugs. PEGylation is a form of conjugation, i.e. the attachment of a polymer to a molecule by a covalent bond. The main effect of the attachment of PEG chains is the so-called "stealth effect", which prevents close approach of and recognition by the immune system and subsequent binding and removal by the reticuloendothelial system (RES) in the liver. More simply, PEG attachment also prevents opsonization by proteins, when attached to the surfaces of nanocarriers for drug delivery. The inhibition of protein adsorption by PEG is further emphasized by fulfillment of the rules for protein-repellent surfaces derived by Whitesides (Yarovsky et al., "Quantitative design rules for protein-resistant surface coatings using machine learning", Scientific Rep. 2019, 9, 265). PEGylation is also used for "stealth liposomes" with long circulation times, low molecular weight drugs as well as for lipid nanoparticles. Such structures are employed for the transport and delivery of mRNA. Here the respective PEG-based lipids play a key role for the vaccination against the COVID-19 pandemic, enabling transport of mRNA to cells, avoiding undesired degradation

processes. The recently approved mRNA vaccines from Moderna and Pfizer-BioNTech require PEGylated lipids to ensure the stability of the mRNA in the lipid-based nanoparticle. PEGylation also prevents coalescence of liposomes and similar structures in aqueous systems. Commonly, molecular weights in the range of 2 to 40 kg/mol are preferred for the PEGylation of drugs or nanocarriers. To sum up, PEG has become a standard for water-soluble medical polymers for a vast variety of medical and pharmaceutical uses, particularly in the therapy of cancer, chronic diseases and recently also for RNA delivery vehicles. The success of PEG may have had several reasons. Among them are commercial availability in sufficient quality and in a wide range of molar masses from the anionic ring-opening polymerization of ethylene oxide as well as its extremely low toxicity and high biocompatibility. Further, PEG can be prepared in narrow molecular weight distributions.

However, an increasing number of studies summarize concerns related to the presence of so-called anti-PEG antibodies (APAs) that are present in a large and constantly growing part of the population. Such antibodies can lead to accelerated clearance of PEGylated drugs from the blood stream, i.e. loss of the stealth effect that is crucial for therapeutic success, allergic reactions and in extreme and rare cases even potentially fatal anaphylactic shock. This undesired effect is observed both for PEGylated peptide drugs, PEGylated liposomes and other PEGylated nanocarriers as well as PEGylated small molecule drugs. Anti-PEG antibodies are also problematic with respect to PEGylated lipids for RNA-transporting lipid nanoparticles, e.g. in the context of COVID-19 vaccines. PEG-antibodies are often mentioned in the context of potential PEG-alternatives as a motivation to look beyond PEG for alternatives. As an estimate, approximately 10% of the population experience allergic reactions when treated with PEGylated formulations. Only recently, the nature of the binding between PEG and anti-PEG antibodies has been studied by Lai et al (Lai et al, „Structure of an anti-PEG antibody reveals an open ring that captures highly flexible PEG polymers.“ *Commun Chem* 2020, *3, 124*). They concluded that binding of PEG is due to an open ring structure of PEG captured by the APAs. By counting the number of monomer repeats of the PEG polymer interacting with the interior and exterior paratope of the Fab, they found the size of the PEG antigen epitope to be ~700 g/mol, equivalent to 16 monomer subunits. Thus, at least 16 ethylene glycol units are required for binding by the APA. Other works suggest that also shorter regular chain segments of PEG as well as the methoxy end group of mPEG (α-methoxy poly(ethylene glycol)) structure play a key role for the recognition. US 8,129,330 B2 therefore discloses methods for the preparation of PEG conjugates that are based on end group modification of the PEG chains. Variation of the end group of PEG is disclosed, aiming at minimizing interaction of for example methoxy end groups with anti-PEG antibodies. The authors disclose conjugates, wherein a hydroxyl group is present on all of the distal polyalkylene glycol termini in said pure conjugate, and wherein

said conjugate exhibits reduced antigenicity compared to mPEG-protein conjugates. It has been reported that antibodies elicited by PEG-OH have similar affinity to both mPEG and PEG-OH, while antibodies induced by mPEG recognize mPEG more effectively than PEG-OH (Sherman et al, „Role of the methoxy group in immune responses to mPEG-protein conjugates." *Bioconjug Chem* 2012, 23(3), 485-499; Sherman et al, „Selectivity of binding of PEGs and PEG-like oligomers to anti-PEG antibodies induced by methoxyPEG-proteins." *Mol Immunol* 2014, 57(2), 236-246.). These results have been obtained by using competitive ELISA and imply that the anti-PEG antibodies elicited by PEG-OH-proteins are directed against the backbone of the PEG (backbone-specific), while antibodies induced by mPEG-protein conjugates are methoxy group specific. It can be concluded that regular segments of at least 4-5 to 16 regularly arranged ethylene glycol units are required to achieve recognition and immunogenic reaction by anti-PEG antibodies. Recent clinical works demonstrated that the presence of antibodies against PEG permits to predict Pegasparagase allergic reactions and failure of rechallenge, emphasizing the clinical importance of anti-PEG antibodies for the success of the treatment of leukemia in this case (Liu et al, "Antibodies Predict Pegasparagase Allergic Reactions and Failure of Rechallenge", *J. Clin. Oncol*. 2019, 37, 2051).

Three strategies for the modification of the PEG structure have been developed to counteract undesired APA interaction of PEGylated therapeutics. Replacing the methoxy end group of mPEG by a hydroxyl group led to a strong decrease in the affinity for anti-PEG antibodies, which was demonstrated by competitive ELISA tests. However, it is obvious that for large scale commercial applications the presence of a hydroxyl group at the terminus would require protected functional initiators, which complicates existing synthetic protocols. A second recent strategy is disclosed in US 2019/0015520 A1 and relies on PEG-bottlebrush structures, i.e. small PEG structures appended to a poly(hydroxyethyl methacrylate) backbone. The inventors state that this type of PEG-architecture minimizes anti-PEG antigenicity, while preserving the desired stealth properties for surface coating. However, the resulting PEG-grafted copolymers exhibit rather broad, multimodal molecular weight distributions, which represent a major obstacle for approval for medical application and PEGylation analogous bioconjugation with peptides or lipids. Narrow distributions ($M_w/M_n < 1.15$) were exclusively feasible by performing a cost- and time-consuming preparative size-exclusion chromatography (SEC).

Another strategy is to exchange PEG with the linear polyether polyglycerol to increase the blood circulation time of liposomes and to avoid accelerated blood clearance (see Abu Lila et al, "*Use of polyglycerol (PG), instead of polyethylene glycol (PEG), prevents induction of*

the accelerated blood clearance phenomenon against long-circulating liposomes upon repeated administration", International Journal of Pharmaceutics, 456 (2013) 235-242). However, the utilization of polyglycerol also results in the introduction of multiple hydroxyl functionalities to the liposome, which is in contrast to the aforementioned rules of Whitesides resulting in complex unspecific recognitions of peptides in the blood stream. Therefore, a targeted use of the conjugated drug or liposomes is not possible with polyglycerol.

Since PEGylated therapeutics are often used for chronic or in many cases otherwise fatal diseases, like in cancer therapy, in many cases repeated doses have to be administered over prolonged periods of time. PEG is a non-biodegradable polymer and has to be eliminated from the body through the kidneys. In studies on the renal filtration of PEGylated drugs, an undesirable accumulation of PEG in the kidneys and the associated pathological changes in the renal system could be demonstrated (see e.g. Bendele, A.; Seely, J.; Richey, C.; Sennello, G.; Shopp, G. Short Communication: Renal Tubular Vacuolation in Animals Treated with Polyethylene-Glycol-Conjugated Proteins. Toxicol.
Sei. 1998, 42, 152-157). The tendency of polyethylene to crystallize can therefore lead to deposits in the kidney. The elimination through the kidneys also limits the molecular weight of PEG for medical therapeutics to the renal cutoff size, which for globular proteins is approximately 50 to 60 kDa.

The present inventors have reported in 2014 on the copolymerization of ethylene oxide with glycidyl methyl ether (GME) by use of the monomer activation method and tetraoctylammonium bromide and tris-*iso*-butylaluminum as initiators (see Frey et al, A Challenging Comonomer Pair: "*Copolymerization of Ethylene Oxide and Glycidyl Methyl Ether to Thermoresponsive Polyethers*", Macromolecules 2014, 47, 5492-5500). Rather broad molecular weight distributions were obtained (dispersity in the range of 1.21 to 1.5), which are clearly not suitable for medical applications. As discussed at the time, with the conventional anionic ring-opening method only molecular weights up to 3000 g/mol and high dispersities have been reported for the polymerization of GME. In previous studies regarding the homopolymerization of GME to poly(glycidyl methyl ether) (PGME) it was generally stated that polymerization causes difficulties, and no molecular weight control can be achieved by anionic ring-opening polymerization as employed for medical PEG (Frey et al., Biomacromolecules 2014, 15, 1935−1954). In all available reports regarding GME polymerization to date, either phosphazene bases were used as a catalyst or aluminum compounds had to be added in the way of a "monomer activated polymerization". None of these polymers or copolymers are suitable for medical applications for several reasons: (i) traces of phosphazene bases lead to toxicity and cannot be removed; (ii) dispersities exceed

1.1, which is prohibitive for most medical applications and (iii) end-group fidelity of the polymers derived from the methods is insufficient for attachment to peptides, drugs or lipids via bioconjugation. Therefore, neither PGME homopolymer nor copolymers of GME have been considered for PEGylation type applications to date.

The retention of polymer end-groups (end-group fidelity) is a critical tool for chain extension and post polymerization reactions. End-group fidelity is also a decisive factor for the use of polymers in bioconjugates for pharmaceutical applications, in which the biomolecules are connected by means of the end-groups. Polymers with low end-group fidelity comprise a large amount of macromolecules that are not bound to the biomolecule and cannot be removed from the mixture without undue expenditure. The formed conjugates do not have the required purity. The loss of end-groups is therefore not desirable, but cannot be completely avoided. End-group fidelity varies greatly depending on the reaction conditions in the preparation of the polymers.

Purpose of the invention

It is the objective of the present invention to provide alternative polymers that are able to replace PEG in its applications and that can alleviate at least some of the aforementioned disadvantages of PEG. The alternative polymer should especially be suited to replace PEG in pharmaceutical applications. It is further an objective to provide polymers with low dispersity. A further objective is to provide polymers with high end-group fidelity. It is also desired to provide a process that allows preparation of such polymers in a simple and commercially feasible way. The alternative polymers should have a low affinity towards anti-PEG antibodies (APAs). A further goal is to provide polymers with a low immunogenicity.

Detailed description

The present invention concerns poly(ethylene glycol) having C1 to C3-alkyloxymethyl side chains. The present invention concerns polyether polymers represented by the following formula [I]:

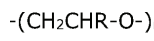

[I]

wherein residues R are independently from each other selected from the group consisting of hydrogen, methoxymethyl, ethoxymethyl, n-propoxymethyl and iso-propoxymethyl; 1

to 100% of the residues R are methoxymethyl; up to 50% of the residues R may be selected from the group consisting of ethoxymethyl, n-propoxymethyl and iso-propoxymethyl; with the proviso that at least one residue R is hydrogen, if at least one residue R is selected from the group consisting of ethoxymethyl, n-propoxymethyl and iso-propoxymethyl; and m is in the range of from 10 to 1000, characterized in that the dispersity is 1.15 or less. Herein the percentages of the residues R are based on the sum of all residues R, i.e. on m. These new polyether polymers are a new type of material, which behaves very different to PEG in regard to the affinity towards anti-PEG antibodies (APAs) and have a low immunogenicity. They also have a low crystallinity. But the polyether polymers of the present invention behave very similar to PEG with respect to various features that are important for pharmaceutical applications, including aqueous solubility, hydration, cell viability and biocompatibility.

Key to the reduced interaction with APAs is the use of substituents on the PEG backbone. The increased spatial requirements of the said PEG copolymers impede or disable interaction with anti-PEG antibodies according to the specific "lock and key principle". Besides the steric impact, the random distribution of the substituents over the polymer backbone and/or the random steric orientation of the substituents furthermore disable the development and formation of specific anti-polymer antibodies.

Key to the similarity of the features of PEG and the inventive polymers is the use of alkoxymethyl side chains. This maintains water solubility and other properties in view of PEG. A repeating group of the present polymer wherein R is a methoxymethyl group, i.e. (-CH_2-CH(-CH_2-OCH_3)-O)-, has the same molecular formula $C_4H_8O_2$ as two repeating units of PEG (-CH_2-CH_2-O)$_2$- and is therefore a constitutional isomer of two main chain repeating units of PEG. It comprises the same number of atoms and very similar functional groups. This leads to similar properties, especially to similar water solubility, which is important for applications in biological systems. The lack of reactive functional groups in the side chain like hydroxy, amino etc. reduces undesired interactions with biological systems.

Ethoxymethyl, n-propoxymethyl and iso-propoxymethyl may be used as residue R to adjust the properties of the polymers further, for example their solubility, interaction with lipids, properties in respect to the passage of biological membranes etc. However, these residues lead to a reduced solubility in water. The choice of such substituents also leads to a deviation from the behavior of PEG for other properties. For this reason, the amount of repeating units with the residues selected from the group consisting of ethoxymethyl, n-propoxymethyl and iso-propoxymethyl is limited to 50% of all residues R of the polymer of formula (I). Also in embodiments of the present invention in which at least one residue R

of the polymers is selected from the group consisting of ethoxymethyl, n-propoxymethyl and iso-propoxymethyl at least one residue R must be hydrogen, preferred at least 5 % are hydrogen in such embodiments, more preferred at least 10 % are hydrogen and most preferred at least 25 % are hydrogen. In a further preferred embodiment up to 20% of the residues R may be selected from the group consisting of ethoxymethyl, n-propoxymethyl and iso-propoxymethyl and even more preferred only up to 5% of the residues R may be selected from this group. These residues are not required for some of the uses of the polymers of the present invention in pharmaceutical applications. For this reason, polymers of the present invention are preferred where R is selected from the group consisting of hydrogen and methoxymethyl. Obviously, ethylene oxide repeating units in the inventive polymers also lead to similar properties with PEG. This selection therefore provides the polymers that are closest in behavior to PEG.

Higher homologues of methoxymethyl, i.e. where R is C4 alkoxymethyl and higher lead to increasingly low solubility in water and other detrimental properties and should therefore generally be avoided. They may however be used in small quantities when required, preferably in amounts of 10 % or less and more preferably in amounts of 3 % or less and most preferred 1 % or less, based on the sum of all residues R selected from the group consisting of hydrogen, methoxymethyl, ethoxymethyl, n-propoxymethyl and iso-propoxymethyl; i.e. on m. If the polyether of the present invention comprises higher homologues of methoxymethyl, where R is C4-alkoxymethyl or higher, the same proviso for the presence of hydrogen applies with the same preferred amounts. Various other co-monomers may be also used in small amounts, i.e. preferably less than 3 wt%, more preferably less than 1 wt% and most preferred in less than 0.1 wt% based on the weight average molecular weight of the polymer of formula [I], if necessary. They may for example be used to introduce functional groups or side chains into the polymer. Best suited for the use in pharmaceutical application are however usually polymers of the present invention that comprise only the repeating units of formula (I).

As mentioned before, ethylene oxide repeating units and glycidyl methyl ether repeating units, i.e. wherein R is methoxymethyl, provide polymers with very similar properties. Because of the very similar properties, the ethylene oxide repeating units in the backbone of PEG may be completely substituted by methoxymethyl substituted repeating units, i.e. 100% of the residues R may be selected from methoxymethyl groups, which constitutes the homopolymer of glycidyl methyl ether. This is however not preferred. The properties of the polymers of the present invention are still closer to the properties of PEG, when at least some of the residues R are selected to be hydrogen. Furthermore, immunogenicity of copolymers will be reduced as compared to the homopolymer of glycidyl methyl ether,

because they do not only differ in the orientation of side groups, but also side groups themselves. Preferred are therefore polymers for the present invention that are copolymers. The largest differences between the side groups and therefore the lowest immunogenicity is provided by polymers in which some of the repeating units have no side groups, i.e. where R is hydrogen. Most effective are therefore polymers of the present invention wherein 3 to 99% of the residues R are hydrogen and 1 to 97% of the residues R are independently from each other selected from the group consisting of methoxymethyl, ethoxymethyl, n-propoxymethyl and iso-propoxymethyl.

More preferred are 5 to 95% of the residues R hydrogen and 5 to 95% of the residues R are independently from each other selected from the group consisting of methoxymethyl, ethoxymethyl, n-propoxymethyl and iso-propoxymethyl. This will ensure a lower immunogenicity. More preferred 10 to 90% of the residues R are hydrogen and 10 to 90% of the residues R are independently from each other selected from the group consisting of methoxymethyl, ethoxymethyl, n-propoxymethyl and iso-propoxymethyl. Even more preferred are 20 to 80% of the residues R are hydrogen and 20 to 80% of the residues R are independently from each other selected from the group consisting of methoxymethyl, ethoxymethyl, n-propoxymethyl and iso-propoxymethyl. The lowest immunogenicity provide polymers of the present invention, where about 50 % of all ethylene oxide repeating units are substituted by alkyl glycidyl ethers. For this reason polymers are preferred where 30 to 70% of the residues R are hydrogen and 30 to 70% of the residues R are independently from each other selected from the group consisting of methoxymethyl, ethoxymethyl, n-propoxymethyl and iso-propoxymethyl and more preferred 40 to 60%. Especially useful in pharmaceutical applications is a polyether polymer of the present invention, wherein the polyether is a poly(glycidyl methyl ether-co-ethylene oxide) copolymer, i.e. wherein the residue R is selected from the group consisting of hydrogen and methoxymethyl. The same preferred ranges apply to embodiments where R is selected from the group consisting of hydrogen and methoxymethyl, i.e. wherein the polyether is a poly(glycidyl methyl ether-co-ethylene oxide) copolymer.

Especially preferred are polyether polymer of the present invention, wherein 30 to 70% of the residues R are hydrogen and the remaining residues R are methoxymethyl. These copolymers comprising repeating units where R is hydrogen combine most of the aforementioned advantageous properties. They have low immunogenicity, good water solubility, low crystallinity and are otherwise very similar to PEG.

m is preferably in the range of 20 to 900 and more preferably in the range of 30 to 800. Most preferably m is in the range of 30 to 700. These ranges correspond to the polymer

weights of PEG that are most suited for medical applications and that are used in existing medical application for PEG. Furthermore, the polymers of the present invention have preferably a molecular weight M_n as determined by MALDI-TOF in the range of 500 to 50.000 g/mol, more preferably in the range of 1.000 to 50.000 g/mol and most preferably in the range of 1.000 to 30.000 g/mol. These ranges apply to all embodiments of the present invention.

Copolymers of the present invention may be random copolymers. Such copolymers provide the lowest immunogenicity, as they do not provide a blueprint for the immune system for antibodies. They are intrinsically resistant to an immune response and are therefore preferred embodiments of the present invention. These polymers may be prepared by a process of the present invention as discussed below.

In one embodiment of the present invention the polymers of the present invention may be block copolymers or may have a block like structure or a tapered or gradient structure. The methods to prepare such polymers are known to the expert in the art. In such embodiments it is preferred that no more than 5% of the macromolecules of the polymers comprise blocks with more than 15 ethylene oxide repeating units, more preferably that no more than 5% of the macromolecules of the polymers comprise blocks with more than 8 ethylene oxide repeating units. This reduces immunogenicity.

As described above, similarity to PEG is an important feature of the polymers of the present invention. This is especially true for the end groups of the polymer. Processing of PEG for the use in the pharmaceutical field, involves regularly the modification of the end groups. For this purpose, any end group known to be used for PEG can also be used for the present polymers. This includes not only the use of all known end groups for PEG, but also their modification including the kind of modification and the process of modification. If necessary, in order to allow the present polymers to function in this regard as similar or in fact identical to PEG, the present polymers may be provided with ethylene oxide repeating units on either end or both ends of the polymer, as depicted in Formula [Ia] to [Ic]. These are preferred embodiments of the present invention.

$$\text{-(CH}_2\text{CH}_2\text{-O-)}_a\text{-(CH}_2\text{CHR-O-)}_m\text{-} \quad [Ia]$$

$$\text{-(CH}_2\text{CHR-O-)}_m\text{-(CH}_2\text{CH}_2\text{-O-)}_a\text{-} \quad [Ib]$$

$$\text{-(CH}_2\text{CH}_2\text{-O-)}_a\text{-(CH}_2\text{CHR-O-)}_m\text{-(CH}_2\text{CH}_2\text{-O-)}_a\text{-} \quad [Ic]$$

In these formulae the partial formulae $\text{-(CH}_2\text{CHR-O-)}_m\text{-}$ depicts a polymer of the present invention as described herein and a may be any number, but is preferable a number in the

range of 1 to 10 and more preferably in the range of 1 to 3. Polymers according to formulae [Ia] to [Ic] allow the modification of the termini of the present polymers exactly as PEG is modified in known processes and especially in present industrial processes. This allows for a smooth transition of established processes from PEG to the polymers of the present invention. Such can be prepared without much additional effort, as will be discussed below.

A further embodiment of the present invention, are polyether polymers represented by any of the following formula [II] and [IIa] to [IIc]:

$$X\text{-}(CH_2CHR\text{-}O\text{-})_m\text{-}CH_2CHR\text{-}Y \quad [II]$$

$$X\text{-}(CH_2CH_2\text{-}O\text{-})_a\text{-}(CH_2CHR\text{-}O\text{-})_m\text{-}CH_2CHR\text{-}Y \quad [IIa]$$

$$X\text{-}(CH_2CHR\text{-}O\text{-})_m\text{-}(CH_2CH_2\text{-}O\text{-})_a\text{-}CH_2CH_2\text{-}Y \quad [IIb]$$

$$X\text{-}(CH_2CH_2\text{-}O\text{-})_a\text{-}(CH_2CHR\text{-}O\text{-})_m\text{-}(CH_2CH_2\text{-}O\text{-})_a\text{-}CH_2CH_2\text{-}Y \quad [IIc]$$

wherein m is 19 to 999 and R is defined as in formula [I] and a is as defined in any of formulae [Ia] to [Ic]. X is the end group derived from the initiator of the reaction and the α-end group (alpha end group) and Y is the ω-end group (omega-end group).

X or Y or both may be chosen from any end group known for use in PEG. The same end groups may also be provided for the polymers of formulae [Ia] to [Ic].

X and Y may independently of each other or both comprise one or more functional group selected from the group consisting of acetal (dialkoxy), aldehyde (formyl), amide (carboxamido), azide, carbonate (alkoxycarbonyl)oxy), carboxyl (carboxy), carboxylic anhydride, ester (alkoxycarbonyl), ether, halo, haloformyl (carbonohaloridoyl), hemiacetal (alkoxyol), hemiketal (alkoxyol), hydroxy, imide (imido), imine (imino), ketal (dialkoxy), ketone (oyl), orthoester (trialkoxy), primary, secondary, tertiary amino group, primary, secondary and tertiary alkoxy group, sulfhydryl (sulfanyl, H-S-), thioether and combinations thereof. In a preferred embodiment X or Y may be selected from the group consisting of alkyl, hydrogen, hydroxy, alkoxy, sulfanyl, phthalimide, amide, amine and combinations thereof. X or Y or both may be a primary alkoxy group selected of the formulae R-CH_n-O-, wherein R is linear, branched or cyclic alkyl or phenyl and n equals 1 to 20. Preferred are X or Y or both selected from the group consisting of methoxy, ethoxy, propoxy, butoxy, pentoxy, hexoxy, heptoxy, octoxy, nonoxy, decanoxy, 3-ethyl-butoxy, 2,3-dialkoxypropoxy and a combination thereof. X or Y or both may also be the alkoxy residue of an alcohol of the following formula:

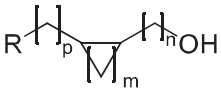

n = 1-20
m = 1-20
p = 0-20
,

wherein R is hydrogen or linear, branched or cyclic alkyl or phenyl. X or Y or both may be the alkoxy residue of a secondary alcohol selected from any of the formulae

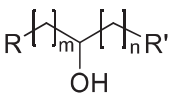

n = 1-20
m = 1-20

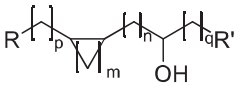

n = 1-20
m = 1-20
p = 0-20
q = 1-20

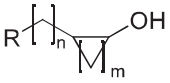

n = 0-20
m = 1-20
,

wherein R and R' are independently from each other hydrogen or linear, branched or cyclic alkyl or phenyl. Among them a secondary alkoxy group is preferred that is selected from the group consisting of 2-propoxy, 2-butoxy, 2-pentoxy, 3-pentoxy, 2-hexoxy, 3-hexoxy, 2-heptoxy, 3-heptoxy, 4-heptoxy and cyclohexyloxy.

X or Y or both may also be selected from primary alkenyloxy groups, which may be linear, branched or cyclic. X or Y or both may also be the alkoxy residue of an alcohol of the following formula:

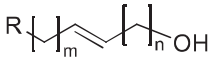

n = 1-20
m = 0-20

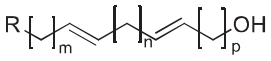

n = 0-20
m = 0-20
p = 1-20
,

wherein R is hydrogen or linear, branched or cyclic alkyl or phenyl. Among them a primary alkenyloxy group is preferred that is selected from the group consisting of 2-propenoxy (allyloxy), 3-butenoxy, 2-butenoxy, 3-methyl-2-butenoxy, 4-pentenoxy, 3-pentenoxy, 2-pentenoxy and 3,5-hexadienoxy.

X or Y or both may further be selected from secondary alkenyloxy groups, which may be branched or cyclic. X or Y or both may be the alkoxy residue of any of the following formulae:

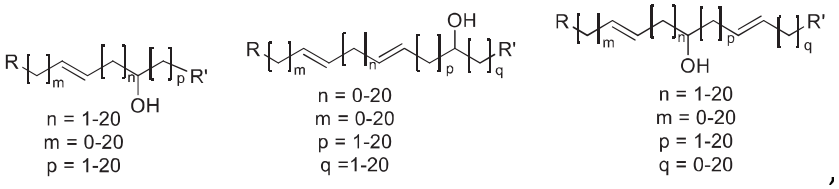

wherein R and R' are independently from each other hydrogen or linear, branched or cyclic alkyl or phenyl. The secondary alkenyloxy group may be of any of the formulae 4-penten-2-oxy, 3-penten-2-oxy, 5-hexen-2-oxy, 4-hexen-2-oxy, 3-hexen-2-oxy, 4,6-heptadien-2-oxy, 1,4-pentadien-3-oxy.

X or Y or both may further be selected from aryloxy and heteroaryloxy groups. Benzyloxy groups are especially preferred. X or Y or both may be the aryloxy or benzyloxy residue of an alcohol of any of the following formulae:

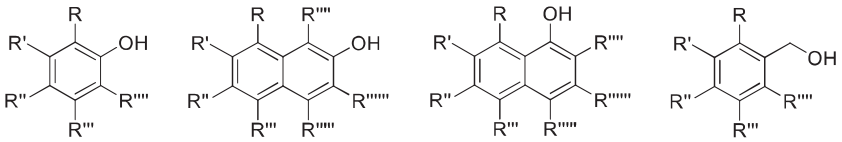

wherein R, R'', R''', R'''' R''''' and R''''''' are independently from each other hydrogen or linear, branched or cyclic alkyl or phenyl. X or Y or both are preferably selected from the group consisting of benzyloxy, phenyloxy and naphthyloxy.

X or Y or both may be multifunctional alkoxy groups, i.e. may have multiple ether bonds to the α- or ω-position of a plurality of macromolecules of the polymers of the present invention according to formulae [II] or [IIa] to [IIc]. Any suitable polyol may be selected therefore. X or Y or both may especially be selected from the group consisting of polyethers of carbohydrates, especially of Ribose, polyethers of 1,1,1-trimethylolpropane, polyethers of glycerol, polyethers of saccharides or hydrogenated saccharides.

Further, Y may be selected from the group consisting of acrylamide, acrylates, aldehyde, alkyne, amine, aminooxy, azide, benzotriazole carbonate, carboxylic acid, chloroformate, cyanuric chloride, dithioester, epoxide, fluorescein, hydrazide, imidazoyl formate, iminoester, isocyanate, maleimide, mesylate, methacrylate, NHS ester, nitrobenzoate, nitrophenylcarbonate, succinimidyl active ester, succinimidyl carbonate, N-succinimidyl carbonate, succinimidyl succinate, thiocarbonate, thiol, thiol carboxylic acid, tosylate, triflate, vinyl sulfone and xanthate.

It is especially preferred that X is selected from the group consisting of hydrogen, alkyl, hydroxy, sulfanyl, C1-C10-alkoxy, C1-C10-thioalkoxy, amino, amino-C1-C10-alkoxy, dibenzylamino-C1-C10-alkoxy, amide, N-heterocyclic carbenes and N-heterocyclic olefins. It is also especially preferred that Y is selected from the group consisting of hydrogen, hydroxy, alkoxy, -CH_2-C(=O)-R wherein R is as defined above, -CHO, alkylcarbonyloxy, alkyoxycarbonyloxy, amine, alkylamine, carboxamido, azide, halogen, sulfanyl, thioalkoxy and sulfonate. In addition, for any alkoxy rest defined herein for the residue X the corresponding thioalkoxy residue may be used, i.e. where a sulfur atom is present instead of the oxygen atom.

Most preferred are polymers of the present invention, where X and/or Y are selected from the group consisting of low molecular weight drugs, nanocarriers, liposomal structures, peptides, polypeptides, glycoproteins, polynucleotide, polysaccharides, lipid structures, liposomes, surfaces and interfaces, which are bonded directly by a covalent bond or by a spacer to the polymer. Nanocarriers usable in the present invention are for example selected from the group consisting of carbon nanotubes (CNT), dendrimers, gold nanorods, lipid nanoparticels, liposomes, micelles, nanocrystals, niosomes, polymeric nanoparticles (PNP), solid lipid nanoparticles (SLNs) and virus-based nanoparticles (VNP).

The polymers of the present invention have dispersities of 1.15 or less. They are suitable for applications where low dispersities are required, as for example in pharmaceutical, medical and biological applications. Dispersity of polymers in pharmaceutical, medical and biological applications is of great importance, as macromolecules of different molecular weight may behave differently in biological systems. They may for example differ in solubility in water, membrane permeability, crystallinity and renal clearance. Since a uniform behavior of all molecules is desired in medical applications, a low dispersity is often required. Most preferred are therefore polymers of the present invention that have a dispersity of 1.10 or less. This applies to all embodiments of the present invention. A dispersity of 1.10 or less is required for most medical and pharmaceutical applications. Most preferred are polymers of the present invention which have a dispersity that is lower than 1.08.

Preferred embodiments of the present invention are polyether polymers represented by the following formula [II]:

$$X\text{-}(CH_2CHR\text{-}O\text{-})_mCH_2CHR\text{-}Y \quad [II]$$

wherein residues R are independently from each other selected from the group consisting of hydrogen, methoxymethyl, ethoxymethyl, n-propoxymethyl and iso-propoxymethyl; 1 to 100% of the residues R are methoxymethyl; up to 50% of the residues R may be selected from the group consisting of ethoxymethyl, n-propoxymethyl and iso-propoxymethyl; with the proviso that at least one residue R is hydrogen, if at least one residue R is selected from the group consisting of ethoxymethyl, n-propoxymethyl and iso-propoxymethyl; X is selected from the group consisting of hydrogen, alkyl, hydroxy, sulfanyl, C1-C10-alkoxy, C1-C10-thioalkoxy, amino, amino-C1-C10-alkoxy, dibenzylamino-C1-C10-alkoxy, amide, N-heterocyclic carbenes and N-heterocyclic olefins; Y is selected from the group consisting of hydrogen, hydroxy, alkoxy, $-CH_2-C(=O)-R$ wherein R is as defined above, -CHO, alkylcarbonyloxy, alkyoxycarbonyloxy, amine, alkylamine, carboxamido, azide, halogen, sulfanyl, thioalkoxy, N-succinimidyl carbonate and sulfonate; X and/or Y may also be selected from the group consisting of low molecular weight drugs, nanocarriers, liposomal structures, peptides, polypeptides, glycoproteins, polynucleotide, polysaccharides, lipid structures, liposomes, surfaces and interfaces, which are bonded directly by a covalent bond or by a spacer to the polymer, m is in the range of from 19 to 999, characterized in that the dispersity is 1.15 or less. Especially preferred is N-succinimidyl carbonate.

An especially preferred embodiment of the present invention is a polyether polymer of the present invention, wherein X is alkoxy and Y is hydroxy. Further preferably X is a C1-C10-alkoxy group and Y is hydroxy and even more preferably X is a C1-C3 linear alkoxy group and Y is hydroxy. These embodiments are analogous to commercially available PEG derivates. Most preferred X is methoxy and Y is OH, which is analogous to mPEG.

As discussed in regard to the dispersity, a unified behavior of all molecules in drugs and excipients used in pharmaceutical and medical applications is preferred. The end-group fidelity of the polymers of the present invention may be determined by MALDI TOF or by a combination of MALDI TOF with ^1H NMR by known methods. The polymers of the present invention have preferably an end-group fidelity of at least 95 % in regard to the group X and more preferably of at least 98 %. In a further embodiment the polymers of the present invention have preferably an end-group fidelity of at least 95 % in regard to the group Y and more preferably of at least 98 %. Even more preferred are polyether polymers of the present invention, wherein the end-group fidelity of the polymer in regard to group X and group Y is at least 95% and most preferably of at least 98 %. Especially preferred are polyether polymers of the present invention, wherein the end-group fidelity of the polymer in regard to group X and group Y is at least 95% and the dispersity is 1.10 or less and most preferred wherein the end-group fidelity of the polymer in regard to group X and group Y is at least 98% and the dispersity is 1.10 or less.

As aforementioned, the polymers of the present invention have similar properties as PEG, especially in biological systems. The present polymers may therefore substitute PEG in most of his applications. The polymers of the present invention are especially designed for use in the pharmaceutical and medical field. They may also be used with the same benefits in veterinary medicine and in other biological applications. In these fields the polymers of the present invention can fulfill the same functions as PEG, but have reduced immunogenicity and antigenicity. Because of their irregular structure, they do not elicit a strong immune response. The inventive polymers show especially a low response to anti-PEG antibodies, as evidenced by ELISA tests. Conjugates used for masking drugs and other pharmaceutically active compounds usually comprise PEG in addition to a physiologically active compound or an adjuvant. The polymers of the present invention may be used instead of PEG in any such application. At the same time the immune response elicited by the present polymers will be weak or non-existent thereby resolving one of the main problems in the use of PEG.

A further embodiment of the present invention is therefore a conjugate comprising a polyether polymer of any of the preceding claims and a substrate. The conjugates of the present invention may in the following also be named polyether-conjugated substrates or polymer-conjugated substrates. In the conjugates of the present invention a polymer of the present invention is bonded to a substrate directly or indirectly by a covalent bond. The polymer of the present invention may be bonded to the substrate by a spacer, which constitutes an indirect bond. The substrate may be selected from the group consisting of a pharmaceutically active compound, an adjuvant, a surface and interfaces. The pharmaceutically active compound is preferably selected from the group consisting of low molecular weight drugs, peptides, polypeptides, proteins, glycoproteins, polynucleotides and polysaccharides. The adjuvant is preferably a vesicle or carrier, which are preferably used to carry a pharmaceutically active compound. The adjuvant is preferably selected from the group consisting of nanocarriers, liposomal structures, lipid structures and liposomes. Nanocarriers usable in the present invention are for example selected from the group consisting of carbon nanotubes (CNT), dendrimers, gold nanorods, lipid nanoparticels, liposomes, micelles, nanocrystals, niosomes, polymeric nanoparticles (PNP), solid lipid nanoparticles (SLNs) and virus-based nanoparticles (VNP). In a further preferred embodiment the substrate is selected from the group consisting of low molecular weight drugs, nanocarriers, liposomal structures, peptides, polypeptides, proteins, glycoproteins, polynucleotides, polysaccharides, lipid structures, liposomes, surfaces and interfaces. Also in these embodiments the substrate may be bonded directly by a covalent bond or by a spacer to the polymer. Especially preferred are conjugates of the present invention with

bovine serum albumin.

The polymer of the present invention may be bonded to the substrate directly by a covalent bond or by a spacer or any kind. Preferably a hydroxy-residue at the ω-terminal of the polymer of the present invention is used to bond a substrate or a spacer to the polymer. This is most economical, as the polymers of the present invention where X is an inert group and Y is OH can be most easily be prepared (see Examples). The conjugation of a substrate to the OH group at the ω-terminal end of PEG is well established. The same processes may be used for the polymers of the present invention. The substrate may however also be bonded to the α-terminal of the polymer. The polymers of the present invention can also be bonded to more than one substrate. This can be done by use of the α-terminal and the ω-terminal of the polymer and by using functional end groups of the polymer or spacer that can bond to a plurality of substrates. This may also be achieved by use of co-monomers with functional groups to which a substrate may be bonded. The bond between the polymers of the present invention and the substrate may be prepared by any means currently used for bonding PEG to substrates. It is also possible to bond a plurality of macromolecules of the polymers of the present invention to one substrate. This is especially useful for vesicle of all kinds including liposomes.

Typical examples for PEG conjugates are the lipid nanoparticles that are essential for vaccines against Covid-19 of the firms BioNTech SE and Pfizer Inc. and Moderna. It comprises a PEG conjugate of lipids, and the lipid nanoparticles (LNPs) are used to encapsulate and protect mRNA, which is the pharmaceutically active substance. The PEG in these conjugates may be substituted by the polymers of the present invention, thereby retaining the effects of the PEG polymer in the conjugate and at the same time reducing the immune response to the conjugate. A further vaccine of this kind is the Covid-19 vaccine of Curevac. Further drugs that comprise PEG conjugates wherein the PEG could be substituted by the present polymers are listed in the following.

Table 1

Trade names	Chemical Structure	Indication
Jivi®	60k-PEG recombinant Factor VII antihemophilic factor	Hemophilia A
Palynziq®	2K-PEG-rhu-Phenylalanine ammonia-lyase, Pegvaliase-pqpz	Phenyl-ketonuria
Adynovate®	20K-PEG-Factor VIII Antihemophilic Factor VIII	Hemophilia A
Revolixys® kit	40K-PEG-RNA aptamer + reverse agent, Factor-IXa blocker, Pegnivacogin /Anivamersen	Anti-coagulation

Onicyde®	2K-PEG-Liposomal irinotecan hydrochloride trihydrate	Metastatic pancreatic cancer
Plegridy®	20k PEG-Interferon β-1a	Relapsing from multiple sclerosis
Movantic®	<1k PEG-Naloxegol	Opioid-induced constipation
Omontys®	40K-PEG-Erythropoietin-mimetic peptide, Peginesatide	Anemia associated with chronic kidney disease
Sylatron®	12K-PEG-Interferon α-2b	Melanoma
Krystexxa®	10k-PEG-Uricase, Pegloticase	Gout
Cimzia®	40k-PEG-Certolizumab	Rheumatoid arthritis, Crohn's disease, Axial spondyloarthritis and psoriatic arthritis
Mircera®	30K-PEG- erythropoietin (epoetin) β	Anemia associated with chronic kidney disease
Macugen®	40K-PEG-anti-VEGF aptamer, Pegaptanib	Age-related macular degeneration
Somavert®	5K-PEG-rhuGH (human growth hormone), Pegvisomant	Acromegaly
Neulasta®	20K-PEG-Granulocyte colony stimulating factor, Pegfilgrastim	Neutropenia
Pegasys®	40K-PEG-interferon α-2	Hepatitis C und B
PegIntron®	12K-PEG-interferon α-2b	Hepatitis C und B
Doxil®/Caelyx®	2K-PEG-Liposomal doxorubicin HCl	Cancer
Oncaspar®	5K-PEGylated L-asparaginase, Pegaspargase	Acute lymphoblastic leukemia
Adagen®	5K-PEG-adenosine deaminase (bovine), Pegademase	Severe combined immunodeficiency disease (SCID)
Irinotecan®	PEGylated liposomal irinotecan hydrochloride trihydrate	Metastatic pancreatic cancer
Lonquez®	20k PEG-rhG-CSF	Neutropenia
Jintrolong®[1]	Branched 40k PEG hGH	hGH deficiency
Neulapeg®	20k-PEG rhG-CSF mutein	Neutropenia
Rebinyn®/ Refixia®	Branched 40k PEG Recombinant factor VIII	Hemophilia B
Asparlas®	5k-PEG L-Asparaginase	Acture lymphoblastic leukemia
Revcovi®	5k-PEG Recombinant B-domain truncated factor VIII	Hemophilia A
Besremi®[3]	Branched 40k PEG Proline-interferon α-2b	Polycythemia vera
PEGPH20®[3]	30k-PEG recombinant human hyaluronidase	Pancreatic cancer
Pegargiminase	20k PEG Arginine deiminase Interleukin-2	Hepatocellular carcinoma
NKTR-214	Branched PEG-20k Fmoc-succinimidyl carbonate	Melanoma, rencal cell carcinoma
PRX-201[3]	Bifunctional PEG2k α-Galactosidase A	Fabry disease
Peginterferon lambda-1a	20k PEG recombinant interferon lambda-1a	Hepatitis C and B[2], Hepatitis D[3]
Abicipar pegol	20k PEG anti-VEGF DARPin	Neovascular age related macular degeneration
TransCon GH®[3]	Four-arm-40PEG spacer hGH	Growth hormone deficiency
AM0010[2]	30k PEG-Interleukin-10	Metastatic pancreatic cancer

Rolontis®[3]	Bifunctional PEG rhG-CSF	Neutropenia
Efpeglenatide[3]	Bifunctional PEG Exendin-4 (glucagon-like peptide-1 receptor agonist)	Type-2 diabetes mellitus
Pegbelfermin[2]	30k PEG fibroblast growth factor-21 mutein	Fibrosis, liver disorders, nonalcoholic steatohepatitis, type 2 diabetes mellitus
Imrestor® (veterinary use)	20k PEG recombinant bovine G-CSF mutein	Reducing risk of clinical mastitis
Pegfilgrastim biosimilars: Fulphila (Mylan®) Lapelga/Pelgraz (Apobiologix®), Udenyca (Coherus Biosciences®), Pelmeg (Mundipharma®), Ziextenzo (Sandoz®)	20K-PEG-Granulocyte colony stimulating factor, Pegfilgrastim, rhG-CSF	Neutropenia
Esperoct®	Branched-PEG40k-SA-CMP, enzymatic glycopegylation at O-glycan on Ser-750	Hemophilia A

[1] only in China
[2] Phase II
[3] Phase III

Process for the preparation of a polyether polymer of the present invention, by anionic ring-opening copolymerization (AROP) comprising the steps of:

- Providing an anion An^-,
- Adding at least one monomer of the formula  -R, wherein R is as defined as described for any of formulae [I] or [II],
- Allowing the polymerization to proceed at a temperature in the range of -10 to 90 °C,

wherein the monomer comprises less than 1 wt% of epichlorohydrin.

In the process of the present invention the anion An^- must be an anion suitable for anionic ring-opening copolymerization (AROP). The expert in the art can easily choose among the known anions for this purpose. The An^- anion may be selected from the groups consisting of alkyl anion, hydride, OH^-, $alkoxy^-$, SH^-, $thioalkoxy^-$, amine anion, amide anion, imide anion and combinations thereof. Alkyl anions and hydride anions may be provided in the form of metal alkyl or metal hydride compounds. The alkoxy anion and the thioalkoxy anion may be the corresponding anion with the same structure as any of the alkoxy groups and aryloxy groups and aralkoxy groups defined herein for the residue X. Preferably however

the alkoxy anion and the thioalkoxy anion are not tertiary alkoxy anions. The imide anion is preferably a phthalimide anion. Polymers of the Formulae [Ia], [Ic], [IIa] and [IIc] may be prepared by first adding the corresponding amount of ethylene oxide to the anion An^- and allowing the polymerization to proceed at a temperature in the range of -10 to 90 °C until all of the ethylene oxide is consumed. Subsequently the steps of adding least one monomer of the formula  -R, and allowing the polymerization to proceed at a temperature in the range of -10 to 90 °C are performed. In this manner the repeating units adjacent to the α-terminal of the polymers of the present invention are provided with exactly the same structure as PEG. Polymers of the Formulae [Ia], [Ic], [IIa] and [IIc] may also be prepared by use of anions of the formulae $X\text{-}(CH_2CH_2\text{-}O\text{-})_a^-$, wherein a is as defined for any of the Formulae [Ia], [Ic], [IIa] and [IIc] and X is any residue as defined herein for X. This is the preferred method. Especially preferred is the use of such anions of the formulae $X\text{-}(CH_2CH_2\text{-}O\text{-})_a^-$, in which X is alkyl, alkoxy, dialkylamin anion or $(RCO)_2N^-$. Even more preferred is the use of anions selected from the group consisting of $MeOCH_2CH_2O^-$, $MeO(CH_2CH_2O)_2^-$, $BenzylOCH_2CH_2O^-$, $BzO(CH_2CH_2O)_2^-$, $(Bz)_2N\text{-}CH_2CH_2O^-$, $(Bz)_2N\text{-}(CH_2CH_2O)_2^-$, phthalimide-$CH_2CH_2O^-$, phthalimide-$(CH_2CH_2O)_2^-$, wherein Me is methyl and Bz is benzyl. Most preferred are $MeO(CH_2CH_2O)_2^-$, $BzOCH_2CH_2O^-$ and $(Bz)_2N\text{-}CH_2CH_2O^-$.

Further, in a final step of the preparation, addition of a small amount of pure EO is possible to ensure primary hydroxyl end groups for the ω-terminal of the polymer that can undergo all established coupling strategies to therapeutic entities. This leads to polymers of the present invention with Formulae [Ib], [Ic], [IIb] and [IIc].

The counter ion to the An^- anion is preferably selected from the group consisting of Na^+, K^+ and Cs^+. The anion An^- may be provided in an inert solvent. The solvent is preferably a non-protic solvent and most preferably cimethyl sulfoxide (DMSO). Also preferably the reaction is performed in the same solvent.

Anionic ring-opening polymerizations with alkyl glycidyl ethers are more prone to undergo chain transfer reactions as follows:

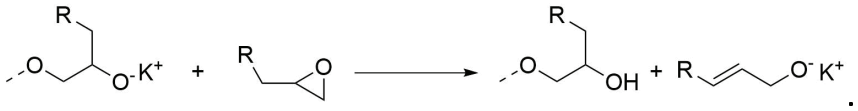

These side reactions increase with the temperature. Therefore, high molecular weight polymers can only be obtained, if the reaction temperature is not above 90°C. The chain transfer reaction results in a broad distribution of molecular weight and therefore in a high dispersity. Therefore, lower polymerization temperatures also provide polymers of the

present invention with lower dispersity. On the other hand, alkyl glycidyl ethers are as reactive in the anionic ring-opening polymerization as ethylene oxide. For this reason the polymerization may be performed at temperatures as low as -10°C. Preferably the polymerization is performed at a temperature in the range of 10 to 70°C and more preferred at a temperature in the range of 10 to 60°C.

A further problem in anionic ring-opening polymerizations is that commercially available alkyl glycidyl ethers are prepared from epichlorohydrin. Part of the epichlorohydrin remains in the alkyl glycidyl ether. Presence of alkyl glycidyl ethers leads to termination reactions as follows:

This in turn leads to low molecular weights and high dispersity of the product. The polymers of the present invention are therefore only accessible by reaction temperatures of -10 to 90°C or less and by the use of alkyl glycidyl ethers that comprise less than 1 wt% of epichlorohydrin. Preferably the alkyl glycidyl ethers comprise less than 0.5 wt% of epichlorohydrin and more preferably less than 0.1 wt%. Most preferably the alkyl glycidyl ether are free of epichlorohydrin. Removal of epichlorohydrin from the glycidyl methyl ether to the extent necessary is impossible, because the glycidyl methyl ether and epichlorohydrin have similar boiling points, e.g. epichlorohydrin 117.9°C, glycidyl methyl ether 110°C. Procedures for the preparation of epichlorohydrin free alkyl glycidyl ethers is provided in Example 1 of the present invention.

Furthermore, high temperatures also lead to side reactions of the starting anion An^- or the group X of the living polymer. Limitation of the temperature in the aforementioned range therefore also improves the end-group fidelity at the α-terminal of the polymers of the present invention and allows for end-group fidelities of 95% or more of the X residue. Other known methods for the polymerization of the alkyl glycidyl ethers do not provide the low dispersity required for the present polymers. They also do not allow for the same high end-group fidelity.

In order to provide random copolymers or the present invention, it is necessary to add at least two different kinds of monomers to the anion. The reactivity ratio for both alkyl glycidyl ether employed and ethylene oxide is in the range of 0.7 to 1.3. For glycidyl methyl ether and ethylene oxide the reactivity ratio is in the range of 0.98 to 1.02. This results in almost ideally random copolymers. Other forms of copolymers i.e. with a block structure, block like structure or a tapered or gradient structure can be prepared according to known

methods. Block copolymers can easily be prepared by subsequent additions of different monomers to the living polymer. Therefore, a process of the present invention is preferred, wherein the step of adding at least one monomer and the step of allowing the polymerization to proceed are repeated at least one time, whereby at least one different monomer is used than the first time.

A further embodiment of the present invention is the use of the polyether polymers of the present invention for the preparation of a conjugate of the polymers with a substrate. The substrate is as defined herein for the conjugates of the present invention. The substrate is preferably a bioactive compound. There is a well-developed chemistry for the preparation of conjugates of PEG, which is known to the expert in the art. The same chemistry may be used for the preparation of a conjugate of the present invention. Preferred is a use of the present invention, for the preparation of conjugated lipids for use in vaccines, in particular based on lipid nanoparticles. These nanoparticles are preferably nanoparticles, as used against COVID-19. Preferred are conjugates of polymers of the present invention with bovine serum albumin (BSA). Especially preferred are conjugates with polymers of the present invention where the y group of the polymer is a N-succinimidyl carbonate group. Even more preferred are conjugates of the present polymer where bovine serum albumin in conjugates by means of such a group Y to a polymer of the present invention. Conjugation of α-BzO-ω-N-succinimidyl carbonate-P(EG-co-GME) to bovine serum albumin if most preferred.

An additional embodiment for the present invention concerns the preparation of conjugates of the present invention. As discussed above, the conjugates may be prepared by any known process for the preparation of conjugates of PEG. The present invention provides additionally a process, where firstly the process for the preparation of the polymers of the present invention is performed and then a substrate is added to the living polymer, wherein the substrate has a functional group that reacts with the living polymer to form a conjugate.

Brief description of the figures:

Figure 1: Figure 1 shows the results of ELISA test of three of the polymers of the present invention and mPEG.

Figures 2 to 8: These figures show the SEC traces of polymers of the present invention and Figure 8 shows in addition the SEC trace of commercially available mPEG.

Figure 9: Figure 9 shows the ^{1}H NMR spectrum of α-BzO-P(EG0.51-co-GME0.49).

Figure 10: Figure 10 shows the MALDI-TOF spectrum of α-BzO-P(EG0.51-co-GME0.49).

Figure 11: Figure 11 shows cloud point of α-BzO-P(EG0.51-co-GME0.49).

Figure 12: Figure 12 shows the MALDI-TOF spectrum of α-DBzN-EtO-PGME, i.e. a homopolymer of the present invention.

Figure 13: Figure 13 shows the MALDI-TOF spectrum of α-MeO-P($PEG_{0.88}$-*b*-$PGME_{0.22}$), i.e. a block copolymer of the present invention.

Figure 14: Figure 14 shows the MALDI-TOF spectrum of α-BzO-ω-Ts-P($EG_{0.93}$-*co*-$GME_{0.07}$), i.e. a copolymer of the present invention that has been further functionalized at the ω-terminal ending.

Figure 15: Figure 15 shows the decreasing ^{1}H NMR signals of monomers during the preparation of a polymer of the present invention.

Figure 16: Figure 16 shows the result of a study of the relative reactivity of ethylene oxide and glycidyl methyl ether in the anionic ring opening polymerization.

Examples:

Reagents:

Chemicals were purchased from TCI, Acros Organics, Roth, Sigma Aldrich and Honeywell, unless otherwise noted. Ethylene oxide was obtained from Air Liquide. Deuterated solvents were purchased from Deutero GmbH. THF was flashed over basic aluminum oxide before usage. Glycidyl methyl ether was dried over CaH_2 and cryo-transferred before the polymerizations.

Measurements:

^{1}H and ^{13}C NMR spectra were recorded on a Bruker Avance III HD 300 spectrometer with 300 MHz and referenced internally to residual proton signals of the deuterated solvent.

Size-exclusion chromatography measurements were performed with dimethylformamide (DMF with 1 g/L LiBr) as the mobile phase (flow rate 1 mL/min) on 2-hydroxyethylmethacrylat (HEMA) 300/100/40 columns at 50 °C. Polymer concentrations were 1 mg/mL. Calibration was carried out using poly(ethylene glycol) standards (from Polymer Standard Service, Mainz, Germany).

Differential scanning calorimetry (DSC) measurements were carried out in the temperature range of -100 to 100 °C with a heating rate of 10 K/min at a PerkinElmer DSC 8500. The

thermal history of the samples was excluded via two cooling and two heating cycles. For each sample, the glass transition and the melting temperatures were obtained from the second heating curve.

MALDI-ToF MS measurements were carried out at a Bruker autoflex maX MALDI-TOF/TOF. The potassium salt of trifluoroacetic acid and trans-2-[3-(4-tert-Butylphenyl)-2-methyl-2-propenylidene]malononitrile (DCTB) were utilized as ionization salt and matrix, respectively.

Example 1: Synthesis of Glycidyl methyl ether (GME)

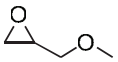

a) Allyl methyl ether (10.0 g, 139 mmol) was dissolved in 274 mL dichloromethane (DCM) and m-chloroperoxybenzoic acid (m-CPBA, 70%, 37.6 g, 153 mmol (based on m-CPBA)) was added to the solution. After stirring overnight, the solution was filtrated and slowly concentrated under reduced pressure. Crude glycidyl methyl ether was separated from solid impurities via cryo-transfer. Slow evaporation of residual dichloromethane in vacuo gave pure glycidyl methyl ether as a colorless liquid; Yield 41%.

b) 1-Chloro-3-methoxy-propan-2-ol (3.00 g, 2.56 mL, 24.1 mmol) and anhydrous sodium sulfate (1.02 g, 7.23 mmol) were added to a flask equipped with a magnetic stirrer and cooled with a water bath. Finely grounded sodium hydroxide (1.25 g, 31.3 mmol) was added under stirring. After complete reaction (TLC control) the crude product was cryo-transferred in vacuo from the reaction flask and dried over CaH2 under cooling. After an additional cryo-transfer, GME was obtained as a colorless liquid with a yield of 93 %.

Example 2: General procedure for the preparation of random copolymers
Synthesis of α-BzO-P(EG-co-GME)

$$Ph\text{-}CH_2\text{-}O\text{-}CH_2\text{-}CH_2\text{-}O\text{-}[CH_2\text{-}CH_2\text{-}O\text{-}]_{98}\text{-}[CH_2CH(CH_2\text{-}O\text{-}CH_3)\text{-}O\text{-}]_8H$$

Potassium tert-butoxide (13.0 mg, 118 µmol) was dissolved in a tetrahydrofuran (THF) - water mixture and transferred into a reaction flask, equipped with a Teflon stopcock and a septum. 2-Benzyloxy-ethanol (20.0 mg, 18.7 µL, 131 µmol) was dissolved in benzene and added to the reaction flask. After slow evaporation of the solvent, the resulting solid was dried at 60 °C under high vacuum overnight. The residue was dissolved in dimethyl sulfoxide (DMSO, 5 mL) and the solution was cooled to -78 °C. Glycidyl methyl ether (119 mg, 122 µL, 1.35 mmol) was added via syringe and ethylene oxide (537 mg, 553 µL,

12.2 mmol) was cryo-transferred into the reaction flask. The solution was heated to 55 °C and stirred for 24 h under vacuum. Afterwards, the solution was poured into excess chloroform and the organic phase was extracted against water (3 times) and brine, dried over $MgSO_4$ and filtrated. After evaporation of the solvent α-BzO-P(EG0.92-co-GME0.08) was obtained as a colorless solid; yield quantitative.

The data of the polymer produced can be found in Tables 2 to 4 below (see entry b). Further examples have been prepared according to this procedure with varying amounts of the monomers (see Tables 2 to 3, entries a to d, f and g). Further, α-MeO-P(EG-co-GME) and α-DBzN-P(EG-co-GME) were prepared according to the same procedure with diethylene glycol monomethyl ether and N,N-dibenzyl-2-aminoethanol as initiators, respectively, instead of benzyloxy-ethanol (entries h and i of Tables 2 to 4).

Example 3: Synthesis of

$$Ph\text{-}CH_2\text{-}O\text{-}CH_2\text{-}CH_2\text{-}O\text{-}[CH_2\text{-}CH_2\text{-}O\text{-}]_{51}\text{-}[CH_2CH(CH_2\text{-}O\text{-}CH_3)\text{-}O\text{-}]_{49}H$$

Cesium hydroxide monohydrate (28.0 mg, 118 µmol) was dissolved in a THF-water mixture and transferred into a reaction flask, equipped with a Teflon stopcock and a septum. 2-Benzyloxy-ethanol (20.0 mg, 18.7 µL, 131 µmol) was dissolved in benzene and added to the reaction flask. After slow evaporation of the solvent, the resulting solid was dried at 60 °C under high vacuum overnight. The residue was dissolved in DMSO (5 mL) and the solution was cooled to -78 °C. GME (367 mg, 374 µL, 4.16 mmol) was added via syringe and EO (183 mg, 189 µL, 4.16 mmol) was cryo-transferred from a graduated ampule into the reaction flask. The solution was stirred for 48 h at room temperature under vacuum. Afterwards, the solution was poured into excess chloroform and the organic phase was extracted against water (3 times) and brine, dried over $MgSO_4$ and filtrated. $P(EG_{0.51}\text{-}co\text{-}GME_{0.49})$ was obtained in quantitative yield as a viscous liquid after evaporation of the solvent and drying under high vacuo. The data of the product can be found in Tables 2 and 3, entry e.

Example 4: Synthesis of glycidyl methyl ether homopolymer

$$\alpha\text{-}Bz_2NCH_2CH_2O(CH_2CH(CH_2OCH_3)\text{-}O)_nH$$

Cesium hydroxide monohydrate (25.0 mg, 149 µmol) was dissolved in a THF-water mixture and transferred into a reaction flask, equipped with a Teflon stopcock and a septum. N,N-Dibenzyl-2-aminoethanol (40.0 mg, 166 µmol) was dissolved in benzene and added to the

reaction flask. After slow evaporation of the solvent, the resulting solid was dried at 60 °C under high vacuum overnight. The residue was dissolved in DMSO (5 mL) and the solution was cooled to -78 °C. Glycidyl methyl ether (GME, 660 mg, 670 µL, 7.46 mmol) was added via syringe. The solution was stirred for 48 h at room temperature under vacuum. Afterwards, the solution was poured into excess chloroform and the organic phase was extracted against water (3 times) and brine, dried over $MgSO_4$ and filtrated. Poly(glycidyl methyl ether) (PGME) was obtained in quantitative yield as a viscous liquid after evaporation of the solvent and drying under high vacuo. The data of this polymer can be found in Table 2 and 3, entry j.

Example 5: Synthesis of α-BzO-P(EG-co-EGE)

$$Ph\text{-}CH_2\text{-}O\text{-}CH_2\text{-}CH_2\text{-}O\text{-}[CH_2\text{-}CH_2\text{-}O\text{-}]_{0.92}\text{-}[CH_2CH(CH_2\text{-}O\text{-}CH_2\text{-}CH_3)\text{-}O\text{-}]_{0.08}H$$

Potassium tert-butoxide (13.0 mg, 118 µmol) was dissolved in a THF-water mixture and transferred into a reaction flask, equipped with a Teflon stopcock and a septum. 2-Benzyloxy-ethanol (20.0 mg, 18.7 µL, 131 µmol) was dissolved in benzene and added to the reaction flask. After slow evaporation, the resulting solid was dried at 60 °C under high vacuum overnight. The residue was dissolved in DMSO (5 mL) and the solution was cooled to -78 °C. Ethyl glycidyl ether (EGE, 270 mg, 260 µL, 2.50 mmol) was added via syringe and ethylene oxide (440 mg, 450 µL, 9.99 mmol) was cryo-transferred from a graduated ampule into the reaction flask. The solution was heated to 55 °C and stirred for 24 h under vacuum. Afterwards, the solution was poured into excess chloroform, and the organic phase was extracted against water (3 times) and brine, dried over $MgSO_4$ and filtrated. P(EG0.92-co-EGE0.08) was obtained as a colorless solid after evaporation of the solvent and drying under high vacuo; yield > 96%. Table 2 and 3, entry k shows the data of this product.

Example 6: Synthesis of mPEG-b-PGME

$$Me\text{-}O\text{-}[CH_2\text{-}CH_2\text{-}O\text{-}]_{0.78}\text{-}[CH_2CH(CH_2\text{-}O\text{-}CH_3)\text{-}O\text{-}]_{0.22}H$$

Potassium tert-butoxide (13.0 mg, 118 µmol) was dissolved in a tetrahydrofuran (THF) - water mixture and transferred into a reaction flask, equipped with a Teflon stopcock and a septum. Methoxypoly(ethylene glycol) (mPEG, M_n 2 kg/mol; 250 mg, 125 µmol) was dissolved in benzene and added to the reaction flask. After slow evaporation, the residue was dried at 80 °C under high vacuum overnight. The residue was dissolved in dimethyl sulfoxide (DMSO, 5 mL) and the solution was cooled to -78 °C. Glycidyl methyl ether (253 mg, 258 µL, 2.88 mmol) was cryo-transferred into the reaction flask. The solution was

heated to 55 °C and stirred for 24 h under vacuum. Afterwards, the solution was poured into excess chloroform and the organic phase was extracted against water (3 times) and brine, dried over $MgSO_4$ and filtrated. mPEG-b-PGME 4k was obtained as a colorless solid after precipitation in ice-cold diethyl ether; yield quantitative. Table 2 and 3, entry j shows the data for this polymer.

Example 7: Synthesis of α-BzO-ω-Ts-P(EG-co-GME)

$$Ph\text{-}CH_2\text{-}O\text{-}CH_2\text{-}CH_2\text{-}O\text{-}[CH_2\text{-}CH_2\text{-}O\text{-}]_{98}\text{-}[CH_2CH(CH_2\text{-}O\text{-}CH_3)\text{-}O\text{-}]_8Ts$$

α-BzO-P(EG-co-GME) (50.0 mg, 4.6 µmol) from Example 2 was dissolved in dichloromethane (DCM) in a flask equipped with a reflux condenser and the solution was cooled to 0 °C. After addition of triethylamine (2.32 mg, 3.18 µL, 22.9 µmol), tosyl chloride (4.37 mg, 22.9 µmol) was added in portions to the solution. The ice-bath was removed and the solution was refluxed overnight. The reaction mixture was extracted with saturated $NaHCO_3$, water and brine, dried over $MgSO_4$ and filtrated. After precipitation in diethyl ether and drying in vacuo, α-BzO-ω-Ts-P(EG-co-GME) was obtained as a white solid; yield quantitative. Tables 2 and 3, entry m shows the data for this polymer.

Example 8: Synthesis of α-BzO-ω-N-succinimidyl carbonate-P(EG-co-GME)

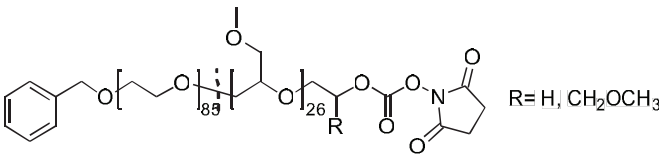

N,N'-disuccinimidyl carbonate (3.5 mg, 13.8 µmol) is added to a stirred solution of α-BzO-P(EG-co-GME) (50.0 mg, 4.6 µmol) from Example 2 in dry CH_3CN (1 ml) at room temperature for 18 h. The reaction mixture was dissolved in dichloromethane extracted with a saturated $NaHCO_3$, water and brine, dried over $MgSO_4$ and filtered. The solvent was removed under reduced pressure and the polymer dried under vacuum. The product was obtained as a white solid; yield quantitative.

Example 9: Conjugation of α-BzO-ω-N-succinimidyl carbonate-P(EG-co-GME) to bovine serum albumin (BSA).

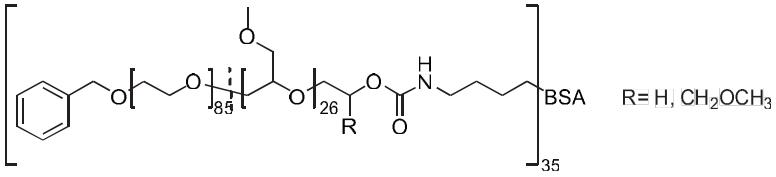

Bovine serum albumin (5 mg, 0.07 µmol) and α-BzO-ω-N-succinimidyl carbonate-P(EG-co-GME) (16.9 mg, 2.6 µmol) from Example 8 were stirred in phosphate-buffered saline (PBS buffer) for 1 h. The unreacted polymer was removed by dialysis in deionized water with a 25 kDa membrane filter. The conjugate was then dried by lyophilization and obtained in quantitative yield. In the preparation of this conjugate, the outer lysing group (30-35) are targeted for the conjugation.

Example 10: Competitive Enzyme-linked Immunosorbent Assay (ELISA)

The interaction of the copolymer samples entry c, d and e were evaluated by a competitive PEG ELISA kit using a murine monoclonal, horseradish peroxidase conjugated anti PEG antibody (HRP anti-PEG) (Life diagnostics, West Chester, PA, USA). Samples of concentrations ranging from 0 to 4600 µg ml-1 were prepared in dilution buffer. Additionally, mPEG with a molecular weight of 5000 g mol-1 was utilized as internal standard for comparison. 50 µl of each prepared sample was dispensed to a PEG pre-coated 96-well plate and 50 µl of HRP anti-PEG was added to each well. The solutions were incubated for 1h at 25 °C with a micro-plate shaker and then washed six times with 400 µl of wash buffer per each well. After removal of residual droplets, 100 µl of 3,3′,5,5′-Tetramethylbiphenyl-4,4'-diamine was added to each well and the solutions were mixed on a micro-plate shaker for 20 min. The reaction was stopped by addition of 100 µl of stop solution and the absorbance at 450 nm was read within 5 minutes.

Analysis of ELISA Data: The determined absorbance values were normalized to visualize the percent of maximal binding. The sample concentrations were transformed to a function of $\log_{10}$. The sigmoidal fits were calculated using the following equation with a representing the upper, b the lower limit, c the inflection point and d the hill slope.

$$y = a + (b-a) / 1 + 10^{(c-x)*d}$$

Example 11: Kinetic of the Synthesis of α-BzO-P(EG-co-GME)

The synthesis of α-BzO-P(EG-co-GME) was repeated in fully deuterated DMSO for an online

in situ ^{1}H NMR kinetic measurement. 95 mg glycidyl methyl ether (95 µl, 1.1 µmol) and 32 mg ethylene oxide (33 µl, 7.1 µmol), i.e. 60% glycidyl methyl ether and 40% ethylene oxide where solved in fully deuterated DMSO. The consumption of ethylene oxide and glycidyl methyl ether over time was measured by ^{1}H-NMR spectroscopy. As measure for the ethylene oxide concentration, the signal of the protons of ethylene oxide at about 2.6 ppm was used. For glycidyl methyl ether the signals of the protons at the oxirane ring with absorptions at about 2.75 and 3.1 ppm were used. Figure 15 shows the decrease of the selected ^{1}H NMR signals of the two monomers over time. Figure 16 shows plot of monomer consumption Mx,t/Mx,t=0 versus total conversion. As can be seen, ethylene oxide and glycidyl methyl ether are consumed at exactly the same rate. This data shows that the copolymers of the present invention are almost ideal random copolymers.

Discussion of the results

Tables 2, 3 and 4 and Figure 1 to 15 show the properties of the polymers prepared. They are discussed in the following.

Table 2: Composition of polymers prepared

Entry (Example)	*Sample*	DP_{EO} NMR	DP_{GE} NMR	*mol*%$_{EO}$ NMR	*mol*%$_{GME}$ NMR
a (2)	α-BzO-P($EG_{0.96}$-*co*-$GME_{0.04}$)	108	4	96	4
b (2)	α-BzO P($EG_{0.92}$-*co*-$GME_{0.08}$)	98	8	92	8
c (2)	α-BzO P($EG_{0.84}$-*co*-$GME_{0.16}$)	112	21	84	16
d (2)	α-BzO P($EG_{0.76}$-*co*-$GME_{0.24}$)	85	26	76	24
e (3)	α-BzO P($EG_{0.51}$-*co*-$GME_{0.49}$)	35	33	51	49
f (2)	α-BzO P($EG_{0.96}$-*co*-$GME_{0.04}$)	223	10	96	4
g (2)	α-BzO P($EG_{0.93}$-*co*-$GME_{0.07}$)	175	13	93	7
h (2)	α-MeO-P($EG_{0.97}$-*co*-$GME_{0.03}$)	147	5	97	3
i (2)	α-DBzN-P($EG_{0.97}$-*co*-$GME_{0.03}$)	142	5	97	3
j (4)	α-DBzN-EtO-PGME	-	45	-	100
k (5)	α-BzO-P($EG_{0.85}$-*co*-$EGE_{0.15}$)	106	18	85	15

l (6)	α-MeO-PEG$_{0.88}$-*b*-PGME$_{0.22}$	50	14	88	22
m (7)	α-BzO-ω-Ts-P(EG$_{0.93}$-*co*-GME$_{0.07}$)	223	10	96	4

GE = Glycidyl ether; *DP* = degree of polymerization

Table 3: Characterization data of polymers prepared

Entry/ (Example)	*Sample*	$M_{n,NMR}$ [kg/mol]	$M_{n,MALDI}$ [kg/mol]	$M_{n,SEC}$ [kg/mol]	PDI_{SEC}	*End-group fidelity* MALDI
a (2)	α-BzO-P(EG$_{0.96}$-*co*-GME$_{0.04}$)	5.3	4.8	3.9	1.04	>99%
b (2)	α-BzO P(EG$_{0.92}$-*co*-GME$_{0.08}$)	5.2	5.3	4.5	1.05	>99%
c (2)	α-BzO P(EG$_{0.84}$-*co*-GME$_{0.16}$)	6.9	4.9	3.7	1.05	>99%
d (2)	α-BzO P(EG$_{0.76}$-*co*-GME$_{0.24}$)	6.0	5.2	3.8	1.06	>99%
e (3)	α-BzO P(EG$_{0.51}$-*co*-GME$_{0.49}$)	4.2	3.8	2.4	1.09	>99%
f (2)	α-BzO P(EG$_{0.96}$-*co*-GME$_{0.04}$)	10.9	8.5	7.5	1.08	>99%
g (2)	α-BzO P(EG$_{0.93}$-*co*-GME$_{0.07}$)	9.0	8.5	7.3	1.05	>99%
h (2)	α-MeO-P(EG$_{0.97}$-*co*-GME$_{0.03}$)	7.0	5.6	4.5	1.10	>99%
i (2)	α-DBzN-P(EG$_{0.97}$-*co*-GME$_{0.03}$)	6.9	5.1	4.0	1.08	>99%
j (4)	α-DBzN-EtO-PGME	4.2	4.0	2.7	1.05	>99%
k (5)	α-BzO-P(EG$_{0.85}$-*co*-EGE$_{0.15}$)	6.7	n.d.	4.2	1.09	n.d.
l (6)	α-MeO-PPEG$_{0.88}$-*b*-PGME$_{0.22}$	3.6	3.7	2.8	1.05	>99%
m (7)	α-BzO-ω-Ts-P(EG$_{0.93}$-*co*-GME$_{0.07}$)	11.1	8.8	n.d.	n.d.	>99%

M_n = molecular weight (number average molar mass), PDI = polydispersity.

Immunogenicity

As can be seen from Table 3, entries a to e show copolymers of the present invention which consisting of ethylene oxide repeating units and glycidyl methyl ether repeating units with about the same molecular weight, i.e. with an M_n of about 4 to 5 kg/mol. The amount of

glycidyl methyl ether repeating units is increasing from a to e from 4 % to 49% (see Table 1, entries a to e). Figure 1 shows the ELISA test results of polymers c to e and of commercially available mPEG. It shows the function of the normalized absorption at a wavelength of 450 nm versus the log10 function of the polymer concentration in nanograms per ml, therefore illustrating the anti-PEG antibody interaction with the investigated polymer concentrations. The ELISA data shows that a strong influence of an increasing concentration of alkyl side chains can be observed (it is important to note that the x-axis has a logarithmic scale). With increasing amount of GME incorporated into the polyether structure, significantly higher polymer concentrations are necessary to observe interactions between the copolymer and the APA. Remarkably, at 49 mol% of GME, absolutely no interaction between APA and the copolymer is present. This means that the respective copolymer cannot be detected by APAs, i.e. it is not immunogenic.

Dispersity

As can be seen from Table 3, entries a to l, all polymers of the present invention have a very low dispersity, i.e. 1.10 or lower. For visualization, the SEC traces of these polymers are shown in Figures 2 to 8. Figure 8 shown in addition the SEC trace of mPEG. It can clearly be seen that the present invention provides polymers with a very narrow molecular weight distribution.

(In Abbildung 2 sollte die rote Linie gegen eine gepunktete Linie oder ähnliches ausgetauscht werden. Die rote Linie wird sonst in der Patentschrift nicht von der schwarzen durchgezogenen Linie unterscheidbar sein.

Preparation and purity of the polymers of the present invention

Figure 9 shows the ^{1}H NMR spectrum of α-BzO P($EG_{0.51}$-*co*-$GME_{0.49}$), i.e. the polymer of Example 3 (entry e of Tables 2 and 3). The product is as obtained from Example 3, without further purification. As can be seen, the present method does not only provide polymers of narrow molecular weight distribution, but also very pure polymers without the need for laborious purification steps. This is an important feature for the use in pharmaceutical applications.

End-group fidelity

As can be seen from Table 3, the end-group fidelity for all polymers of the present invention is nearly 100%. Figure 10 shows the MALDI TOF mass spectrum of α-BzO P($EG_{0.51}$-*co*-

$GME_{0.49}$), i.e. the polymer of Example 3 (entry e of Tables 2 and 3) with potassium and sodium cations. The only peaks visible here are the peaks of the product molecule. There are no peaks form macromolecules with a different end group. This shows that end-group fidelity of the polymers of the present invention is very high. In addition, the spectrum confirms the narrow molecular weight distribution.

Solubility

Figure 4 shows the cloud point measurement of α-BzO-P(EG0.51-co-GME0.49), i.e. the polymer of Example 3 (entry e of Tables 2 and 3). The cloud point determines the temperature at which immiscibility in water / in aqueous solution is observed upon heating. As an example, for the copolymer with 49% GME, the cloud point can be observed at 95 °C, showing excellent water solubility of the Poly(GME-co-EO) copolymers. The homopolymer PEG shows a cloud point of ca. 100°C. All other copolymers of the present invention with 26-49% GME are in between PEG and this copolymer, showing cloud points of 96-100°C. For copolymers of 25 mol% GME incorporation and lower no cloud point was detected in water at temperatures ranging from 0 to 99 °C. Thus, GME copolymerization hardly affects water solubility, which is a feature of the similar structure of polyethylene glycol and methyl ethyl ether. This is an important feature of the polymers of the present invention as it shows that they can substitute PEG in aqueous systems without causing problems with phase separation or even precipitation.

Homopolymers

Figure 12 shows the MALDI-TOF spectrum of the homopolymer of Example 4. The spectrum shows not only that the polymer has a low dispersity, but also that it is free from impurities deriving different end groups. The fact that besides the peaks of the product only white noise is visible shows that the end-group fidelity is about 100 %. Glycidyl methyl ether homopolymer has so far not been produced with these specifications.

Comparison of dispersity of end group fidelity of the polymers of the present invention with that of mPEG

Figure 13 shows an overlay of MALDI TOF spectra of commercially available mPEG and a block copolymer of the present invention (polymer of Example 6 (entry l of Tables 2 and 3). As can be seen, a clear shift between the macroinitiator mPEG and entry l is observed, indicating a successful block copolymer synthesis. Absence of macroinitiator in the MALDI-ToF MS of entry l further proves quantitative block copolymer formation. This is further proven by a distance of the signals of 44 g mol-1.

Modification of end groups

Figure 14 shows the MALDI TOF spectrum of α-BzO-ω-Ts-P(EG-co-GME), i.e. the polymer of Example 7 (see Tables 2 and 3, entry). In this polymer the ω-end group OH has been modified to a tosyl group. As can be seen from the spectrum, the modified polymer has the same narrow molecular weight distribution and the same high end-group fidelity. This shows that the polymers of the present invention can be modified as known for PEG.

Crystallinity

Table 4 shows thermal properties of some of the polymers of Tables 2 and 3:

Sample	T_g [°C]	T_m [°C]	ΔH_{PEG} [J/g]	$X_{c,PEG}$
a	-56	46	88.63	0.45
b	-56	45	76.79	0.39
c	-59	37	56.26	0.29
f	-59	35	58.22	0.30
g	-61	7	32.62	0.17
k	-56	46	88.63	0.45
l	-59	45	80.16	0.41

T_g = Glass transition temperature; T_m = Melting point; ΔH_{PEG} = Enthalpy of fusion; X_c = Crystallinity (all measurements by DSC)I

As can be seen, crystallinity of the inventive polymers is low. This prevents for example accumulation of the polymers in the kidney or in the liver.

Claims

1. Polyether polymers represented by the following formula [I]:

$$-(CH_2CHR-O-)_n-$$

[I]

wherein

- residues R are independently from each other selected from the group consisting of hydrogen, methoxymethyl, ethoxymethyl, n-propoxymethyl and iso-propoxymethyl;
- 1 to 100% of the residues R are methoxymethyl;
- up to 50% of the residues R may be selected from the group consisting of ethoxymethyl, n-propoxymethyl and iso-propoxymethyl;
- with the proviso that at least one residue R is hydrogen, if at least one residue R is selected from the group consisting of ethoxymethyl, n-propoxymethyl and iso-propoxymethyl; and
- m is in the range of from 10 to 1000,

characterized in that

the dispersity is 1.15 or less.

2. Polyether polymer according to claim 1, wherein 5 to 95% of the residues R are hydrogen and 5 to 95% of the residues R are independently from each other selected from the group consisting of methoxymethyl, ethoxymethyl, n-propoxymethyl and iso-propoxymethyl.

3. Polyether polymer according to any of the preceding claims, wherein the polyether is a poly(glycidyl methyl ether-co-ethylene oxide) copolymer.

4. Polyether polymer according to any of the preceding claims, wherein 30 to 70% of the residues R are hydrogen and the remaining residues R are methoxymethyl.

5. Polyether polymer according to any of the preceding claims, wherein the polymer is a random copolymer.

6. Polyether polymers according to any of the preceding claims represented by the following formula [II]:

$X-(CH_2CHR-O-)_mCH_2CHR-Y$ [II]

wherein X is selected from the group consisting of hydrogen, alkyl, hydroxy, sulfanyl, C1-C10-alkoxy, C1-C10-thioalkoxy, amino, amino-C1-C10-alkoxy, dibenzylamino-C1-C10-alkoxy, amide, N-heterocyclic carbenes and N-heterocyclic olefins;
Y is selected from the group consisting of hydrogen, hydroxy, alkoxy, $-CH_2-C(=O)-R$ wherein R is as defined above, -CHO, alkylcarbonyloxy, alkyoxycarbonyloxy, amine, C1-C10-alkylamine, carboxamido, azide, halogen, sulfanyl, thioalkoxy, N-succinimidyl carbonate and sulfonate;
X and/or Y may also be selected from the group consisting of low molecular weight drugs, nanocarriers, liposomal structures, peptides, polypeptides, proteins, glycoproteins, polynucleotide, polysaccharides, lipid structures, liposomes, surfaces and interfaces, which are bonded directly by a covalent bond or by a spacer to the polymer,
m is in the range of from 9 to 999,

characterized in that

the dispersity is 1.15 or less.

7. Polyether polymer according to claim 6, wherein X is alkoxy and Y is hydroxy.

8. Polyether polymer according to any of claims 6 or 7, wherein end-group fidelity of the polymer in regard to group X and/or in regard to group Y is at least 95%.

9. Conjugate, comprising a polyether polymer of any of the preceding claims and a substrate.

10. Conjugate according to claim 9, wherein the substrate is selected from the groups consisting of low molecular weight drugs, nanocarriers, liposomal structures, peptides, polypeptides, proteins, glycoproteins, polynucleotides, polysaccharides, lipid structures, liposomes, surfaces and interfaces.

11. Process for the preparation of a polyether polymer according to any of claims 1 to 8, by anionic ring-opening copolymerization comprising the steps of:

- Providing an anion An^-,
- Adding at least one monomer of the formula  -R, where in R is as defined in any

of claims 1 to 8,

- Allowing the polymerization to proceed at a temperature in the range of -10 to 90 °C

wherein the monomer comprises less than 1 wt % of epichlorohydrin.

12. Process according to claim 11, wherein the step of adding at least one monomer and the step of allowing the polymerization to proceed are repeated at least one time, whereby at least one different monomer is used than the first time.

13. Process according to any of claims 11 or 12, wherein the counter ion to the An^- anion is selected from the group consisting of Na^+, K^+ and Cs^+.

14. Use of the polyether polymers according to any one of claims 1 to 8 for the preparation of a conjugate of the polymers with a bioactive compound.

15. Use according to claim 14 for the preparation of conjugated lipids for use in vaccines, in particular based on lipid nanoparticles, wherein these nanoparticles are preferably nanoparticles, as used against COVID-19.

Abstract

The present invention concerns polyether polymers represented by the following formula [I]:

$$-(CH_2CHR\text{-}O\text{-})_m-$$

[I],

wherein residues R are hydrogen or C1-C3 alkoxymethyl, 1 to 100 % are methoxymethyl and up to 50% of R may be C2-C3 alkoxymethyl with the proviso that at least one R is hydrogen, if at least one R is C2-C3 alkoxymethyl; and m is in the range of from 10 to 1000, wherein the dispersity is 1.15 or less. The invention further concerns a process for their preparation, conjugates thereof and the use thereof.

2020-104 UMZ

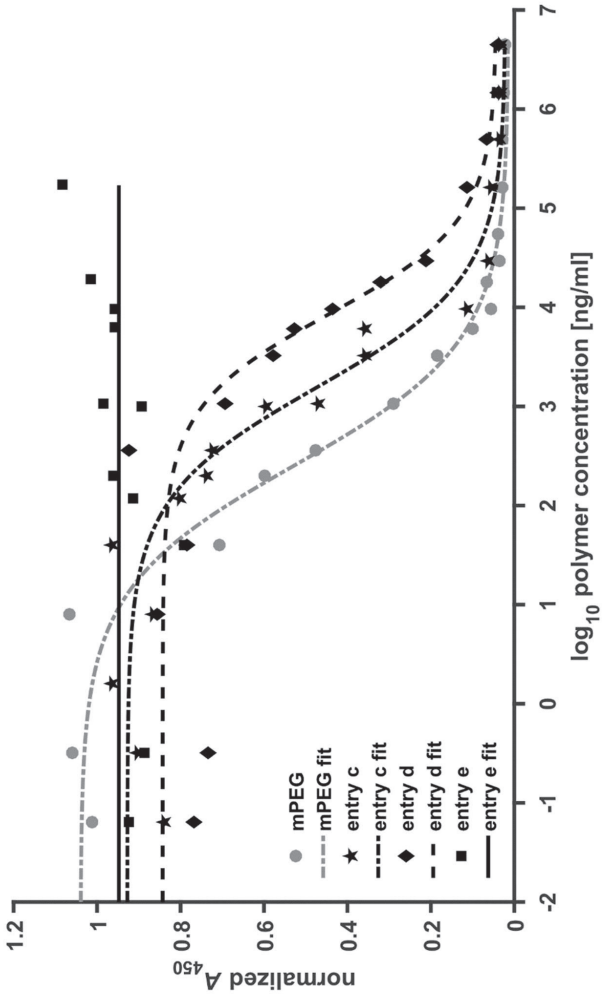

Figure 1

1

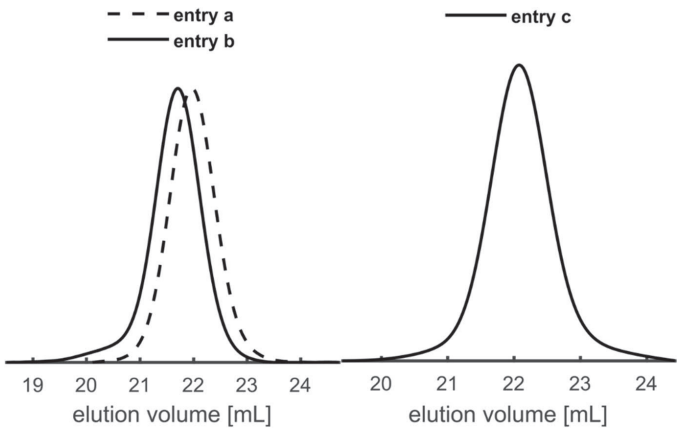

Figure 2

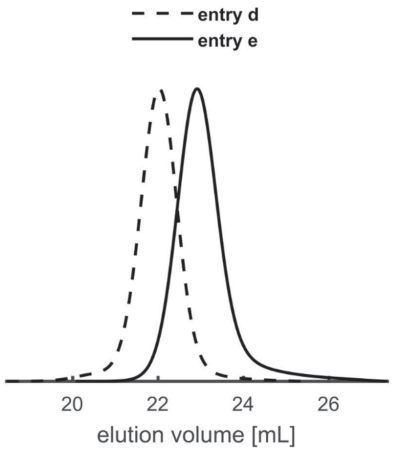

Figure 3

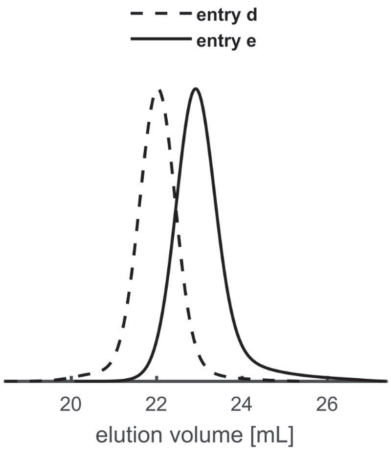

Figure 4

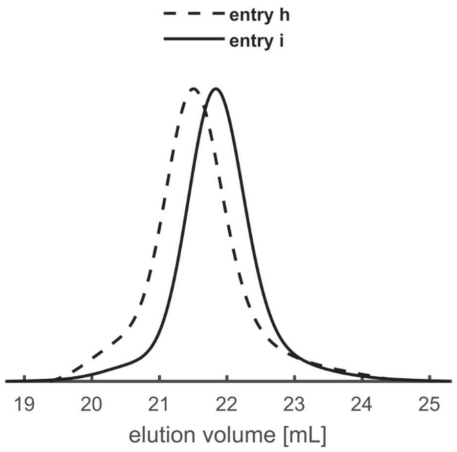

Figure 5

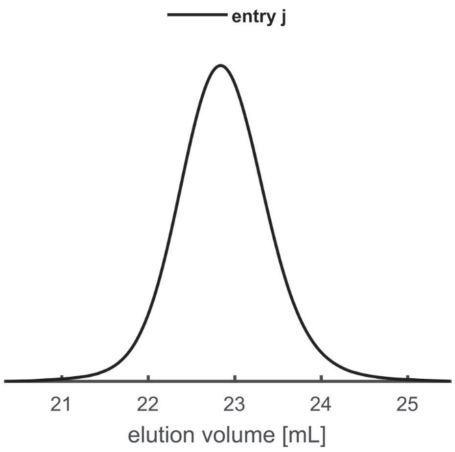

Figure 6

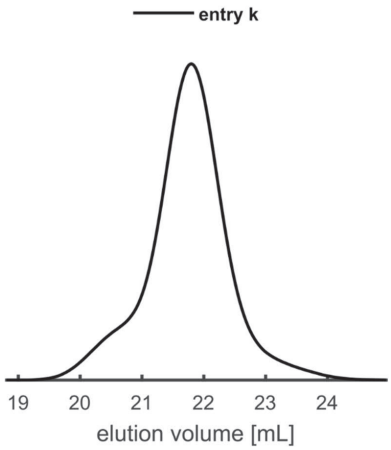

Figure 7

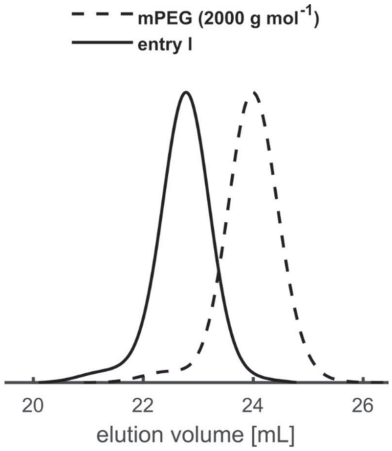

Figure 8

3

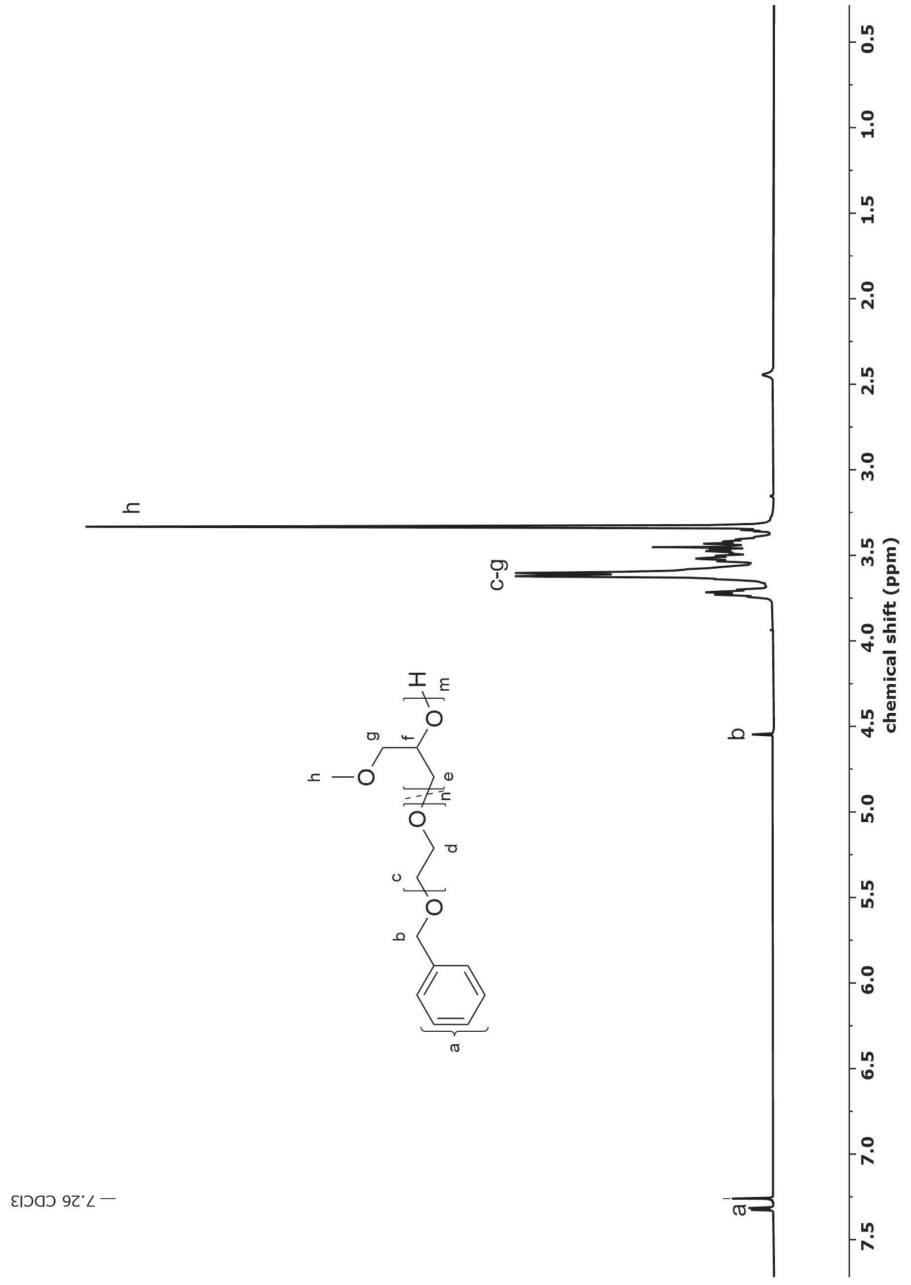
h
c-g
b
a
7.26 CDCl3
chemical shift (ppm)
7.5
7.0
6.5
6.0
5.5
5.0
4.5
4.0
3.5
3.0
2.5
2.0
1.5
1.0
0.5

Figure 9

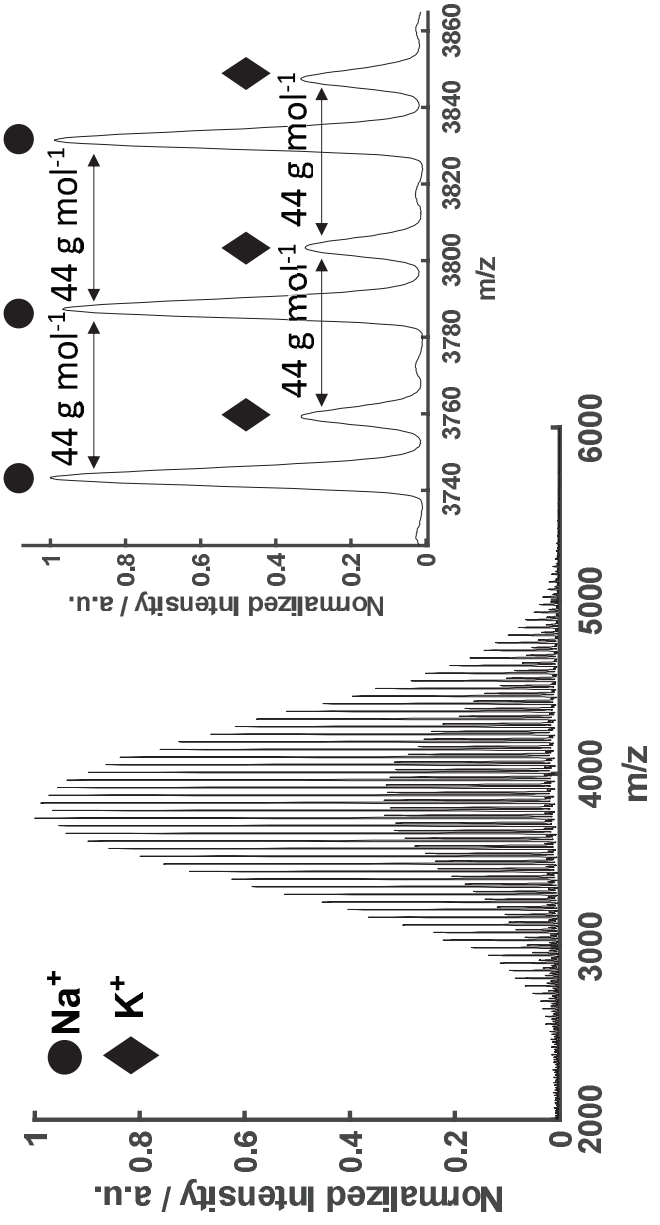
Normalized Intensity / a.u.
m/z
Na+
K+
44 g mol-1
44 g mol-1
44 g mol-1
44 g mol-1

Figure 10

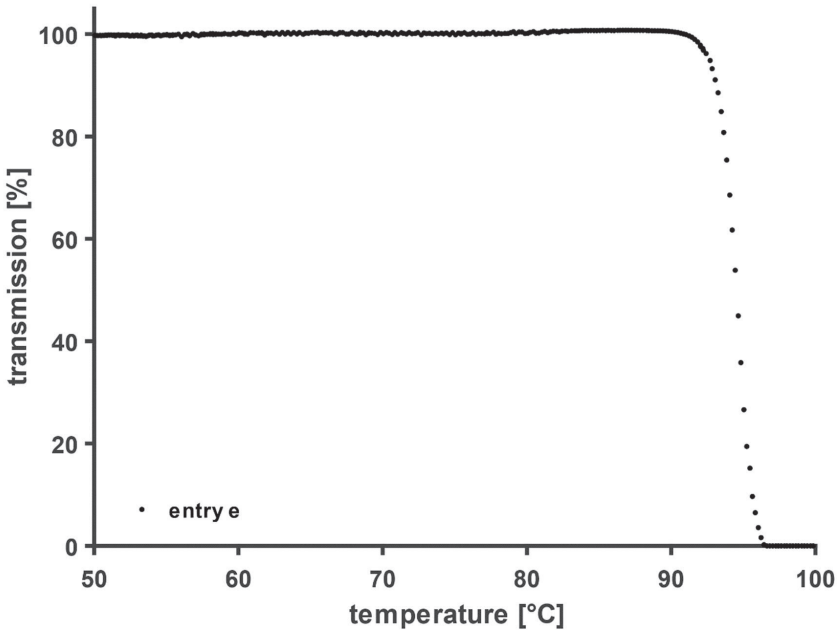
100
80
60
40
20
0
transmission [%]
entry e
50
60
70
80
90
100
temperature [°C]

Figure 11

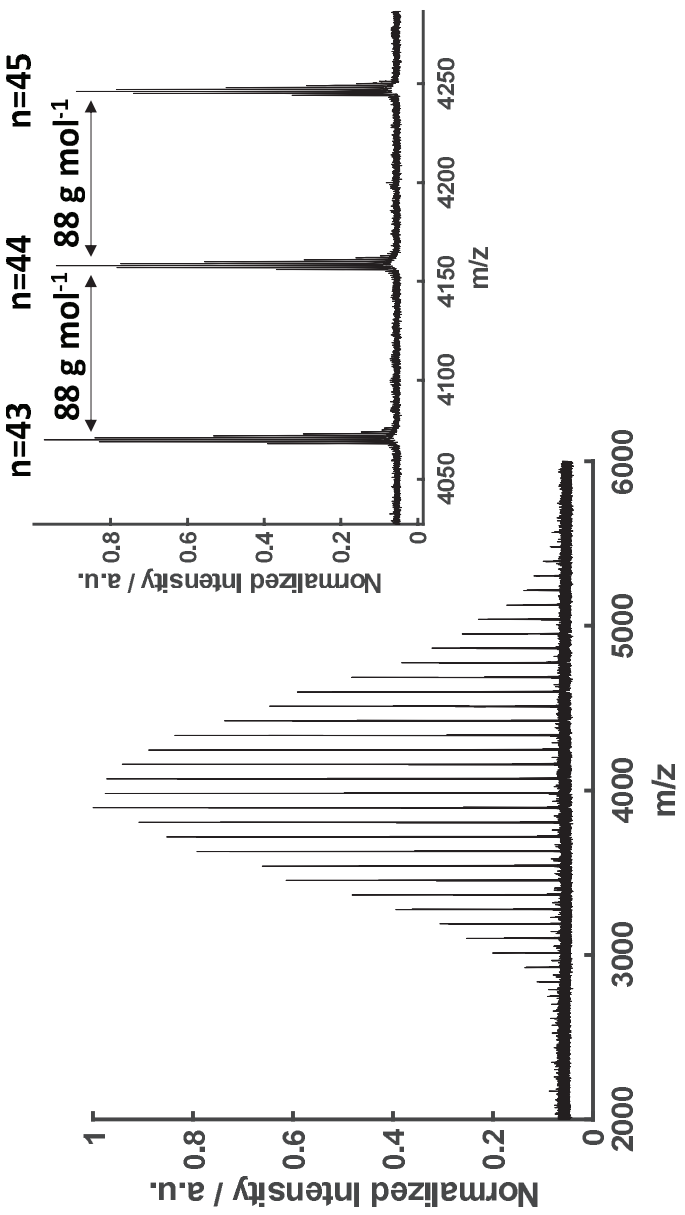

Figure 12

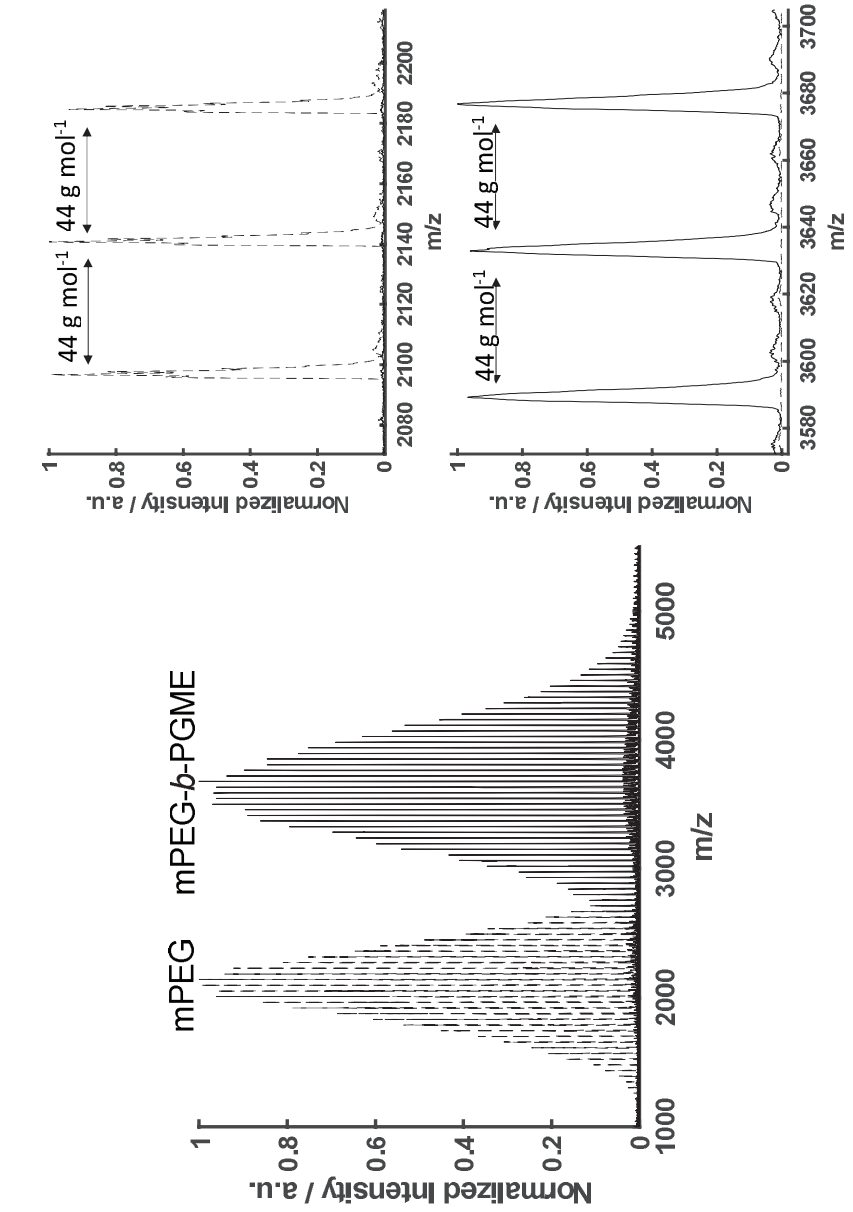
Normalized Intensity / a.u.
m/z
mPEG
mPEG-b-PGME
44 g mol-1
44 g mol-1
44 g mol-1
44 g mol-1

Figure 13

8

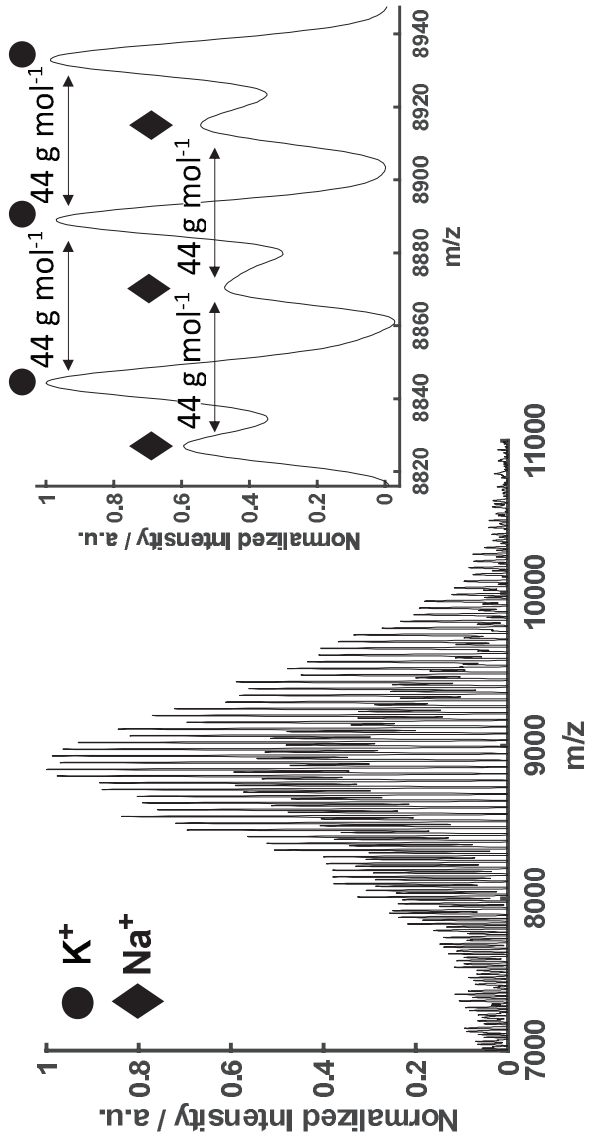
Normalized Intensity / a.u.
m/z
K+
Na+
44 g mol-1
44 g mol-1
44 g mol-1
44 g mol-1

Figure 14

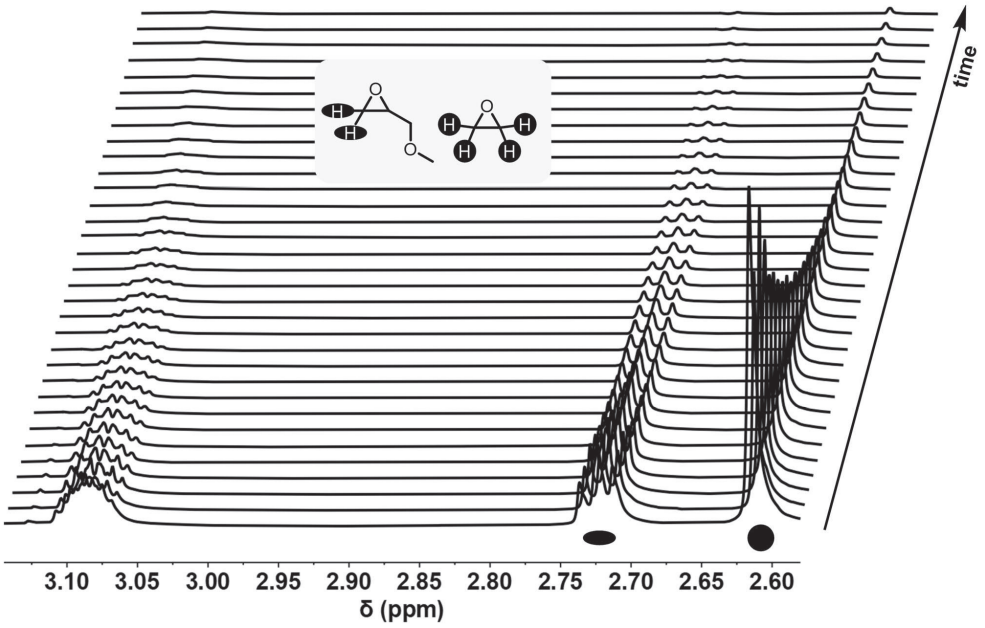

Figure 15

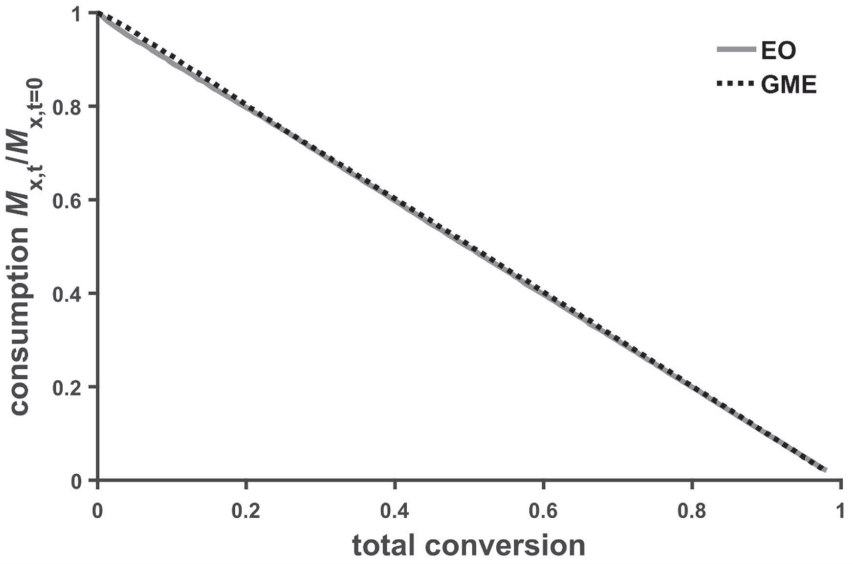

Figure 16

Curriculum vitae - Philip Reinhard Dreier

Personal Data

Address	Mombacher Straße 67a 55122 Mainz
Phone	+49 178 8799913
E-Mail	philip.dreier22@gmail.com
Date and Place of Birth	22.12.1990 / Worms

Education and Work Experience

02/2018 - today	**Doctoral Candidate** in Polymer Chemistry, Research Group of Prof. Dr. Frey
10/2011 - 02/2018	**Master of Science** (1.9), Chemistry, University of Mainz • Master Thesis (2017) in Polymer Chemistry, Research Group of Prof. Dr. Frey • Bachelor Thesis (2014) in Polymer Chemistry, Research Group of Prof. Dr. Frey
04/2016 - 09/2016	**Semester abroad**, ERASMUS+ Internship, University of Warwick, England, Polymer Chemistry, under Supervision of Prof. Dr. Perrier and Prof. Dr. Cameron

Languages and Skills

Languages	**German** (native speaker), **English** (fluent)
IT	**MATLAB**, **Origin**, **LATEX**, **Chemdraw**, **MestReNova**, **Office**
Certified Competences	**Certified Project Manager Business Chemistry**, GDCh **Business Administration for Chemists**, GDCh-Training **"Allgemeines Promotionskolleg"**, University of Mainz
Social Service	**Community Service**, Diakoniestation Lampertheim

List of Publications

Contribution as first author or equally

2021, submitted

Dreier, P.; Matthes, R.; Barent, R. D.; Schüttner, S.; Müller, A. H. E.; Frey, H. In situ Kinetics is Indispensable: Influence of Solvents and Monomers on Anionic Ring-Opening Copolymerization of Epoxides *Macromolecules*, **submitted**.

2021, to be submitted

Matthes, R.; Dreier, P.; Fuß, F.; Bros, M.; Barent, R. D.; Schüttner, S.; Frey, H. Questioning a Paradigm: Random PEG Copolymers for a Better PEGylation?, **to be submitted.**

Dreier, P.; Ahn, J.; Chang, T.; Frey, H. Epoxide Functionalization of Polystyryl-Anions Studied via Solvent Gradient Interaction Chromatography. *Polymer Chemistry*, **to be submitted**.

Dreier, P.; Mathes, R.; Frey, H. Introduction of Multiple Charged Trifluoromethanesulfonamide Groups into Poly(ethylene oxide) Blocks of Polystyrene-Poly(ethylene oxide) Block Copolymer Electrolytes via the Mitsunobu Reaction, **to be submitted**.

Dreier,P.; Steube,M.; Floudas, G; Frey, H. High Yield Peptide Synthesis Strategies for Complex Block Terpolymers: Amphiphilic Thermoplastic Elastomers and their Application as Solid Polymer Electrolytes, **to be submitted**.

Patents, submitted

Dreier, P.; Mohr, R.; Frey, H. Poly(ethylene glycol) having C1 to C3-alkyloxymethyl side chains, bioconjugates thereof, process for its preparation and its use, **submitted**.

Contribution as coauthor

2020

Verkoyen, P.; Dreier, P.; Bros, M.; Hils, C.; Schmalz, H.; Seiffert, S.; Frey, H. "Dumb" pH-Independent and Biocompatible Hydrogels Formed by Copolymers of Long-Chain Alkyl Glycidyl Ethers and Ethylene Oxide. *Biomacromolecules* **2020**, *21*, 3152–3162.

2017

Schubert, C.; Dreier, P.; Nguyen, T.; Maciol, K.; Blankenburg, J.; Friedrich, C.; Frey, H. *Polymer* **2017**, *121*, 328–339.

Conferences

09/2020 **Macrosymposium Freiburg, Germany**

Poster: Amphiphilic Thermoplastic Elastomers with Adjustable Mechanical Properties and their Application as Solid Polymer Electrolytes

09/2019 I**onic Polymerization, Beijing, China**

Poster: Multiaminofunctional Polyethers as Potential Polymer Electrolytes for Lithium Metal Batteries